Volume 23 Number 6

1955

by the

JOURNAL OF CHEMICAL PHYSICS

EDITORS

CLYDE A. HUTCHISON, JR., *Editor*

Associate Editors

Term ending December 31, 1950

RICHARD M. BADGER
DAVID M. DENNISON
JOHN G. KIRKWOOD
G. B. KISTIAKOWSKY
A. W. LAWSON
K. S. PITZER
H. M. SCOTT

Term ending December 31, 1952

CURTIS T. CRAWFORD, JR.
H. S. GUTOWSKY
WILLIAM N. LIPSCOMB
ELLIOTT W. MONTROLL
GEORGE SCATCHARD
J. W. STOUT
GREGORY H. WANNIER

Term ending December 31, 1954

JAMES R. ARNOLD
JACOB BIGELEISEN
WALTER GORDY
ALVIN H. NIELSEN
EARLE K. PLYLER
WAYNE H. SHAFFER
T. F. YOUNG

The Journal of Chemical Physics is published monthly by the American Institute of Physics. Its purpose is to bridge the gap between journals of physics and those of chemistry. The artificial boundary between physics and chemistry has now been in actual fact completely eliminated, and a large and active group is engaged in research which is as much the one as the other. It is to this group that the Journal is rendering its principal service and finding its greatest appeal, both as a prompt and efficient medium for publication of research and as a convenient and carefully edited assemblage of pertinent information.

Instructions for Contributors

Send manuscripts to Clyde A. Hutchison, Jr., Editor, *The Journal of Chemical Physics*, Institute for Nuclear Studies, University of Chicago, Chicago 37, Illinois. Unless otherwise stated submission of a manuscript is a representation that it has been neither copyrighted, published, nor submitted for publication elsewhere. Textual material (abstract, body of the paper, tabular material, references, and figure captions) must be in English, typewritten (except mathematical expressions) double spaced with wide margins on durable, white paper, preferably bond. The original copy, not the carbon, should be submitted. For general style, spellings, abbreviations, and form, consult recent issues of this journal. The authors' institutions are requested to pay a publication charge of $15.00 per page which, if honored, entitles them to 100 free reprints. Instructions will be sent with galley proofs.

An abstract must accompany each article. It should be adequate as an index and as a summary.

Type but the simplest mathematical expressions should be carefully printed in by hand. Be sure to distinguish between capital and small letters. Indicate clearly superscripts and subscripts by inverted carets and carets, respectively. Avoid complicated superscripts and subscripts. Avoid repetition of a complicated expression by representing it by a symbol. Identify in the margin Greek letters and unusual symbols. Use fractional exponents instead of root signs. Use the solidus (/) for fractions wherever its use will save vertical space.

References should appear as footnotes, numbered consecutively. Literature citations of technical journals should be in the form indicated in the Style Manual of the American Institute of Physics and Chemical Abstracts (Chem. Abstracts 45, I-CCLV (1951)).

Tables may be typewritten on sheets separate from the running text. Each table must have a caption which will make the data in the table intelligible without reference to the text. Avoid complicated column headings.

Wherever possible figures should be planned for the width of a column (3 in.). A convenient reduction ratio is about 2:1 or 3:1. Lettering should be large enough on the original that when reduced it shall not be less than about 1/16 in. (~1.5 mm). Line drawings must be in *india ink* on white paper or tracing cloth. Coordinate paper is not desirable but if used must be blue lined and the coordinate lines which are to show must be inked over. Pictures of apparatus, etc., should be glossy prints and should have maximum black and white contrast. Identify each original drawing or photograph on the back with the author's name and the figure number. Figures should be numbered consecutively. Captions should be typed on a separate sheet of paper.

A limited number of alterations in proof are unavoidable, but the cost of making extensive alterations after the article has been set in type will be charged to the author.

Proof and all correspondence concerning papers in the process of publication should be addressed to the Publication Manager, American Institute of Physics, 57 East 55 Street, New York 22, New York.

Subscription Price

	U. S. and Canada	Elsewhere
To members of the American Institute of Physics and Affiliated Societies	$12.00	$13.00
To all others	15.00	17.00

Back Number Prices

Yearly rate when complete year is available: $18.00.
Single copies: $1.75 each.

Subscriptions, renewals, and orders for single copies should be addressed to the American Institute of Physics, 57 East 55 Street, New York 22, New York.

Changes of address should be sent to the American Institute of Physics.

The Journal of Chemical Physics is published monthly by the American Institute of Physics at Prince and Lemon Streets, Lancaster, Pennsylvania.

Entered as second-class matter December 20, 1932, at the Post Office at Lancaster, Pa., under the Act of August 24, 1912. Acceptance for mailing at special rate of postage provided for in paragraph (d-2), section 34.40, P. L. & R. of 1948, authorized February 5, 1933.

THE JOURNAL
OF
CHEMICAL PHYSICS

VOLUME 23, NUMBER 6 JUNE, 1955

Statistical Mechanics of Polymer Solutions. Parts I and II

MICHIO KURATA AND MIKIO TAMURA, *Department of Industrial Chemistry, Faculty of Engineering, Kyoto University, Kyoto, Japan*

AND

TATSURO WATARI, *Faculty of Liberal Arts and Education, Yokohama University, Kamakura, Japan*

(Received July 10, 1953)

Some contributions are made to the refining of the lattice model theory of Flory of chain polymer solutions by introducing the idea used in the recent theory of regular assembly that combinatory factor constructed in terms of multiple site clusters can be properly used to take long-range correlations between a given site and its far distant neighbors into account.

In Part I, the combinatory factors of Flory and others in current use are reconstructed to exemplify the pseudo-assembly method which has been presented by Kikuchi and the present authors for an easy construction of combinatory factors of higher-order approximation for regular assembly, and to give a thorough understanding of the succeeding uses in Part II.

In Part II, a refined theory of chain polymer solutions is developed. The final expressions for the entropy of dilution and the osmotic pressure depend on the flexibility and the degree of branching of the polymer chain, and give a better agreement with observed data even at high dilution.

PART I. PSEUDO-ASSEMBLY METHOD FOR CHAIN POLYMER SOLUTION

A. Introduction

ALTHOUGH the pioneering work of Flory[1] to extend the theory of strictly regular solutions to polymer solutions has been succeeded and improved by various authors,[2–8] the essential features of the original theory of Flory remains almost unchanged, and its inconformity with observed thermodynamic data at high dilutions remains unsolved in the successive lattice model theories. The underlying assumptions of these theories are: (a) the type of the lattice can be specified only by its coordination number, and (b) long-range correlations between far distant segments of a given polymer, or long-range deviations from a random distribution of segments, can be ignored in the process of constructing the combinatory factor which gives the configurational entropy of the system. Both of these assumptions are mere successions of the Bragg and Williams or the Bethe assumption for regular assemblies such as the Ising ferromagnet, alloys, and strictly regular solutions.

In this decade, theories of regular assembly have been refined with respect to the assumptions mentioned above by several authors[9–14] who have used the probabilities of appearance of various configurations of larger clusters, such as triangles or squares, to obtain a more exact expression for the combinatory factor. The refinement is chiefly due to the possibility of taking account of long-range correlations between a given molecule and its far distant neighbors which are entirely ignored in the Bragg-Williams and the Bethe theories. Such correlations become certainly more important in

[1] P. J. Flory, J. Chem. Phys. **10**, 51 (1942); **12**, 425 (1944).
[2] M. L. Huggins, J. Phys. Chem. **46**, 151 (1942).
[3] R. Fujishiro, J. Chem. Soc. Japan **65**, 519 (1944) (in Japanese).
[4] A. R. Miller, Proc. Cambridge Phil. Soc. **39**, 54, 131 (1943); see also A. R. Miller, *The Theory of Solutions of High Polymers* (Oxford University Press, London, 1948).
[5] E. A. Guggenheim, Proc. Roy. Soc. (London) **A183**, 203, 213 (1944); Trans. Faraday Soc. **41**, 107 (1945).
[6] E. A. Guggenheim, *Mixtures* (Oxford University Press, London, 1952).
[7] W. J. Orr, Trans. Faraday Soc. **40**, 320 (1944).
[8] J. Alfrey and P. Doty, J. Chem. Phys. **18**, 77 (1945).
[9] C. N. Yang, J. Chem. Phys. **13**, 66 (1945); Y. Y. Li, J. Chem. Phys. **17**, 447 (1949) and Phys. Rev. **76**, 972 (1949).
[10] T. L. Hill, J. Chem. Phys. **18**, 988 (1950).
[11] E. A. Guggenheim and M. L. McGlashan, Trans. Faraday Soc. **47**, 929 (1951).
[12] J. A. Barker, Proc. Roy. Soc. (London) **A216**, 45 (1953).
[13] R. Kikuchi, Phys. Rev. **81**, 988 (1951).
[14] Kurata, Kikuchi, and Watari, J. Chem. Phys. **21**, 434 (1953). This paper will be cited as TCP III.

the case of polymer solutions where, even at high dilutions, each of the polymer molecules occupies a long sequence of lattice sites. Hence, the introduction of the improved theory of regular assembly to polymer statistics seems to be effective in refining the lattice model theories of Flory and others.

In this series, the authors make some contributions to the refining of the lattice model theory of polymer solutions by introducing the idea of the recent theories of regular assembly reviewed in the foregoing. Fortunately, the pseudo-assembly method,[14] which has been presented by Kikuchi and the authors for an easy construction of combinatory factors of higher-order approximation, proves very convenient to this purpose. In Part I of this article, a short sketch of the method is given in an appropriate form for the present purpose, and some of the combinatory factors of polymer solutions already given by various authors are reconstructed to exemplify the method, on the one hand, and to investigate the nature of these combinatory factors from a unified standpoint, on the other. In Part II, a refined theory of chain polymer solution is given and the entropy of dilution is calculated to make comparison with experimental data. The effects of the flexibility and branching of the polymer chain on thermodynamic properties are also considered somewhat in detail.

It seems to be worth while to re-examine the lattice model theory at the present stage when the theories of gaslike model,[15–18] though elegant, are confronted with mathematical difficulties in the case of chain polymer solutions, or are forced to involve more or less phenomenological treatments.*

B. Combinatory Factors of Regular Solution

We begin with the illustration of the combinatory factors of regular solution in an appropriate form for immediate use in the case of polymer solutions.

Consider a regular solution with $(p+1)$ components of N single-site molecules, the number of molecules of species j $(j=0,1,\cdots,p)$, being N_j. Hence,

$$\sum_{j=0}^{p} N_j = N. \tag{B.1}$$

If we denote the probability of appearance of a j molecule on a lattice point by x_j, and that of a j-k pair of molecules on a pair of neighboring lattice points by y_{jk}, we have

$$x_j = N_j/N = \sum_{k=0}^{p} y_{jk}. \tag{B.2}$$

Now, introducing the abbreviated notations,[19]

$$[\text{point}]_L \equiv L!/\prod_{j=0}^{p} (x_jL)! \tag{B.3}$$

and

$$[\text{bond}]_L \equiv L!/\prod_{j=0}^{p}\prod_{k=0}^{p} (y_{jk}L)!, \tag{B.4}$$

we can write the well-known combinatory factors of the zeroth (Bragg-Williams) and the first (Bethe) approximations, $G_1^{(1)}$ and $G_\omega^{(2)}$, as follows[20]:

$$G_1^{(1)} = [\text{point}]_N, \tag{B.5}$$

$$G_\omega^{(2)} = [\text{point}]_N \cdot ([\text{bond}]_{\omega N}/[\text{point}]_{2\omega N}) \tag{B.6a}$$

$$= ([\text{point}]_N)^{1-2\omega} \cdot ([\text{bond}]_N)^{\omega}, \tag{B.6b}[21]$$

where 2ω is the coordination number of the lattice. Although the detail of the derivation of $G_\omega^{(2)}$ by the pseudo-assembly method[14] is not reproduced here, it will be noted that Eq. (B.6a) has obtained from

$$G_\omega^{(2)} = G_1^{(1)} \cdot ([\text{bond}]_{\omega N}/\textstyle\sum_y [\text{bond}]_{\omega N}), \tag{B.7}$$

and

$$\textstyle\sum_y [\text{bond}]_{\omega N} = [\text{point}]_{2\omega N}. \tag{B.8}$$

Here the summation extends over all of possible sets of y_{jk} for a given set of x_j.

As was pointed out in Sec. G of TCP III, the second approximation is attained by constructing the combinatory factor in terms of a cluster closed with respect to bonds; such clusters are *triangular* in the case of the face-centered cubic lattice, and *square* in the case of the simple cubic lattice. As a preparation for Part II, we will list here the combinatory factors of the second (Kikuchi) approximation without reproducing their

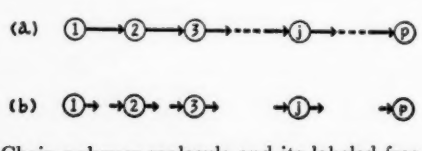

FIG. 1. Chain polymer molecule and its labeled free segments. An arrow represents a chemical bond or a chemical-bond-residue. (a) Chain polymer molecule; (b) labeled free segments.

[15] B. M. Zimm, J. Chem. Phys. **14**, 164 (1946).
[16] A. Isihara, J. Chem. Phys. **18**, 1446 (1950); **19**, 397 (1951).
[17] P. J. Flory, J. Chem. Phys. **13**, 453 (1945); P. J. Flory and W. R. Krigbaum, J. Chem. Phys. **18**, 1086, (1950).
[18] T. B. Grimley, Proc. Roy. Soc. (London) **A212**, 339 (1952).
* *Note added February* 15, 1954.—In a paper just received [Disc. Faraday Soc. **15**, 57 (1953)], Rushbrooke, Scoins, and Wakefield present conclusions similar to ours by direct counting of β_K, which is the analog of Mayer's *irreducible integral*. However, the overlap between their theory and ours is only slight.

[19] Throughout the subsequent analysis, the abbreviated notations such as $[\text{point}]_L$, $[\text{bond}]_L$, $\cdots$, are used to represent "the number of ways of distributing on L sites the cluster indicated in the brackets." They are connected with the notations X_L, Y_L, $\cdots$, or $\{\text{point}\}_L$, $\{\text{bond}\}_L$, $\cdots$ used in TCP III by $[\text{point}]_L = L!/X_L = L!/\{\text{point}\}_L$, $[\text{bond}]_L = L!/Y_L = L!/\{\text{bond}\}_L$, and so on.
[20] The indices written on G represent that, for example, $G_\omega^{(2)}$ is constructed in terms of a "2"-molecular (bond) cluster whose total number is "ω"N.
[21] As we are interested in assemblies with sufficiently large N, we can safely use the Stirling formula and obtain

$$[\text{point}]_{2\omega N} = ([\text{point}]_N)^{2\omega}, \quad [\text{bond}]_{\omega N} = ([\text{bond}]_N)^{\omega}, \cdots.$$

Relations of this kind will be frequently used without remarks.

derivations.

(1) Lattice with ωN Bonds and νN Triangular Cells

$$G_\nu^{(3)}=[\text{point}]_N\left\{\frac{[\text{bond}]_{\omega N}}{[\text{point}]_{2\omega N}}\right\}\times\left\{\frac{[\text{triangle}]_{\nu N}}{[\text{point}]_{3\nu N}([\text{bond}]_{3\nu N}/[\text{point}]_{6\nu N})}\right\} \quad \text{(B.9a)}$$

$$=([\text{point}]_N)^{1-2\omega+3\nu}([\text{bond}]_N)^{\omega-3\nu}([\text{triangle}]_N)^{\nu}. \quad \text{(B.9b)}$$

(2) Lattice with ωN Bonds and μN Square Cells

$$G_\mu^{(4)}=[\text{point}]_N\left\{\frac{[\text{bond}]_{\omega N}}{[\text{point}]_{2\omega N}}\right\}\times\left\{\frac{[\text{square}]_{\mu N}}{[\text{point}]_{4\mu N}([\text{bond}]_{4\mu N}/[\text{point}]_{8\mu N})}\right\} \quad \text{(B.10a)}$$

$$=([\text{point}]_N)^{1-2\omega+4\mu}([\text{bond}]_N)^{\omega-4\mu}([\text{square}]_N)^{\mu}. \quad \text{(B.10b)}$$

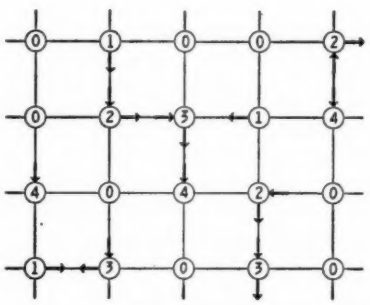

FIG. 2. $G_1^{(1)}$ configuration of hypothetical solution of *free* segments, when $\omega=2$ and $p=4$.

The face-centered cubic and the simple cubic lattices are specified by $\omega=6$, $\nu=8$, and by $\omega=\mu=3$, respectively.

C. First Approximation of Chain Polymer Solution

Consider a polymer solution composed of N_0 solvent molecules and of N_p chain polymers; the latter consists of p-segments which are connected by $p-1$ chemical bonds and are labeled by $j=1,2,\cdots,p$, from the head to the tail as shown in Fig. 1(a). A segment occupies one lattice point as well as a solvent molecule does. As the first step in investigating the chain polymer solution, we consider a hypothetical system composed of solvent molecules and of labeled *free segments* which are shown in Fig. 1(b). For the sake of convenience, we call the j-segment-side-residue of the j-$(j+1)$ chemical bond the "*forward* bond," and that of the $(j-1)$-j chemical bond the "*backward* bond" of the j-segment; these are indicated, in Fig. 1, by arrows away from and toward the j-segment, respectively.

TABLE I. Types and probabilities of appearance of pair clusters in hypothetical solution of free segments. An arrow represents a chemical-bond-residue.

Pair	Prob.	Pair	Prob.
(j)—(k) j - k	y_{jk}	(j)→←(k) j>- k>	$y_{j>k>}$
(j)—←(k) j - k>	$y_{jk>}$	(j)→→(k) j>- <k	$y_{j><k}$
(j)—→(k) j - <k	$y_{j<k}$	(j)←←(k) <j - <k	$y_{<j<k}$

Figure 2 shows a configuration of this hypothetical system in which six types of pair clusters are in existence. The probabilities of appearance of these pair clusters are given in Table I, where $j>$ or $<j$ represents a particle with a forward or backward bond, and j represents a particle without bond residue. If the probability that a particle of the indicated type will appear on one end of bond is denoted by ξ, we have

$$x_j=\xi_j+\xi_{j>}+\xi_{<j}, \quad \text{(C.1)}$$

and

$$\xi_j=\sum_{k=0}^{p}(y_{jk}+y_{jk>}+y_{j<k}),$$

$$\xi_{j>}=\textstyle\sum_k(y_{j>k}+y_{j>k>}+y_{j><k}), \quad \text{(C.2)}$$

$$\xi_{<j}=\textstyle\sum_k(y_{<jk}+y_{<jk>}+y_{<j<k}),$$

with the convention that ξ and y with the subscripts, $0>$, <0, <1, and $p>$ are identically zero.

In the case of the chain polymer solution, however, the pair clusters of such types as j-$k>$ or $j>$-$k>$ can never exist, and the number of the chemical bonds connecting the j-segment with the $(j+1)$-segment is obviously equal to the number of polymers N_p. Therefore, if the volume fraction of polymer molecule is denoted by v_p, we obtain

$$x_0=N_0/N=1-v_p,$$
$$x_j=N_p/N=v_p/p, \quad (j=1,2,\cdots,p), \quad \text{(C.3)}$$

and

$$\begin{cases} y_{j><j+1}\omega N=y_{<j+1,\,j>}\omega N=N_p/2 \\ \qquad\qquad =(v_p/2p)N, & \text{if } j\neq 0,\ p; \\ y_{j><k}=0, & \text{if } k\neq j+1; \\ y_{<jk>}=0, & \text{if } k\neq j-1; \\ y_{jk>}=y_{j<k}=y_{j>k>}=y_{<j<k}=0, & \text{for all pairs of } j \text{ and } k. \end{cases} \quad \text{(C.4)}$$

Equation (C.4) with Eq. (C.2) gives

$$\xi_{j>}=\xi_{<j+1}=0, \quad \text{if } j=0,p;$$
$$=v_p/2\omega p, \quad \text{if } j\neq 0,p; \quad \text{(C.5)}$$

$$\xi_j=\sum_{k=0}^{p}y_{jk}=1-v_p, \quad \text{if } j=0;$$

$$=\{1-(1/2\omega)\}(v_p/p), \quad \text{if } j=1,p; \quad \text{(C.6)}$$

$$=\{1-(1/\omega)\}(v_p/p), \quad \text{if } j=2,3,\cdots,(p-1);$$

and

$$\sum_{j=0}^{p} \xi_j = \sum_{j,k=0}^{p} y_{jk} = 1-(a/\omega)v_p, \tag{C.7}$$

where

$$a \equiv 1-(1/p). \tag{C.8}$$

As the hypothetical system does not differ from the regular solution discussed in Sec. B, except that it consists of asymmetric particles, or particles with bond residue, and as the chain polymer solution can be regarded as a special case of the hypothetical system with the restrictions of Eqs. (C.3) to (C.6), we can safely apply the method outlined in Sec. B to the present system without essential alteration. Then, using the abbreviations,

$$[\text{point}]_N \equiv N!/\prod_{j=0}^{p} (x_j N)!$$
$$= N!/\{(1-v_p)N\}!\{(v_p N/p)!\}^p, \tag{C.9}$$

$$[\text{point}']_{2\omega N} \equiv (2\omega N)!/\prod_{j=0}^{p} \{(\xi_j 2\omega N)!$$
$$\times (\xi_{j>} 2\omega N)!(\xi_{<j} 2\omega N)!\}$$
$$= (2\omega N)!/\{\textstyle\prod_j (\xi_j 2\omega N)!\}$$
$$\times \{(v_p N/p)!\}^{2(p-1)}, \tag{C.10}$$

and

$$[\text{bond}]_{N\omega} \equiv (\omega N)!/\prod_{j,k=0}^{p} \prod_{a=j,j>,<j} \prod_{b=k,k>,<k} (y_{ab}\omega N)!$$
$$= (\omega N)!/\{\prod_{j,k=0}^{p} (y_{jk}\omega N)!\}$$
$$\times \{(v_p N/2p)!\}^{2(p-1)}, \tag{C.11}$$

and keeping in mind the relation corresponding to Eq. (B.8),

$$\textstyle\sum_y [\text{bond}]_{\omega N} = [\text{point}']_{2\omega N}, \tag{C.12}$$[2]

we can obtain

$$G_1^{(1)} = [\text{point}]_N R, \tag{C.13}$$

and

$$G_\omega^{(2)} = ([\text{point}]_N R)([\text{bond}]_{\omega N}/[\text{point}']_{2\omega N}) \tag{C.14a}$$
$$= \frac{N!}{\{(1-v_p)N\}!\{(v_p N/p)!\}^p} \times \frac{\prod_j \{(\xi_j \omega N)!\}^2 \{(v_p N/2p)!\}^{2(p-1)}}{\prod_{j,k} (y_{jk}\omega N)!(\omega N)!} R, \tag{C.14b}$$

where ξ_j's are given by Eq. (C.6), and R represents the number of distinguishable arrangements of bond residue. In the case of flexible chain polymers, R is given by

$$R = (2\omega)^{pN_p}(2\omega-1)^{(p-2)N_p}$$
$$= (2\omega)^{v_p N}(2\omega-1)^{\{1-(2/p)\}v_p N}. \tag{C.15}$$

The combinatory factor $G_\omega^{(2)}$ thus obtained is identical with those of Miller[4] and of Oyama and Matsuo.[23]

When athermal solution is concerned, we obtain

$$y_{jk} = \xi_j \xi_k / \textstyle\sum_{j=0}^{p} \xi_j = \xi_j \xi_k / \{1-(a/\omega)v_p\} \tag{C.16}$$

by maximizing $G_\omega^{(2)}$ with respect to y_{jk}. The substitution of Eqs. (C.6) and (C.16) into Eq. (C.14b) gives

$$G_\omega^{(2)} = \frac{N!}{\{(1-v_p)N\}!\{(v_p N/p)!\}^p} \times \frac{[\{1-(a/\omega)v_p\}\omega N]!\{(v_p N/2p)!\}^{2(p-1)}}{(\omega N)!} R, \tag{C.17}$$

which is just the combinatory factor already given by Huggins.[2]

Although we have derived Eq. (C.17) as a special case of Eq. (C.14b), we can obtain the same result directly as follows. In athermal solution, the disappearance of the short-range order due to van der Waals' interaction permits us to construct $G_\omega^{(2)}/G_1^{(1)}$ in terms of chemical bonds, or of $y_{j><j+1}$ and $\xi_{j>}$, alone, keeping unspecified both y_{jk} and ξ_j. Thus, denoting the number of ways of distributing $\xi_{j>}L$ and $\xi_{<j}L$ particles with bond residue on L sites by $[\text{point}^*]_L$ and those of distributing $y_{j><j+1}L$ and $y_{<j+1,j>}L$ chemical bonds on L sites by $[\text{bond}^*]_L$, and remembering Eqs. (C.4) and (C.5), we obtain[24]

$$[\text{point}^*]_L = [\text{bond}^*]_L = L!/[\{1-(a/\omega)v_p\}L]!$$
$$\times \{(v_p L/2\omega p)!\}^{2(p-1)}. \tag{C.18}$$

Using $[\text{point}^*]_L$ and $[\text{bond}^*]_L$ instead of $[\text{point}']_L$ and $[\text{bond}]_L$ in Eq. (C.14a), we recover Eq. (C.17) at once; that is, we can write it formally as

$$G_\omega^{(2)} = [\text{point}]_N \cdot ([\text{bond}^*]_{\omega N}/[\text{point}^*]_{2\omega N}) \cdot R. \tag{C.19}$$

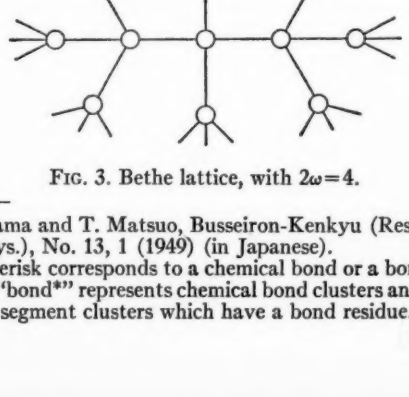

FIG. 3. Bethe lattice, with $2\omega = 4$.

[22] The summation extends over all of possible sets of y's for a given set of ξ's.

[23] T. Oyama and T. Matsuo, Busseiron-Kenkyu (Researches on Chem. Phys.), No. 13, 1 (1949) (in Japanese).

[24] An asterisk corresponds to a chemical bond or a bond residue. Therefore "bond*" represents chemical bond clusters and "point*" represents segment clusters which have a bond residue.

As is well known, the osmotic pressure π of athermal solution is given by

$$\pi\bar{V}_0/\mathbf{R}T=\bar{S}_0^{(2)}/\mathbf{R}=(\partial \ln G_\omega^{(2)}/\partial N_0)_{N_p}$$
$$=(1/p)v_p+\{\tfrac{1}{2}-(a^2/2\omega)\}v_p^2+\cdots, \quad \text{(C.20)}$$

where $\bar{V}_0$ is the partial molar volume of the solvent, $\mathbf{R}$ is the gas constant, T is the absolute temperature and $\bar{S}_0^{(2)}$ is the entropy of dilution of the first approximation. It will be noted here that the second coefficient in Eq. (C.20) is overestimated for flexible chain polymers except for rodlike molecules.

Strictly speaking, as was pointed out in TCP III, the theory of the first approximation is nothing but the theory of the Bethe (dendritic) lattice which has no cell closed in form with respect to bonds as shown in Fig. 3. Since the discrimination whether a polymer chain is flexible or not loses its proper meaning utterly on the Bethe lattice, we cannot discuss the effect of flexibility of chain by the first approximation. This consideration naturally leads us to the second approximation, in which closed cell clusters are introduced in order to construct improved combinatory factors.

PART II. AN IMPROVED THEORY OF CHAIN POLYMER SOLUTIONS (SECOND APPROXIMATION OF ATHERMAL SOLUTION)

In the present part, we shall develop, using the method outlined in Part I, an improved theory of athermal solution of chain polymers, and compare the theory with experimental data of the osmotic pressure. The effects of flexibility and branching of the polymer chain on the entropy of dilution are also discussed in some detail.

D. Face-Centered Cubic Lattice and Two-Dimensional Triangular Lattice

We begin with the lattice composed of N lattice points, ωN bonds, and νN triangular cells, which was adopted in Sec. B as an example of the second approximation of the regular assembly. The face-centered cubic and the two-dimensional triangular lattices are specified by $\omega=6$, $\nu=8$, and by $\omega=3$, $\nu=2$, respectively.

Let us denote the probabilities of appearance of three kinds of configurations of triangular cluster by z's as given in Table II, where $j>$ or $<j$ in the subscript of z represents the particle of species j with the *forward* or *backward* bond, and $<j>$ represents the j particle with both of the bonds. In treating a problem of athermal system, we can use the clusters given in the right half of the table as basic clusters, because the probabilities of appearance of particles with no arrow (or with no chemical-bond-residue) can be left unspecified as was shown in Sec. C [see Eq. (C.19)]. Without loss of generality, we can put

$$z_{j><j+1><j+2}=z_{<j+1><j+2,\,j>}=z_{<j+2,\,j><j+1>}$$
$$=z_{j><j+2<j+1>}=z_{<j+1>j><j+2}=z_{<j+2<j+1>j>}, \text{ etc., (D.1)}$$

TABLE II. Types and probabilities of appearance of triangular clusters. An empty circle represents a lattice point occupied by a particle of any kind, and an arrow represents a chemical bond.

Triangle	Probability	Triangle	Probability
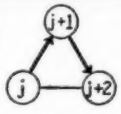	$z_{j><j+1><j+2}$	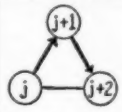	$z_{j><j+1><j+2}$
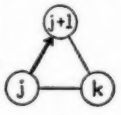	$z_{j><j+1,k}$	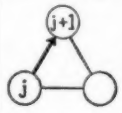	$\sum_{k=0}^{p} z_{j><j+1,k}$
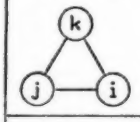	z_{jki}	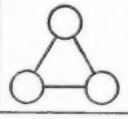	$\sum_{j,k,i=0}^{p} z_{jki}$
General Solution		Athermal Solution	

because of their symmetry. The z's are normalized by

$$\sum_{j,k,i=0}^{p} z_{jki}+6\sum_{j=0}^{p}\{z_{j><j+1><j+2}+\sum_{k=0}^{p} z_{j><j+1,k}\}=1, \quad \text{(D.2)}$$

and they are related to $y_{j><j+1}$ [see Eq. (C.4)] by

$$y_{j><j+1}=\sum_{k=0}^{p} z_{j><j+1,k}+z_{j><j+1><j+2}+z_{j-1><j><j+1}$$
$$=0 \qquad (j=0,p) \qquad \text{(D.3)}$$
$$=v_p/2\omega p \quad (j=1,2,\cdots,p-1),$$

where v_p is the volume fraction of the polymer.

The number of the subchain composed of three consecutive segments, say j-, $(j+1)$- and $(j+2)$-segment, is obviously equal to the number of polymer molecules N_p. Hence, if β is the probability that the bond angle becomes $\frac{1}{3}\pi$, we can write

$$6z_{j><j+1><j+2}\nu N=\beta N_p=(\beta v_p/p)N$$
$$(j=1,2,\cdots,p-2) \quad \text{(D.4)}$$
$$=0 \qquad (j=0,\,p-1,\,p),$$

in which the numerical factor 6 represents the number of ways of orientating a given cluster [see Eq. (D.1)]. Using this relation and Eq. (D.3), we have

$$\sum_{k=0}^{p} z_{j><j+1,k}=\{(1/2\omega)-(\beta/3\nu)\}(v_p/p)$$
$$(j=2,3,\cdots,p-2)$$
$$=\{(1/2\omega)-(\beta/6\nu)\}(v_p/p) \qquad \text{(D.5)}$$
$$(j=1,\,p-1)$$
$$=0 \qquad (j=0,p),$$

TABLE III. Types and probabilities of appearance of one-point clusters. An empty circle represents a lattice point occupied by a particle of any kind, and an arrow represents a chemical-bond-residue.

Point	Prob.	Point	Prob.
$\textcircled{j}\leftarrow$ or $\textcircled{j}\rightarrow$	$\eta_{<j>}$	$\textcircled{j}\rightarrow$	$\overline{\overline{\eta}}_{j>}$
$\textcircled{j}\nwarrow$ or $\textcircled{j}\rightarrow$	$\eta_{j>}$	$\textcircled{j}\leftarrow$	$\overline{\overline{\eta}}_{<j}$
$\textcircled{j}\nwarrow$ or $\textcircled{j}\leftarrow$	$\eta_{<j}$	$\textcircled{j}-$	$\overline{\overline{\eta}}_{j}$
$\textcircled{j}\leftarrow$	η_j		
$\nwarrow$	$\sum_{j=0}^{p}\eta_j$	$\circ-$	$\sum_{j=0}^{p}\overline{\overline{\eta}}_j$

and, combining Eqs. (D.2), (D.4) with Eq. (D.5), we obtain

$$\sum_{j,k,i} z_{jki}=1-\{(3a/\omega)-(b/\nu)\}v_p, \tag{D.6}$$

with the abbreviations,

$$a\equiv 1-(1/p) \quad \text{and} \quad b\equiv\beta\{1-(2/p)\}. \tag{D.7}$$

For the sake of convenience, let us introduce the probability η that a particle of the indicated type will appear on a corner of a triangular cell as shown in Table III. The definition of η gives, with Eq. (D.4) to (D.6), the following relations:

$$\begin{aligned}\eta_{<j>}&=z_{j-1><j><j+1}=\beta v_p/6\nu p && (j=2\sim p-1)\\ &=0 && (j=0,1,p),\end{aligned} \tag{D.8a}$$

$$\begin{aligned}\eta_{<j}&=\sum_k z_{j-1><j,k}+z_{j-2><j-1><j}\\ &=\{(1/2\omega)-(\beta/6\nu)\}(v_p/p) && (j=2\sim p-1)\\ &=v_p/2\omega p && (j=p)\\ &=0 && (j=0,1),\end{aligned} \tag{D.8b}$$

$$\begin{aligned}\eta_{j>}&=\sum_k z_{j><j+1,k}+z_{j><j+1><j+2}\\ &=\{(1/2\omega)-(\beta/6\nu)\}(v_p/p) && (j=2\sim p-1)\\ &=v_p/2\omega p && (j=1)\\ &=0 && (j=0,p),\end{aligned} \tag{D.8c}$$

$$\begin{aligned}\eta_j&=\sum_{k,i} z_{jki}+2\sum_k z_{k><k+1,j}\\ &=\{1-(2/\omega)+(\beta/3\nu)\}(v_p/p) && (j=2\sim p-1)\\ &=\{1-(1/\omega)\}(v_p/p) && (j=1,p)\\ &=1-v_p && (j=0),\end{aligned} \tag{D.8d}$$

$$\begin{aligned}\Sigma_j\eta_j&=1-2\Sigma_j(\eta_{j>}+\eta_{<j}+\eta_{<j>})\\ &=1-\{(2a/\omega)-(b/3\nu)\}v_p.\end{aligned} \tag{D.8e}$$

η's are related to ξ's by

$$\xi_j=\eta_j+\eta_{j>}+\eta_{<j}, \quad \xi_{j>}=\eta_{j>}+\eta_{<j>},$$
$$\text{and} \quad \xi_{<j}=\eta_{<j}+\eta_{<j>}. \tag{D.9}$$

The combinatory factor of the second approximation $G_\nu^{(3)}$ of the present system can be written in the form analogous to Eq. (B.9a),

$$G_\nu^{(3)}=\{[\text{point}]_N R\}\left\{\frac{[\text{bond}^*]_{\omega N}}{[\text{point}^*]_{2\omega N}}\right\}\times\left\{\frac{[\text{triangle}_*^*]_{\nu N}}{[\text{point}_*^*]_{3\nu N}([\text{bond}^*]_{3\nu N}/[\text{point}^*]_{6\nu N})}\right\}, \tag{D.10}$$

with the abbreviations,

$$\left\{\begin{aligned}&[\text{point}]_L\equiv L!/\textstyle\prod_j(x_jL)!,\\ &[\text{point}^*]_L\equiv L!/(\textstyle\sum_j\xi_jL)!\\ &\qquad\times\textstyle\prod_j\{(\xi_{j>}L)!(\xi_{<j}L)!\},\\ &[\text{point}_*^*]_L\equiv L!/(\textstyle\sum_j\eta_jL)!\textstyle\prod_j\{(\eta_{j>}L)!\\ &\qquad\times(\eta_{<j}L)!(\eta_{<j>}L)!\}^2,\\ &[\text{bond}^*]_L\equiv L!/(\textstyle\sum_{j,k}y_{jk}L)!\\ &\qquad\times\textstyle\prod_j\{(y_{j><j+1}L)!\}^2,\\ &[\text{triangle}_*^*]_L\equiv L!/(\textstyle\sum_{j,k,i}z_{jki}L)!\\ &\qquad\times\textstyle\prod_j\{(\sum_k z_{j><j+1,k}L)!\\ &\qquad\times(z_{j><j+1><j+2}L)!\}^6.\end{aligned}\right. \tag{D.11}$$

Although derivation of Eq. (D.10) will not be given here, it is noted that the equation can be derived from considerations quite similar to those given in Secs. B and C, and that the first two terms in the right-hand side of the equation correspond to $G_\omega^{(2)}$ already given by Eq. (C.19). Substituting Eqs. (C.4) to (C.7) and (D.1) to (D.9) into Eq. (D.10), we find the explicit expression for $G_\nu^{(3)}$,

$$\begin{aligned}G_\nu^{(3)}=&\left\{\frac{N!}{\{(1-v_p)N\}!\{(v_pN/p)!\}^p}R\right\}\\ &\times\left\{\frac{\{(1-a\omega^{-1}v_p)\omega N\}!\{(v_pN/2p)!\}^{2(p-1)}}{(\omega N)!}\right\}\\ &\times\left\{\frac{(\nu N)!}{[\{1-(3a\omega^{-1}-b\nu^{-1})v_p\}\nu N]!Z_{\nu N}^*}\right.\\ &\left.\cdot\frac{[\{1-(2a\omega^{-1}-\frac{1}{3}b\nu^{-1})v_p\}3\nu N]!H_{3\nu N}^*}{\{(1-a\omega^{-1}v_p)3\nu N\}!Y_{3\nu N}^*}\right\},\end{aligned} \tag{D.12}$$

with

$$Z_{\nu N}^{*}\equiv\left[\left\{\left(\frac{1}{2\omega}-\frac{\beta}{6\nu}\right)^{\frac{v_p}{p}\nu N}\right\}!\right]^{12}\times\left[\left\{\left(\frac{1}{2\omega}-\frac{\beta}{3\nu}\right)^{\frac{v_p}{p}\nu N}\right\}!\right]^{6(p-3)}\times\left\{\left(\frac{\beta v_p}{6p}N\right)!\right\}^{6(p-2)},$$

$$Y_{3\nu N}^{*}\equiv\left\{\left(\frac{v_p}{2\omega p}3\nu N\right)!\right\}^{2(p-1)}, \tag{D.13}$$

$$H_{3\nu N}^{*}\equiv\left\{\left(\frac{v_p}{2\omega p}3\nu N\right)!\right\}^{4}\times\left[\left\{\left(\frac{1}{2\omega}-\frac{\beta}{6\nu}\right)^{\frac{v_p}{p}3\nu N}\right\}!\right]^{4(p-2)}\times\left\{\left(\frac{\beta v_p}{2p}N\right)!\right\}^{2(p-2)}.$$

As will be shown later, the explicit forms of $Z_{\nu N}^{*}$, $Y_{3\nu N}^{*}$, and $H_{3\nu N}^{*}$, Eq. (D.13), do not appear in the final equation of the entropy of dilution.

From Eq. (D.12), we can derive at once the following expression for the entropy of dilution $\bar{S}_0^{(3)}$,

$$\begin{aligned}\bar{S}_0^{(3)}/\mathbf{R}&\equiv(\partial\ln G_\nu^{(3)}/\partial N_0)_{N_p}\\&=-\ln(1-v_p)+\omega\ln(1-a\omega^{-1}v_p)\\&\quad-\nu[\ln\{1-(3a\omega^{-1}-b\nu^{-1})v_p\}\\&\quad-3\ln\{1-(2a\omega^{-1}-\tfrac{1}{3}b\nu^{-1})v_p\}\\&\quad+3\ln(1-a\omega^{-1}v_p)].\end{aligned} \tag{D.14}$$

Expanding this equation in power series of v_p, we have

$$\bar{S}_0^{(3)}/\mathbf{R}=b_1v_p+b_2v_p^2+\cdots, \tag{D.15}$$

with

$$b_1=1/p \tag{D.16}$$

and

$$b_2=\tfrac{1}{2}-(a^2/2\omega)-b\{(a/\omega)-(b/3\nu)\}.$$

Accordingly, the present approximation does not agree with the first approximation because $b\neq0$, in general [see Eq. (D.7)]. When p is large enough so that $1/p\ll1$, we can put $a=1$ and $b=\beta$. Since β increases, according to its definition, from zero to unity with increasing flexibility of polymer chain, we obtain

$$\left.\begin{aligned}&b_2=5/12\sim7/24 \text{ when } \omega=6 \text{ and } \nu=8\\&\qquad\text{(the face-centered cubic lattice),}\\&\text{and}\\&b_2=\tfrac{1}{3}\sim\tfrac{1}{6} \text{ when } \omega=3 \text{ and } \nu=2\\&\qquad\text{(the two-dimensional triangular lattice).}\end{aligned}\right\} \tag{D.17}$$

Although these values are still overestimated in comparison with experimental results, $b_2=0.1\sim0.2$, the fact that b_2 of the present theory decreases remarkably with increasing flexibility, or with increasing β, encourages our intention to refine the lattice model theory. When the bond angle is fixed to π and, accordingly, $b=0$, i.e., when the solution is composed of rodlike polymers, b_2 of the second approximation reduces to that of the first approximation. This result also seems to be reasonable, because b_2 of the lattice solution of rod-like polymers is counted rigorously by the first approximation, as will be shown in the Appendix.

Let us reserve more detailed comparison of the theory with observed data for Sec. F.

TABLE IV. Types and probabilities of appearance of square clusters. An empty circle represents a lattice point occupied by a particle of any kind, and an arrow represents a chemical bond.

Square	Probability	Square	Probability
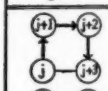	$W_{j<j+1<j+2<j+3}$		$W_{j<j+1<j+2<j+3}$
	$W_{j<j+1<j+2,\ell}$		$\sum_{\ell=0}^{p} W_{j<j+1<j+2,\ell}$
	$W_{j<j+1,k<k+1}$		$W_{j<j+1,k<k+1}=\lambda_{jk}V_p^2$
	$W_{j<j+1<k+1,k>}$		$W_{j<j+1<k+1,k>}=\chi_{jk}V_p^2$
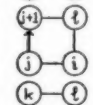	$W_{j<j+1,\ell i}$		$\sum_{\ell,i=0}^{p} W_{j<j+1,\ell i}$
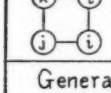	$W_{jk\ell i}$	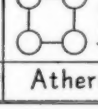	$\sum_{j,k,\ell,i=0}^{p} W_{jk\ell i}$
General Solution		Athermal Solution	

E. Simple Cubic Lattice and Two-Dimensional Square Lattice

Now we proceed to another interesting example, simple cubic lattice. As was pointed out in Sec. B, the second approximation of the lattice composed of N lattice points, ωN bonds, and μN squares is attained when we adopt square clusters as the basic cluster. Table IV shows the basic clusters and their probabilities of appearance. In the case of athermal solution, we can develop the second approximation by using the basic clusters given in the right half of the table.

Without loss of generality, we can put

$$w_{jkli}=w_{klij}=w_{lijk}=w_{ijkl}=w_{ilkj}=w_{lkji}=w_{kjil}=w_{jilk}, \tag{E.1}$$

because of the symmetry of the clusters. For simplicity's sake, let us define new variables λ and κ by

$$\left.\begin{aligned}&\lambda_{jk}\equiv w_{j><j+1,k><k+1}/v_p^2, && \kappa_{jk}\equiv w_{j><j+1<k+1,k>}/v_p^2,\\&\lambda_j\equiv\sum_{k=0}^{p}\lambda_{jk}, && \kappa_j\equiv\sum_{k=0}^{p}\kappa_{jk},\\&\lambda\equiv\textstyle\sum_j\lambda_j, && \kappa\equiv\textstyle\sum_j\kappa_j.\end{aligned}\right\} \tag{E.2}$$

With these notations, the normalization condition of w's and the relation of w's to y's can be written as follows:

$$\sum_{j,k,l,i=0}^{p} w_{jkli}+4(\lambda+\kappa)v_p^2+8\sum_{j=0}^{p}\{w_{j><j+1><j+2><j+3}+\sum_{l=0}^{p} w_{j><j+1><j+2,l}+\sum_{l,i=0}^{p} w_{j><j+1,li}\}=1, \quad \text{(E.3)}$$

and

$$y_{j><j+1}=\sum_{k=j-2}^{j} w_{k><k+1><k+2><k+3}+\sum_{l=0}^{p}\sum_{k=j-1}^{j} w_{k><k+1><k+2,l}+\sum_{l,i=0}^{p} w_{j><j+1,li}+(\lambda_j+\kappa_j)v_p^2. \quad \text{(E.4)}$$

Before we construct the combinatory factor of the second approximation $G_\mu^{(4)}$, let us derive the relations of w's to v_p.

Consider the subchains composed of three consecutive segments, say j-, $(j+1)$-, and $(j+2)$-segment, and of four consecutive segments, say j-, $(j+1)$-, $(j+2)$-, and $(j+3)$-segment, and call them the "three-segment subchain" and the "four-segment subchain," respectively, both of which are obviously equal to the number of the polymer molecules N_p. We then obtain

$$\begin{aligned} w_{j><j+1><j+2><j+3}+w_{j-1><j><j+1><j+2}+\sum_l w_{j><j+1><j+2,l} &=0 \qquad (j=0,\ p-1,\ p)\\ &=\beta v_p/8\mu p \quad (j=1,2,\cdots,p-2), \end{aligned} \quad \text{(E.5)}$$

and

$$\begin{aligned} w_{j><j+1><j+2><j+3} &=0 \qquad (j=0,\ p-2,\ p-1,\ p)\\ &=\gamma v_p/8\mu p \quad (j=1,2,\cdots,p-3), \end{aligned} \quad \text{(E.6)}$$

where β and γ represent the probabilities that the bond angle will become $\frac{1}{2}\pi$, and that the four-segment subchain coils in the form of square, respectively. Substituting Eqs. (E.6) into (E.5), we have

$$\begin{aligned} \sum_{l=0}^{p} w_{j><j+1><j+2,l} &=0 \qquad (j=0,\ p-1,\ p)\\ &=(\beta-\gamma)v_p/8\mu p \quad (j=1,\ p-2)\\ &=(\beta-2\gamma)v_p/8\mu p \quad (j=2,3,\cdots,p-3), \end{aligned} \quad \text{(E.7)}$$

and, substituting again Eqs. (E.6) and (E.7) into (E.4), we have

$$\sum_{l,i=0}^{p} w_{j><j+1,li}=\zeta_j-(\lambda_j+\kappa_j)v_p^2, \quad \text{(E.8)}$$

with

$$\begin{aligned} \zeta_j &=0 \qquad (j=0,p)\\ &=\{(1/2\omega)-(\beta/8\mu)\}(v_p/p) \quad (j=1,\ p-1)\\ &=[(1/2\omega)-\{(2\beta-\gamma)/8\mu\}](v_p/p)\\ &\qquad (j=2,3,\cdots,p-2). \end{aligned} \quad \text{(E.9)}$$

Then, defining c by

$$c\equiv\gamma\{1-(3/p)\}, \quad \text{(E.10)}$$

and using a and b defined by Eq. (D.7), we obtain

$$\zeta\equiv\sum_j \zeta_j=\{(a/2\omega)-(b/4\mu)+(c/8\mu)\}v_p, \quad \text{(E.11)}$$

and, substituting Eqs. (E.6) to (E.11) into (E.3), we find

$$\sum_{j,k,l,i} w_{jkli}=1-\{(4a/\omega)-(b/\mu)\}v_p+4(\lambda+\kappa)v_p^2. \quad \text{(E.12)}$$

For the sake of convenience, let us again denote by η the probability that a particle of the indicated type will appear on a corner of square cell. This definition of η gives, in the present case, the following relations:

$$\begin{aligned} \eta_{<j>}&\equiv\sum_l w_{j-1><j><j+1,l}+w_{j-1><j><j+1><j+2}+w_{j-2><j-1><j><j+1}\\ &=0 \qquad (j=0,1,p)\\ &=\beta v_p/8\mu p \qquad (j=2,3,\cdots,p-1), \end{aligned} \quad \text{(E.13a)}$$

$$\begin{aligned} \eta_{j>}&\equiv\sum_{l,i} w_{j><j+1,li}+(\lambda_j+\kappa_j)v_p^2+\sum_l w_{j><j+1><j+2,l}+w_{j><j+1><j+2><j+3}\\ &=0 \qquad (j=0,p)\\ &=v_p/2\omega p \qquad (j=1)\\ &=\{(1/2\omega)-(\beta/8\mu)\}(v_p/p) \quad (j=2,3,\cdots,p-1), \end{aligned} \quad \text{(E.13b)}$$

$$\begin{aligned} \eta_{<j}&=0 \qquad (j=0,1)\\ &=v_p/2\omega p \qquad (j=p)\\ &=\{(1/2\omega)-(\beta/8\mu)\}(v_p/p) \quad (j=2,3,\cdots,p-1), \end{aligned} \quad \text{(E.13c)}$$

$$\sum_j \eta_j=1-2\sum_j(\eta_{j>}+\eta_{<j}+\eta_{<j>})=1-\{(2a/\omega)-(b/4\mu)\}v_p, \quad \text{(E.13d)}$$

and

$$\xi_j=\eta_j+\eta_{j>}+\eta_{<j}, \quad \xi_{j>}=\eta_{j>}+\eta_{<j>}, \quad \text{(E.14)}$$

and

$$\xi_{<j}=\eta_{<j}+\eta_{<j>}.$$

Using the notations given in the foregoing and defining the abbreviations,

$$[\text{point}^{*}_{*}]_L \equiv L!/(\sum_j \eta_j L)!\prod_j\{(\eta_{<j}L)!\times(\eta_{j>}L)!(\eta_{<j>}L)!\}^2,$$

$$[\text{square}^{**}_{*}]_L \equiv L!/(\sum_{j,k,l,i} w_{jkli}L)!\times\prod_j\{(w_{j><j+1><j+2><j+3}L)!\times(\sum_k w_{j><j+1><j+2,k}L)!\times(\sum_{k,i} w_{j><j+1,ki}L)!\}^3\times\prod_{j,k}\{(\lambda_{jk}v_p{}^2L)!(\kappa_{jk}v_p{}^2L)!\}^4, \quad \text{(E.15)}$$

we can write the combinatory factor of the second approximation $G_\mu{}^{(4)}$ of the present lattice as

$$G_\mu{}^{(4)} = \{[\text{point}]_N R\}\left\{\frac{[\text{bond}^{*}]_{\omega N}}{[\text{point}^{*}]_{2\omega N}}\right\}\times\left\{\frac{[\text{square}^{**}_{*}]_{\mu N}}{[\text{point}^{*}_{*}]_{4\mu N}([\text{bond}^{*}]_{4\mu N}/[\text{point}^{*}]_{8\mu N})}\right\}, \quad \text{(E.16)}$$

which is the analog of Eq. (B.10a), and gives, with Eqs. (E.1) to (E.13), the more explicit expression,

$$G_\mu{}^{(4)} = \left\{\frac{N!}{\{(1-v_p)N\}!\{(v_pN/p)!\}^p}R\right\}\left\{\frac{\{(1-a\omega^{-1}v_p)\omega N\}!\{(v_pN/2p)!\}^{2(p-1)}}{(\omega N)!}\right\}\times\left\{\frac{(\mu N)![\{1-(2a\omega^{-1}-\frac{1}{4}b\mu^{-1})v_p\}4\mu N]!H_{4\mu N}}{[\{1-(4a\omega^{-1}-b\mu^{-1})v_p+4(\lambda+\kappa)v_p{}^2\}\mu N]!W_{\mu N}\{(1-a\omega^{-1}v_p)4\mu N\}!Y_{4\mu N}}\right\}, \quad \text{(E.17)}$$

with

$$W_{\mu N} \equiv \{(\gamma v_pN/8p)!\}^{8(p-3)}[\{(\beta-\gamma)v_pN/8p\}!]^{16}[\{(\beta-2\gamma)v_pN/8p\}!]^{8(p-4)}\times\prod_j[\{(\zeta_j-\lambda_jv_p{}^2-\kappa_jv_p{}^2)\mu N\}!]^8\prod_{j,k}\{(\lambda_{jk}v_p{}^2\mu N)!(\kappa_{jk}v_p{}^2\mu N)!\}^4. \quad \text{(E.18)}$$

Here, $H_{4\mu N}$ and $Y_{4\mu N}$ are again given by the similar equations to Eq. (D.13).

The variables, λ_{jk} and κ_{jk}, which remain undetermined in $G_\mu{}^{(4)}$, can be determined by the equations of equilibrium condition,

$$\left(\frac{\partial \ln G_\mu{}^{(4)}}{\partial\lambda_{jk}}\right)_{v_p,\beta,\gamma}=0 \quad \text{and} \quad \left(\frac{\partial \ln G_\mu{}^{(4)}}{\partial\kappa_{jk}}\right)_{v_p,\beta,\gamma}=0. \quad \text{(E.19)}$$

Remembering the definition of λ's, Eq. (E.2), and using the condition of symmetry, $\lambda_{jk}=\lambda_{kj}$, we obtain from Eqs. (E.19) and (E.17)

$$\{1-(4a\omega^{-1}-b\mu^{-1})v_p+4(\lambda+\kappa)v_p{}^2\}\lambda_{jk}v_p{}^2 = \{\zeta_j-(\lambda_j+\kappa_j)v_p{}^2\}\{\zeta_k-(\lambda_k+\kappa_k)v_p{}^2\}. \quad \text{(E.20)}$$

Similarly, we find for κ

$$\{1-(4a\omega^{-1}-b\mu^{-1})v_p+4(\lambda+\kappa)v_p{}^2\}\kappa_{jk}v_p{}^2 = \{\zeta_j-(\lambda_j+\kappa_j)v_p{}^2\}\{\zeta_k-(\lambda_k+\kappa_k)v_p{}^2\}. \quad \text{(E.21)}$$

From these two equations, we obtain at first

$$\lambda_{jk}=\kappa_{jk} \quad \text{and, then,} \quad \lambda_j=\kappa_j, \quad \lambda=\kappa. \quad \text{(E.22)}$$

Substituting these relations into Eq. (E.21), and making the summations over k and j, we obtain

$$\{1-(4a\omega^{-1}-b\mu^{-1})v_p+8\lambda v_p{}^2\}\lambda_jv_p{}^2 = (\zeta-2\lambda v_p{}^2)(\zeta_j-2\lambda_jv_p{}^2)$$

and

$$\{1-(4a\omega^{-1}-b\mu^{-1})v_p+8\lambda v_p{}^2\}\lambda v_p{}^2=(\zeta-2\lambda v_p{}^2)^2, \quad \text{(E.23)}$$

the latter of which gives

$$\lambda v_p{}^2 = 2\zeta^2/[1-(2a\omega^{-1}-b\mu^{-1})v_p+\{(1-2a\omega^{-1}v_p+b\mu^{-1}v_p)^2+16\zeta^2\}^{\frac{1}{2}}]. \quad \text{(E.24)}$$

At high dilutions, we can write λ in the power series of v_p,

$$8\lambda = 2(a\omega^{-1}-\tfrac{1}{2}b\mu^{-1}+\tfrac{1}{4}c\mu^{-1})^2\times\{1+(2a\omega^{-1}-\tfrac{1}{2}c\mu^{-1})v_p+\cdots\}. \quad \text{(E.25)}$$

From Eq. (E.23), we can easily obtain

$$\lambda_j=\lambda(\zeta_j/\zeta). \quad \text{(E.26a)}$$

The substitution of this relation into the quotient of Eq. (E.20) by (E.23) gives

$$\lambda_{jk}=\lambda(\zeta_j\zeta_k/\zeta^2). \quad \text{(E.26b)}$$

Let us now compute the mixing entropy $S^{(4)}$ and the entropy of dilution $\bar{S}_0{}^{(4)}$ by using $G_\mu{}^{(4)}$ given in the foregoing. Assuming that β is independent of v_p, we find from Eqs. (E.17) and (E.26)

$$\begin{aligned}S^{(4)}/\mathbf{R} = &-\{(1-v_p)\ln(1-v_p)+v_p\ln v_p\}\\ &+\{\omega(1-a\omega^{-1}v_p)\ln(1-a\omega^{-1}v_p)+av_p\ln v_p\}\\ &-\mu\{1-(4a\omega^{-1}-b\mu^{-1})v_p+8\lambda v_p{}^2\}\\ &\times\ln\{1-(4a\omega^{-1}-b\mu^{-1})v_p+8\lambda v_p{}^2\}\\ &-8\mu(\zeta-2\lambda v_p{}^2)\ln(\zeta-2\lambda v_p{}^2)-8\mu\lambda v_p{}^2\ln(\lambda v_p{}^2)\\ &-2(\beta-\gamma)(v_p/p)\ln\{(\beta-\gamma)v_p/8\mu p\}\\ &-(\beta-2\gamma)\{1-(4/p)\}v_p\ln\{(\beta-2\gamma)v_p/8\mu p\}\\ &-cv_p\ln(\gamma v_p/8\mu p)+4\mu\{1-(2a\omega^{-1}\\ &-\tfrac{1}{4}b\mu^{-1})v_p\}\ln\{1-(2a\omega^{-1}-\tfrac{1}{4}b\mu^{-1})v_p\}\\ &-4\mu(1-a\omega^{-1}v_p)\ln(1-a\omega^{-1}v_p)\\ &+(4a\mu\omega^{-1}-b)v_p\ln v_p. \quad \text{(E.27)}\end{aligned}$$

TABLE V. Comparison of b_2 of the second approximation with its rigorous values. The symbols bp and cp represent the numbers of the subchains with the figures, ∟ and □, per molecule, respectively; r and q are defined by Eq. (H.3) in appendix.

Two-dimensional Square Lattice, $\omega=2, \mu=1$							Simple Cubic Lattice, $\omega=\mu=3$						
p	Molecule	r	q	b_2	bp	cp	b_2	p	Molecule	r	q	b_2	bp	cp	b_2
3		2	14	0.389	0	0	0.389	3		3	23	0.426	0	0	0.426
		4	27	0.385	1	0	0.385			12	91	0.421	1	0	0.421
4		2	23	0.359	0	0	0.359	4		12	132	0.344	2	1	0.351
		4	42	0.328	2	0	0.328			8	98	0.383	3	0	0.383
		4	36	0.281	2	1	0.289								
5		2	34	0.340	0	0	0.340	7		1	25	0.255	12	0	0.255
		8	132	0.330	1	0	0.335								
		8	126	0.315	2	0	0.320								
		8	106	0.265	3	1	0.270	8		12	324	0.211	6 (6)	3 (5)	0.277 (0.228)
		8	106	0.265	3	1	0.270								
		1	13	0.210	4	0	0.210	12		12	564	0.163	10 (10)	5 (9)	0.254 (0.182)
		rigorous value			2nd Approx.					rigorous value			2nd Approx.		

The quantity $\bar{S}_0^{(4)}$ is derived from $S^{(4)}$, after simple rewritings with Eqs. (E.20) and (E.21), as

$$\begin{aligned}\bar{S}_0^{(4)}/\mathbf{R}=&-\ln(1-v_p)+\omega\ln(1-a\omega^{-1}v_p)\\&-\mu\ln\{1-(4a\omega^{-1}-b\mu^{-1})v_p+8\lambda v_p^2\}\\&+4\mu\ln\{1-(2a\omega^{-1}-\tfrac{1}{4}b\mu^{-1})v_p\}\\&-4\mu\ln(1-a\omega^{-1}v_p).\end{aligned}\tag{E.28}$$

Expanding this equation in the form of Eq. (D.15), we have

$$\begin{aligned}&b_1=1/p,\\&b_2=\tfrac{1}{2}-\tfrac{1}{2}a^2\omega^{-1}-\{ac\omega^{-1}-\tfrac{1}{4}bc\mu^{-1}+\tfrac{1}{8}(b-c)^2\mu^{-1}\}.\end{aligned}\tag{E.29}$$

Accordingly, b_1 and b_2 of the second approximation reduce to those of the first approximation only when the solution is composed of rod-like polymers or $b=c=0$.

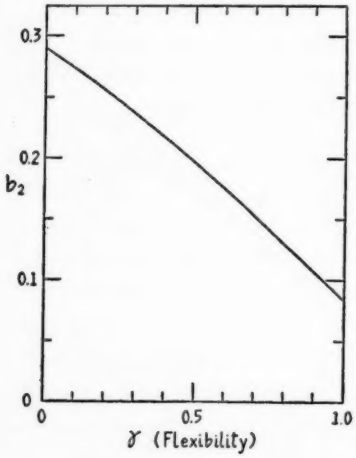

FIG. 4. Relation of the second virial coefficient of the entropy of dilution b_2 to flexibility of polymer chain γ.

F. Nature of the Second Approximation and Comparison with Experimental Data

We shall now investigate the nature of the second approximation in detail in two ways: (1) by making comparison with the rigorous values of b_2, its value of the second approximation is examined to reveal the nature of the approximation, and (2) the entropy of dilution is compared with the observed data.

We shall adopt the lattice discussed in Sec. E as an example. Equations (D.7) and (E.10) can be rewritten in the forms

$$bp=\beta(p-2) \quad \text{and} \quad cp=\gamma(p-3). \tag{F.1}$$

Remembering the definitions of β and γ, and taking into consideration that $(p-2)$ and $(p-3)$ represent the number of the three- and the four-segment subchain in each of the polymer molecules, we can interpret bp and cp as the numbers of the subchains with the figures, ∟ and □, per molecule, respectively. Therefore, when p is not so large that one can easily compute bp and cp from the shape of molecule, we can obtain, using Eq. (E.29), b_2 of the solution of the polymer of the given shape. As will be explained in Sec. G, this method of computing b_2 can be applied without any essential alteration to the solutions of branched chain polymers, in which b and c are again given by

$$\begin{aligned}bp&=\text{number of the subchains, ∟, per molecule,}\\cp&=\text{number of the subchains, □, per molecule.}\end{aligned}\tag{F.2}$$

In Table V, b_2 thus obtained are shown with the shape of molecules and with the rigorous values of b_2 which are determined by the method given in the Appendix. From this table, we find that b_2 of the second approximation agrees well with its rigorous values for all of the examples except the last two, and that the effects

of flexibility and branching of the chain on b_2, accordingly on the entropy of dilution, are taken into account with sufficient accuracy by this approximation, at least when p is not so large. As was pointed out in TCP III,[14] the correlations having figures *open* with respect to square can be taken into account rigorously by the second approximation, but the correlations of *closed* figures are only approximately taken into account. This nature of the second approximation gives us an explanation of the aforementioned result, that Eq. (E.29) gives somewhat disagreeing values of b_2 in the last two examples in Table V, where the polymer chain coils into closed shape with respect to square. Such a defect of the second approximation may be improved by proceeding to the third approximation in which the cubic cell is adopted as the basic cluster. However, we continue our study within the limit of the second approximation in order to avoid mathematical difficulties of higher approximations. Assuming that γ is a parameter adjustable between zero and one, and that it increases to one when polymer chains coil up tightly as in the last two examples, we obtain the values given in parentheses for b_2, which agree tolerably with the rigorous values. Therefore, taking an optimistic view, we may conclude that the second approximation is available to quantitative discussions of the solutions of highly flexible chain molecules when we shift the effect of flexibility on the parameter γ.

When p is sufficiently large and $1 \gg 1/p$, we can put $a=1$, $b=\beta$, and $c=\gamma$. If we consider that the bond angle is $\frac{1}{2}\pi$, hence $\beta=1$, and if we adopt the simple cubic lattice ($\omega=\mu=3$), Eqs. (E.28) and (E.29) can be written in the following forms:

$$\begin{aligned}\bar{S}_0^{(4)}/\mathbf{R} &= -\ln(1-v_p) - 9\ln(1-\tfrac{1}{3}v_p) \\ &\quad + 12\ln(1-7/12v_p) - 3\ln(1-v_p+8\lambda v_p^2), \\ 8\lambda v_p^2 &= 16\zeta^2/[1-\tfrac{1}{3}v_p+\{(1-\tfrac{1}{3}v_p)^2+16\zeta^2\}^{\frac{1}{2}}], \\ 4\zeta &= \tfrac{1}{6}(2+\gamma)v_p,\end{aligned} \tag{F.3}$$

and

$$b_2 = \tfrac{1}{3} - (1/24)\{6\gamma+(1-\gamma)^2\}. \tag{F.4}$$

This relation of b_2 to γ are shown in Fig. 4, from which we find that the theoretical value of b_2 decreases from 0.292 to 0.083 with increasing flexibility γ of the chain, and that the values of b_2 cover the range, from 0.08 to 0.18, which has been expected from various experimental data of the osmotic pressure.

Next, let us calculate from Eqs. (F.3) the reduced partial molal entropy (RPME) which is defined by

$$\mathrm{RPME} = (\bar{S}_0/v_p) - \lim_{v_p \to 0}(\bar{S}_0/v_p). \tag{F.5}$$

In Fig. 5, we plot by white circles the theoretical values of RPME against v_p, which are obtained by Eqs. (F.5) with (F.3) and with $\gamma=\frac{1}{2}$. These values show satisfactory agreement with the experimental values over whole range of concentration, v_p; the smoothed experimental curve is adopted from the data obtained for benzene solution of rubber by Gee and Treloar.[25] In the figure, RPME of the Flory approximation is also plotted by the dotted line. The theoretical values of b_2 are 0.5 in the Flory approximation, 0.20 in the second approximation, and its experimental value is 0.18. We show in Fig. 6 two kinds of ratios, $(\bar{S}_0)_{\mathrm{Flory}}/(\bar{S}_0)_{\mathrm{exp}}$ and $(\bar{S}_0)_{\mathrm{Flory}}/\bar{S}_0^{(4)}$, by the solid and the dotted lines, respectively. According to Flory, $(\bar{S}_0)_{\mathrm{Flory}}/(\bar{S}_0)_{\mathrm{exp}}$ represents the ratio of dimension of the segment to that of solvent molecule, and decreases to one with increasing v_p. This tendency is also expressed satisfactorily on the whole by $(\bar{S}_0)_{\mathrm{Flory}}/\bar{S}_0^{(4)}$ or by the second approximation as shown in Fig. 6. The aforementioned results show that the second approximation can be reasonably adapted for quantitative discussion of the solutions of chain polymer.

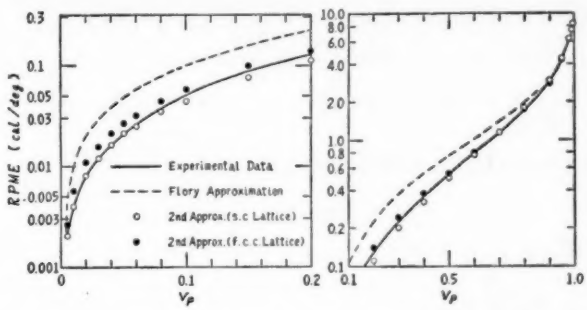

FIG. 5. Reduced partial molal entropy (RPME) for benzene solution of rubber at 25°C and its theoretical values.

However, strictly speaking, we must determine γ from the equilibrium condition that $(\partial S^{(4)}/\partial\gamma)_{v_p}=0$. In this case, we find, from Eq. (E.27),

$$(\beta-2\gamma)^2 = (8\mu/v_p)\gamma(\zeta-2\lambda v_p^2). \tag{F.6}$$

With another equilibrium condition, Eq. (E.23), we

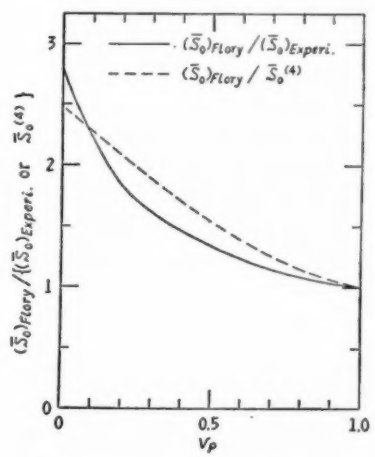

FIG. 6. Ratio of the entropy of dilution of Flory's approximation $(\bar{S}_0)_{\mathrm{Flory}}$ to its experimental data $(\bar{S}_0)_{\mathrm{exp}}$.

[25] G. Gee and L. R. G. Treloar, Trans. Faraday Soc. **38**, 147 (1942).

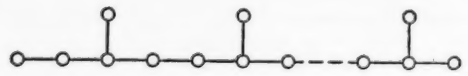

FIG. 7. Branched chain polymer molecule, with $\rho=\frac{1}{3}$.

can write γ in power series of v_p,

$$\gamma=\gamma_0+\gamma_1 v_p+\cdots, \tag{F.7}$$

with

$$\begin{aligned}\gamma_0&=\tfrac{1}{3}\{(\beta+2\mu\omega^{-1})-(4\mu^2\omega^{-2}+4\mu\omega^{-1}-2\beta^2)^{\frac{1}{2}}\},\\ \gamma_1&=\gamma_0(4\mu\omega^{-1}-2+\gamma_0)^2/4\mu(4\mu\omega^{-1}+2-6\gamma_0).\end{aligned} \tag{F.8}$$

Therefore, we find

$$\begin{aligned}&\gamma_0=0.33\dot{3}, \quad \gamma_1=0.0046, \quad b_2=0.083 \\ &\qquad\qquad \text{(two-dimensional square lattice)},\\ &\gamma_0=0.1835, \quad \gamma_1=0.0148, \quad b_2=0.260 \\ &\qquad\qquad \text{(simple cubic lattice)},\end{aligned} \tag{F.9}$$

when $\beta=1$. This value, 0.260, of b_2 is somewhat large in comparison with its experimental value. Accordingly, in this sense, the second approximation seems to be still defective.

If the face-centered cubic lattice ($\omega=6$ and $\nu=8$) is adopted, and if p is large enough so that $a=1$ and $b=\beta$, we obtain, from Eq. (D.14), the values of RPME, shown in Fig. 5 by black circles, for the solution of highly flexible polymers ($\beta=1$). The agreement of these values with the experimental data (the solid line in Fig. 5) is fairly improved in comparison with that of the Flory approximation, though it seems not to be enough, especially at high dilutions. The theoretical value of b_2 is 0.29 in the present case.

When the solution is not athermal, the heat of mixing may contribute to Eq. (F.6) and, as a result, b_2 may depend on temperature.

G. Effect of Branching of the Chain

We shall now discuss the effect of branching of the chain. Consider the polymer molecule having side chains at intervals of f-segments, each of which is composed of one segment as shown schematically in Fig. 7. Representing the number of segments in the principal chain by p^* and the total number of segments in one molecule by p, and assuming that both p^* and p are large enough so that one can safely ignore the end effect, we have

$$p=p^*(1+\rho), \quad \rho\equiv 1/f, \tag{G.1}$$

where ρ represents the ratio of the number of the side chains to p^* and will be called hereafter the "degree of branching." As the numbers n_3 and n_4 of the three- and the four-segment subchains per molecule are given by

$$\begin{aligned}n_3&=p^*\{1-(2/p^*)\}+2\rho p^*\doteqdot(1+2\rho)p^*,\\ n_4&=p^*\{1-(3/p^*)\}+2\rho p^*\doteqdot(1+2\rho)p^*,\end{aligned} \tag{G.2}$$

respectively, we find, by the substitution of Eqs. (G.1) into (G.2),

$$n_3=n_4=\{(1+2\rho)/(1+\rho)\}p. \tag{G.3}$$

Hence, the numbers of the clusters with the figures, ∟ and □, in the solution are given as shown in Table VI where the numbers of the similar clusters in the solution of linear chain molecules are also given for comparison. From this table we find that the effect of branching on the numbers of the clusters can be taken into account only by rewritings such as $\beta\to\beta'$ and $\gamma\to\gamma'$. As the number of chemical bonds is independent of the branching, and as thermodynamic properties of the solutions depend only on the total numbers of clusters of each kind in the whole system (for example, they depend on $\lambda=\sum_{j,k}\lambda_{jk}$, but not on an individual of λ_{jk}), we can conclude that, if one makes the rewritings that $\beta\to\beta'$ and $\gamma\to\gamma'$, the results obtained for the solution of linear chain molecules are applicable to the solution of molecules with side chains; and, then, we have

$$b_2=\tfrac{1}{2}-\tfrac{1}{2}\omega^{-1}-\{\gamma'\omega^{-1}-\tfrac{1}{4}\beta'\gamma'\mu^{-1}+\tfrac{1}{8}(\beta'-\gamma')^2\mu^{-1}\}. \tag{G.4}$$

Therefore, we can say that the increases of β' and of γ' due to the increase of the degree of branching ρ contribute the similar effect to b_2, or to the second virial coefficient of the osmotic pressure, as the increase of flexibility of the chain β and γ does. This conclusion has already been presented by Zimm,[15] who gave a qualitative discussion on the effect of branching.

If we put $\beta=1$ or $\beta'=(1+2\rho)/(1+\rho)$, Eqs. (F.8) and (F.9) can be rewritten, in the case of the simple cubic lattice, into the forms:

$$\begin{aligned}\gamma_0'&=\{(1+2\rho)/(1+\rho)\}\gamma_0\\ &=\{3+4\rho-(6+12\rho+4\rho^2)^{\frac{1}{2}}\}/3(1+\rho),\end{aligned} \tag{G.5}$$

and

$$\begin{aligned}b_2=\tfrac{1}{3}-[\{&(28\rho^2+60\rho+30)\\ &-(9+4\rho)(6+12\rho+4\rho^2)^{\frac{1}{2}}\}/108(1+\rho)^2].\end{aligned} \tag{G.6}$$

Table VII shows this relation of b_2 to ρ, from which we find that the effect of branching on b_2 cannot be ignored in general. The similar consideration as given in the foregoing is also applicable to the solutions of molecules having many branches at a segment or having

TABLE VI. Effect of branching of polymer chain on the numbers of the three-segment and of the four-segment subchains with the indicated figures.

Subchain	Total Number of the Subchains	
	Linear Polymer	Branched Polymer
	$\beta(p-3)N_p\doteqdot\beta pN_p$	$\beta\{\frac{1+2\rho}{1+\rho}\}pN_p=\beta' pN_p$
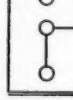	$\{\alpha(p-2)-2\beta(p-3)\}N_p$ $\doteqdot(\alpha-2\beta)pN_p$	$(\alpha-2\beta)\{\frac{1+2\rho}{1+\rho}\}pN_p$ $=(\alpha'-2\beta')pN_p$

multifunctional segments. Some examples have been given in Table V.

In conclusion, we are indebted to Dr. Ryoichi Kikuchi of the University of Tokyo for his kind encouragement, and to members of the Research Group on Polymer Science at Kyoto, especially to Dr. Ei Teramoto, for stimulating discussions. Thanks are tendered also to the Ministry of Education of the Japanese Government for a grant-in-aid. One of the authors (T.W.) wishes to express his sincere thanks also to Professor San-ichiro Mizushima and Dr. Taro Kihara of the University of Tokyo, who gave him the opportunity of studying, with ever increasing interest, at their laboratories.

APPENDIX

H. Method of Computing the Rigorous Values of b_2 for Lattice Solutions

If we represent by ϕ_i the number of ways of putting the ith polymer molecule on the lattice partly occupied by $(i-1)$ polymer molecules in advance, the combinatory factor G of the system containing N_p polymers is given by

$$G=\Big(\prod_{i=1}^{N_p}\phi_i\Big)/(N_p!\sigma^{N_p}), \tag{H.1}$$

where σ is the symmetrical number of the polymer. Let us consider, as an example, the two-dimensional square-lattice solution of the tetramer which is shown in Fig. 8. As the molecule takes four orientations at a cell and other molecules are excluded from the nine cells shaded in the figure, we can put

$$\phi_i=4\{N-9(i-1)\}, \tag{H.2}$$

if the excluded volume of individual molecules does not overlap each other. Although the overlapping of the excluded volumes must be correctly taken into account in order to obtain the rigorous expression for the combinatory factor, we can safely ignore this overlapping effect so far as b_1 and b_2 are concerned, because the effect contributes, in the expansion of $\bar{S}_0$, only to higher terms than v_p^2. Accordingly, writing ϕ_i in general cases as

$$\phi_i=rN-(i-1)q, \quad (i=1,2,\cdots,N_p), \tag{H.3}$$

we obtain from Eq. (H.1)

$$G=(rN/q)!q^{N_p}/[\{(rN/q)-N_p\}!N_p!\sigma^{N_p}], \tag{H.4}$$

and

$$\frac{\bar{S}_0}{\mathbf{R}}=\left(\frac{\partial \ln G}{\partial N}\right)_{N_p}=-\frac{r}{q}\ln\left(1-\frac{qv_p}{rp}\right)$$
$$=\frac{1}{p}v_p+\frac{q}{2rp^2}v_p^2+\cdots. \tag{H.5}$$

Since r and q can be easily obtained for molecules with small p by geometrical considerations, we can get the rigorous values of b_2 from Eq. (H.5), which have been shown with r and q in Table V.

Similarly, we can obtain the rigorous value of b_2 of the lattice solution of rod-like polymers. In this case, we have

$$r=2\omega, \quad q=2\{p^2\omega-(p-1)^2\}, \tag{H.6}$$

and

$$b_2=\tfrac{1}{2}-\tfrac{1}{2}\{1-(1/p)\}^2\omega^{-1};$$

this value of b_2 is just the one obtained by the first approximation [see Eq. (C.20)].

TABLE VII. Effect of branching (ρ) of polymer chain on the second virial coefficient (b_2).

ρ	γ_0'	b_2
0	0.1835	0.260
$\frac{1}{8}$	0.222	0.247
$\frac{1}{4}$	0.266	0.237
$\frac{1}{2}$	0.311	0.221
1	0.385	0.201

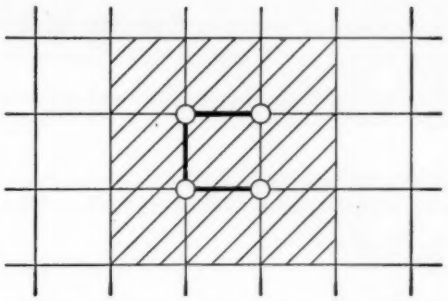

FIG. 8. Excluded volume of a tetramer with the figure of square, in the two-dimensional square-lattice solution. Shaded area is the excluded volume.

Spectra of Transition-Metal Complexes*

L. E. ORGEL
Gates and Crellin Laboratories of Chemistry, California Institute of Technology, Pasadena, California
(Received October 11, 1954)

The electronic transitions observed in complexes of the transition-metal ions are interpreted in terms of a slightly modified crystal-field theory. Parameters of chemical interest are derived.

THE absorption bands of transition-metal complexes are commonly of two kinds: those due to charge-transfer processes and those arising from transitions which, to a good approximation, can be considered as taking place within the *d*-shell of the ion. It is usually possible to decide to which class an observed band belongs[1,2] although in certain complexes, where the interaction between the metal ion and the ligands is particularly strong, the two types of transition are no longer even approximately distinct and the theoretical treatment is then more complicated e.g., in the MnO_4^- ion.[3] In this paper we shall discuss only those transitions which are localized on the metal ion.

The general theory of the energy-levels for *d*-electrons in transition-metal complexes was first developed by Van Vleck[4] and by Schlapp and Penney.[5] Since then many applications of their theory to the magnetic properties of complexes and a few to the optical properties have been made.[6,7] We shall extend the methods of a previous paper on this subject,[8] developing a slightly different interpretation of crystal-field theory, and then derive certain quantities of chemical interest from a detailed study of the spectra of transition-metal complex ions.

We shall calculate the energy-level diagrams of a number of complex ions as a function of a parameter Dq which depends on the geometry of the ion. The energy levels which must be compared with the calculated diagram are those which correspond to the stable geometric configuration of the ground-state of the ion being maintained in the excited states. We shall be concerned, therefore, with the maxima of absorption bands, not with 0—0 bands.

Since, in discussing the intensities of transitions our interests will be qualitative we shall quote values of ϵ_{max}, the value of the molecular extinction coefficient at the absorption maximum, rather than attempt to calculate oscillator strengths.

THE EFFECT OF ENVIRONMENT ON THE *d*-ORBITALS OF TRANSITION-METAL IONS

The degeneracy of the *d*-orbitals of a transition-metal ion is removed, more or less completely, when the ion becomes part of a crystal or is solvated in solution. Only those ions or molecules attached directly to the metal atom are normally important in determining the coarse structure of the energy-level scheme of the ion so that the broad features of the spectrum of a complex ion in solution are similar to those of the same ion in a crystal. For this reason we shall be concerned only with the central metal atom and its immediate neighbors.

It has been usual to regard the splitting of the degeneracy of the *d*-orbitals as a consequence of the electrostatic field set up by the ligands. However, in view of the complexity of chemical-bonding phenomena, it seems surprising that so crude a picture is capable of giving a good basis for detailed calculations of magnetic properties. The reason for this success is, however, readily understood: the magnetic and optical properties depend on the wave functions and stationary state energy-levels of the *d*-electrons and not on the detailed form of the interaction of the ion with its environment. In most of the calculations, group theory is used to determine the symmetry type of the orbitals, but the energies are derived from empirical data, sometimes supported by qualitative arguments. Thus although the approach adopted is formally based on electrostatics, in practice the results are quite general and apply to any mechanism which removes the degeneracy of the *d*-orbitals.

It has been shown that the description of transition-metal complexes in terms of covalent and ionic bonds is almost equivalent to the crystal-field theory in which polarization of the ligands is taken into account. It was also suggested that double-bonding may be important in determining the energy-levels of the complex, an approach recently developed by Stevens.[9] It follows that the empirical pattern of energy levels must give information which will be useful in the interpretation of bond properties.

* Contribution No. 1945 from Gates and Crellin Laboratories of Chemistry, California Institute of Technology, Pasadena, California.

[1] E. Rabinowitch, Revs. Modern Phys. **14**, 112 (1942).
[2] L. E. Orgel, Quarterly Revs. (London) **8**, 422 (1954).
[3] M. Wolfsberg and L. Helmholz, J. Chem. Phys. **20**, 837 (1952).
[4] J. H. Van Vleck, *Theory of Electric and Magnetic Susceptibilities* (Oxford University Press, London, 1932).
[5] R. Schlapp and W. G. Penney, Phys. Rev. **42**, 666 (1932).
[6] B. Bleaney and W. K. Stevens, Repts. Progr. Phys. **16**, 108 (1953).
[7] H. Hartmann and H. L. Schläfer, Z. Naturforsch. **6A**, 760 (1951).
[8] L. E. Orgel, J. Chem. Soc. 4756 (1952).
[9] W. K. Stevens, Proc. Roy. Soc. (London) **219A**, 542 (1953).

THE STATE OF IONIZATION OF THE METAL IN TRANSITION-METAL COMPLEXES

The conventional description of a hydrated or complex ion used in crystal-field theory is that of a single metal ion carrying a positive charge equal to the formal valency of the metal, surrounded by a group of negative ions or neutral dipoles. The success of quite detailed calculations[10] in which the energy-level diagrams for the ion in the crystal is taken as identical with that of the free ion seems at first to argue against covalent bonding, even in such stable, highly charged complexes as $[Cr(H_2O)_6]^{+++}$. However, a detailed comparison of the intervals between the states arising from the configurations d^n, d^ns, and d^ns^2 shows that only slight changes occur as the charge decreases, at least for the elements with several d-electrons.[11] This shows that the $4s$ electrons do not shield the $3d$-electrons to any important extent and, *a fortiori*, we should expect the same to be true of the $4p$-electrons. It follows that covalent bonding in which the $4s$- and $4p$-orbitals are partially filled is not precluded by the success of calculations in which it is neglected. Conversely, we are justified in using the levels of the free ion as a basis for calculations, even if there is reason to believe that "covalent bonding" is involved. In more accurate calculations, particularly on ions of high charge which have few d-electrons, corrections for the slight changes in the intervals which occur between d^n-, d^ns-, and d^ns^2-configurations might be made e.g., in V^{+++}.

While we have presented arguments suggesting that, apart from the effect of the environment on the degeneracy of the d-orbitals, the energy-level diagram for the states of one configuration of the free ion is adequate in discussing the states of the complex, it must be emphasized that the relative positions of different configurations will be profoundly changed by complex formation. Just as we have to introduce a splitting of the degenerate d-orbitals, so we need to introduce a change in the basic separation between the d- and s-levels. This has many important consequences, e.g., simple cuprous salts are colorless although, in the free ion, the transition from the $d^{10}\,{}^1S$ state to the $d^9s\,{}^3D$ and ^1D states occur at 22 000 cm^{-1} and 26 000 cm^{-1} respectively.[12] If it were not for an increase in the interval between the d^{10} and d^9s configurations certain components of these transitions would occur in the visible. In general the interval between configurations d^n and $d^{n-1}s$ or $d^{n-1}p$ in tetrahedral or octahedral complexes is expected to be greater than in the free ions.

THE CONFIGURATIONS d^1 AND d^9

In the most general environment the degeneracy of the d-orbitals is removed completely. There are five separate levels and transitions are possible between the ground state and any of the other four states. Fortunately many of the most important complexes have some elements of symmetry or near symmetry which greatly simplify their spectra.

The simplest and commonest type of complex is that in which the central ion is surrounded by an octahedron of ligands. If the octahedron is regular and the six ligands are identical it has been shown by Schlapp and Penney[5] that the d-orbitals are split into a stable triply degenerate t_{2g} orbital and a less stable doubly degenerate e_g orbital. The only transition possible is from the T_{2g} to the E_{2g} state and it, like all transitions within the d-shell, is a $g-g$ transition and is therefore forbidden.

The only example of a regular octahedrally coordinated ion with one $3d$-electron whose spectrum has been studied is $[Ti(H_2O)_6]^{+++}$[13] and the theory has been discussed in some detail.[14] The ion has a single, weak absorption band whose maximum is at 20 400 cm^{-1}. The source of the absorption intensity is not understood, but, arguing by analogy with the spectra of other tightly bound molecules, it is probably due to the coupling of electronic and vibrational motion rather then to a quadrupole or magnetic dipole transition. If, in order to follow the convention introduced by Schlapp and Penney,[5] we take the separation between the t_{2g} and e_g orbitals as 10 Dq, then $Dq=2040$ cm^{-1}. A number of ions such as $TiCl_3(C_2H_5OH)_3$ has also been studied. They have a single absorption maximum, at longer wavelengths than that of $[Ti(H_2O)_6]^{+++}$.

In tetrahedral complexes the simple crystal-field theory predicts a splitting similar to that in octahedral complexes, but of the opposite sign, i.e., the e level is below a t_1 level.[15] However, the assumption that we may restrict our discussion to the d-orbitals is no longer valid. In the absence of a center of symmetry the t_1 component of the d-orbitals can mix with the $4p$-orbitals. Thus for a single d-electron the orbital for the ground state is nearly a pure $3d$-orbital, but in the excited state there is a considerable $4p$-component. We, therefore, expect a more intense transition than is found in octahedral complexes. The only substance of the kind which has been studied is VCl_4. It has an absorption maximum at about 9000 cm^{-1} with $\epsilon_{max}=110$.[16] It should be noted that the split between the e and t_1 orbital is much smaller than is usual for octahedrally coordinated ions of high valency. It is not at all clear that the quantity Dq has any significance for complexes in which p and d

[10] R. Finkelstein and J. H. Van Vleck, J. Chem. Phys. **8**, 790 (1940).
[11] L. E. Orgel, J. Chem. Phys. (to be published).
[12] Data on atomic spectra are taken from Atomic Energy Levels, National Bureau of Standards, Washington 1949, 1952.
[13] H. Hartmann and H. L. Schläfer, Z. physik. Chem. **197**, 116 (1951).
[14] F. E. Ilse and H. Hartmann, Z. physik. Chem. **197**, 239 (1951).
[15] It must be noted that the representations of the octahedral (O_h) and tetrahedral (T_d) groups are related in the following way:

O_h	A_{1g}	A_{1u}	A_{2g}	A_{2u}	E_g	E_u	T_{1g}	T_{1u}	T_{2g}	T_{2u}
T_d	A_1	A_1	A_2	A_2	E	E	T_2	T_1	T_1	T_2.

[16] A. G. Whittaker and Don M. Yost, J. Chem. Phys. **17**, 188 (1949).

orbitals are mixed, but a simple application of the formula gives $Dq=900$ cm^{-1}. The intensity is quite large, particularly for an infrared band, but still very much weaker than that in certain other tetrahedral complexes, e.g., $[CoCl_4]^{--}$.

From a chemical viewpoint the mixing of d and p orbitals is the d-p hybridization postulated by Pauling.[17] Orbitals whose maximum concentrations are near the ligands are used in bonding, while the remaining hybrids, which are automatically removed as far as possible from the ligands, contain any nonbonding electrons. The very high intensities and anomalous positions of the absorption bands of tetrahedral complexes, particularly of Co^{++}, is evidence for d-p hybridization.

The d^9 configuration, i.e., the d-shell with one vacancy, behaves like a single d-electron when the degeneracy of the d-orbitals is removed except that all the splittings are reversed. A similar relation holds between other d^n and d^{10-n} configurations. In octahedral d^9 complexes we expect a single $E-T_{2g}$ transition. The cupric complexes, which are the only extensively studied ions with this configuration, do not have a simple octahedral environment, but the central atom is attached to four nearest neighbors in a plane and often to two more distant groups which complete a distorted octahedron.[18] The energy levels are split as shown in Fig. 1 by the deviation from a regular octahedron. Clearly as many as three transitions may occur in the visible and near infrared if the splitting is large enough.

The cupric ion in solution, which is presumably $[Cu(H_2O)_6]^{++}$ has a very broad absorption band with a maximum close to 8000 A and $\epsilon_{max}=11$.[19] Hydrated cupric sulfate crystals have a very similar absorption band, but recent work suggests that as many as three transitions of different polarizations may be involved.[20]

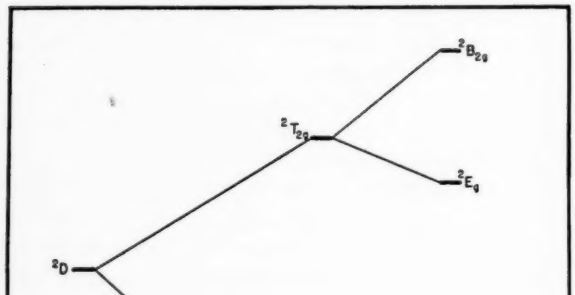

FIG. 1. Energy level diagram for the d^9 configuration.

Replacement of coordinated water molecules by ammonia leads to a steady shift of the absorption maximum to shorter wavelengths until four ammonia molecules are present, when $\lambda_{max}=5900$A and $\epsilon_{max}=50$. The addition of a fifth ammonia molecule caused the maximum to move to 6600 A[21] i.e., to a longer wavelength; no evidence for the addition of a sixth ammonia molecule could be obtained even in liquid ammonia. Ethylene diamine complexes behave similarly, while pyridine does not seem to form complexes with an amine-copper ratio of greater than four to one. In octahedral complexes we usually find that successive replacement of water by ammonia causes the crystal field splitting to increase steadily, so that a special explanation of the effect of the fifth ammonia molecule on the cupric ion spectrum must be found. It seems probable that the first four ammonia molecules are added in a plane, say along the x- and y-axes of a coordinate system centered on the Cu^{++} ion. This results in a progressive destabilization of the $d_{x^2-y^2}$ orbital with respect to all other orbitals and also to a weakening of the bonding to the water molecules in the z-direction which stabilizes the d_{z^2}, d_{xz}, and d_{yz} orbitals. Thus the transitions from the d_{z^2}, d_{xz}, and d_{yz} to the half-empty $d_{x^2-y^2}$ move to shorter wavelengths. The fifth ammonia molecule must be attached in the z-direction and so will destabilize the d_{z^2}, d_{xz}, and d_{yz} orbitals while leaving the $d_{x^2-y^2}$ orbital little changed. Any second-order effect will be to weaken the bonds in the xy plane and so to stabilize the $d_{x^2-y^2}$ orbitals. In each case the result is to move the absorption band to longer wavelengths. Any distortion of the structure towards a tetragonal pyramid would have the same effect.

In presumably nonoctahedral complexes such as $[Cu(H_2O)_6]^{++}$ one is clearly not justified in associating the position of maximum absorption with the center of gravity of the states arising from the splitting of the T_{2g} level relative to the E_g level, for the latter level is itself split. Consequently the value of $Dq=1250$ cm^{-1} obtained by the direct application of the simple theory is not comparable with values obtained for octahedral complexes. For the same reason we shall not discuss the spectra of other cupric complexes in detail. In general we find that the magnitude of the splitting produced by different ligands increases in the order

chloride < water < pyridine < ammonia < ethylene diamine.

In complexes whose stereochemistry deviates very markedly from the regular octahedral arrangement,

[17] L. Pauling, J. Am. Chem. Soc. **53**, 1367 (1931).
[18] A. F. Wells, *Structural Inorganic Chemistry* (Oxford University Press, New York, 1950).
[19] R. Mecke and H. Leg, Z. physik. Chem. **111**, 392 (1924).
[20] D. McClure, private communication.
[21] Z. Bjerrum and E. G. Nielsen, Acta Chem. Scand. **2**, 297 (1948).

particularly in planar complexes, it should be possible to resolve the visible absorption into two or more bands. This has in fact been done for a number of planar organic derivatives of cupric copper, e.g., cupric acetylacetonate by Calvin and Belfort.[22]

THE CONFIGURATIONS d^2 AND d^8

These configurations are the simplest in which we have to consider the simultaneous effects of the removal of the d-electron degeneracy and of the electrostatic interaction between the d-electrons. The way in which the crystal field splits the ^3F ground states of these configurations is well known.[5] We shall develop the slightly more general theory which includes the mixing together of the different atomic states by the crystal-field for all the singlet and triplet levels. The d^2 ions have not been studied at all extensively so we shall restrict our numerical calculations on them to the triplet states of V^{+++}; the Ni^{++} ion will be treated in more detail since a good deal of experimental evidence is available and calculations are made very easily.

We have followed closely the procedure of Finkelstein and Van Vleck.[10] The matrix elements of V expressed as multiples of Dq are for Ni^{++}

$^1A_{1g}$		^1E_g		$^1T_{2g}$	
^1S	^1G	^1D	^1G	^1D	^1G
0	$4\sqrt{6}$	24/7	$\frac{40\sqrt{3}}{7}$	−16/7	$\frac{20\sqrt{3}}{7}$
$4\sqrt{6}$	4	$\frac{40\sqrt{3}}{7}$	4/7	$\frac{20\sqrt{3}}{7}$	−26/7

$^1T_{1g}$	$^3T_{1g}$		$^3T_{2g}$	$^3A_{2g}$
^1G	^3F	^3P	^3F	^3F
2	−6	4	2	12
	4	0		

In the d^2 configurations the signs of the diagonal elements must be reversed.

We shall consider first the spectrum of the $[V(H_2O)_6]^{+++}$ ion.[23] In the V^{+++} ion the separation between the ^3F and ^3P states is 13 000 cm^{-1}, and using this quantity we are able to calculate the energy level diagram of Fig. 2 in which the position of each level is plotted against Dq. The transitions $^3T_{1g}-^3T_{2g}$ and $^3T_{1g}-^3A_{2g}$ depend on the $^3F-^3P$ separation of the free ion only to second order, while the $^3T_{1g}-^3T_{1g}$ transition depends on it to first order. We therefore choose Dq to fit the experimental separation between the $^3T_{1g}$ and $^3T_{2g}$ levels, a value of $Dq=1900$ cm^{-1} being appropriate. The transitions to the T_{1g} and A_{2g} states are then predicted at 28 500 cm^{-1} and 36 000 cm^{-1}. The transition observed is at 25 000 cm^{-1} while the 36 000 cm^{-1} neighborhood is completely covered by a strong charge-transfer transition. The discrepancy between the observed and predicted positions of the second transition is rather large. It is probable that part of it is due to the $^3F-^3P$ interval of the hydrated ion being less than that for the free ion. We have already remarked that shielding effects will be particularly important in highly charged ions with few d-electrons such as the V^{+++}.

Finkelstein and Van Vleck[10] have commented on the fact that even with comparatively large octahedral fields the Russell-Saunders coupling is not much affected in V^{+++} complexes. In tetrahedral fields the mixing of the two T_1 states is important even for fairly small values of Dq, as is shown by Fig. 2.

The singlet states of the Ni^{++} ion, whose positions are required to compute the energy-level diagram for nickelous complexes, have not been observed experimentally. However, we may extrapolate from values for Ni^+ d^8s and Ni d^8s^2 to obtain values of 12 000 cm^{-1} and 21 000 cm^{-1} for the energies of the ^1D and ^1G states above the ^3F ground state. The ^1S state has not been observed for any related ion, since it is far above the rest of the configuration. Using values of $F_2=1560$ cm^{-1} and $F_4=110$ cm^{-1} for the Slater-Condon parameters[11] we estimate that it lies 49 000 cm^{-1} above the ground state. Although this figure is subject to a considerable error it will affect our calculation only in second order, since we will not be interested in the upper A_{1g} level.

The final energy level diagram, excluding the upper A_{1g} level which lies far above the remaining levels, is shown in Fig. 3. We find that three triplet-triplet transitions, $^3A_{2g}-^3T_{2g}$, $^3A_{2g}-^3T_{1g}$, and $^3A_{2g}-^3T_{1g}$ should occur in that order for octahedral complexes. In addition there should be a number of much weaker triplet-singlet transitions.

The hydrated nickel ion, $Ni(H_2O)_6^{++}$ in aqueous solution has three main absorption bands at 8500 cm^{-1},[24] and 14 000 cm^{-1} and 26 000 cm^{-1} [25] with ϵ_{max} values of 2, 1.8, and 6 respectively. If we choose $Dq=850$ to fit the first transition we expect further transitions at 14 000 cm^{-1} and 27 000 cm^{-1} in good agreement with experiment.

A detailed examination of the published spectra of Ni^{++} in solution suggests that there is a further weak peak at 19 000 cm^{-1} and that the 26 000 cm^{-1} band lies over and partially obscures weak bands at 22 500 cm^{-1} and 30 000 cm^{-1}. Crystal absorption spectra[26] confirm the existence of weak discrete transitions at 22 500 cm^{-1} and in the region from 17 500–20 500 cm^{-1}. The peak at 30 000 cm^{-1} may correspond to a transition to the $^1E_{1g}$ state at 29 500 cm^{-1} while the 22 500 cm^{-1} band

[22] M. Calvin, private communication.
[23] S. C. Furman and S. Garner, J. Am. Chem. Soc. **72**, 1785 (1950).
[24] T. Dreisch and W. Trommer, Z. physik. Chem. **B37**, 37 (1937).
[25] A. Kiss and R. Szabo, Z. anorg. Chem. **252**, 172 (1943).
[26] G. Gielessen, Ann. Physik **5**, 22, 537 (1935).

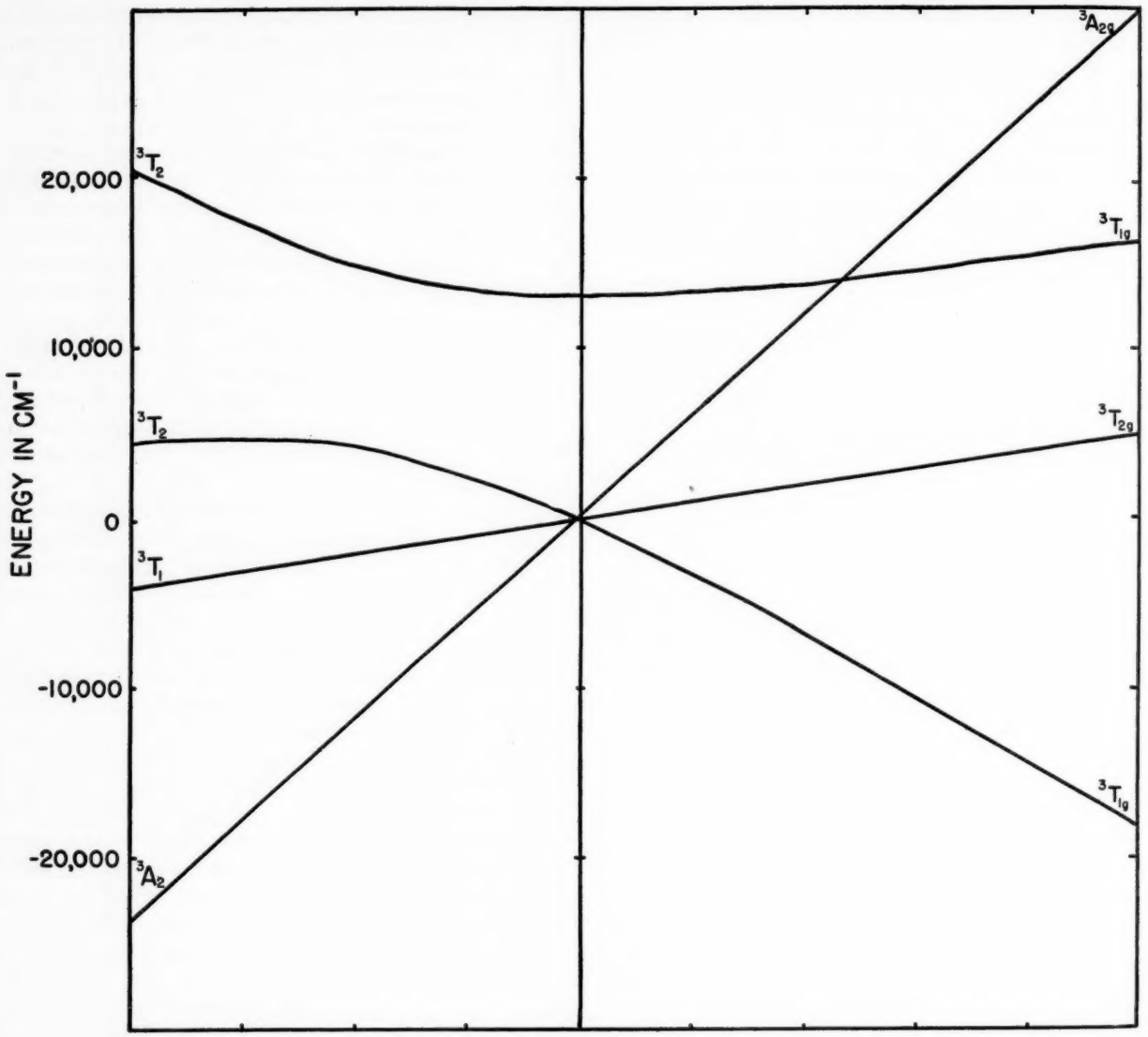

FIG. 2. Energy level diagram for the V^{+++} ion. The intervals indicated along the Dq-axis each represent 500 cm^{-1}.

would correspond exactly to the transition to a $^1T_{1g}$ state. The band close to 19 000 cm^{-1} does not correspond very well with any level on our diagram.

The identification of two of the bands as intercombinations suggested above is very tentative, since they are very much weaker than their triplet-triplet neighbor, and might represent vibrational structure in the latter. Further studies of a number of different complexes would be required to settle the assignments.

The infrared band of the hexamine nickel ion has its maximum at 10 600 cm^{-1}.[24] Taking $Dq=1060$ cm^{-1} to fit it, we predict further bands at 17 500 cm^{-1} and 29 200 cm^{-1}, in reasonable agreement with the observed bands at 16 700 cm^{-1} and 27 400 cm^{-1}.[27]

The corresponding peaks for tris ethylene-diamine nickel are observed at 11 200 cm^{-1}, 18 300 cm^{-1}, and 29 000 cm^{-1}, respectively.[27] Taking $Dq=1120$ cm^{-1} the calculated values are 11 200 cm^{-1}, 19 100 cm^{-1}, and 31 000 cm^{-1} respectively. In the tris-*o*-phenanthroline complex only two bands have been observed at 12 700 cm^{-1} and 19 000 cm^{-1}.[27] Bands are predicted at 12 700 cm^{-1} and 20 200 cm^{-1} if we use $Dq=1270$ cm^{-1}.

From the position of the first visible absorption peaks the following order of increasing Dq has been deduced for Ni^{++} complexes.[28]

Methyl alcohol < water < oxalate < pyridine
< ammonia < ethylenediamine < *o*-phenathroline.

[27] G. L. Roberts and F. H. Field, J. Am. Chem. Soc. **72**, 4232 (1950).

[28] Russell, Cooper, and Vosbergh, J. Am. Chem. Soc. **65**, 1301 (1943).

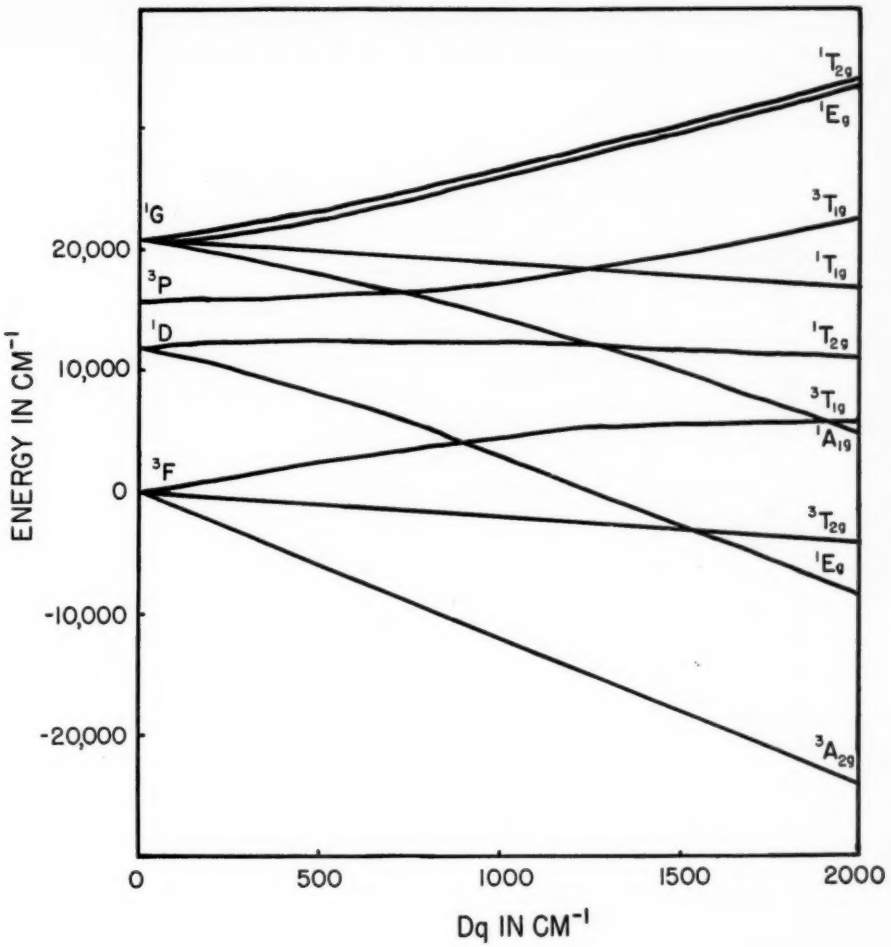

FIG. 3. Energy level diagram for the Ni^{++} ion.

A considerable number of octahedral compounds in which the ligands are not identical have been studied, in particular the ions $[Ni(H_2O)_n(NH_3)_{6-n}]^{++}$ with $n=0, 1, 2, 3, 4, 5, 6$.[29] Experimentally it is found that the visible-band shifts steadily to shorter wavelengths as the number of molecules of ammonia in the complex increases, but that no splitting of the band occurs. Theoretically we would expect that this band, like the analogous band in the Cr^{+++} ion, would be split for certain of the complexes. The absence of such a splitting is due to two factors. Firstly, the expected splitting is small compared with the total width of the band and secondly, due to the mobility of the system, a mixture of stereoisomers is always present for the complexes with $n=2$, 3, and 4. The observed shift to the blue with increasing n is the shift of the center of gravity of the bands of all the complexes with a given n.

The electronic spectra of tetrahedral nickel complexes have not been investigated. The planar, diamagnetic complexes of divalent nickel are characterized by strong absorption bands with their maxima close to 4000 A and with ϵ_{max} values ranging from 2000 to 10 000.[30] It seems unlikely that this transition is a simple transition within the d-shell in view of its very high intensity. Two other explanations seem plausible, namely that it is a transition which is not approximately localized on the nickel ion or that it is a transition from a $3d$-orbital to the unoccupied $4p$-orbital of the Ni^{++} ion. We are inclined to think that the latter explanation is the more probable one. It would be interesting to know whether there are any weak bands at longer wavelengths than the strong 4000 A band in these nickel complexes, corresponding to the expected transitions within the $3d$-shell.

THE CONFIGURATIONS d^3 AND d^7

The d^3 configuration has been discussed in detail by Finkelstein and Van Vleck, who have obtained the matrix elements of the cubic field for the quartet and doublet states.[10] They have applied their theory to the hydrated chromic ion and have shown that the lowest doublet state is brought to the observed position if a value of 1820 cm^{-1} is taken for Dq. We have identified the two strongest long wavelength absorption

[29] J. Bjerrum, *Metal Ammine Formation in Aqueous Solution* (Copenhagen, 1941).

[30] McKenzie, Mellon, Mills, and Short, Proc. Roy. Soc., New South Wales **58**, 70 (1944).

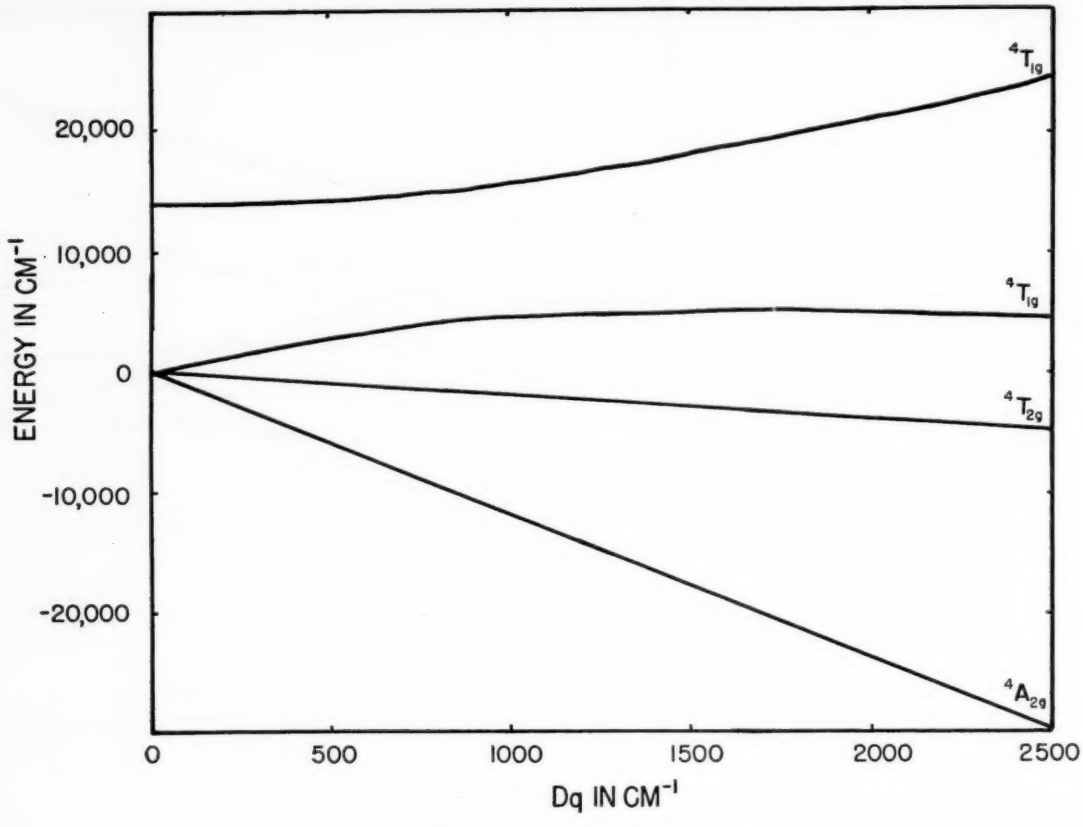

FIG. 4. Energy level diagram for the Cr^{+++} ion.

bands of trivalent chromium complexes as quartet-quartet transitions within the d^3 configuration.[8] The energy level diagram for the quartet states of the chromic ion in octahedral coordination is given in Fig. 4. Using a value of 1720 cm^{-1} for Dq we predict absorption maxima at 17 200 cm^{-1} and 25 700 cm^{-1} compared with the experimental values of 17 200 cm^{-1} and 25 600 cm^{-1}.[31] Thus a value of 1770 cm^{-1} for Dq would give good agreement with both the singlet and triplet states.

The energy level diagram of $[Cr(NH_3)_6]^{+++}$ does not agree quite so well with experiment. If we take $Dq=2150$ cm^{-1}, to give the lower transition correctly at 21 500 cm^{-1}, then we predict an upper transition at 30 500 cm^{-1} compared with the observed value of 28 500 cm^{-1}.[32]

The successive substitution of ammonia molecules for water in $[Cr(H_2O)_6]^{+++}$ results in a progressive shift of the absorption maxima to longer wavelengths,[31] but there is no resolution of any of the absorption bands into two or more components.

A general survey of mono and polysubstituted chromium complexes[33,34] shows that the value of Dq increases in the order

Iodide < bromide < chloride < thiocyanate < oxalate < water < ammonia < ethylenediamine.

We have shown that in mono-substituted and particularly in *trans*-disubstituted chromic complexes the lowest absorption band should be split into two components while the upper band should, to a first approximation, remain unsplit.[8] With the knowledge of the relative size of Dq contributions which we have derived we can see that if the substituent has a smaller Dq value than the other ligands the short wavelength component of the split band, since it is degenerate, should be twice as strong as the long wavelength component. If the substituent has a larger Dq value than the other ligand the order of intensities should be reversed. We shall discuss this point in more detail in connection with cobaltic complexes, and here will only note that the theory seems to be qualitatively correct for chromium complexes.

The spectrum of the hydrated vanadous ion has been studied by Dreisch and Kallscheuer,[35] who found a band with its maximum at about 11 600 cm^{-1} and by Kato,[36] who found bands with maxima at 12 200 cm^{-1}

[31] R. I. Colmar and F. W. Schwartz, J. Am. Chem. Soc. **54**, 3204 (1932).
[32] M. Linhard, Z. Electrochem. **50**, 224 (1944).
[33] M. Linhard and M. Weigel, Z. anorg. Chem. **266**, 49 (1951).
[34] W. Kuhn, Z. anorg. Chem. **216**, 321 (1934).
[35] T. Dreisch and O. Kallscheuer, Z. physik. Chem. **B45**, 19 (1939).
[36] S. Kato, Sci. Papers Inst. Phys. Chem. Research (Tokyo) **13**, 49 (1930).

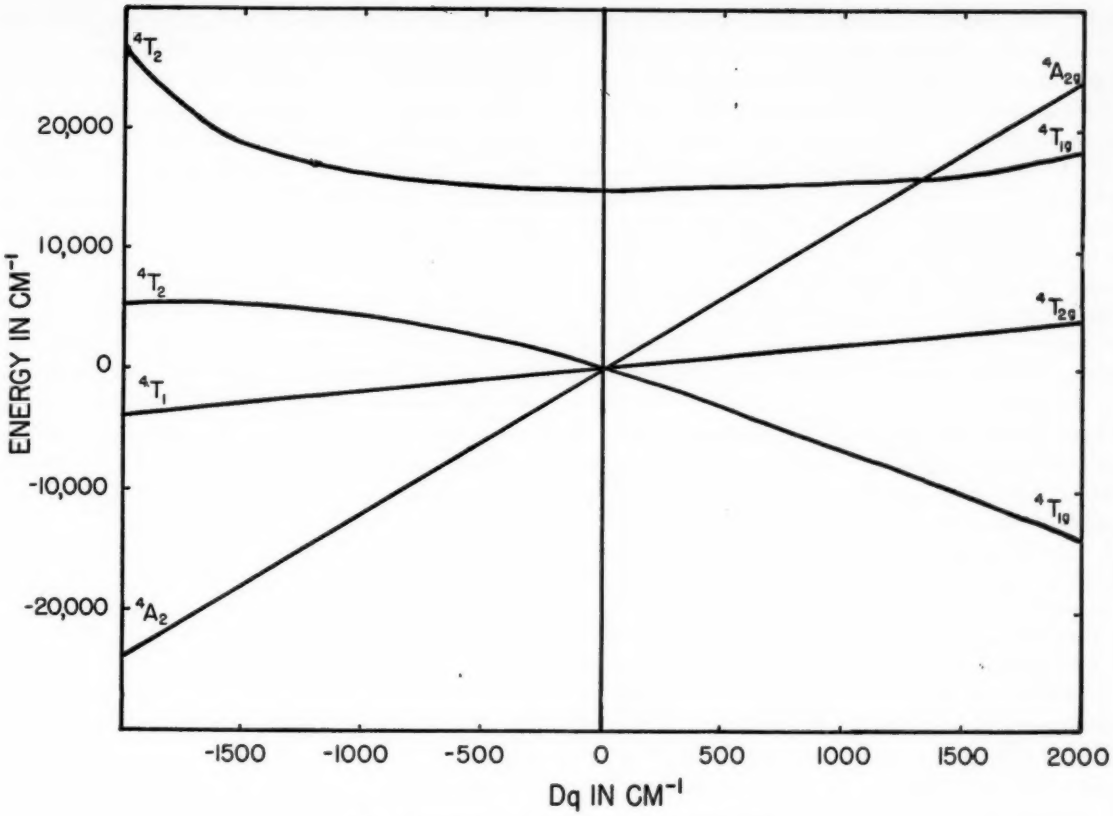

FIG. 5. Energy level diagram for the Co^{++} ion.

and 17 900 cm^{-1}. Taking a value of $Dq = 1220\ cm^{-1}$ we predict levels at 12 200 cm^{-1} and 18 700 cm^{-1}, in satisfactory agreement with experiment. No other vanadous complexes seem to have been studied.

The spectra of a number of cobaltous salts have been recorded. Those of the regular octahedral and tetrahedral complexes, in which the cobalt ion has a quartet ground state, are the most important from our point of view. The energy level diagram for the d^7 configuration may be obtained from the matrix-elements given by Finkelstein and Van Vleck. The energy-level diagram for the quartet states in both octahedral and tetrahedral complexes is shown in Fig. 5.

The hydrated cobaltous ion, $[Co(H_2O)_6]^{++}$, in aqueous solution has an absorption band in the infrared with its maximum at 8100 cm^{-1} [24] and a broad, complex band whose maximum is at 19 600 cm^{-1} and which stretches from about 15 000 cm^{-1} to about 28 000 cm^{-1}.[37] If we take $Dq = 970\ cm^{-1}$ we predict transitions at 8100 cm^{-1}, 17 500 cm^{-1}, and 22 000 cm^{-1}. We think it probable that the 19 600 cm^{-1} band of the cobaltous ion includes both of the shorter wavelength quartet-quartet transitions and, in addition, some quartet-doublet transitions.

The $[Co(NH_3)_6]^{++}$ ion has an absorption maximum at about 20 200 cm^{-1} while the corresponding ethylenediamine complex has two maxima at 20 800 cm^{-1} and 28 100 cm^{-1}.[27] In view of the great similarity of other spectra of ammonia and ethylenediamine complexes we assume that the two bands near 20 000 cm^{-1} have the same origin, namely in the $T_{1g} - A_{2g}$ transition. This would correspond to a value of 1130 cm^{-1} for Dq in the ethylenediamine complex and slightly less in that of ammonia.

The analysis of the spectra of the tetrahedral cobaltous complex ions $[COCl_4]^{--}$, $[CoBr_4]^{--}$, $[CoI_4]^{--}$ and $[Co(CNS)_4]^{--}$ presents a number of difficulties. Each of the halides has an absorption band in the infrared, the maxima being at 6300 cm^{-1}, 5300 cm^{-1}, and 5000 cm^{-1} with ϵ_{max}'s of 15 100 and 160 for the chloride, bromide, and iodide, respectively. In the visible there are a number of absorption bands, but one of these is always stronger than any other. This strong band is at 15 000 cm^{-1} in the chloride, at 13 700 cm^{-1} in the bromide, at 12 500 cm^{-1} in the iodide[37] and at 17 000 cm^{-1} in the thiocyanate.[38] The extinction coefficient is as high as 2500 in $[Co(CNS)_4]^{--}$ while in $[CoCl_4]^{--}$ ϵ_{max} is about 600.

The energy-level diagram for tetrahedral Co^{++} (Fig. 5) shows that the two strong bands do not correspond in position to the two lowest predicted transitions, for if we fit the lowest transition correctly in

[37] A. Kiss and P. Csokan, Z. physik. Chem. **A186**, 239 (1940).

[38] W. R. Brode and R. A. Morton, Proc. Roy. Soc. (London) **120**, 21 (1928).

$[CoCl_4]^{--}$ we predict the next transition at 11 000 cm^{-1}, which is much *below* the observed transition.

The two observed bands are much stronger than those of divalent transition-metal ions in octahedral coordination. This we believe to be due to the mixing together of the $3d_{xy}$, $3d_{xz}$, and $3d_{yz}$ orbitals and the $4p$ orbitals, which is possible since the tetrahedron of ligands has no center of symmetry and can therefore cause the mixing of orbitals which are of g and u symmetry in the free atom. The transition from the A_2 ground-state to the two T_2 upper states are formally allowed on symmetry grounds, while the transition to the T_1 state is forbidden. It seems plausible to assume that the two strong observed transitions are in fact the allowed transitions. If we do this we find $Dq=375$ cm^{-1} in $[CoCl_4]^{--}$ in order to account for the infrared band, and then predict a second band at 19 500 cm^{-1}. This value again disagrees rather badly with the experimental value. It is possible that this assignment is nevertheless correct and that the discrepancy is due to the depression of the upper T_2 state by a nearby state of the d^2p configuration. If this is so there should be a forbidden transition in the infrared to a state only about 3500 cm^{-1} above the ground state. The spectra of the bromide and iodide complexes interpreted in this way give values of 310 cm^{-1} and 290 cm^{-1} for Dq. Any other interpretation of these spectra would also require a small Dq value. A possible explanation of the low values of Dq will be given in the next paper.

THE CONFIGURATIONS d^4 AND d^6

Very little information is available concerning the spectra of the complexes which have the d^4 configuration, i.e., chromous and manganic complexes. Aqueous solutions of chromous chloride have an absorption band with its maximum at about 12 600 cm^{-1} which almost certainly belongs to the $[Cr(H_2O)_6]^{++}$ ion.[35] The energy level for the quintet states of d^4 is identical with that of d^9 and so we find a value of $Dq=1260$ cm^{-1}. It should be noted that although the chromous solutions studied were not very stable, the position of the band maximum would not be affected since the chromic ion does not absorb in the same region as the chromous.

The Mn^{+++} hydrated ion has an absorption maximum at 4750 A,[7] corresponding to a Dq value of 2100 cm^{-1}. No other manganic complexes seem to have been investigated.

The configuration d^6 occurs in the ferrous and cobaltic complexes. The energy diagram for the quintet states is identical with that for a single d-electron, so that the absorption maximum of the hydrated ferrous ion, which occurs at 10 500 cm^{-1} [35] corresponds to $Dq=1050$ cm^{-1}. No other ferrous complexes with quintet ground states have been examined.

The spectra of the few diamagnetic ferrous complexes which have been studied e.g., $[Fe(CN)_6]^{4-}$ and $[Fe(Phenanthroline)_3]^{++}$ do not fit into the present theoretical scheme at all well. This may be connected with the strong double bond formation which must occur in them.

The complexes of trivalent cobalt, with the exception of the $[CoF_6]^{3-}$ ion, are diamagnetic i.e., they have singlet ground states. Unfortunately the calculation of the energy-level diagram for the singlet states would be extremely lengthy, there being as many as seven $^1T_{2g}$ states. Instead we shall discuss the spectra in a qualitative way.

We have shown that the close similarity between the spectra of chromic and cobaltic complexes is due to the fact that when the splitting of the $3d$-orbitals becomes very large compared with the electrostatic interactions between $3d$-electrons the energy diagrams for the three lowest singlet states of Co^{+++} and for the three lowest quartet states of Cr^{+++} are essentially identical.[8] The two strong absorption bands correspond to transitions from the state $(t_{2g})^3\,{}^4A_{2g}$ to the states $(t_{2g})^2(e_g)^1\,{}^4T_{1g}$ and $^4T_{2g}$ in Cr^{+++}[39] and from the state $(t_{2g})^6\,{}^1A_{1g}$ to the states $(t_{2g})^5(e_g)^1\,{}^1T_{1g}$ and $^1T_{2g}$ in Cr^{+++}. The energy level diagram for Co^{+++} will differ somewhat from that of Cr^{+++} in fact, because "configuration interaction" is possible in the former e.g., between $(t_{2g})^6\,{}^1A_{1g}$ and $(t_{2g})^4(e_g)^2\,{}^1A_{1g}$, which is impossible in the latter.

The similarity between the strongest transitions in cobaltic and chromic complexes does not extend to the intercombinations. The reason for this is clearly that the lowest quartet-doublet transitions in Cr^{+++} are essentially those within the $(t_{2g})^3$ configuration. In Co^{+++} the lowest triplets belong to the $(t_{2g})^5(e_g)^1$ configuration.

A very large variety of cobaltic complexes has been studied, so that although we cannot get accurate values of Dq we can find the order of increasing Dq for a variety of ligands.

From the work of Kiss and Czegledy[40,41] we may deduce the following order of Dq contributions:

$$CO_3^{--}<OH^-<NO_3^-=SO_3^{--}<CNS^-<H_2O$$
$$<\text{Oxalate}<NH_3<\text{ethylene diamine}<NO_2^-<CN^-.$$

The measurements of Linhard and Weigel[42] give the following order of increasing Dq

$$I^-<Br^-<Cl^-<N_3^-<R\cdot CO_2^-<F^-<NH_3<NO_2^-.$$

The two orders cannot be brought together with certainty since there are small differences between the positions of the maxima found by the different workers.

Perhaps the most interesting conclusion to be drawn from these spectra is that the cyanide ion produces a much bigger splitting than any other ion. The first

[39] We use small letters to designate orbitals in accordance with Professor Mulliken's recommendations on spectroscopic nomenclature. This involves a change from the notation of our earlier paper.

[40] A. Kiss and D. Czegledy, Z. anorg. Chem. **235**, 407 (1937).

[41] A. Kiss, Z. anorg. Chem. **246**, 28 (1941).

[42] M. Linhard and M. Weigel, Z. anorg. Chem. **264**, 321 (1951); **266**, 49 (1951); **267**, 113 (1952); **267**, 121 (1952).

maximum of $[Co(NH_3)_6]^{+++}$ is at 21 000 cm^{-1} while that of $[Co(CN)_6]^{---}$ is at 32 000 cm^{-1}. This is consistent with the very marked double-bond character of the transition-metal to cyanide bonds.

We have shown that the longest wavelength absorption band in monosubstituted cobaltic complexes is split into two components[8] and that if Dq for the substituent is less than it is for the other ligand then the long wavelength component should be twice as strong as the other. If Dq is greater for the substituent then the order of intensities should be reversed. Furthermore, it is readily seen that the magnitude of the splitting should be proportional to the difference in Dq values for the substituent and for the other ligand. These relations are in general found to be correct.[42]

In disubstituted complexes we would predict that the splitting of the longest wavelength transition would be much more marked in the *trans*-complexes than in the *cis*. This is completely confirmed by the measured spectra.[42]

THE CONFIGURATION d^5

The matrix-elements of the cubic field for the triplet states of the d^5 configuration have been calculated in the usual way. The elements which do not vanish through symmetry are given below.

E_1	^4P	^4F	^4G
^4P	0	0	$4\sqrt{5}$
^4F	0	0	$2\sqrt{5}$
^4G	$4\sqrt{5}$	$2\sqrt{5}$	0

E_2	^4D	^4F	^4G
^4D	0	$20/\sqrt{7}$	0
^4F	$20/\sqrt{7}$	0	$10\sqrt{3/7}$
^4G	0	$10\sqrt{3/7}$	0

E	^4D	^4G
^4D	0	0
^4G	0	0

It should be noted that all diagonal elements are zero. The energy level diagram for Mn^{++} in octahedral or tetrahedral coordination is shown in Fig. 6. An analogous diagram applies to Fe^{+++}. We will not reproduce it here as it may easily be obtained by solution of the appropriate secular equations using the extrapolated values of 32 000 cm^{-1}, 35 000 cm^{-1}, 38 500 cm^{-1}, and 52 000 cm^{-1} for the energies of the ^4G, ^4P, ^4D, and ^4F states of Fe IV(d^5).[43]

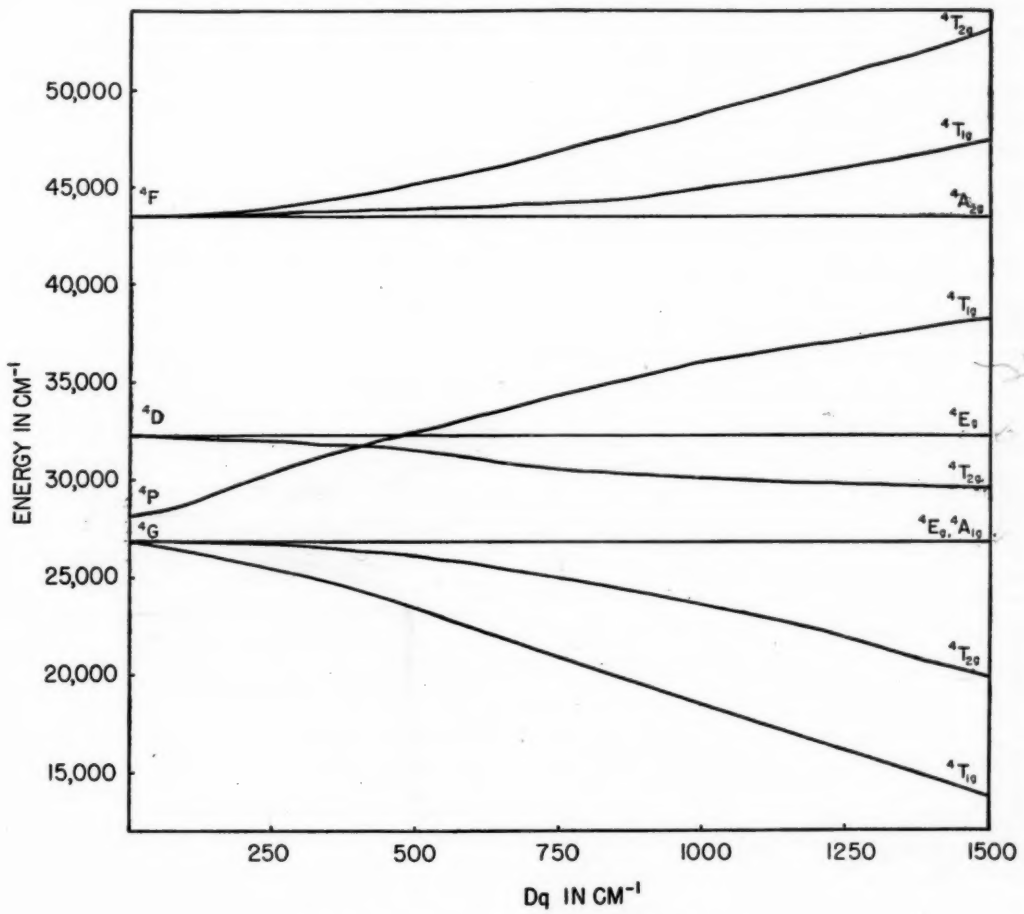

FIG. 6. Energy level diagram for the Mn^{++} ion.

[43] Edlen, *Actualities Scientifiques et Industrielles* (Hermann & Cie, Paris, 1941), No. 895, Part I.

The configuration d^5 is exceptional in that no spin-allowed transitions are to be expected, since the ^6S ground state is not split significantly by the field, and all excited states are of lower multiplicity. It follows that only very weak absorption corresponding to sextet-quartet transitions is to be expected. The sextet-doublet transitions are almost certainly too weak to appear in absorption.

It is found experimentally that $[Mn(H_2O)_6]^{++}$ exhibits very weak discrete absorption between 24 500 cm^{-1} and 25 500 cm^{-1}.[26] The ultraviolet region does not seem to have been investigated. If we assume a Dq value of about 1000 cm^{-1} we predict a number of transitions between 18 000 cm^{-1} and 35 000 cm^{-1} followed by a further series of transitions which begins at 43 000 cm^{-1}. The data available are not sufficient to make any definite assignment. We are inclined to think that the observed transition is not the lowest $^6S-{}^4G(T_{1g})$ transition but that the upper state is $^4G(A_{1g})$, $^4G(E_g)$ or possibly $^4G(T_{2g})$. A number of compounds in which the octahedron of ligands surrounding the manganous ion includes two or more species have been studied. They show a number of bands between 23 000 and 40 000 cm^{-1}.[26] This is consistent with the theoretical scheme, but the energy-level diagram is so complicated that no assignments can be made. An experimental study of the $[Mn(H_2O)_6]^{++}$ ion would be particularly valuable.

The spectrum of $[Fe(H_2O)_6]^{+++}$ has been studied in some detail by Rabinowitch and Stockmayer.[44] They find very weak bands at 24 500 and 18 400 cm^{-1} and a further band with a maximum at less than 14 000 cm^{-1}. Infrared studies show that maximum of the latter band is near 13 000 cm^{-1}. These observations are not easily explained since theoretically there should be only two transitions much below 32 000 cm^{-1}, the position of the ^4G state. Using a reasonable value of 2100 for Dq we predict $^4G(T_{1g})$ and $^4G(T_{2g})$ levels at 13 300 and 20 700 cm^{-1} respectively, in rough agreement with experiment, but the band at 24 500 remains completely unexplained. It might be a strongly forbidden charge-transfer band, but this seems unlikely in view of its sharpness. Until further evidence is available both the values of Dq and the assignments of the two long wavelength bands are tentative. It is interesting that complex-formation with ammonia or aliphatic amines should shift the two long wavelength bands of Fe^{+++} to *lower* energies.

[44] E. Rabinowitch and W. H. Stockmayer, J. Am. Chem. Soc. **64**, 335 (1942).

The tetrahedral ion $[FeCl_4]^-$ has been studied under a variety of conditions.[45] It has a broad very weak absorption band from 6000–8000 A with maxima at about 7500, 6900, and 6100 A, and sharper peaks at 5250 A and 6500 A. Like the spectra of other tetrahedral complexes these cannot be explained quantitatively by our theory. It is not clear whether the observed transitions are internal transitions of the iron atom or spin-forbidden charge-transfer bands.

CONCLUSIONS

We have shown that many features of the absorption spectra of transition-metal complexes may be understood in terms of crystal-field theory. A number of interesting regularities are evident when the Dq values are compared. In particular:

(1) The values of Dq for hydrated divalent ions are close to 1000 cm^{-1}, falling from 1220 cm^{-1} for V^{++} and 1260 cm^{-1} for Cr^{++} to 850 cm^{-1} for Ni^{++}.

(2) The values of Dq for hydrated trivalent ions are close to 2000 cm^{-1}.

(3) The common ligands may be arranged in a squence in such a way that the Dq values for their complexes with any metal ion increase as we go from left to right. Such a sequence is:

I^- Br^- Cl^- F^- H_2O oxalate pyridine
NH_3 ethylene diamine NO_2^- CN^-.

(4) The little evidence available suggests that Dq is much smaller for tetrahedral complexes than for corresponding octahedral complexes.

We shall defer the discussion of the importance of these regularities in understanding the chemistry of transition-metal complexes to a subsequent paper.

The identification of excited electronic states of many complexes and the estimation of Dq values should prove helpful in interpreting paramagnetic susceptibility data and paramagnetic resonance spectra. In many cases the values of Dq assumed at present are very different from those derived in this work.

I am indebted to Dr. D. McClure for communicating results on the crystal spectra of hydrated transition-metal ions, prior to publication. His interpretation of these spectra is in substantial agreement with that presented in this paper.

[45] H. L. Friedman, J. Am. Chem. Soc. **74**, 5 (1952).

Studies of the Interaction between Stable Molecules and Atoms. I. A Molecular Orbital Theory of the Activation Energy between Molecules and Atoms*

VIRGINIA GRIFFING
Department of Chemistry, Catholic University of America, Washington, D. C.
(Received June 22, 1954)

The molecular orbital method of calculation is applied to the interaction between closed-shell species; the results discussed in this paper and presented in the following papers of this series indicate that this method will yield quantitative results for energies of a system as function of internuclear parameters if one is interested in the differences in energy for two different geometric ground state configurations of the system. The molecular orbitals are used as a basis of constructing correlation diagrams for predicting mechanisms and calculating activation energies for chemical reactions. The orbitals of the reactants and products are correlated with the orbitals of a state defined as the ambivalent complex. The low-lying excited states of the interacting molecules seem to be of importance in determining the activation energy of a chemical reaction. Considerable qualitative insight into the activation process is gained by this method; the relative values of the activation energies for the interaction between two closed-shell molecules, a molecule and a radical, and two radicals are predicted in agreement with experiment.

I. INTRODUCTION

THIS paper is the first in a series of studies of "atomic complexes" with the method of molecular orbitals which have been completed in our laboratories. Papers II to VI present actual numerical calculations on systems which are simple enough that they can be studied as function of internuclear parameters. These simple systems must be understood before results obtained in more complicated systems can be interpreted. In addition these systems have been chosen so as to represent certain idealized models of chemical interaction. In this first paper it is shown that these calculations can be used to predict the mechanism of simple chemical reactions, by considering the least energy necessary to form a possible intermediate complex.

The ideas are not entirely new insofar as they apply the well-known self-consistent field molecular orbital[1] approximation to a system of n-electrons for different geometrical configurations of the nuclei (both stable and unstable configurations). However, the emphasis is somewhat different here. It is shown that general principles which have long been useful and widely accepted in the discussion of the ground state electronic structure and in the interpretation of electronic spectra of stable molecules are also useful in deciding which interactions of stable molecules bring about chemical reactions. This series of papers would seem to settle the question of the usefulness of the molecular orbital approach in studying chemical kinetics.

It is believed that this discussion gives considerable physical insight into the approximate values and nature of activation energies; e.g., one can see from a consideration of the molecular orbitals of a bimolecular complex why the activation energy between most saturated molecules is so high that free radical mechanisms must predominate in the thermal decomposition of these molecules. It further explains the low activation energy for a reaction between a molecule and a radical and the nearly zero energy of activation for reaction between two radicals equally as well as the bond picture. In addition, an explanation is suggested for the fact that $H_2+I_2\rightarrow 2HI$ proceeds by a bimolecular mechanism, while the reaction $H_2+Cl_2\rightarrow 2HCl$ proceeds by an atomic mechanism.

We are going to use simple determinants built up from one-electron wave functions, which are linear combinations of atomic orbitals (LCAO); the coefficients are calculated according to the well-known self-consistent field methods.

We do so according to the following general assumptions:

1. The description by one-electron molecular orbitals is adequate for discussing possible chemical interactions between molecules.
2. The chemical interaction between saturated molecules can be treated as a four-electron problem.
3. The symmetry properties of the molecular orbitals reduce the number of possibilities to be considered.

II. DISCUSSION OF THESE ASSUMPTIONS

(1) Even though the SCF-molecular orbitals may not be the best wave functions for giving numerical answers, we believe that greater physical insight can be obtained by using the best single determinant wave function inasmuch as the Pauli principle then appears in its naive form in which only two electrons can occupy the same molecular orbital. If greater numerical accuracy is required it can be obtained by including a limited amount of configuration interaction. From the point of view of economy of calculation, this is probably the best method of approach (even though many con-

* Supported by the Office of Naval Research.
[1] For discussion of molecular orbital theory see C. C. J. Roothaan, Revs. Modern Phys. **23**, 69 (1951); R. S. Mulliken, J. chim. phys. **46**, 497 (1949); **46**, 675 (1949); J. E. Lennard-Jones, Proc. Roy. Soc. (London) **A198**, 1 (1949), and other papers in this series with Pople, Hall; J. F. Mulligan, J. Chem. Phys. **19**, 347 (1951).

figurations are included) as long as the distances between atoms are of the same order of magnitude as those occurring in stable molecules.

(2) It is further assumed that the activation process between two saturated molecules can be treated as a four-electron problem† to a good first approximation. This is justified by the fact that molecules are in some ways simpler than atoms, in particular since they nearly always have paired electron ground states with the full symmetry of the nuclear framework. In order to simplify the discussion, we discuss here no molecules with double bonds. Then, it would seem, any chemical interaction between two saturated molecules will essentially be determined by the interaction between the outermost molecular orbital of one molecule with the outermost molecular orbital of the other. The lowest orbital of the complex will have a density maximum between the two interacting molecules corresponding to a "bonding orbital" in ordinary molecule formation. The second orbital of the complex will have a node between the two molecules corresponding to antibonding. In addition there is an increase in energy due to additional nuclear repulsions. When there are two electrons in each of these orbitals this leads to a higher energy than that of the separated molecules, i.e., an activation energy. Therefore it is assumed that the activation process for molecule interaction can be treated as a four-electron problem to a good first approximation.

(3) The symmetry properties of the molecular orbitals of the separated molecules and of the complex can be used to draw some general conclusions about possible reaction mechanisms; further, the number of geometrical configurations‡ that must be considered in constructing a potential energy surface can be drastically reduced. Thus, this is actually a generalization of the Hund-Mulliken coordination schemes for diatomic molecules to form correlation diagrams for polyatomic systems. In the case of diatomic molecules, Hund and Mulliken have correlated the one-electron orbitals of "separated atoms," "diatomic molecule," and "united atom." There are two rules which govern these coordination schemes[2]: (a) As the interatomic distance is changed the symmetry properties of the molecular states must remain unchanged. (b) Two different molecular states of the same symmetry may not have the same energy for any internuclear distance. The second of these rules prohibits the occurrence of degeneracy in the case of diatomic molecules.

The reason for this is that the mathematical requirements of degeneracy cannot be satisfied by changing a single parameter, i.e., the internuclear distance. Even though one can get a bond-like interaction between two He atoms if one supplies enough energy to excite electronically one of the He atoms, according to Hund's rule[2] this state cannot cross over the nonbonding ground state for He_2 for any value of the internuclear parameter. Therefore it is a consequence of the two rules that the stable state of He_2 is of necessity an electronically excited state of the molecule. Thus, the critical energy that must be supplied to bring about "chemical interaction" between two He atoms is an electronic energy and can be compared with that in processes which occur in photochemistry.

However, Teller[2] has shown that degeneracy can be established by adjusting two parameters in the absence of magnetic forces. From this we draw the following conclusions. If one considers a generalized two-center system in which the two parameters, (a) internuclear distance and (b) nuclear charge, are varied one can obtain the entire set of homonuclear diatomic molecules predicting the electronic structure of their ground states and in principle their chemical properties.

In polyatomic systems, one usually has two or more geometrical parameters that can be independently varied thus bringing about a crossing over of potential energy surfaces.

Teller has discussed the conditions that must be fulfilled to bring about the intersection of the ground state potential energy surface of a polyatomic molecule with one of the excited electronic states of the same molecule (internal conversion). This discussion can be equally well applied to a polyatomic system made up of two molecules, except that in this case one needs to consider the intersection of potential energy surfaces of a particular kind of complex which we shall designate as the "ambivalent complex," rather than those of a stable molecule. The "ambivalent complex" is defined in the following way: If a complex of particular size and shape can be formed from one set of closed-shell molecules (say AB and CD) and can decompose into products different from those (say $AC+BD$ or $A+BC+D$), then for this particular geometrical arrangement of the atoms it must be possible to describe the electronic wave functions of the complex in two different ways, as a linear combination of the electronic wave functions of AB and CD and as a linear combination of the electronic wave functions of say AC and BD. It is one of the fundamental points of this paper that the path of the direct reaction $AB+CD \rightarrow AC+BD$ must go through the complex ambivalent in respect to these two states.

In some cases the "ambivalent orbitals" are also degenerate. In this case the complex is called a "degenerate complex." If the "ambivalent orbital" is also degenerate, the ambivalence property is also exhibited when the ambivalent orbital is expressed as a linear combination of atomic orbitals. That is, there are two independent linear combinations of the atomic orbitals which equally well describe the state. If the orbital of the "ambivalent complex" is nondegenerate, the orbital

† Eyring has made this assumption in much of his work but has used the electrons localized in particular bonds rather than moving in the entire field of the nuclear framework.

‡ These ideas have probably been used intuitively by a number of investigators but have not been previously formalized in this way so far as we know.

[2] E. Teller, J. Phys. Chem. 41, 109 (1937).

has a unique form when expressed as a linear combination of atomic orbitals. It will be shown that a "degenerate complex" arises in the case where

$$AB+CD \rightarrow AC+BD,$$

while the "ambivalent complex" arises in the case where

$$AB+CD \rightarrow A+BC+D,$$

and the degeneracy occurs for some other internuclear distances along the path of decomposition of the complex.[3]

This "ambivalent complex" is related to the activated complex of Eyring except that our attention is directed to the forms of the one-electron wave functions as functions of internuclear coordinates. The minimum energy that must be supplied to the initial molecules to get them into this ambivalent configuration is called the "ambivalent complex energy." The formation of the "ambivalent complex" is specified as a minimum condition which must be met before a chemical interaction will take place. The "ambivalent complex energy" will be related to the experimental energy of activation of an elementary chemical reaction.

In the following, the application of the molecular orbital theory to construct correlation diagrams for the chemical interactions between two saturated molecules is first illustrated by considering two different reaction paths for the interaction of two hydrogen molecules. This example was chosen as a model because the molecular orbitals in the separated molecules are of σ type and a four-electron problem includes all the electrons. Thus, the interpretation of the results will not be complicated by any errors due to the neglect of the effects of electrons moving in inner closed-shell molecular orbitals. Further, this is the simplest model one can assume and have two independent geometrical parameters.

III. QUADRATIC H_4 AMBIVALENT COMPLEX

In the first example, the two molecules are brought together along a path such that the four hydrogen atoms form a rectangle. There are four independent orthonormal one-electron molecular orbitals that can be formed from the four atomic orbitals.[4] Since there are only four electrons, two electrons are fed into each of the two lowest energy molecular orbitals. The other two orbitals are occupied only in excited states of the complex. The coefficients of the atomic wave functions in the orbitals are completely determined in this case by symmetry and the energy will be a function of two parameters, i.e., the two sides of the rectangle. In order for chemical interaction (i.e., formation of AC and BD out of AB and CD) to take place, the two sides of the rectangle must be equal, the second and third molecular orbitals are now degenerate, i.e., a degenerate state is reached and could accommodate the four electrons of the complex; however, there is a lower-lying totally symmetrical molecular orbital which will accommodate two electrons. This leaves two electrons in the twofold orbitally degenerate level.

The planar H_4 complex which would have the lowest energy with reference to nuclear repulsion would be the square configuration belonging to the symmetry D_{4h}. The lowest lying molecular orbital corresponds to a totally symmetrical a_{1g} level. The second molecular orbital is a twofold degenerate e_u orbital. If one assumes that the ground state of the degenerate complex is given by placing two electrons with paired spins in the a_{1g} and either of the e_u molecular orbitals, the total electron configuration is a ^1E_u state.§ Energy in the vibrational degrees of freedom of the structure described above would immediately carry it into one of the following structures: (a) It could go back to the original rectangular form which would mean a return to the two original molecules and no reaction. (b) The system could go into the other rectangular form in which atoms have exchanged partners and decompose into two stable molecules, and chemical reaction has taken place; however, the energy to produce the degenerate symmetrical state must first be supplied. (c) The system could go from the square to the rhombic form (D_{2h}) which could be stable from symmetry considerations; thus this configuration could be a stable dimer or it could decompose along some normal coordinate of the rhombic form. (d) Similarly, the square degenerate form could go into the nonplanar form belonging to the group C_{2v} in which three atoms lie at the corners of an isosceles right triangle and the fourth is on the perpendicular bisector of the hypotenuse at the vertex of a congruent isosceles triangle. (e) Finally, the complex could belong to symmetry T_d in which the four atoms are at the corners of an equilateral tetrahedron, but in this case the nuclear repulsion would be much greater and consequently even more energy would be required unless the orbitals were directed. This might be a possible complex in which $2p$ electrons are important.

Now consider what this discussion means. The interaction (a) is uninteresting from the point of view of bimolecular interactions bringing about decomposition. The mechanism (b) has to go through the degenerate

[3] This theory is an extension of the concept of "internal conversion" introduced by J. Franck and H. Sponer in *Contribution a L'Etude de la Structure Moleculaire*, Victor Henri Memorial Volume (Maison Desoer, Liege, 1947–1948). These authors suggest this approach to reaction kinetics.

[4] See paper III of this series [V. Griffing and A. Macek, J. Chem. Phys. **23**, 1029 (1955)].

§ The energy level scheme for quadratic H_4 is given in paper III and, if one neglects configuration interaction on the ground state of the complex, is orbitally degenerate. To get any quantitative information about the energy and the total electron configuration of this ambivalent complex, one must include configuration interaction because the shell is not filled. The configuration interaction splits the degeneracy of the single determinantal wave function into two nondegenerate states. However, for our purposes, the existence of the degenerate orbital is still of of importance and will be discussed in detail later.

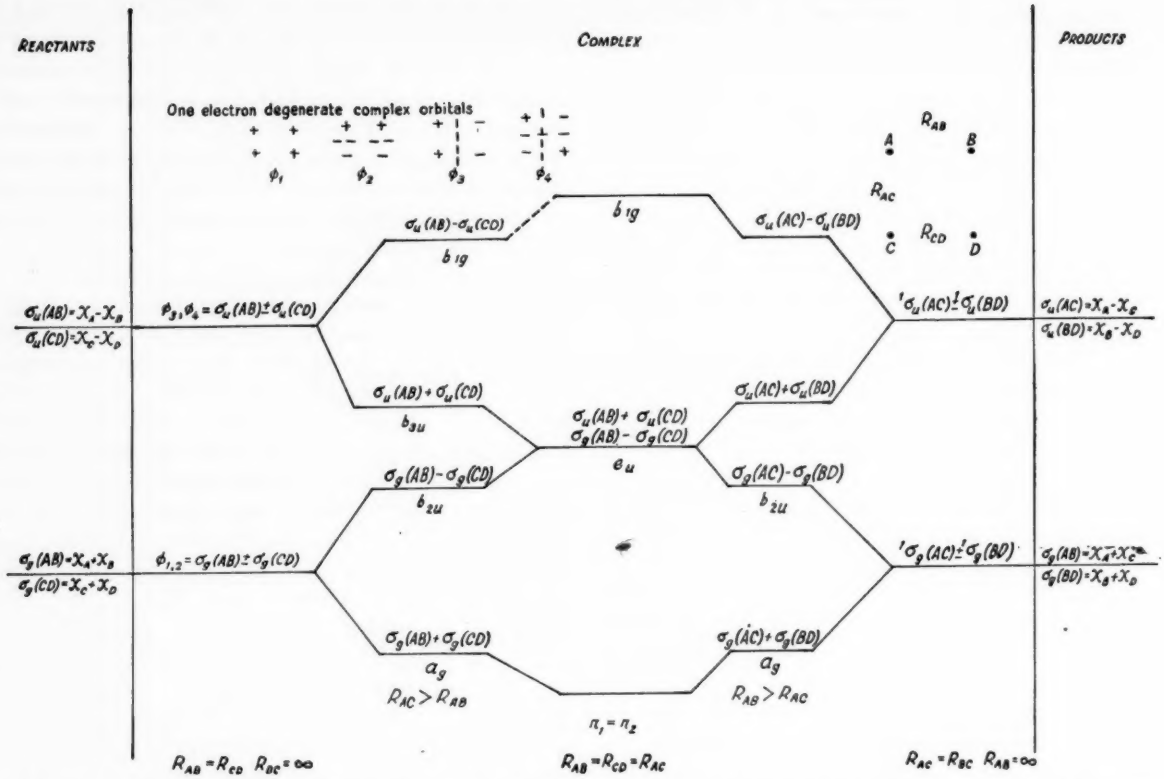

FIG. 1. Correlation diagram for quadratic H_4. The molecular orbitals of the separate molecules $H_2(AB)$ and $H_2(CD)$ are correlated with the products, $H_2(AC)$ and $H_2(BD)$ through a rectangular complex ($R_{AC}>R_{AB}$) and the degenerate ambivalent complex ($R_{AB}=R_{AC}$).

point and is the only possible path for a true bimolecular kinetics which would bring about the direct molecular exchange between

$$\begin{matrix} AB & CD & AC & BD \\ H_2 & + H_2 & \rightarrow H_2 & + H_2. \end{matrix}$$

The energy to produce the symmetrically degenerate state would be the degenerate complex energy that must be supplied to bring about such a mechanism and there would be equal *a priori* probability that once in this state the molecules would return to their original configuration or go into reaction with exchange of atoms. The correlation diagram for this case is given in Fig. 1.

In Fig. 1, the molecular orbitals of the separated hydrogen molecules AB and CD are shown at the left side of the diagram. The ground state molecular orbitals are represented by $\sigma_g(AB)=C(1s_A+1s_B)$ and $\sigma_g(CD)=C(1s_C+1s_D)$ and the excited state molecular orbital for a hydrogen molecule is represented by $\sigma_w(AB)=C(1s_A-1s_B)$ and $\sigma_w(CD)=C(1s_C-1s_D)$. Considered from the point of view of the degenerate system $ABCD$ these first two orbitals are degenerate when $R_{BC}=\infty$, because in this configuration the degenerate complex molecular orbitals can be represented equally well by

$$\phi_1=C_1\{\sigma_g(AB)+\sigma_g(CD)\}$$

and

$$\phi_2=C_2\{\sigma_g(AB)-\sigma_g(CD)\};$$

the excited state degenerate complex molecular orbitals can be replaced by $\phi_3=C_3\{\sigma_w(AB)+\sigma_w(CD)$ and $\phi_4=C_4\{\sigma_w(AB)-\sigma_w(CD)\}$. ϕ_1, ϕ_2, ϕ_3, and ϕ_4 are shown in the upper left-hand corner of Fig. 2. As the intermolecular distance $R_{AC}=R_{BD}$ is decreased along a rectangular path, this degeneracy is split and for an arbitrary geometrical arrangement $R_{AC}=R_{BD}=R$ and $R_{AB}=R_{CD}=R'$ the one-electron orbitals of the complex are nondegenerate and belong to the irreducible representations of the group D_{2h}. However, if $R_{AC}=R_{DB}=R_{AB}=R_{CD}$ the lowest orbital is totally symmetric and is nondegenerate, and the second and third molecular orbitals ϕ_2 and ϕ_3 are now doubly degenerate. The electronic structure of the degenerate complex is then given by placing two electrons with paired spins in ϕ_1 and two electrons with paired spin in either ϕ_2 or ϕ_3. One can see qualitatively from this diagram why there is high activation energy for this type of reaction. In the first place the four atoms must be moved into that geometrical configuration which brings about a crossing of the molecular orbitals made up from the ground state of the separated hydrogen molecules and the high lying excited state of the separated hydrogen molecules. From this diagram one might expect the sum of the energies at $R_{AC}=R_{BD}=\infty$, $R_{AB}=R_{CD}=R_0$ to be equal to the sum of the energies at $R_{AC}=R_{AB}$, but when the complex is square the energy of the degenerate com-

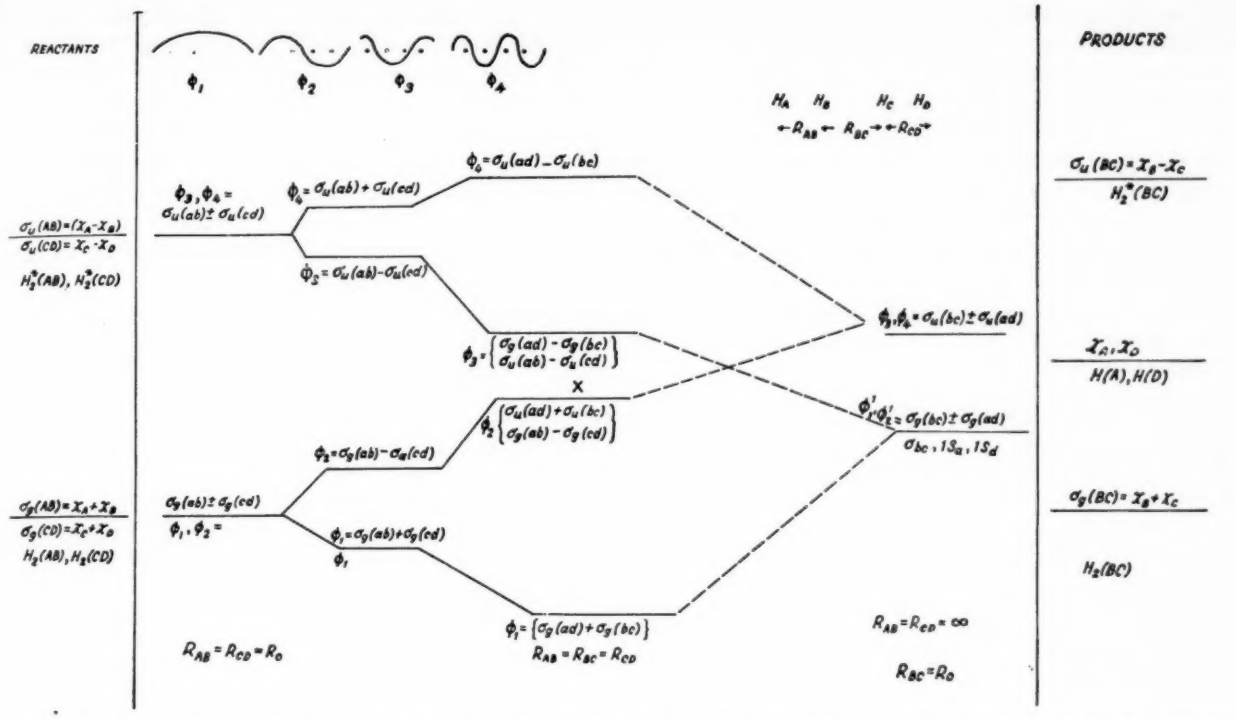
REACTANTS
PRODUCTS
ϕ_1 ϕ_2 ϕ_3 ϕ_4
H_A H_B H_C H_D
$\leftarrow R_{AB} \leftarrow$ $R_{BC} \rightarrow \leftarrow R_{CD} \rightarrow$
$\phi_5 = \sigma_u(ad) - \sigma_u(bc)$
$\phi_6 = \sigma_u(ab) + \sigma_u(cd)$
$\phi_3, \phi_4 = \sigma_u(ab) \pm \sigma_u(cd)$
$\phi_2 = \sigma_u(ab) - \sigma_u(cd)$
$\sigma_u(AB) = (\chi_A - \chi_B)$
$\sigma_u(CD) = \chi_C - \chi_D$
$H_2^*(AB), H_2^*(CD)$
$\phi_3 = \begin{Bmatrix} \sigma_g(ad) - \sigma_g(bc) \\ \sigma_u(ab) - \sigma_u(cd) \end{Bmatrix}$
$\phi_2 = \begin{Bmatrix} \sigma_u(ad) + \sigma_u(bc) \\ \sigma_g(ab) - \sigma_g(cd) \end{Bmatrix}$
$\phi_3, \phi_4 = \sigma_u(bc) \pm \sigma_u(ad)$
$\phi_2', \phi_3' = \sigma_g(bc) \pm \sigma_g(ad)$
$\sigma_{bc}, 1s_a, 1s_d$
$\sigma_u(BC) = \chi_B - \chi_C$
$H_2^*(BC)$
χ_A, χ_D
$H(A), H(D)$
$\sigma_g(BC) = \chi_B + \chi_C$
$H_2(BC)$
$\sigma_g(AB) = \chi_A + \chi_B$
$\sigma_g(CD) = \chi_C + \chi_D$
$H_2(AB), H_2(CD)$
$\sigma_g(ab) \pm \sigma_g(cd)$
$\phi_1, \phi_2 =$
$\phi_1 = \sigma_g(ab) + \sigma_g(cd)$
$\phi_1 = \{\sigma_g(ad) + \sigma_g(bc)\}$
$R_{AB} = R_{CD} = R_0$
$R_{AB} = R_{BC} = R_{CD}$
$R_{AB} = R_{CD} = \infty$
$R_{BC} = R_0$

FIG. 2. Correlation diagram for linear H_4. The molecular orbitals of the two H_2 molecules are correlated with the molecular orbitals of the newly formed $H_2(BC)$ molecule and the two H atoms through those of the ambivalent complex (X). The degeneracy in this diagram occurs for values of the internuclear parameters differing from values for the ambivalent complex.

plex is pushed upward by the increased nuclear repulsions and the increase in electron-electron interaction energy. The second half of the diagram is a mirror image of the first half except that reaction has taken place and one now has molecules AC and BD, the degenerate complex decomposing along the coordinate $R_{AB}=R_{CD}\rightarrow\infty$ and $R_{AC}=R_{BD}\rightarrow R_0$. One calculates the degenerate complex energy as the difference in energy for the states at $R_{AB}=R_0$, $R_{AC}=\infty$, and for such $R_{AB}=R_{AC}=R_{BD}=R_{CD}$ at which the energy is a minimum. In the square case, for all values of the internuclear parameter below 2.2 a.u. the calculated energy of the complex is at least 3 ev above the energy of the four hydrogen atoms infinitely separated from each other. If one compares the calculated value for the square case at $R=2.2$ a.u. with the molecular orbital calculated value of two hydrogen molecules, one obtains an activation energy of about 9 ev.‖

If the rhombic or nonplanar configurations have the lowest energy (case c or d), then the energy of either of these forms would have to be considerably lower than the square form to be stable. Otherwise, vibrational energy concentrated in the proper normal mode of vibration would carry it into the unstable square form, which would then carry it through the degenerate point to reaction. Again, the critical energy to form the square complex would need to be supplied; however, if the reaction path were directly from the two molecules into either the rhombic or nonplanar form and then by vibrational excitation into the square form, there would probably be a time lag before the energy is concentrated in the proper normal vibration to bring about the square form and to decomposition.

If the energy of a rhombus or nonplanar form is considerably lower than that of the square—so that vibration would be unlikely to produce the square—the system would probably not decompose into two H_2 molecules but into one H_2 molecule and two H atoms (for the rhombus the molecule would be formed by the atoms on the shorter diagonal, the free atoms by those on the longer diagonal). In this case, the free atom mechanism would predominate after the initial step. However, the process $2H_2\rightarrow H_2+2H$ occurs with a much lower activation energy from a linear complex of two H_2 molecules than from the rhombic complex, because in the linear complex the nuclear repulsion is smaller.

IV. LINEAR H_4 AMBIVALENT COMPLEX

Calculations for the linear case have been made[5] and will now be discussed. One starts out with two hydrogen molecules in their ground state and brings them together along a line in such a way that initially the two inter-

‖ If one includes configuration interaction between the two degenerate orbitals, this value is lowered by about 1.6 ev. Other configurations, not yet included in our calculation, will probably lower it to values below the dissociation into four hydrogen atoms, but the activation energy will still be so high that this mechanism can probably be ruled out as a likely one.

[5] See paper IV of this series [V. Griffing and J. T. Vanderslice, J. Chem. Phys. **23**, 1035 (1955)].

nuclear distances R_{AB} and R_{CD} are equal and the distance between the centers of gravity of the two molecules is large. Then one calculates the energy of the configuration $R_{AB}=R_{BC}=R_{CD}$. Although in practice one does not need to require that $R_{AB}=R_{CD}$ along the reaction path, this does not place any restriction on the calculation since we are only interested in the energy difference between the two separated H_2 molecules in their ground state and the symmetrical configuration having the lowest energy. If one considers the one electron molecular orbitals for the four-center linear case, one finds that they have the following properties. Consider the structure

$$H_A-H_B-H_C-H_D.$$

The lowest molecular orbital is totally symmetrical and is represented by an electron moving in a path such that the probability of the electron being on H_B and H_C is equal and the probability of the electron being on H_A and H_D is also equal. The ground state wave functions of the two separated molecules $\sigma_g(AB)=\sigma_g(CD)$ must from the symmetry of the complex now form a wave function of the form

$$\phi_1=a_{11}\sigma_g(AD)+a_{12}\sigma_g(BC),$$

where in general $a_{11}\neq a_{12}$. The second molecular orbital will have a node between H_B and H_C. But here again, from the symmetry of the complex, the atoms H_B and H_C must be equivalent. In this case one cannot preserve the symmetry of the wave function and write the second one-electron molecular orbital as $\phi_2'=a_{21}\sigma_g(AD)-a_{22}\sigma_g(BC)$, but it becomes $\phi_2=a_{21}\sigma_w(AD)-a_{22}\sigma_w(BC)$. The situation is best illustrated if one approximates the one-electron molecular orbitals as a linear combination of hydrogen atom ground state atomic orbitals. If one writes to a first approximation $\sigma_g(AB)=1/N(1s_A+1s_B)$ and $\sigma_g(CD)=1/N'(1s_C+1s_D)$, where N is a normalization constant, one cannot build up the one-electron functions for the complex as linear combinations of the H_2 molecular orbitals σ_g as in the quadratic case, but must have wave functions in which the coefficient on each atomic orbital is varied independently keeping the functions orthonormal and so that they belong to the irreducible representation of $D_{\infty h}$.[5] One gets

$$\phi_1=a_{11}(1s_A+1s_D)+a_{12}(1s_B+1s_C)$$
$$\phi_2=a_{21}(1s_A-1s_D)+a_{22}(1s_B-1s_C),$$

where the coefficients have been varied for minimum energy in the SCF calculation according to the method of Roothaan. The first molecular orbital of the complex can be considered as a linear combination of the ground state H_2 molecular orbital of a hydrogen molecule with internuclear distance R_{AD} and the second H_2 molecular orbital with internuclear distance R_{BC}. The second molecular orbital can only be considered as built up as a linear combination of the excited state H_2 molecule molecular orbitals like $\sigma_w(AB)=1/N'(1s_A-1s_B)$. However, in this case the complex is not orbitally degenerate but the second orbital ϕ_2 is an "ambivalent orbital." This orbital is formed as the wave form continually shifts as the two molecules are brought together. The ambivalent complex is the totally symmetrical linear form in which the three internuclear distances are all equal (i.e., $R_{AB}=R_{BC}=R_{CD}$). At a critical value of this internuclear parameter, i.e., $R_{AB}=2.1$ a.u., $a_{21}=a_{22}$ and the second orbital can be represented in two alternative forms, i.e.,

$$a_{21}\sigma_w(AD)+a_{22}\sigma_w(BC)=a_{21}\sigma_g(AB)-a_{22}\sigma_g(CD)$$

or, in terms of atomic orbitals,

$$\phi_2=C(1s_A+1s_B-1s_C-1s_D).$$

This is the "ambivalent complex" and if one calculates the energy of the complex as function of the internuclear parameter, varying the coefficients for self-consistency, one finds a minimum in the electronic energy of the complex for the particular value of the internuclear parameter. In order to determine the energy along the reaction coordinate before the "ambivalent complex" is formed, one would have to do a self-consistent field calculation using a wave function having the form

$$\phi_2=a_{21}\sigma_g(AB)-a_{22}\sigma_g(CD).$$

The wave form of this orbital beyond this point, as the "ambivalent complex" decomposes into products, is given by

$$\phi_2=a_{21}\sigma_w(AD)+a_{22}\sigma_w(BC).$$

This situation is analogous to that of the approach along one rectangle through the square and decomposition along the other rectangular coordinate, but in this case the ambivalent complex is reached without the occurrence of orbital degeneracy; thus the interaction with the first excited state has not yet occurred and one can intuitively describe the activation energy as that energy necessary to replace the two hydrogen molecules by one hydrogen molecule vibrationally excited to a distance $R_{BC}=2.1$ a.u. and a second hydrogen molecule in which the internuclear distance is $3R_{BC}$. The correlation diagram for this case is given in Fig. 2. At the left of the diagram, the initial molecular orbitals are the same as those in Fig. 1. However, as the two molecules are brought together along the reaction path, keeping the system always linear and symmetrical (i.e., preserving symmetry $D_{\infty h}$), four one-electron states of the "ambivalent complex" orbitals are formed by a splitting of two degenerate (for $R_{BC}=\infty$) orbitals. In this case (in contrast with the rectangular path) the coefficients are no longer completely determined by symmetry. The "ambivalent complex" is formed as indicated at the center of the diagram by X at values of the internuclear parameter $R_{AB}=R_{BC}=R_{CD}=2.1$ a.u., that value that gives a minimum for the

TABLE I.

	KE(ϕ_1)	KE(ϕ_2)	Electron-nuclei attraction ϕ_1 H_1	Electron-nuclei attraction ϕ_2 H_2	Nuclei repulsions	Electron-electron interaction G	Total energy
H−H−H−H	17.190	28.02	−(46.05)2	−(40.56)2	58.93	57.80	−56.50
H−H | | H−H	16.18	41.12	−(53.46)2	−(42.36)2	73.64	68.12	−51.43

"ambivalent complex energy." In contrast with the square case, there has been no mixing with the excited orbital ϕ_3 even though one can represent the orbital as a linear combination of "excited state" orbitals of the two hydrogen molecules H_{AD} and H_{BC}. As the equivalent "ambivalent complex" now decomposes along a path in which $R_{BC}\rightarrow R_0$ and $R_{AB}=R_{CD}\rightarrow\infty$, the states represented by ϕ_2 and ϕ_3 must cross. This becomes evident if one considers the symmetry properties and nodes of the wave functions. ϕ_1 (together with ϕ_3) can go directly into the doubly degenerate ground state of the complex for $R_{AB}=\infty$ which is the ground state of the hydrogen molecule BC and two hydrogen atoms A and D. However, ϕ_2 has a node between atoms B and C and must converge to the excited state orbital of the hydrogen molecule BC; the energy curve for this orbital is crossed over by that for the orbital ϕ_3 which has a node between atoms A and B and a second node between atoms C and D. However as $R_{AB}\rightarrow\infty$, these two nodes move to infinity and this state converges to the lowest degenerate orbital of the complex, as represented on the right. Thus there is a mixing in of the excited states in this case, but it is after the formation of the "ambivalent complex" and at large internuclear distances as the two hydrogen atoms, H_A and H_D, move away. The middle pair of hydrogen atoms, H_B, H_C are moving during this process to the equilibrium configuration of the hydrogen molecule. Thus the energy of the complex must decrease beyond the point X, and the minimum point in the curve $E(r)$ for the symmetrical configuration $R_{AB}=R_{BC}=R_{CD}$ must be the "ambivalent complex energy." The calculated value of this barrier is 18 kcal/mole above the dissociation energy of a hydrogen molecule if one uses a SCF molecular orbital calculation to determine the energy of the complex and also the energy of the two separated hydrogen molecules. One can see qualitatively, in terms of the MO picture, two explanations for the much lower energy required for interaction along this path in comparison with the rectangular path leading to the square complex. In the first place, the nuclear repulsions are smaller by about 20 percent, and, secondly, the orbital degeneracy in the square case requires that the excited state be mixed in, but only at large internuclear distances where the energy of the excited state of the hydrogen molecule has become much lower.

V. DISCUSSION OF THE GENERAL THEORY

One can now generalize the theory. These generalizations are based in part on the calculations for the two different configurations of H_4. The numerical values of the various parts of the energy are given in electron volts. The situation is similar for all values of the internuclear parameter (Table I).

The general picture is based on the symmetry properties of the eigenfunction when one replaces the $3N$—dimensional Schroedinger equation by N three-dimensional equations—i.e., the orbital picture. In addition it is based on the assumption that the one-electron orbitals vary continuously as one changes the internuclear parameters, so that a twofold degenerate orbital can only occur when a higher energy orbital and a lower energy orbital intersect. This probably applies only if σ functions alone are involved, not when directed wave functions are available since these will give maximum interaction along a particular direction. Further calculations are in progress on other atomic complexes involving other types of symmetry and wave-functions made up of p and d functions which produce molecular orbitals with degeneracies of another kind (e.g., II orbitals).

One assumes that the SCF orbitals of the two separated molecules all remain essentially the same except for the outermost orbital ϕ_M and $\phi_{M'}$ on each molecule. This then reduces to a four-electron problem for interactions between saturated molecules. (This is comparable to using only the valence electrons in considering formation of molecules from atoms.¶) However, in setting up the one-electron functions of the complex, one cannot use simple $\phi_M\pm\phi_{M'}$, but one must also include the first excited state orbitals $\phi_M{}^*\pm\phi_{M'}{}^*$, where those excited states having the proper symmetry must be chosen. In practice this is most easily done by using the atomic orbitals and calculating the four one-

¶ The mathematical formulation for this theory is exactly the same as the LCAO-SCF method applied to the formation of molecules from atoms. In this case one uses linear combinations of molecular orbitals and must include unfilled molecular orbitals in the calculation. In the case of using the LCAO method to describe stable molecules, the unfilled orbitals usually have about the same energy as some of the filled ones; thus the interaction can produce binding. In considering the interaction between closed-shell molecules, the unfilled molecular orbitals are higher energy excited states; thus the interaction requires an activation energy. Mulliken had suggested that activation energy was a "promotion energy" many years ago according to a private communication from Eyring.

electron self-consistent field functions of the complex. From this one can get a qualitative picture of the relative order of magnitude of the activation energy of various systems. In the interaction between two closed-shell molecules one must place two electrons in the lowest ambivalent complex orbital, which can be considered as a bonding state made up of a symmetrical linear combination of the ground state MO's of the molecules; however, the second pair of electrons must be placed in the second ambivalent complex orbital which is a less symmetrical linear combination of a mixture of the ground states and excited states of the separated molecules and is thus antibonding. However, if one considers the interaction between a radical and a closed-shell molecule, two electrons go in the lowest bonding orbital of the ambivalent complex and only one electron in the second antibonding orbital. Thus this would require a lower energy of activation. In the case of the interaction between two radicals, the two electrons can both be placed in the bonding orbital and one would expect this process to require a very small or zero energy of activation.

If one considers Table I, one sees that the KE of the lowest filled (bonding) orbital is not much different for the two ambivalent complexes of different symmetry. On the other hand, the KE of the antibonding orbitals is much higher in the square. The combination of electron-nuclear and nuclear-nuclear interaction acts in the same direction as the KE of the antibonding orbitals, although not as strongly.

One can draw the following qualitative conclusion: As long as one has more bonding than antibonding orbitals, the more symmetrical configuration is more stable. If one has more antibonding orbitals, the less symmetrical configuration is more stable. Thus, one should choose a geometrical configuration, where the atoms are placed in the critical spatial configuration with a minimum symmetry, as the ambivalent complex which will allow the reaction between closed-shell molecules to take place.

One says "minimum symmetry" for if the ambivalent complex is also degenerate, the activation energy is higher than when a nondegenerate ambivalent complex enables the molecules to react. This is the result of higher electron and nuclear repulsions and the higher kinetic energies in the geometrically symmetrical arrangement necessary for degeneracy.

This explains why free-radical mechanisms predominate in the kinetics of thermal decompositions inasmuch as the ambivalent complex (square) leading to elementary bimolecular second-order kinetics requires a high degree of symmetry. Even a bimolecular collision producing two radicals in a single step requires a lower energy (e.g., linear H_4 compared with the square H_4)** because of lower symmetry. In case of higher symmetry, in which degenerate molecular orbitals appear, one has to take the final n-electron configuration into account. The degeneracy is split by the electron-electron interactions bringing about a lowering of the energy of the ground state of the complex, but this is not sufficient (only 1.6 ev in square H) to compensate for the additional repulsions. In the case of π type functions, this lowering may be sufficient to compensate for the higher positive energies in symmetrical complexes (e.g., this kind of splitting is responsible for O_2 having a triplet groundstate).

** If one includes the $\infty-$fold axis then $D_{\infty h}$ is more symmetrical than D_{4h}, but in these cases the $\infty-$axis does not affect the eigenfunctions.

VI. TRIPLET STATES. APPLICATION OF THE THEORY TO HYDROGEN-HALOGEN REACTIONS

Up to now, we have focused our attention on the one-electron orbitals of the ambivalent complex, with two electrons with paired spins placed in each orbital. However, there is one point in which the total n-electron configuration becomes important even qualitatively and must be discussed further. If the outermost ambivalent orbital is orbitally degenerate (as in the quadratic H_4 case), then one has six ways of choosing the electronic configuration in these orbitals, depending upon the additional degeneracy introduced by spin. In particular, the electrons placed in an orbitally degenerate orbital may have their spins either parallel or antiparallel; then there is a singlet-triplet splitting such that the triplet is represented by the antisymmetric linear combination of the product of the two degenerate orbitals; the singlet is represented by symmetric linear combinations of the products of the degenerate orbitals. In this case, the triplet usually lies lower than the singlet (Hund's rule) and the lowest electronic configuration of the ambivalent complex would be a triplet. Since most molecules have a singlet ground state and are thus required to interact along a singlet path, this low-lying triplet state will not be of any importance in chemical reactions. However, when molecules are considered in which $j-j$ coupling exists, the reaction could proceed from an initial singlet state in which the two infinitely separated reactants have singlet ground states through the lower triplet complex and by a second triplet-singlet transition back to the singlet states of the products. Thus, if the singlet-triplet transition *could* be allowed, the bimolecular reaction could go by a path that lies considerably lower than the orbitally degenerate singlet state. This suggests a possible explanation of certain results that have been obtained in the experimental study of the kinetics of the hydrogen-halogen reactions. It is generally accepted that one must postulate an atomic mechanism for the reaction between molecular hydrogen and molecular chlorine or bromine, i.e., a chain mechanism where

$$Cl_2 \rightarrow 2\,Cl$$
$$Cl + H_2 \rightarrow HCl + H$$

in order to explain the experimental rate data. On the other hand, the rate data for the hydrogen-iodine reaction has led to acceptance of the following bimolecular mechanism:

$$\begin{array}{c} \text{H}-\text{H} \\ \text{H}_2+\text{I}_2 \rightarrow \vert \quad \vert \rightarrow 2\,\text{HI}. \\ \text{I}-\text{I} \end{array}$$

This difference can now be interpreted in the following manner. Since Cl_2 and Br_2 are relatively light molecules for which Russell-Saunders coupling between orbit and spin is a better approximation, the singlet-triplet transitions are not allowed and thus the bimolecular mechanism would need to proceed along the singlet surface which would require considerably more activation energy than that required to dissociate the Cl_2 or Br_2 molecule. On the other hand, the H_2+I_2 reaction can proceed by way of the triplet ambivalent complex, as iodine is sufficiently heavy that the triplet-singlet transition is no longer forbidden. In this case spin-orbit interaction would have to be considered. Teller has shown that a minimum of three independent parameters must be varied in this case to bring about the necessary orbital degeneracy. However, there are three independent parameters in this case, the H—H distance, the I—I distance, and the H—I distance. This suggestion is based on the results of the calculations of the hydrogen model which is a very crude approximation to this case, but an attempt is now being made to test this explanation by applying the methods outlined in this paper to a more realistic model.

CONCLUSIONS

From the results discussed in this paper and presented in the following papers one can make the following conclusions:

The single-determinant molecular orbital method can be used as a basis for constructing correlation diagrams between the molecular orbitals of reactants and products with a state defined as the ambivalent complex, the orbitals of which can be determined by the same method as an intermediate. From a consideration of the symmetry properties of the molecular orbitals and the symmetry properties of the ground electronic states of the molecules and a few selected ambivalent complexes, considerable insight into the nature of the activation process is obtained. The interaction of the low-lying excited electronic states of the separated molecules seem to be of importance in determining the activation energy of a chemical reaction.

Even though the LCAO molecule orbital method converges upon dissociation to excited electronic states of atoms, this difficulty is minimized in calculating activation energies for closed-shell molecules because one can take the difference between two LCAO-molecular orbital calculations, i.e., the one for the reactant molecules and the one for the ambivalent complex. In each case the internuclear parameters are of the same order as interatomic distances in molecules. In this study it has been further assumed that activation processes can be considered as two, three, and four electron problems; this is based on the assumption that inner-shell interactions can be neglected. This assumption needs to be investigated and will be considered later. However, this assumption will only affect the numerical results obtained in this study, but in no way affects the general picture of the relative activation energies required for the interaction between two closed-shell molecules (4 electrons), the interaction between a molecule and a radical (3 electrons), and the the interaction between two radicals (2 electrons). That is, in the case of molecules, two electrons are placed in a bonding ambivalent complex orbital which can compensate for the additional nuclear repulsions that become important as the two molecules approach, and two electrons are placed in an antibonding ambivalent complex orbital. For the case of a molecule and a radical, only one electron needs to be placed in the antibonding ambivalent complex orbital. Finally, in considering interaction between two radicals, the two electrons can both go into the lowest bonding complex orbital and the excited states do not need to be mixed in. These conclusions, however, are dependent on the assumption that eigenfunctions having the correct symmetry properties are obtained when one replaces the $3N$-dimensional Schroedinger equations by N 3-dimensional equations of the Hartree-Fock type.

In addition, a plausible explanation is suggested to explain the differences observed in the experimental study of the H_2+Cl_2 and the H_2+I_2 reactions.

Studies of the Interaction between Stable Molecules and Atoms. II. Interaction between Two He Atoms*

VIRGINIA GRIFFING AND J. F. WEHNER
Department of Chemistry, The Catholic University of America, Washington, D. C.

(Received June 22, 1954)

The repulsive energy of two helium atoms has been calculated using molecular orbital theory. The equations of Roothaan were used to break down the energy into integrals involving atomic orbitals. The necessary integrals are tabulated in the literature for a wide range of parameter which enabled the potential energy curve to be calculated from $R=0.6$ to 7.0 a_0. The Slater $(1s)$ orbital with effective nuclear charge $Z=27/16$ was used. The potential curve is lower at all distances from those of other investigators in the range where Van der Waals forces give attraction although the curves agree at closer distances. Ionization energies have been calculated over these distances and extrapolated to infinity to give a value which is much better than that calculated with the same orbital by ordinary means. The addition of $2p\sigma$ character to the molecular orbitals by constructing hybrid orbitals of the type $N\{(1s)+\lambda(2p\sigma)\}$ and the determination of λ by a SCF calculation according to the scheme of Roothaan, gives an attractive energy of 2.14×10^{-5} a.u. with $\lambda=1.4\times10^{-3}$ at $R=3.11$ A. Experimental values are approximately 3×10^{-5} a.u. The calculated results are compared with experimental data in the exchange and Van der Waals region of the values of the internuclear parameter.

A STUDY of diatomic helium was undertaken in order to test the usefulness of the molecular orbital method in calculating the interaction energy between two closed-shell systems. He_2 is not only a closed-shell system but made up of two rare-gas atoms and thus the molecular orbital description should converge to the correct values at large distance. Thus this seemed to be an ideal system for calculating interaction energies over a wide range of internuclear parameters by a single method.

The system can be considered as consisting of doubly charged helium nuclei a and b separated by a distance R with four electrons; each moving in the field of the nuclei and the average field of the other electrons. The assumption is made that the molecular orbitals can be formed as independent linear combinations of atomic orbitals.[1] The total wave function is then assumed to be an antisymmetrized product of orthonormal molecular spin orbitals (MSO). A MSO is a product of the MO with the usual spin eigenfunction.

The AO's used in this calculation were simple Slater-type $1s$-functions (hydrogen functions)

$$\chi_a=\left(\frac{Z^3}{\pi}\right)^{\frac{1}{2}}e^{-Zr_a},$$

where Z, the effective nuclear charge, is 27/16 according to a variational calculation on the atom,[2] and r_a is the distance of the electron from nucleus a.

The only possible linear combinations of the AO's are:

$$\varphi_1=N_1(\chi_a+\chi_b);\quad \sigma_g,$$

$$\varphi_2=N_2(\chi_a-\chi_b);\quad \sigma_u,$$

where

$$N_1=(2+2S_{ab})^{-\frac{1}{2}},\quad N_2=(2-2S_{ab})^{-\frac{1}{2}},\quad S_{ab}=\int\chi_a\chi_b d\tau.$$

These orbitals are very similar to the molecular orbitals used in the ground-state calculation of H_2, differing only in the fact that an effective nuclear charge is used instead of the actual nuclear charge. A good description of the properties of these orbitals is given by Slater.[3]

The molecular wave function is thus:

$$\psi=\frac{1}{(24)^{\frac{1}{2}}}\sum_\lambda(-1)^\lambda P_\lambda[(\varphi_1\alpha)^1(\varphi_1\beta)^2(\varphi_2\alpha)^3(\varphi_2\beta)^4],\quad(1)$$

where P_λ is the operation permuting the superscripts which denote electrons, and α and β are the usual orthonormal spin eigenfunctions. The available orbitals are thus filled and any configuration interaction would have to involve excited states, which lie much higher. Therefore this form of ψ should be applicable even at large distances. This behavior is different from that of H_2,

TABLE I. Interatomic potential for He_2.

R(A)	LCAO (27.2 ev)	R(A)	Slater	Rosen
0.3136	4.2909	0.311	4.220	5.389
0.4704	1.9053	0.467	2.065	2.717
0.6272	0.9137	0.622	1.022	1.360
0.9408	0.2283	0.850	0.358	0.489
1.2544	0.05790	1.245	0.0573	0.0882
1.5680	0.014174	1.560	0.0136	0.0221
1.8816	0.0031120	1.866	0.00332	0.00577
2.1952	0.000733	2.178	0.000783	0.00147
2.5088	0.000156	2.489	0.0001871	0.000371
3.136	0.00000293	3.110	0.00001162	0.0000242
3.763	0.00000025	3.75	0.000000566	0.000001441
∞	0	∞	0	0

* This work was supported by Contract Nonr-1220(00).

[1] C. C. J. Roothaan, Revs. Modern Phys. **23**, 69 (1951).

[2] Eyring, Walter, and Kimball, *Quantum Chemistry* (John Wiley and Sons Inc., New York, 1944) or any elementary text on quantum mechanics.

[3] J. C. Slater, Technical Report No. 3, Solid-State and Molecular Theory Group, Massachusetts Institute of Technology.

where φ_2 is not filled at small distance, but configurations containing φ_2 become important for large distances.

The operator for this problem is

$$H=\sum_{\mu=1}^{4} H^{\mu}+\sum_{\mu>\nu=1}^{4}\frac{1}{r^{\mu\nu}}+\frac{4}{R},$$

where

$$H^{\mu}=-\tfrac{1}{2}\nabla_{\mu}^{2}-\frac{2}{r_{a\mu}}-\frac{2}{r_{b\mu}}.$$

According to Roothaan,[1] the total energy for the system is

$$E=\int\psi H\psi d\tau$$
$$=2H_1+2H_2+J_{11}+4J_{12}+J_{22}-2K_{12}+4/R, \quad (2)$$

where

$$H_i=\int\varphi_i^{\mu}H^{\mu}\varphi_i^{\mu}d\tau^{\mu}$$

$$J_{ij}=\int\varphi_i^{\mu}\varphi_j^{\nu}\frac{1}{r^{\mu\nu}}\varphi_i^{\mu}\varphi_j^{\nu}d\tau^{\mu\nu}$$

$$K_{ij}=\int\varphi_i^{\mu}\varphi_j^{\nu}\frac{1}{r^{\mu\nu}}\varphi_j^{\mu}\varphi_i^{\nu}d\tau^{\mu\nu}.$$

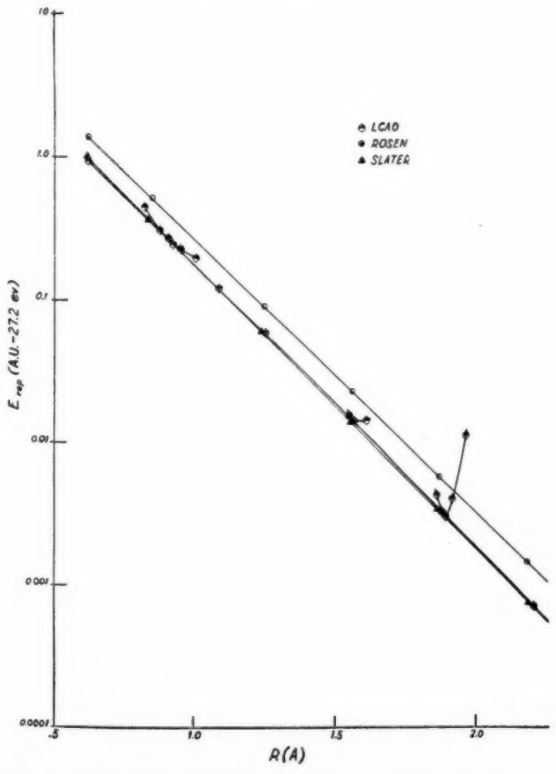

FIG. 1. A semilogarithmic plot of the repulsive energy of two helium atoms as calculated by the LCAO method, Slater (reference 4), and Rosen (reference 5) for the range 0.5 to 2.25 A. The parabola-like curves which are approximately tangent to the LCAO curve are the result of a variation of Z for constant $\rho=ZR$. They show that the value of Z giving a minimum for isolated atoms is good enough for all distances.

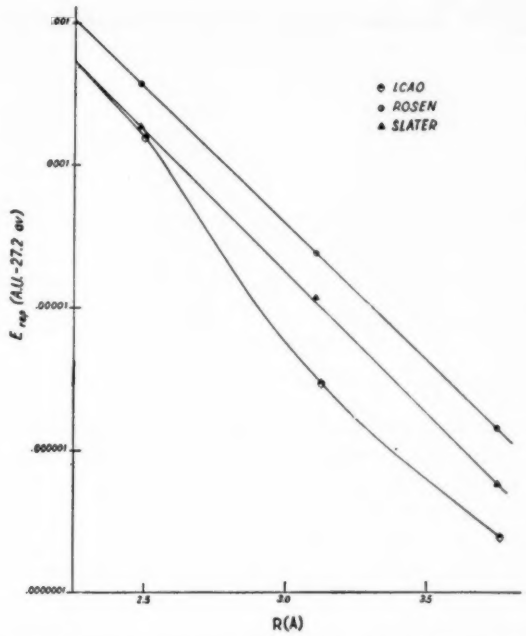

FIG. 2. A semilogarithmic plot of the repulsive energy of two helium atoms as calculated by the LCAO method, Slater (reference 4), and Rosen (reference 5) for the range 2.25 to 3.75 A which includes the Van der Waals region.

The internuclear separation in Bohr radii (0.5292 A) is R and the unit of energy is the Hartree (27.204 ev). The integrals are function of R. (For a breakdown into basic orbitals see the appendix.) The interatomic potential energy is defined as the total energy E (Eq. 2) minus the energy of 2 He atoms calculated using the same atomic orbitals. The interatomic potential is given in Table I and plotted in Figs. 1 and 2.

The results agree closely with previous calculations done by the Heitler-London[4] and the bond eigenfunction method,[5] except in the neighborhood of the Van der Waals minimum, where the MO method gives a lower energy. The calculation is much less complicated by the MO method than by the other methods.

The results of other investigations were expressed in an analytical form, and the actual calculations may have agreed with ours even in the Van der Waals region.

Seitz[6] has shown that the determinantal wave function of the MO calculation may be obtained from the wave function of the Heitler-London calculation by adding and subtracting certain rows or columns provided of course that the same analytical form of the orbitals are used. In a paper pointing out the proper expression to use for the interaction energy in a Heitler-London calculation, Margenau and Rosen[7] have calculated this energy using the same orbitals as in this calculation for several parameters and these points lie on our curve.

[4] J. C. Slater, Phys. Rev. **32**, 349 (1928).
[5] P. Rosen, J. Chem. Phys. **18**, 1182 (1950).
[6] F. Seitz, *Modern Theory of Solids* (McGraw-Hill Book Company, Inc., New York, 1940).
[7] H. Margenau and P. Rosen, J. Chem. Phys. **21**, 394 (1953).

TABLE II. Ionization energies and potential energy of He_2^+.

R(A)	ϵ_1	ϵ_2	$V_{He_2^+}$
0.3136	−1.8468	0.5221812	2.8722
0.6272	−1.3714	−0.300953	0.3182
0.9408	−1.1293	−0.620545	−0.0477
1.0976	−1.06527	−0.7127023	−0.0707
1.2544	−1.016693	−0.7654065	−0.0732
1.56799	−0.9549542	−0.8339992	−0.048311
1.8816	−0.9228665	−0.8684849	−0.024888
2.1952	−0.9089955	−0.8834904	−0.012261
2.5088	−0.90218893	−0.8906695	−0.0056589
3.136	−0.8975947	−0.8953658	−0.0011157
3.763	−0.8966890	−0.8962797	−0.0002044
∞	−0.8964844		0

An attempt was made to improve the calculation by minimizing the energy with respect to the effective nuclear charge for each distance. The energy expression may be written as a function of Z and $\rho=ZR$ which consists of a sum of complicated functions of ρ, each multiplied by either Z or Z^2 so that ρ may be held constant and Z varied. If the results are plotted against R (see Fig. 1) a parabola-like curve is obtained for each ρ and the best energy curve is the envelope of these curves. The envelope curve is almost coincident with the curve determined with $Z=27/16$, so that the variation of effective nuclear charge is unimportant in the He_2 problem from the viewpoint of decreasing the energy.

The ionization energy of each of the molecular orbitals was calculated using Roothaan's scheme. There is no variation of coefficients necessary as the coefficients were completely determined by the orthonormality conditions. The MO's are redefined as $\varphi_i=a_{ia}\chi_a+a_{ib}\chi_b$: where a_{in} is either $\pm N_i$ as previously defined.

Thus the ionization energies ϵ_i are the roots of the determinantal equation

$$|H+G-\epsilon S|=0,$$

where H, G, and S are matrices of order 2 having elements defined by

$$H_{pq}=\int \chi_p^{\mu} H^{\mu} \chi_q^{\mu} d\tau^{\mu}; \quad S_{pq}=\int \chi_p^{\mu}\chi_q^{\mu} d\tau^{\mu},$$

$$G_{pq}=\sum_i \sum_{r,t} a_{ip}[2(pq:rt)-(pt:rq)]a_{iq} \text{ (see appendix)}$$

$$(pq:rt)=\int \chi_p^{\mu}\chi_r^{\nu}\frac{1}{r^{\mu\nu}}\chi_q^{\mu}\chi_t^{\nu} d\tau^{\mu\nu}.$$

The expression for ϵ_i is very simple in this case,

$$\epsilon_1,\epsilon_2=\frac{(H_{11}+G_{11})\pm(H_{12}+G_{12})}{1\pm S_{12}}.$$

The values of ϵ_i are plotted as a function of R (Fig. 3) and it is seen that by letting $R\to\infty$ (where all two center integrals are zero) that $\epsilon_1=\epsilon_2=H_{11}(\infty)+G_{11}(\infty)$ $=24.39$ ev, an error of 0.19 ev from the experimental value. This method gives a better result than the value 23.05 calculated by subtracting the energy of an He^+ ion from the total energy of He calculated with this same AO[2].

In Fig. 4, the repulsive energy calculated by the LCAO method is compared with the experimental results of Amdur.[8] Amdur's results are plotted from the following expressions given by Amdur:

$$V(R)=\frac{4.62\times10^{-12}}{R^{1.79}} \text{ ergs} \quad 0.52<R<1.02 \text{ A},$$

and

$$V(R)=\frac{7.55\times10^{-12}}{R^{5.94}} \text{ ergs} \quad 1.27<R<1.59 \text{ A}$$

(1 a.u. (i.e., 27.204 ev) $=4.355\times10^{-12}$ ergs).

In Fig. 5 the dotted curves are the experimental curves given by Hirschfelder *et al.*[9] The full line curves are the calculated curves plus a c/r^6 term for different values of c. For $c=1.39$ and our interaction potential, the curve falls much too low; $c=1.041$ gives the best fit. This calculation thus also presents a method for calculating the potential energy curve of He_2. If one

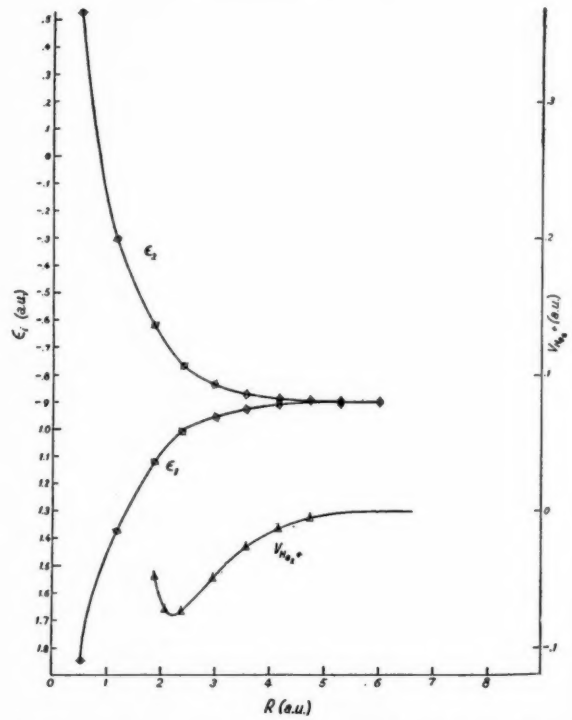

FIG. 3. ϵ_1 and ϵ_2 are the ionization energies of the bonding and antibonding orbitals respectively as a function of distance and $V_{He_2^+}$ is the potential-energy curve for the helium-molecule ion as calculated by the LCAO method.

[8] I. Amdur, J. Chem. Phys. **17**, 190 (1948); I. Amdur and A. L. Harkness, J. Chem. Phys. **22**, 664 (1954).

[9] Hirschfelder, Curtiss, Bird, and Spotz, *The Properties of Gases* (University of Wisconsin Press, Madison, Wisconsin, 1952), Chap. 14.

considers that in He_2, two electrons are in the lowest MO of He_2 and that the third electron is in the second orbital, it can be shown[1] that the total energy calculated by taking an antisymmetrized product of these orbitals is equal to the total energy of He_2 minus the ionization energy of the second orbital. The potential energy determined by this method is given in Table II and plotted in Fig. 2. The $V_{He_2^+}$ form was obtained by subtracting ϵ_2 from the LCAO interactomic potential and adding $\epsilon_2(\infty)$ to give a He atom and a He^+ ion as the zero of energy. The minimum is approximately 2.07 ev at an internuclear distance of 1.20 A, which is only slightly less accurate than the calculation of Weinbaum[10] and Pauling,[11] in which they used the Heitler-London method and minimized with respect to the effective nuclear charge, which was not done here. The spectroscopic value as reported in Weinbaum's paper is 2.5 ev at 1.09 A.

Since the spherically symmetrical 1*s*-functions do not have any flexibility which would permit the inclusion of polarization along the internuclear axis it is not surprising that this simple MO calculation failed to give

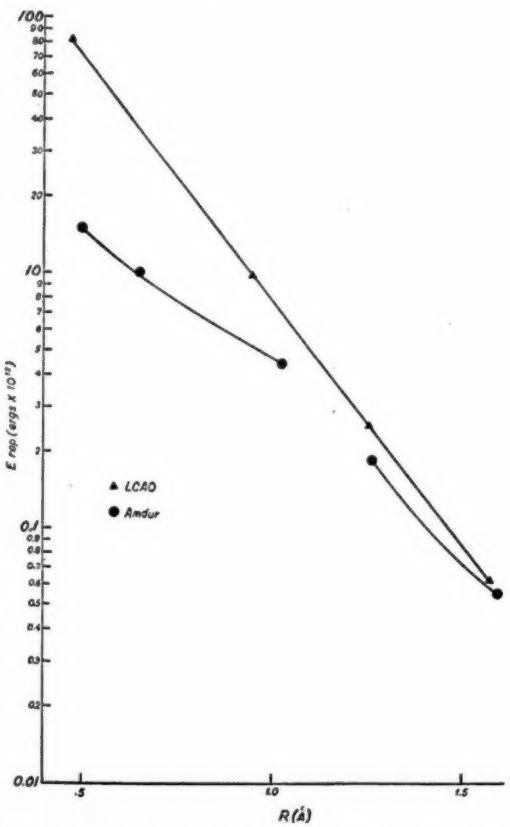

FIG. 4. A semilog plot of the repulsive energy *versus* internuclear distance as calculated by the LCAO method and the experimental results of Amdur (reference 8) for the range $R=0.47$ to 1.5 A. The results of Amdur are expressed as

$4.62\times10^{-12}/R^{1.79}$ ergs $\quad 0.52<R<1.02$ A
$7.55\times10^{-12}/R^{5.94}$ ergs $\quad 1.27<R<1.59$ A.

[10] S. Weinbaum, J. Chem. Phys. **3**, 547 (1935).
[11] L. Pauling, J. Chem. Phys. **1**, 56 (1933).

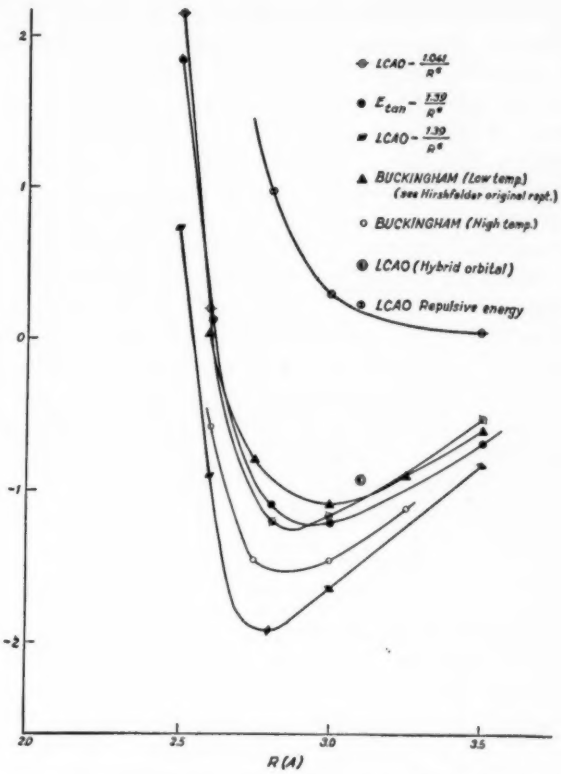

FIG. 5. The He—He interaction energy is plotted as a function of distance in the Van der Waals region. Various Van der Waals potentials have been added to the calculated curves for the interaction energy and the results are compared with experimental curves.

the Van der Waals attractive energy. It was decided to distort the spherical 1*s*-charge distribution by adding some *p*-character to the orbitals in an attempt to improve the calculation.

Consider the four orbitals, $1s_a$, $1s_b$, $2pz_a$, $2pz_b$ where z is along the internuclear axis. Call them χ_1, χ_2, χ_3, χ_4 respectively. The matrix

$$\mathbf{U}=\frac{1}{\sqrt{2}}\begin{pmatrix}1 & 1 & 0 & 0\\ 0 & 0 & 1 & 1\\ 1 & -1 & 0 & 0\\ 0 & 0 & 1 & -1\end{pmatrix}$$

will transform the vector of the orbitals (χ) into four symmetry orbitals

$$\sigma_1=\frac{1}{\sqrt{2}}(\chi_1+\chi_2),\quad \sigma_2=\frac{1}{\sqrt{2}}(\chi_3+\chi_4)$$

$$\sigma_3=\frac{1}{\sqrt{2}}(\chi_1-\chi_2),\quad \sigma_4=\frac{1}{\sqrt{2}}(\chi_3-\chi_4).$$

These symmetry orbitals can be used to form the two molecular orbitals

$$\varphi_1=N_1(\sigma_1+\lambda_1\sigma_2);\quad \varphi_2=N_2(\sigma_3+\lambda_2\sigma_4)$$

which have the same symmetry as the initial MO's σ_g and σ_u. The constants λ_1 and λ_2 must be determined by variation, keeping the MO's orthonormal. This can be done conveniently in the self-consistent field procedure of Roothaan using a single-determinantal wave function. The (4×4) matrices **H**, **G**, and **S** are set up, using assumed values of λ_1 and λ_2 to calculate **G**. They are put into block form by unitary transformation with the matrix **U** and the two resulting (2×2) determinants are solved by the quadratic formula, each giving a low-energy orbital and an excited orbital. A calculation attempting to add $2p$ character to the atomic orbitals of the isolated atom in a similar fashion gives a minimum energy for $\lambda=0$, so that a finite value of λ_1 and λ_2 at finite distances seems to be the result of the polarization of the atoms.

The $2pz$ orbital used was

$$2pz_a=\left(\frac{Z^5}{\pi}\right)^{\frac{1}{2}} r_a \cos\theta_a e^{-Zr_a},$$

where the same Z was used as in the $1s$-orbital to simplify the integrals. The calculation was done at 3.110 A which is near the minimum on the Van der Waals energy curve. An attractive energy of 2.14×10^{-5} a.u. with $\lambda_1=-\lambda_2=1.4\times10^{-3}$ was obtained. The experimental values are approximately 3.4×10^{-5} a.u.[9]

CONCLUSION

With comparatively little calculation, the LCAO–SCF MO method yields a good potential energy curve for the interaction between two He atoms. The same calculation also gives the vertical ionization energies ϵ_1 and ϵ_2 for a single electron from each of the MO's making it possible to calculate the first ionization energy for the He atoms as that limiting value to which the ϵ_1 and ϵ_2 converge as the internuclear distance goes to infinity. This method gives a value of 24.39 ev compared with 24.58 from experiment. In addition, the value of ϵ_2 as a function of distance can be subtracted from the potential energy curve for He_2 yielding the potential energy curve for He_2^+ from the same calculation.

In addition, it was shown by mixing in some $2p$ character that one could obtain an attractive energy about two-thirds the experimental attractive energy at Van der Waals distances. This could perhaps be improved by varying the screening constant in the p-orbital.

The molecular orbital method has thus been shown to yield much information from comparatively simple calculations for a rare-gas system.

APPENDIX

Expressions for the internuclear potential:

$$H_1=2N_1^2\left[\int \chi_a^\mu H^\mu \chi_a^\mu d\tau^\mu+\int \chi_a^\mu H^\mu \chi_b^\mu d\tau^\mu\right]$$

$$H_2=2N_2^2\left[\int \chi_a^\mu H^\mu \chi_a^\mu d\tau^\mu-\int \chi_a^\mu H^\mu \chi_b^\mu d\tau^\mu\right]$$

$$J_{11}=N_1^4[2(aa:aa)+8(aa:ab)+4(ab:ab)+2(aa:bb)]$$

$$J_{12}=N_1^2N_2^2[2(aa:aa)+2(aa:bb)-4(ab:ab)]$$

$$J_{22}=N_2^4[2(aa:aa)-8(aa:ab)+4(ab:ab)+2(aa:bb)]$$

$$K_{12}=N_1^2N_2^2[2(aa:aa)-2(aa:bb)].$$

For the ionization energy:

$$a_{1a}=a_{1b};\quad a_{2a}=-a_{2b}$$

$$G_{11}=G_{22}=(a_{1a}^2+a_{2a}^2)[(aa:aa)+2(aa:bb)-(ab:ab)]+2(a_{1a}^2-a_{2a}^2)(aa:ab)$$

$$G_{12}=G_{21}=2(a_{1a}^2+a_{2a}^2)(aa:ab)+(a_{1a}^2-a_{2a}^2)[3(ab:ab)-(aa:bb)].$$

These integrals may be found in the literature for the necessary parameters.[12]

[12] J. O. Hirschfelder and J. W. Linnett, J. Chem. Phys. **18**, 130 (1950).

Studies of the Interaction between Stable Molecules and Atoms. III. A Molecular Orbital Treatment of the Quadratic Form of H_4

VIRGINIA GRIFFING AND ANDREJ MAČEK
Department of Chemistry, Catholic University of America, Washington, D. C.
(Received June 22, 1954)

Molecular orbital calculations of the quadratic arrangement of four hydrogen atoms have been carried out as a function of the internuclear distance. It is shown that the complex has orbital degeneracy in the ground state. An approximation, which includes the lowest orbital and the degenerate orbitals only, yields a triplet and three singlet states, the triplet being the lowest one in accordance with Hund's rule. The actual calculations show that the quadratic H_4 is unstable with respect to a totally symmetrical displacement at all points of the potential energy surface.

1. INTRODUCTION

THIS is the third in a series of papers in which three- and four-electron problems are considered with a view toward gaining an understanding of the interactions between atoms and molecules. The transition state of the bimolecular H_2+H_2 exchange reaction consists of four electrons moving in the field of a geometrically symmetric arrangement of four protons. The problem of interaction of four hydrogen atoms at short distances was treated first by Eyring[1] for various nuclear arrangements; and more recently by Taylor[2] for a linear form.

Eyring's calculations are semiempirical. This means that, in addition to working with the approximate London formula, one obtains the exchange energy contributions as the difference between the experimental total energy (from spectra) and the calculated Coulombic energy; furthermore, the ratio of Coulombic energy to exchange energy is assumed to be constant for all internuclear distances. Eyring found that by varying this ratio through a reasonable range, the calculated value of the energy for the quadratic H_4 complex can be made to fall very near the experimental activation energy of the reaction (around 60 kcal). Thus he inferred that the activated complex consists of four protons placed in four corners of a square, the side of which is 1.20 A. Critical discussions of Eyring's method are found in the literature.[3] Taylor, on the other hand, took the problem *ab initio* using the MO method. His interest was in developing a model for solids. The calculation shows that the energy of the linear H_4—the distances between adjacent atoms being equal to the equilibrium distance of the hydrogen molecule—is between that of four separated hydrogen atoms and that of two separated hydrogen molecules. When configurational interaction between neighboring states is included, the energy of the system is computed and is 4 ev above the energy of two hydrogen molecules calculated by the same method.

[1] H. Eyring, J. Am. Chem. Soc. **53**, 2537 (1931).
[2] R. Taylor, Proc. Phys. Soc. (London) **64A**, 249 (1951).
[3] A. S. Coolidge and H. M. James, J. Chem. Phys. **2**, 811 (1934); and J. O. Hirschfelder, J. Chem. Phys. **9**, 645 (1941).

1. MO DESCRIPTION OF QUADRATIC H_4

Molecular orbitals will be formed as linear combinations of hydrogenic 1*s*-orbitals. Denoting the four nuclei by *a*, *b*, *c*, and *d*, one can write the *i*th MO:

$$\varphi_i=\sum_p \chi_p c_{pi}. \tag{1}$$

Here $\sum_p$ indicates summation over the nuclei, and the χ_p are:

$$\chi_p=\frac{1}{\sqrt{\pi}}e^{-\mu_p}.$$

The total 4-electron wave function $\bar{\psi}$ will then be an antisymmetrized product[4] of the MO, and the total energy of any one electronic configuration will be given by

$$E=\int\bar{\psi}\mathcal{H}\psi d\tau.$$

Complex conjugates are denoted by barred quantities.

Let us consider first a rectangular nuclear configuration of two interacting hydrogen molecules

$$\begin{array}{ccc} \circ H_d & & \circ H_a \\ | & & | \\ \circ H_c & & \circ H_b \end{array}.$$

During the exchange reaction, which can be written

$$H_aH_b+H_cH_d\rightarrow H_aH_d+H_bH_c,$$

we expect the distances *ab* and *cd* to increase as *ad* and *bc* decrease, until all the four distances become equal; this then will be the "activated complex." According to (1) the four MO's of the rectangular system are:

$$\varphi_1'=c_1'(\chi_a+\chi_b+\chi_c+\chi_d) \quad \text{of symmetry } a_g$$
$$\varphi_2'=c_2'(\chi_a+\chi_b-\chi_c-\chi_d) \quad \text{of symmetry } b_{2u}$$
$$\varphi_3'=c_3'(\chi_a-\chi_b-\chi_c+\chi_d) \quad \text{of symmetry } b_{3u}$$
$$\varphi_4'=c_4'(\chi_a-\chi_b+\chi_c-\chi_d) \quad \text{of symmetry } b_{1g}.$$

The types of symmetry of the φ_i are given by repre-

[4] M. Goeppert-Mayer and A. L. Sklar, J. Chem. Phys. **6**, 645 (1938).

sentations[5] of the symmetry group D_{2h}. All the coefficients c_i corresponding to the ith MO are numerically equal, since we are using only one kind of AO. The formation of the MO can be interpreted as follows:

A molecular orbital of symmetry a_g arises out of the MO of two molecules H_aH_b and H_cH_d, both in their bonding states, when these come together to form a nodeless state. The orbital energy ϵ_1 corresponding to φ_1' must be expected to be the lowest one.

A molecular orbital of symmetry b_{2u} arises out of the MO of H_aH_b and H_cH_d, both in bonding states, when these come together in such a way as to form a nodal plane between them. The orbital energy corresponding to φ_2' is ϵ_2.

A molecular orbital of symmetry b_{3u} arises out of the MO of H_aH_b and H_cH_d, both in antibonding states, when these come together without formation of additional nodal planes. The corresponding orbital energy ϵ_3 will in general be different from ϵ_2.

A molecular orbital of symmetry b_{1g} arises out of the MO of H_aH_b and H_cH_d, both in antibonding states, when these come together with the formation of a nodal plane between them. We should expect φ_4' to have the highest orbital energy.

Now it is clear that as a symmetric transition state is formed, the rectangular nuclear configuration becomes a quadratic one, and φ_2' and φ_3' become degenerate. The two representations b_{2u} and b_{3u} of the symmetry group D_{2h} merge into the degenerate representation e_u of the symmetry D_{4h}.[5] The four MO's of the quadratic system are:

$$\left.\begin{aligned}
&\varphi_1=c_1(\chi_a+\chi_b+\chi_c+\chi_d) && \text{of symmetry } a_{1g};\\
&\varphi_2=c_2(\chi_a-\chi_c)\\
&\varphi_3=c_3(\chi_b-\chi_d)\end{aligned}\right\} \quad \text{of symmetry } e_u; \qquad (2)$$
$$\varphi_4=c_4(\chi_a-\chi_b+\chi_c-\chi_d) \quad \text{of symmetry } b_{1g}.$$

2. FIRST APPROXIMATION. SINGLE DETERMINANT WAVE FUNCTION WITH PAIRED ELECTRONS IN ONE OF THE ORBITALLY DEGENERATE ORBITALS

There are two degenerate electronic configurations in which four electrons are paired in the two lowest orbitals, i.e., φ_1 and φ_2 or φ_3. These configurations belong to the E_u[6] irreducible representation of the symmetry group D_{4h}. Since the electrons are paired in both φ_1 and φ_2 or φ_3, the complex can be treated by Roothaan's matrix method.[7] To this end the AO and the MO are written as row vectors connected by the matrix of coefficients Cpi of formula (1):

$$(\boldsymbol{\varphi})=(\boldsymbol{\chi})(\mathbf{C}). \qquad (1')$$

(**C**) is an $n\times m$ matrix, where n is the AO number and m the MO number. Dividing, as usual, the total electronic Hamiltonian operator into a one-electron and a two-electron part,

$$\mathfrak{H}=\sum_\mu H^\mu+\tfrac{1}{2}\sum_{\mu\neq\nu}\frac{1}{r^{\mu\nu}}, \qquad (2')$$

the MO energies, ϵ_i, are obtained from the matrix equation,[7]

$$(\mathbf{H}+\mathbf{G})\mathbf{c}_i=\epsilon_i(\mathbf{S})\mathbf{c}_i. \qquad (3)$$

Elements of (**H**) are one-electron nuclear field integrals defined in terms of AO:

$$H_{pq}=\int\bar{\chi}_p{}^\mu H^\mu\chi_q{}^\mu d\tau^\mu. \qquad (4)$$

Elements of (**G**) are two-electron integrals:

$$G_{pq}=\sum_i\sum_{rt}\bar{c}_{ri}G_{prqt}c_{ti}, \qquad (5)$$

where i indicates the summation over the filled MO. The terms of (5) are $G_{prqt}=2J_{prqt}-J_{prtq}$, where

$$J_{prqt}=\int\bar{\chi}^\mu\bar{\chi}^\nu\frac{1}{r^{\mu\nu}}\chi_q{}^\mu\chi_t{}^\nu d\tau^\mu d\tau^\nu. \qquad (6)$$

The elements G_{pq} can be collected conveniently by a method especially developed to handle systems involving many particles.[8]

(**S**) is the matrix of overlap integrals:

$$S_{pq}=\int\bar{\chi}_p{}^\mu\chi_q{}^\mu d\tau^\mu. \qquad (7)$$

The problem of varying the coefficients c_{ai} of Eq. (1) (or c_i of Eq. (2) simultaneously to attain self-consistency does not arise here, since they are determined uniquely by the conditions of orthonormality of the MO:

$$\sum_{pq}\bar{c}_{pi}S_{pq}c_{qj}=\delta_{ij}. \qquad (8)$$

The problem is now reduced to evaluation of overlap, one-electron and two-electron integrals. This is discussed in Appendix I. According to (3), orbital energies ϵ_i and coefficients are obtained from the determinantal equation:

$$\mathrm{Det}[(\mathbf{H}+\mathbf{G})-\epsilon(\mathbf{S})]=0. \qquad (3')$$

Solution of this fourth-degree equation can be simplified if matrix elements of (**S**), (**H**), and (**G**) are expressed in terms of symmetry orbital integrals. Due to geometric symmetry, any matrix (**M**) of a rectangular nuclear configuration of the system (involving one kind of atomic orbital only) will consist of four elements recurring symmetrically:

$$(\mathbf{M})=\begin{array}{c|cccc} & a & b & c & d\\ a & M_p & M_q & M_r & M_q\\ b & M_q & M_p & M_q & M_s\\ c & M_r & M_q & M_p & M_q\\ d & M_q & M_s & M_q & M_p\end{array}$$

[5] See, for instance, G. Herzberg, *Infra-Red and Raman Spectra* (D. Van Nostrand Company, Inc., New York, 1946), Chap. 2.

[6] Configuration interaction (resulting from the quadratic potential field of the nuclei) will split these configurations into two nondegenerate states of the complex. In order to get good numerical values this will need to be taken into account and will be discussed later.

[7] C. C. J. Roothaan, Revs. Modern Phys. **23**, 69 (1951).

[8] P. F. Wacker, thesis, The Catholic University of America, 1954. For a discussion see Appendix IIa.

We now define an orthogonal matrix (**U**) which transforms the four AO into four symmetry orbitals σ_i, given by four types of symmetry of (2):

$$(\sigma)=(\chi)(\mathbf{U})=(\chi_a\chi_b\chi_c\chi_d)=\begin{pmatrix} \frac{1}{2} & \frac{1}{2} & \frac{1}{\sqrt{2}} & 0 \\ \frac{1}{2} & -\frac{1}{2} & 0 & \frac{1}{\sqrt{2}} \\ \frac{1}{2} & \frac{1}{2} & -\frac{1}{\sqrt{2}} & 0 \\ \frac{1}{2} & -\frac{1}{2} & 0 & -\frac{1}{\sqrt{2}} \end{pmatrix}. \tag{9}$$

The matrix (**M**) when transformed by (**U**) is reduced to the form:

$$(\mathbf{M}^\sigma)=(\mathbf{U})^*(\mathbf{M})(\mathbf{U})=\begin{pmatrix} M_p+2M_q+\frac{1}{2}(M_r+M_t) & \frac{1}{2}(M_r-M_t) & 0 & 0 \\ \frac{1}{2}(M_r-M_t) & M_p-2M_q+\frac{1}{2}(M_r+M_t) & 0 & 0 \\ 0 & 0 & (M_p-M_r) & 0 \\ 0 & 0 & 0 & (M_p-M_t) \end{pmatrix}. \tag{10}$$

The matrices ($\mathbf{S}^\sigma$), ($\mathbf{H}^\sigma$), and ($\mathbf{G}^\sigma$) being reduced, Eq. (3′) can be solved very quickly and without recourse to mechanical equation solvers. In order to calculate the total energy E, one does not need to calculate the ϵ_i, but only the molecular orbitals. However, this matrix formulation is a convenient one to use, and these orbital energies may be of significance in certain problems.

The total electronic energy of the system is given by the sum of all one-electron and all two-electron integrals defined in terms of $2m$ molecular spin-orbitals ψ_i[9]

$$E=\sum_i H_i^\psi+\tfrac{1}{2}\sum_{ij}(J_{ij}^\psi-K_{ij}^\psi), \tag{11}$$

where

$$H_i^\psi=\int\bar{\psi}_i^\mu H^\mu\psi_i^\mu d\tau^\mu,$$

$$J_{ij}^\psi=\int\bar{\psi}_i^\mu\bar{\psi}_j^\nu\frac{1}{r^{\mu\nu}}\psi_i^\mu\psi_j^\nu d\tau^\mu d\tau^\nu,$$

$$K_{ij}^\psi=\int\bar{\psi}_i^\mu\bar{\psi}_j^\nu\frac{1}{r^{\mu\nu}}\psi_i^\nu\psi_j^\mu d\tau^\mu d\tau^\nu. \tag{12}$$

It can be shown easily that when all the electrons are paired in m molecular orbitals φ_i, (11) becomes

$$E'=2\sum_i H_i^\varphi+\sum_{ij}(2J_{ij}^\varphi-K_{ij}^\varphi). \tag{11′}$$

MO integrals defined by (12) are combinations of AO integrals defined by Eqs. (4), (5), and (6). Contributions to the total electronic energy were collected in Wacker's[8] notation discussed in Appendix IIb. MO coefficients c of Eq. (2), orbital energies ϵ_i for orbitals φ_1 and φ_2, and the total electronic energy E' of the paired electron configuration are given in Table I. The same results, of course, are obtained when φ_3 is substituted for φ_2, because the two configurations $\begin{pmatrix}\varphi_1 & \varphi_1 & \varphi_2 & \varphi_2\\ \alpha & \beta & \alpha & \beta\end{pmatrix}$ and $\begin{pmatrix}\varphi_1 & \varphi_1 & \varphi_3 & \varphi_3\\ \alpha & \beta & \beta & \alpha\end{pmatrix}$ are degenerate.

Because of the degeneracy of φ_2 and φ_3, the energies given in Table I are energies of configurations, but do not correspond to any possible physical state of the system. The two orbitally degenerate configurations interact with each other and are split into nondegenerate states as discussed in the next section.

3. COMPLETE DISCUSSION OF THE GROUND STATE

From the foregoing description of the MO, it follows that the ground state of the quadratic H_4 involves orbital degeneracy. Two electrons are paired in the lowest orbital φ_1, while the other two go into degenerate orbitals φ_2 and φ_3. The situation is thus similar to that encountered in the MO description of the oxygen molecule. According to the theory of spin degeneracy

TABLE I.[a]

$R_{ab}=R_{bc}=\cdots$	c_1	c_2	ϵ_1	ϵ_2	E'
1.606	0.2933	1.0153	−22.9	−7.5	−45.0
2.000	0.3127	0.9009	−19.7	−8.0	−49.9
2.097	0.3178	0.8804	−19.0	−7.9	−50.4
2.276	0.3271	0.8506	−17.9	−7.7	−51.4
5.000	0.4536	0.7146	−10.5	−6.8	−45.7

[a] Distances in units: 1 a.u. =0.5293 A; Energy in ev.

[9] See, for instance, R. S. Mulliken, J. chim. phys. **46**, 675 (1949).

TABLE II.

	I	II	III	IV	V	VI
φ_2	$\alpha\beta$		α	β	α	β
φ_3		$\alpha\beta$	α	β	β	α

of two electrons, the best single determinant wave function of the system is one corresponding to a triplet which is formed by the interaction of the two spin degenerate configurations.

The ground state can be completely described by considering six configurations corresponding to six possible ways of distributing two electrons into two degenerate orbitals φ_2 and φ_3. The other two electrons are paired in the totally symmetric molecular orbital. The two electrons in φ_2 and φ_3 can be distributed as shown in Table II.

The first two degenerate configurations, I and II, interact and yield two singlet states.[6] The off-diagonal element between I and II is the exchange integral K_{23}. Hence

$$E_{\mathrm{I\,I}}=E_{\mathrm{II\,II}}=E';$$
$$E_{\mathrm{I\,II}}=E_{\mathrm{II\,I}}=K_{23}{}^{\varphi};$$
$$E({}^1B_{1g},{}^1A_{1g})=E'\pm K_{23}{}^{\varphi}.$$

These energies are given in Table III.

The four configurations III to VI give two states, a triplet and a singlet,[10] the triplet being the lower one in accordance with Hund's rule. The energies of these two states are:

$$\begin{aligned}E({}^1B_{2g},{}^3B_{2g})&=2H_1{}^{\varphi}+H_2{}^{\varphi}+H_3{}^{\varphi}+J_{11}{}^{\varphi}+2J_{12}{}^{\varphi}-K_{12}{}^{\varphi}\\&\quad+2J_{13}{}^{\varphi}-K_{13}{}^{\varphi}+J_{23}{}^{\varphi}\pm K_{23}{}^{\varphi}\\&=E'-(J_{22}{}^{\varphi}-J_{23}{}^{\varphi})\pm K_{23}{}^{\varphi}.\end{aligned}\qquad(11'')$$

All the off-diagonal elements between I and II on one side and III to VI on the other side,

$$E_{\mathrm{I\,III}}=E_{\mathrm{I\,IV}}=\ldots=\sqrt{2}(H_{23}+J_{23}{}^{11}+J_{23}{}^{22}+J_{12}{}^{13}),$$

vanish, as shown by expanding them in terms of AO integrals. The notation

$$H_{23}=\int\bar{\varphi}_2{}^{\mu}H^{\mu}\varphi_3{}^{\mu}d\tau^{\mu};$$

$$J_{ij}{}^{kl}=\int\bar{\varphi}_i{}^{\mu}\bar{\varphi}_k{}^{\nu}\frac{1}{r^{\mu\nu}}\varphi_j{}^{\mu}\varphi_l{}^{\nu}d\tau^{\mu}d\tau^{\nu}$$

TABLE III.

Energy	1.606	2.000	2.097	2.276	5.000
${}^1B_{1g}$	−44.6	−49.7	−49.9	−51.1	−45.7
${}^1A_{1g}$	−45.4	−50.1	−50.9	−51.7	−45.7

[10] J. C. Slater, *The Quantum Theory of Matter* (The McGraw-Hill Book Company, Inc., 1951), pp. 195–197.

is taken from Taylor's work.[2] The MO description of the quadratic H_4 thus yields a triplet and three singlets in analogy with the MO treatment of cyclobutadiene.[11] The state energies of Eq. (11'') are given in Table IV.

4. ENERGY OF EXCITED STATES

When the calculation of Sec. 2 is repeated for orbitals a_{1g} and b_{1g}, i.e., for the configuration $\begin{pmatrix}\varphi_1 & \varphi_1 & \varphi_4 & \varphi_4\\ \alpha & \beta & \alpha & \beta\end{pmatrix}$, the orbital energy ϵ_4, for the first parameter ($R=1.606$), is equal to about 21 ev, which means that it is antibonding to about the same extent to which ϵ_1 is bonding. The system then is barely stable with respect to dissociation into protons and electrons; its energy is more than 40 ev higher than the corresponding total energies involving the degenerate orbital e_u. Analogous calculations for $R=2.097$ give the results, $\epsilon_4\sim 4.5$ ev, and a total energy of about −27 ev, almost 25 ev above the total energy of configurations involving e_u. Configurations including φ_4 can probably be omitted from calculations without introducing any appreciable errors, even though they may have the same symmetry as one of the low-lying singlet excited state.

TABLE IV.

R energy	1.606	2.000	2.097	2.267	5.000[a]
${}^1B_{2g}$	−45.9	−51.9	−52.2	−53.7	−50.6
${}^3B_{2g}$	−47.2	−52.3	−53.1	−54.2	−50.6

[a] The method is probably not good at this large distance and the energy converges to the value −54.4 for the 4 separated atoms.

Recent valence-bond calculations for cyclobutadiene including singly- and doubly-charged polar structures indicate that the lowest-energy singlet state is a ${}'B_{1g}$ state[12] rather than the triplet as occurs here. However, in the case of H_4 the excited B_{1g} state lies so high that it is not likely that configuration interaction will alter the order of the energy levels. Cyclobutadiene is a system of pure π electrons, which can move freely through an extended space and have directional properties, while H_4 is a pure s-electron system; thus this difference might be expected.

CONCLUSIONS

Tables I and III show that there is no minimum in the energy of either the singlet or the triplet states of quadratic H_4. The curves are similar to the one obtained by Hirschfelder[13] for equilateral-triangular nuclear arrangements of H_3. Thus we conclude that, due to large nuclear repulsion, the quadratic H_4 is not a

[11] A. W. Wheland, Proc. Roy. Soc. (London) **164A**, 397 (1938); R. McWeeny (to be published) (by private communication).
[12] R. McWeeny, reference 11.
[13] J. O. Hirschfelder, J. Chem. Phys. **6**, 795 (1938).

probable structure for the transition state of the molecular reaction. Because of selection rules the transition state would have to be the singlet which lies about ½ ev above the triplet ground state. The low energy resulting from Eyring's semiempirical calculation is probably due to approximations inherent in that procedure, since it is not likely that even the complete configurational interaction treatment (which should give the same results as an extended valence bond treatment) would lower the total energy to the value quoted by Eyring.[1]

This view is supported by the fact that even the simple MO method does yield considerably lower energy for linear H_4 complexes,[2] where the nuclear repulsion is about 20 percent lower than for the corresponding quadratic-nuclear form for the same distance between adjacent nuclei. Furthermore, Griffing and Vanderslice[14] have shown that even lower values (about −57 ev) are obtained for the linear molecule, if a self-consistent field LCAO procedure is adopted. Since in the case of a quadratic-nuclear form the average distances between interacting atoms are smaller than for the corresponding linear case, a MO treatment in the former case should be as good as in the latter, or better. This suggests that, quite apart from absolute values obtained by MO treatments, the linear complex is the one of less energy and hence is a more probable structure of the transition state.

APPENDIX I. EVALUATION OF INTEGRALS

(a) One-Electron Integrals

Overlap integrals S_{pq} were evaluated from integrated forms given in standard texts on quantum mechanics and checked against tables of Mulliken *et al.*[15]

Integrals of (H) are two types; kinetic energy integrals,

$$\int \bar{\chi}_p{}^\mu(-\tfrac{1}{2}\Delta)\chi_q{}^\mu d\tau^\mu,$$

and nuclear field integrals,

$$\int \frac{1}{r_a}\bar{\chi}_p{}^\mu\chi_q{}^\mu d\tau^\mu.$$

All the one-center integrals were integrated directly in spherical coordinates. Two-center nuclear field integrals have to be integrated in elliptical coordinates.[16] Two-center kinetic-energy integrals reduce to linear combinations of two-center nuclear-field integrals and two-center overlap integrals.[17]

Three-center nuclear field integrals for 1*s*-functions have been tabulated[18] for all nuclear configurations. Interpolation in tables yields somewhat high values. This was corrected by comparison with the error introduced by interpolation of two-center integrals whose exact values are known.

The pqth element of the $(\mathbf{H})$ matrix is:

$$H_{pq}=-\tfrac{1}{2}\int \bar{\chi}_p{}^\mu\Delta\chi_q{}^\mu d\tau^\mu+\sum_{a=a,b\ldots}\int\frac{1}{r_a}\bar{\chi}_p{}^\mu\chi_q{}^\mu d\tau^\mu.$$

(b) Two-Electron Integrals

The one-center integral can be evaluated directly in spherical coordinates.[19] Its value is 0.625 a.u. where 1 a.u. = 27.204 ev.

Integrated forms of two-center integrals have been collected by Slater.[20] A comparison of exact values with values obtained from Mulliken's approximations[9] shows that the latter are quite accurate at our distances, and they were therefore used to approximate multicentered integrals.

Mulliken's approximation for the 4-center integral is:

$$\int \bar{\chi}_p{}^\mu\bar{\chi}_r{}^\nu\frac{1}{r^{\mu\nu}}\chi_q{}^\mu\chi_t{}^\nu d\tau^\mu d\tau^\nu \sim\tfrac{1}{4}S_{pr}S_{qs}(J_{pq}+J_{ps}+J_{qr}+J_{rs}),$$

where

$$J_{pq}\equiv\int \bar{\chi}_p{}^\mu\bar{\chi}_q{}^\nu\frac{1}{r^{\mu\nu}}\chi_p{}^\mu\chi_q{}^\nu d\tau^\mu d\tau^\nu.$$

The same formula was used to approximate three-centered integrals.

APPENDIX II. WACKER'S MATRIX NOTATION

(a) The (G) Matrix

Elements G_{prqt} of Sec. 2 are arranged in a $4^2\times4^2$ matrix denoted by

$$(\mathbf{g})=(2\mathbf{j}-\mathbf{k}),$$

where $(\mathbf{j})$ is the matrix of elements J_{prqt} and $(\mathbf{k})$ the matrix of elements J_{prtq} [Eq. (6)].

The matrix elements G_{pq} are now expanded according to (5);

[14] V. Griffing and J. T. Vanderslice, J. Chem. Phys. **23**, 1035 (1955).
[15] Mulliken, Rieke, Orloff, and Orloff, J. Chem. Phys. **17**, 1248 (1949).
[16] See, for instance, Eyring, Walter, and Kimball, *Quantum Chemistry* (John Wiley and Sons, Inc., New York, 1944).
[17] C. C. J. Roothaan, J. Chem. Phys. **19**, 1445 (1951).
[18] J. O. Hirschfelder and C. Weygandt, J. Chem. Phys. **6**, 806 (1938).
[19] L. Pauling and E. B. Wilson, *Introduction to Quantum Mechanics* (McGraw-Hill Book Company, Inc., New York, 1935), p. 446.
[20] J. C. Slater, Technical Report No. 3, Massachusetts Institute of Technology, February 15, 1953.

$$G_{pq}=\sum_{i=1,2}\sum_{rt}\bar{c}_{ri}G_{prqt}c_{ti}$$

$$=(\bar{c}_{a1}c_{a1}+\bar{c}_{a2}c_{a2})G_{paqa}+(\bar{c}_{a1}c_{b1}+\bar{c}_{a2}c_{b2})G_{paqb}+(\bar{c}_{a1}c_{c1}+\cdots\cdots$$
$$+(\bar{c}_{b1}c_{a1}+\bar{c}_{b2}c_{a2})G_{pbqa}+(\bar{c}_{b1}c_{b1}+\bar{c}_{b2}c_{b2})G_{pbqb}+\cdots\cdots \quad (13)$$
$$+\cdots\cdots$$
$$+\cdots\cdots+(\bar{c}_{d1}c_{d1}+\bar{c}_{d2}c_{d2})G_{pdqd}.$$

It can be seen by inspection of this expanded form that, to collect an element G_{pq}, one has to multiply every element of the pqth submatrix of (**g**)—the submatrix consisting of elements G_{prqt} of constant p and q—by the corresponding element of the matrix ($\bar{\mathbf{C}}\mathbf{C}^{+}$), constant for all pairs of p and q, and add the products; + signifies the transpose of the matrix. This is equivalent to taking the trace of the product of the pqth submatrix of (**g**) and a constant matrix (**ϱ**),

$$(\boldsymbol{\varrho})\equiv(\bar{\mathbf{C}}\mathbf{C}^{+})^{+}=(\mathbf{C}\mathbf{C}^{*}), \quad (14)$$

where the asterisk denotes the Hermitian conjugate. The array of traces determined by pairs of p and q is the two-electron (**G**) matrix. Since the submatrices of (**g**) are obtained by keeping the first and the third subscripts of G_{prqt} constant, the operation of obtaining (**G**) is written:

$$(\mathbf{G})\equiv tr_{2,4}[(\mathbf{g})_{2,4}(\rho)]. \quad (15)$$

(**ϱ**) is obtained directly from the matrix of coefficients (**C**).

As an illustration of the symmetry of the electron-nuclear and electron-electron potentials, the (**H**) and the (**G**) matrices for one parameter, $R=1.606$ a.u., are given in Table V.

TABLE V.[a]

		a	b	c	d
(**H**)=	a	−2.040	−1.567	−1.225	−1.567
	b		−2.040	−1.567	−1.225
	c			−2.040	−1.567
	d				−2.040
		a	b	c	d
(**G**)=	a	1.363	0.941	0.685	0.941
	b		1.363	0.941	0.611
	c			1.363	0.941
	d				1.363

[a] The matrix elements are given in Hartree units.

(b) Total Energy for Paired Electrons

To collect the one-electron contribution $2\sum_i Hi^{\varphi}$ to the total energy E',

$$E'=2\sum_{i}^{2}Hi^{\varphi}+\sum_{ij}^{2}(2J_{ij}^{\varphi}-K_{ij}^{\varphi}), \quad (11')$$

one has to multiply the matrix (**H**) by appropriate coefficients c_{ai}. Defining a matrix ($\mathbf{H}^{\varphi}$) in terms of MO, analogous to the AO (**H**) matrix of Sec. 2 (Eq. 4), we can write in the matrix notation:

$$(\mathbf{H}^{\varphi})=\int\varphi^{*\mu}H^{\mu}\varphi^{\mu}d\tau^{\mu}. \quad (16)$$

Substituting for φ the definition of the MO (1′),

$$(\mathbf{H}^{\varphi})=\int(\mathbf{c})^{*}\mathbf{x}^{*\mu}H^{\mu}\chi^{\mu}(\mathbf{c})d\tau^{\mu}$$
$$=(\mathbf{C})^{*}(\mathbf{H})(\mathbf{C}).$$

Then, introducing (14),

$$\sum_i H_i^{\varphi}=tr(\mathbf{H}^{\varphi})=tr[(\mathbf{C})^{*}(\mathbf{H})(\mathbf{C})]=tr[(\mathbf{H})(\rho)]. \quad (17)$$

TABLE VI.[a]

R	1.606	2.000	2.097	2.267	5.000
E_T	64.5	57.3	56.0	53.9	49.5

[a] R in a.u. =0.5293 A; Energy in ev.

In an analogous way, one deduces for the two-electron contribution:

$$\sum_{ij}(2J_{ij}^{\varphi}-K_{ij}^{\varphi})\equiv tr[(\mathbf{G})(\boldsymbol{\varrho})]$$
$$=tr\{tr_{2,4}[(2\mathbf{j}-\mathbf{k})_{2,4}(\boldsymbol{\varrho})](\boldsymbol{\varrho})\}. \quad (18)$$

The total energy is obtained from (17) and (18):

$$E'=tr\{[2(\mathbf{H})+(\mathbf{G})](\mathbf{p})\}. \quad (11')$$

Energies E' are listed in Table I.

Other quantities can be computed in a similar way. Thus the kinetic energy E_T of electrons is obtained quickly by defining a matrix (**T**):

$$T_{pq}=\int\bar{\chi}_p^{\mu}(-\tfrac{1}{2}\Delta)\chi_q^{\mu}d\tau^{\mu},$$
$$E_T=2tr[(\mathbf{T})(\boldsymbol{\varrho})]. \quad (19)$$

The kinetic energies for four parameters are tabulated in Table VI.

Studies of the Interaction between Stable Molecules and Atoms. IV. The Energy of the Linear H_4 Complex*

VIRGINIA GRIFFING AND JOSEPH T. VANDERSLICE
Department of Chemistry, The Catholic University of America, Washington, D. C.
(Received June 22, 1954)

Roothaan's LCAO–SCF treatment has been applied to the linear symmetrical H_4 complex in an attempt to test this method for calculating the energies of activated complexes. Calculations have been made for internuclear distances of 1.4, 1.6, 2.0, and 2.2 a.u. The SCF method gives a lower value for the energy of 1.4 a.u. than was obtained by a simple molecular orbital method without configuration interaction, but gives a higher value than the best configuration interaction treatment. The values of the energies that were obtained are −55.48, −55.99, −56.50, and −56.54 ev at distances of 1.4, 1.6, 2.0, 2.2 a.u., respectively. The changes in the wave functions as one adiabatically changes the internuclear distance are of particular interest. Although the results cannot be directly compared with experiment, reasonable values for the energy are obtained indicating that the molecular orbital SCF method with a limited amount of configuration interaction is a promising method for treating closed-shell molecules and interactions between such molecules for small values of the internuclear parameters.

THIS is the fourth paper in this series which was designed to study the application of the LCAO–SCF method of molecular orbitals as developed by Roothaan[1] to the interaction between two separate chemical species. This method has been applied by a number of workers[2] to calculate the ground states and low-lying electronically excited states of stable molecules yielding good results for the ground state and fair results for the excited states. In all these calculations, the equilibrium internuclear distances were obtained from experiment and in most cases only part of the electrons were included in the calculation. However, very little work has been done in which an attempt is made to calculate the energy of the ground state of a molecule as function of internuclear distance; in addition this method has not been applied to the study of the interaction of two systems to form an unstable complex. Thus this study was undertaken in order to test the method for the calculation of intermolecular potential energy curves as function of distance in the range of internuclear parameters in which chemical forces are important. Further, it was hoped that the variation of self-consistent field coefficients as function of distance would yield valuable information about their significance in understanding molecular structure. In particular, in view of the general method outlined in Paper I of this series[3] for calculation of activation energies of chemical reactions, four-electron problems become quite important.

The linear H_4 system was chosen because this is the simplest case of an interaction between two molecules with closed-shell ground states in which the one-electron molecular orbitals could be chosen as an arbitrary linear combination of 1*s*-atomic orbitals.[4] Also, the coefficients are not entirely determined by symmetry and orthonormality conditions. All of the electrons in this system could be conveniently included and the solutions could be compared with the molecular orbital calculation for the H_2 molecule[5] in order to calculate an activation energy. In addition, Taylor[6] has calculated the energy of this system for one value of the internuclear distance by the molecular orbital method including configuration interaction; thus, this system is an ideal one for testing the effect of determining the coefficients by a Hartree-Fock type calculation for a many-centered case. The system was simple enough to calculate the energy as function of internuclear distances and thus the variation with distance of the SCF parameters could be determined. This calculation will also yield a value for the activation energy of the bimolecular exchange between two hydrogen molecules.

Furthermore, we believe that simple idealized interacting systems must be understood before one can hope to develop satisfactory methods for adequately studying more complicated systems in which more drastic assumptions must be made.

THE LCAO–SCF METHOD

An excellent outline of Roothaan's methods has been given by Mulligan.[2] The molecular orbitals ϕ_i are represented by LCAO's, i.e.,

$$\phi_i=\sum_p a_{ip}\chi_p, \tag{1}$$

where the i numbers the MO's, p the AO's, and the a_{ip}'s are the undetermined coefficients. To obtain the best set of MO's, one has to solve the following matrix equation

$$(\mathbf{H}+\mathbf{G})a_i=\epsilon_i\mathbf{S}a_i. \tag{2}$$

The column vectors a_i give the coefficients of the AO's in the i'th MO while $\mathbf{S}$ is a Hermitian overlap

* Supported by the Office of Naval Research.
[1] C. C. J. Roothaan, Revs. Modern Phys. **23**, 69 (1951).
[2] R. G. Parr and R. S. Mulliken, J. Chem. Phys. **18**, 1338 (1950); J. F. Mulligan, J. Chem. Phys. **19**, 347 (1951).
[3] V. Griffing, J. Chem. Phys. **23**, 1015 (1955).
[4] Since only 1*s*-orbitals are required, dependable values of the three- and four-center integrals could be calculated.
[5] C. A. Coulson, Proc. Camb. Phil. Soc. **34**, 204 (1938).
[6] R. Taylor, Proc. Phys. Soc. **A64**, 249 (1951).

TABLE I. The S matrix.[a]

R	1.4	1.6	2.0	2.2
$S_{11}=S_{22}=S_{33}=S_{44}$	1.000	1.000	1.000	1.000
$S_{14}=S_{41}$	0.166	0.110	0.047	0.030
$S_{12}=S_{43}=S_{21}=S_{34}=S_{23}=S_{32}$	0.753	0.694	0.586	0.533
$S_{13}=S_{42}=S_{24}=S_{31}$	0.390	0.307	0.533	0.146

[a] In a.u. (1 a.u. = 13.602 ev).

matrix with elements given by

$$S_{pq}=\int \bar{\chi}_p \chi_q d\tau. \tag{3}$$

Furthermore, **H** is the bare nuclear field orbital energy matrix with elements

$$H_{pq}=\int \bar{\chi}_p H \chi_q d\tau, \tag{4}$$

where H includes the kinetic energy of the electrons and their potential energy in the field of the four nuclei. The symbol **G** denotes the electronic interaction matrix with elements

$$G_{pq}=\sum_{irt} \bar{a}_{ir} G_{prqt} a_{it}, \tag{5}$$

where i runs only over filled shells and

$$\begin{aligned} G_{prqt}&=2J_{prqt}-J_{prtq} \\ J_{prqt}&=e^2\int \frac{\bar{\chi}_p{}^{\mu}\bar{\chi}_r{}^{\nu}\chi_q{}^{\mu}\chi_t{}^{\nu}}{r^{\mu\nu}} d\tau^{\mu\nu}. \end{aligned} \tag{6}$$

Equation (2) can be written in the form

$$\mathbf{L}a_i=\epsilon_i \mathbf{S}a_i, \tag{7}$$

where $\mathbf{L}=\mathbf{H}+\mathbf{G}$. This means that the best LCAO–MO's are eigenfunctions of the Hermitian operator **L**. The problem reduces to solving the secular equation (7) for the undetermined coefficients a_i, and the orbital energies ϵ_i. Since **G** and consequently **L** depend on the a_i's, it is necessary to use a self-consistent field procedure.

Once the self-consistent a_i's have been obtained, the total energy is given by

$$E=2\sum_i H_i+\sum_{ij}(2J_{ij}-K_{ij})+V, \tag{8}$$

TABLE II. The H matrix.[a]

R	1.4	1.6	2.0	2.2
$H_{11}=H_{44}$	−3.400	−3.147	−2.780	−2.632
$H_{14}=H_{41}$	−0.730	−0.448	−0.177	−0.125
$H_{12}=H_{43}=H_{21}=H_{34}$	−3.060	−2.710	−2.028	−1.776
$H_{13}=H_{42}=H_{24}=H_{31}$	−1.703	−1.343	−0.707	−0.469
$H_{22}=H_{33}$	−4.144	−3.846	−3.392	−3.202
$H_{23}=H_{32}$	−3.323	−2.932	−2.185	−1.904

[a] In a.u. (1 a.u. =13.602 ev).

where

$$\left.\begin{aligned} H_i&=\int \bar{\phi}_i H \phi_i d\tau \\ J_{ij}&=e^2\int \frac{\bar{\phi}_i{}^{\mu}\bar{\phi}_j{}^{\nu}\phi_i{}^{\mu}\phi_j{}^{\nu}}{r^{\mu\nu}} d\tau^{\mu\nu} \\ K_{ij}&=e^2\int \frac{\bar{\phi}_i{}^{\mu}\bar{\phi}_j{}^{\nu}\phi_j{}^{\mu}\phi_i{}^{\nu}}{r^{\mu\nu}} d\tau^{\mu\nu} \end{aligned}\right\}, \tag{9}$$

and V equals the potential energy of the nuclei alone and the i and j run over filled shells.

APPLICATION TO THE H_4 SYSTEM

The H_4 system was taken as being linear. The distance between nearest neighbors was considered to be a constant for all four nuclei. The energy was calculated for values of this distance of 1.4 (the normal internuclear distance of H_2), 1.606, 2.0, and 2.2 atomic units. The interaction between all electrons and nuclei were considered. Numbers 1 and 4 refer to the outermost nuclei, 2 and 3 to the inner nuclei. Nuclei 1 and 2 are adjacent.

TABLE III. The G matrix.[a]

R	1.4	1.6	2.0	2.2
$G_{11}=G_{44}$	2.317	2.201	2.019	1.946
$G_{14}=G_{41}$	0.340	0.227	0.083	0.056
$G_{12}=G_{43}=G_{21}=G_{34}$	1.796	1.534	1.105	0.940
$G_{13}=G_{42}=G_{24}=G_{32}$	0.893	0.636	0.313	0.221
$G_{22}=G_{33}$	2.787	2.611	2.461	2.385
$G_{23}=G_{32}$	2.100	1.794	1.428	1.260

[a] In a.u. (1 a.u. = 13.602 ev).

The MO's were made up of Slater type $1s$-orbitals.[7] In this case we have with $Z=1$,

$$(1s)=(Z^3/\pi)^{\frac{1}{2}}\exp(-Zr).$$

DETERMINATION OF THE LCAO–MO'S

To obtain the best LCAO–MO's it was necessary to solve Eq. (7) for the LCAO coefficients a_i. The overlap matrix **S** was first evaluated and the results are given in Table I. Then the bare nuclear-field orbital-energy matrix **H** was evaluated. The results are given in Table II. The electronic interaction matrix presented the most difficulty, not only because it contains three- and four-center integrals, but also because its elements depend on the undetermined a_i's. After the necessary integrals had been evaluated and multiplied by the assumed a_i's, the matrix **G** could be evaluated and the secular equation solved for the a_i's.

The procedure followed was first to assume values of the a_i's consistent with the orthonormality conditions.[1] The matrix **G** was evaluated and the secular equation

[7] J. C. Slater, Phys. Rev. **36**, 57 (1930).

(7) solved for the a_i's using the potentiometric linear-equation solver of the type designed by Filler, Cowan, and Roothaan.[8] When the assumed a_i's agreed with the calculated a_i's self-consistency was attained and the best LCAO–MO's and the total energy could then be obtained. The elements of the matrix **G** using the self-consistent a_i's are given in Table III.

RESULTS

The molecular orbitals were chosen as orthonormal linear combinations of the atomic orbitals $1s_1$, $1s_2$, $1s_3$, and $1s_4$ and have the following forms belonging to the irreducible representations of the symmetry group $D_{\infty h}$ which represents the symmetry of the Hamiltonian operator

$$\phi_1=a_{11}(1s_1+1s_4)+a_{13}(1s_2+1s_3),$$
$$\phi_2=a_{21}(1s_1-1s_4)+a_{23}(1s_2-1s_3),$$
$$\phi_3=a_{31}(1s_1+1s_4)-a_{33}(1s_2+1s_3),$$
$$\phi_4=a_{41}(1s_1-1s_4)-a_{43}(1s_2-1s_3).$$

Thus by symmetry one can reduce to half the number of coefficients that must be determined. Then by the self-consistent field calculation and normalization conditions the four undetermined coefficients in the first two ground-state molecular orbitals were determined. A set of coefficients in ϕ_3 and ϕ_4 are also determined; these are not self-consistent solutions but do represent a crude approximation of the excited orbitals of the system. The self-consistent field coefficients for the ground-state orbitals are plotted as function of internuclear distance in Fig. 1. It is interesting to note that the coefficients in the totally symmetrical bonding orbital ϕ_1 show a smooth variation as function of internuclear distance while the coefficients describing the antibonding orbital ϕ_2 vary widely as function of the internuclear parameters and cross over for a value of $R=2.1$ a.u. In spite of the wide variation of the coefficients, the energy as function of the internuclear parameter shows smooth variation such as one would expect. With zero being taken as four nuclei and four electrons infinitely far apart, the total energy is plotted against internuclear distance in Fig. 2. The energy continually decreases out to distances of 2.0 a.u. We see that at all distances the system is stable against dissociation into four H atoms which would have a combined energy of -54.15 ev but not against dissociation into two H_2 molecules which would have a combined energy of 60.37 ev[5] as calculated by the molecular orbital method. The total energy obtained by this method at a distance of 1.4 a.u. has a value lower by 0.89 ev than that obtained by Taylor[6] without configuration interaction. When he included configuration interaction, the energy decreased below our value by 0.92 ev. The values of the energy at $R=2.0$ and $R=2.2$ a.u. are equal within the accuracy of the calculation indicating a minimum in

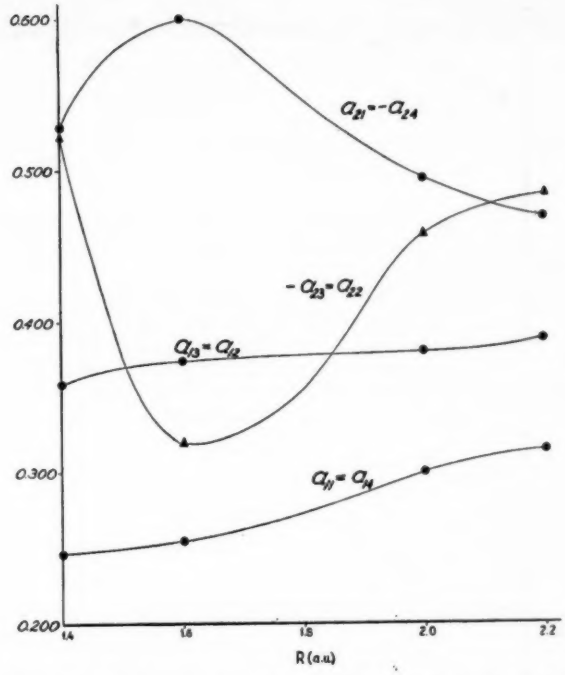

FIG. 1. The self-consistent field coefficients for the wave functions of the filled orbitals in linear H_4 are plotted as function of the internuclear distance.

between at $R\sim2.1$ a.u. The coefficients a_{21} and a_{23} that occur in ϕ_2 also cross at this point. This kind of a complex has been defined as an "ambivalent complex" in Paper I[3] of this series.

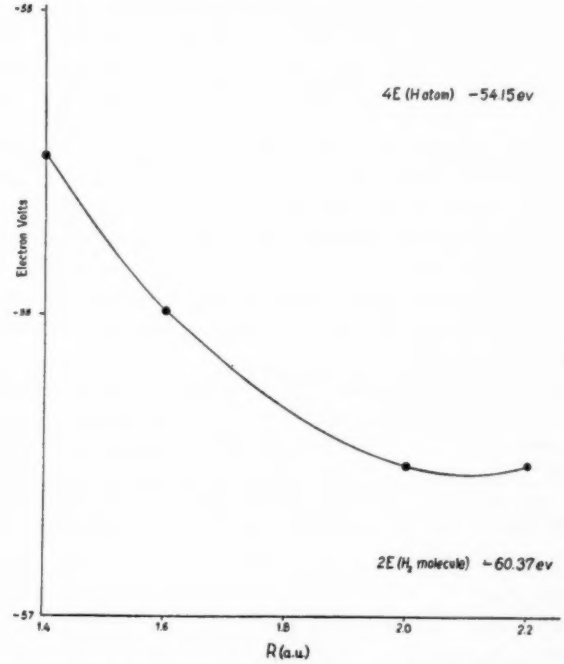

FIG. 2. The total energy in electron volts of linear H_4 is plotted as function of the internuclear distance. The zero is taken as 4H nuclei and 4 electrons infinitely separated from each other. The internuclear distance is plotted in a.u. (i.e., R/a_0).

[8] Filler, Cowan, and Roothaan, Office of Naval Research Technical Report from the University of Chicago for the period September 1, 1948 to May 31, 1949; Contract N6ori-20 T.O. nine.

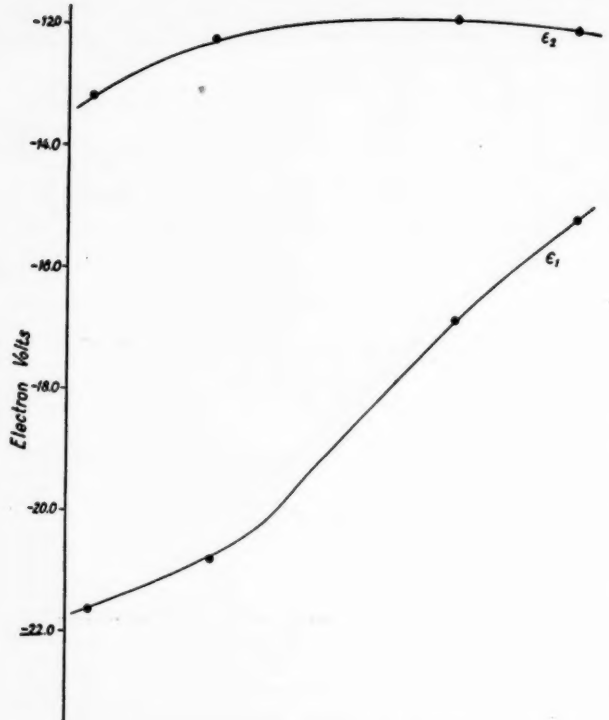

FIG. 3. The Hartree-Fock eigenvalues (vertical ionization energies) are plotted as function of the internuclear distance.

The eigenvalues of the Hartree-Fock operator, ϵ_1 and ϵ_2 are plotted as function of the internuclear parameter in Fig. 3. These have been identified by previous investigations[1] with the vertical ionization energies; although it is not possible to compare these with experiment, their relative values seem reasonable and, for these distances, seem to be converging to a correct value for the hydrogen atom at large internuclear distances; however, if the calculation was extended to larger values of the internuclear parameter, the validity of the molecular orbital calculation would probably break down and these values would converge to some average between the ground and excited states of the hydrogen atoms.

Previous investigators[9] have worked on the quantum-mechanical calculation of the interaction energy of two hydrogen molecules. However, their results cannot be compared with the present work, since these workers were interested in energy values for different values of the internuclear parameters and larger values of the intermolecular distances. Furthermore, the present results cannot be compared with the semiempirical results of Hirschfelder, Bird, and Spotz[10] nor with those of de Boer and Michels,[11] not only for the above reasons but also because it would be necessary to average over different orientations, whereas only the linear case has been considered here.

[9] J. de Boer, Physica **9**, 363 (1942); H. Margenau, Phys. Rev. **64**, 131 (1943); and A. Evert and H. Margenau, Phys. Rev. **90**, 1021 (1953).

CONCLUSION

From this work, we conclude that the LCAO–SCF method should yield fairly reliable results when used as a basis for calculation of interaction energies for closed-shell molecules as long as internuclear distances are not too large. It is also shown that the SCF calculation introduces a considerable improvement over the simple molecular orbital calculation as made by Taylor. Furthermore this work indicates that considerable insight into the nature of chemical binding and the interaction between molecules in their closed-shell ground state can be obtained by a "best" single determinant molecular orbital calculation. Furthermore it seems likely that the LCAO–SCF method with a limited amount of configuration interaction will prove to be the simplest and best method for calculating the ground states of stable molecules and the interaction energy at small internuclear distances between stable molecules.

APPENDIX I

Integrals

All the integrals have been evaluated exactly when possible. Tables and formulas for overlap integrals are given by Mulliken *et al.*[12] The kinetic energy integrals were obtained from Roothaan's formulas.[13] The one electron bare nuclear field, the exchange, and the hybrid Coulomb-exchange integrals were obtained from Hirschfelder and Weygandt's work.[14] The three- and four-center integrals were obtained using Mulliken's approximation formula.[15]

[10] Hirschfelder, Bird, and Spotz, J. Chem. Phys. **16**, 968 (1948).
[11] J. de Boer and A. Michels, Physica **5**, 945 (1938).
[12] Mulliken, Rieke, Orloff, and Orloff, J. Chem. Phys. **17**, 1248 (1949).
[13] C. C. J. Roothaan, J. Chem. Phys. **19**, 1445 (1951).
[14] J. O. Hirschfelder and C. N. Weygandt, J. Chem. Phys. **6**, 806 (1938).
[15] R. S. Mulliken, J. Chim. Phys. **46**, 497 (1949).

Studies of the Interaction between Stable Molecules and Atoms. V. Molecular Orbital Approach to the $H+H_2$ Reaction*

VIRGINIA GRIFFING AND JOSEPH T. VANDERSLICE
Department of Chemistry, The Catholic University of America, Washington, D. C.
(Received June 22, 1954)

In an attempt to find a relatively simple way of calculating activation energies for chemical reactions, Roothaan's LCAO-SCF method has been applied to the linear H_3 complex. Since Roothaan's method has been developed for closed shells, a self-consistent field treatment has been done on the linear H_3^- complex. According to Roothaan, the energy of the H_3 should be equal to a first approximation to the energy of the H_3^- minus the energy required to remove one electron. Calculations have been made at distances ranging from 1.4 to 2.5 atomic units and for various values of the screening constant. Correlation diagrams for the reaction $H+H_2$ have been constructed and the activation energy calculated. The method gives considerable insight into charge distribution but is unsatisfactory for calculating good energy values. The results are compared with experiment and with values calculated by the MO-configuration interaction method which yields a value of 8.76 kcal/mole.

INTRODUCTION

THE reaction of a hydrogen atom with a hydrogen molecule is one of the simplest but still unsolved problems in reaction kinetics. Many attempts have been made to treat this reaction by *a priori* theoretical calculations.[1] So far all these have failed to give reliable quantitative results and not even a satisfactory qualitative understanding has been forthcoming. In earlier papers, Hirschfelder[2] and co-workers have calculated the energy of H_3 and H_3^+ for the linear complex in both the symmetrical and some unsymmetrical configurations. In contrast to the results of the semiempirical theory, these papers predicted a symmetrical activated state. Later Hirschfelder[3] calculated the energies of nonlinear H_3 and H_3^+ by both the molecular orbital and homopolar bond methods. He found the MO method to be inferior to the homopolar bond method for the symmetrical triatomic configuration. This result is not surprising in view of the fact that the MO theory, using a single determinant, is now known to be dependable only for closed-shell electronic configurations. Furthermore, Hirschfelder has calculated the energy of nonlinear H_3 as function of the angle between the nuclei and has established that the orbitally-degenerate electronic state for the equilateral configuration of the nuclei is unstable, in agreement with the Jahn-Teller theorem.[4] Even though Hirschfelder's results[3] could be improved by using a more general set of eigenfunctions, it seems likely that the relative values of the energies for various geometrical configurations of the nuclei are valid. Thus, in view of Hirschfelder's calculations and the general results given in the first four papers[5] of this series, an LCAO-SCF calculation of the linear symmetrical H_3 negative ion has been undertaken with the hope that the calculated ionization energy could be subtracted away, giving good results for the H_3 complex. Even though the quantitative results of our calculations are not satisfactory, we believe this study shows that the molecular-orbital theory of chemical binding does give an excellent qualitative understanding of the problem, as well as reliable quantitative data in many cases, if one takes into account the fact that this approach gives good results for energy differences even though the absolute values may be in error. In this case one must use configuration interaction to get good quantitative results because H_3 does not have a closed-shell ground state. A correlation diagram following the general scheme recently developed by Griffing and co-workers[5] will be drawn and reasons advanced why the activation energy of the process is so small.

OUTLINE OF THEORY

The theoretical approach is described in papers by Griffing and co-workers.[5] Essentially, it consists in looking at the reactants and products of a chemical reaction, constructing a correlation diagram depicting the symmetry of the one-electron orbital and then showing how these wave functions change during the reaction. One of the essential points in this scheme is that an "ambivalency" and "degeneracy" has to occur during the course of the chemical reaction which allows for a continuous transition from the initial to the final state. Furthermore, the fact that the molecular orbital theory does not give good absolute values but only good values of energy differences is recognized. These points of the theory will be illustrated for the $H+H_2$ reaction.

* Supported by the Office of Naval Research.

[1] Glasstone, Laidler, and Eyring, *The Theory of Rate Processes* (McGraw-Hill Book Company, Inc., New York, 1941).

[2] Hirschfelder, Eyring, and Rosen, J. Chem. Phys. **4**, 121, 130 (1936); Hirschfelder, Diamond, and Eyring, J. Chem. Phys. **5**, 695 (1937); and Stevenson and Hirschfelder, J. Chem. Phys. **5**, 933 (1937).

[3] J. O. Hirschfelder, J. Chem. Phys. **6**, 795 (1938).

[4] Jahn and Teller, Proc. Roy. Soc. (London) **A161**, 200 (1937).

[5] See Papers I to IV of this series [V. Griffing *et al.*, J. Chem. Phys. **23**, 1015 (1955); **23**, 1024 (1955); **23**, 1029 (1955); **23**, 1035 (1955)].

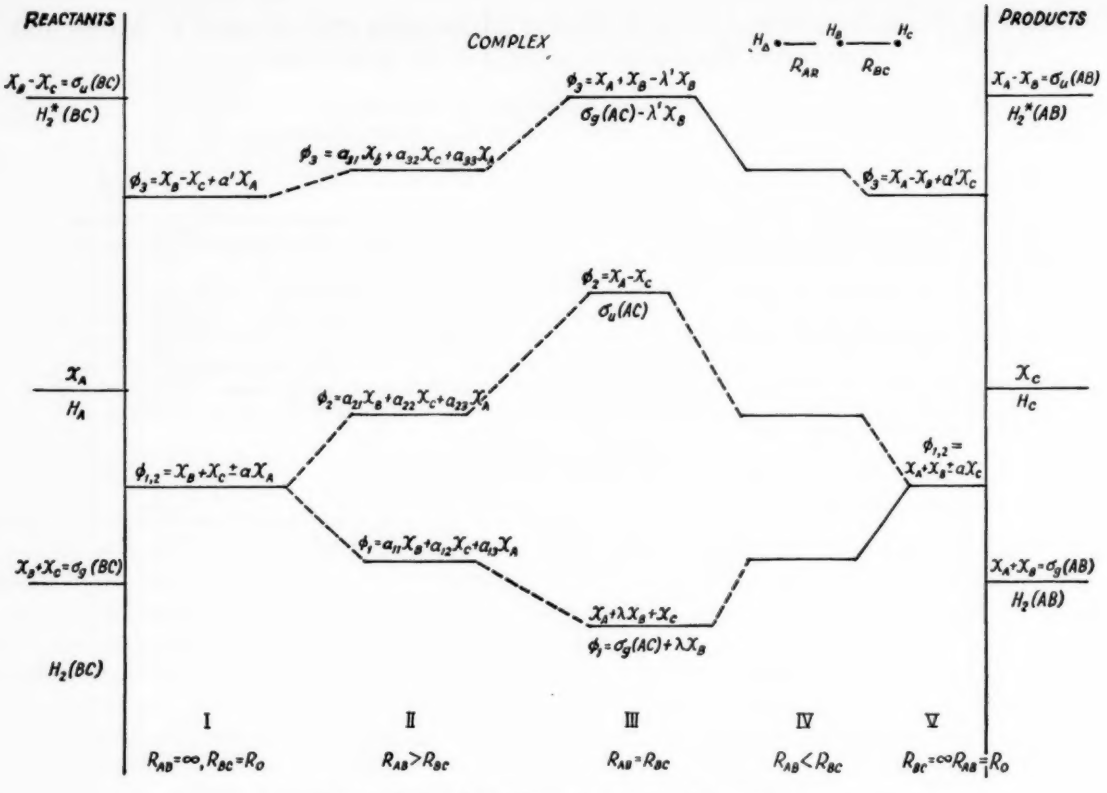

FIG. 1. Correlation diagram for the $H+H_2$ reaction.

CORRELATION DIAGRAM FOR THE REACTION

It has been assumed that the intermediate "ambivalent complex" is a linear one with the internuclear distances equal. The energy of the triangular H_3 complex is much higher than the linear complex[3] and hence would not be expected to be the "degenerate complex" for the reaction. The correlation diagram is illustrated in Fig. 1 where χ_A, χ_B, and χ_C are the 1*s*-atomic orbitals on atoms H_A, H_B, and H_C, respectively, and χ_{BC} is the ground-state molecular orbital for H_2. The reaction is assumed to be

$$H_A+H_2{}^{BC}\rightarrow H_A-H_B-H_C\rightarrow H_2{}^{AB}+H_C.$$

When the H_A atom and the $H_2{}^{BC}$ molecule are infinitely separated, the situation may be represented by State I. Here there is no interaction between the various levels, i.e., the H_A atom has no influence on the levels in the $H_2{}^{BC}$ molecule. As the H_A atom approaches the $H_2{}^{BC}$ molecule along the internuclear axis line of centers, the situation represented as State II appears in which there is interaction among the original levels of State I to give the levels of State II. When the "degenerate complex" is formed in State III, the three possible levels made up out of 1*s*-function for H_3 appear. As the H_C atom starts to move away from the newly formed $H_2{}^{AB}$ molecule, a situation represented by State IV occurs which is similar to the situation in State II. It is to be noted that the second-lowest level in State II has now passed over into the second-lowest level in State IV in a continuous manner. Both of these levels go into the second-lowest level in State III as the internuclear distances are made equal. In this sense, these levels become degenerate and ambivalent when the complex is formed. The same argument applies to the lowest-lying level in States II, III, and IV. It is interesting to see how the orbital electronic densities change during the process. This is illustrated in Fig. 2. This figure shows that the densities change in the manner that one would expect.

CALCULATION OF THE ACTIVATION ENERGY

Since the best possible LCAO–molecular orbital calculations have been done on H_2[6] and H_3,[7] one can use those values to obtain the activation energy for the reaction. This has already been pointed out by Griffing and Vanderslice.[8] The best possible molecular orbital calculations require the use of configuration interaction. If one uses Walsh and Matsen's value[7] for the energy of H_3 and subtracts from that the energy of H_2 obtained by Slater[6] using configuration interaction and the energy of a hydrogen atom, one obtains for the activation energy a value of 8.76 kcal which is to be compared

[6] J. C. Slater, "Electronic Structure of Atoms and Molecules," Technical Report No. 3 of the Solid State and Molecular Theory Group, Massachusetts Institute of Technology.
[7] J. M. Walsh and F. A. Matsen, J. Chem. Phys. **19**, 526 (1951).
[8] V. Griffing and J. T. Vanderslice, J. Chem. Phys. **23**, 1035 (1955).

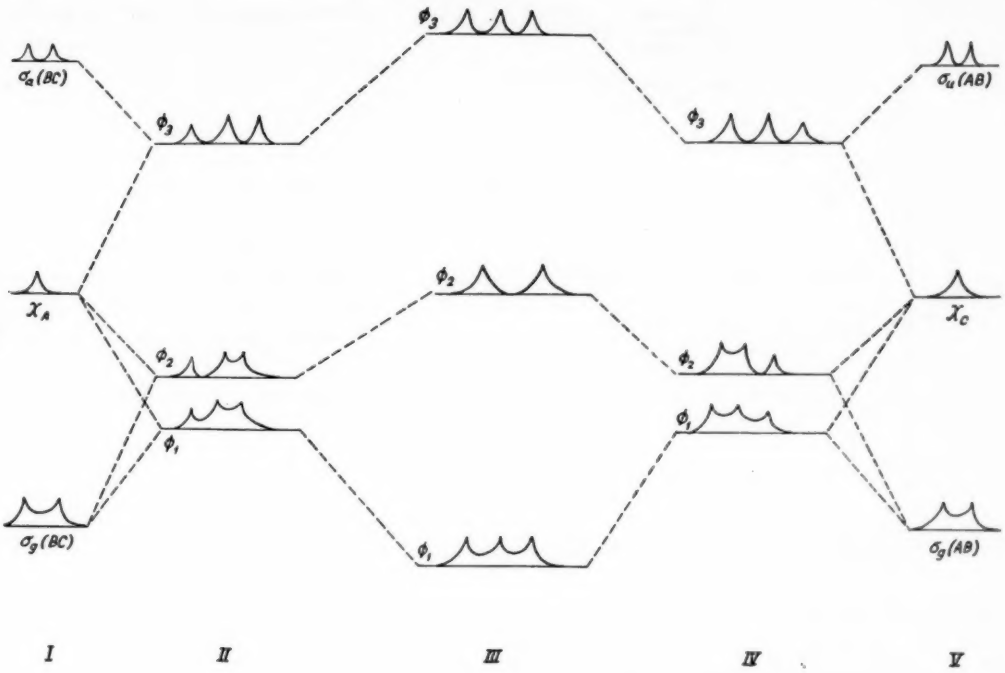

FIG. 2. Electronic densities corresponding to states appearing in correlation diagram.

with the experimental value of about 5–10 kcal.[9] One might reasonably object that in the quantitative treatment, configuration interaction was included whereas in the correlation diagram, the simple molecular orbital picture has been used. Such an objection is a valid one. However, if one includes configuration interaction in the correlation diagram it would lose its essential simplicity while on the other hand, if one uses the simple molecular orbital treatment for the calculation, good numerical results are not obtained.

If one does use the best simple molecular orbital calculation, i.e., without configuration interaction for the energy H_3[5], and subtracts from that the energy of a hydrogen molecule[10] and a hydrogen atom one obtains a value of 22 kcal for the activation energy. In an attempt to improve this value and still keep the calculation simple, the energy of the H_3^- species was calculated. Since the simple MO method is known to give good results for closed shells, and since the energy of the H_3 should be given to a good approximation by subtracting the first ionization of H_3^- from the total energy of H_3^-,[11] it was hoped that better results would be obtained from the activation energy. Unfortunately, this was not the case. Roothaan's self-consistent field method[11] for closed shells was applied to the species H_3^- at distances from 1.4 to 2.5 a.u. and for various values of the screening constant. The results obtained are recorded in Table I. If one picks the minimum value of the energy at each distance and plots the results, the curve shown in Fig. 3 is obtained. The energy at the minimum of the curve is −3.086 a.u. which corresponds to an activation energy of 41 kcal. Apparently this method cannot be used for species with a small number of electrons, but may still be useful for more complicated molecules in excited states.

It is to be emphasized that the approach used above differs considerably from the semiempirical method of Eyring and Polanyi to obtain numerical results. The

TABLE I. Energies of H_3 as a function of ξ and R[a].

R(a.u.)	ξ	$E(H_3^-)$(a.u.)	ϵ_2(a.u.)	$E(H_3)$(a.u.)
1.4	0.714	−2.365	−0.089	−2.276
	0.857	−2.694	0.098	−2.792
	1.000	−2.645	0.231	−2.876
	1.143	−2.509	0.432	−2.941
	1.429	−1.855	0.914	−2.769
1.6	0.750	−2.724	−0.069	−2.655
	0.875	−2.805	0.026	−2.831
	1.000	−2.792	0.182	−2.974
	1.250	−2.481	0.516	−2.997
	1.375	−2.239	0.666	−2.905
2.0	0.800	−2.909	−0.076	−2.833
	0.900	−2.936	0.018	−2.954
	1.000	−2.944	0.099	−3.043
	1.100	−2.923	0.163	−3.086
	1.250	−2.559	0.443	−3.002
2.2	0.950	−2.957	0.038	−2.994
	0.955	−2.972	0.039	−3.011
	1.000	−3.023	0.040	−3.063
	1.136	−2.791	0.236	−3.027
2.5	0.800	−2.972	−0.116	−2.856
	0.960	−2.982	0.005	−2.987
	1.000	−2.955	0.053	−3.008
	1.200	−2.482	0.379	−2.861

[a] 1 a.u. = 13.602 ev.

[9] A. Farkas and L. Farkas, Proc. Roy. Soc. (London) **152A**, 124 (1935).
[10] C. A. Coulson, Trans. Faraday Soc. **33**, 1479 (1937).
[11] C. C. J. Roothaan, Revs. Modern Phys. **23**, 69 (1951).

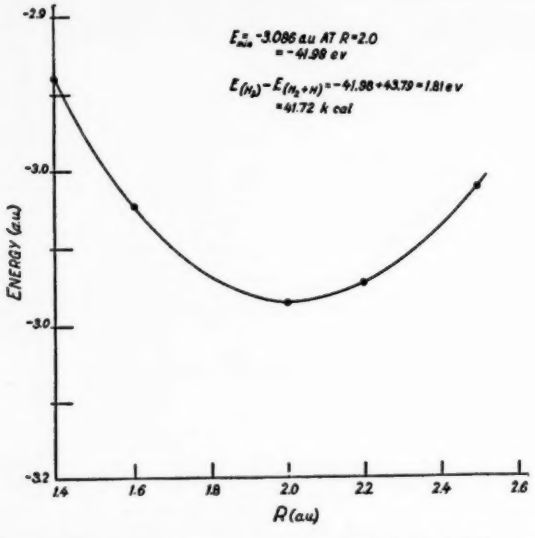

FIG. 3. Energy of H_3 as a function of internuclear distance.

latter used Morse potential functions along with spectroscopic data as well as the assumption that the Coulombic energy is 20 percent of the binding energy. The present method involves only the assumptions in the molecular orbital method with no dependence on experimental quantities.

DISCUSSION

As was pointed out by Griffing, the correlation diagram may be used to give some insight into the reasons why the activation energy for this reaction is so small. In this case, we have only three electrons taking part in the chemical reaction. Thus, in the "degenerate ambivalent complex," there are two electrons in the lowest orbital and only one in the second-lowest orbital. This means that the electronic energy of this ambivalent complex is much lower than for cases where four electrons play an essential part in the chemical reaction. Griffing has assumed that reactions between closed-shell molecules can be treated as a four-electron problem and therefore, in these cases, all four electrons have to be considered in the reaction. Since in the present reaction, only three electrons are involved and the electronic energy is thereby lower, it is to be expected that the activation energy for this process will be much smaller than for reactions between closed-shell molecules. Such an argument would apply to any atomic mechanism which would involve only three electrons. The argument can easily be extended to the interaction of two atoms where the activation energy is even smaller ($\sim$0) than for this case. These conclusions are borne out by experiment.

CONCLUSION

Using the simple molecular orbital theory, one can set up a correlation diagram connecting the energy levels of the initial, intermediate, and final stages of the $H+H_2$ process. This picture gives some insight into the behavior of the levels and also allows one to get a qualitative reason why the activation energy for an atomic mechanism is smaller than that for a molecular mechanism. It also shows that an ambivalent degeneracy in the levels appears as the "ambivalent degenerate complex" is formed. One may also get a qualitative picture how the orbital electronic distribution changes during the reaction. Finally, if one uses the LCAO molecular orbital calculations including configuration interaction, one can calculate an activation energy for this reaction of 8.76 kcal. It is expected that the picture presented here can be used for more complicated reactions.

ACKNOWLEDGMENTS

The authors would like to thank Dr. G. W. Castellan for many interesting and helpful discussions.

Long Time Phosphorescence of Organic Crystals*

HARTMUT KALLMANN, *New York University, Physics Department, Washington Square, New York, New York*
BERNARD KRAMER, *New York University, Physics Department, Washington Square, New York, New York,*
AND *Hunter College, Physics Department, Bronx, New York,*

AND

EUGENE SUCOV, *New York University, Physics Department, Washington Square, New York, New York*
(Received July 7, 1954)

Long time phosphorescence (of the order of minutes) of anthracene, stilbene, durene, and naphthalene crystals at room temperature is reported. The decays are approximately hyperbolic and the observed phosphorescence is shifted to longer wavelengths than the usual fluorescent emission. This phosphorescence is not induced by the light strongly absorbed in the substance but mainly by the weak absorption of light of wavelengths corresponding to their own fluorescent light. There are indications that this phosphorescence stems from an approximately uniform, continuous trap distribution and that such a mechanism permits a description of some of the observed behavior. Wavelength measurements seem to indicate that this phosphorescent light emission does not originate from triplet to ground transitions.

INTRODUCTION

THE light flashes in organic crystals such as anthracene and stilbene are known to decay in about 10^{-8} sec.[1] A further "long time" decay has been observed[1,2] with anthracene; several percent of the total emission is emitted after 10^{-6} to 10^{-4} sec. Longer decays (of the order of seconds) have been observed[3–5] using such organic materials dispersed in rigid media; such experiments are done at liquid nitrogen temperatures and the phosphorescence observed is ascribed to metastable triplet transitions since the phosphorescence occurs at greater wavelenths than the usual fluorescence.

The experiments reported in this paper describe a long time phosphorescence (of the order of minutes) at room temperature with single crystals of anthracene, stilbene, naphthalene, and durene.

EXPERIMENTAL

A. Apparatus

The experimental apparatus is shown in Figs. 1 and 2. A 1P28 photomultiplier was operated at 600 v, and the anode resistance could be varied from 10^{10} to 10^5 ohms. A ganged circuit to compensate for the dark current at the three upper ranges was used; in this way the sensitivity could be varied over the entire range without further shifting of the dc bias. The voltage across the anode resistor was placed at the grid of a Raytheon electrometer tube, and the output, in turn, was fed to a Sanborn dc Amplifier-Recorder. Thus the final recording showed the phosphorescent light emission as a function of time.

A double shutter arrangement was used to excite the crystal while the photomultiplier was shielded, and to shield the crystal from the exciting source while opening the photomultiplier to the phosphorescent radiation. Since only long time decays were recorded, the shutters were operated manually, so that the first points on the phosphorescent curve are of the order of a fraction of a second after excitation. Corning glass filters and Wratten neutral filters could be placed directly before the source or immediately under the crystal being investigated so that the wavelength and intensity of the exciting radiation could be varied, and the spectrum of the phosphorescent emission could be investigated.

The source of excitation was a 250 watt G.E. Uviarc mercury discharge tube. The intensity incident upon the crystal is shown in column 2 of Table I for the wavelength range used.

B. Effects of Exposure Time, Wavelength, and Intensity of the Incident Radiation

An anthracene crystal about 2 cm×2 cm×1 cm was excited by ultraviolet for varying amounts of time and exciting intensities. The resultant phosphorescent decay was recorded and plotted on a log-log scale. If the decay follows a law given by $I=K/t^n$, then a slope of 45° indicates $n=1$ or a hyperbolic decay, while steeper curves have $n>1$ and shallower curves have $n<1$. Figure 3 shows the results of exposure times of 1 sec, 30 sec, and 3 min on the above described crystal with ultraviolet excitation. The curves are all linear and at 45° angles, indicating hyperbolic decay. The phosphorescence due to 3 min exposure was roughly three times the phosphorescence due to 1 sec exposure throughout the entire decay interval of four minutes. With 3 percent exciting intensity the phosphorescent emission is not measurably different when the exposure time is decreased from 3 min to 30 sec and is about three times greater than that due to the one-second exposure time. (See Table I for these and follow-

* This work was supported by the Signal Corps Engineering Laboratories, Evans Signal Laboratory, Belmar, New Jersey.
[1] Bittman, Furst, and Kallmann, Phys. Rev. **87**, 83 (1952).
[2] F. B. Harrison, Nucleonics, March 1954, p. 24.
[3] G. N. Lewis and M. Kasha, J. Am. Chem. Soc. **66**, 2100 (1944).
[4] Lewis, Lipkin, and Magel, J. Am. Chem. Soc. **63**, 3005 (1941).
[5] D. S. McClure, J. Chem. Phys. **17**, 905 (1949) [see also P. Debye and J. O. Edwards, J. Chem. Phys. **20**, 236 (1952)].

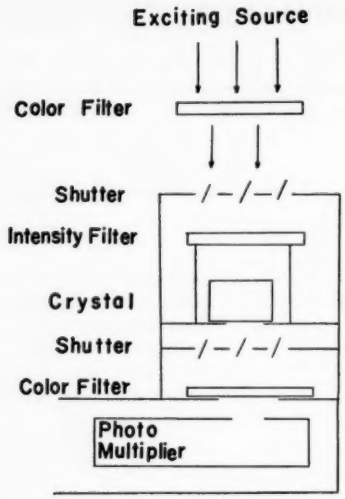

FIG. 1. Experimental arrangement for studying characteristics of phosphorescence in organic crystals.

ing results.) With one percent exciting intensity the exponent is smaller than 1 (~0.8) and there is a slight drop in phosphorescence between 3-min and 30-sec exposure time. The phosphorescence induced by a 1-sec exposure is too small to be measured. Comparing the longest exposure at 100 percent ultraviolet intensity with that 1000 times weaker, it is noted that the decrease in phosphorescent intensity is of the order of 20 for short decay times and of the order of ten for longer decay times.

Similar series of experiments were carried out with exciting light of wavelengths above 4000 A (3–74 Corning filter in front of the Hg arc) and of wavelengths above 4600 A (3–71 Corning filter in front of the Hg arc) and the results are shown in Table I. These longer wavelengths are much less absorbed than the shorter ones and excite the normal fluorescence spectrum much less. Since the excitation of the phosphorescence by ultraviolet is completely due to the absorption of the produced fluorescence and not due to the ultraviolet excitation directly (see next paragraph), the results obtained with longer wavelengths can be best understood as an excitation with much weaker intensity (less energy absorbed). In all cases two saturation phenomena of the phosphorescence are apparent: saturation with increasing intensity and with increasing exposure time. With decreasing excitation the exponent of the decay law becomes smaller. The intensities obtained with 4600 A light were too weak to allow a complete series of measurements.

Similar experiments with a small anthracene flake, about 0.5 mm thick and 1 cm² in area gave quite different results under 3660 A excitation. Although its fluorescent emission was greater than that of the large anthracene crystal, the phosphorescent yield was barely detectable under the same conditions. This small flake however, could be used for producing the phosphorescence of the large crystal, by placing it in front of the large crystal and irradiating both flake and crystal. Under these conditions, the phosphorescence of the latter was the same as when the crystal was directly irradiated (flake removed). This shows that the phosphorescence of the large crystal was not produced by the ultraviolet light directly but rather by the visible fluorescent radiation emitted from a thin layer of the crystal at the side of the incident radiation in which practically all ultraviolet light is absorbed.

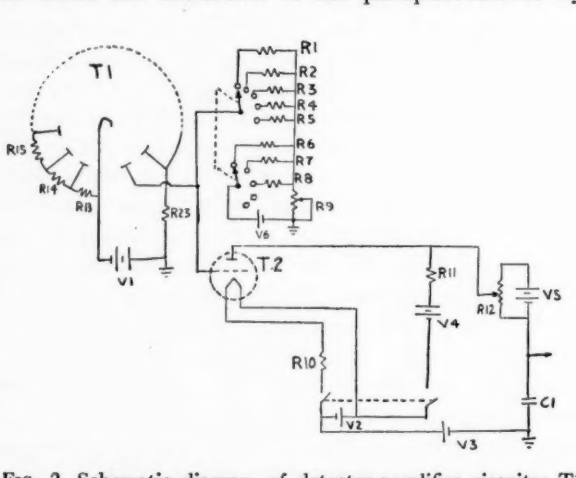

FIG. 2. Schematic diagram of detector-amplifier circuits: T1 Photomultiplier 1P28; T2 Electrometer Tube CK 5697; C1 1 microfarad; V1 600 v; V2 1.5 v; V3 1.5 v; V4 22.5 v; V5 22.5 v; V6 45 v; R1 10^{10} Ω; R2 10^{9} Ω; R3 10^{8} Ω; R4 10^{7} Ω; R5 10^{6} Ω; R6 10^{5} Ω; R7 10^{4} Ω; R8 10^{5} Ω; R9 200 Ω; R10 50 Ω; R11 47K Ω; R12 50K Ω; R13–R23 100K Ω.

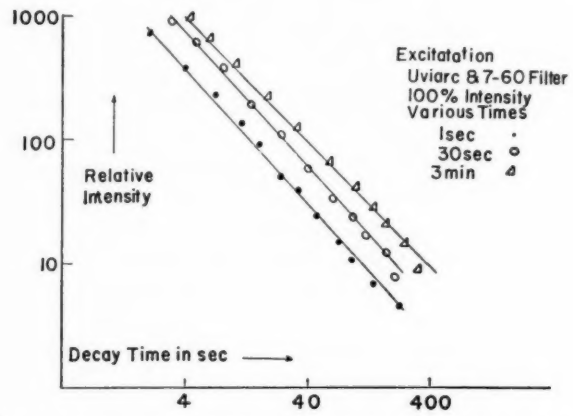

FIG. 3. Phosphorescent decay curves for anthracene under various conditions (uv full intensity).

Three other crystals were also investigated but not as thoroughly as anthracene. The data for a durene crystal (2 cm×1 cm×1 cm), stilbene crystal (3 cm radius, 3 cm thick), and naphthalene crystal (2 cm ×1 cm×0.5 cm) are given in Table I (see also Figs. 4 and 5). In these cases the 3660 A band is not strongly absorbed but falls within the fluorescent spectra of these materials.

The same saturation phenomenon with respect to exciting intensities was observed as in anthracene, and the phosphorescence is of the same order of magnitude.

TABLE I. Comparison of phosphorescent light intensities for various organic crystals.

Crystal	Type of light	Incident intensity	Exposure time	Phosphorescence after decay times of 4 sec	40 sec	200 sec	n
Anthracene	3660 A (uv)	100% (5×10^{-3} watt/cm²)	3 min	1000	100	20	1
			30 sec	750	60	10	1.1
			1 sec	355	30	5	1.03
		3%	3 min	300	30	6	1
			30 sec	300	30	6	1
			1 sec	130	9	···	1.17
		0.1%	3 min	52	8.2	···	0.80
			30 sec	40	6.3	···	0.79
	3–74 filter above 4000 A (visible)	100% (11.6×10^{-3} w/cm²)	3 min	600	50	9	1.08
			30 sec	600	50	9	1.08
			1 sec	270	25	5	1.03
		10%	3 min	220	30	7.5	0.86
			30 sec	200	25	7.5	0.90
		1%	3 min	32	7	···	0.66
			30 sec	32	7	···	0.66
				8 sec	40 sec		
	3–71 filter above 4600 A (visible)	100% (8×10^{-3} w/cm²)	3 min	15	4.5	···	0.75
			30 sec	15	4.5	···	0.75
		10%	3 min	7	2.8	···	0.56
			30 sec	7	2.8	···	0.56
				1 sec	4 sec		
Durene	3660 A (uv)	100%	1 min	7000	900		1.48
		3%	1 min	4800	390		1.81
				1.6 sec	4 sec	40 sec	
Stilbene	3660 A (uv)	100%	1 min	650	280	40	0.85
		3%	1 min	650	90	10	nonlinear
				4 sec	40 sec		
Naphthalene	3660 A (uv)	100%	1 min	500	26		1.28
		3%	1 min	140	10		1.15

It is also interesting to note that while anthracene and naphthalene indicate decreasing n with decreasing excitation intensity, durene shows an n which increases under these conditions.

With solid phenyl ether whose melting point is near room temperature, a noticeable phosphorescence was observed which, however, disappeared upon liquification. No spectral or intensity investigations were carried out.

C. Spectral Distribution of Phosphorescence

The spectral distribution of the emitted phosphorescence was measured by interposing a series of cut-off Corning color filters between the excited crystal and the photomultiplier. The difference of phosphorescent light output for two filters, reduced to the same photomultiplier sensitivity, supplies the phosphorescence emitted in the wavelength range transmitted by one of the filters and not by the other. The crystal was again exposed for one minute, and approximately 0.5 second later the phosphorescent emission was allowed to pass through the filter and into the photomultiplier. The following general results were obtained.

(1) For all crystals the log-log decay curves are linear and parallel (except for durene) and an approximately hyperbolic decay is observed for all wavelengths of phosphorescence.

(2) Comparing the results obtained for various filters and taking the wavelength dependence of the photomultiplier into account, a maximum in the phosphorescent intensity is found around 5200 A for all these crystals, while very little intensity is observed below 5000 A or over 6000 A.

The light which excites the phosphorescence of these crystals also produces a fluorescence which was found to be different from the normal fluorescent spectrum†; it was shifted toward longer wavelengths. For anthra-

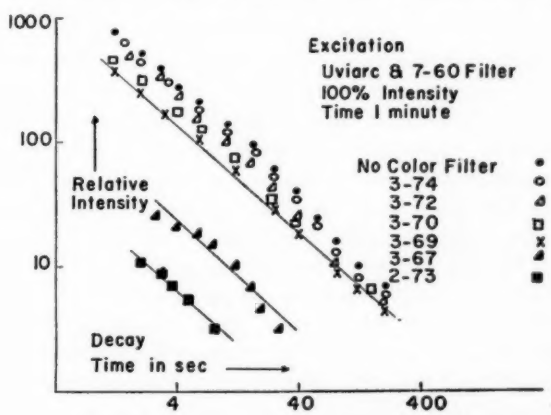

FIG. 4. Phosphorescence decay curves for stilbene in various spectral regions.

† Measured with a Bausch and Lomb monochromator.

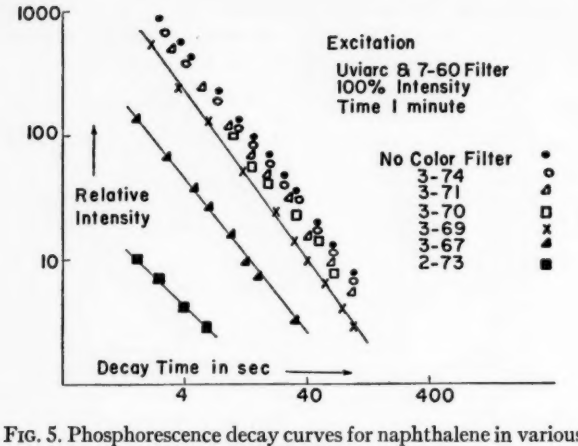

FIG. 5. Phosphorescence decay curves for naphthalene in various spectral regions.

cene, stilbene, and naphthalene it was in the same wavelength region as the respective phosphorescence; for durene this fluorescence was shifted to the ultraviolet.

CONCLUSIONS

From the foregoing results it is seen that (a) a long-time, approximately hyperbolic phosphorescence (of the order of minutes) exists in a number of organic materials; (b) this phosphorescence is of a longer wavelength than the usual fluorescent emission and is mainly excited by radiation of longer wavelengths than that necessary to excite the normal fluorescent band; (c) two saturation effects exist such that the increase in phosphorescent emission is appreciably less than proportional to the increase in excitation intensity and to the increase in exposure time; (d) the spectrum of the observed phosphorescence is not appreciably changed during the decay.

Two possible mechanisms leading to hyperbolic decay will be noted here. First, there may be a continuous distribution of trap levels each containing the same number of traps. If the trapped energy is released to emission centers by thermal vibrations of the lattice, a hyperbolic decay will result.[6] Actually a number of discrete levels with a suitable number of traps can lead to practically the same decay. Second, there may be N excited centers and two possibilities of recombination; one monomolecular, proportional to N, and one bimolecular recombination, proportional to N^2. If the monomolecular recombination ($\alpha_1 N$) is radiative, while the other ($\alpha_2 N^2$) is nonradiative but much more frequent, a hyperbolic light decay will be obtained, since the light emission is proportional to N.

The continuous trap level mechanism seems to be the better choice. It explains not only the almost hyperbolic decay, but also the observed dependence on intensity and exposure time (see appendix). The monomolecular plus bimolecular mechanism always leads to the same absolute value of phosphorescence for a given substance (given by $\alpha_1/\alpha_2 t$) when the hyperbolic portion is reached, independent of excitation intensity and exposure time. Deviations from the hyperbolic law should occur mostly at short decay times and for short exposure times for this mechanism. This is not borne out by the observations.

The shift of this long time phosphorescence to longer wavelengths may be interpreted as an emission from a long-living triplet state whose energy is below the singlet state (fluorescent emission). However, these known triplet levels differ appreciably depending on the organic crystals investigated[5,7]; anthracene should have a phosphorescence in the infrared while durene should be in the visible. The experiments do not display such a shift. Although the described method of checking the spectrum of the phosphorescence is not very exact,‡ the difference to be expected on the basis of the triplet theory should be easily discernible.

In investigations concerning the triplet state it is assumed that it is reached via the singlet due to the small probability of the excited singlet molecules going over into the triplet state. If this would be true, strong phosphorescence should be associated with strong fluorescence. This, however, is not the case, as the experiments with the anthracene flake indicate. The latter showed a barely observable phosphorescence but even a larger fluorescence than the crystal.

Thus these experiments show that the long-living state is excited directly. Again one could conjecture that the absorption leading to the phosphorescence emission goes to the triplet state. The wavelengths mainly responsible for the phosphorescence in anthracene seem to exclude this possibility. The phosphorescence reported in this paper was observed at room temperatures and may not be related to the low temperature phosphorescence previously observed.[5]

No experiments were performed to decide the question of whether the energy levels responsible for phosphorescence are due to impurities or lattice defects. It may only be remarked that because of the weak absorption of the light producing phosphorescence in these crystals, such levels whether intrinsic or due to impurities, must have a concentration less than 10^{16} molecules per gram.

APPENDIX

If there are N_i occupied traps per cm^3 and per energy level of width dE_i, and the electron (or hole) is released directly to emission centers (negligible or constant retrapping) the following equation is obtained[6] for L, the number of quanta emitted in the phosphorescence,

$$L=\frac{N_i kT}{t}\left[e^{-t/\tau_D}-e^{-t/\tau_s}\right], \qquad (1)$$

[6] J. T. Randall and M. H. F. Wilkins, Proc. Roy. Soc. (London) A184. 347 (1945).

[7] J. R. Platt, J. Chem. Phys. 17, 484 (1949).

‡ The phosphorescent intensity is limited since the saturation effect discussed above prevents an appreciable increase in phosphorescent intensity thus making more accurate measurements extremely difficult.

where N_i is the same for all levels of the different energy E; where τ_D and τ_s are lifetimes of the deepest and shallowest traps, respectively, and where for a trap level E_i the lifetime is given by $\tau_i=\tau_0 e^{E_i/kT}$ (τ_0 assumed the same for all traps). For $\tau_D \gg t \gg \tau_s$ this reduces to

$$L=N_i kT/t. \tag{2}$$

The filling of the individual trap levels will now be considered. Let N_i be the number of filled traps of the ith level, N_{0i} the total number of traps/cm³ of the ith level, and assume (a) that incident radiation (I) fills the traps directly, and (b) that the rate of release from the traps is proportional to N_i. Then we may write

$$\dot{N}_i=\alpha I(N_{0i}-N_i)-\delta_i N_i, \tag{3}$$

where $\delta_i=1/\tau_i$ and αI is the number of excitations/cm³ sec.

Solving:

$$N_i=\frac{\alpha I N_{0i}}{\alpha I+\delta_i}[1-e^{-(\alpha I+\delta_i)t_{\exp}}], \tag{4}$$

where $t_{\exp}$ is the exposure time. This gives the number of occupied traps (after the time $t_{\exp}$) in the ith level.

Saturation due to prolonged exposure time is obtained when $t_{\exp}(\alpha I+\delta_i)$ is large compared to 1 for all δ_i which contribute to the phosphorescence in the observed time interval. When this occurs, the expression for N_i becomes

$$N_i=\alpha I N_{0i}/(\alpha I+\delta_i).$$

Thus, for αI large compared to δ_i, N_i becomes independent of the intensity and equal to N_{0i} so that all traps are filled uniformly, satisfying the conditions for (2). If, however, αI is small compared to δ_i, the expression becomes

$$N_i=\alpha I N_{0i}/\delta_i.$$

In this case the number of occupied traps in any level is proportional to the exciting intensity and depends on the depth of the level (through δ_i). Thus the traps are not filled uniformly, and a departure from a hyperbolic decay would be obtained. According to these considerations, such a departure should begin to occur when deviations from saturation begin to become noticeable for long exposure times because of low intensity. This may be the reason for the observed decrease in slope with decreasing intensities. As long as $\alpha I \gg \delta$ for all δ_i contributing to (2), uniform trap distributions are obtained for all exposure times, but the occupation of the traps and thus the intensity of the phosphorescence would depend on the intensity and the exposure time. The hyperbolic decay law would still hold. For very short exposure time the uniform trap distribution and thus the hyperbolic decay law would even prevail when $\alpha I<\delta_i$, as long as $t_{\exp}\delta_i<\frac{1}{2}$, since for this condition

$$N_i \cong \alpha I N_{0i} t_{\exp},$$

again yielding a uniform trap distribution, but now proportional to both the excitation and exposure time. It is a peculiarity of the uniform trap distribution that it provides for a hyperbolic decay law for quite different types of excitations.

Since the spectral distribution of the phosphorescence does not change during the decay, it must be assumed that all traps empty to the same band of emission levels; that is, the terms $\delta_i N_i$ in (3) are transitions to the same levels independent of the trap level.

THE JOURNAL OF CHEMICAL PHYSICS VOLUME 23, NUMBER 6 JUNE, 1955

Infrared Absorption Spectra of Monodeuterated Pyridines

F. Allan Andersen, Børge Bak, Svend Brodersen, and John Rastrup-Andersen
Chemical Laboratory of the University of Copenhagen, Copenhagen, Denmark

(Received October 18, 1954)

For this work 2*D*-, 3*D*-, and 4*D*-pyridine have been prepared from corresponding halogen compounds. The infrared spectra of the compounds in the liquid phase are reported over the spectral range 400–3200 cm⁻¹. Interpretation of the spectra is carried through by analogy with the spectra of isotopic benzenes, pyridine, and pyridine-d_5.

In connection with microwave studies of the monodeuterated pyridines reported elsewhere,[1] infrared absorption curves of these compounds in the liquid state were simultaneously taken, primarily in order to check the purity of the samples. Since the spectra obtained were pretty different without showing signs of being spectra of mixtures (except for a small contamination with ordinary pyridine) we throught it worthwhile to study them in further detail. The present paper will demonstrate that these spectra can be interpreted within the general frames known to work so well for benzene and its deuterated species[2,3] and it will also

[1] Bak, Hansen, and Rastrup-Andersen, J. Chem. Phys. **22**, 2013 (1954).

[2] A. Langseth and R. C. Lord, Kgl. Danske Vidensk. Selskab, Mat.-fys. Medd. **16**, No. 6 (1938).

[3] C. K. Ingold *et al.*, J. Chem. Soc. (London) **1946**, 222 and following papers.

TABLE I. Observed infrared spectra of liquid 2, 3, and 4 deuteropyridine.

2*D*-pyridine Frequency cm^{-1}	*D*	3*D*-pyridine Frequency cm^{-1}	*D*	4*D*-pyridine Frequency cm^{-1}	*D*
405	∞	404	∞		
600	0.88	599	0.76	597	0.83
620–70	∞ at 638	620–70	∞ at 632	620–70	∞ at 633
748	1.4	688	0.12	743	0.22
814	∞	717	∞	834	0.09
834	0.2	796	0.07	862	∞
901	0.55	823	1.2	*ca.* 890	0.1
970	0.06	848	0.76	968	0.09
989	0.83	902	0.01	980	0.15
ca. 997	0.3	938	0.06	989	1.1
1029	0.58	965	0.12	1012	0.85
1059	0.63	980	0.73	1015	0.81
1100–15	0.07	1033	0.75	1068	0.56
1149	0.53	1050	0.16	1086	0.26
1212	0.02	1086	0.09	1121	0.06
1294	0.44	1108	0.32	1193	0.04
1357	0.04	1128	0.15	1215	0.52
1378	0.06	1195	0.53	1237	0.03
ca. 1400	0.09	*ca.* 1200	0.4	1269	0.01
1424	∞	1217	0.08	1347	0.05
1461	0.88	1242	0.02	1374	0.06
1565–85	∞	1262	0.02	*ca.* 1390	0.06
1590	0.85	1337	0.09	1413	∞
1629	0.08	*ca.* 1367	0.05	1476	0.97
1716	0.05	*ca.* 1390	0.15	1559	1.3
1783	0.03	1416	∞	1575	∞
1798	0.03	1468	1.0	1591	1.0
1867	0.05	1560–80	∞	1604	0.20
1894	0.04	1586	1.3	1744	0.07
1927	0.04	1632	0.06	1825	0.04
1960	0.07	1760	0.02	1861	0.05
1987	0.05	1785	0.04	1948	0.11
2165	0.02	1869	0.03	2074	0.02
2235	0.07	1896	0.07	2153	0.01
2258	0.57	1928	0.09	2198	0.02
2300	0.04	1949	0.08	2225	0.01
2362	0.02	1976	0.04	2270	0.09
2412	0.01	2013	0.02	2285	0.15
2445	0.01	2029	0.01	2300	0.06
2483	0.01	2234	0.02	2335	0.02
2534	0.01	2253	0.04	2399	0.02
2596	0.01	2289	0.08	2425	0.02
2859	0.03	2389	0.02	2473	0.01
2911	0.09	2439	0.01	2545	0.01
2928	0.05	2458	0.01	2563	0.01
ca. 2961	0.08	2542	0.01	2625	0.01
ca. 2977	0.14	2595	0.01	2641	0.01
ca. 2989	0.25	2855	0.03	2657	0.01
3000	0.50	2876	0.07	2686	0.01
ca. 3040	0.36	2904	0.06	2872	0.09
3051	0.49	2918	0.08	*ca.* 2920	0.05
ca. 3068	0.50	2927	0.08	2940	0.09
3075	0.53	2976	0.29	2968	0.37
3137	0.10	2993	0.29	2992	0.23
3165	0.07	3004	0.36	3008	0.42
		3022	0.53	3019	0.57
		3038	0.90	3033	0.71
		3053	0.63	3069	0.80
		3077	0.41	*ca.* 3125	0.04
		3133	0.08	*ca.* 3140	0.03
		3151	0.05		

build on the paper by Lord and collaborators on pyridine and "heavy" pyridine,[4] being in almost every respect consistent with this work. The present investigation suffers from the fact that because of lack of equipment neither the infrared spectra of the vapors, nor the Raman spectra could be obtained, but it is felt that this default may be less important because of the existing elaborate investigations on benzene, pyridine, and their deuterated species already referred to.

[4] Corrsin, Fax, and Lord, J. Chem. Phys. **21**, 1170 (1953).

PREPARATIONS AND INFRARED SPECTRA

The preparations are described in the paper on the microwave absorption.[1] Both microwave and infrared spectra showed that the samples were pure except for a trace of ordinary pyridine. The infrared spectra referred to earlier[1] were recorded on a Beckmann I.R. 2 instrument with NaCl optics. The spectra to be discussed here were taken on a Beckmann I.R. 3 under successive application of KBr, NaCl, and LiF optics so that the 400–3200 cm^{-1} spectral region was covered. The effective slit width was 2–5 cm^{-1}. The cell thickness applied was constantly 0.03 mm. We had to refrain from varying the cell thickness since the amount of sample was small (0.3 cc) and had to be conserved for studies of ultraviolet absorption. The true shape of a few strong bands, the optical densities of which are given as "∞" in Table I, is therefore unknown to us but lack of this information did not prove to be serious. The curves recorded experimentally are plotted in Fig. 1, only the dotted part of the curves represent calculated *D*-values. The measurements were made without a reference cell so that the densities include the reflexion and absorption losses in the cell. The frequencies of all the bands observed, which are thought to be good to ± 1 cm^{-1}, are reported in Table I together with the optical densities at the maxima. These densities were calculated by subtracting probable values of the density of the cell from the directly read *D*-values so that they represent, of course, only a rough measure of the true intensity, especially for overlapping lines. In order to obtain optimal conditions for a comparison with the spectrum of ordinary pyridine this substance was reinvestigated with the same technique previously used. The result was a nice confirmation of the observations made by Lord and collaborators.[4] Additional weak lines were found at 1207, *ca* 1407, 1947, 2038, 2136, 2212, 2258, 2269, 2365, 2426, 2487, 2600, 2628, 2831, 2855, 2921, 2931, 2987, and 3145. The strong line observed by Lord at 3036 was found to be split in two lines at 3025 and 3032 cm^{-1}.

DISCUSSION OF SPECTRA

Table II gives the assignments of the normal vibration frequencies for the monodeuterated pyridines together with the corresponding assignments for C_6H_6, C_6D_6, C_5H_5N, and C_5D_5N adopted by Lord[4] and the assignments for C_6H_5D, $C_6H_4D_2$(*para*-), and $C_6H_2D_4$-(*para*-) given by Ingold and collaborators.[3] The criteria used for assigning the frequency of an observed line to a particular normal vibration are the usual ones. (1) The frequency must lie inbetween the corresponding frequencies for "light" and "heavy" pyridine. Exceptions to this rule are known from other cases but they are

rare. (2) The intensity of the line must be compatible with the intensity of the corresponding line in the spectra of the various isotopic benzenes and pyridines (with due regard to differences in selection rules). (3) If the "parent" normal vibration is a "carbon"-vibration, the normal vibration frequency of a monodeuterated species must lie close to the corresponding pyridine frequency. If it is a "hydrogen" vibration it must be chosen in a way consistent with the corresponding choice made in the case of the partly deuterated benzenes. (4) If the line in question cannot possibly be interpreted as a combination or overtone, it must be one of the normal vibrations of the molecule. (5) Any complete set of normal vibration frequencies chosen must obey the Teller-Redlich product rule.

In the spectrum of 4*D-pyridine* the assignment of the fifteen vibrations number 1, 6a, 8a, 9a, 12, 18a, 19a, 6b, 8b, 15, 18b, 19b, 4, 10b, and 11 is evident according to the criteria (1), (2), and (3). Of the remaining twelve normal vibrations, five are hydrogen or deuterium stretching frequencies which are going to be discussed separately together with the corresponding vibrations in 3*D*- and 2*D*-pyridine. It remains to explain the assignment of the seven normal vibrations number 3, 14, 10a, 16a, 16b, 17a, and 5.

ν_3

Both ν_3 and ν_{9a} have been located at 1215, largely for the same reasons as given by Lord for pyridine where the line at 1218 also has been interpreted as double. The assignment gets important support from the fact that *pairs* of lines are observed in the spectra of 3*D*-pyridine (1217, 1195) and 2*D*-pyridine (1212, 1149).

ν_{14}

This vibration is a typical carbon vibration. The assignment given for all three monodeuterated pyridines is mainly based on the observation of the line at 1337 in the spectrum of 3*D*-pyridine as the prominent line in this spectra region. This assignment may be slightly incompatible with Lord's assignment for pyridine but harmony may be achieved if for pyridine $\nu_{14}=1357$ (likewise observed by Lord) and if the line at 1375 in pyridine is interpreted as 16b+17a=405 +981=1386.

ν_{10a}

This vibration is an out-of-plane hydrogen deformation frequency. Teller's product rule shows ($\tau=1.00$) that all three vibrations of the A_2 class must lie close to the corresponding pyridine frequencies. Here it is convenient also to discuss ν_5, which, in the deuterated pyridine species must be located in the 800–900 interval. Furthermore ν_{10a} and ν_5 in pyridine (886, 942) are weak, and therefore they must also be expected to be weak in the 4*D*-pyridine spectrum. The two *weak* lines, 890 and 834 observed in the 4*D*-spectrum

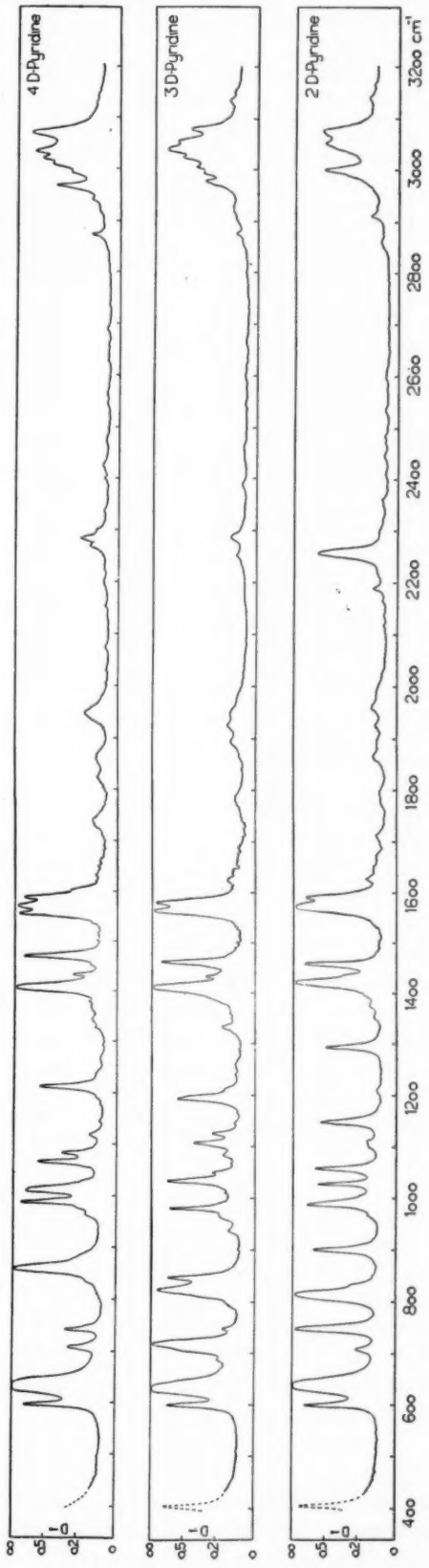

FIG. 1. Infrared spectra of 2*D*-, 3*D*-, and 4*D*-pyridine.

TABLE II. Compilation of normal vibration frequencies for C_6H_6, C_6H_5D, $C_6H_4D_2$(*para*-), $C_6H_2D_4$(*para*-), C_6D_6, C_5H_5N, C_5D_5N together with assignment here suggested for monodeuterated pyridines.

Vib. No.	Species $D_{6h}C_{2v}V_hC_s$	C_6H_6	C_6H_5D	$C_6H_4D_2$	$C_6H_2D_4$	C_6D_6	C_5H_5N	C_5D_5N	4*D*-Py	3*D*-Py	2*D*-Py
1	$A_{1g}A_1A_gA'$	992	980	978	961	945	992	962	989	980	989
2	$A_{1g}A_1A_gA'$	3062	3055	3055	2285	2293	3054	2293	3033[a]	3038[a]	3040[a,b]
6a	$E_g^+A_1A_gA'$	606	601	597	589	579	605	582	597	599	600
7a	$E_g^+A_1A_gA'$	3048	3060	2280	3045	2266					
8a	$E_g^+A_1A_gA'$	1595	1591	1587	1572	1553	1580	1530	1575	1570	1576[b]
9a	$E_g^+A_1A_gA'$	1178	1176	1173	862	869	1218	887	1215	1195	1149
12	$B_{1u}A_1B_{2u}A'$	1010	1007	992	977	962	1029	1006	1015	1033	1029
13	$B_{1u}A_1B_{2u}A'$	3060	2269	2275	3078	2290	3054	2270	2285	3053[a]	3051[a]
18a	$E_u^-A_1B_{2u}A'$	1035	1031	1033	819	813	1068	823	1068	1050	1059
19a	$E_u^-A_1B_{2u}A'$	1485	1480	1469	1353	1333	1482	1340	1476	1468	1461
20a	$E_u^-A_1B_{2u}A'$	3080	3066	3060	2280	2294	3036	2254	3019[a]	3022[a]	2258[a]
3	$A_{2g}B_1B_{1g}A'$	1326	1292	1309	1255	1037	1218	908	1215	1217	1212
6b	$E_g^+B_1B_{1g}A'$	606	603	601	586	579	652	625	645[b]	650[b]	640[b]
7b	$E_g^+B_1B_{1g}A'$	3048	3041	3042	2272	2266	3054	2285	3069[a]	2289[a]	3068[b]
8b	$E_g^+B_1B_{1g}A'$	1595	1574	1569	1564	1553	1572	1542	1559	1570	1570[b]
9b	$E_g^+B_1B_{1g}A'$	1178	1076	909	954	869					
14	$B_{2u}B_1B_{3u}A'$	?				?	1375	1322	1347	1337	1357
15	$B_{2u}B_1B_{3u}A'$	1160	1158	1106	1057	830	1148	887	1086	1108	1112[b]
18b	$E_u^-B_1B_{3u}A'$	1035	858	814	812	813	1068	833	862	848	834
19b	$E_u^-B_1B_{3u}A'$	1485	1450	1413	1439	1333	1439	1301	1413	1416	1424
20b	$E_u^-B_1B_{3u}A'$	3080	3079	3079	2280	2294	3083	2293	3069[a]	3077[a]	3075[a]
10a	$E_g^-A_2B_{2g}A''$	850	850	850	664	664	886	690	890[b]	823	814
16a	$E_u^+A_2A_uA''$	405	405	405	352	350	374	329	365[b]	350[b]	360[b]
17a	$E_u^+A_2A_uA''$	970	970	970	793	790	981	798	968	965	970
4	$B_{2g}B_2B_{3g}A''$	703	698	634	615	601	675	625	660–70	670[b]	660–70
5	$B_{2g}B_2B_{3g}A''$	993	995	967	930	827	942	762	834	902	901
10b	$E_g^-B_2B_{3g}A''$	850	778	736	767	664	749	567	743	717	748
11	$A_{2u}B_2B_{1u}A''$	671	608	597	548	497	703	530	633	632	638
16b	$E_uB_2B_{1u}A''$	405	380	367	383	350	405	371	383[b]	404	405
17b	$E_uB_2B_{1u}A''$	970	922	876	925	790					

[a] Assignment only tentative.
[b] Frequency value only approximate.

which cannot be overtones, are accordingly interpreted as ν_{10a} and ν_5, respectively. Support for this assignment is obtained when the 3*D*- and 2*D*-spectra are considered. Here, ν_{10a} (which is forbidden by symmetry in pyridine and 4*D*-pyridine and conceivably only appears because the spectra of *liquids* are investigated) is allowed, so that the strong lines at 823(3*D*) and 814(2*D*) may be interpreted as ν_{10a}. Correspondingly, there is a weak line at 902 in the 3*D*-spectrum which may conveniently be assigned to ν_5. In the 2*D*-spectrum, $\nu_5=901$, in spite of the fact that this line is strong (see later). Teller's product rule then gives $\nu_{16b}=383$ cm^{-1}.

ν_{17a}

From the spectra of the isotopic benzenes it is seen that this frequency must be close to the pyridine frequency 981. The observed 4*D*-spectrum offers a choice between lines at 980 and 968. Since in the 3*D*- and 2*D*-spectra only one possibility exists for ν_{17a} (965, 970, respectively), we prefer 968 as the ν_{17a} for 4*D*-pyridine while 980 may be interpreted as a combination tone (see the aforementioned and later).

ν_{16a}

Although unobserved by us this frequency is certain to be located in the 374–329 region (not examined by us). Since the two remaining fundamentals in the A_2 class are fixed at 890 and 968, ν_{16a} may be calculated by the product rule. This results in $\nu_{16a}=376$ cm^{-1}. Its real value is probably close to 360-65.

In the spectrum of *3D-pyridine* assignments of vibrations number 1, 6a, 8a, 12, 18a, 19a, 6b, 8b, 14, 18b, 19b, 10a, 17a, 4, 5, 10b, 11 and 16b (18 vibrations) seem undisputable according to the criteria (1), (2), (3), and the previous discussion for 4*D*-pyridine. The discussion concerning the hydrogen and deuterium stretching vibrations is postponed, so that here only comments on the vibrations number 3, 9a, 15, and 16a are necessary. Both ν_3 and ν_{9a} are planar hydrogen deformation vibrations. Experience from the deuterated benzenes suggest that they must lie close to the pyridine frequencies, *viz.* 1218 (double). Experimental frequencies at 1217 and 1195 are at disposal. In the 2*D*-spectrum the corresponding possibilities are 1212 and 1149. It seems difficult to make a rational choice between the two possibilities for an assignment. If one considers the

TABLE III. Summary of observed (strong) lines in the 3020–3080 cm^{-1} region in the pyridine and the monodeuterated pyridine spectra.

Pyridine	4*D*-Py	3*D*-Py	2*D*-Py
3025	3019	3022	No strong line
3032	3033	3038	3040
3053	No strong line	3053	3051
3079	3069	3077	3068
			3075

TABLE IV. Possible assignments for overtones.

Assignment	Pyridine Obs.	Pyridine Calc.	4D-pyrid. Obs.	4D-pyrid. Calc.	3D-pyrid. Obs.	3D-pyrid. Calc.	2D-pyrid. Obs.	2D-pyrid. Calc.	Pyridine-d_5 Obs.	Pyridine-d_5 Calc.
2×16b	810	810	···	780	796	808	[814]	810	···	742
16a+11	[1068][a]	1077	980	998	[980]	982	997	998	···	859
2×16a	[749]	748	···	730	688	700	707[b]	720	···	658
16a+6a	inact.	979	inact.	962	938	949	[970]	960	inact.	911
16b+11	···	1108	1012	1023	1033	1036	[1029]	1043	[908]	901
16a+10b	···	1123	[1086]	1108	1086	1067	1103	1108	[886]	896
16b+10b	[1148]	1154	1121	1133	1128	1121	1149	1153	···	938
2×6a	1207	1210	1193	1194	1200	1198	···	1200	1143[c]	1164
6a+11	1296	1308	1237	1230	1242	1231	···	1238	···	1112
16b+5	[1357]	1347	[1215]	1224	···	1306	1294	1306	1143[c]	1133
16b+17a	1375	1386	[1347]	1358	1367	1369	1378[c]	1375	···	1169
2×11	1407[c]	1406	1269	1266	1262	1264	···	1276	1043	1060
4+10b	1407[c]	1424	1390[c]	1403–13	1390	1387	1400	1408–18	···	1192
16b+12	[1441]	1434	1390[c]	1405	1438[b]	1437	1436[b]	1434	1364	1377
11+10b	[1441]	1452	1374	1376	[1337]	1349	1378[c]	1386	···	1097
16a+3	[1583]	1592	[1575]	1580	[1570]	1567	[1576]	1572	1228	1237
6a+1	1599	1597	1591	1586	1586[c]	1579	1590[c]	1589	1550	1544
6a+12	1633	1634	1604[c]	1612	1632	1632	1629	1629	1581[c]	1588
11+17a	1682	1684	1604[c]	1601	1586[c]	1597	1590[c]	1608	[1322]	1328
14+16a	···	1731	···	1712	···	1687	1716	1717	1645	1651
10b+12	···	1778	1744	1758	1760	1750	1783[c]	1777	1581[c]	1573
1+10a	inact.	1878	inact.	1879	1785	1803	1798	1803	inact.	1652
16b+19a	1872	1887	1861	1866	1869	1872	1867	1866	···	1711
9a+11	1923	1921	1825	1848	···	1827	1783[c]	1787	1414	1417
9a+10b	1947	1967	1948[c]	1958	1896	1912	1894	1897	1450	1454
8a+16b	1987	1985	1948[c]	1965	1976	1974	1960	1981	1918	1901
10a+15	2038[c]	2034	···	1976	1928	1931	1927[c]	1926	1581[c]	1577
6a+19b	2038[c]	2044	···	2010	2013	2015	···	2024	1863	1883
1+15	2136	2140	2074[c]	2075	···	2088	···	2101	1850	1849
6a+8b	···	2177	2153	2156	···	2169	2165[c]	2170	2117	2124
15+18b	2212	2216	1948[c]	1948	1949	1956	1927[c]	1946	···	1720
9a+12	2258	2247	2225	2230	2234	2228	2165[c]	2178	···	1893
8a+11	2269	2283	2198	2208	···	2202	···	2214	2042	2060
9a+18b	2293	2286	2074[c]	2077	2029	2043	1987	1983	···	1720
9a+15	2365	2366	2300	2301	[2289]	2303	[2258]	2261	···	1774
2×3	2426	2436	2399	2430	2439[c]	2434	2412	2424	1806	1818
8b+10a	2454[c]	2458	2425	2449	2389	2393	2362	2384	···	2232
1+19a	2454[c]	2474	2473[c]	2465	2439[c]	2448	2445	2450	[2285]	2302
18b+19b	2487[c]	2507	2270	2275	2253	2264	2235	2258	2117[c]	2134
18a+19b	2487[c]	2507	2473[c]	2481	2458	2466	2483	2483	2117[c]	2124
18b+19a	···	2550	2335	2338	[2289]	2316	2300	2295	···	2173
1+8a	···	2572	2545	2564	2542	2550	2534	2565	2460	2492
8b+12	2600	2601	2563	2574	2595[c]	2603	2596[c]	2599	2566	2548
8b+18a	2628[c]	2640	2625	2627	2595[c]	2620	2596[c]	2629	···	2365
8a+18a	2628[c]	2648	2641	2643	2595[c]	2620	···	2635	···	2353
9a+19a	···	2700	2686	2691	···	2663	2596[c]	2610	···	2227
8a+15	···	2728	2657	2661	···	2678	···	2688	2389	2417
19a+19b	2908	2921	2872[c]	2889	2855	2884	2859[c]	2885	···	2641
6a+13			2872[c]	2882					···	
6a+7b					2876	2888				
6a+20a							2859[c]	2858		
8b+14	2921	2929	2920[c]	2906	2918	2907	2911[c]	2927	···	2864
8a+14	2931	2937	2920[c]	2922	2904	2907	2928	2933	···	2852
2×19a	2960	2964	2940	2952	2927	2936	2911[c]	2922	···	2680
8b+19b	2987	3011	2968	2972	2976[c]	2986	2977	2994	···	2843
8a+19b	3004	3019	2992	2988	2976[c]	2986	2989	3000	···	2831
8b+19a	[3032]	3054	3008	3035	3004	3038	3000	3031	···	2882
8a+8b	3145[c]	3152	3125	3134	3133	3140	3137	3146	···	3072
2×8a	3145[c]	3160	3140	3150	3151	3140	3165	3152	···	3060

[a] The symbol [ ] indicates obscured by normal vibration frequency.
[b] Obscured by impurity of pyridine.
[c] More than one combination assigned to this frequency.

corresponding frequencies in the benzene series it is noted that ν_{9a} is the more sensitive to isotopic substitution. Based on this and remembering that 1195(3*D*) and 1149(2*D*) are both strong while 1217(3*D*) and 1212(2*D*) are weak the assignment in Table II has been chosen.

ν_{15}

Corresponding to the three experimental frequencies 1086, 1108, and 1128 we can place two combination tones in addition to the fundamental in this spectral region. The combinations are 16a+10b=1067 (or the almost coinciding 16b+4=1074) and 16b+10b=1121.

Therefore, either 1108 or 1128 must be a fundamental. Since 1108 is by far the stronger we put $\nu_{15}=1108$.

ν_{16a}

Its position may be estimated in much the same way as done for 4*D*-pyridine. Also, we think that the line observed at 688 may be the first overtone, so that $\nu_{16a}=ca$ 350.

In the spectrum of *2D-pyridine* assignment of the frequencies number 1, 6a, 8a, 9a, 12, 18a, 19a, 3, 6b, 8b, 14, 15, 18b, 19b, 10a, 17a, 4, 10b, 11, and 16b (20 lines) is not subject to discussion because of criteria (1), (2), (3), and arguments already presented. It remains to discuss ν_{16a} and ν_5. The magnitude of ν_{16a} is inferred from the observed combinations 16a+11=997, 16a+10b=1103, and 11+10b=1378. The reason for mentioning ν_5 separately is not dictated by its position, which is quite suitable, but by its measured intensity. The line observed is *strong* compared with the corresponding *weak* lines in pyridine, 4*D*- and 3*D*-pyridine. We are unable to explain this sudden increase in intensity but we are forced to maintain the interpretation given because it is impossible to place a combination frequency in this spectral interval. Also, no alternative line which could be called ν_5 is observed. The phenomenon that isotopic substitution has a great effect on spectral activity is by no means unparallelled. To take the present material it suffices to refer to the observed great intensity of the deuterium stretching frequency in 2*D*-pyridine as compared with the corresponding lines in the 3*D*- and the 4*D*-compounds. The great intensity of the combination 16b+5 in 2*D*-pyridine is another but may be less convincing example.

In the assignment of the *hydrogen and deuterium stretching frequencies* one suffers from the lack of a rational guidance for a definite choice. The observed frequencies which we (somewhat arbitrarily) want to use in the discussion are summarized in Table III. First, our choice between fundamentals and combination tones is a matter of observed intensity. Secondly, we want to make use of the fact that no hydrogen stretching frequency in the isotopic benzenes has been put lower than about 3040. In the pyridine spectrum, the 3040–3100 region may be expected to be rather free of overtones. Both intensity relationships and the criterium (4), therefore, indicate that the fundamentals are to be found in the *upper* parts of the line-rich regions of the hydrogen stretching vibrations.

In pyridine and 4*D*-pyridine, ν_{7b} and ν_{20b} must be expected to be of highest frequency because of their low symmetry. Since the line 3069 in the 4*D*-spectrum has a comparatively isolated position we put $\nu_{7b}=\nu_{20b}=3069$ while, in pyridine, $\nu_{7b}=3053$ and $\nu_{20b}=3079$ (or vice versa) provided nothing else indicates (compare below) that in pyridine $\nu_{7b}=\nu_{20b}$. From the spectra of the deuterated benzenes it follows that ν_2 is rather insensitive to isotopic substitution, so that we can choose $\nu_2=3032$, 3033, 3038, and 3040 in pyridine and the 4*D*-, 3*D*-, and 2*D*-derivatives. Now, from the vibration pictures for C_6H_5D and $C_6H_4D_2$(*para*) given by Ingold[3] it seems to follow that it must be ν_{13} which is most sensitive to isotopic substitution in the 4-position. Therefore, $\nu_{13}(4D)=2285$. As a consequence, $\nu_{13}(\mathrm{Py})=3053$, $\nu_{13}(3D)=3053$, and $\nu_{13}(2D)=3051$. This again forces one to assume that $\nu_{7b}(\mathrm{Py})=\nu_{20b}(\mathrm{Py})=3079$. Then, $\nu_{20a}(\mathrm{Py})=3025$, $\nu_{20a}(4D)=3019$, $\nu_{20a}(3D)=3022$, and $\nu_{20a}(2D)=2258$. We must then set $\nu_{7b}(2D)=3068$ and $\nu_{20b}(2D)=3075$ (similar to the benzenes), $\nu_{20b}(3D)=3077$ and $\nu_{7b}(3D)=2289$. Of course this consideration ignores possible effects of Fermi resonance and other interactions which make any attempt to an assignment almost hopeless.

Generally, the *assignment of overtones* for a particular compound may be possible in a variety of ways. This is also the case for the spectra here studied but if the principle be accepted that *corresponding* fundamentals must preferably be used when spectra of isotopic molecules are analyzed for overtones, the number of acceptable combinations decreases very rapidly. In Table IV our proposal for the interpretation of overtones in our observed pyridine, 4*D*-, 3*D*-, and 2*D*-pyridine spectra and the pyridine-d_5 spectrum given by Lord is stated. Only one intensity irregularity is worth while pointing out. In the 2*D*-spectrum the strong line at 1294 has been assigned to 16b+5 although the corresponding combinations in the remaining isotopic species are weak. We are unable to explain this irregularity, but it has its parallels as already mentioned.

ACKNOWLEDGMENTS

We are indebted to Professor Richard C. Lord, Massachusetts Institute of Technology, for a discussion of the results presented here and to Professor Langseth, University of Copenhagen, for the loan of the Beckmann I.R. 3 spectrograph.

Vibrational Spectra of Molecules and Complex Ions in Crystals. VIII. The Infrared Spectrum of a Mixed Crystal of 1-Deutero-Ammonia and 2-Deutero-Ammonia*

F. P. REDING† AND D. F. HORNIG
Metcalf Chemical Laboratories, Brown University, Providence, Rhode Island
(Received August 23, 1954)

The infrared spectrum of a mixed crystal containing NH_3, NH_2D, ND_2H, and ND_3 was observed at $-190°C$. All of the fundamental frequencies of NH_2D and ND_2H were assigned. A calculation of the 12 frequencies of these two molecules was made, using the four nonzero force constants previously obtained from NH_3 and ND_3. The average deviation from the observed frequencies was 0.6 percent and the maximum deviation 1.6 percent. It is shown that the coupling between the motions of the various molecules can be neglected.

IN previous papers the infrared and Raman spectra of crystalline NH_3 and ND_3 have been reported.[1,2] Both the infrared and Raman spectra showed effects which are characteristic of crystalline spectra, (a) a change in the internal frequencies of vibration from the gas values, (b) evidence of coupling between the motions of the molecules, and (c) the presence of lattice frequencies. However, the splitting of vibrational lines amounted only to a few wave numbers, and the frequency separation between lattice and internal frequencies was so great that in the normal coordinate analysis of the internal modes of vibration effects (b) and (c) were neglected. This analysis resulted in a potential function for the ammonia molecule in the crystalline state which reproduced all of the eight frequencies of the two molecules within one percent.

Certain problems remained however. It is always possible to obtain more than one potential function which can reproduce the frequencies equally well. Each of them corresponds to a different allocation of frequencies to normal modes of motion. A choice between them can only be made if further frequencies from isotopically substituted molecules can be checked. In the case of the ammonia molecule, the most general potential function contains six independent force constants. The two molecules, NH_3 and ND_3, have eight frequencies between them, but since those frequencies are connected by two Teller-Redlich ratios, only six independent frequencies are available to determine the six independent force constants. Hence no checks were possible from NH_3 and ND_3 alone. The twelve frequencies of NH_2D and NHD_2, however, provide a very strong check on the potential function proposed.

In addition, a study of a mixed crystal provides a check on the previous conclusion that coupling between NH_3 molecules may be neglected. Coupling between molecules has the effect that to each vibration of an isolated molecule there corresponds a band of frequencies. In a pure crystal only those members of the band for which all unit cells vibrate in the same phase may give rise to spectral activity.[3,4] In an isotopically mixed crystal the potential function should be the same as in the pure crystal but the concept of a unit cell breaks down; instead the spectrum may be thought of as a superposition of spectra of single molecules, pairs, clusters of three and so forth. Consequently, if the effects of coupling are of any consequence we should find that (a) the frequencies of the NH_3 and ND_3 molecules will differ slightly in the mixed crystal from their value in the pure crystals, (b) the line widths for dilute components, which exist chiefly as single molecules, should be less than in the pure crystal, and (c) the widths of the lines from more concentrated components should be greater than in the pure crystal.

With these things in mind we have studied the infrared spectrum of crystals containing about 10 percent NH_3, 40 percent NH_2D, 40 percent NHD_2, and 10 percent ND_3. We have compared the frequencies observed with those calculated from the potential function previously derived[1] and have studied the spectrum for the other effects mentioned.

EXPERIMENTAL

The spectrum of a mixed crystal of the four ammonias, NH_3, NH_2D, NHD_2, and ND_3 was obtained at $-190°C$ using a cell similar to that described by Wagner and Hornig.[5] The results are shown in Fig. 1 and Table I. The curves are experimental and have not been corrected for scattering nor has the noise level been appreciably smoothed. The resolution of the spectrometer used,[6] is indicated in three different spectral regions by the vertical parallel lines. The spectrum from 800 to 2000 cm^{-1} was obtained from a film approximately one and a half times thicker than that from 2000 to 3500 cm^{-1}.

The sample was prepared by admitting one part ND_3

* Based on a thesis submitted by F. P. Reding in partial fulfillment of the requirements for the Ph.D. degree, Brown University, 1951. This work was supported by the Office of Naval Research.

† Present address: Research and Development Department, Carbide and Carbon Chemicals Company, South Charleston, West Virginia.

[1] F. P. Reding and D. F. Hornig, J. Chem. Phys. **19**, 594 (1951).
[2] F. P. Reding and D. F. Hornig, J. Chem. Phys. **22**, 1926 (1954).
[3] D. F. Hornig, J. Chem. Phys. **16**, 1063 (1948).
[4] H. Winston and R. S. Halford, J. Chem. Phys. **17**, 607 (1949).
[5] E. L. Wagner and D. F. Hornig, J. Chem. Phys. **18**, 296 (1950).
[6] Hornig, Hyde, and Adcock, J. Opt. Soc. Am. **40**, 497 (1950).

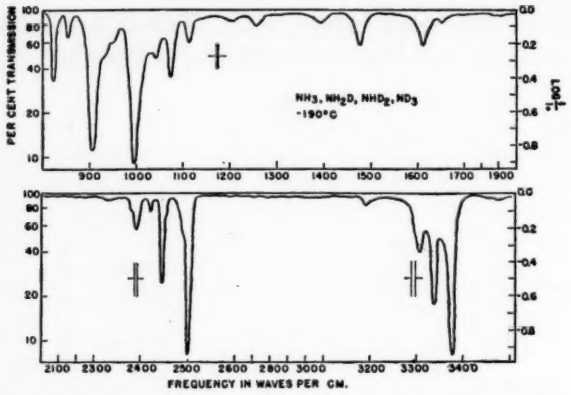

FIG. 1. The infrared spectrum of a mixed crystal containing approximately 10 percent NH_3, 40 percent NH_2D, 40 percent ND_2H, and 10 percent ND_3 at $-190°C$.

and one part NH_3 into an evacuated storage flask. To insure complete mixing the gases were frozen and evaporated several times. The mixed gases were then allowed to exchange for a week at room temperature after which time the composition, as determined from the spectrum, was approximately 10: 40: 40; 10 of NH_3, NH_2D, ND_2H, and ND_3 respectively.

The bands at 824 and 1069 cm^{-1} which arise from the symmetrical bending vibration, ν_2, in ND_3 and NH_3 are 7 cm^{-1} and 9 cm^{-1} higher in frequency than the infrared active components in their respective pure crystals and 15 cm^{-1} higher than the lowest-frequency Raman-active component. Similarly, the antisymmetrical bending frequency, ν_4, occurs at frequencies 3 cm^{-1} higher in ND_3 and 5 cm^{-1} higher in NH_3 than in the pure crystals. The experimental error in determining the band centers in this region is less than one wave number. Since both these molecules are present in the mixed crystal lattice to the extent of only 10 percent each, the resultant breakdown in vibrational coupling between like neighboring molecules probably accounts for the small shift. The ND_2H frequencies at 905, 1255, 1476, 2389, and 3338 cm^{-1} differ from those found when ND_2H is present as a dilute solution in ND_3 by +4, +8, −1, +4, and +3 cm^{-1}. This evidence further suggests the absence of much coupling in the present crystal.

The bands at 2500 and 3378 cm^{-1} are at the same frequencies as the antisymmetrical stretching vibration ν_3 in the spectrum of crystalline ND_3 and NH_3, respectively. However, in the spectrum of pure crystalline ND_3 ν_2 at 815 cm^{-1} is more intense than ν_3 at 2500 cm^{-1} and in NH_3 ν_2 at 1060 cm^{-1} is more intense than ν_3 at 3378 cm^{-1}. In the mixed spectrum it is seen that the bands at 2500 and 3378 cm^{-1} are much more intense than those at 824 and 1060 cm^{-1} and must arise primarily from NH_2D and ND_2H vibrations. We attribute the weak absorption around 2350 cm^{-1} to atmospheric carbon dioxide, since the intensity of this band decreased when dry nitrogen was blown into the spectometer.

The widths of ν_2 from both NH_3 (10 cm^{-1}) and ND_3 (16 cm^{-1}) are definitely less than in the pure substances. This result is similar to that found in dilute solutions of HCl and DCl.[7] However, the lines from NHD_2 and NDH_2 are also surprisingly sharp. All bending vibrations of both molecules have a width of about 25 cm^{-1} and the stretching vibrations have widths ranging from 10 cm^{-1} to 30 cm^{-1}.

NORMAL COORDINATE ANALYSIS

In the spectra of crystalline NH_3 and ND_3 the hydrogen atoms have been shown to conform to the reported x-ray structure[8,9] with cubic-space group symmetry T^4 ($P2_13$) containing four molecules per unit cell. In the mixed crystal only the nitrogen lattice complex will retain the cubic symmetry. Undoubtedly, the type of molecules surrounding a given molecule in the crystal will be completely random as will be the orientations of the hydrogen and deuterium atoms in the three possible "hydrogen" positions for a given NH_2D or ND_2H molecule. Since the mixed crystal has a composition of approximately 10 percent NH_3, 40 percent NH_2D, 40 percent ND_2H, and 10 percent ND_3 most of the neighboring molecules of a given molecule will on the average be of a different type. This should result in an almost complete breakdown in the coupling between the internal modes of like molecules. Consequently the different frequencies of vibration for a given internal mode arising from the various phases of coupling between like molecules will largely disappear and only one spectral line should be observed for each internal mode. Since both NH_2D and ND_2H are present to the extent of 40 percent, however, it is possible that some structure may appear on the shoulders of their bands due to coupling.

TABLE I. Vibrational frequencies of a mixed crystal of NH_3, NH_2D, NHD_2, and ND_3.[a]

Observed frequency cm^{-1}	Assignment	Observed frequency cm^{-1}	Assignment
824	$\nu_2(ND_3)$	1651	$\nu_4(NH_3)$
854	$\nu_2(ND_3)$+lattice	1890	?
905	$\nu_2(ND_2H)$	2350	atmos CO_2
936	$\nu_2(ND_2H)$+lattice	2378	?
953	$\nu_2(ND_2H)$+lattice	2389	$\nu_1(ND_2H)$
993	$\nu_2(NH_2D)$	2420	$\nu_1(ND_2H)$+lattice
1039	$\nu_2(NH_2D)$+lattice	2444	$\nu_1(NH_2D)$
1069	$\nu_2(NH_3)$	2453	?
1113	$\nu_2(NH_3)$+lattice	2487	$2\nu_{4'}(ND_2H)$
1202	$\nu_4(ND_3)$	2500	$\nu_{3''}(ND_2H)$
1255	$\nu_{4'}(ND_2H)$	3188	$2\nu_{4'}(NH_2D)$
1393	$\nu_{4''}(NH_2D)$	3307	$\nu_{3'}(NH_2D)$
1476	$\nu_{4''}(ND_2H)$	3338	$\nu_{3'}(ND_2H)$
1609	$\nu_{4'}(NH_2D)$	3378	$\nu_{3''}(NH_2D)$
		3450	Various possibilities

[a] Here $\nu_{i'}$ and $\nu_{i''}$ refer to the A' and A'' vibrations of NH_2D and ND_2H under the point group C_s.

[7] G. L. Hiebert and D. F. Hornig, J. Chem. Phys. **20**, 918 (1952).
[8] H. Mark and E. Pohland, Z. Krist. **61**, 532 (1925).
[9] J. de Smedt, Bull. Class. Sci. Acad. Roy. Belg. **11**, 655 (1925).

Since there is such a complete breakdown of crystal symmetry, no unit cell group exists and the crystalline selection rules[3,4] do not apply. It is probable that the selection rules for the free molecules approximate the present situation. Vibrations of all symmetry species may give rise to an infrared spectrum in both point groups C_{3v} (NH_3 and ND_3) and C_s (NH_2D and ND_2H); consequently, 20 fundamentals may be observed in the mixed crystal spectrum.

The point group C_s contains the irreducible representations A' and A''. In both molecules there are four vibrations of symmetry A' corresponding to ν_1 and ν_2 and one component each of the split degenerate vibrations ν_3 and ν_4 (hereafter designated as $\nu_{3'}$ and $\nu_{4'}$). There are two vibrations of Species A'' corresponding to the second two components of the split degenerate vibrations (hereafter designated as $\nu_{3''}$ and $\nu_{4''}$). Consequently, following the method of Wilson,[10] six symmetry coordinates, four which transform like A' and two like A'', are required. A satisfactory set of symmetry coordinates is:

$$\begin{aligned}
&\text{Species } A' \qquad S_1=d\\
&\qquad\qquad\ S_2=\alpha\\
&\qquad\qquad\ S_3=(r_1+r_2)/2^{\frac{1}{2}}\\
&\qquad\qquad\ S_4=(\beta_1+\beta_2)/2^{\frac{1}{2}}\\
&\text{Species } A'' \qquad S_5=(\beta_1-\beta_2)/2^{\frac{1}{2}}\\
&\qquad\qquad\ S_6=(r_1-r_2)/2^{\frac{1}{2}}.
\end{aligned} \tag{1}$$

In these equations d represents the change in the bond distance between the nitrogen and the odd atom (the N−H bond in ND_2H and the N−D bond in NH_2D), r_1 and r_2 the change in bond distances between the nitrogen and the two like atoms, α the change in the angle defined by the two like atoms and the nitrogen, and β_1 and β_2 the change in the angles between the two different atoms and the nitrogen.

If the potential function is not affected by isotopic substitution, the most general potential function for these molecules is[11,12]:

$$\begin{aligned}
2V=&f_d(d^2+r_1^2+r_2^2)+d_0^2f_\alpha(\alpha^2+\beta_1^2+\beta_2^2)\\
&+2f_{dd}(dr_1+dr_2+r_1r_2)+2d_0^2f_{\alpha\alpha}(\alpha\beta_1+\alpha\beta_2+\beta_1\beta_2)\\
&+2d_0f'_{\alpha d}(\alpha d+\beta_1r_1+\beta_2r_2)+2d_0f_{\alpha d}\\
&\times[\alpha(r_1+r_2)+\beta_1(d+r_2)+\beta_2(d+r_1)].
\end{aligned} \tag{2}$$

TABLE II. Force constants of the most general valence force potential function for the internal vibrations of crystalline ammonia and 3-deutero-ammonia ($\times 10^{+5}$ dyne/cm).

$f_d=6.130$	$f_{\alpha\alpha}=-0.0492$
$f_{dd}=-0.0712$	$f_{\alpha d}=0.00$
$f_\alpha=0.5835$	$f'_{\alpha d}=0.00$

[10] E. B. Wilson, Jr., J. Chem. Phys. **7**, 1047 (1939); **9**, 76 (1941).
[11] M. Hemptinne and J. Delfosse, Ann. Soc. Sci. Brus. **56**, 373 (1936).
[12] J. Duchesne and J. Ottelet, J. Chem. Phys. **17**, 1354 (1949).

TABLE III. Calculated and observed values of the special A'' fundamental frequencies of crystalline 1-deutero-ammonia and 2-deutero-ammonia.

Vibration	NH_2D frequencies (cm^{-1}) Calculated	Observed	ND_2H frequencies (cm^{-1}) Calculated	Observed
$\nu_{3''}$	3381	3378	2497	2500
$\nu_{4''}$	1413	1393	1478	1476

After transforming to symmetry coordinates and noting that $f_{\alpha d}$ and $f'_{\alpha d}$ were found to equal zero in the previous work we have for species A':

$$F_{A'}=\begin{vmatrix} f_d & 0 & 2^{\frac{1}{2}}f_{dd} & 0\\ 0 & d_0^2f_\alpha & 0 & 2^{\frac{1}{2}}d_0^2f_{\alpha\alpha}\\ 2^{\frac{1}{2}}f_{dd} & 0 & (f_d+f_{dd}) & 0\\ 0 & 2^{\frac{1}{2}}d_0f_{\alpha\alpha} & 0 & d_0^2(f_\alpha+f_{\alpha\alpha}) \end{vmatrix} \tag{3}$$

and for species A''

$$F_{A''}=\begin{vmatrix} (f_d-f_{dd}) & 0\\ 0 & d_0^2(f_\alpha-f_{\alpha\alpha}) \end{vmatrix}. \tag{4}$$

The G-matrix for NH_2D for species A' is

$$G_{A'}=\begin{vmatrix} g_d{}^{\mathrm{D}} & g_{\alpha d} & 2^{\frac{1}{2}}g_{\alpha d} & 2^{\frac{1}{2}}g'_{\alpha d}\\ g_{\alpha d} & g_\alpha{}^{\mathrm{H}} & 2^{\frac{1}{2}}g'_{\alpha d} & 2^{\frac{1}{2}}g_{\alpha\alpha}{}^{\mathrm{H}}\\ 2^{\frac{1}{2}}g_{dd} & 2^{\frac{1}{2}}g_{\alpha d} & (g_d{}^{\mathrm{H}}+g_{dd}) & (g'_{\alpha d}+g_{\alpha d})\\ 2^{\frac{1}{2}}g'_{dd} & 2^{\frac{1}{2}}g_{\alpha\alpha}{}^{\mathrm{H}} & (g'_{\alpha d}+g_{\alpha d}) & (g_\alpha{}^{\mathrm{HD}}+g_{\alpha\alpha}{}^{\mathrm{D}}) \end{vmatrix} \tag{5}$$

and for species A'' is

$$G_{A''}=\begin{vmatrix} (g_d{}^{\mathrm{D}}-g_{dd}) & (g'_{\alpha d}-g_{\alpha d})\\ (g'_{\alpha d}-g_{\alpha d}) & (g_\alpha{}^{\mathrm{HD}}-g_{\alpha\alpha}{}^{\mathrm{H}}) \end{vmatrix}. \tag{6}$$

The g-elements, except for $g_\alpha{}^{\mathrm{HD}}$, are the same as those used in the normal coordinate treatment of crystalline NH_3 and ND_3.[1] Those elements with the superscript D or H indicate that the deuterium or hydrogen mass, respectively, was used in their calculation; those elements without superscripts involve only the nitrogen mass. The G-matrices for ND_2H may simply be obtained by interchanging the superscripts H and D. The element $g_\alpha{}^{\mathrm{HD}}$ is given by the expression,[13]

$$g_\alpha{}^{\mathrm{HD}}=\frac{1}{d_0^2}[\mu_{\mathrm{H}}+\mu_{\mathrm{D}}+2(1-\cos\alpha)\mu_{\mathrm{N}}]$$
$$=9.800\times10^{39}\ \mathrm{g\ cm^{-2}}.$$

The numerical values of the force constants, taken from NH_3 and ND_3, which were used in calculating the frequencies are given in Table II. The secular equation, $|F_{A''}G_{A''}-E\lambda|=0$, for the A'' vibrations is a quadratic expression and is simply solved. The values of $\nu_{3''}$ and $\nu_{4''}$ for both NH_2D and ND_2H are listed in Table III; the experimental frequencies which most nearly correspond to the calculated frequencies are listed for comparison.

The secular equation, $|F_{A'}G_{A'}-E\lambda|=0$, for the A'

[13] J. C. Decius, J. Chem. Phys. **16**, 1025 (1948).

TABLE IV. Calculated and observed values of the species A' fundamental frequencies of crystalline 1-deutero-ammonia and 2-deutero-ammonia.

Vibration	NH_2D frequencies (cm^{-1}) Calculated	Observed	ND_2H frequencies (cm^{-1}) Calculated	Observed
ν_1	3283	3307	2372	2389
ν_2	986	994	891	905
$\nu_{3'}$	2431	2444	3331	3378
$\nu_{4'}$	1615	1609	1251	1255

vibrations had a dimensionality of four. This determinant was expanded into minors, which were in turn expanded and the terms collected into a quartic equation in the λ's. It was solved by trial and error. The calculated values of the fundamental frequencies of species A' for both molecules are listed in Table IV; again the experimental frequencies which most nearly correspond are listed.

The average deviation of the calculated from the experimentally observed frequencies in Tables III and IV is only 0.6 percent and the maximum deviation is only 1.6 percent. From this excellent agreement it must be concluded that the force constants for the crystalline ammonias given in Table II are the true force constants of the system and the potential function given by Eq. (3) describes the system quite well.

It is of interest that there is such excellent agreement between the observed and calculated frequencies when the cross-term force constants f_{ad} and f'_{ad} are zero. However, these two force constants cannot be determined with any precision since they enter the equations for the frequencies either as squares or with very small coefficients so that the calculated frequencies are very insensitive to these constants. This same difficulty occurs in determining these cross terms in the potential function of gaseous NH_3 or any other similar molecule such as AsH_3. Consequently, the conclusion of Duchesne and Ottelet[11] that in gaseous NH_3 and AsH_3 the cross term f_{dd} is small whereas f_{ad} is quite large is doubtful.

ASSIGNMENT OF THE OBSERVED SPECTRUM

The excellent agreement between the calculated frequencies of NH_2D and ND_2H and the frequencies observed in the mixture spectrum permits an assignment of the bands. The assignment of the six fundamental frequencies of both NH_2D and ND_2H on the basis of the calculated frequencies is open to little doubt. It is most improbable that the excellent correlations for all twelve frequencies can be coincidental.

On the basis of the spectra of pure NH_3 and ND_3[1] the bands at 824, 1069, 1202, and 1651 cm^{-1} certainly arise from the NH_3 and ND_3 vibrations assigned to them in Table I. As mentioned before they vary slightly in frequency from the bands in the pure crystals because of the breakdown in crystalline coupling in going to the mixed crystal. In addition some of the intensity of the bands at 2500 and 3378 cm^{-1} arises from ν_3 in ND_3 and NH_3, respectively. The spectrum of the mixed crystal removes any remaining doubt as to the frequency of ν_4 in crystalline NH_3 and ND_3; in the pure crystals ν_4 was overlapped by the strong combination of ν_2 with the torsional lattice modes.

The bands at 854, 936, 953, 1039, and 1113 cm^{-1} on the high-frequency shoulders of the four bands arising from the symmetrical bending vibration ν_2 are apparently combination bands of these fundamentals with very low-frequency lattice vibrations such as those found in NH_3 and ND_3. However, it is possible that they arise instead from reflection maxima or impurities in the ND_3 (perhaps N_2D_4). In this connection it should be pointed out that extra peaks of medium intensity were observed in the spectrum of the pure ND_3 at 849, 934, and 950 cm^{-1} although the amount of ND_2H present was very small.

The band at 3188 cm^{-1} has been assigned to the first overtone of $\nu_{4'}$, NH_2D, at 1609 cm^{-1}. The corresponding first overtone of $\nu_{4'}$ in ND_2H at 1255 cm^{-1} may be the band near 2487 cm^{-1} on the low-frequency shoulder of the strong band at 2500 cm^{-1}. This absorption may also arise from ν_3 of ND_3 or from an intermolecular coupling component of adjacent ND_2H molecules. It is probable that such coupling of like neighboring molecules accounts for the absorption near 2378 and 2453 cm^{-1} on the low- and high-frequency shoulders of the peaks at 2389 and 2444 cm^{-1}.

CONCLUSION

The potential function of the crystalline ammonia system is adequately and accurately described by the force constants listed in Table II. In terms of these four force constants it is possible to calculate the twenty fundamental vibrations of the ammonia systems and accurately assign the spectrum of the mixed crystals. The coupling between ammonia molecules is certainly weak. It is probable that potential functions which neglect intermolecular coupling and lattice vibrations are adequate to describe internal vibrations in many simple molecular crystals.

Calculation of Thermodynamic Properties of Polyelectrolytes

R. A. Marcus
Department of Chemistry, Polytechnic Institute of Brooklyn, Brooklyn 1, New York
(Received October 7, 1954)

Expressions are derived which introduce an appreciable simplification into the calculation of the thermodynamic properties of solutions of polyelectrolytes in certain cases. For example, for a certain class of theoretical models of these systems it is found that the square of the mean ion activity coefficient of a univalent salt in the presence of polymeric ions is $V^2/\int e^{-e\psi/kT}dV \cdot \int e^{e\psi/kT}dV$, the integration of the potential ψ being over a region whose volume is the volume of solution per macro-ion, V, and whose symmetry is that assumed for the polyelectrolyte. The osmotic pressure of a salt-polyelectrolyte system is, ignoring the contribution of the macro-ion, estimated to be $\sum_i c_i^s kT$, where $\sum_i c_i^s$ is the sum of the concentrations of all ions at the surface bounding the previously defined volume V. Other relations and various applications are given. The activity coefficient of salt in the presence of polyelectrolytes, calculated by extending the "parallel rod" picture of polymeric ions, is found to be in reasonable agreement with the experimental data. The use of the Poisson-Boltzmann equation to estimate ψ in these systems is shown not to render inconsistent several alternative expressions for the electrostatic contribution to the free energy.

INTRODUCTION

THE strong electrostatic fields in the neighborhood of polymeric ions have been established experimentally and their theoretical description [1–8] has been the subject of a number of recent communications. Relevant thermodynamic data include osmotic pressures, activity coefficients of salts, and titration behavior of polymeric acids and bases. Usually these properties are calculated theoretically by differentiation of a free-energy expression into which parameters of the models have been introduced. Because of the frequent complex dependence of these parameters on the thermodynamic variables such as the moles of the components and the volume of the solution, the differentiation may become a lengthy process. A somewhat different procedure is employed here for a certain class of models, in that the last two steps are reversed—expressions are set up for various thermodynamic properties by differentiation of the free energy, these are then simplified and the parameters are introduced as a final step. This procedure effects a considerable simplification of the calculation in various cases.

THEORETICAL

1. General

A number of theoretical models of polyelectrolytes have been advanced[1–8]; several of these have in common the following assumptions:

(1) The interaction between polymeric ions is neglected except insofar as the concentration of these ions determines the size of the electrically neutral volume V assigned to each polymeric ion (total volume of solution divided by number of such ions).

(2) The electrostatic interaction between all ions in this subvolume obeys the Poisson-Boltzmann equation

$$\nabla^2\psi = -\frac{4\pi}{D}(\rho+\rho_p) \tag{1}$$

where the charge density of mobile ions ρ equals $\sum_i c_i e_i$. The charge of ions of the ith type is e_i, and c_i, their local concentration, is given by

$$c_i = \frac{n_i \exp(-e_i\psi/kT)}{\int \exp(-e_i\psi/kT)dV} \tag{2}$$

where n_i is the number of these ions in V. The volume charge density of ions fixed on the polymeric ion ρ_p is sometimes replaced by a surface charge density. That is, $\nabla^2\psi = -4\pi\rho/D$ is used instead of (1) and a boundary condition relating the potential gradient and the charge per unit area at the surface of the polymeric ion is given. The present approach will apply to both treatments. The subvolume V and the model are chosen with a certain degree of symmetry such that on the boundary of the electrically neutral volume V the potential gradient is zero.

In Eq. (2) the concentration c_i and the potential ψ acting on a mobile ion are assumed to be a function only of the three coordinates defining the position of the ion in space, the macro-ion being held fixed in this space. Actually, more rigorously, the potential is a function not only of these three coordinates but also of the instantaneous configuration of the other mobile ions. Similar remarks may be made about the concentration c_i; the local concentration gradients about each mobile ion should be considered explicitly. The assumption made here thus treats the mutual interaction of the

[1] Kuhn, Künzle, and Katchalsky, Helv. Chim. Acta **31**, 1994 (1948).
[2] J. J. Hermans and J. T. G. Overbeek, Rec. trav. chim. **67**, 761 (1948).
[3] Alfrey, Berg, and Morawetz, J. Polymer Sci. **7**, 543 (1951).
[4] Fuoss, Katchalsky, and Lifson, Proc. Natl. Acad. Sci. U. S. **37**, 579 (1951).
[5] Kimball, Cutler, and Samelson, J. Phys. Chem. **56**, 57 (1952).
[6] P. J. Flory, J. Chem. Phys. **21**, 162 (1953).
[7] Osawa, Imai, and Kagawa, J. Polymer Sci. **13**, 93 (1954).
[8] F. E. Harris and S. A. Rice, J. Phys. Chem. **58**, 725 (1954); R. A. Marcus, J. Phys. Chem. **58**, 621 (1954).

mobile ions in a more or less approximate manner.[7] Correspondingly, the Poisson-Boltzmann equation, as used here, will give best results when the mobile ion interacts more with the macro-ion and the many distant mobile ions than with a local mobile ion. This will occur when the mobile ions are dilute, which does not imply that $|e\psi/kT|$ must be small compared with unity.

This viewpoint may also be inferred from the behavior of the activity coefficient of added salt calculated on the basis of Eqs. (1) and (2). At a given polyelectrolyte concentration it tends toward unity as the salt concentration is increased, inasmuch as a given mobile ion is increasingly shielded by the salt from the influence of the macro-ion. In dilute solutions experimental data support this expectation. Nevertheless, for a given polyelectrolyte concentration, as the salt concentration increases the magnitude of the activity coefficient should ultimately approach that observed for the same salt solution containing no polyelectrolyte, rather than unity. This discrepancy is due to the fact that the local concentration gradients in the vicinity of each ion are but approximately taken into account.

(3) Calculations of the electrostatic potential are frequently made for some average configuration of the polymer rather than for all possible ones. This assumes that all important configurations of the polymer have about the same electrostatic free energy arising from the interaction of the charges fixed on the polymer with each other and with the mobile ions in solution.

(4) It will be assumed that the configurational entropy of the polymer chain S_p and the average local concentration $C_p(\mathbf{r})$ of groups, neutralized plus unneutralized, fixed on the chain depend upon only one quantity, h, the configurational variable. This variable may be an average end-to-end distance or the average radius of the polymer, assumed coiled, and its value will depend on the thermodynamic state of the system. It will, for example, increase with increasing charge density along the chain, i.e., with increasing degree of neutralization, and will decrease with increasing shielding of these charges from each other, i.e., with increasing salt concentration. The effect of using a different assumption will be discussed at the end of this section.

In treating this class of models the following contributions to the free energy of a macro-ion and its accompanying mobile ions present in V will be considered:

(a) S_p, the configurational entropy of the polymer chain, which is related[1] to the number of configurations of the polymer consistent with a given value of h.

(b) S_m, the entropy of mixing of the charged and uncharged groups along the chain.

(c) S_{id}, the ideal entropy of mixing of the mobile ions.

(d) F_e, the free energy associated with the reversible charging of the mobile ions and of the macro-ion, during which process the polymer configuration and the number and spatial distribution of ionized groups on the macro-ion are held fixed.

(e) $\sum_i n_i\mu_i^0$, where μ_i^0 is the standard free energy of the mobile ion of the ith kind while n_i is the number of such ions in V.

(f) $m[\alpha\mu_A{}^0+(1-\alpha)\mu_{HA}{}^0]$, where $\mu_A{}^0$ and $\mu_{HA}{}^0$ are the standard free energies of the neutralized and unneutralized groups, respectively, α is the degree of neutralization, and m is the total number of groups on the polymer chain.

The expression for the free energy may therefore be written as

$$F=-TS_p-TS_m+F_e-TS_{id}+\sum_i n_i\mu_i{}^0 +m[\alpha\mu_A{}^0+(1-\alpha)\mu_{HA}{}^0] \quad (3)$$

where S_m is given by

$$S_m=-k\int C_p[\alpha_r \ln\alpha_r+(1-\alpha_r)\ln(1-\alpha_r)]dV \quad (4)$$

where C_p is the local concentration of the groups on the polymer while α_r is the local fraction of these groups which are neutralized. Furthermore, α_r is related to the charge density ρ_p due to ions fixed on the polymer by the relation, $\alpha_r C_p e_p=\rho_p$, where e_p is the charge of an ion attached to the polymer.

If the simplifying assumption is made that the neutralized and unneutralized groups are randomly mixed then α_r becomes independent of position and equal to α, the degree of neutralization. Thus, S_m becomes

$$S_m=-mk[\alpha\ln\alpha+(1-\alpha)\ln(1-\alpha)]. \quad (5)$$

While the calculations given below will, in general, be performed without making this assumption, the effect of employing it will be discussed.

Various expressions may be used to estimate the electrostatic contribution F_e to the Helmholtz free energy. Neglecting electrostriction the equations given below also represent the corresponding contribution to the Gibbs free energy. F_e may be calculated in the following way[9] from the reversible work to charge the entire system in V at constant configuration and charge distribution of the macro-ion, constant volume, and temperature. The charging process is performed in a manner such that at any stage all ions have the same fraction λ of their final charge. The corresponding values of ψ, ρ, ρ_p, c_i, etc. are indicated by the superscript, $'$. The charge per unit volume, $\rho'+\rho_p'$, is $(\sum_i c_i'e_i\lambda+\alpha_r C_p e_p\lambda)$. When the charge on each ion is increased by a fraction $d\lambda$, the charge of those ions in a volume element dV is increased by $(\sum_i c_i'e_i+\alpha_r C_p e_p)d\lambda dV$; that is, by $(\rho'+\rho_p)(d\lambda/\lambda)dV$. Since the local value of the potential is ψ', an element of work $\psi(\rho'+\rho_p')(d\lambda/\lambda)dV$ is done. Summing this work over all ions, i.e., integrating over V, the total work done during the complete charging process from $\lambda=0$

[9] See E. J. W. Verwey and J. T. G. Overbeek, *Theory of Stability of Lyophobic Colloids* (Elsevier Publishing Company, Inc., New York, 1948), p. 58.

to $\lambda=1$ is

$$F_e=\int_{\lambda=0}^{\lambda=1}\int_V \psi'(\rho'+\rho_p')\frac{d\lambda}{\lambda}dV=\int_\lambda 2E_e'\frac{d\lambda}{\lambda} \quad (6)$$

where E_e' is the electrostatic energy [see Eq. (7)]. If the polymeric ion had been regarded as forming a surface charge density σ over its surface instead of a volume density ρ_p, then the integral of $\psi'\rho_p'$ over the volume would become an integral over the surface A of the polymer, $\int_\lambda\int_A\psi'\sigma'(d\lambda/\lambda)dA$. Similar remarks will apply to all electrostatic expressions throughout this paper. The final equations for the thermodynamic properties will be the same regardless of which picture is used.

A second expression for F_e may be obtained from the Gibbs-Helmholtz equation together with an equation for the electrostatic energy, E_e.

$$E_e=\tfrac{1}{2}\int\psi(\rho+\rho_p)dV \quad (7)$$

$$F_e=T\int_{T=\infty}^{T=T}E_e d\left(\frac{1}{T}\right). \quad (8)$$

The integration in (8) is performed at constant dielectric constant,[10] and at constant average configuration and charge distribution of the macro-ion. We note that the lower limit arises from the condition that $F_e/T=0$ when $T=\infty$.

A third expression for F_e may be found by combining the equation for E_e with a suitable equation for the entropy of mixing, S, of the mobile ions in V.

$$S=-k\textstyle\sum_i\displaystyle\int(c_i\ln c_i-c_i)dV \quad (9)$$

where the summation is over all mobile ions. If the total number of ions of type i in the volume V is n_i, then the ideal entropy of mixing is

$$S_{id}=-k\textstyle\sum_i\left(n_i\ln\dfrac{n_i}{V}-n_i\right). \quad (10)$$

This equation follows from Eq. (9) when one sets c_i equal to its average value n_i/V. The deviation of the entropy of mixing from its ideal value is $(S-S_{id})$ and we may write as a third expression for F_e,

$$F_e=E_e-T(S-S_{id}). \quad (11)$$

In view of the questions which can be raised concerning the internal consistency of solutions of the Poisson-Boltzmann equation, it is of interest to examine the extent to which the various expressions for F_e are exactly equal when solutions of this equation are introduced into them. In Appendix I it is shown that they are equal.

The third expression for the electrostatic free energy, Eq. (11), is the most convenient one for the present purposes and will be used. Before proceeding it is first observed that Poisson's equation (1) may be written[11] in the integral form:

$$\psi(\mathbf{r})=-\frac{1}{D}\int\frac{\rho(\mathbf{r}'')+\rho_p(\mathbf{r}'')}{|\mathbf{r}-\mathbf{r}''|}dV. \quad (12)$$

Equation (12) will be used in some of the proofs given in Appendix I.

In general a thermodynamic function of the system can be expressed in the terms of partial derivatives of the free energy, and a first partial derivative can for example be calculated by estimating the change in free energy corresponding to an appropriate change in the thermodynamic state. The calculation is simplified by observing that in any reversible change of thermodynamic state the contributions to the free energy change arising from a change in configurational variable h, a change in the fraction α of the groups on the macro-ion which are neutralized, and a change in the relative distribution of the charges over the chargeable sites on this polymer are each equal to zero. This circumstance arises since the change in h, α, and in the relative distribution of the charges, occurs automatically with the reversible change of state and so contributes nothing to the work done and therefore nothing to the free energy change. The statement concerning h and α is readily established by observing that the equilibrium values of h and α satisfy the equations $(\partial F/\partial h)_\alpha=0$ and $(\partial F/\partial\alpha)_h=0$, all thermodynamic variables being held constant. Thus the change in free energy corresponding to a reversible change of state equals that calculated at a given h and α, for

$$\delta F=\frac{\partial F}{\partial\alpha}\delta\alpha+\frac{\partial F}{\partial h}\delta h+(\delta F)_{\alpha,h}=(\delta F)_{\alpha,h}. \quad (13)$$

The statement concerning the relative distribution function, α_r/α, of charges on the polymer is verified rigorously for the present model in Appendix II. This has the consequence that the free-energy change equals that estimated at fixed h, α, and α_r/α. Equations are also derived in Appendix II for α_r/α and for the relation satisfied by the equilibrium value of h.

[10] A few remarks concerning this restriction of integration at constant dielectric constant are perhaps in order. If E_e were the total electrostatic contribution E to the energy of the system, then the restriction would be unnecessary, but E_e is actually only a portion of E. It can be shown that while $\partial(F_e/T)/\partial(1/T)=E$, $[\partial(F_e/T)/\partial(1/T)]_D=E_e$. Conversely, in order to obtain F_e from E_e by integration with respect to $1/T$, it is necessary to hold D constant. The difference between E and E_e has been discussed by N. Bjerrum, Z. physik. Chem. **119**, 145 (1926). E may be calculated by imagining an isothermal process in which the ions are held motionless throughout and estimating the reversible work done w_r by the system and the heat absorbed q_r by the system in bringing the ions from infinity to their final equilibrium positions. w_r is simply $-E_e$ while q_r was computed by Bjerrum from the temperature dependence of w_r using the second law of thermodynamics to be $-w_r\partial\ln D/\partial\ln T$ whence $E=q_r-w_r=E_e(1+\partial\ln D/\partial\ln T)$.

[11] E.g., J. C. Slater and N. H. Frank, *Introduction to Theoretical Physics* (McGraw-Hill Book Company, Inc., New York, 1933), p. 217.

We shall conclude this section with an amplification of the assumptions (3) and (4) made earlier, and with a brief inquiry into the extent to which the equations deduced here for various thermodynamic properties remain valid when assumption (4) concerning S_p and C_p is either dropped or replaced by another. First it is observed that for a given polymer molecule many polymer configurations are important and contribute to the configurational entropy S_p. If these all have substantially the same electrostatic free energy (really, the same $F+TS_p$), as postulated in assumption (3), then S_p will depend only on the same parameter, here h, which characterizes S_p for the uncharged polymer. That is, assumptions (3) and (4) are not mutually inconsistent. If, further, many of these configurations are substantially different so that appreciable fluctuations of the configuration of a polymer molecule from the average configurational distribution function, $C_p(\mathbf{r})$, occurs in time, then it is the parameter h, rather than the function $C_p(\mathbf{r})$ which maximizes the free energy. That is, in the expression for δF, the coefficient of δh rather than of δC_p is set equal to zero at equilibrium.

Consider now a different model, one in which all the important configurations of a polymeric molecule are very similar so that only small fluctuations from the distribution function $C_p(\mathbf{r})$ occur. It is expected that these configurations will have substantially the same electrostatic free energy, and assumption (3) thus remains valid. In this model C_p is calculated by maximizing the free energy. That is, C_p describes that distribution of groups on the polymer which maximizes the free energy. This has the immediate consequence that in a reversible change of state this spatial distribution function of groups on a polymer will automatically adjust itself and, like the redistribution of the charges on these groups, contribute nothing to δF. This may be verified by writing, in contrast to the previous model where S_p and C_p were only indirectly related (through h), for this case $S_p=\int g(C_p)dV$, where g is a function of C_p alone and introducing this into Eq. (56) for the free energy in Appendix II. The procedure used there is then followed except that the variation of the free energy is computed in terms of δC_p instead of δh. As before $\partial F/\partial\alpha=0$ and it is concluded that in this alternative model the free-energy change equals that estimated at fixed α, α_r/α and C_p. These restrictions are equivalent to constant α, α_r/α, and h, since when h is constant, C_p is constant. Thus, the various equations deduced below for the thermodynamic properties remain valid if this alternative model of polyelectrolytes be assumed.

2. Calculation of Activity Coefficients

The chemical potential, and hence the activity coefficient, of added salt may be calculated by differentiating the sum of all contributions to the free energy with respect to amount of salt. According to the discussion in the previous section, only the derivative at constant degree of neutralization, at constant polymer configuration, and fixed distribution of polymer charges need be calculated. When these variables are held constant S_p and S_m do not change and, as seen from Eq. (3), it is sufficient to calculate the changes in F_e, $-TS_{id}$ and $\sum_i n_i\mu_i^0$.

Inasmuch as (F_e-TS_{id}) equals (E_e-TS), Eq. (11), the changes in E_e and S will be determined rather than the changes in F_e and S_{id}. According to Eq. (7) the change in E_e with amount of added salt at constant volume V may be written as

$$\delta E_e=\tfrac{1}{2}\int[\psi(\delta\rho+\delta\rho_p)+(\rho+\rho_p)\delta\psi]dV$$

$$=\int(\rho+\rho_p)\delta\psi dV=\int\psi(\delta\rho+\delta\rho_p)dV. \qquad (14)$$

The second equation may be established by writing ψ and $\delta\psi$ in terms of the ρ's and $\delta\rho$'s using Eq. (12). At constant polymer configuration and distribution of polymer charges $\delta\rho_p=0$ so that

$$\delta E_e=\int\psi\delta\rho dV. \qquad (15)$$

The change in S at constant volume may be estimated from (9) to be

$$\delta S=-k\textstyle\sum_i\int\ln c_i\delta c_i dV. \qquad (16)$$

Using the Boltzmann expression (2) and denoting $\int\exp(-e_i\psi/kT)dV$ by V_i, it follows that

$$\delta S=-k\textstyle\sum_i\int\left(-\frac{e_i\psi}{kT}+\ln\frac{n_i}{V_i}\right)\delta c_i dV$$

$$=\frac{1}{T}\int\psi\delta\rho dV-k\textstyle\sum_i\left(\ln\frac{n_i}{V_i}\right)\int\delta c_i dV \qquad (17)$$

since $\delta\rho=\sum_i e_i\delta c_i$. It is noted that n_i/V_i is independent of position and hence has been removed from the second integral.

At constant volume $\delta n_i=\int\delta c_i dV$ so that from Eqs. (14) and (17) we have

$$\delta(E_e-TS)=kT\textstyle\sum_i\ln\frac{n_i}{V_i}\delta n_i. \qquad (18)$$

The change in the term $\sum_i n_i\mu_i^0$ caused by the addition of salt is $\sum_i\mu_i^0\delta n_i$.

Thus the chemical potential of any mobile ion of the type j in V is

$$\mu_j=\frac{\partial}{\partial n_j}(E_e-TS+\textstyle\sum_i n_i\mu_i^0)=\mu_j^0+kT\ln\frac{n_j}{V_j}. \qquad (19)$$

The chemical potential of any salt, one mole of which dissociates into ν_+ moles of cations and ν_- moles of anions in this sytem, is therefore

$$\mu=\nu_+\mu_+^0+\nu_-\mu_-^0+kT\ln\left(\frac{n_+}{V_+}\right)^{\nu_+}\left(\frac{n_-}{V_-}\right)^{\nu_-} \quad (20)$$

where the subscripts + and − correspond to the cations and anions, respectively.

Defining the mean ion activity coefficient $f_\pm$ by the equation

$$\mu=\nu_+\mu_+^0+\nu_-\mu_-^0+kT\ln\left(\frac{n_+}{V}\right)^{\nu_+}\left(\frac{n_-}{V}\right)^{\nu_-}f_\pm^{\nu} \quad (21)$$

where $\nu=\nu_++\nu_-$, it follows that

$$f_\pm^{\nu}=\left(\frac{V}{V_+}\right)^{\nu_+}\left(\frac{V}{V_-}\right)^{\nu_-}. \quad (22)$$

It may be verified that making an additional assumption of random mixing of neutralized and unneutralized groups on the polymer, i.e., setting $\alpha_r=\alpha$ everywhere and so using Eq. (5) for S_m instead of (4), leaves Eq. (22) unaltered.

It is interesting to observe that this equation can also be obtained in a somewhat different, though less rigorous, way. Let us assume that this salt-polyelectrolyte solution is in equilibrium with an ideal salt solution containing no polyelectrolyte, where the concentration of ions of the ith type is $\bar{c}_i$, the two phases being separated by a membrane impermeable to the macro-ion in order to maintain equilibrium. That is, a type of Donnan membrane equilibrium is set up. Then it is reasonable to expect that the concentration of ions of type i in any local region of the subvolume V in the polyelectrolyte phase will be given by $c_i=\bar{c}_i\exp(-e_i\psi/kT)$ since $c_i=\bar{c}_i$ in the ideal solution where $\psi=0$. Thus $n_i=\bar{c}_i\int\exp(-e_i\psi/kT)dV$. At equilibrium the activity of a salt is the same in both phases. That is,

$$f_\pm^{\nu}(n_+/V)^{\nu_+}(n_-/V)^{\nu_-}=(\bar{c}_+)^{\nu_+}(\bar{c}_-)^{\nu_-}.$$

Since, as just stated, $n_i=\bar{c}_iV_i$, Eq. (22) immediately follows.

That the mean ion activity coefficient, calculated on this basis, is always equal to or less than unity when both ions of the salt have the same valence, may be shown by application of Schwarz's inequality[12]: $\int f^2dV\cdot\int g^2dV\geq(\int fgdV)^2$. Setting $f=\exp(-e_+\psi/2kT)$ and $g=\exp(-e_-\psi/2kT)$ it follows that $fg=1$ when $e_+=-e_-$. The integral on the right-hand side of the inequality then becomes V^2 while the product on the left-hand side is V_+V_-. That is, $V_+V_-\geq V^2$ and, since $\nu_+=\nu_-$ here, $f_\pm$ is seen from Eq. (22) to be equal to or less than unity.

[12] H. Margenau and G. M. Murphy, *The Mathematics of Physics and Chemistry* (D. Van Nostrand Company, Inc., New York, 1943), p. 130.

A few applications, considered below, may serve to indicate the ease of a calculation based on Eq. (22) as compared with one involving a differentiation of the free energy into which parameters of the models have been previously introduced.

Applications

A coiled model of polyelectrolytes.—The Poisson-Boltzmann equation has been solved[7] for a spherically symmetrical model of a polyelectrolyte, using the approximation that a large number of mobile ions lie within the coils such that this region is about electrically neutral. The result obtained by these authors for the chemical potential of added salt [their Eqs. (32) and (33)] may also be obtained in a very straightforward manner by using Eq. (22) here and their Eqs. (23) and (24). This procedure avoids an awkward integration and differentiation. Actually these two values for μ differ roughly by an additive constant due to a slight difference in the definition of the entropy.[13]

"Parallel rod" model of polyelectrolytes.—Recently the Poisson-Boltzmann equation has been solved[3,4] exactly for the cylindrically symmetric case, no added salt, in which the polymeric ion assumed to be rod-like lies along the axis. No exact solution for ψ is available for the important case of added salt. Nevertheless the solution of these authors can also be applied to the calculation of the activity coefficient of infinitesimal amounts of such salt, inasmuch as such minute traces do not affect ψ. These authors, however, did not concern themselves with added salt and did not calculate any activity coefficient. Using their expression for ψ [Eq. (33) of reference 4], the product V_+V_- was calculated and it is found after considerable simplification that for a uni-univalent salt

$$f_\pm^2=2\frac{1-(a/R)^2}{\lambda^*[f_1-(a/R)^4f_2]} \quad (23)$$

where a=radius of the rod, R=radius of the cylinder (πR^2 is the volume of solution per macro-ion per unit length of the macro-ion), $\lambda^*=e^2\nu^*/DkTh^*$, there being ν^* ions fixed on a macro-ion of length h^*, β is the solution of $\lambda^*=(1+\beta^2)/\{1-\beta\cot[\beta\ln(a/R)]\}$ and f_1 and f_2 are functions of β. Thus

$$f_1=\frac{13+\beta^2}{(4+\beta^2)(1+\beta^2)},\qquad f_2=\frac{(\lambda^*-3)^2+4+\beta^2}{(4+\beta^2)[(\lambda^*-1)^2+\beta^2]}. \quad (24)$$

Depending on the magnitudes of the parameters λ^* and a/R, β may become imaginary. When β becomes

[13] Osawa *et al.* use a definition of the entropy of mixing based on mole fractions while here a definition based on concentrations is used. The latter is more simply related to the definitions of E_s and F_s while the former is more exact but also more awkward. In dilute solution they differ by an additive constant. In very concentrated solutions where a significant difference occurs neither presumably is especially correct, the effect of hydration and restricted volume on this entropy becoming very important then.

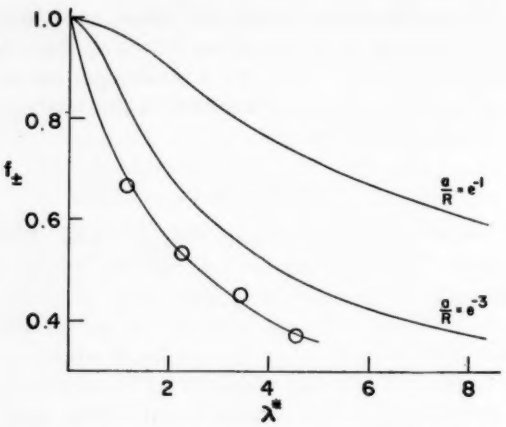

FIG. 1. The dependence of the activity coefficient $f_\pm$ of vanishingly small amounts of added salt on the charge parameter λ^* of the polyelectrolyte: theoretical, —— calc for $a/R=e^{-1}$ and for $a/R=e^{-3}$; experimental, -⊖- data of $f_\pm$ *vs* α are plotted on this graph using $\lambda^*=5.9\alpha$ as the conversion factor (see text).

imaginary it should be replaced in all these equations by $i|\beta|$ and we observe that

$$\cot(i|\beta|\ \ln a/R)=-i\coth(|\beta|\ \ln a/R).$$

Reasonable estimates of λ^* and of a/R may be made although some uncertainty arises because of the kinked nature of the polymeric ion. As the degree of neutralization α of polymethacrylic acid, say, increases, the polymeric ion becomes more highly charged and stretches due to the repulsion of its charges. When α exceeds about 0.35 viscosity and light scattering measurements[14] indicate that the dimensions change relatively little with increasing α. The viscosity data[14] suggest that for these values of α the head-to-tail length of the molecule is about half that of the linear chain length; that is, half the value it would have were it fully stretched. The question arises as to which length to use for h^*. The effective surface charge density acting on mobile ions at appreciable distances from the macro-ion should be that corresponding to the value estimated from observed head-to-tail length while the effective density acting on mobile ions very near the macro-ion might approximately be that estimated from the total linear chain length.

This uncertainty in h introduces a corresponding one in a/R and λ^*. The calculated values of $f_\pm$ are relatively insensitive to such errors in a/R while the effect of $f_\pm$ of an uncertainty in λ^* of a factor of 2 may be inferred from Fig. 1. In the present calculation we shall use the observed head-to-tail length, so that $h/\nu^*=1.25$ A. When the concentration of polyelectrolyte is c_0 equivalents per liter, then $\pi R^2h^*c_0=\nu^*$, so that when R and h are in A, we find $R=20.6/\sqrt{c_0}$ A. When $c_0=0.05\ M$, as in the following data, when $R=92$ A. The radius, a, of the cylindrical, charged rod is essentially the distance of closest approach of the mobile ions to a carboxyl ion fixed on the polymer chain. If a is about 6 A, then $a/R=e^{-2.75}$. Other reasonable choices of a will have only a minor effect on the calculated values of the activity coefficient. When α exceeds 0.35 we estimate from the previously mentioned head-to-tail length $\lambda^*=5.7\alpha$, approximately.

In Fig. 1 the mean ion activity coefficients of traces of salt in the presence of polyelectrolyte, estimated from Eq. (23), are given as a function of λ^* for $a/R=e^{-1}$ and $a/R=e^{-3}$. In performing these calculations, λ^* was calculated for various values of β, for these two values of a/R, using the equation relating λ^* to β, rather than solving this transcendental equation for β. A graphical representation for the dependence of λ^* on β has been given by Lifson and Katchalsky.[15]

Experimental activity coefficients[16] have been determined for various amounts of added salt as a function of the degree of neutralization. These data extrapolated to zero concentration of added salt are plotted in the form $f_\pm$ *vs* λ^* in Fig. 1 assuming $\lambda^*=5.7\alpha$. The agreement with the curve for $a/R=e^{-3}$ is reasonably good considering the nature of the approximations and the fact that no adjustable parameters were used. To obtain exact agreement an arbitrary choice of $\lambda^*=9.5\alpha$ is necessary.

3. Calculation of Osmotic Pressure

The osmotic pressure of a salt-polyelectrolyte system may be calculated by differentiating the free energy, as given by Eq. (3), with respect to volume keeping the amounts of polyelectrolyte and added salt constant. Recalling from the discussion in Sec. 1 that this derivative equals that at constant polymer configurational variable h, fixed polymer charge distribution and fixed degree of neutralization, the contributions to the free energy which may change with volume under these restrictions are $-TS_m$, E_e and $-TS$ as defined in Eqs. (4), (7), and (9), respectively. The changes in these quantities will now be calculated. The contribution of the motion of the macro-ion to the osmotic pressure will, however, be neglected for the present purposes.

A change in volume δV will change the potential, the charge density and the upper limit of integration of the expressions for S_m, E_e, and for S. The contribution to δS_m arising from a change in the upper limit of integration in (4) is zero since the polymer lies within V rather than on the bounding surface S of this volume. At fixed distribution of polymer charges, α_r does not change so that the change in the integrand of the expression for S_m is also zero. That is, δS_m is zero.

Indicating the values of ψ and ρ on the surface of the volume V by a superscript s we have

$$2\delta E_e=\int\psi(\delta\rho+\delta\rho_p)dV+\int(\rho+\rho_p)\delta\psi dV+\psi^s(\rho^s+\rho_p{}^s)\delta V. \quad (25)$$

[14] See A. Oth and P. Doty, J. Phys. Chem. **56**, 43 (1952).

[15] S. Lifson and A. Katchalsky, J. Polymer Sci. **13**, 43 (1954).

[16] A. Katchalsky and S. Lifson, J. Polymer Sci. **11**, 409 (1953).

By expressing $\delta\psi$ and ψ in terms of the ρ's using Eq. (12), it is found that

$$\delta E_e = \int (\rho+\rho_p)\delta\psi dV$$

$$= \int \psi(\delta\rho+\delta\rho_p)dV + \psi^s(\rho^s+\rho_p{}^s)\delta V. \quad (26)$$

At fixed polymer configuration and polymer charge distribution $\delta\rho_p=0$ and since ρ_p lies within V rather than on its surface S, $\rho_p{}^s=0$. Thus it follows that

$$\delta E_e = \int \psi\delta\rho dV + \psi^s\rho^s\delta V. \quad (27)$$

We also have from (9)

$$\delta S = -k\textstyle\sum_i (c_i{}^s \ln c_i{}^s - c_i{}^s) - k\sum_i \int \ln c_i \delta c_i dV. \quad (28)$$

Using the Boltzmann expression for c_i, we obtain

$$T\delta S = \rho^s\psi^s\delta V - kT\textstyle\sum_i \left(c_i{}^s\delta V + \int \delta c_i dV\right) \ln\frac{n_i}{V_i}$$

$$+ \int \psi\delta\rho dV + kT\textstyle\sum_i c_i{}^s\delta V. \quad (29)$$

The change in the number of mobile ions of the ith type δn_i is equal to $(c_i{}^s\delta V + \int \delta c_i dV)$ and is zero. It thus follows that

$$\delta F = \delta E_e - T\delta S = -kT\textstyle\sum_i c_i{}^s\delta V. \quad (30)$$

The introduction of solvent to increase the volume also results in another free-energy change which in dilute solution becomes $\mu_w{}^0\delta n_w$ to a good approximation, $\mu_w{}^0$ being the chemical potential of pure solvent. Inclusion of this in (30) and division of the equation by δn_w yields for the chemical potential of the solvent $\mu_w = \mu_w{}^0 + (\partial F/\partial V)\bar{V}_w$, $\bar{V}_w$ being the partial molar volume of solvent. Inasmuch as the osmotic pressure π equals $(\mu_w{}^0 - \mu_w)/\bar{V}_w$ in dilute solutions, we have

$$\pi = -\frac{\partial F}{\partial V} = kT\textstyle\sum_i c_i{}^s. \quad (31)$$

It may be verified that the additional assumption of random mixing of the neutralized and unneutralized groups on the polymer chain leads to the same equation for π.

The result (31) for the contribution of the mobile ions is quite reasonable. The potential gradient at the boundary of the volume V is zero so that the ions there are, according to the present formalism, not acted on by any electrostatic forces. That is, the solution at the boundary is an "ideal solution," and the osmotic pressure of an ideal solution is kT multiplied by the total concentration of its solute.[17] Since the concentration at the boundary is $\sum_i c_i{}^s$ the osmotic pressure is $kT\sum_i c_i{}^s$. This sum is, at least in the absence of added salt, less than the average total concentration in the solution so that the osmotic pressure is less than the value it would have if the solution were everywhere ideal. When the solution becomes ideal the concentration of an ion at the boundary becomes equal to its average concentration, n_i/V, and the osmotic pressure assumes its ideal value $\sum_i (n_i/V)kT$.

As an application of (31), we consider the derivation of an expression obtained for the osmotic pressure using the "parallel rod" picture. By computing the electrostatic free energy in terms of the parameters, a/R and λ^*, of this model and differentiating it with respect to the volume, Katchalsky and Lifson[15] calculated the osmotic pressure. The differentiation is, however, a particularly tedious one and an equation for the osmotic pressure can be obtained much more simply using (31) and their expression for the concentration. Thus we find immediately

$$\pi = \nu^* kT(1-\beta^2)n_p/2\lambda^* \quad (32)$$

where $n_p = 1/\pi R^2 h^*$, the number of macro-ions per cc, and β, ν^*, and λ^* have been defined earlier. Actually this equation is slightly different from Eq. (34) of their paper. This difference arises from a minor error in the definition there of the osmotic pressure of the uncharged system, π_i [their Eq. (30)] which does not take into account the volume of the solution unavailable to the mobile ions. Their value of π_i should be multiplied by the factor $R^2/(R^2-a^2)$.

Finally it is to be observed that Eq. (31) is independent of Eq. (22) which was derived in the previous section. These equations are related to the chemical potentials of solvent and added salt, respectively, and these are independent. However, any expression derived for the chemical potential of the polyelectrolyte would not be independent of these since the Gibbs-Duhem equation connects all three chemical potentials.

4. Calculation of Titration Curves

It will be assumed for simplicity in this section that the protons attached to some of the basic groups in these polybasic acids (or bases) are randomly distributed among all groups. That is, Eq. (5) for S_m will be used rather than Eq. (4). This may be regarded as a type of Bragg-Williams approximation used in the treatment of order-disorder phenomena. The error inherent in this assumption for the case where nearest neighbor interaction between the charged groups of polyelectrolytes predominates has been considered elsewhere.[18] Under the experimental conditions discussed there (appreciable added salt present) it appeared to be a fairly good approximation. In the present

[17] This argument was suggested to the writer by Dr. H. Morawetz.

[18] R. A. Marcus, J. Phys. Chem. 58, 621 (1954).

model the assumption will be the more appropriate the less ψ (and therefore, according to (65), α_r) varies over the space occupied by the macro-ion.

It will be recalled that the equilibrium value of the degree of neutralization α is determined by setting the variation in the free energy equal to zero, the volume, salt, number of available protons, and polymer configuration being held fixed. The change in the various contributions to F, listed in Eq. (3), will now be estimated. At constant polymer configuration S_p is constant. The term (F_e-TS_{id}) equals (E_e-TS). At constant volume, δE_e and δS are given by Eqs. (14) and (17), respectively. With the added restriction of constant salt concentration it thus follows that

$$\delta(E_e-TS)=\int\psi\delta\rho_p dV+kT\ln\frac{n_H}{V_H}\delta n_H. \qquad (33)$$

At constant polymer configuration and assumed random distribution of neutralized and unneutralized groups ρ_p changes only because of a change in the total number of ionized groups. Since the ionized groups are assumed to be randomly distributed the local concentration of the ionized groups on the polymer is proportional to the sum of the concentrations of all groups, neutralized plus unneutralized. Therefore the fractional change in the charge density $\delta\rho_p/\rho_p$ with change in α is constant throughout the polymer and is, in fact, equal to the over-all fractional change in the number of ionized groups, $\delta\alpha/\alpha$. That is, $\delta\rho_p$ in Eq. (33) is related to $\delta\alpha$ according to the equation

$$\frac{\delta\rho_p}{\rho_p}=\frac{\delta\alpha}{\alpha}. \qquad (34)$$

The change in S_m, given by (5) is

$$\delta S_m=-mk[\ln(\alpha/1-\alpha)]\delta\alpha,$$

while the variation in $\sum_i n_i\mu_i^0$ at constant salt is $\mu_H{}^0\delta n_H$. Observing that $\int\delta\rho_p dV=e_p m\delta\alpha=-e_H\delta n_H$ it then follows, if the individual ions on the polymer are univalent anions, say, $(e_p=-e_H)$, that

$$\delta F=\left[kT\ln\frac{\alpha}{1-\alpha}+(\mu_H{}^0+\mu_A{}^0-\mu_{HA}{}^0)+\frac{\int\psi\delta\rho_p dV}{m\alpha}+kT\ln\frac{n_H}{V_H}\right]\delta n_H \qquad (35)$$

i.e.,

$$-\ln\frac{\alpha n_H}{(1-\alpha)V_H}=\frac{\Delta\mu^0}{kT}+\frac{\int\psi\rho_p dV}{m\alpha kT}. \qquad (36)$$

Equation (36) may be used, in conjunction with Eq. (22) for the mean ion-activity coefficient, to estimate the activity of some acid such as HCl in the presence of a polymeric acid as a function of the latter's degree of neutralization, α. For example, the logarithm of the activity of HCl is

$$\ln a_{HCl}=\ln\frac{n_H n_{Cl} f_\pm{}^2}{V_H V_{Cl}}=-\frac{\Delta\mu^0}{kT}-\frac{\int\psi\rho_p dV}{m\alpha kT}+\ln\left[\frac{(1-\alpha)n_{Cl}}{\alpha V_{Cl}}\right] \qquad (37)$$

where $V_{Cl}=\int\exp(e\psi/kT)dV$.

Alternatively, Eq. (36) may be used to obtain an expression for the dependence of pH on α but there is some uncertainty arising from the liquid junction potential, E_L, present in the electrochemical cell used to define the pH. If in the presence of salt E_L is reasonably independent of the degree of neutralization, α, of the polymeric acid or base, then a calculation of the change of pH with α only involves an estimate of the change in $-\log a_H$ with α, for then the $p\mathrm{H}=-\log a_H$ +constant. According to Eq. (19) previously given for the chemical potential of an ion, $-\log a_H=-\log n_H/V_H$ and it therefore follows from (36) that

$$p\mathrm{H}=\log\frac{\alpha}{1-\alpha}+\frac{\Delta\mu^0}{2.3kT}+\frac{\int\psi\rho_p dV}{2.3m\alpha kT}+\text{constant}. \qquad (38)$$

Defining the pK of the polymeric acid as $p\mathrm{H}-\log\alpha/1-\alpha$ we have to the same degree of approximation

$$pK=\frac{\Delta\mu^0}{2.3kT}+\frac{\int\psi\rho_p dV}{2.3m\alpha kT}+\text{constant}. \qquad (39)$$

When the ions fixed on the polymer chain are regarded as forming a surface charge density σ rather than a volume charge density ρ_p, the integral in (38) and (39) should be replaced by the surface integral $\int_A\psi\sigma dA$.

When no added salt is present, it is possible that depending upon the conditions the change of ionic concentration accompanying neutralization may have a somewhat larger effect on the liquid junction potential than is the case when salt is present. However, in the absence of added salt the repulsion of the like charges on a macro-ion is usually poorly shielded and the change of pK with α is generally quite large. Changes in E_L with α are presumably of a smaller order of magnitude. In that case Eq. (39) may again be used.

If in this treatment the simplifying assumption of random mixing of neutralized and unneutralized groups had not been made, then an equation similar to (38) would have been obtained, but with the exception that $(\int\psi\rho_p dV)/(m\alpha)+kT\ln(\alpha/1-\alpha)$ would have been replaced by $kT\ln D$ where D is defined in (66).

5. Note on the Equilibrium Configuration

In the calculation of the various thermodynamic properties a knowledge of the polymer configuration is necessary. Making certain assumptions, a parameter roughly defining this configuration may be estimated from viscosity or light scattering measurements, say. This parameter may, for example, be the radius of the polyelectrolyte, assumed to be coiled. If, instead, the polymer is assumed to be rod-like no such additional information is necessary.

On the other hand, the equilibrium value of a configurational variable such as radius of polymer or average end-to-end distance may be calculated by setting the change in the free energy F equal to zero for any deviation of this variable from its equilibrium value, at constant composition, volume, temperature, and degree of neutralization. In Appendix II it has been shown in this manner that the equilibrium value of h satisfies the relation

$$kT\int \ln(1-\alpha_r)\frac{dC_p}{dh}dV = T\frac{dS_p}{dh}. \tag{40}$$

A knowledge of the dependence of α_r and ψ on position and on h, and of C_p and S_p on h, is needed to solve this equation. Thus α_r is related to ψ by the relation (65), $\alpha_r = De^{-e_p\psi/kT}/(1+De^{-e_p\psi/kT})$, which can be introduced into the Poisson-Boltzmann equation. This latter equation may then be solved for $\psi(r,h)$. Estimates of the dependence of C_p and S_p on h for the uncharged polymer can be made and, according to assumption (3), of the first section, these could be used for the macro-ion in order to solve Eq. (40) for h.

When random mixing of the neutralized and unneutralized groups on the polymetric molecule is assumed, then it may be verified by using the same procedure as in Appendix II, only setting $\alpha_r=\alpha$ in Eq. (56) for the free energy there, that h is the solution of

$$\alpha e_p\int \psi\frac{dC_p}{dh}dV = T\frac{dS_p}{dh}. \tag{41}$$

Alternatively, it can readily be shown with the aid of (65) that (40) reduces to this equation when ψ varies but little over the space occupied by the polymer.

ACKNOWLEDGMENTS

The writer would like to express his appreciation to Dr. E. M. Loebl and Dr. H. Morawetz of this institute who read the manuscript critically and offered a number of helpful comments.

APPENDIX I

Comparison of Various Expressions for Fe

(i) Comparison of Eqs. (6) and (8).

When the degree of charging of the entire system is λ the corresponding value of the electrostatic free energy will be denoted by F_e'. That is, $F_e'=F_e$ when $\lambda=1$. Accordingly, we may rewrite these equations in terms of F_e':

$$F_e' = \int_{\lambda=0}^{\lambda=1} 2E_e'\frac{d\lambda}{\lambda}, \tag{6'}$$

$$F_e' = T\int_{T=\infty}^{T=T} E_e' d\left(\frac{1}{T}\right), \tag{8'}$$

where the integration in (8') is to be performed at constant dielectric constant D. The superscript $'$ will be used to signify the values of ψ, ρ, etc. when $\lambda\neq 1$. Differentiating the first expression with respect to λ we have

$$\left(\frac{\partial F_e'}{\partial\lambda}\right)_T = \frac{2E_e'}{\lambda}$$

and therefore

$$\left(\frac{\partial(F_e'/T)}{\partial\lambda}\right)_T = \frac{2E_e'}{\lambda T}.$$

Deriving the second with respect to $1/T$ at constant D we have

$$\left(\frac{\partial(F_e'/T)}{\partial(1/T)}\right)_{\lambda,D} = E_e'.$$

To show the equivalence of Eqs. (6) and (8) it is sufficient, therefore, to show that

$$\left(\frac{\partial(F_e'/T)}{\partial\lambda}\right)_T = \frac{2}{\lambda T}\left(\frac{\partial(F_e'/T)}{\partial(1/T)}\right)_{\lambda,D}.$$

If at constant D, F_e' depends on λ and T only through a variable λ^2/T, then this equation can readily be derived by expressing each partial in terms of the derivative with respect to λ^2/T:

$$\left(\frac{\partial F_e'/T}{\partial\lambda}\right)_T = \left(\frac{\partial F_e'/T}{\partial\lambda^2/T}\right)_D\left(\frac{\partial\lambda^2/T}{\partial\lambda}\right)_T = \frac{2\lambda}{T}\frac{\partial F_e'/T}{\partial\lambda^2/T}, \tag{42}$$

$$\left(\frac{\partial F_e'/T}{\partial 1/T}\right)_{\lambda,D} = \left(\frac{\partial F_e'/T}{\partial\lambda^2/T}\right)_D\left(\frac{\partial\lambda^2/T}{\partial 1/T}\right)_\lambda = \lambda^2\frac{\partial F_e'/T}{\partial\lambda^2/T}. \tag{43}$$

The elimination of $\partial F_e'/T/\partial\lambda^2/T$ from these equations yields the desired equation. As expected, at constant D the statistical mechanical expression for F_e'/T,

$$F_e' = -kT\ln\left[\int\cdots\int\exp\left(-\sum_{>i}\frac{\lambda^2 e_i e_j}{|\mathbf{r}_i-\mathbf{r}_j|DkT}\right)\times dV_1\cdots dV_N/V^N\right] \tag{44}$$

depends on λ and T only through a dependence on λ^2/T and so fulfills this equation. The integration is over the coordinates of all mobile ions in V but the i and j refer to the coordinates of all ions.

The Poisson-Boltzmann equation can be shown to yield the same dependence of F_e'/T on λ and T. We first observe that

$$\psi'(\mathbf{r})=-\frac{1}{D}\int\frac{\rho'(\mathbf{r}'')+\rho_p'(\mathbf{r}'')}{|\mathbf{r}-\mathbf{r}''|}dV'' \qquad (12')$$

where $\rho'=\lambda\sum_i e_i c_i'$. Since c_i' depends on λ and T only through the variable $\lambda\psi'/T$, according to the Boltzmann expression, $c_i'=n_i\exp(-\lambda e_i\psi'/kT)/\int\exp(-\lambda e_i\psi'/kT)dV$, it follows that ρ' equals λ times a function of $\lambda\psi'/T$. Let $\rho'=\lambda f(\lambda\psi'/T)$. Throughout, regardless of the value of λ and T, the polymer configuration and its charge distribution are held constant in integrating these expressions for F_e'; that is, $\rho_p'/\lambda=\alpha_r C_p$ is independent of λ and of T. Thus it follows from

$$\frac{\lambda\psi'}{T}=-\frac{1}{D}\int\frac{\lambda^2}{T}\left[\frac{f(\lambda\psi'/T)+\rho_p'/\lambda}{|\mathbf{r}-\mathbf{r}''|}\right]dV \qquad (45)$$

that $\lambda\psi'/T$ depends only on λ^2/T at constant D.

Since $E_e'=\frac{1}{2}\int\psi'(\rho'+\rho_p')dV$ we conclude from

$$\frac{E_e'}{T}=\frac{1}{2}\int\frac{\lambda\psi'}{T}[f(\lambda\psi'/T)+\rho_p'/\lambda]dV \qquad (46)$$

that E_e'/T is a function only of $\lambda\psi'/T$ and therefore, at constant D, only a function of λ^2/T. Since

$$F_e'/T=\int_{\lambda=0}^{\lambda=\lambda}\frac{2E_e'}{T}\frac{d\lambda}{\lambda},$$

F_e'/T is, at constant D, only a function of λ^2/T, since $d\lambda/\lambda$ can for integration purposes be expressed in terms of the derivative of a function (logarithm) of λ^2/T. This establishes the statement that the assumption of the Poisson-Boltzmann equation does not affect the equality of Eqs. (6) and (8).

(ii) Comparison of Eqs. (6) and (11)

It has been established in the previous section that the use of the Poisson-Boltzmann Eq. (1) does not affect the identity

$$E_e=\left(\frac{\partial F_e/T}{\partial 1/T}\right)_D=F_e-\left(\frac{\partial F_e}{\partial T}\right)_D,$$

where F_e is given by Eq. (6). Using this result it may be concluded that it is sufficient to show that $[\partial F_e/\partial T]_D=-(S-S_{id})$ in order to demonstrate that the use of Eq. (1) does not render Eqs. (6) and (11) inconsistent. The entropy difference $(S-S_{id})$ is computed from Eqs. (9) and (10). In the following proof all differentiations with respect to T will be performed at constant λ and D, and those with respect to λ, at constant T and D.

We have from the differentiation of (6)

$$\frac{\partial F_e}{\partial T}=\int\int\left[(\rho'+\rho_p')\frac{\partial\psi'}{\partial T}+\psi'\left(\frac{\partial\rho'}{\partial T}+\frac{\partial\rho_p'}{\partial T}\right)\right]\frac{d\lambda}{\lambda}dV. \qquad (47)$$

Expressing ψ' and $\partial\psi'/\partial T$ in terms of ρ' and $\partial\rho'/\partial T$ with the aid of (12'), it may be verified that Eq. (47) becomes

$$\frac{\partial F_e}{\partial T}=2\int\int\psi'\left(\frac{\partial\rho'}{\partial T}+\frac{\partial\rho_p'}{\partial T}\right)\frac{d\lambda}{\lambda}dV. \qquad (48)$$

Since the polymer configuration is kept constant in integrating the expression for F_e, $\partial\rho_p'/\partial T=0$ and

$$\frac{\partial F_e}{\partial T}=2\int\int\psi'\frac{\partial\rho'}{\partial T}\frac{d\lambda}{\lambda}dV. \qquad (49)$$

Since ρ' is λ times a function of λ^2/T, it may be verified that

$$\frac{1}{\lambda}\frac{\partial\rho'}{\partial T}=\frac{\partial}{\partial T}(\rho'/\lambda)=-\frac{\lambda}{2T}\frac{\partial}{\partial\lambda}(\rho'/\lambda) \qquad (50)$$

by expressing each partial derivative in terms of a derivative with respect to λ^2/T. Substituting this into Eq. (49) and integrating by parts, we have

$$\frac{\partial F_e}{\partial T}=-\frac{\int\rho\psi dV}{T}+\int\int\left(\frac{\rho'}{T}\frac{\partial\psi'}{\partial\lambda}+\frac{\rho'\psi'}{\lambda T}\right)d\lambda dV. \qquad (51)$$

This expression may be simplified by employing the following identity [established by carrying out the differentiation on the left-hand side of (52) and then introducing the Boltzmann expression for c_i']:

$$k\frac{\partial}{\partial\lambda}\sum_i n_i\ln V_i'=-\int\left(\frac{\rho'}{T}\frac{\partial\psi'}{\partial\lambda}+\frac{\rho'\psi'}{\lambda T}\right)dV. \qquad (52)$$

Integrating this from $\lambda=0$ to $\lambda=1$ the left-hand side becomes $k\sum_i n_i\ln(V_i/V)$ since $V_i'=V_i$ when $\lambda=1$ and $V_i'=V$ when $\lambda=0$. Thus from Eqs. (51) and (52) it follows that

$$\frac{\partial F_e}{\partial T}=-\frac{\int\rho\psi dV}{T}-k\sum_i n_i\ln\frac{V_i}{V}. \qquad (53)$$

Since according to (2)

$$-\frac{\rho\psi}{kT}=-\frac{\sum_i e_i c_i\psi}{kT}=\sum_i c_i\ln\frac{c_i V_i}{n_i} \qquad (54)$$

it follows that from (53)

$$\frac{\partial F_e}{\partial T}=k\sum_i \int c_i \ln c_i dV - k\sum_i n_i \ln\frac{n_i}{V}$$

$$=k\sum_i \int (c_i \ln c_i - c_i)dV - k\sum_i\left(n_i \ln\frac{n_i}{V}-n_i\right),$$

$$=-(S-S_{id}). \tag{55}$$

APPENDIX II

Calculation of Distribution Functions and of Effect of Redistribution of Groups on δF

It will be shown here that the redistribution of the charges on the polymer and, incidentally, the change in the configurational variable h, both of which accompany a reversible change in state, contribute nothing to the calculated free-energy change δF, so that δF equals that estimated at fixed relative distribution, α_r/α and at fixed h.

On the basis of Eq. (3) for F and the various equations given in the text for the terms which occur there, we may write

$$F=\int K dV - TS_p \tag{56}$$

where

$$K=kTC_p[\alpha_r \ln\alpha_r+(1-\alpha_r)\ln(1-\alpha_r)]$$

$$+\tfrac{1}{2}\psi(\textstyle\sum_i c_i e_i+\alpha_r C_p e_p)+kT\sum_i (c_i \ln c_i - c_i)$$

$$+\textstyle\sum_i c_i\mu_i^0+C_p[\alpha_r\mu_A{}^0+(1-\alpha_r)\mu_{HA}{}^0]. \tag{57}$$

It follows from $\alpha_r C_p=(\alpha_r/\alpha)C_p\alpha$ and $c_i=(c_i/n_i)n_i$ that $\delta(\alpha_r C_p)=\alpha C_p\delta(\alpha_r/\alpha)+(\alpha_r/\alpha)C_p\delta\alpha+\alpha_r\delta C_p$ and $\delta c_i=n_i\delta(c_i/n_i)+(c_i/n_i)\delta n_i$. That is, the change in c_i for example may be written as the sum of a change in n_i at fixed relative distribution c_i/n_i, plus a change in the relative distribution. We may then write for δF,

$$\delta F=\int\left[\frac{\partial K}{\partial(\alpha_r/\alpha)}\delta\left(\frac{\alpha_r}{\alpha}\right)\right.$$

$$\left.+\textstyle\sum_i\dfrac{\partial K}{\partial(c_i/n_i)}\delta\left(\dfrac{c_i}{n_i}\right)+\dfrac{\partial K}{\partial C_p}\dfrac{dC_p}{dh}\delta h\right]dV$$

$$+\delta\int (K)_{\alpha_r/\alpha,c_i/n_i,C_p}dV-T\frac{dS_p}{dh} \tag{58}$$

where in the partial derivative $\partial K/\partial(\alpha_r/\alpha)$, for example, α, c_i/n_i, n_i, C_p and all thermodynamic variables are held fixed. The variation in the second integral is performed at fixed α_r/α, c_i/n_i, and C_p, as indicated by the subscripts, and only differs from zero when there is a change in α or in the thermodynamic state. Actually, because of the equilibrium relation $\partial F/\partial\alpha=0$, it follows therefore, that in a given thermodynamic state it equals zero. At equilibrium in a specified thermodynamic state δF equals zero and the variations in α_r/α, c_i/n_i and C_p are subject to the restrictions of constant number of each type of ion, and constant number of neutralized and of unneutralized groups on the polymer. Therefore, in a given state

$$\left.\begin{aligned}&\frac{1}{\alpha}\int\delta(\alpha_r C_p)dV=0\\&\frac{1}{n_i}\int\delta c_i dV=0\quad\text{for all } i\\&\int\delta C_p dV=0\end{aligned}\right\}. \tag{59}$$

Multiplying these equations by the constants A, B_i, and C, the Lagrangian multipliers, and adding to (58), where the second integral and δF are set equal to zero, it follows that the coefficients of $\delta(\alpha_r/\alpha)$, $\delta(c_i/n_i)$ and δh are zero since this new equation is obeyed for arbitrary variations in α_r/α, c_i/n_i, and h. [At least these variations in α_r/α and c_i/n_i are arbitrary subject to (59) and this limitation may be removed by imagining V spanned by cells, the integral of K over V becoming a sum over cells, and choosing A, and B_i so that the coefficient of the variations in a particular cell is zero. The variations in α_r/α and c_i/n_i in the other cells are arbitrary so that the coefficients of these variations must equal zero in these cells too if the equation is to be obeyed for all variations.] By this process Eqs. (60), (61), and (62) defining the equilibrium α_r/α, c_i/n_i, and h are obtained

$$\frac{\partial K}{\partial(\alpha_r/\alpha)}+C_p A=0 \tag{60}$$

$$\frac{\partial K}{\partial(c_i/n_i)}+B_i=0 \tag{61}$$

$$\int\left(\frac{\partial K}{\partial C_p}+A\frac{\alpha_r}{\alpha}+C\right)\frac{dC_p}{dh}dV-T\frac{dS_p}{dh}=0. \tag{62}$$

Introducing these results for $\partial K/\partial(\alpha_r/\alpha)$ and $\partial K/\partial C_p$ etc., into (58) it follows that

$$\delta F=-A\int\delta\left(\frac{\alpha_r C_p}{\alpha}\right)dV-C\int\delta C_p dV$$

$$+\delta\int(K)_{\alpha_r/\alpha,C_p}dV \tag{63}$$

where we have combined the term involving $\partial K/\partial(c_i/n_i)$ with the last term in Eq. (58). In Eq. (63) the first term is really $-A$ multiplied by $m\delta(\alpha/\alpha)$, which always

equals zero[19] while the second term is also always zero. Therefore,

$$\delta F=\delta\int(K)_{\alpha_r/\alpha,C_p}dV=\delta(F)_{\alpha_r/\alpha,C_p} \tag{64}$$

which establishes the desired result.

Introducing expression (57) for K into (60), (61), and (62) it follows that α is given by Boltzmann expression (2), that α_r is given by (65), where D is a constant estimated by multiplying

$$\alpha_r=\frac{De^{-e_p\psi/kT}}{1+De^{-e_p\psi/kT}} \tag{65}$$

both sides of (65) by C_pdV and integrating over V,

$$m\alpha=\int C_p\alpha_r dV=D\int\frac{e^{-e_p\psi/kT}}{1+De^{-e_p\psi/kT}}dV \tag{66}$$

and that h is the solution of

$$\int(kT\ln\alpha_r+e_p\psi)\frac{dC_p}{dh}dV=T\frac{dS_p}{dh}. \tag{67}$$

[19] Actually,

$$0=m\delta(\alpha/\alpha)=\delta\int(C_p\alpha_r)/\alpha dV=\alpha_r{}^sC_p{}^s\delta V/\alpha+\int\delta(\alpha_rC_p/\alpha)dV$$

and $C_p{}^s$ equals zero since the polymer lies within V and not on the bounding surface, S, of this volume, so that this expression for $m\delta(\alpha/\alpha)$ becomes $\int\delta(\alpha_rC_p/\alpha)dV$.

THE JOURNAL OF CHEMICAL PHYSICS VOLUME 23, NUMBER 6 JUNE, 1955

Photochemical Studies of the Porphyrins. III. Photoreduction of a Porphyrin by Benzoin

GILBERT R. SEELY* AND MELVIN CALVIN
Department of Chemistry and Radiation Laboratory,† University of California, Berkeley, California

(Received October 18, 1954)

An examination of the kinetics of the photoreduction of zinc tetraphenylporphin by benzoin is reported. The products are successively the dihydro- (chlorin) derivative; a tetrahydro-derivative and possibly a hexahydro compound as well. It is demonstrated that the primary requirement is the photoactivation of the benzoin; a secondary reaction, involving photoactivated porphyrin as well, is also demonstrated. The quantum yield based on light absorbed by benzoin varies between 0.01 and 0.06.

WORK has been previously reported from this laboratory[1–3] on the photochemical oxidation of zinc dihydrotetraphenylporphin, also known as zinc tetraphenylchlorin. Due to interest in the role of chlorophyll in photosynthesis, and the possibility that reduction or oxidation of chlorophyll may have a function in that role, we have continued study of photochemical reactions of simple porphyrins.

Since zinc tetraphenylchlorin had been quantitatively oxidized to the porphin by quinone,[1] when irradiated by light absorbed by the chlorin, we sought to reverse this reaction by photochemically reducing zinc tetraphenylporphin. It was found that, using the following reducing agents in deoxygenated benzene, alcohol, or pyridine solutions, reduction could be detected spectroscopically after exposure to sunlight: benzoin, *p*-dimethylaminobenzoin, ascorbic acid, dihydroxyacetone, dioxymaleic acid, reductone, hydrazobenzene, semicarbazide, *n*-hexyl mercaptan, 1,2-ethanedithiol and arabinose. The rapidity and extent of reduction varied greatly with the reducing agent used; with benzoin, reduction was spectroscopically complete after 15 or 20 minutes of sunlight. The mercaptans and arabinose produced only a trace of zinc tetraphenylchlorin after days of exposure to sunlight. The hydrazines worked very little faster, and the hydroxyketones listed (except benzoin), required several hours, or even days for significant reduction.

In general, reduction was found to occur in two steps. At first, a band near 625 mμ, indicative of zinc tetraphenylchlorin, was seen to emerge. Later, a band near 600 mμ intensified, which is indicative of a compound which will be identified as a zinc tetraphenyltetrahydroporphin. On prolonged exposure to light, this band, too, fades, leaving a washed-out spectrum.

The reduction by benzoin was the only one fast enough to permit kinetic measurements under artificial illumination, so this reagent was used throughout, for determination of the quantum yield and the mechanism of the reduction.

* This paper was abstracted from the thesis of Gilbert R. Seely, submitted in partial fulfillment of the requirement for Doctor of Philosophy, University of California, Berkeley, February, 1954. Present address: 9771 TSU, Det. 3, Dugway Proving Grounds, Utah.

† The work described in this paper was supported by the U. S. Atomic Energy Commission.

[1] G. D. Dorough, Ph.D. thesis, University of California, Berkeley, 1947; M. Calvin and G. D. Dorough, J. Am. Chem. Soc. **70**, 699 (1948); G. D. Dorough and M. Calvin, Science **105**, 433 (1947).

[2] Ball, Calvin, and Dorough, J. Am. Chem. Soc. **68**, 2278 (1946).

[3] F. M. Huennekens, Ph.D. thesis, University of California, Berkeley, 1948; F. M. Huennekens and M. Calvin, J. Am. Chem. Soc. **71**, 4024, 4031 (1949).

EXPERIMENTAL

Zinc tetraphenylporphin was prepared directly by heating 5 cc pyrrole, 10 cc benzaldehyde, and 5 g zinc acetate in 15 cc of pyridine for four days at 180°C in a sealed tube. On cooling, the product separates as purple crystals, which may be filtered from the tarry by-products, and washed with a mixture of acetone and ether.[1]

Before use, this crude material must be purified by chromatography. The most convenient way was found to be as follows: crude porphin is dissolved in benzene, and put onto a column composed of a mixture of ignited magnesia and Hy-flo Super Cel. Development is continued with benzene until the purple, fastest moving layer, which is porphin, is sufficiently separated from the green layer of zinc chlorin. Sometimes a trace of pyridine in the developer was found helpful in later stages. The column is then extruded, and the part containing the porphin treated with water. Slaking releases a solution of zinc porphin in benzene, which is decanted, filtered, and evaporated. Stock solutions were made up in benzene, and were stable indefinitely, kept dark. If pyridine is used in the development, the zinc porphin pyridinate complex crystallizes out, which can be made to lose its pyridine by drying in a vacuum oven above 100°C. The benzoin used for the reductions was recrystallized from alcohol-water.

In order for reduction to take place, oxygen must be completely absent; if present, a side reaction occurs. Standard solutions of zinc porphin and of benzoin in benzene are measured into a square pyrex tube, of 1 cm sides, having two opposite faces ground optically flat. Extra benzene is added, the spectrum is taken, and the contents of the tube are flushed, near the boiling point of benzene, with nitrogen which has been freed of oxygen by passing it through two bottles containing Fieser's solution and one containing sodium benzophenone ketyl in toluene. The tube is cooled, covered with a head, and evacuated as an extra precaution. During this procedure, the volume of the contents of the tube is reduced by about one-third.

The concentration of zinc porphin is obtained from the spectrum, taken after flushing and evacuation. From the concentration of the benzoin before flushing, and the spectra of porphin before and after flushing, the concentration of benzoin after flushing may be obtained. Such a large excess of benzoin is used that its concentration remains essentially constant during the course of the reaction.

The contents of the tube are now irradiated, and at intervals the spectrum is taken, for from the rate of fall of the absorption bands characteristic of the porphin the rate of reduction may be found. Light from a General Electric Reflector Sunlamp is passed through a large aperture, focused by a condensing lens onto the receptive surface of a Kurlbaum large area bolometer, and the reaction tube placed in a water thermostat equipped with a diaphragm, so that all light reaching

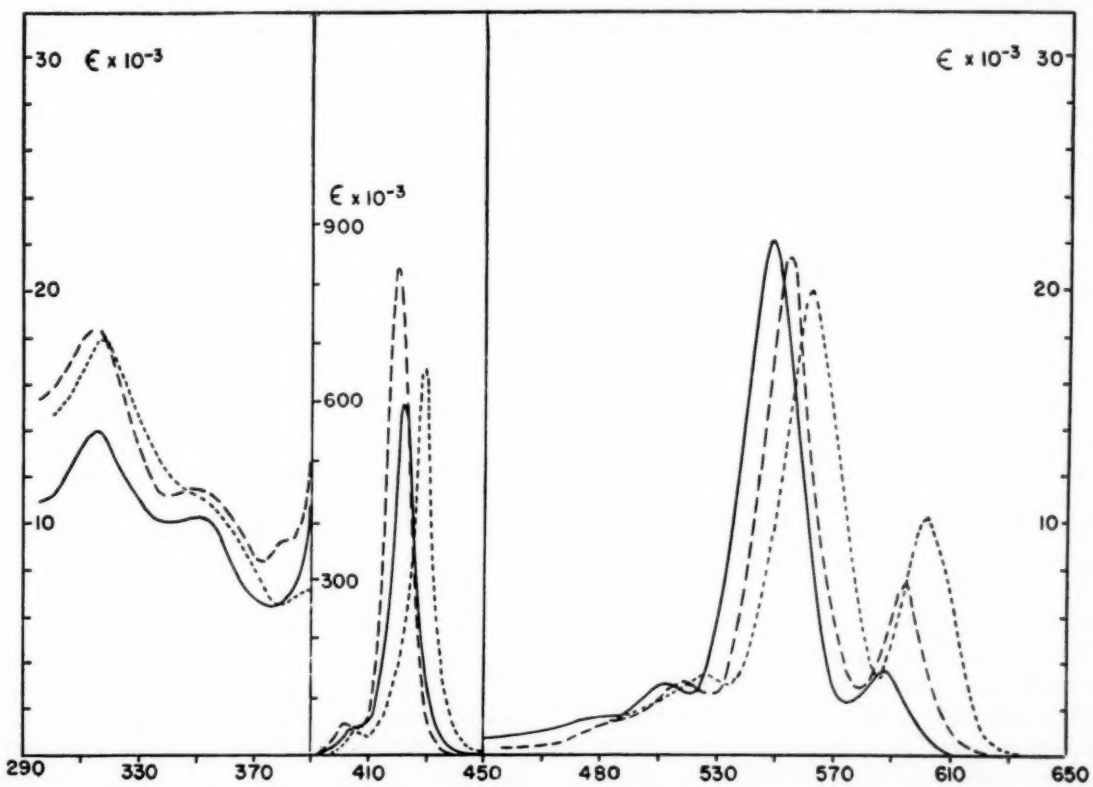

FIG. 1. Spectra of zinc tetraphenylporphin in three solvents: ——— benzene; - - - - ethanol; ····· pyridine.

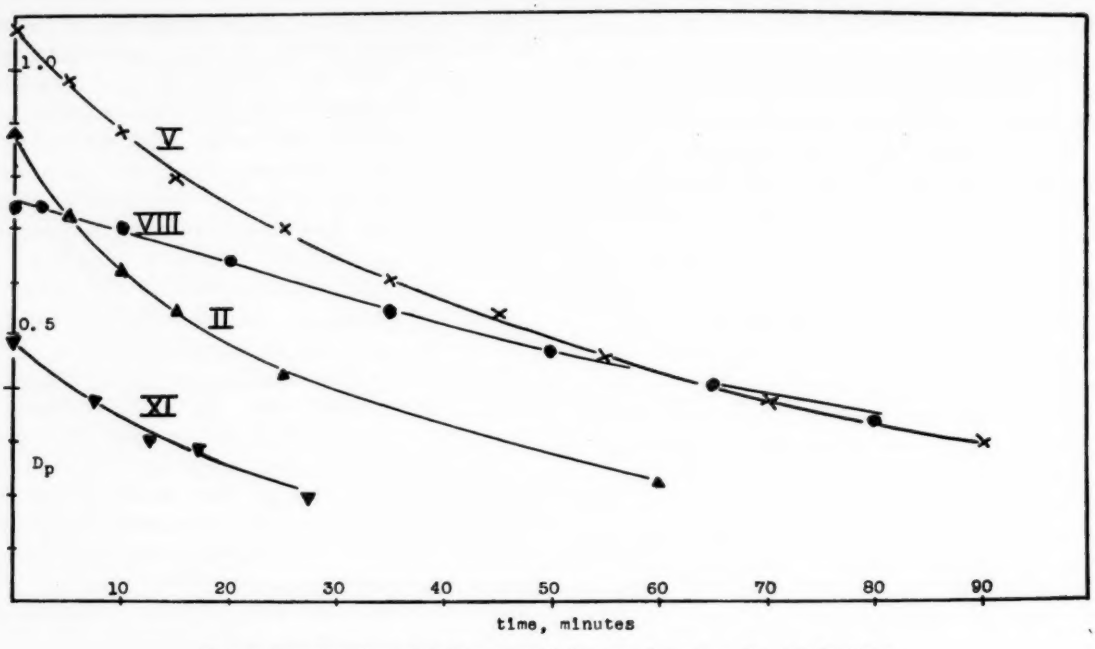

FIG. 2. Density-time plots for some of the experiments as listed in Table I.

the bolometer must first pass through the tube. In this way, a high level of light intensity could be obtained and measured. The bolometer was calibrated against a primary standard lamp furnished by the National Bureau of Standards, and showed linear response in the range of operation. The intensity of light incident on the tube could be decreased by the use of screens over the aperture between the sunlamp and the condensing lens and a place was provided between aperture and lens for interposing color filters. The temperature of the water in the thermostatted jacket, which was just wide enough to allow the reaction tube to fit inside, was maintained at 25° for all of the runs.

Spectra were taken at convenient intervals of the region from 450 to 650 mμ, on a Cary Recording Spectrophotometer (Fig. 1). This region provides enough information to enable calculation of the concentrations of all the principal porphyrins present. Spectra thus obtained show, in addition to the absorption of zinc porphin, bands characteristic of zinc chlorin, zinc tetrahydroporphin, and traces of oxidation products formed by side reactions involving the remnant of oxygen present. The quantity desired is the optical density due to porphin at 550 mμ, which, divided by the extinction coefficient, 22 200, yields the concentration of porphin. Since all the other compounds mentioned absorb at this wavelength, their contribution to the measured optical density must be taken into account. This correction is straightforward, for their spectra are all known, and they all have characteristic intense absorption bands elsewhere in the region 450 to 650 mμ.

The optical density of zinc porphin at 550 mμ was plotted as a function of time (Fig. 2), at constant incident light intensity, and the initial rate of reduction found from the slope at zero time by dividing the rate of change of optical density by the molar extinction coefficient of zinc porphin at 550 mμ, which is 22 200. Only initial rates were used, owing to the complication of the spectrum as the reaction progresses, and consequent uncertainties introduced into the amount of light usefully absorbed.

RESULTS AND DISCUSSION

The mechanism of the photo-oxidation of chlorin by quinones is well established. Absorption of light by the chlorin may be followed by a nonradiative transition from the short-lived singlet state to the long-lived triplet state, in which it has time to donate hydrogens to a quinone molecule. It was expected that the reduction of zinc porphin might proceed similarly, and that the rate would therefore depend on the amount of light absorbed by the porphin, and be practically independent of the benzoin concentration. The results, however, showed a behavior almost opposite to this.

The light energy of the General Electric Sunlamp in the visible and ultraviolet region is concentrated almost entirely in the six mercury emission lines at 365, 405, 436, 545, 576, and 622 mμ. It could be shown beyond a doubt by means of appropriate colored filters, that no reaction whatsoever occurred unless light of the 365 mμ line was permitted to reach the cell, and that light of this wavelength alone is sufficient for relatively rapid reaction. Both porphin and benzoin absorb at this wavelength, the former rather more than the latter, and it could be demonstrated that the rate of reaction was directly proportional to the amount of light absorbed by the benzoin over a fairly wide range of

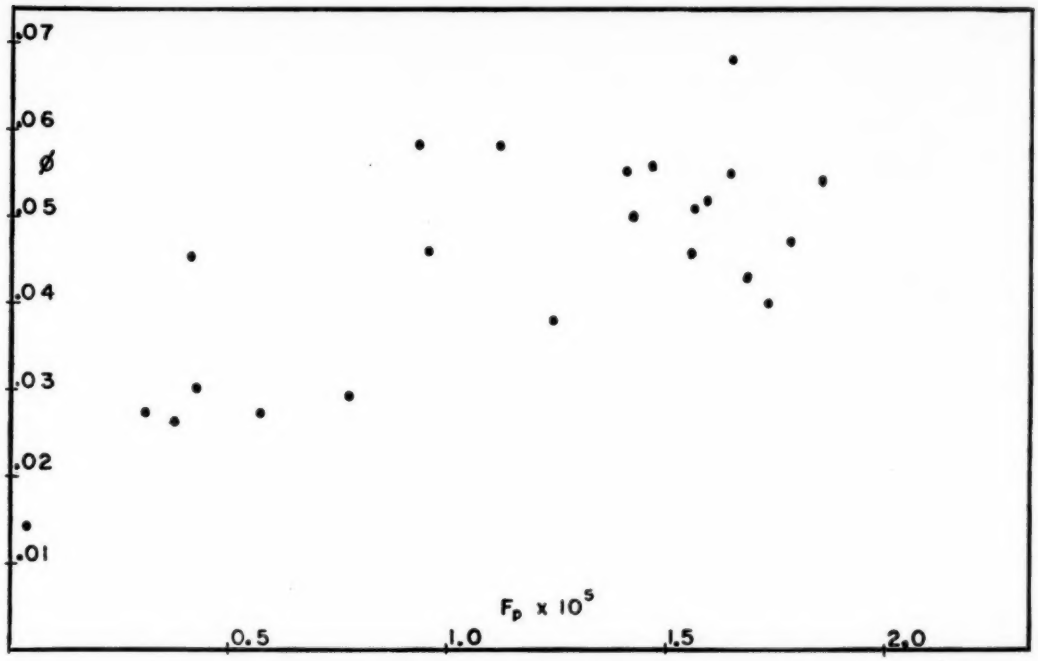

FIG. 3. Quantum yield against total light absorbed by porphin.

benzoin and porphin concentrations. The quantum yield for the reaction was therefore defined as the rate of reduction divided by the rate of light absorption by benzoin.

It had been shown that light in the lines at 405, 436, 545, and 576 mμ, which are absorbed by porphin, is insufficient for reaction. However, by experiments in which the light intensity of the unfiltered mercury lamp was varied by means of screens, the rate of reduction was found to be of order greater than first with respect to the light intensity, that is, the quantum yield increased with increasing light intensity. Experiments in which the aperture was covered half by a yellow filter, which passed light absorbed only by the porphin, and half by a filter passing only ultraviolet light in the region of absorption by benzoin, showed that although light absorbed by the porphin was ineffective alone, when used in conjunction with light absorbed by the benzoin, the quantum yield was augmented. A few more experiments were run in which the amount of light absorbed by the porphin was varied, and from a plot of quantum yield against rate of absorption of light by porphin (Fig. 3) it could be seen that at zero light absorption by porphin, the quantum yield falls to about 0.02. At high light absorption by porphin, the quantum yield rises to about 0.05.

The tabulation of the results is shown in Table I. In it are listed the concentrations of zinc porphin and of benzoin, the flux in watts per liter through the tube (F), the initial rate of reduction of zinc porphin (R), the light absorbed by benzoin in einsteins per liter per second (F_b), the light absorbed by porphin in the same units (F_p) and the quantum yield (ϕ) based on light absorbed by benzoin. ϕ is found by dividing the reduction rate by the light absorbed by the benzoin. This tabulation also includes runs during which high and low light intensities were used alternately, the initial rates obtained by extrapolation to zero entered as separate rows for the two light intensities. One of the experiments in which the aperture was covered by two filters is also included.

The behavior described suggested that reduction was taking place by two parallel mechanisms, one linear in light intensity, and the other quadratic; more precisely, a rate law of the form:

$$R = aF_b + bF_bF_p$$

where F_b and F_p are respectively the rates of light absorption by benzoin and porphin. The implication of this law is that benzoin reacts, when in a long-lived excited state, both with porphin in its ground state, and in its long-lived excited state, the latter reaction predominating at high light intensities. It has been possible to derive a rate law based on this implication, which fits the data as well as can be expected, considering the experimental accuracy.

Two data are the foundations of the derivation. Even though the concentration of excited porphin is minute compared with that of unexcited porphin, about two-thirds of the reaction, at the high light intensities, goes via excited porphin. Second, at a given level of light intensity, the reduction rate is apparently independent of the porphin concentration. The first datum implies that an excited benzoin molecule may collide with hundreds, or perhaps thousands, of unexcited porphin molecules without either reacting, or

TABLE I. Summary of results of rate runs on reduction of zinc porphin by benzoin.

Run No.	Porphin conc. molar	Benzoin conc. molar	F, watts/liter	F_b[a] einsteins/liter·sec	F_p[b] einsteins/liter·sec	R, initial rate moles/sec	ϕ quantum yield R/F_b
I	5.1×10^{-5}	3.3×10^{-3}	6.9	6.7×10^{-8}	1.40×10^{-5}	3.7×10^{-9}	0.055
II	4.5×10^{-5}	32.0×10^{-3}	6.7	55.0×10^{-8}	1.24×10^{-5}	21.0×10^{-9}	0.038
III	5.75×10^{-5}	0.75×10^{-3}	8.8	1.9×10^{-8}	1.85×10^{-5}	1.03×10^{-9}	0.054
IV	4.7×10^{-5}	18.2×10^{-3}	8.8	43.0×10^{-8}	1.73×10^{-5}	17.1×10^{-9}	0.040
V	5.1×10^{-5}	9.6×10^{-3}	8.1	21.0×10^{-8}	1.64×10^{-5}	14.2×10^{-9}	0.068
VI	5.4×10^{-5}	6.2×10^{-3}	8.0	13.7×10^{-8}	1.65×10^{-5}	7.6×10^{-9}	0.055
VII	5.75×10^{-5}	1.0×10^{-3}	6.9	3.6×10^{-8}	1.46×10^{-5}	2.0×10^{-9}	0.056
VIII	6.94×10^{-5}	5.3×10^{-3}	7.0	9.4×10^{-8}	1.56×10^{-5}	4.8×10^{-9}	0.058
IX	6.6×10^{-5}	6.9×10^{-3}	7.2	13.0×10^{-8}	1.59×10^{-5}	6.8×10^{-9}	0.052
X	2.4×10^{-5}	7.9×10^{-3}	7.9	21.5×10^{-8}	1.12×10^{-5}	12.4×10^{-9}	0.058
XI	2.25×10^{-5}	7.9×10^{-3}	6.8	19.0×10^{-8}	0.93×10^{-5}	11.1×10^{-9}	0.058
XII	5.55×10^{-5}	9.2×10^{-3}	8.1	18.0×10^{-8}	1.68×10^{-5}	7.8×10^{-9}	0.043
XIII	5.6×10^{-5}	26.1×10^{-3}	6.8	42.0×10^{-8}	1.42×10^{-5}	21.0×10^{-9}	0.050
	5.6×10^{-5}	26.1×10^{-3}	2.05	12.6×10^{-8}	0.43×10^{-5}	3.8×10^{-9}	0.030
XIV	5.1×10^{-5}	16.5×10^{-3}	...[b]	12.9×10^{-8}	0.04×10^{-5}	1.76×10^{-9}	0.014
	5.1×10^{-5}	16.5×10^{-3}	...[c]	12.9×10^{-8}	0.38×10^{-5}	5.2×10^{-9}	0.026
XV	4.85×10^{-5}	18.0×10^{-3}	7.8	37.5×10^{-8}	1.55×10^{-5}	17.3×10^{-9}	0.046
	4.85×10^{-5}	18.0×10^{-3}	1.55	7.5×10^{-8}	0.31×10^{-5}	2.1×10^{-9}	0.027
XVI	11.4×10^{-5}	15.0×10^{-3}	7.2	20.0×10^{-8}	1.78×10^{-5}	9.4×10^{-9}	0.047
XVII	2.44×10^{-5}	1.30×10^{-3}	6.7	4.5×10^{-8}	0.96×10^{-5}	2.07×10^{-9}	0.046
XVIII	2.63×10^{-5}	7.9×10^{-3}	2.75	7.4×10^{-8}	0.41×10^{-5}	3.3×10^{-9}	0.046
XIX	5.0×10^{-5}	16.1×10^{-3}	2.9	12.3×10^{-8}	0.58×10^{-5}	3.3×10^{-9}	0.027

[a] Determined for $\lambda=365$ mμ, from the incident wattage and the absorption coefficients of benzoin and porphin at this wavelength.
[b] Determined as a sum over the wavelength lines 365 (7.6 percent), 405 (6.9 percent), 436 (15.2 percent), 545 (22.3 percent), 576 (22.7 percent), 622 (3.2 percent) which constitute the bulk of the incident beam intensity, and the absorption coefficients of the porphin at each of these wavelengths.
[c] Color filters were used during this run, and the calculation modified accordingly.

becoming deactivated. The second implies that in the absence of excited porphin molecules an excited benzoin molecule has a long enough life-time that it will ultimately almost surely react with porphin in the ground state. These, in turn, suggest that we may postulate an activated complex involving excited benzoin and ground-state porphin, formed by collision, in which, upon decomposition, either the porphin has been reduced, or the benzoin has been deactivated without reduction of porphin. Not every collision between excited benzoin and ground-state porphin leads to an activated complex, but only, on the average, one in some number "n." We may well assume that every collision between excited benzoin and excited porphin leads to an activated complex, for if nothing else happened, the two molecules in their paramagnetic triplet states would quench each other.

We wish first to calculate the steady-state concentration of benzoin in its triplet excited state. If F_b is the light absorbed by the benzoin, expressed in einsteins per liter per second, and α_b is the fraction of singlet excited benzoin molecules passing over into the triplet excited state, then the rate of formation of triplet excited benzoin is $\alpha_b F_b$. Excited benzoin decays by three paths: (1) natural decay, with lifetime τ_b and rate B'/τ_b, where B' represents the concentration of excited benzoin; (2) collision with ground-state porphin to form an activated complex; (3) collision with excited porphin.

The number of collisions between excited benzoin and ground-state porphin, expressed in "moles" per liter per second, $Z=cB'P$, where P is the porphin concentration, and "c" a kinetic constant with the proper dimensions. The number of collisions between excited benzoin and excited porphin, $Z'=cB'P'$, where P' is the concentration of triplet excited porphin. Remembering that only one in "n" of the former collisions leads to an activated complex, for steady-state conditions,

$$\frac{dB'}{dt}=\alpha_b F_b-\frac{B'}{\tau_b}-\frac{cB'P}{n}-cB'P'=0.$$

The steady-state concentration of excited benzoin is therefore

$$B'=\frac{\alpha_b F_b}{\frac{1}{\tau_b}+\frac{cP}{n}+cP'}.$$

Now let β be the fraction of activated complexes involving ground-state porphin which decompose with reduction of the porphin and β' be the fraction of collisions between excited benzoin and excited porphin which lead to reduction. Then the rate of reduction of porphin will be

$$-\frac{dP}{dt}=\frac{\beta Z}{n}+\beta' Z'=\frac{\beta cB'P}{n}+\beta' cB'P'.$$

The concentration of triplet excited porphin is

$$P'=\alpha_p \tau_p F_p,$$

where τ_p is the lifetime of triplet excited porphin and α_p is the fraction of singlet excited porphin molecules which pass into the triplet state.

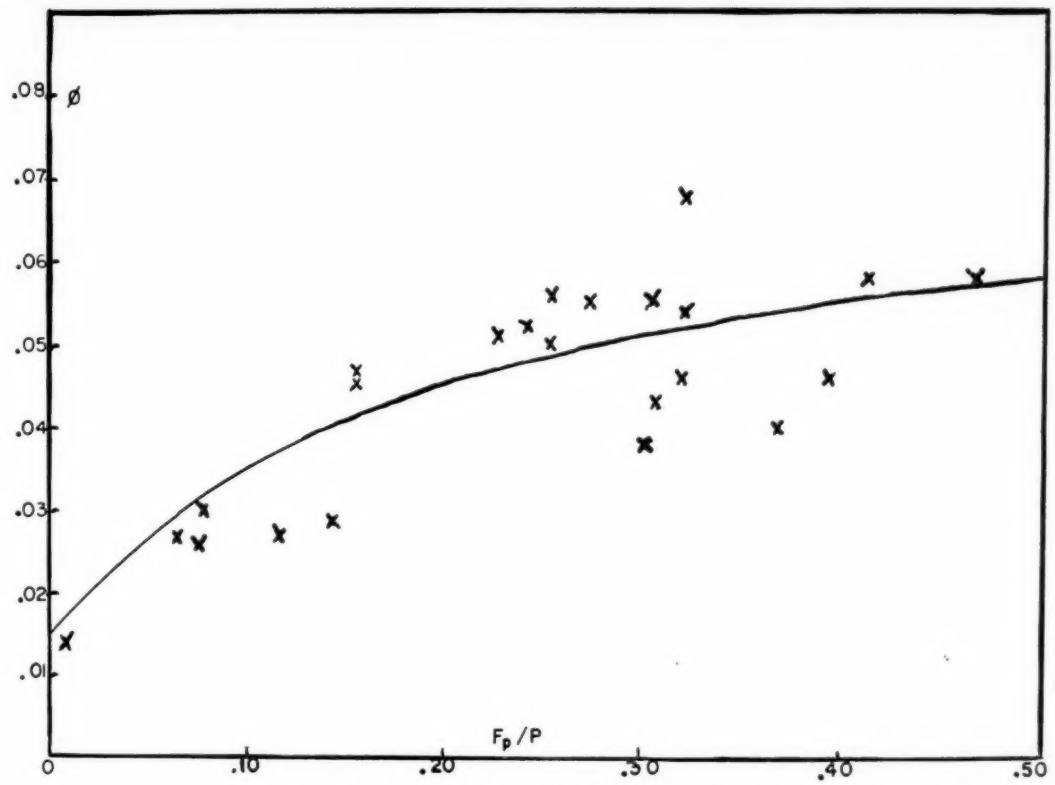

FIG. 4. Quantum yield *vs* specific absorption by porphin.

We may now write the expression for the quantum yield, as it has been defined:

$$\phi=\frac{1}{F_b}\left(-\frac{dP}{dt}\right)=\frac{\alpha_b\left(\dfrac{\beta cP}{n}+\beta' c\alpha_p\tau_p F_p\right)}{\dfrac{1}{\tau_b}+\dfrac{cP}{n}+c\alpha_p\tau_p F_p}.$$

Now the observed essential independence of the quantum yield of the porphin concentration means that the term involving the life-time of excited benzoin is small compared to the rest of the denominator. Considerable simplification may be obtained by dropping this term:

$$\phi=\frac{\alpha_b(\beta+n\beta'\alpha_p\tau_p F_p/P)}{1+n\alpha_p\tau_p F_p/P}.$$

The quantum yield is now seen to be a function of only one variable, F_p/P, and a plot of quantum yield against this variable is shown (Fig. 4). The expression for the quantum yield is of the form:

$$\phi=\frac{a+bc(F_p/P)}{1+c(F_p/P)}.$$

The scatter of the points makes it difficult to obtain reliable values for the constants a, b, and c, but for sake of illustration a curve has been drawn through the points with $a=0.015$, $b=0.075$, and $c=5.8$.

The scatter of points is explicable on three grounds. The primary data are differences between optical densities after successive intervals, and these were subject to random machine error of the Cary spectrophotometer, amounting perhaps to 10 percent of the difference. This leads to an uncertainty of the rate at all times during a given run. Further, the presence of oxygen in traces gave rise to a side reaction which increased the apparent rate. Again, accumulation of reaction products and by-products which absorb in the visible region retard the apparent rate of reduction.

The Hydrogenated Porphyrin Series

It has been possible, by photochemical hydrogenation, to prepare three identifiable reduction products of zinc tetraphenylporphin, and arrange them uniquely according to extent of reaction.

The first reduction product has been identified by its spectrum as zinc dihydrotetraphenylporphin (zinc tetraphenylchlorin) (Fig. 5). Its presence can be detected in all reductions of the porphin. It is the first product to form, but is usually reduced rapidly to the second reduction product. If a base such as pyridine is present in the solution, chlorin tends to accumulate, being reduced more slowly. It has been previously reported that quinones can oxidize chlorin photochemically back to porphin.

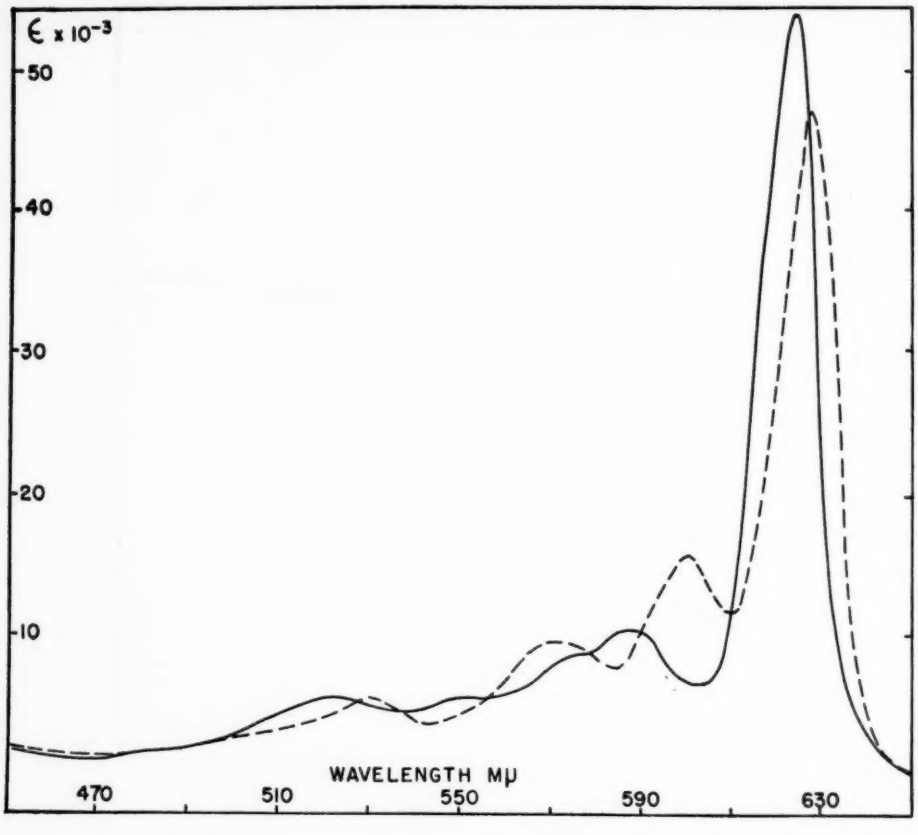

FIG. 5. Spectra of zinc tetraphenylchlorin: ——— benzene; - - - - pyridine.

If reduction of porphin proceeds to any extent, the second reduction product is always the most abundant, the highest yield of 60 percent having been obtained with dihydroxyacetone in alcohol plus a trace of piperidine, after an hour's sunlight. Formed this way, it is apparently free from contaminants absorbing in the visible region, and its spectrum may be obtained with some accuracy. This compound undergoes slow photoreduction, faster in the absence of base. In the presence of air and light, the compound is rapidly destroyed, its bluish-green solution, with red fluorescence, fading to a straw-colored solution without distinct absorption bands. It is stable for short periods in the dark, in contact with air, but is slowly destroyed with formation of a small amount of chlorin. This oxidation is more rapid on an absorbing surface, and attempts to purify the compound by chromatography failed for this reason. Both the spectra of the zinc complex and of the free base agree with those of a compound which has been prepared by catalytic hydrogenation of porphin[4] (Fig. 6). It was also found that the quinones, phenanthraquinone and *o*-naphthoquinone, oxidize the reduction product quantitatively back to porphin. The mechanism of this reaction is apparently the same as that of the well-known photo-oxidation of chlorin, that is, the rate was found to depend linearly on the rate of light absorption by the porphyrin, and to be otherwise independent of porphyrin and quinone concentrations. The quantum yield was found to be about 3.6×10^{-4}, and thus quite a bit smaller than that for oxidation of chlorin, *ca* 0.02. This accounts for the fact that no chlorin can be observed as an intermediate in the oxidation.

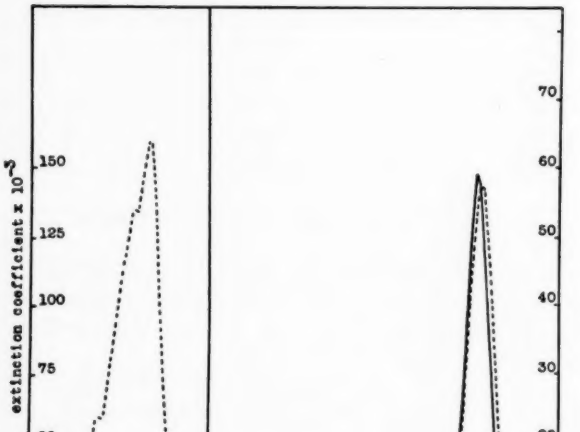

FIG. 6. Spectra of zinc tetrahydrotetraphenylporphin: ——— benzene; - - - - pyridine.

[4] G. D. Dorough and J. R. Miller, J. Am. Chem. Soc. **74**, 6106 (1952).

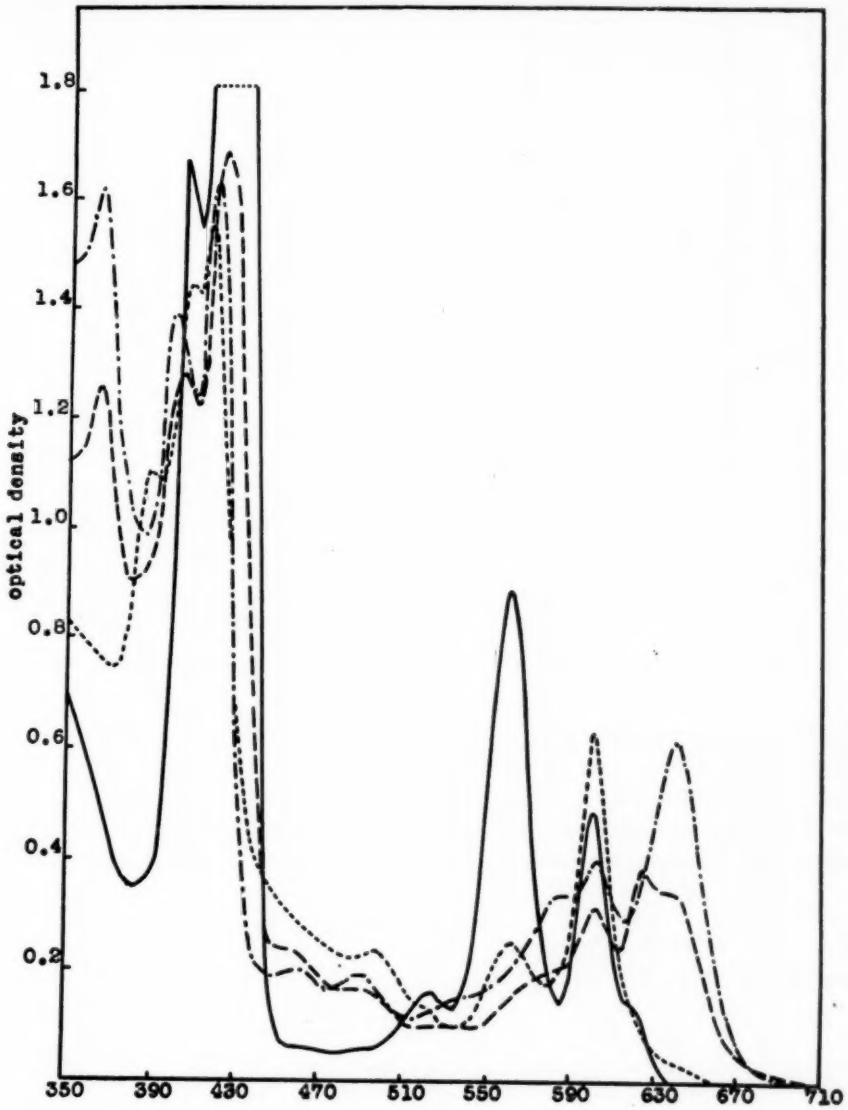

FIG. 7. Photoreduction of zinc tetraphenylporphin by benzoin in benzene plus ½ percent piperidine, in sunlight: ——— at start; – – – – 3½ minutes sunlight; –·–·–·– 12 minutes more sunlight; emergence of hexahydroporphin band; ····· overnight in dark with oxygen; regeneration of tetrahydroporphin.

The third reduction product of this series is extremely evanescent, and has only been observed occasionally when porphin is reduced by benzoin in benzene containing a trace (about 0.5 percent) of piperidine. This compound, whose spectrum is characterized by a band at 642 mμ, is apparently a further (third) reduction product of the second reduction product, for its band has been observed when a solution of the second reduction product is reduced by benzoin in benzene plus pyridine (see Figs. 7 and 8). The compound, on exposure to air in the dark for a day, is cleanly oxidized to the second reduction product which, in turn, is oxidized much more slowly. A qualitative spectrum for this compound could be obtained by differences during the air oxidation.

These three compounds, which are connected so intimately by oxidations and reductions, also have spectral characteristics in common (Fig. 9). All exhibit the two-band systems typical of porphyrins, the intense system near 400 mμ and the system of spaced bands in the green and red regions. If we are correct to attribute these band systems to the presence of conjugation throughout the great ring of the porphyrins, all these compounds must have this conjugation essentially intact. The successive formation of these compounds by hydrogenation suggests that they differ by successive additions of two hydrogen atoms to the ring. Since chlorin is dihydroporphin, the second reduction product should be a tetrahydroporphin, and the third reduction product should be a hexahydroporphin. In this last compound, if we disregard the unlikely possibility that the benzene rings have become hydrogenated under the conditions of the reaction, the only way hydrogens may be added to the porphin ring, and still maintain an essential type of conjugation for the ionic forms is to put them on the beta positions of the pyrrole rings. Resonance structures can be drawn for such a hexa-

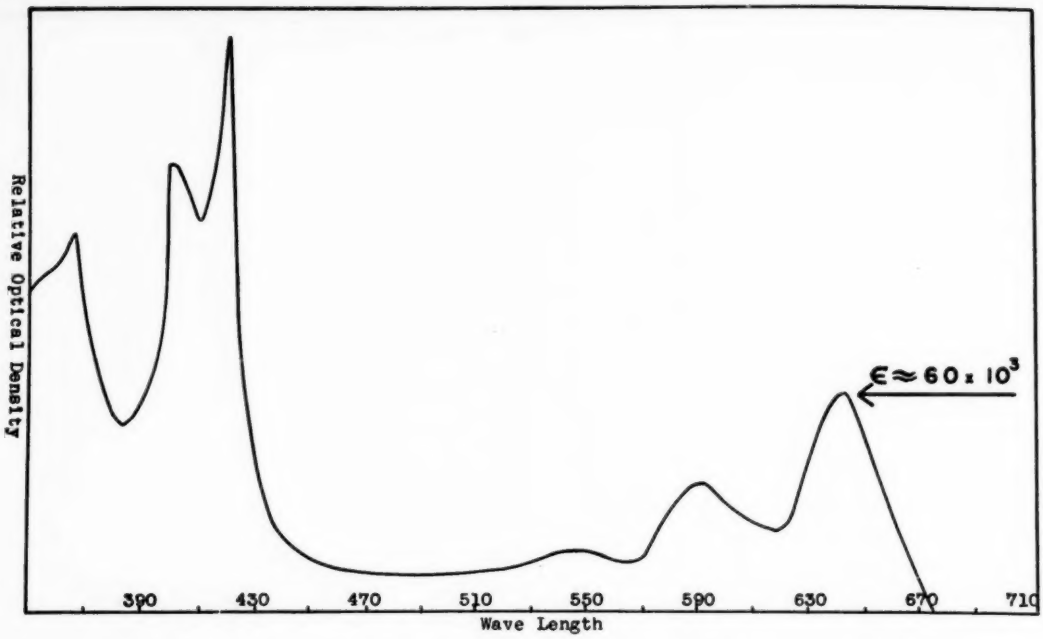

FIG. 8. Sketch of spectrum of zinc hexahydroporphin in benzene plus ½ percent piperidine.

hydroporphin (Fig. 10); some of these are shown, and indicate that some degree of stability might be expected for the compound. No such resonance structures can be drawn for an octahydroporphin, so such a compound should not be expected to absorb in the visible.

The Benzoin-Catalyzed Degradation of Zinc Porphin by Oxygen

It has been previously mentioned that presence of oxygen in tubes containing a solution of zinc porphin and benzoin leads to a side reaction. The course and

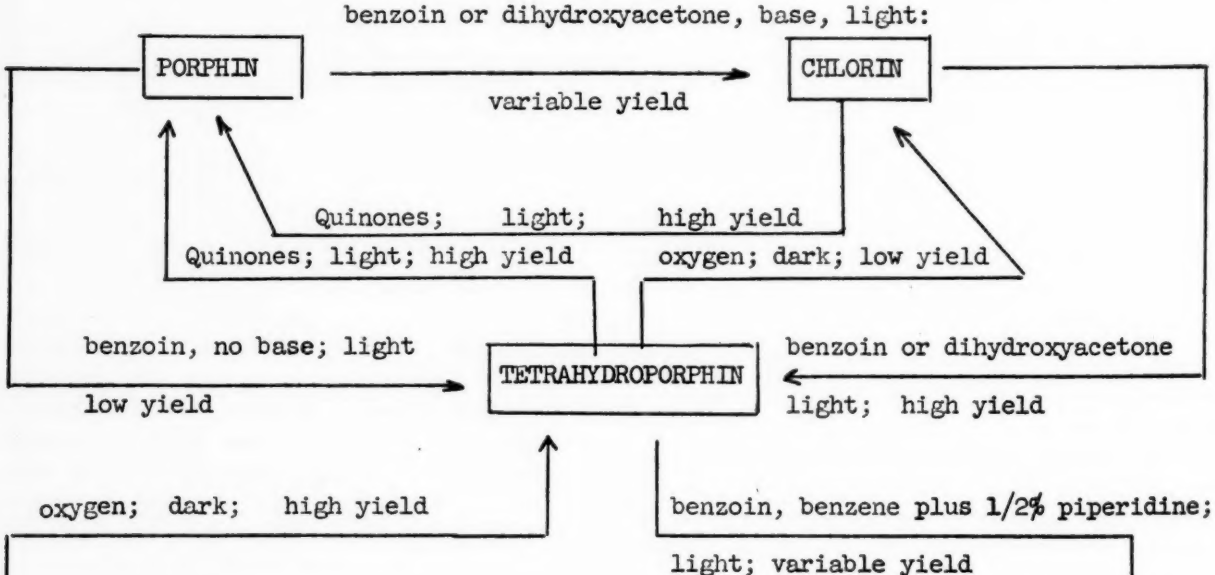

FIG. 9. Redox relations among the zinc tetraphenylporphyrins.

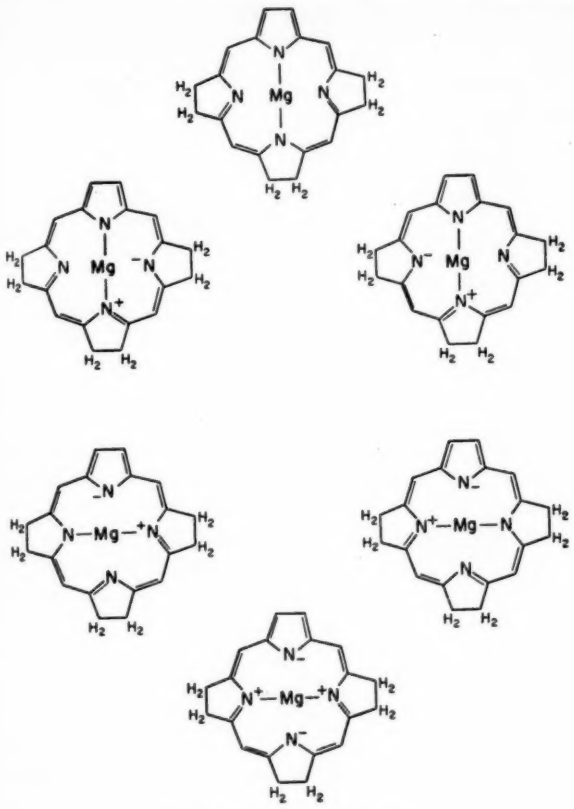

FIG. 10. Hexahydroporphin.

kinetics of this reaction have been investigated as well as the reduction.

It has been long known that zinc porphin in solution is slowly decomposed by oxygen in the presence of sunlight over a period of many days (Figs. 11 and 12). The first product, or products, formed by this degradation absorb in the blue part of the spectrum, with maximum near 490 mμ. This product would be destroyed by further exposure to sunlight, but if it is allowed to stand in the dark for two or three days, it is converted into a blue compound, with an intense peak at 628 mμ. This blue compound is not very sensitive to light, and its concentration may be built up by alternately exposing the tube to light and letting it stand in the dark. A drop of pyridine added to a benzene solution of the blue compound shifts the absorption peak from 628 to 632 mμ; the compound is stable to 3 *N* HCl, but 6 *N* HCl liberates a beautiful purple free base, stable to alkali. The original compound, a zinc complex, may be regenerated by adding a solution of zinc acetate to the free base, in pyridine. The easy

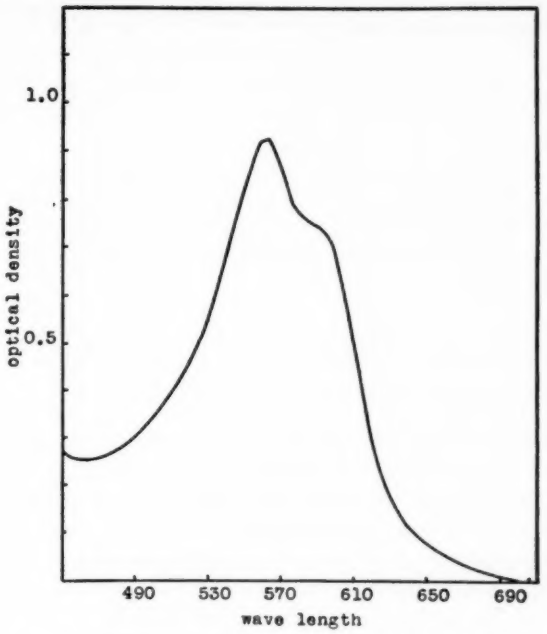

FIG. 12. Spectrum of free base of blue oxidation product of zinc tetraphenylporphin.

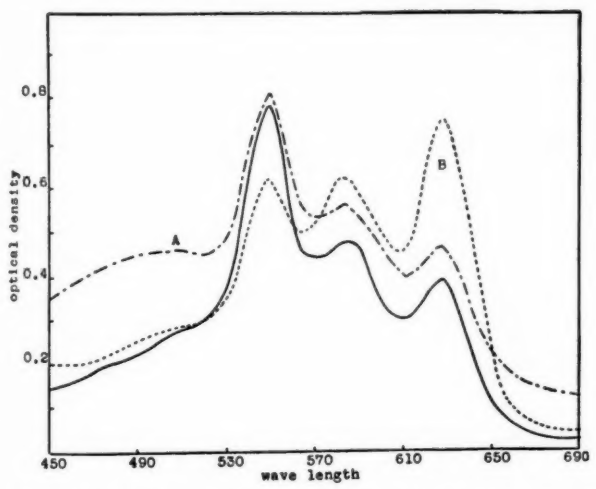

FIG. 11. Reaction of zinc tetraphenylporphin with oxygen in benzene solution. ——— At start; -·-·-·- after 1½ hours sunlight through filter No. 9782; - - - - after standing several days in darkness. At start, the porphin has already been partially destroyed. Irradiation brings about build-up of first degradation products at *A*. Standing in the dark, these change into a product with band at *B*.

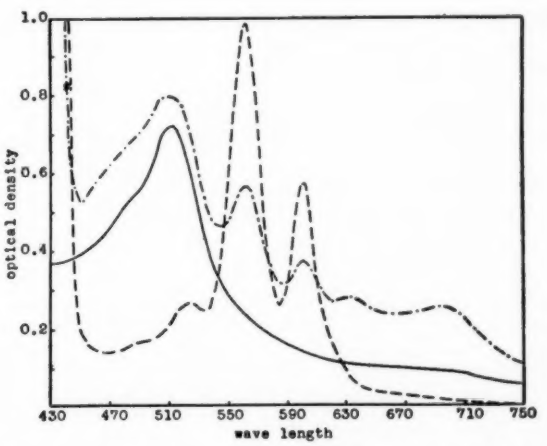

FIG. 13. Destructive oxidation of zinc tetraphenylporphin catalyzed by benzoin. Light source: AH-4 mercury lamp. - - - - At start; -·-·-·- after 5 minutes; ——— after 12 minutes.

TABLE II. Rate run results: benzoin-catalyzed degradative oxidation of porphin.

Run No.	Porphin conc. molar	Benzoin conc. molar	O_2 pressure atmos.	Init. rate moles/sec	F_b, $\frac{\text{einsteins}}{\text{liter}\cdot\text{sec}}$	Quantum yield
I	5.5×10^{-5}	7.2×10^{-3}	0.2	1.46×10^{-8}	13.0×10^{-8}	0.112
II	4.35×10^{-5}	3.15×10^{-3}	0.2	0.63×10^{-8}	6.4×10^{-8}	0.098
III	4.2×10^{-5}	17.1×10^{-3}	0.2	3.0×10^{-8}	26.2×10^{-8}	0.115
IV	4.5×10^{-5}	10.1×10^{-3}	0.2	0.64×10^{-8}	6.0×10^{-8}	0.107
V	2.3×10^{-5}	7.4×10^{-3}	0.2	1.64×10^{-8}	16.7×10^{-8}	0.089
VI	6.65×10^{-5}	9.1×10^{-3}	0.2	1.21×10^{-8}	15.3×10^{-8}	0.079
VII	4.9×10^{-5}	9.1×10^{-3}	1.0	1.84×10^{-8}	18.0×10^{-8}	0.102
VIII	4.25×10^{-5}	1.57×10^{-3}	0.2	0.38×10^{-8}	3.4×10^{-8}	0.112
						Av. 0.103±0.011
	Cu porphin					
IX	5.4×10^{-5}	10.4×10^{-3}	0.2	3.75×10^{-8}	21.5×10^{-8}	0.174

interconversion between complex to free base indicates that the cyclic structure is still intact, but the absence of a Soret band near 400 mμ indicates that the porphyrin conjugation is probably broken.

The course of degradative oxidation in the presence of benzoin seems to be different. The most prominent oxidation product (or products), in this case, have peak absorption at 530 mμ when formed in benzene, and at 510 mμ, when formed in the presence of pyridine (Fig. 13). There is nothing corresponding to the blue compound mentioned above. Benzoin shares the ability to "induce" oxidative destruction of zinc porphin with benzil, acetophenone, benzaldehyde, desoxybenzoin, butyl phenylketone, *p*-dimethylaminobenzoin, anthracene, phenanthraquinone, and possibly some mercaptans. No such catalyzed degradation was observed in the presence of benzophenone, naphthalene, diphenyl disulfide, and *p*-azoanisole. Rate of destruction varied considerably among the effective ones, and the colors of the products were not the same in every case. Many of the "catalysts" are seen to possess the COC_6H_5 radical. The copper and nickel porphin complexes are as susceptible to this degradation as is the zinc complex.

Because benzoin had been used in rate of reduction experiments, this reagent was also used in experiments on rate of degradation of zinc porphin. The setup for these experiments was the same as for the reductions, except that the tubes were neither evacuated nor flushed with nitrogen, so that a fifth of an atmosphere of oxygen remained. It was found that light absorbed by the benzoin was necessary and sufficient for maximum rate of reaction, light absorbed by porphin had no effect, and the quantum yield was independent of porphin and benzoin concentrations (see Table II).

The interpretation of this reaction rests on papers recently published by Schenck.[5] He cites evidence that many compounds, including some which catalyze the degradation of zinc porphin, are able to form addition compounds with oxygen when irradiated, and, moreover, are able to transfer this oxygen to other compounds on collision. Applied to this reaction, benzoin, irradiated, forms an oxygen addition product, and on collision with a molecule of zinc porphin transfers that oxygen to the porphin ring. The kinetics can be understood, if we acknowledge that every benzoin molecule passing into the triplet state will have ample opportunity to pick up oxygen, and the compound so formed is sufficiently stable to have ample time to react with porphin. Thus the reaction rate depends only upon the number of benzoin molecules excited into the triplet state.

[5] Schenck, Kinkel, Mertens, Eggert, Denk, Schmidt-Thomee, and Ziegler, Liebig's Ann. **584**, 126–219 (1953).

On the Logarithmic Rate Law in Chemisorption and Oxidation

P. T. LANDSBERG*
Westinghouse Electric Corporation, Research Laboratories, East Pittsburgh, Pennsylvania
(Received September 13, 1954)

It is shown that the logarithmic rate law is found very widely in chemisorption and oxidation. A theory of this law is offered, and comparison with experiment leads to reasonable values for the parameters. Although the theory is very elementary, it is hoped that the physical interpretation it provides of experimentally determined parameters will encourage a more detailed study of these, for instance as a function of temperature and ambient pressure.

I. INTRODUCTION

THE purpose of this paper is to unify the study of those phenomena relating to the chemisorption of gases on solid surfaces and the oxidation of metals, which can be described by logarithmic rate laws. A study of the experimental facts reveals some striking analogies between these two fields of study, which have often been treated separately. By offering an elementary theory of such rate laws, it is hoped that a physical interpretation of the parameters which occur in them will emerge, and that further study of these parameters under varying external conditions will thus be encouraged.

II. THE LOGARITHMIC LAW IN CHEMISORPTION

The chemisorption of gases on solid surfaces has been the subject of considerable study in recent years. In spite of some doubts,[1] it does appear that a large portion of the experimental data can be represented by the equation

$$bq=\log\frac{t+t_0}{t_0}. \qquad (1)$$

q is the number of particles chemisorbed per unit area at time t after the beginning of the experiment. b and t_0 are constants for given conditions. Other rate laws are also known, but (1) is one of the most common ones. A difficulty with regard to (1) is the lack of a satisfactory theoretical basis. A semiquantitative attempt to arrive at (1) has been made by some Russian workers,[2] but they do not claim to have given a satisfactory proof. More recently some German workers[3] have attempted a deduction on the basis of barrier layer theory, but they arrive at different rate laws for adsorption on n-type as against adsorption on p-type semiconductors. There does not appear to be any evidence at this time to bear out this conclusion. A simple theoretical model which leads to (1) will be given later. It is, however, of some importance to show first that the published literature reveals (1) as a reasonably well-established empirical relationship.

Equation (1) was first shown to apply to the catalytic oxidation of CO on MnO_2 between -78°C and 39°C.[4] The effect of pressure on the oxidation of CO by oxygen on MnO_2 was discussed later,[5] and a study was made of the chemisorption of CO and CO_2 on MnO_2 at low pressures.[6] Again, Eq. (1) was verified. By now these workers had recognized that the central stage in the catalytic oxidation of CO was the adsorption of CO on MnO_2, and experiments were next made at higher initial pressures of the gas mixtures (30 mm to 500 mm Hg), and at temperatures from -38.8°C to 17°C.[7] Equation (1) was again obeyed. In more widely known papers[8]† the validity of Eq. (1) was established for the chemisorption, between -23°C and 50°C, of hydrogen and of ethylene on a catalyst of reduced NiO. Again, it was found that oxidation of CO by oxygen at room temperatures below 2 mm Hg pressure was accelerated by the presence of NiO, and that for very active catalysts the amount of material oxidized satisfied Eq. (1).[9] A law (1) was again observed in the catalytic oxidation of propylene on Pt.[10] The subject was taken up in the United States, Britain, and Germany.

In the United States, Taylor and Thon[11] found that the law (1) is valid in many other chemisorption experiments, and they analyzed a great deal of previously published information. They found the law to

* Westinghouse Electric Corporation, Research Laboratories, East Pittsburgh, Pennsylvania. On leave of absence from the University of Aberdeen, Aberdeen, Scotland.

[1] K. J. Laidler, in *Catalysis* (Reinhold Publishing Corporation, New York, 1954), Vol. I, p. 189–191.

[2] F. Characorin and S. Elowitz, Acta Physicochim. U.R.S.S. **5**, 325 (1936).

[3] H.-J. Engell and K. Hauffe, Z. Elektrochem. **57**, 762 (1953).

[4] J. Zeldowitch, Acta Physicochim. U.R.S.S. **1**, 449 (1934–35); S. Roginsky and J. Zeldowitch, *ibid.* **1**, 554 and **1**, 559 (1934–35).

[5] Characorin, Elowitz, and Roginsky, Acta Physicochim. U.R.S.S. **3**, 502 (1935).

[6] F. Characorin and S. Elowitz, Acta Physicochim. U.R.S.S. **5**, 325 (1936); S. Elowitz and L. A. Kachur, J. Gen. Chem. (U.S.S.R.) **9**, 714 (1939).

[7] S. Elowitz and S. Roginsky, Acta Physicochim. U.R.S.S. **7**, 295 (1937).

[8] S. Y. Elovich and G. M. Zhabrova, Zhur. Fiz. Khim. **13**, 1761 and 1775 (1939).

† It is on the basis of these papers that the name "Elovitch equation" has been given to Eq. (1) in the Anglo-Saxon literature. In view of the papers in reference 4, this would appear to be a misnomer. It should also be noted that the person whose Russian name is currently translated in the West as "Elovich," wrote his German papers (see references 5 and 6) under the name "Elovitz."

[9] S. Roginsky and T. F. Tselinskaya, Zhur. Fiz. Khim. **22**, 1360 (1948).

[10] P. Y. Butyagin and S. Y. Elovich, Doklady Akad. Nauk. S.S.S.R. **75**, 711 (1950).

[11] H. A. Taylor and N. Thon, J. Am. Chem. Soc. **74**, 4169 (1952); N. Thon and H. A. Taylor, J. Am. Chem. Soc. **75**, 2747 (1953).

be valid in the chemisorption of H_2 on $2MnO \cdot Cr_2O_3$,[12] H_2 on Pt,[13] H_2 and D_2 on Ni,[14] C_2H_4 on Ni,[15] O_2 on CoO,[16] H_2 on Cu,[17] CH_4 on Ni,[18] N_2 on Fe,[19] H_2 on ZnO,[20] and H_2 on $ZnO \cdot MoO_3$.[21] Melnick[22] found recently that the law applied also to the chemisorption of O_2 on ZnO, and gave a simple model for this process. In the references 20 and 21 some discontinuities in the slope of the graph of q against $\log t$ were noticed. In Britain, Porter and Tompkins[23] studied the kinetics of chemisorption of H_2 and of CO on evaporated iron films at liquid-air temperatures and again verified Eq. (1). They also gave a theoretical discussion assuming (*a*) variation of activation energy with coverage and (*b*) surface heterogeneity.

In Germany, Engell and Hauffe[3] found that the law (1) also applied to the chemisorption of O_2 on NiO between the temperatures of 300°C and 700°C, and an oxygen pressure of 60 mm of Hg. For *lower* temperatures, however, a discontinuity developed in the slope of the curves. On the other hand, Taylor and Thon observed[11] that in references 19 and 20 there was evidence that the law (1) would fail as the temperature was *increased* beyond a certain critical range.

III. LOGARITHMIC LAW IN OXIDATION

A logarithmic rate law of the form (1) is also known in the oxidation of metals. The situation here is not unlike that in chemisorption. The original work is in this case of German origin,[24] and is older than the corresponding Russian work on chemisorption.‡ Again the work was taken up in other countries only after a considerable time-lag when earlier work by Vernon[25] on the oxidation of iron between 50°C and 195°C was found[26] to satisfy the law (1). The same was found to be true for the oxidation of zinc[26] in air between 25°C and 400°C. The fit to Eq. (1) was not always perfect, and in some instances the experimental results could be represented better by two intersecting straight lines. Nonetheless, since gravimetrical methods were used, the work was regarded as more reliable than Tammann's original work, which depended on a method utilizing interference colors. In view of the later confirmation of some of his results, it may be mentioned that the law (1) was found to apply to the oxidation in air of Fe, Co, Ni, Mn, Cr, Cu, Sb, Bi, Sn, Pb, Zn, Cd. In iron, for example, it was valid at least between 0.1 and 1.0 min and between 252°C and 385°C. In nickel it applied at least between 0.1 and 10 min and between 485°C and 645°C. Sometimes intersecting straight lines were obtained. However, this was regarded as an exception. Early experiments by Steinheil on the oxidation of aluminum[27] were also found to be in agreement with (1).[28] Lustman and Mehl[28] found that the oxidation of copper at about 118°C satisfied the Eq. (1). They used a polarimetric method, as did also Winterbottom[29] who verified (1) for the oxidation in dry air, and at 14°C, of Cu, Fe, and Al. Some of these results have been confirmed by an electron diffraction technique[30] and an electrolytic reduction method.[31]

More recently, it has been found that the logarithmic law held in the case of oxidation of stainless steel[32] and of zinc foil between 300°C and 350°C,[33] by measuring the volumetric intake of oxygen; in the case of the oxidation of tantalum between 220°C and 320°C,[34] using both a spectrophotometric and a gravimetric method; and in the case of the oxidation of titanium near 325°C.[35]

In the case of oxide films, as in the case of chemisorption, if a logarithmic relationship has been found, increase of temperature tends to destroy its validity. Zn, Ta, and Ti are cases in point, which have been studied in the references cited above. Another example is Ni, which has been shown to follow a logarithmic up to 302°C.[32] In this paper, using data of Gulbransen and Andrew[36] on high purity Ni, the law will be shown

[12] A. T. Williamson and H. S. Taylor, J. Am. Chem. Soc. **53**, 2168 (1931).
[13] B. Maxted and C. H. Moon, J. Chem. Soc. 1542 (1936).
[14] S. Iijima, Rev. Phys. Chem. Japan **12**, 1 (1938).
[15] S. Iijima, Rev. Phys. Chem. Japan **14**, 68 (1940).
[16] J. C. W. Frazer and L. Heard, J. Phys. Chem. **42**, 865 (1938).
[17] T. Kwan, J. Research Inst. Catalysis, Hokkaido, Univ. **1**, 95 (1949).
[18] M. Kubokawa, Rev. Phys. Chem. Japan **12**, 157 (1938).
[19] P. H. Emmett and S. Brunauer, J. Am. Chem. Soc. **56**, 35 (1934).
[20] D. V. Sickman and H. S. Taylor, J. Am. Chem. Soc. **54**, 602 (1932); C. D. Strother and H. S. Taylor, J. Am. Chem. Soc. **56**, 586 (1934).
[21] G. Ogden and H. S. Taylor, Trans. Faraday Soc. **30**, 1178 (1934); M. V. C. Sastri and K. V. Ramanathan, J. Phys. Chem. **56**, 220 (1952).
[22] D. Melnick, Ph.D. thesis, University of Pennsylvania, 1954.
[23] A. S. Porter and F. C. Tompkins, Proc. Roy. Soc. (London) **A217**, 529 (1953).
[24] G. Tammann and W. Köster, Z. anorg. u. allgem. Chem. **123**, 146 (1922); Tammann, Stahl, and Eisen, **42**, 615 (1922); Z. anorg. u. allgem. Chem. **124**, 25 (1922); G. Tammann and Schröder, Z. anorg. u. allgem. Chem. **128**, 179 (1923); G. Tammann and G. Seibel, Z. anorg. u. allgem. Chem. **148**, 297 (1925) and **152**, 149 (1926).
‡ Should the two rate laws turn out to be independent discoveries of the same basic physical process, a case could then be made out to name the statement (1) "the Tammann Rate Equation."
[25] W. H. J. Vernon, Trans. Faraday Soc. **31**, 1668 (1935).
[26] Vernon, Akeroyd, and Stroud, J. Inst. Metals **65**, 301 (1939).
[27] A. Steinheil, Ann. phys. **19**, 455 (1934).
[28] B. Lustmann and R. F. Mehl, Metals Technol., April, 1941, or Am. Inst. Mining and Met. Engrs., Tech. Publs. No. 1317 (1941); B. Lustmann, Trans. Electrochem. Soc. **81**, 359 (1942).
[29] A. B. Winterbottom, Trans. Electrochem. Soc. **76**, 326 (1939).
[30] A. H. White and L. H. Germer, Trans. Electrochem. Soc. **81**, 305 (1942).
[31] A. L. Dighton and H. A. Miley, Trans. Electrochem. Soc. **81**, 321 (1942).
[32] W. E. Campbell and N. B. Thomas, Trans. Electrochem. Soc. **91**, 623 (1947).
[33] W. J. Moore and J. K. Lee, Trans. Faraday Soc. **47**, 501 (1951).
[34] Waber, Sturdy, Wise, and Ripton, J. Electrochem. Soc. **99**, 121 (1952).
[35] J. T. Waber, J. Chem. Phys. **20**, 734 (1952).
[36] E. A. Gulbransen and K. F. Andrew, J. Electrochem. Soc. **101**, 128 (1954).

to be valid up to 500°C; at higher temperatures the parabolic rate law holds.[36]

As in the case of chemisorption, when the logarithmic law had been found, the question has occasionally been asked whether some other law might not express the data equally well. For instance, Gulbransen found the logarithmic law for the formation of thin oxide films on iron between 300°C and 400°C,[37] but could not be sure that it was the only likely law to correlate his data. It is also relevant to observe that Rhodin[38] found that the logarithmic law was satisfied in the oxidation of copper between −95°C and 62°C, although his primary purpose was to check a theoretical equation,

$$dq/dt \propto \exp(A/q), \quad A \text{ independent of } t, \qquad (2)$$

which was derived by Cabrera and Mott.[39] He found reasonably good agreement with both Eq. (1) and Eq. (2). Thus, while there is room for doubt in some individual cases as to whether law (1) is really valid, its simplicity and the weight of evidence in its favor make its study desirable.

It has been remarked (for instance, by Evans[40] and by Gulbransen[41]) that the logarithmic growth of oxide films has not so far received an explanation which will satisfactorily account for its widespread occurrence. The theoretical situation is here therefore similar to that of the logarithmic law in the field of chemisorption. There are certain theories, believed to be outdated, which depended on the existence of an exponential concentration gradient of ions in the film.[24,26] There is also the important point, first made by Mott,[42,43,39] that growth of a film by tunnel effect would follow a logarithmic law. He also proposed[43] that in the case of thicker films a logarithmic growth law might be due to a continuous recrystallization of the oxide film. Evans[44] has advocated repeated mechanical breakdown as a mechanism that might account for the logarithmic rate law. It appears, however, that these explanations, in spite of their undoubted relevance, have not so far commanded general agreement, or at least are not believed to represent physical mechanisms which are at work *in the majority* of instances quoted above.

[37] E. A. Gulbransen, Trans. Electrochem. Soc. **81**, 327 (1942); Cf. also B. Lustmann, Trans. Electrochem. Soc. **83**, 313 (1943).

[38] T. N. Rhodin, J. Am. Chem. Soc. **72**, 5102 (1950); see also T. N. Rhodin, Advances in Catalysis **5**, 40 (1953).

[39] N. Cabrera and N. F. Mott, Repts. Progr. Phys. **12**, 163 (1949).

[40] U. R. Evans, Trans. Electrochem. Soc. **91**, 547 (1947).

[41] E. A. Gulbransen, Trans. Electrochem. Soc. **91**, 575 (1947).

[42] N. F. Mott, J. Inst. Metals **65**, 333 (1939); Trans. Faraday Soc. **35**, 1175 (1939).

[43] N. F. Mott, Trans. Faraday Soc. **36**, 472 (1940).

[44] U. R. Evans, Trans. Electrochem. Soc. **83**, 335 (1943); Trans. Faraday Soc. **41**, 365 (1945); Nature **157**, 732 (1946); *Metallic Corrosion, Passivity and Protection* (Edward Arnold, London, England, 1948), p. 136; *Introduction to Metallic Corrosion* (Edward Arnold, London, England, 1948), p. 194.

IV. AN ELEMENTARY THEORY OF THE LOGARITHMIC RATE LAWS

It appears from the striking similarity between the evidence from chemisorption and the evidence from the formation of oxide films on metals, that

(a) the logarithmic rate law is not too sensitive either to the nature of the gas or to the nature of the surface;

(b) the logarithmic rate law in oxidation may occur under conditions when the chemisorption of the oxygen on the surface is the rate-controlling factor, so that the basic mechanisms in the two cases may in fact be essentially the same.

In this section tentative suggestions will be presented to account for the general form of the rate law. These suggestions are sufficiently general to be applicable perhaps to other systems having similar features. For instance, the corrosion film formation of copper in aqueous solution satisfies also the logarithmic law.[45]

Suppose that at time $t=0$ we have a surface with adsorption sites in contact with a gas. The nature of these sites, and their mode of generation, is not specified by the theory, nor is the amount of gas already adsorbed on the surface at time $t=0$ of importance. The sites may be due to the properties of that part of the surface which has not yet been covered by adsorbed molecules, they may be produced by the action of the already adsorbed molecules on the surface,[46] and they might even be offered by adsorbed molecules themselves. At this time let there be s_0 sites per unit area, and let there be s sites per unit area at an arbitrary time t. Let there be N impacts by gas molecules with the surface, expressed per unit area and per unit time. Let a be the effective contact area between a molecule and the surface upon collision, so that as is the fraction of impacts that could be effective in trapping a molecule. One may expect a to be roughly of the order of a molecular cross section. The probability that a molecule sticks upon impact is proportional to as, i.e.,

$$p=Cas, \qquad (3)$$

where C is a constant. The number of molecules sticking per unit area per unit time is

$$dq/dt=CasN. \qquad (4)$$

Let b be the effective area over which sites become invalidated by the adsorption of a single molecule. b is not necessarily of the same order as a. The actual area b_1 over which sites become invalidated is presum-

[45] G. R. Hill, J. Electrochem. Soc. **100**, 345 (1953).

[46] F. F. Volkenstein, Zhur. Fiz. Khim **23**, 917 (1949); see also H. S. Taylor, Discussions Faraday Soc. **8**, 9 (1950); D. J. M. Bevan and J. S. Anderson, Discussions Faraday Soc. **8**, 238 (1950); Gatner, Gray, and Stone, Discussions Faraday Soc. **8**, 246 (1950); M. J. Boudort, J. Am. Chem. Soc. **74**, 1531 (1952); S. R. Morrison and P. H. Miller, Tech. Rept. No. 6, Contract N6-onr-24914 (1952).

ably larger, or of the same order, as a.§ However, b_1 must be reduced by an area b_2 to yield b. The origin of b_2 resides in the fact that an adsorbed molecule may sometimes be expected to generate some new sites (though not as many as it has invalidated) by one of a variety of mechanisms. In particular, it is liable to cause a displacement of atoms, and other changes in the electronic structure of the surface, which lead to the formation of new sites. The density of newly created sites over the area b_2 is unlikely to be very different from the average areal density of already existing sites, at the time when the sites are generated. It is reasonable, therefore, to put $b_2 s$ for the number of sites generated by an adsorbed particle. While this will be assumed, extensions of this procedure will be studied on a subsequent occasion. The number of sites invalidated per unit area per unit time is therefore

$$-\frac{ds}{dt}=CNas\cdot bs. \tag{5}$$

Integration of the differential equation for s, yields

$$\frac{s_0}{s}=1+CNabs_0 t. \tag{6}$$

Inserting this into the differential equation for q, yields

$$q=\frac{1}{b}\log\left(1+\frac{t}{t_0}\right), \quad t_0=\frac{1}{CNabs_0}. \tag{7}$$

This is the required law.

V. DISCUSSION OF THE THEORY

The above deduction in spite of its extreme simplicity, introduces a somewhat novel feature by taking explicit account of cooperative effects among the sites. They cooperate to retain a molecule, and if one site is occupied, other sites are affected. The basic assumptions are the constancy of C and of b with time, although all parameters may be expected to depend on the temperature. It is to be hoped that the dependence of b and t_0 (which are susceptible of direct experimental determination as will be discussed below), on pressure and temperature will be tested, and throw some light on the tentative suggestions made here. So far, no extensive study has been made of these factors. The considerations of the previous section suggest that t_0 should decrease as the pressure of the gas phase is increased, since N occurs in the denominator of t_0. This appears to be borne out by experiments[47] on the chemisorption of H_2 on Cr_2O_3. In this case the law (1) holds again with the parameters given in Table I. However, since pt_0 is not a constant, it would appear that (if the theory of Sec. IV is a reasonable approximation) the product $Cabs_0$ decreases as the pressure is increased.

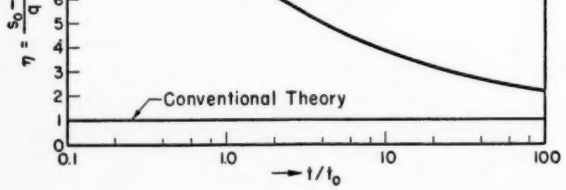

FIG. 1. Adsorption at constant pressure. Number of sites invalidated per absorbed particle as a function of time ($bs_0=10$).

§ The idea that an area with the properties of b_1 may play a part in chemisorption phenomena is due to Melnick (see reference 22).

A comparison between the present suggestions and current theory would be premature and may be reserved for a future occasion. It suffices to point out that current theory leads to the result

$$\frac{d\Theta}{dt}=\alpha P(1-\Theta)^n \exp\left(-\frac{E}{kT}\right), \tag{8}$$

where $n=1$ or 2, P is the pressure of the gas phase, E is the energy of activation, and Θ is the coverage.

TABLE I. Parameters of logarithmic law (1). H_2 on Cr_2O_3 after H. A. Taylor.[a]

p (atmos)	0.125	0.25	0.5	1.0
t_0 (min)	32	32	22	18
pt_0 (atmos-min)	4	8	11	18

[a] H. A. Taylor, private communication.

Θ is the fraction of occupied sites to originally valid sites, and can be related to our q by $\Theta=q/s_0$, provided the generation of sites is neglected ($b_2=0$).

However, the notion of "coverage" is modified even if there is no site generation. To illustrate this, define an efficiency $\eta\equiv(s_0-s)/q$ which measures the number of sites invalidated per absorbed particle. η is proportional to bs_0 and Fig. 1 shows its dependence on time for $bs_0=10$. If $bs_0=100$, the point $\eta=10$ becomes $\eta=100$. As adsorption proceeds, areas of inhibition (b) start to overlap until the adsorbed layer is packed as closely as is compatible with the lattice parameter of the solid surface and the atomic or molecular diameter of the adsorbed particles. Although there is nothing in the mathematics to indicate this, the process must then terminate. For at this time the effect of desorption will become non-negligible and would have to be introduced into the differential equations for s and q. Now, $\eta=bs_0$ at $t=0$, so that if the sites were regularly arranged and there were no generation of sites, no amount of overlapping of areas of inhibition could reduce η below $(1/2)bs_0$ or, perhaps, $(2/5)bs_0$, and for the theory to be

[47] R. L. Burwell and H. S. Taylor, J. Am. Chem. Soc. 58, 697 (1936).

consistent, adsorption should then cease. The times at which this effect should occur are given by $4t_0$ and $8.5t_0$ respectively. In fact, however, logarithmic rate laws are known to extend beyond such periods.

In order to account for this fact, it is sufficient to assume that the sites are not quite uniformly arranged, while retaining the assumption that no sites are generated. The chance (p) of a molecule sticking in an area with a relatively large density of sites is, by (3), relatively large. A site in such an area will therefore tend to be occupied first, and a comparatively large number of sites will be invalidated. Hence the high value of η at the beginning of the experiments. Particles absorbed late in the experiment will settle in areas in which the density of valid sites is small, since p is small for such areas, and there will then be a depression of η. The small density of sites in these remaining areas may be due either to an initial small density, or else because areas of inhibition have already protruded into this region in virtue of previous adsorption.

The distribution of sites must not be too non-uniform, however. For instance, if all valid sites were concentrated within an area of inhibition, there would be practically no adsorption, and a discrepancy would develop between our physical picture and the mathematical equations. The reason is that our variables are assumed to be continuous functions of the time, and the distribution of sites must be sufficiently uniform to validate this assumption.

It is clear that in the absence of generation of sites, η can reach unity only in exceptional cases, and can never decrease below this value since each absorbed particle uses up at least one site. According to conventional ideas of adsorption, however, η is always unity, since each adsorbed atom invalidates exactly one site:

$$s+q=s_0. \tag{9}$$

Since $\eta<1$ if $bs_0<1$, it follows that such cases have no physical meaning *in the absence of site generation*. This can be understood by noting that the relation $bs_0<1$ implies that an area of inhibition is smaller than the average area surrounding one site on the original surface. If $bs_0>1$, however, there is in general one single time t_1, in addition to the time $t=0$, at which (9) is satisfied. It is clear that, in the absence of site generation, the length of time for which a logarithmic rate law can be valid must be smaller than t_1. For we have

$$s+q<s_0 \quad \text{for} \quad t<t_1, \quad s+q>s_0 \quad \text{for} \quad t>t_1,$$

and, in the absence of site generation, the second case is clearly impossible. By (6) and (7) the equation for t_1 is

$$\exp\frac{(bs_0)}{(1+t_0/t_1)}=1+\frac{t_1}{t_0}. \tag{10}$$

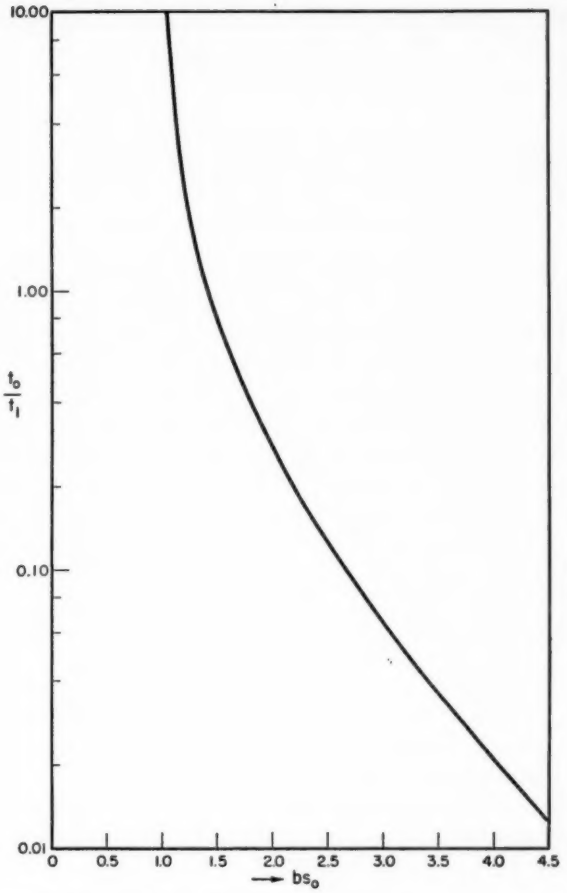

FIG. 2. Adsorption at constant pressure. The graph gives the solution curve of Eq. (10), showing how the ratio of the times t_0/t_1, depends on the parameter bs_0 of the system.

The solution of this equation is shown in Fig. 2 and may be supplemented by the approximate formulas

$$\frac{t_1}{t_0}=\begin{cases}2[bs_0-1] & (1\leqslant bs_0\leqslant 1.05),\\ \exp(bs_0)-1 & (4.5\leqslant bs_0).\end{cases} \tag{10a}$$

We have $t_1>t_0$ if, and only if, $bs_0>1.386$.

The idea that (9) is violated at almost all times, even in the absence of generation of sites, may seem strange. However, a logarithmic rate law contradicts at least one of the more usual ideas of adsorption. We shall regard as "usual" the two relations

$$s+q=s_0, \quad dq/dt=As. \tag{11a,b}$$

(11a) stipulates constancy in time of the number of occupied sites plus the number of available sites, (11b) stipulates a rate of adsorption proportional to the available number of sites. If, then, a logarithmic rate law (7) is supposed to be valid, and (11a) is supposed to hold, it follows that

$$s_0-s=\frac{1}{b}\log\left(1+\frac{t}{t_0}\right),$$

and

$$\frac{dq}{dt}=\frac{1}{bt_0}\frac{1}{1+t/t_0}=B\exp(bs),$$

where B is independent of time. Hence (11b) fails. Similarly, if (7) and (11b) both hold, it follows that

$$b(s+q)=A^{-1}(t+t_0)^{-1}+\log(1+t/t_0),$$

so that (11a) is violated. Thus a logarithmic rate law must violate (11a) or (11b), and our present suggestion is based on the idea that (11b) is valid, but (11a) fails.

We have seen that, in the absence of site generation, the mathematical equations may be expected to apply for times smaller than t_1. Suppose, however, that the equations are found to be valid over a longer period. One then has $s+q>s_0$ for $t>t_1$, so that adsorption sites must have been generated,‖ and $b_2>0$. In this case mechanisms which have been discussed elsewhere[46,11] must operate. In particular, if there is a diffusion of ions as a result of chemisorption, and a chemical reaction occurs, it is conceivable that adsorption sites are supplied for considerable periods. The constant $b=b_1-b_2$ would then presumably be rather small. This is the situation which one would expect in the growth of oxide films. Empirical evidence in favor of these ideas is presented in Sec. VII.

Some inadequacies of current ideas, as based on (8), may also be shown up on purely empirical grounds. For when a law (1) holds, and (8) is applied to the data, it is often found that such a considerable dependence on "coverage" is contained in α and in E. that the variation implied by the term $(1-\Theta)^n$ can be neglected in comparison. This suggests that one may in these cases be attempting to force experimental results into comparison with a theory which is not well adapted to explain them.

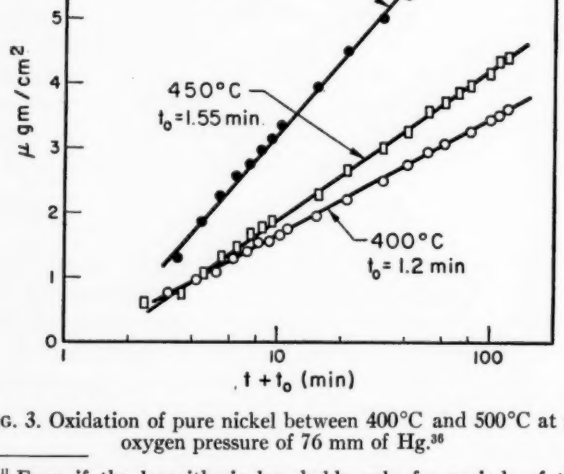

FIG. 3. Oxidation of pure nickel between 400°C and 500°C at an oxygen pressure of 76 mm of Hg.[36]

‖ Even if the logarithmic law holds only for periods of the order of t_1, it is clear that sites must have been generated.

Comparison with the absolute reaction-rate theory[48] would also be premature. However, it may be observed that in the cases where a logarithmic law holds, the agreement with that theory is not always very satisfactory.[49]

VI. REMARKS ON RELATED FIELDS OF STUDY

If Eq. (1) is differentiated with respect to time, it is found that

$$\frac{dq}{dt}=\frac{1}{bt_0}\exp(-bq). \tag{12}$$

It was just a law of this type which had to be postulated to the account for the rate of formation of ammonia,[50] assuming that the rate-controlling step was the adsorption of nitrogen on the iron catalyst. The law (12) is equivalent to the law (1), since either can be deduced from the other. Its approximate validity in this case has been confirmed by other workers.[49,51] Together with a rate of desorption $\beta\exp(\gamma q)$,[52] (12) forms an empirical basis for the derivation of an adsorption isotherm due to Slygin and Frumkin,[53] and evidence coming from work related to these fields may therefore also be relevant to the range of validity of the law (1).

VII. NUMERICAL CONSIDERATIONS

In order to plot experimental results so as to obtain a simple evaluation of the constants, one may use either of two methods. One may either plot q as a function of $\log(t+t_0)$ as indicated by Eq. (1); this has the disadvantage that it is not easy to obtain a unique value of t_0. Or, one may plot $\log(dq/dt)$ as a function of q; in this case intercept and slope yield b and t_0, but a graphical differentiation is involved.

As an example we consider recently published data for the chemisorption of nitrogen on iron (reference 50, Fig. 4, Sample I, 199°C). The straight-line law is not exactly obeyed in this case. But by concentrating on the earlier stage of the adsorption, a straight line may definitely be drawn (adsorption up to 1 cc). The rate of adsorption at the beginning of the experiment (i.e. at $t=0$, $q=0$) can be estimated to be about 0.2 cc of gas adsorbed per minute, or 4.19×10^{11} molecules adsorbed per cm² per second. Since the number of

[48] Laidler, Glasstone, and Eyring, J. Phys. Chem. **8**, 659, 667 (1940).

[49] P. Zwietering and J. J. Roukens, Trans. Faraday Soc. **50**, 178 (1954).

[50] M. Temkin and V. Pyzhev, Acta Physicochim. U.R.S.S. **12**, 327 (1940).

[51] For instance, by the work of Brunauer, Love, and Keenan, J. Am. Chem. Soc. **64**, 751 (1942), on the earlier experimental data obtained by P. H. Emmett and S. Brunauer, J. Am. Chem. Soc. **56**, 35 (1934). Compare also P. H. Emmett and J. T. Kummer, Ind. Eng. Chem. **35**, 677 (1943).

[52] I. Langmuir, J. Am. Chem. Soc. **54**, 2798 (1932).

[53] A. Slygin and A. Frumkin, Acta Physicochim. U.R.S.S. **3**, 791 (1935).

TABLE II.

Temperature (°C)	t_0 (Min)	Slope (μ gm/cm²)	$b(A^2)$
400	1.20	0.77	0.34
450	1.55	1.17	0.23
500	1.40	1.73	0.15

molecules of gas striking a square cm of the surface per second should in the case of this curve be about 2.98×10^{23}, it follows that the probability (p_0) per impact of a molecule sticking at the surface at the beginning of the experiment is 1.41×10^{-12}. This figure depends only on the experimental results and kinetic theory, and is independent of our more specialized model of adsorption. Using Eq. (3), therefore, $p_0 = Cas_0 = 1.41 \times 10^{-12}$. Since as_0 may be expected to be of order unity, this is also a rough estimate for the dimensionless constant C. This deals with the intercept of the straight line. The slope of the line is approximately -1.72 reciprocal cc of gas adsorbed, or, equivalently, 1.37×10^{-14} reciprocal number of atoms adsorbed per cm² of surface. The constant $b = b_1 - b_2$ has therefore the value 1.37×10^{-14} cm², so that the radius of an area of influence of an adsorbed atom turns out to be $r = 6.59\ A$, or, if $b_2 > 0$, then $r > 6.59\ A$. This inequality would hold if there was site-generation.

This figure may be checked as follows: Taking the mean distance between iron atoms somewhat arbitrarily as $\sqrt{(12)}\ A$, the mean distance between adsorbed nitrogen atoms on a fully covered surface is $3.46\ A$. However, at the end of the experiment under consideration only a fraction $1.6/6.5 = 0.25$ of the available surface was covered, so that the mean distance between adsorbed nitrogen atoms at the end of the experiment must have been equal to $d = 6.92\ A$. This figure cannot be expected to be accurate, however, since the sites are unlikely to form an exact lattice. Thus the inequality $d > r$, which is required by our model, is still fulfilled at the end of the experiment ($t \sim 600$ min). However, d and r are not very different at this stage, so that our model would predict a breakdown of the logarithmic law at this time, and this is borne out by the experiment. In fact, since it appears to have already failed at this time, one may in fact have $t > 6.59\ A$, so that a small amount of site generation cannot be excluded.

The value of t_0 is found to be 2.9 min, in general agreement with the kind of values given by Taylor and Thon.[11] We do not therefore wish to give here an equally detailed analysis of other available data. It may, however, be observed that if the number of available sites per cm² at the beginning of the experiment (s_0) exceeded 10^{14}, then the time t_1 satisfies $t_1 > t_0$. If we make the arbitrary assumption that $s_0 \sim 7.3 \times 10^{14}$ cm^{-2}, then $t_1 \sim 6.4 \times 10^4$ min, which represents about a hundred times the length of the actual experiment.

Figure 3 gives a plot of q as a function of $\log(t+t_0)$ for the oxidation of pure nickel at elevated temperatures, using data given by Gulbransen and Andrew.[36] The values of the parameters are given in Table II, and show that the efficiency of site generation increases with temperature.

A possible physical picture for the formation of oxide films is therefore as follows: there are two basic mechanisms which tend to promote film growth: chemisorption and ionic motion. Now, chemisorbed layers are liable to give rise to an electric field near the surface, due to attendant charge separation, and these fields may eventually be strong enough to cause ionic motion. On the other hand, ionic motion tends to remove ions from chemisorption sites, and tends to generate new sites. In this way it encourages additional chemisorption. It is clear therefore that the two mechanisms aid each other. At lower temperatures chemisorption is liable to be dominant and to cause by the attendant electric fields, ionic motion in excess of what one would expect on the grounds of temperature alone.¶ As the temperature is raised, desorption increases in importance, and opposes chemisorption, while ionic motion becomes easier. At this stage the logarithmic law tends to go over into the parabolic law, since a diffusion mechanism[39,42,43] begins to control the rate of the

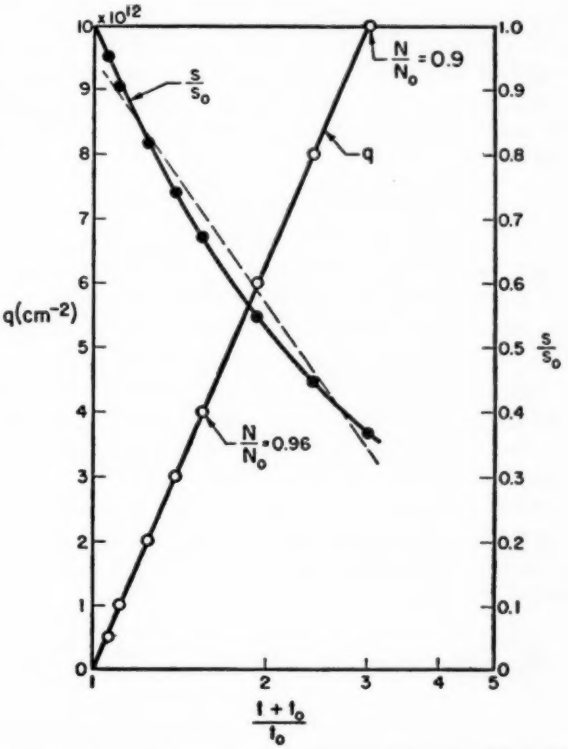

FIG. 4. Adsorption at constant volume. The graph shows the increase in the number of adsorbed molecules per unit area, and the fractional decrease in the number of available sites with lapse of time. It is assumed that $(b/A)\times$ the total number of molecules which were present in the fixed volume V at time $t=0$ has the value 10, and that $b = 10^{-13}$ cm².

¶ This effect should show up in a plot of the parabolic rate constant against $1/T$, and is found for instance in the oxidation of nickel (reference 36, Fig. 5).

reaction. The transition region deserves careful study as it is not clear at present how the two factors cooperate in this range of temperatures. It is hoped to return to this question in the future. It seems likely that the probability of sticking, Eq. (3), ceases to be proportional to the number of available sites s, at the higher temperatures when there are plenty of sites.

This view appears to differ from that of Mott and Cabrera only in its emphasis on the chemisorption stage of the growth process. It depends crucially on the assumption that some understanding of the logarithmic growth law of chemisorption can be gained along the lines indicated in Sec. IV, and it then relies on a modification of this mechanism. A statement of the merits of this point of view would include its simplicity, its ability to correlate data on oxide films with chemisorption data, the circumstance that the theoretical treatment is susceptible of considerable generalization, and the circumstance that it leads to logarithmic rate laws of oxidation for films thicker than those covered in Cabrera and Mott's treatment. Thus the maximum thickness of film attained in the experiments illustrated in Fig. 3 is about $7\mu g/cm^2$, or about $D=440$ A, and growth was still continuing, whereas Cabrera and Mott state that their theory can be expected to apply only to thicknesses $D \ll X_1$, where $X_1 \sim 100$ A to 1000 A. The main drawback of the present suggestions is that the constants which occur are not at present related to atomic constants, as they are in Cabrera and Mott's treatment, but such developments should also be possible.

VIII. GENERALIZATIONS

The theory of Sec. IV must be criticized for utilizing rather crude assumptions. It is, for instance, unlikely that all sites within a circle of area b_1 will be equally and completely invalidated by the adsorption of an atom. In a better theory b_1 may be replaced by a probability distribution function, which states the probability that a further molecule can be adsorbed at a distance γ from a molecule which has already been adsorbed. It might be thought at first sight that this procedure would be equivalent to introducing an activation energy which depends on coverage. But this has already been done, in effect, since by (8) and (12), putting $\Theta=q/s_0$,

$$\frac{d\Theta}{dt}=\alpha P(1-\Theta)^n \exp\left(-\frac{E}{kT}\right)=\frac{1}{bs_0t_0}\exp(-bs_0\Theta).$$

In terms of the conventional model this identification leads immediately to the linear dependence of activation energy on coverage. Our interpretation of this effect is that the exponential factor arises from an overlap of areas of inhibition brought about by increasing adsorption.

The theory of Sec. IV can also be criticized for neglecting the influence of molecular velocities on the probability of sticking, and for the lack of an atomic theory of the factor C. These and other mathematical complications would however tend to confuse a basically simple point of view, and may therefore be held over.

We shall, however, deal at the same elementary level with another physical situation that may arise, in order to illustrate our belief that the treatment of Sec. IV can be generalized in several directions. Consider the case of chemisorption at a surface from a gas which is not kept at constant pressure (as in Sec. IV) but at constant volume, so that the number of collisions with the surface decreases as gas becomes chemisorbed. Equations (4) and (5) remain valid, but N is now a function of the time. Nonetheless, by taking the ratio of (5) to (4), so that N disappears, one finds

$$ds/dq=-bs, \quad s=s_0\exp(-bq); \tag{13}$$

equations which hold also in the constant pressure case. As an additional equation for N, we take

$$\rho V+qA=\text{constant}, \tag{14}$$

which expresses conservation of the number of molecules. ρ is the number of molecules per unit volume, and may be equated to $6N/c$, c being the most probable molecular velocity, since in this elementary theory, we neglect the velocity distribution of the molecules. N has the previous significance (Sec. IV). V is the fixed volume of the gas phase, A the effective area of the surface.** If N_0 be the value of N at $t=0$, (14) becomes simply

$$N_0-N=(cA/6V)q. \tag{15}$$

Differentiating (15) with respect to time, and using (4), (13), and (15), one finds

$$Ei(-\lambda N)-Ei(-\lambda N_0)=\frac{\exp(-\lambda N_0)}{\lambda t_0 N_0}, \tag{16}$$

where

$$Ei(\chi)\equiv\int_{-\infty}^{\chi}(e^t/t)dt, \quad \lambda\equiv 6bV/cA. \tag{17}$$

Under ordinary conditions the dimensionless quantity λN is of order 10 to 1000 for a volume V of order 10 cc to 1000 cc. For large positive χ, the asymptotic expansion

$$Ei(-\chi)\sim -e^{-\chi}\left[\frac{1}{\chi}-\frac{1}{\chi^2}+\frac{2!}{\chi^3}-\frac{3!}{\chi^4}+\cdots\right]$$

holds. Using this in (16), the solution of the problem can be summarized by (13) and the equations

$$\nu\exp(\gamma\nu)=e^{\gamma}/(1+\tau), \tag{18}$$

$$q=(\gamma/b)(1-\nu), \tag{19}$$

where

$$\nu\equiv N/N_0, \quad \tau\equiv t/t_0, \quad \gamma=\lambda N_0=(b/A)\rho_0 V. \tag{20}$$

** A must contain a correction factor if the gas is chemisorbed in atomic form.

For given parameters, (18) gives N (and hence the density ρ of the gas phase) as a function of time, and then (19) and (13) give q and s as a function of time. Since the exponential term dominates in (18), the multiplying factor ν can often be neglected, when (19) is again a law of the precise form of (1), with the same constants, except that now

$$t_0 = 1/(CN_0 abs_0), \tag{21}$$

in obvious generalization of (7).

To illustrate these equations, Fig. 4 shows typical curves for q and s as a function of $1+\tau$ using (13), (18), and (19). It is clear that it is impossible, for the parameters chosen, to distinguish experimentally the curve of Eq. (1) from that of Eq. (19). The rate of adsorption is therefore in effect again logarithmic, in agreement with experiment. It is seen from Fig. 4 that the number of sites s does not obey a logarithmic law In particular, it shows that after the pressure has fallen by 10 percent due to adsorption, the number of available sites has already decreased to one-third the original value.

ACKNOWLEDGMENTS

The writing of this paper affords the author a welcome opportunity to express his sincere appreciation of the kindness and hospitality which he has experienced during his year's stay in the United States. Thanks are due to Professor W. Ufford and the Physics Department of the University of Pennsylvania, and in particular to Professor P. H. Miller, Jr., to whom the author is also indebted for first drawing his attention to the problems of chemisorption; to the Westinghouse Research Laboratories, where most of this paper was written; to Dr. P. H. Emmett and Dr. E. A. Gulbransen for stimulating discussions on chemisorption and the growth of oxide films; he has also benefited from correspondence with Dean H. S. Taylor and Professor H. A. Taylor, and earlier discussions with Dr. D. Melnick.

THE JOURNAL OF CHEMICAL PHYSICS VOLUME 23, NUMBER 6 JUNE, 1955

Method of Calculating Cross Sections for Molecular Collisions*

ERNEST BAUER
Institute of Mathematical Sciences, New York University, New York, New York
(Received September 10, 1954)

The calculation of cross sections for slow inelastic collisions of molecules, such as occur in chemical reactions, shows an interesting combination of classical and quantum-mechanical features. The de Broglie wavelength is small compared with the range of the intermolecular potential so that there exists a relatively well-defined quasi-classical orbit; but in some cases the coupling constant is small compared with unity, and this gives the problem certain quantum-mechanical characteristics. On account of the condition relating to the de Broglie wavelength, a calculation of the total collision cross section requires the knowledge of the partial waves for a large number of values of the angular momentum $l\hbar$.

A method is devised to suit these different features. The WKB method lends itself well to this application, with a quasi-classical amplitude and a quantum-mechanical phase for the wave function. We also use the concept of an impact parameter b rather than the orbital quantum number l: this is well suited to describing a quasi-classical orbit, and hence for calculating the total cross section in a case like the present one. As an example of the method, the cross section for excitation of the first vibrational state of a hydrogen molecule resulting from collision with another hydrogen molecule is calculated.

I. INTRODUCTION

WE wish to calculate the cross section for the excitation of molecular vibrations by collision between two molecules, or an atom and a molecule, at energies so low that the translational and vibrational energies are of the same order of magnitude. Processes of this kind are basic to many gas phase chemical reactions[1,2] and also to phenomena such as the "vibrational relaxation" that has been suggested as a mechanism for the large absorption of high-frequency sound in gases.[3]

Numerous quantum-mechanical calculations of this kind of process have been made[4–8] and the correct order

* This work was supported in part by Contract No. AF-19(122)-463 with the U. S. Air Force through sponsorship of the Geophysics Research Directorate of the Air Force Cambridge Research Center, Air Research and Development Command.

[1] Mott and Massey, *Theory of Atomic Collisions* (Oxford University Press, London, England, 1949), second edition, p. 294.

[2] Fowler and Guggenheim, *Statistical Thermodynamics* (Cambridge University Press, Cambridge, England, 1939), ch. 12.

[3] W. T. Richards, Revs. Modern Phys. **11**, 36 (1939).

[4] Excitation of molecular vibration and rotation by collision: one-dimensional treatment of the translational motion. C. Zener, Phys. Rev. **37**, 556; **38**, 277 (1931); J. M. Jackson and N. F. Mott, Proc. Roy. Soc. (London) **A137**, 702 (1932); Schwartz, Slawsky, and Herzfeld, J. Chem. Phys. **20**, 1591 (1952); K. Takayanagi, Progr. Theoret. Phys. (Japan) **8**, 111 (1952); H. Aroeste, J. Chem. Phys. **21**, 870 (1953); J. C. Beckerle, J. Chem. Phys. **21**, 2034 (1953).

[5] Vibrational dissociation by collision: one-dimensional treatment of the translation. E. Bauer, Phys. Rev. **84**, 315 (1951); **85**, 277 (1952).

[6] Chemical reactions: one-dimensional treatment of the transla-

of magnitude for the cross section has been obtained. The problem of measuring cross sections for this kind of process experimentally is a very difficult one because of the low energy of translation, so that no detailed numerical data such as angular distributions can be expected; from a theoretical standpoint there are serious difficulties connected with the form of the intermolecular potential, and also with the mathematical treatment of the translational motion.

On account of the complexity of the problem, which arises from the large number of electrons and nuclei involved, it has not been possible to give convincing quantitative calculations of the intermolecular (van der Waals) potential for any but the very simplest systems.[9] The quantitative knowledge that is available on the van der Waals potentials of most molecules[10] has been derived from a knowledge of macroscopic properties of the gas, such as the viscosity and the second virial coefficient, by means of various statistical-mechanical models. From a logical standpoint this is a very unsatisfactory method of proceeding, both because many different models could give the same value for the macroscopic constants, and also, more specifically, because viscosity and other such properties depend on the behavior of a gas in near-equilibrium, when the molecules are mostly far apart from one another; in studying collisions, on the other hand, we are interested in the characteristics of the intermolecular potential at the opposite extreme, namely when the molecules are in close proximity.[11] In the present work we shall make heuristic assumptions regarding the form of the potential, similar to those that have been made previously.[6] As far as this aspect of the problem is concerned, it seems that at present one cannot hope for any radically improved results. However, with a reasonably reliable and rapid method of calculation it might be possible to consider a program of determining the potential from the value of the cross section, by varying the parameters involved in the potential in a systematic way, or conceivably even by more sophisticated methods.

The central aim of this work is the presentation of a relatively rapid method for calculating the cross sections for slow inelastic collisions in which the Born approximation is not valid and where it is not possible to restrict oneself to the calculation of a relatively small number of partial waves.

The problem is this. We wish to make a perturbation calculation of the cross section for the transfer of energy between two degrees of freedom.[12] The Hamiltonian H of the system consists of an unperturbed part

$$H^0=T^0+V^0$$

(T=kinetic energy; V=potential energy), and a small perturbation V' that provides a coupling between the different degrees of freedom.[13]

Now we must be more specific. We consider the transfer of energy between translational ("external") and internal degrees of freedom of the system. The internal motion considered here is vibration, but one could equally well consider rotation. In any case, the internal motion is quite well understood, and will not be discussed here: the problem is to give a suitable treatment for the translational motion. The translational motion is characterized by a reduced mass M_e ("e" for "external"), an energy $E=\hbar^2k^2/2M_e$, and an impact parameter b related to the angular momentum $\hbar l$ by the relation

$$\hbar l=\hbar kb. \tag{1}$$

The potential V^0 is made up of two parts, namely V_i which determines the internal motion, and V_e^0 which acts on the translational degrees of freedom. The potential V_e^0 has a definite range R, and the perturbation potential V' also has a definite range, $R'\gtrsim R$, in the translational coordinate.

The essential character of the translational motion is defined in terms of two conditions. First, the de Broglie wavelength $\lambda\!\!\!^{-}=1/k$ is very much smaller than R:

$$\lambda\!\!\!^{-}=1/k\ll R. \tag{2}$$

This condition arises from the large value of the particle mass M_e, which gives large values for k even for small energies E. The physical meaning of the condition (2) is that there exists an orbit for our colliding particles in something like the classical sense: there is a diffuseness in this orbit of order $\lambda\!\!\!^{-}=1/k$, but this is small compared with the "natural length" R for the problem.

There is yet a second condition, concerning the mag-

tion. E. Bauer and Ta-You Wu, J. Chem. Phys. **21**, 726, 2072(L) (1953).

[7] Vibrational excitation: three-dimensional classical treatment of the translation. B. Widom and S. H. Bauer, J. Chem. Phys. **21**, 1670 (1953).

[8] Vibration and rotation: three-dimensional quantum mechanical treatment of the translation. K. Takayanagi, Progr. Theoret. Phys. (Japan) **8**, 497 (1952); K. Takayanagi and T. Kishimoto, Progr. Theoret. Phys. (Japan) **9**, 578 (1953); Schwartz and Herzfeld, J. Chem. Phys. **22**, 767 (1954); R. Brout, J. Chem. Phys. **22**, 934, 1189 (1954).

[9] A. A. Evett and H. Margenau, Phys. Rev. **90**, 1021 (1953).

[10] Hirschfelder *et al.* Chem. Revs. **44**, 205 (1949).

[11] A typical example is the Lennard-Jones 6–12 form $(a/r^{12}-b/r^6)$ normally used for the van der Waals potential; while this is adequate at large intermolecular separations and does reproduce the known minimum in the potential, it is entirely unsatisfactory at small separations, where the potential is known to behave like $1/r$ rather than like $1/r^{12}$ (see reference 6).

[12] The "perturbation" character is inherent not only in the present (and all previous) methods of calculation, but even in the qualitative description of the system in terms of separate degrees of freedom. The underlying reason for this arises from the fact that it is in general impossible to solve problems involving several degrees of freedom exactly, such as even the classical three-body problem.

[13] If we introduce the notation

$$a\ll^* b$$

for "a is very much less than b almost everywhere," then the perturbation approach will be valid if the condition

$$V'\ll^* H^0$$

is satisfied, and slow collisions may be defined by the condition

$$T^0\ll^* V^0.$$

nitude of the momentum transferred in a collision in relation to the uncertainty principle. Roughly, we may say that the momentum transferred is given by the expression

$$\delta p \sim \int \text{grad} V' dt, \tag{3}$$

where the integration extends over the whole collision, so that

$$\delta p \sim (V'/R)\cdot(RM_e/\hbar k) = V'M_e/\hbar k. \tag{3a}$$

We now ask: what is the order of magnitude of the expression[14]

$$\delta p R/\hbar \sim V'RM_e/\hbar^2 k. \tag{4}$$

If the expression (4) is much larger than unity, then the effect of the uncertainty principle—or quantum-mechanical effects generally—will be small, so that we may treat the translational motion classically. If (4) is very much less than unity, we must treat the translational motion in terms of quantum mechanics, even though the orbit may be well defined, in view of condition (2).[15]

It turns out that in the present problem (4) is frequently small compared with unity (see Table I), so that a strictly classical treatment of the translational motion[7] is not completely satisfactory.

The two conditions involving (2) and (4) are basic to the present problem. It is clear from (1) and (2) that one must consider values of the impact parameter $b \lesssim R$, corresponding to angular momenta $l\hbar \lesssim l_1\hbar$, where

$$l_1 = kR \gg 1. \tag{5}$$

Actually $l_1 \sim 10$–100 in the present case (see Table I), and this determines the method of attack: basically we use perturbation theory,[16] but in a different representation from that usually employed. Normally one would expand the solution in spherical harmonics of order l $(=0,1,2,\cdots)$, solve the radial equation (an ordinary differential equation) for each value of l, and then sum the contributions for all $l \lesssim l_1$ to give the total cross section. This procedure would clearly be exceedingly lengthy in the present case, and thus we use wave functions characterized by the impact parameter b rather than by l; to obtain the total cross section, we integrate over all $b \lesssim R$.

Here we use the WKB method in an impact parameter formulation. The WKB method is essentially an asymptotic expansion in powers of $\hbar$ or $1/k$ or $1/M_e$—depending on how one chooses to regard it—and involves a wave function of form $A\exp(iS/\hbar)$, where $|A|^2$ is a density function, and S a phase. In view of condition (2) the density $|A|^2$ just follows the classical orbit, described in terms of the impact parameter b, with the quantum width $\lambda\!\!\!^{-} = 1/k \ll R$; the phase S is a solution of the Hamilton-Jacobi equation of the problem.

[14] For Coulomb scattering, $V' = Ze^2/r$, so that if we are willing to speak of a range R in this case, the expression (4) is just $Ze^2/\hbar v$.

[15] There is no inconsistency here because (2) involves k and R, whereas (4) involves V', R, M_e, and k, so that (2) and (4) are essentially different.

[16] See reference 1, chapter VIII: "Method of Distorted Waves."

TABLE I. The total cross section.

E_0 $(10^{-3}\ e^2/a_0)$	20	20.27	30	40	60	80
σ_C'' $(10^{-19}$ cm$^2)$	0	1.5	6.7	4.4	1.7	1.2
σ_Q'' $(10^{-19}$ cm$^2)$	0	0.02	3.8	3.1	1.6	1.2
σ_Q'' has its maximum for $l=l_m$: $l_m=$		4	15	23	24	22
σ_Q'' is essentially zero for $l>l_0$: $l_0=$		6	30	47	67	75
$\lambda\!\!\!^{-}_f/d$ (expression (2))		0.18	0.03	0.02	0.015	0.012
$\delta p R/\hbar$ (expression (4))						
(a) evaluated at $r=d$		0.5	0.08	0.06	0.04	0.03
(b) evaluated at r corresponding to $l=l_m$		0.02	0.5	0.9	1.4	1.8

(i) $E_0 = 20.27\times10^{-3}\ e^2/a_0$ is too close to the threshold for the present method to yield reliable results, on account of the small number of phases that contribute to σ''.

(ii) There are considerable differences in the value of the expression (4), depending on just how one evaluates it. The basic point is that the expression is of the order unity but somewhat smaller, so that one would expect the result for σ'' to lie somewhere between the C- and Q-values.

II. SPECIFICATION OF THE PROBLEM

We consider a molecule AB which is excited in collision with an atom (or molecule) C. Each atom is regarded as a "particle" of respective mass M_A, M_B, M_C; each such "particle" is essentially the nucleus with a given potential field determined by the orbital electrons, which themselves are not explicitly considered here. This "adiabatic" separation of the electronic from the nuclear motions is justified in the present problem because it follows from the low energies of the heavy-particle motions under discussion that the velocities of the heavy particles are several orders of magnitude smaller than the electronic velocities, so that there is practically no possibility of transferring energy between electronic and nuclear (translational, rotational, vibrational) modes of motion.

In discussing total collision cross sections, it is convenient to eliminate the motion of the center of mass, and thus we use the following coordinates:

$$\begin{aligned} \boldsymbol{\varrho} &= \mathbf{r}_{AB} \\ \mathbf{r} &= \mathbf{r}_C - (M_A\mathbf{r}_A + M_B\mathbf{r}_B)/(M_A+M_B) \\ \mathbf{R} &= (M_A\mathbf{r}_A + M_B\mathbf{r}_B + M_C\mathbf{r}_C)/(M_A+M_B+M_C). \end{aligned} \tag{6}$$

Here $\boldsymbol{\varrho}$ is the internuclear separation of the molecule AB and describes its internal motion (rotation, vibration); $\mathbf{r}$ is the coordinate of the incident particle C relative to the center of mass of the molecule AB and describes the translational motion. $\mathbf{R}$ is the coordinate of the center of mass of the system as a whole: it is irrelevant to the present discussion, and will not be used here.

We must specify the reduced masses in the coordinates $\boldsymbol{\varrho}$ and $\mathbf{r}$; they are, respectively,

$$M_i = M_AM_B/(M_A+M_B),$$

and

$$M_e = M_C(M_A+M_B)/(M_A+M_B+M_C). \tag{7}$$

We shall consider the case when $A=B$, and $C=AB$; then

$$M_i=\tfrac{1}{2}M_A, \quad \text{and} \quad M_e=M_A. \tag{7a}$$

We are concerned with a transition in which the system goes from one state 0 to another state f. Any given state j of the system as a whole is characterized by specifying both the internal (vibrational and rotational) and external (translational) motions; this may conveniently be done by giving the internal energy $\epsilon_j=\hbar\omega_j$ for a pure vibration, and the momentum $\hbar\mathbf{k}_j$, which is related to the translational energy E_j by $E_j=\hbar^2k_j^2/2M_e$. It is clear that if no rotational transitions occur between our states 0 and f, we have conservation of energy in the form

$$\hbar(\omega_f-\omega_0)=(k_0^2-k_f^2)\hbar^2/2M_e. \tag{8}$$

TABLE II. The van der Waals potential V_e for two hydrogen molecules (see reference 9) (see Eqs. (12), (13), (14)).

$U_e^0=4.18\times10^{-4}$	e^2/a_0
$a=0.916$	a_0^{-1}
$\rho_0=1.40$	a_0
$d=5.67$	a_0
$U'a\rho_{01}=5.87\times10^{-6}$	e^2/a_0
$z_0=6.87$	a_0

It should be noted that conservation of linear momentum is ensured automatically because we have eliminated the motion of the center of mass of the system as a whole; conservation of angular momentum will have to be considered separately (see Sec. V).

In the present work we are concerned explicitly with a transition involving only translational and vibrational motion, and in particular the normal and first excited vibrational states of the molecule in question. The method can obviously be applied to other processes, such as the excitation of rotation by collisions, but at least for an initial discussion it is desirable to have the internal and external modes of motion as different in character as possible, because they are treated on a rather different basis.

III. THE POTENTIAL

We wish to express the potential energy of the system $AB+C$ in terms of the coordinates $\boldsymbol{\varrho}$, $\mathbf{r}$ in such a way that we may write[17]

$$V=V(\boldsymbol{\varrho},\mathbf{r})=V_i^0(\boldsymbol{\varrho},\mathbf{r}_0)+V_e^0(\boldsymbol{\varrho}_0,\mathbf{r})+V'(\boldsymbol{\varrho}-\boldsymbol{\varrho}_0,\ \mathbf{r};\ \boldsymbol{\varrho}_0). \tag{9}$$

At this point we neglect any noncentral characteristics of V and proceed as follows. Consider our three particles A, B, C in a straight line, and assume that all interactions may be represented as those between two atoms. Then

$$V=V(r_{AB})+V(r_{BC})+V(r_{CA}). \tag{10}$$

[17] For a symmetrical way of treating $\boldsymbol{\varrho}$ and $\mathbf{r}$, see reference 6.

$V(r_{AB})$ is the internal potential energy of the AB-molecule, and thus its quantitative character is well known from spectroscopic evidence: we call it $V_i^0(\boldsymbol{\varrho},\mathbf{r}_0)$, since $\boldsymbol{\varrho}=\mathbf{r}_{AB}$. For the external (van der Waals) potential between the atoms, i.e.,

$$V_e=V_e^0+V'=V(r_{BC})+V(r_{CA}), \tag{11}$$

we substitute Morse expressions

$$V(x)=U_0[e^{-2a(x-x_0)}-e^{-a(x-x_0)}] \tag{12}$$

rather than the conventional Lennard-Jones 6–12 form.[11,17a]

We now take the case $A=B$, $C=AB=A_2$, with the three particles A, B, C in a straight line, so that

$$r_{BC}=r-\tfrac{1}{2}\rho; \quad r_{CA}=r+\tfrac{1}{2}\rho. \tag{6a}$$

Substituting (6a) and the form (12) for $V(r_{BC})$, $V(r_{CA})$ into (11), we finally get the result

$$V_e^0(\rho_0,r)=U_e^0[e^{-2a(r-d)}-e^{-a(r-d)}],$$

$$U_e^0=U_0\frac{2[\cosh(\frac{1}{2}a\rho_0)]^2}{\cosh(a\rho_0)};$$

$$d=x_0+(1/a)\log\left[\frac{\cosh(a\rho_0)}{\cosh(\frac{1}{2}a\rho_0)}\right], \tag{13}$$

$$V'(d\rho,r)=U'ad\rho[e^{-2a(r-z_0)}-e^{-a(r-z_0)}],$$

$$U'=U_0\frac{[\sinh(\frac{1}{2}a\rho_0)]^2}{2\sinh(a\rho_0)};$$

$$z_0=x_0+(1/a)\log\left[\frac{2\sinh(a\rho_0)}{\sin(\frac{1}{2}a\rho_0)}\right]. \tag{14}$$

We still have the problem of determining the correct numerical values of the constants U_0, a, ρ_0, x_0. These must be chosen to give the correct equilibrium nuclear separation ρ_0, and also the correct van der Waals potential V_e^0. The numerical values chosen for the case of two hydrogen molecules colliding are listed in Table II. They are essentially the quantum-mechanical results of Evett and Margenau[9] but these agree very well with the empirical values obtained from viscosity and second virial coefficients.[10]

It must be stressed that the present discussion of the potential is far from being self-consistent or satisfactory. There is a lack of consistency in the fact that the internal potential $V_i^0(\boldsymbol{\varrho},\mathbf{r}_0)=V(r_{AB})$ and the external potential $V_e=V_e^0+V'$ are treated in completely different ways. We see empirically that one cannot use the expression (12) with the same set of constants U_0, a, x_0, ρ_0 for both V_i^0 and V_e^0, because the numerical values of the two potentials are so different: in particular, the well depth in V_i is of the order 4.5 ev for hydrogen as against 0.01 ev in the case of V_e. This quantitative

[17a] A detailed discussion of the bound states associated with van der Waals potentials in the 6–12 form has been given by J. E. and M. F. Kilpatrick, J. Chem. Phys. **19**, 930 (1951).

difference is entirely understandable in terms of the distortion of the "electron cloud" of the molecule at close nuclear separations, and the attendant complications, but it does show clearly the heuristic character of the present derivation of V_e^0 and V'. The numerical values of V_e^0 used here are reasonably satisfactory, but it is clear that the numerical values used for V', depending as they do on the differentiation of the function V_e^0, cannot be expected to be accurate.

The purpose of this work is essentially the derivation of a method for calculating cross sections, and in view of this the aim of the present section is merely to arrive at a potential which is sufficiently plausible in its qualitative and semiquantitative aspects so that the numerical values of the cross section resulting from the calculation shall have some sort of meaning.

IV. THE PERTURBATION SCHEME

Disregarding the motion of the center of mass of the system, we may write the total Hamiltonian H as

$$H=H(\boldsymbol{\varrho},\mathbf{r})=T_i(\boldsymbol{\varrho})+T_e(\mathbf{r}) +V_i^0(\boldsymbol{\varrho})+V_e^0(\mathbf{r})+V'(\boldsymbol{\varrho},\mathbf{r}), \quad (15)$$

where the kinetic energy terms T are given by the usual expressions

$$T_i(\boldsymbol{\varrho})=-(\hbar^2/2M_i)\nabla_{\boldsymbol{\varrho}}^2; \quad T_e(\mathbf{r})=-(\hbar^2/2M_e)\nabla_r^2, \quad (16)$$

and the potential energy terms V have the values of Sec. III and Table II.

We treat V' as a small perturbation, and describe eigenstates of the unperturbed system as

$$\phi_j(\boldsymbol{\varrho})\chi_j(\mathbf{r}),$$

where $\phi_j(\boldsymbol{\varrho})$, $\chi_j(\mathbf{r})$ are, respectively, solutions of

$$[T_i(\boldsymbol{\varrho})+V_i^0(\boldsymbol{\varrho})-\hbar\omega_j]\phi_j(\boldsymbol{\varrho})=0 \quad (17)$$

and

$$[T_e(\mathbf{r})+V_e^0(\mathbf{r})-\hbar^2k_j^2/2M_e]\chi_j(\mathbf{r})=0. \quad (18)$$

In the present work we treat the $\phi_j(\boldsymbol{\varrho})$ as known functions: the central problem is to find suitable functions $\chi_j(\mathbf{r})$ by solving Eq. (18), and in particular to find an expression for the transition matrix element $(f|V'|0)$.

V. THE ORBIT

On account of condition (2), we can speak of an orbit which follows the classical path, but has a width λ arising from the uncertainty principle. Accordingly, we consider first the classical motion of a particle C moving with momentum $\hbar\mathbf{k}_0$ towards the molecule AB, exciting this molecule into a vibrational state f, and then leaving with momentum $\hbar\mathbf{k}_f$. The initial orbit of C is a straight line asymptotically, and the length of the perpendicular from the center of mass of the molecule AB onto the continuation of this straight line is known as the "impact parameter" b_0 of the initial orbit. Similarly, we define an impact parameter b_f for the final orbit (see Fig. 1).

We now ask the following question: given the initial and final asymptotic orbits, what is the actual orbit which links them? For definiteness, we suppose

(i) that the scattering potential is central. This enables us to locate the classical motion in a plane.

(ii) That no rotational motion is excited, so that angular momentum is conserved. The condition for conservation of angular momentum is[18]

$$\hbar k_0 b_0=\hbar k_f b_f=\hbar l. \quad (19)$$

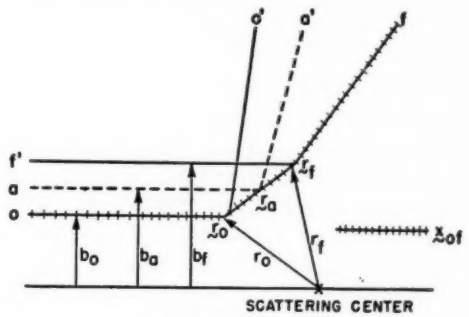

FIG. 1. The orbit.

(iii) that the potential $V_e^0(\mathbf{r})$ which determines the orbit has a short range. This assumption is again convenient but, like the other conditions, it is not necessary in principle.

It is evident from physical considerations that in the classical case the actual orbit passes continuously through all classical orbits a which satisfy

$$\hbar k_a b_a=\hbar k_0 b_0=\hbar k_f b_f \quad (20)$$

and

$$k_f^2\leq k_a^2\leq k_0^2. \quad (21)$$

If the potential V_e^0 is of sufficiently short range, the orbit will in fact pass through the locus of the turning points $\mathbf{r}_a$ of all orbits a satisfying the conditions (20) and (21). This situation is illustrated in Fig. 1.

The orbit $0\mathbf{r}_0\mathbf{r}_a\mathbf{r}_f f$ shown in Fig. 1 is the classical one, $\mathbf{x}_{0f}$. We consider our particle C as moving along it with appropriate speed, and producing a potential $V'(\boldsymbol{\varrho},\mathbf{x}_{0f}(t))$ at the position of the molecule AB. This potential $V'=V'(\boldsymbol{\varrho},t)$ now induces transitions in the internal state of AB. Explicitly, in the classical limit for the expression (4) the potential inducing transitions in AB is

$$V'(\rho,\mathbf{x}_{0f})=\int d^3\mathbf{r}\delta(\mathbf{r}-\mathbf{x}_{0f})V'(\boldsymbol{\varrho},\mathbf{r}), \quad (22)$$

where the particle C runs through the orbit $\mathbf{x}_{0f}$ with known speed, so that $V'(\boldsymbol{\varrho},\mathbf{x}_{0f})$ represents a function of

[18] If J quanta of angular momentum (molecular rotation) are excited, we have

$$\hbar k_0 b_0-\hbar k_f b_f=\hbar J$$

instead of (19), but this does not change the method fundamentally.

ϱ and of the time t, but not of any dynamical variable of the relative motion.

In the present, quasi-classical case we may still speak of an orbit, but it is now blurred rather than sharp as in the classical case just discussed. We specify our set of states precisely as in the classical case, except that now we cannot give a sharp value for the impact parameter b_j, but can only specify it to within the quantum uncertainty:

$$\delta b_j \sim \lambda\!\!\!^{-}_j = 1/k_j \quad (j=0,a,f). \tag{23}$$

We shall discuss wave functions which follow the classical orbits but have the quantum width δb_j. These functions will be determined by the *WKB* method, as outlined in the next section.

When a particle moves in a short-range potential V_e^0, its orbit can be split up into the asymptotic portions $0\mathbf{r}_0$ and $\mathbf{r}_f f$ beyond the turning points of the initial and final orbits, and into the region $\mathbf{r}_0\mathbf{r}_a\mathbf{r}_f$ between these turning points (see Fig. 1). It is the latter region between the turning points that is important in the present case, on account of the short range of the perturbation potential V'.

The turning points of the orbits are readily characterized by the classical distances of closest approach, r_j. These are the appropriate solutions of[19]

$$E_j(1-b_j^2/r_j^2)-V_e^0(r_j)=0. \tag{24}$$

At the distance of closest approach the momentum $\hbar k_j$ is diminished to a value $\hbar q_j(r_j)$ given by

$$q_j(r_j)=k_j b_j/r_j. \tag{25}$$

It should be noted here that for a quantum-mechanical orbit characterized by k_j, b_j, r_j, the actual particle density $|\chi_j|^2$ has its maximum not at the point $\mathbf{r}_j$, but at a point $r_j'=r_j+\lambda\!\!\!^{-}_j$ in distance from the molecule AB.[20] Accordingly, in evaluating matrix elements, the perturbation potential and the effective wave numbers will be evaluated at this point $\mathbf{r}_j'$ rather than at $\mathbf{r}_j$.

VI. APPLICATION OF THE WKB METHOD[21]

A simple and convenient expression for the translational wave function $\chi_j(\mathbf{r})$ is given by the WKB solution of the wave equation (18), namely

$$\chi_j(\mathbf{r})=A_j(\mathbf{r})\exp\{iS_j(\mathbf{r})/\hbar\}, \tag{26}$$

where $S_j(\mathbf{r})$ satisfies the Hamilton-Jacobi equation corresponding to (18), namely

$$(\mathrm{grad}S_j)^2+2M_eV_e^0(\mathbf{r})=\hbar^2k_j^2, \tag{27}$$

and $|A_j|^2$ satisfies the equation of conservation of particle flux:

$$\mathrm{div}[\{\hbar\mathbf{q}_j(\mathbf{r})/M_e\}|A_j|^2]=0, \tag{28}$$

where $\mathbf{q}_j(\mathbf{r})$ is the effective wave number defined in Eq. (29) below.

We can always make an ansatz of the form (26) for the wave function. If we then make asymptotic expansions of S_j and A_j in powers of $\hbar$ or $1/k_j$ or $1/M_e$, the leading terms for S_j and A_j are given respectively by (27) and (28).

The action function $S_j(\mathbf{r})$ is given by an expression of the form

$$S_j(\mathbf{r})=\int d\mathbf{r}\cdot\mathbf{q}_j(\mathbf{r}), \tag{29}$$

where

$$q_j(\mathbf{r})^2=k_j^2-(2M_e/\hbar^2)V_e^0(\mathbf{r}). \tag{30}$$

We choose the density function $A_j(\mathbf{r})$ to satisfy the following conditions:

(i) $\chi_j(\mathbf{r})$ shall follow the classical orbit, but with the quantum width $\delta b_j \simeq 1/k_j$. For simplicity we shall assume that χ_j has a rectangular profile as a function of b_j.

(ii) $\chi_j(\mathbf{r})$ shall be normalized per unit energy range, and also with respect to impact parameter (i.e., angular momentum).

A detailed discussion of the normalization is given elsewhere[22]; here we merely quote the result:

$$|A_j(\mathbf{r})|^2=\begin{cases} M_e/\{\hbar^2\pi q_j(\mathbf{r})4\pi b_j\delta b_j\} & \text{along the classical orbit } (b_j\pm\tfrac{1}{2}\delta b_j) \\ 0 & \text{off the orbit.}\end{cases} \tag{31}$$

VII. PERTURBATION MATRIX ELEMENTS

Consider the internal (vibrational) state of the molecule AB. In a collision this is perturbed by a potential arising from the passage of the third particle C. In particular, the actual perturbation potential $V_{0f}'(\varrho)$ acting on the ϱ coordinate is

$$V_{0f}'(\rho)=\int d^3\mathbf{r}V'(\rho,\mathbf{r})\begin{cases}\delta(\mathbf{r}-\mathbf{x}_{0f}) & \text{classical case, } C\text{: expression (4)}\gg 1 \\ \chi_f^*\chi_0 & \text{quantum case } Q\text{: expression (4)}\ll 1\end{cases} \tag{32}$$

[19] The physical meaning of Eq. (24) is that the point of closest approach is characterized by the condition that the potential energy, increasing with decreasing separation r, has diminished the total kinetic energy until its net value, $E_j-V_e^0(r)$, is just balanced by the energy arising from the rotational motion connected with the angular momentum $\hbar l=\hbar k_j b_j$, namely $\hbar^2 l(l+1)/2M_e r^2$, or $\hbar^2 k_j^2 b_j^2/2M_e r^2$.

[20] This is due to the behavior of the wave function near a turning point. For one-dimensional examples, see reference 5 (first paper), Sec. VI (a), or reference 6, Fig. 3.

[21] The idea of using the WKB method in impact parameter formulation for three-dimensional problems was suggested to me by Professor J. B. Keller, cf. T. Takabayasi, Progr. Theoret. Phys. (Japan) 8, 143 (1952).

[22] E. Bauer, Research Report CX-17, Division of Electromagnetic Research, Institute of Mathematical Sciences, New York University (1954).

$\mathbf{x}_{0f}$ is the classical particle orbit, here interpreted as a function of time alone. In the present case we know that the actual orbit follows the classical orbit $\mathbf{x}_{0f}$, but has the quantum width λ. In view of the form of the wave function χ $(=A\exp\{iS/\hbar\})$, we shall take for the total matrix element,

$$(f|V'|0)=\int d^3\varrho\phi_f^*\phi_0 V_{0f}'(\varrho), \tag{33}$$

the expression

$$(f|V'|0)=\int\int d^3\varrho d^3\mathbf{r}\phi_f^*\phi_0 V'(\varrho,\mathbf{r})A_f^*(\mathbf{r})A_0(\mathbf{r})\begin{cases}1 & \text{case } C\\ \exp\{i(S_0-S_f/\hbar\}, & \text{case } Q\end{cases}. \tag{34}$$

The present calculations have been carried out for both the cases C and Q, i.e. for $\delta pR/\hbar$ both very much greater, and very much less, than unity.

We may simplify Eq. (34):

(i) From the discussion of Sec. V we know that the volume integration over $d^3\mathbf{r}$ may be reduced to a line integration over $d\mathbf{x}_{0f}$, evaluated with the appropriate width $\delta b_j\simeq\lambda_j$. This is the fundamental simplification of the present method: it may perhaps be compared in some very rough way with the fact that the expression for $\sin\delta_l$ given by the standard "method of phases"[23] is in the form of a single integral. In addition to this basic simplification there are several of a more technical nature, arising from the character of the phase S_j of the wave function.

(ii) On account of the short range of the potential V', the line integration over $d\mathbf{x}_{0f}$ does not have to be taken over the whole orbit, but only over a finite and rather short portion near the turning points. In particular, we shall take the integral only over the nonasymptotic portion of the orbit, which is roughly the region $\mathbf{r}_0\mathbf{r}_a\mathbf{r}_f$ of Fig. 1. The line element in this "effective region of interaction is denoted by $d\mathbf{x}$, and because the whole region is relatively short, we shall replace the expression (29) for S_j by the simpler form

$$S_j(\mathbf{x})=\mathbf{q}_j(\mathbf{x})\cdot\mathbf{x}. \tag{35}$$

We shall make yet a further simplification here, and write

$$\{S_0(\mathbf{x})-S_f(\mathbf{x})\}/\hbar=\{\mathbf{q}_0(\mathbf{r}_0')-\mathbf{q}_f(\mathbf{r}_f')\}\cdot\mathbf{x}=q_{0f}'x, \tag{36}$$

bearing in mind the discussion of Sec. V that the particle density has its maximum at a point distant $r_j'=r_j+1/k_j$ from the scattering center.

Let the length of the "effective region of interaction" be x_m. Then it turns out that the relation

$$q_{0f}'x_m\gg 2\pi \tag{37}$$

is satisfied, so that the exponential phase in the wave function makes a relatively large number of oscillations over the interaction region. On account of this one may neglect other, less rapid, variations in functional behavior inside the integral over dx, in comparison with that of $\exp\{i(S_0-S_f)/\hbar\}$. In particular:

(iii) The amplitude function $A_j(\mathbf{r})$ is not a very rapidly varying function of $\mathbf{r}$ along the orbit, and thus we may replace it by its value at the point $\mathbf{r}_j'$, namely $A_j(\mathbf{r}_j')$.

(iv) Similarly, over the effective region of interaction $V'(\mathbf{x})$ is a relatively slowly varying function, and thus we may replace the function $V'(\varrho,\mathbf{x})$ inside the $\mathbf{x}$-integral by $[V'(\varrho,\mathbf{r}_0')V'(\varrho,\mathbf{r}_f')]^{\frac{1}{2}}$ outside this integral.

Combining all these approximations, we arrive at the expression

$$(f|V'|0)=\int d^3\varrho\phi_f^*(\varrho)\phi_0(\varrho)[V'(\varrho,\mathbf{r}_0')V'(\varrho,\mathbf{r}_f')]^{\frac{1}{2}}A_f^*(\mathbf{r}_f')A_0(\mathbf{r}_0')2\pi(b_0\delta b_0 b_f\delta b_f)^{\frac{1}{2}}\begin{cases}x_m, & \text{case } C\\ (2/q_{0f}')\sin(q_{0f}'x_m/2), & \text{case } Q\end{cases} \tag{38}$$

which may be simplified further by using the expression (31) for $A_j(\mathbf{r})$, and (14) for $V'(\varrho,\mathbf{r})$.

VIII. THE TOTAL CROSS SECTION

Equation (38) gives the transition matrix element $(f|V'|0)$ for given wave numbers k_0, k_f as a function of the impact parameter. The formulation is of course inherently symmetrical in b_0 and in b_f, but for definiteness we write everything in terms of b_f, which is related to b_0 by Eq. (19). The total cross section is then given by the expression

$$\sigma_{0f}''=\int_0^\infty 2\pi b_f db_f|(f|V'|0)|^2, \tag{39}$$

where $(f|V'|0)$ is taken as a function of b_f.

It is clear that (39) is to be considered as an approximation to the function

$$\sigma_{0f}'=\sum_{l=0}^{\infty}\frac{4\pi}{k_0k_f}(2l+1)|(f|V'|0)|^2, \tag{40}$$

[23] See reference 1, Chapters II, VI. It should be noted that the method of phases as such only exists for the case of elastic scattering.

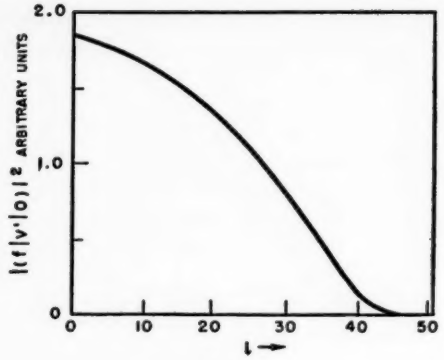

(a)

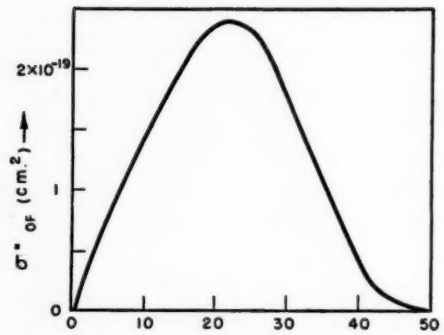

(b)

FIG. 2. Dependence of the partial cross section on the angular momentum $l=kb$: Q-approximation, $E_0=40\times10^{-3}\ e^2/a_0$. (a) The square of the transition matrix element, $|(f|V'|0)|^2$, expressed in arbitrary units, as a function of l. (b) The partial cross section $\sigma_{0f}''(l)$ as a function of l.

where now $(f|V'|0)$ is the conventional transition matrix element, regarded as a function of l. One would expect the replacement of (40) by (39) to be satisfactory for $l\gg1$, where the relative step size $\delta l/l$ is small; in the present case the most important contribution to σ_{0f} comes from relatively large l (see Table II, Fig. 2) so that one may safely use (39) instead of (40).[24]

[24] Detailed comparisons of the partial cross sections $\sigma_{0f}'(l)$ and $\sigma_{0f}''(l)$ have been made for a number of values of l and of the energy, and the orders of magnitude of the results of the two methods are in good agreement. The actual calculation of the partial cross sections $\sigma_{0f}'(l)$ shows clearly the usefulness of the present method of calculation, as the evaluation of any one $\sigma_{0f}'(l)$ requires about as much time as does the total cross section σ_{0f}''. For a typical energy value one has to consider some 60 phases, so that the present method cuts down the work by a factor of the order ten over the conventional method.

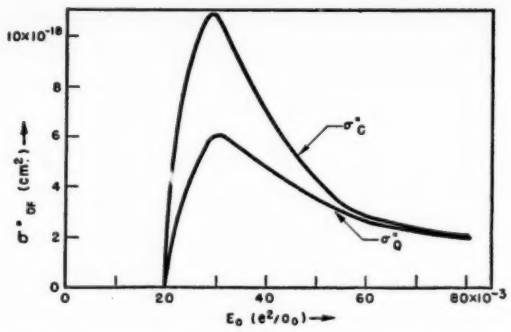

FIG. 3. The total cross section σ_{0f}'' as a function of energy, in the C- and Q-approximations.

The results for σ_{0f}'' as a function of energy in the C- and Q-limits of expression (4) are listed in Table I, and shown in Fig. 3. The character of the results is reasonable in both the energy dependence and the general order of magnitude: it is well known empirically[3] that the cross section for excitation of the vibration is rather small. It is clear that one would expect the C-results to be greater than the Q-results. Superficially it seems strange that the C- and Q-results differ most at the lowest energies, but this feature can be understood by recalling that a measure of the difference between the C- and Q-results is given by k_0-k_f, which of course decreases with increasing energy.

A more detailed discussion of some features of the present method, and its relation to previous calculations, is given elsewhere.[22] The aim of the present work is essentially the presentation of a method of calculation which is free from some of the objections that can be raised against the previous, essentially one-dimensional calculations.[4–6] The approximations made here are largely of a kind whose effect can be calculated explicitly, and it should be possible to use the present method to recalculate the cross sections for a number of related processes.

I should like to thank Dr. A. B. Bhatia, Professor J. B. Keller, and Dr. Ta-You Wu for numerous discussions.

Note added in proof.—The numerical values of the cross section $\sigma_{0f}''(l)$ in Fig. 2(b), and σ_{0f}'' in Fig. 3, are too large by a factor 16. The values given in Table I are correct.

Resistance in a Liquid-Liquid Interface. III. The Effect of Molecular Properties*

J. H. SINFELT AND H. G. DRICKAMER
Department of Chemistry and Chemical Engineering, University of Illinois, Urbana, Illinois
(Received October 20, 1954)

The diffusion of molecular sulfur across a saturated liquid-liquid interface has been investigated for several molecular pairs, using a method previously described. The interfacial resistance does not directly depend on polarity of the liquids, nor can it be correlated with interfacial tension. High resistances are associated with liquids which show a high degree of hydrogen bonding. With suitable assumptions it is possible to calculate a free energy of activation for transfer across the interface. It appears that transfer in systems involving negligible resistance is analogous to van der Waals adsorption, while for systems involving high resistance the process is comparable to chemisorption.

THE effect of an interface between phases on molecular motion is a problem of both theoretical and practical importance. So far, although indications of resistance to mass transfer through the interface have been found under several circumstances,[1–4] it has not been possible to establish just what conditions produce this resistance. In this investigation the effect of several molecular properties on interfacial resistance was studied. Specifically, variations in polarity, in interfacial tension, and in degree of hydrogen bonding were introduced.

In all cases binary mixtures of partially miscible liquids were employed, and the rate of transfer of sulfur between the layers was measured.

The experimental method employed was essentially identical to that described previously,[2] but the principle will be outlined here. A mixture of two liquid components containing also the sulfur was shaken thoroughly and equilibrated in a temperature bath. After at least twenty-four hours the layers were separated. A similar mixture containing radioactive sulfur was treated in the same manner. The two hydrocarbon rich layers were contacted in the diffusion apparatus and the concentration of radioactive sulfur at one end was measured as a function of time by means of a scintillation counter utilizing a cadmium tungstate crystal. The experiment was repeated for the other layer, and then for the system involving the interface. The method of calculating the diffusion coefficients was described in previous publications.[1,2,5] The results are expressed in terms of D_1 and D_2 for the two layers, D(apparent) for the interfacial system, and an interfacial transfer coefficient α which is defined by the equation

$$\mathbf{J}=\alpha[C(0^-,t)-mC(0^+,t)] \qquad (1)$$

where $\mathbf{J}$ is net flux of molecules across unit area of interface, $C(0^-,t)$, $C(0^+,t)$ are concentrations on either side of the interface at time t, and m is equilibrium distribution of sulfur. Furthermore α has the dimension of a velocity and is clearly infinite for the case of no resistance in the interface. Actually the values of α which were numerically larger than a few hundred times the average value of D for the two layers gave no resistance distinguishable in our experiments.

The systems studied are listed in Table I. The components of the aniline-methylcyclohexane solutions were mixed in such a proportion that the resulting mixture had the same composition as that corresponding to the critical solution temperature. The composition at the critical solution temperature is 47 weight percent aniline. For the other systems the compositions corresponding to the critical solution temperature were not known. The nitrobenzene and normal heptane were mixed in a 50-50 ratio by weight, while the components of the other systems were mixed in a 50-50 ratio by volume, since the critical solution temperature usually corresponds to a composition not far from 0.50 volume fraction.

Since methylcyclohexane is less dense than aniline, the interfacial runs for this system were made with the methylcyclohexane rich layer containing radioactive sulfur as the upper cell, and the aniline rich layer containing only nonradioactive sulfur as the lower cell. For the other systems the *n*-heptane rich layer was always the upper cell in interfacial runs. The tagged component was usually in the upper half of the cell initially. Two runs were made on formic acid-heptane with the tagged sulfur initially below. The results did

TABLE I.

System	Critical solution temperature °C
1. aniline-methylcyclohexane	40.9
2. nitrobenzene-*n*-heptane	20.0
3. nitromethane-*n*-heptane	70.0
4. aniline-*n*-heptane	115
5. phenol-*n*-heptane	52.9
6. formic acid-*n*-heptane	185

* This work was supported in part by the U. S. Atomic Energy Commission.

[1] Scott, Tung, and Drickamer, J. Chem. Phys. **19**, 1075 (1951).
[2] L. H. Tung and H. G. Drickamer, J. Chem. Phys. **20**, 10, 13 (1952).
[3] J. T. Davies, J. Phys. and Colloid Chem. **54**, 185 (1950).
[4] R. E. Emmert and R. L. Pigford, Chem. Eng. Progr. **50**, 87 (1954).
[5] K. D. Timmerhaus and H. G. Drickamer, J. Chem Phys. **19**, 1242 (1951).

TABLE II.

Temperature °C	$D_1 \times 10^6$ cm²/sec	$D_2 \times 10^6$ cm²/sec	$D_a \times 10^6$ cm²/sec	m	$\alpha \times 10^6$ cm/sec
		Aniline-methylcyclohexane			
0.0	4.35	0.795	0.714	0.637	13.2
16.5	5.60	2.40	2.32	0.890	60.5
37.3	12.9	6.85	4.24	0.935	65.5
		Nitrobenzene-*n*-heptane			
0.0	7.17	3.66	3.61	0.506	112
16.5	7.55	6.90	6.53	0.750	529
		Aniline-*n*-heptane			
17.3	6.50	1.27	1.01	0.360	18.5
32.2	7.26	3.05	2.68	0.426	64.0
		Nitromethane-*n*-heptane			
17.7	10.9	4.16	4.20	4.16	125
		Phenol-*n*-heptane			
40.6	21.0	2.93	1.87	0.86	25.8
		Formic acid-*n*-heptane			
17.3	6.83	0.927	0.364	20.8	0.442

not differ from the above but the runs were somewhat erratic and a small effect could have been present.

The radioactive S^{35} was obtained from the Oak Ridge National Laboratory in the form of a benzene solution. The purity of the radioactive sulfur was greater than 99.5 percent. The S^{35} was obtained by evaporating the benzene. The *n*-heptane was pure grade (99 mole percent minimum), as produced by the Phillips Petroleum Company. The phenol was reagent grade and was obtained from Merck and Company. The melting point of the phenol was 42°C. The formic acid was C.P. grade (98–100 percent), as produced by the General Chemical Division of the Allied Chemical and Dye Corporation. The methylcyclohexane, aniline, nitrobenzene, and nitromethane were obtained from the University of Illinois Chemical Stores and were redistilled with a Vigreux column. In each case approximately the middle third of the distillate was collected and used in the experiments. The observed boiling points were 99°C for the methylcyclohexane, 182°C for the aniline, 210°C for the nitrobenzene, and 100°C for the nitromethane.

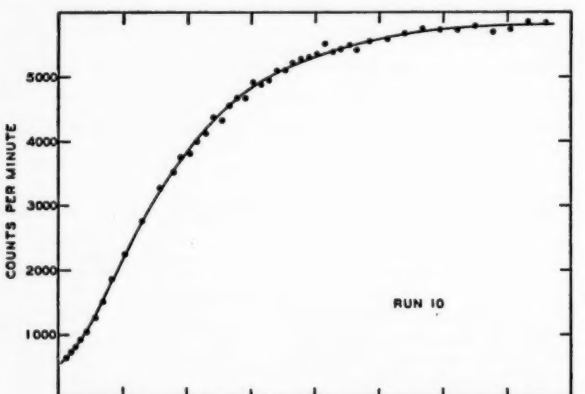

FIG. 1. Counts per minute *versus* time, typical run.

An interfacial active agent was used with the formic acid-*n*-heptane system and with the nitromethane-*n*-heptane system to reduce the interfacial tension and to determine the effect on the interfacial resistance. The agent used was polyoxethylene sorbitan monolaurate, also known by the trade name of Tween 20. It was furnished by the Atlas Powder Company.

The experimental results are shown in Table II. The diffusion coefficients are reproducible within 3–4 percent. The accuracy of α is harder to estimate. For high resistances it is reproducible within 5 percent. For low resistances it is less accurate, but our discussion hinges on its magnitude and not its exact value. In each case D_1 is the diffusion coefficient in the hydrocarbon rich layer, and D_2 is for the other layer while D_a is the apparent diffusion coefficient for the interfacial runs. The values of D_1, D_2, and D_a are the average values of two or more runs. The distribution coefficient

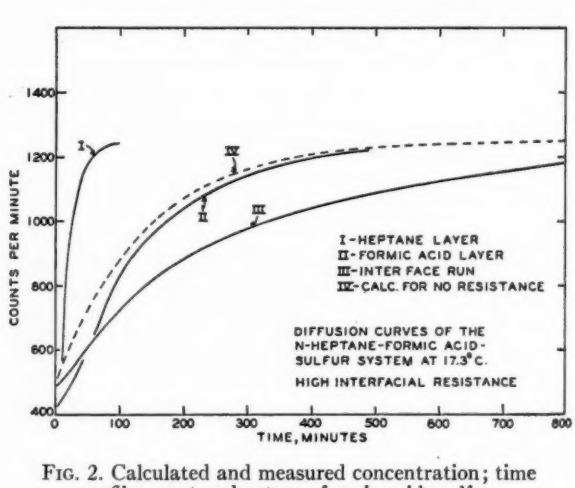

FIG. 2. Calculated and measured concentration; time profiles; system heptane; formic acid; sulfur.

m is the ratio of the sulfur concentration in cell 1 to that in cell 2 at equilibrium. It was measured by counting the radioactivity of each of the two layers. The difference of radioactive absorption in the two layers was neglected. Thus for the aniline-methylcyclohexane system

$$m = \frac{\text{(no. of counts in MCH rich layer-background)}}{\text{(no. of counts in aniline rich layer-background)}}.$$

A typical run is shown in Fig. 1 to illustrate the technique. The existence of the resistance is strikingly illustrated in Figs. 2 and 3, the former for a system of high resistance, the latter for a system with negligible resistance.

I. THE EFFECT OF POLARITY ON INTERFACIAL RESISTANCE

All of the systems in this work contained one polar liquid. The nonpolar liquid in five of the systems is

n-heptane. For the methylcyclohexane-aniline system the methylcyclohexane is essentially nonpolar, since the dipole moment of the methyl group is very small. Table III lists the systems and the corresponding values of the interfacial transfer coefficient α. For each system the dipole moment of the polar component is also listed. The dipole moments were taken from LeFevre.[6] From Table III it is apparent that high-interfacial resistance does not necessarily correspond to high values of the dipole moment. Here the systems showing the least interfacial resistance were actually the most polar. The formic acid-*n*-heptane system has the highest interfacial resistance, but the dipole moment of the formic acid is only 1.2 debye units.

II. THE EFFECT OF INTERFACIAL TENSION

Values of the interfacial tension γ are listed in Table IV for several of the systems, with and without interfacial agents present. The values of α, the interfacial transfer coefficient, are also listed. The interfacial tensions were determined by a drop weight method. Table IV indicates that interfacial resistance cannot be explained on the basis of interfacial tension alone. The formic acid-*n*-heptane system had the highest interfacial tension and the highest interfacial resistance, but the nitromethane-*n*-heptane system, with an intermediate value of the interfacial tension, had the lowest interfacial resistance. When the interfacial agent (Tween 20) was added to the formic acid-*n*-heptane system, the interfacial tension was practically cut in half, but there was no change in the interfacial transfer coefficient α. The interfacial agent was added to the *n*-heptane-nitromethane system to determine whether the agent might actually increase the interfacial resistance of a system which had a comparatively small resistance. Again the interfacial agent had no effect on the interfacial diffusion rate. These results cast considerable doubt on the explanation that the large organic molecules of a wetting agent hinder the molecules from crossing the interface. The observed effects of wetting agents in reducing mass transfer rates in wetted-wall columns and other mass transfer equipment are probably the result of the elimination of rippling and other hydrodynamic effects. The recent data of Emmert and Pigford[4] support the latter statement.

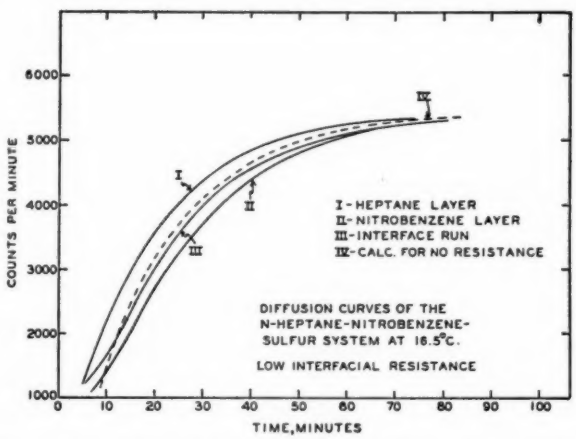
COUNTS PER MINUTE
TIME, MINUTES
I - HEPTANE LAYER
II - NITROBENZENE LAYER
III - INTERFACE RUN
IV - CALC. FOR NO RESISTANCE
DIFFUSION CURVES OF THE N-HEPTANE-NITROBENZENE-SULFUR SYSTEM AT 16.5°C.
LOW INTERFACIAL RESISTANCE

FIG. 3. Calculated and measured concentration; time profiles; system; heptane-nitrobenzene; sulfur.

TABLE III. Dipole moments and interfacial transfer coefficients.

System	Temperature °C	Dipole moment debye units	$\alpha \times 10^6$ cm/sec
1. nC_7–nitrobenzene	16.5	4.23	529
2. nC_7–nitromethane	17.7	3.0	125
3. nC_7–phenol	40.6	1.7	25.8
4. nC_7–aniline	17.3	1.55	18.5
5. nC_7–formic acid	17.3	1.2	0.44
6. MCH–aniline	16.5	1.55	60.5

III. THE EFFECT OF HYDROGEN BONDING

It has been shown that the dipole moments do not give an explanation of interfacial resistance. However, the systems which showed the high interfacial resistances all had a component which was capable of forming hydrogen bonds. Table V lists the systems in the order of increasing hydrogen bonding, and gives the corresponding values of the interfacial transfer coefficient. In the absence of any exact quantitative measure of hydrogen bonding, the solubilities in water, which is strongly hydrogen bonding, illustrate the relative extents of this effect. The solubility data listed in Table VI are taken from Hildebrand.[7] Tables V and VI show that the interfacial resistance increases as the extent of hydrogen bonding increases. The *n*-heptane-phenol system seems to be slightly out of order, since its interfacial transfer coefficient is larger than the interfacial transfer coefficient of the *n*-heptane-aniline system. However, the *n*-heptane-phenol measurements were made at a higher temperature, since phenol forms a solid phase at the lower temperatures. The decrease in α with lowering of temperature would easily remove the slight discrepancy from Table V.

The dipole moment itself is not a complete measure of orientation. Molecules which hydrogen bond exhibit

TABLE IV. Interfacial tensions and interfacial transfer coefficients.

System	Temperature °C	γ dynes/cm	$\alpha \times 10^6$ cm/sec
1. nC_7–aniline	17.3	2.7	18.5
2. nC_7–nitromethane	17.7	7.0	125
nC_7–nitromethane +Tween 20	17.7	4.5	125
3. nC_7–formic acid	17.3	12.2	0.44
nC_7–formic acid +Tween 20	17.3	6.6	0.44

[6] R. J. W. LeFevre, *Dipole Moments* (Methuen and Company, Ltd., London, England, 1948), second edition.

[7] J. H. Hildebrand and R. L. Scott, *Solubility of Non-Electrolytes* (Reinhold Publishing Corporation, New York, 1950).

TABLE V. Hydrogen bonding and interfacial resistance.

System	Temperature °C	$\alpha \times 10^8$ cm/sec
1. nC_7–nitrobenzene[a]	16.5	529
2. nC_7–nitromethane[a]	17.7	125
3. nC_7–aniline	17.3	18.5
4. nC_7–phenol	40.6	25.8
5. nC_7–formic acid	17.3	0.44

[a] No hydrogen bonding.

TABLE VI. Solubility in water at 20°C.

Compound	Solubility, mole percent
Nitrobenzene	0.028
Aniline	0.70
Phenol	1.7
Formic acid	completely miscible

a high degree of hindered relative molecular rotation. This hindered molecular rotation would be very significant at an interface, and the strong orientation would lead to interfacial resistance to diffusion, since only those diffusing molecules with certain preferred orientations would not be retarded at the interface. Oster and Kirkwood[8] explain that hydrogen bonding molecules show greater hindered molecular rotation because the charge distribution is exposed, so that neighboring molecules can assume relative configurations in which there is very strong interaction. Molecules like nitrobenzene have a shielded charge distribution, and the intermolecular repulsive forces prevent significant orientation.

IV. THE ENERGY BARRIER AT THE INTERFACE

The diffusion of molecules across an interface may be visualized as a process involving an intermediate activated state. Of the molecules striking the interface, only those with sufficient energy to surmount the energy barrier will penetrate the interface. By means of the theory of absolute reaction rates, a treatment of diffusion in solutions has been developed.[9] According to this theory, the diffusion coefficient is given by

$$D=l^2\frac{kT}{h}\exp\left(-\frac{\Delta F^{\ddagger}}{RT}\right) \qquad (2)$$

where l is the distance between equilibrium positions in the liquid, kT/h is a frequency factor, and $\Delta F^{\ddagger}$ is the magnitude of the free-energy barrier for diffusion. By an analogous treatment the interfacial transfer coefficient α is given by

$$\alpha=l\frac{kT}{h}\exp\left(-\frac{\Delta F^{\ddagger}}{RT}\right). \qquad (3)$$

[8] G. Oster and J. G. Kirkwood, J. Chem. Phys. **11**, 175 (1943).
[9] Glasstone, Laidler, and Eyring, *Theory of Rate Process* (McGraw-Hill Book Company, Inc., New York, 1941).

Here the exponential factor represents the probability that a molecule striking the interface will possess sufficient free energy to surmount the energy barrier. Equation (3) breaks down in the limiting case of no interfacial resistance ($\alpha\rightarrow\infty$). [It may also be that Eq. (1) is a poor defining equation at low resistance.] For this case $\Delta F^{\ddagger}$ is zero, and Eq. (3) gives a finite value for α, which, however, is 10^8 to 10^{10} times as large as the diffusion coefficient D. Thus Eq. (3) [or (1)] is not valid for extremely small resistances.

The free energy of activation for diffusion across the interface may be associated with the energy of adsorption. The molecules in one of the phases must surmount an energy barrier to be adsorbed on the surface of the other phase. The process is similar to adsorption on the surface of a solid. In the case of liquids with no hydrogen bonding the process is like van der Waals adsorption, i.e., a physical transfer. For associated liquids the process approaches chemisorption.

The value of the free energy of activation can be calculated from Eq. (3) if l is approximated by $(V/N)^{\frac{1}{3}}$ where V is the molal volume (average for the system) and N is Avogadro's number. From the table of values of $\Delta F^{\ddagger}$ (Table VII), it can be seen that the free-energy barrier to diffusion through the interface is large. The $\Delta F^{\ddagger}$ values for ordinary diffusion in a single phase are much lower. Consider the *n*-heptane-nitrobenzene system as an example. The free energy of activation for diffusion in the *n*-heptane rich layer, is 4640 calories per mole. This is considerably below the value of 11 720 calories per mole for diffusion across the *n*-heptane-nitrobenzene interface. And it must be remembered that the *n*-heptane-nitrobenzene system had the smallest interfacial resistance of any of the systems studied. The effect is thus even more striking for systems with large interfacial resistance. These high values of $\Delta F^{\ddagger}$ for interfacial diffusion indicate that only an extremely small fraction of the molecules striking the interface are able to cross it.

The values of $\Delta F^{\ddagger}$ calculated from Eq. (3) are only approximate, but they are useful in comparing one system with another. From the results in Table VII it is apparent that the free-energy barrier at the interface must be quite large before a diffusional resistance

TABLE VII. $\Delta F^{\ddagger}$ for interfacial diffusion of S^{35}.

System	Temperature °C	$\Delta F^{\ddagger}$ cal/mole
1. nC_7–nitrobenzene	0.0	11 880
	16.5	11 720
2. nC_7–nitromethane	17.7	12 620
3. nC_7–aniline	17.3	13 710
	32.2	13 690
4. nC_7–phenol	40.6	14 650
5. nC_7–formic acid	17.3	15 920
6. MCH–aniline	0.0	13 000
	16.5	12 900
	37.3	13 880

at an interface can even be detected. The $\Delta F^{\ddagger}$ values for interfacial diffusion increase as the extent of hydrogen bonding increases, and again it is apparent that the interfacial resistance is high for systems which show considerable hydrogen bonding.

Interfacial diffusion involves adsorption of diffusing molecules from one phase onto the surface of the other phase. For the systems with low interfacial resistance the adsorption is of the van der Waals type, whereas for systems with high interfacial resistance the adsorption is probably similar to chemisorption, and occurs at a finite rate.

The effect of temperature on interfacial resistance was studied for several of the systems, and in each case the resistance decreased with temperature. The variation of $\Delta F^{\ddagger}$ with temperature seems to be small.

The authors wish to acknowledge the assistance and advice of Dr. Lu Ho Tung.

THE JOURNAL OF CHEMICAL PHYSICS VOLUME 23, NUMBER 6 JUNE, 1955

One-Dimensional Model of the Hydrogen Bond

ELLIS R. LIPPINCOTT AND RUDOLPH SCHROEDER
Department of Chemistry, Kansas State College, Manhattan, Kansas
(Received October 11, 1954)

A one-dimensional model for hydrogen bonding is proposed based on the potential function $V=D[1-\exp(-n\Delta r^2/2r)]$. The energy associated with both the weak and strong bonds of the configuration $RO-H---OR_2$ is obtained through application of this function. A repulsive Van der Waals potential and an attractive electrostatic potential are also assumed to exist between the two electronegative atoms of the hydrogen bond. Through application of the conditions describing a stable equilibrium, relations are obtained which permit a calculation of OH frequency shifts, OH bonded distances, hydrogen bond energies and k_{O---O} force constants, all as a function of the O---O distance R. The calculated quantities agree well with those obtained from neutron diffraction, infrared, and other experimental studies. Because of the assumptions involved, this model is best used to describe the properties of hydrogen bonds in crystals. The model is also capable of extention to describe the properties of other types of hydrogen bonds such as HFH, NHN, NHO, OHN, etc.

INTRODUCTION

THERE is no complete agreement as to the nature of the hydrogen bond. A large number of investigators favor an electrostatic model while others favor a quantum-mechanical explanation. However, no theory has explained quantitatively the main features of hydrogen bonding.[1] Any adequate model should quantitatively describe such features as the OH frequency shift, hydrogen bond energy, bonded OH distance, and the like.

Recently Rundle and Parasol[2] and Lord and Merrifield[3] have published results of infrared studies on strong hydrogen bonds in crystals. Both groups were able to demonstrate experimentally a definite relationship between OH frequency shift and O---O distance. Their data are quite significant in that from them a check may readily be made of any proposed theory of the hydrogen bond.

The success with which a number of bond properties in both diatomic and polyatomic molecules have been correlated and predicted by means of a potential function recently presented by one of us has led us to attempt to formulate a one-dimensional model of the hydrogen bond based on the same potential function.[4]

Cross, Burnham, and Leighton[5] have previously used a potential function to describe a number of properties associated with hydrogen bonding in ice and water, but did not extend it to other types of O—H---O hydrogen bonding. Our proposed model is different from theirs in that a function has been used which describes bond properties more accurately than the Morse function, that a Van der Waals repulsion term between the oxygen atoms has been introduced in a different manner and that an electrostatic attraction term is used.

A MODEL BASED ON A POTENTIAL FUNCTION

For a model we propose to use the potential function

$$V=D[1-\exp(-n\Delta r^2/2r)] \qquad (1)$$

where D=bond dissociation energy, $\Delta r=r-r_0$, and $n=k_0r_0/D$. In the above form the function is applicable to bonds in diatomic and polyatomic molecules and should form a basis for a model of hydrogen bonding provided that it can be modified suitably.

To make the problem tractable we make the following assumptions, which are illustrated in Fig. 1 for OH---O bonding.

[1] Several reviews on hydrogen bonding have been published. M. Davies, Chem. Soc. Ann. Repts. **43**, 1 (1946); L. Hunter, *ibid.* **43**, 141 (1946); L. Kellner, Repts. Progr. in Phys. **15**, 1 (1952).
[2] R. E. Rundle and M. Parasol, J. Chem. Phys. **20**, 1487 (1952).
[3] R. C. Lord and R. E. Merrifield, J. Chem. Phys. **21**, 166 (1953).
[4] E. R. Lippincott, J. Chem. Phys. **21**, 2070 (1953).
[5] Cross, Burnham, and Leighton, J. Am. Chem. Soc. **59**, 1134 (1937).

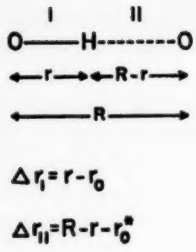

FIG. 1. The asterisk will be used to identify the properties of bond II, if it were an unperturbed OH bond.

(a) The hydrogen atom is located along the line of centers between the two electronegative atoms making up the bond. (b) Bond I is equivalent to a slightly stretched typical covalent bond, the amount of stretching being $r-r_0$. (c) Bond II is a weak bond which is equivalent to a highly stretched bond, the amount of stretching being $R-r-r_0^*$. (d) There is a Van der Waals repulsion between the two oxygen atoms, which may be described by an exponential potential. (e) There is an electrostatic potential between the two oxygen atoms which may be represented as $-B/R^m$. (f) The potential energy of stretching in both bonds may be obtained through application of the simple potential function (1).

Because of these assumptions our model will better approximate a hydrogen bond in the crystalline state than one in the liquid or vapor state; therefore any comparison with experimental data will be based on studies of the hydrogen bond in crystals. This model should be more applicable to hydrogen bond dimers than polymers.

The potential energy for this model consists of the sum of four terms

$$V=V_1+V_2+V_3(\text{repulsion})+V_4(\text{electrostatic}). \quad (2)$$

It is convenient to choose $V=0$ when the molecules are completely separated. From the above assumptions

$$V_1=D[1-\exp(-n\Delta r^2/2r)] \quad (3)$$

$$V_2=D^*\{1-\exp[-n^*(R-r-r_0^*)^2/2(R-r)]\}$$
$$-D^*=-D^*\{\exp[-n^*(R-r-r_0^*)^2/2(R-r)]\} \quad (4)$$

$$V_3=Ae^{-bR} \qquad V_4=-B/R^m. \quad (5)$$

Before this potential function may be applied, it is necessary to have some knowledge of the properties of bonds I and II in their unperturbed or unstretched configurations. As the potential function (1) is assumed applicable to both bonds in their unstretched configurations the following relations hold. $nD=k_0r_0$ and $n^*D^*=k_0^*r_0^*$. Since bond I is essentially a slightly stretched OH bond, the values for n, D, k_0, and r_0 may be taken from the corresponding values for the H_2O molecule. For bond II a knowledge of the quantities n^*, D^*, k_0^*, and r_0^* is not readily available. This bond is more properly considered as a highly stretched HO^+R_2 bond rather than as a highly stretched HOR bond. Because the parameter, n, is related to atomic ionization potentials of the atoms making up the bond[4] we would expect $n^*\neq n$. Furthermore, although the bond lengths associated with H$-$OR and H$-$O$^+R_2$ are not quite the same, we will assume that $r_0=r_0^*$ for lack of information. Likewise, although k_0^* is not necessarily the same as k_0 we will assume $k_0^*=k_0$ for lack of further information. These assumptions imply that $n^*D^*=nD$. Since all properties of bonds I and II in their unperturbed positions may now be evaluated except n^*, we write

$$n^*=gn \quad (6)$$

where g is chosen such that the best results are obtained. A suitable value of g is 1.45. The evaluation of g in principle requires the use of one frequency shift or one OH bond length.

Other schemes may be chosen to evaluate the properties of bond II in the unperturbed position. For example one might put n^* equal to some function of $R-r$. The scheme used here has the advantage of simplicity and makes use of only one empirically evaluated parameter. Any other method would of necessity involve at least one or more such parameters.

For motion of the nuclei along the axis of the hydrogen bond the following conditions characteristic of a stable equilibrium are applicable.

$$\left(\frac{\partial V}{\partial r}\right)_{eq}=0 \quad (7)$$

$$\left(\frac{\partial^2 V}{\partial r^2}\right)_{eq}=k_H \quad (8)$$

$$\left(\frac{\partial V}{\partial R}\right)_{eq}=0 \quad (9)$$

$$\left(\frac{\partial^2 V}{\partial R^2}\right)_{eq}=k_{O---O} \quad (10)$$

where k_H is the force constant associated with the notion of the hydrogen atom and k_{O---O} is the force constant associated with the motion of the oxygen atoms.

Before we use these conditions it will be convenient to modify the repulsion and electrostatic terms, so that they contain two constants and not three. To do this we write

$$V_3+V_4=V_0\left\{2\exp[-b(R-R_0)]-\left(\frac{R_0}{R}\right)^m\right\} \quad (11)$$

where V_0 is equal to V_3+V_4 when $R=R_0$. On comparing (11) with (5) one has

$$A=2V_0e^{+bR_0} \quad (12)$$

$$B=V_0R_0^m. \quad (13)$$

By dividing (13) by (12) one obtains B in terms of A and Eq. (5) becomes on substitution:

$$V_3+V_4=A[e^{-bR}-(\tfrac{1}{2})(R_0/R)^m e^{-bR_0}]. \quad (14)$$

The constant A may be evaluated by using the condition $(\partial V/\partial R)=0$, while b can be evaluated through the use of a known hydrogen bond energy.

It is necessary to choose a value for the exponent m in the electrostatic term. For hydrogen bond dimers, involving nonequivalent oxygen atoms, such as one has with the carboxylic acids, m may be given a value of 1 since the oxygen atoms carry fractional charges. For bonds involving equivalent oxygen atoms such as in ice, a more suitable value of m can be chosen between 3 and 6. Since the electrostatic term does not appear in the equations used to determine the O—H distance or O—H frequency shifts and gives only a minor contribution to the energy and k_{O---O} force constant, we will uniformly choose $m=1$. Although for particular cases of O—H---O hydrogen bonding a more suitable electrostatic potential may be chosen, the one used here has the advantage of simplicity. We have used a value of $m=6$ and the results are nearly as good as those with $m=1$.

THE DEPENDENCES OF r ON THE O---O DISTANCE

This elementary model is now capable of predicting a relation between the OH bond distance and the O---O distance for hydrogen bonds. From (2) and the condition that $(\partial V/\partial r)=0$, we have on solving for Δr

$$\Delta r=(\{\exp[-n^*(R-r-r_0^*)^2/2(R-r)]\}/\exp(-n\Delta r^2/2r))\times[r^2(R-r-r_0^*)(R-r+r_0^*)/(R-r)^2(r+r_0)]. \quad (15)$$

Since R_0, r_0, and n are known from experimental data and $r_0^*=r_0$ and $n^*=gn$, Eq. (15) is suitable for calculating Δr as a function of R_0 by the method successive approximations.

$$r_0=0.97\cdot10^{-8}\text{ cm}$$
$$n=k_0r_0/D=9.18\cdot10^8\text{ cm}^{-1} \quad (16)$$
$$n^*=(1.45\times n)=13.32\cdot10^8\text{ cm}^{-1}.$$

In Table I the calculated values of Δr for given values of R_0 are tabulated. A graph of r *versus* R_0 is shown in Fig. 2. Fortunately recent neutron diffraction measurements by Peterson and Levy on ice and KH_2PO_4 have been given which enable us to check these predictions.[6]

TABLE I. Calculated r and $\Delta\omega$ values.

R in A	r in A	$\Delta\omega$ in cm^{-1}
2.40	1.163	1510
2.45	1.151	1900
2.50	1.115	1785
2.55	1.079	1445
2.60	1.051	1110
2.70	1.019	680
2.80	0.998	400
2.90	0.986	240
3.00	0.980	150
3.10	0.976	90

[6] S. W. Peterson and H. A. Levy, J. Chem. Phys. **21**, 2084 (1953); Phys. Rev. **92**, 1082(A) (1953).

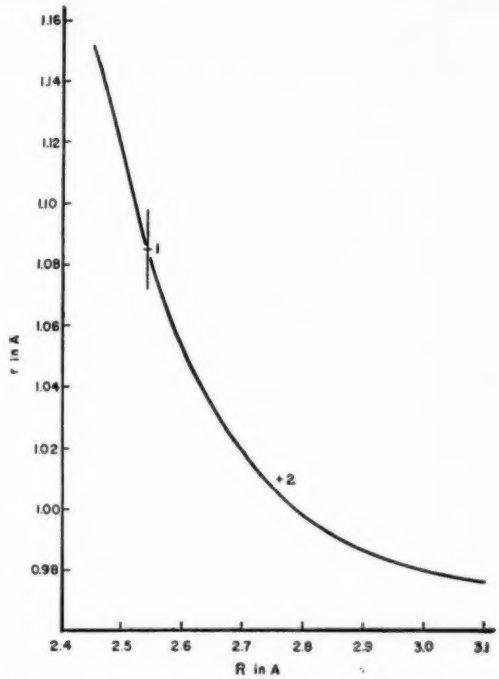

FIG. 2. O—H distance as a function of O---O distance for hydrogen bonds. 1. KH_2PO_4, 2. Ice.

The agreement between the observed and predicted results is excellent.

THE RELATIONSHIP BETWEEN OH FREQUENCY SHIFT AND O---O DISTANCE

One of the most characteristic properties of the hydrogen bond is the relatively large frequency shift associated with the OH stretching mode of vibration. Through application of Eq. (8) this OH frequency shift may be predicted as a function of R_0. By using (2) with (8) one obtains

$$k_H=(nD/r^3)[\exp(-n\Delta r^2/2r)]\times[r_0^2-(n\Delta r^2/4r)(r+r_0)^2]+[n^*D^*/(R-r)^3]\times\{\exp[-n_e^*(R-r-r_0^*)/2(R-r)]\}\times[r_0^{*2}-n^*(R-r-r_0^*)^2(R-r+r_0^*)^2/4(R-r)]. \quad (17)$$

One may apply $n^*D^*=nD$ and the condition that $nD=k_0r_0$. Since the mass of the oxygen atoms are large compared to that of the hydrogen atom it is a reasonable assumption that

$$k_0=4\pi^2\mu\omega^2c^2$$
and that (18)
$$k_H=4\pi^2\mu\omega_H^2c^2.$$

These combined with (17) give

$$\omega_H/\omega=\left\{\begin{array}{l}\{\exp[-n\Delta r^2/2r)]\}(r_0/r^3)\\ \quad\times[r_0^2-(n\Delta r^2/4r)(r+r_e)^2]\\ \quad+(r_0^*/(R-r)^3)\\ \{\exp[-n^*(R-r-r_0^*)^2/2(R-r)]\}\\ \quad\times[r_0^{*2}-n^*(R-r-r_0^*)^2\\ \quad\times(R-r+r_0^*)^2/4(R-r)]\end{array}\right\}^{\frac{1}{2}} \quad (19)$$

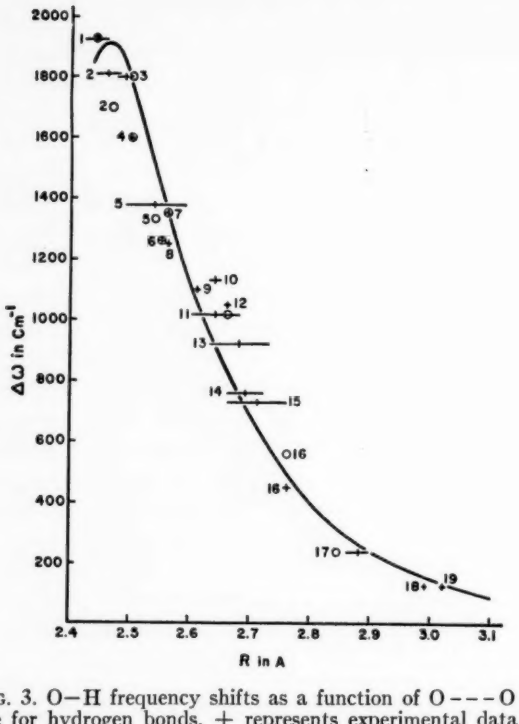

FIG. 3. O—H frequency shifts as a function of O - - - O distance for hydrogen bonds. + represents experimental data obtained from reference 3 in text. ○ represents experimental data obtained from reference 4 in text. 1. Ni-dimethylglyoxime. 2. Maleic acid. 3. Oxalic acid·$2H_2O$. 4. Ureaoxalate. 5. KH_2PO_4. 6. $NaHCO_3$. 7. *N*-acetylglycine. 8. Phloroglucinol. 9. $KHCO_3$. 10. Salicylic acid. 11. Succinic acid. 12. Resorcinol. 13. Adipic acid. 14. Pentaerythritol. 15. Diaspore. 16. Ice. 17. Oxalic acid·$2H_2O$. 18. LiOH·$2H_2O$. 19. NaOH.

From (16) and from the previous calculations of r as a function of R illustrated in Fig. 2 the information is available to calculate ω_H/ω as a function of R. The frequency of the unbonded OH stretching mode was taken as 3700 cm^{-1}. In Fig. 3 we give a plot of $\Delta\omega$ *versus* R by using Eq. (19).

Rundle and Parasol[2] as well as Lord and Merrifield[3] have published infrared studies on strong hydrogen bonds in crystals. Both groups have given plots showing the experimental dependence of frequency shift on O - - - H—O distance, as determined from x-ray diffraction studies. In Fig. 3 we have plotted their experimental points. The agreement between experimental and predicted frequency shifts is satisfactory and within the experimental error of measuring the frequency shifts. Such measurements are subject to considerable error first because of the width of the bands and second because a number of them have more than one main component.

In so far as the geometry is concerned, the maximum in the predicted curve at 2.45 A corresponds to the case of symmetrical hydrogen bonding. It thus appears that most cases of O—H - - O hydrogen bonding are asymmetrical but both oxalic acid and nickel dimethylglyoxime examples which are not far from the symmetrical case.

L. Kuhn[7] has given an experimental curve of $\Delta\omega$ as a function of H - - - O distance for weak intra- and intermolecular hydrogen bonds in alcohols. Since most of the examples given by his studies would correspond to bent bonds and because his work was done in solution, a comparison with his results cannot be readily made. The model used here assumes that the hydrogen bond is linear.

The successful prediction of the O—H distances and the OH frequency shifts as a function of R, is sufficient evidence that the proposed hydrogen bond potential function is essentially correct in its dependence on r, the bonded OH distance. We must still demonstrate that its dependence on R, the O - - - O distance is correct.

THE DEPENDENCE OF HYDROGEN BOND ENERGY ON O - - - O DISTANCE

There is a considerable amount of information available on OH - - - O hydrogen bond energies. These energies have been estimated from measurements on heats of sublimation, heats of vaporization, monomer-dimer equilibrium studies, etc.[1] A prediction of these may be made from Eq. (2) through the application of Eqs. (3), (4), (14), and (15). The constant B has been obtained in terms of the constant A. The latter is readily evaluated from the condition $(\partial V/\partial R)=0$, from which it follows that

$$A=\frac{n^*D^*}{2}\left[1-\left(\frac{r_0^*}{R_0-r}\right)^2\right]\times\exp[-n^*(R_0-r-r_0^*)^2/2(R_0-r)]/(e^{-bR_0})(b-1/2R_0). \quad (20)$$

A remains constant for a wide range of R_0 values. The only quantity which remains unknown is the repulsion constant b. This has a value of $4.8\cdot10^8$ cm^{-1} and was chosen to give the best agreement with the predicted energies. As Eq. (2) is presented, no correction has been made for the change of translational and rotational degrees of freedom on dissociation of the hydrogen bond. We have used a correction of $3RT/2$. (For this model the bending modes associated with the hydrogen bond would have zero frequency.)

A plot of predicted hydrogen bond energy as a function of R is given in Fig. 4. The commonly accepted values of the energies for oxalic acid, carboxylic acids, alcohols, and ice are included for a comparison. The predicted curve does not seem to have a curvature which would give the best agreement with the experimental values. However, since these latter are probably not known with an accuracy of greater than ±1 kcal/mole, the predicted values are considered acceptable, but part of any discrepancy may be due to our failure to introduce a proper Van der Waals repulsion term into

[7] L. P. Kuhn, J. Am. Chem. Soc. **74**, 2492 (1952).

our model. A curve based on $m=6$ has been calculated, but is indistinguishable from Fig. 4. The use of $m=6$ gives reasonable values for the energies but does not give as satisfactory values for the O---O force constants as does $m=1$.

CALCULATION OF THE O---O FORCE CONSTANT

Since the model now behaves properly to a fair approximation in both r and R, it is possible to use Eq. (10) to calculate k_{O---O}. From (2) and (10) the following expression is obtained:

$$k_{O---O}=\partial^2V_2/\partial R^2+(\partial V_2/\partial R)\times(b^2R_0^2-1)/R_0(bR_0-\tfrac{1}{2}). \quad (21)$$

In Table II we have tabulated k_{O---O} and the corresponding O---O frequencies for ice, formic acid, and oxalic acid. This frequency has been observed for ice, formic acid, and acetic acid from Raman studies.[5,8–10] The agreement between the calculated and observed frequencies is quite reasonable.

TABLE II. Calculated values for the O---O force constants and frequencies.

	R Angstroms	$k\cdot10^{-5}$ dynes/cm	ω(calc) cm^{-1}	ω(obs) cm^{-1}
Ice	2.76	0.220	204	210[b]
Formic acid	2.78[a]	0.175	161	189±80[c,d]
	2.73[a]	0.281	204	
	2.68[a]	0.455	259	
Oxalic acid	2.50	2.49	434	

[a] J. W. Karle and L. O. Brockway, J. Am. Chem. Soc. **66**, 574 (1941).
[b] See reference 5.
[c] See reference 8.
[d] Value given is for formic acid in the liquid state.

CALCULATION OF THE EFFECTIVE CHARGE ON THE OXYGEN ATOMS

If we interpret the proposed potential functions as being consistent with a resonance model illustrated by the structures:

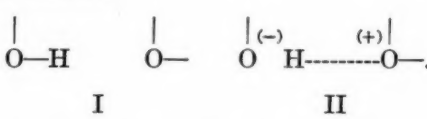

I II

The constant, B, in the electrostatic term, $-B/R$, can be regarded as the product of the effective charges on the oxygen atoms. One then has a means of representing the relative importance of structure II. For smaller values of R, structure II is increasingly important. Consistent with this is the fact that B is a function R which increases when R decreases. Writing $B=N(ae)^2$ where N is Avogadro's number and a represents the fractional charge, it is possible to calculate a as a function of R_0. The results are given in Fig. 5. It should be emphasized that this curve is only applicable to cases of hydrogen bonding involving dimers where the oxygen atoms may be regarded as nonequivalent. The curve would not be applicable to ice, where the oxygen atoms are equivalent as far as hydrogen bonding is concerned.

The role of the electrostatic term in hydrogen bonding

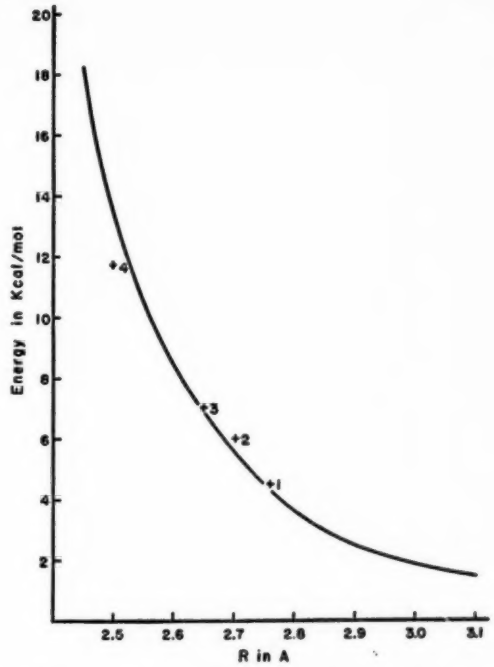

FIG. 4. Hydrogen bond energy as a function of O---O distance, $m=1$. 1. Ice. 2. Alcohols. 3. Carboxylic acid dimers. 4. Oxalic acid.

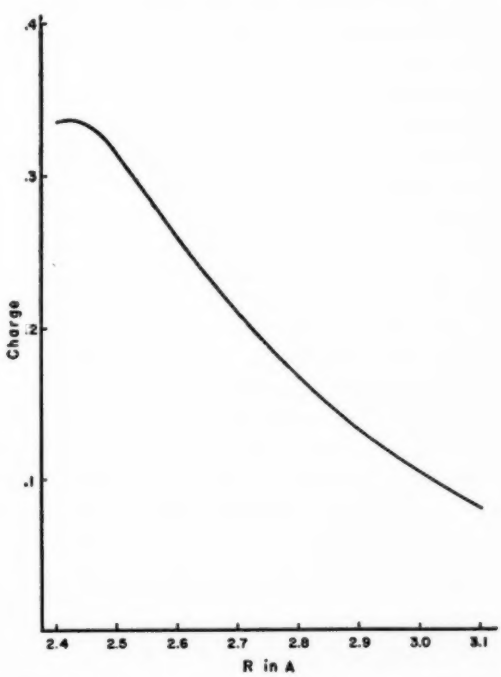

FIG. 5. Fractional charge on oxygen atoms as a function of O---O distance for hydrogen bond dimers involving nonequivalent oxygen atoms.

[8] Gupta, Indian J. Phys. **10**, 117 (1936).
[9] Ganesan and Venkateswaran, Indian J. Phys. **4**, 196 (1924).
[10] Ghosh and Kar, J. Phys. Chem. **35**, 1735 (1931).

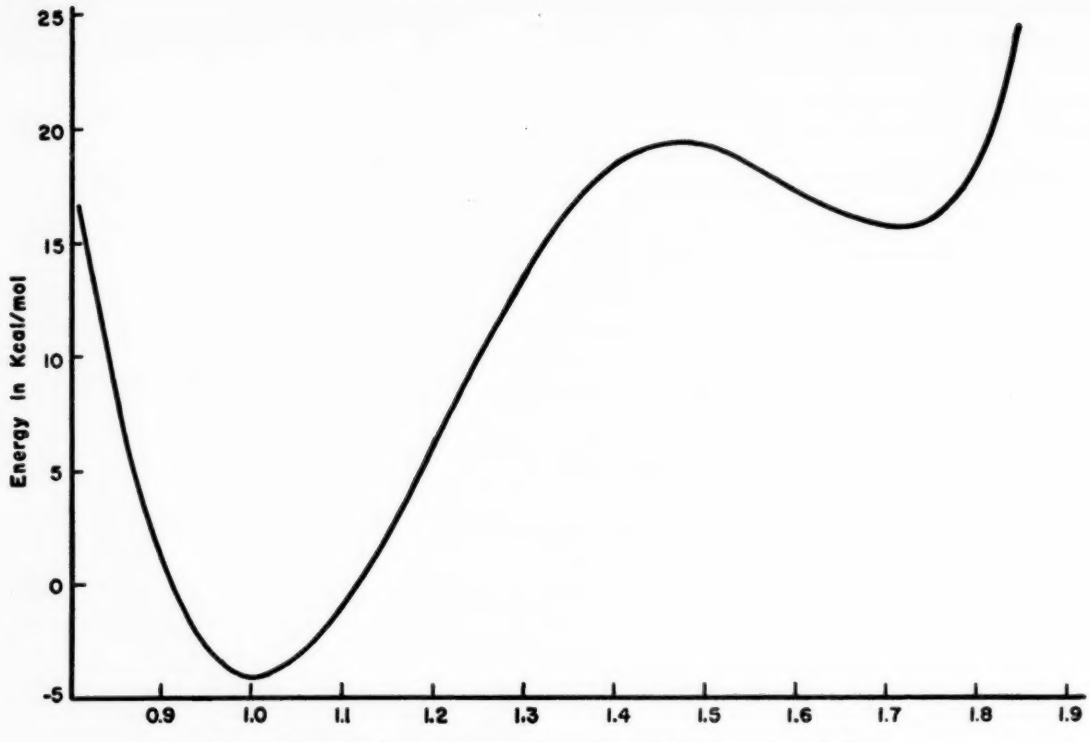

FIG. 6. The potential energy curve for motion of hydrogen atoms in ice.

may be studied by considering the effect on V of increasing B (thus an increase of charge on the oxygen atoms). Since A is constant for all O—H - - - O bonds, the conditions that $(\partial V/\partial R)_{eq}=0$ may be used to calculate the value of R_0 at equilibrium. This new R_0 will be smaller. The effect on the terms of the potential, $V=V_1+V_2+V_3+V_4$, is as follows. V_1 is slightly larger indicating a stretching of bond I in Fig. 1. V_2 is proportionately much smaller indicating a gain in stability due to formation of a stronger bond II in Fig. 1. V_3 is proportionately much larger, because of the large Van der Waals repulsion. V_4 is slightly larger. The important point is that the major changes in V are in V_2 and V_3 and not in the electrostatic term. The reason for this is that distance factors are more important in V_2 and V_3 than they are in the electrostatic term. The latter is important not because it gives a major contribution to the energy but because it allows a relatively close approach of the oxygen atoms. Hydrogen bonds between donor atoms of low ionization potential and acceptor atoms of large electron affinity would favor structure II and these have a smaller R_0 and larger energy. This of course is one of the common observations made in hydrogen bond studies.

POTENTIAL CURVES FOR THE HYDROGEN BOND

Since the proposed model adequately describes a number of properties associated with hydrogen bonding, one can obtain potential curves for the motion of the hydrogen atom and also for that of the oxygen nuclei. The former may be obtained by using (2) to obtain V as a function of r, all other quantities remaining constant, and the latter by using (2) to obtain V as a function of R, all other quantities remaining constant. These curves are shown in Figs. 6, 7, 8, and 9 for ice and oxalic acid respectively. In the curves for motion of the H atom, ice shows a maximum while that for oxalic acid does not although the curve is quite asym-

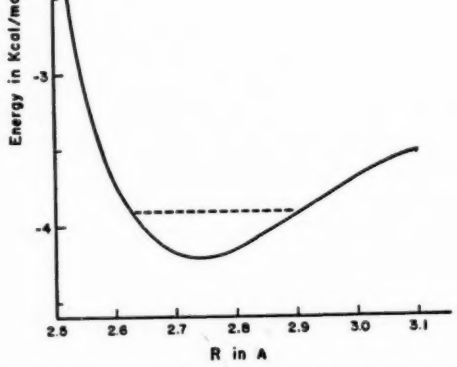

FIG. 7. The potential energy curve for the O - - - O motion of hydrogen bonds in ice.

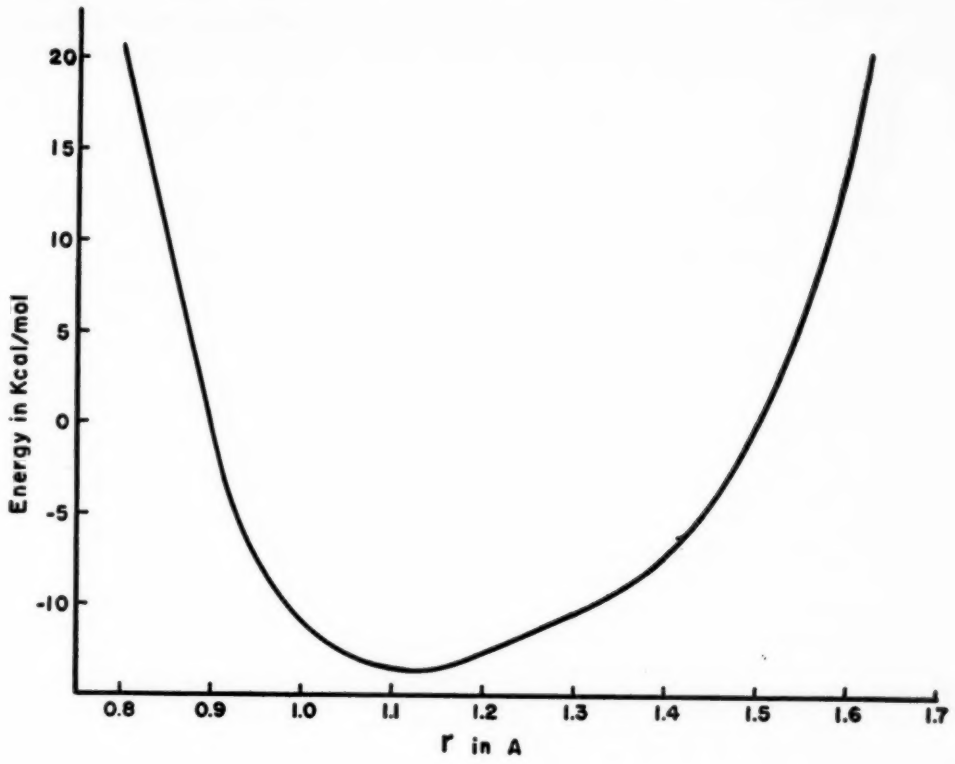

FIG. 8. The potential energy curve for the motion of the bonded hydrogen atoms in oxalic acid.

metric. The second potential minimum in ice lies nearly 20 kcal above the first minimum. These curves clearly indicate that there should be considerable anharmonicity associated with the bonded OH frequency. This anharmonicity can be calculated if one uses this potential as an anharmonic oscillator and solves the Schroedinger wave equation for the energy levels by means of the W.B.K. approximation method.

The curves for the motion of the oxygen nuclei are significant in that they show the importance of the Van der Waals repulsion term. Actually this repulsion term is necessary to make the model mechanically stable. Without it the hydrogen bond would collapse. Again the potential curve is very anharmonic. For convenience the ground state has been drawn in for the ice curve.

Classically one can use the k_{O---O} force constant to estimate the mean displacement of the oxygen atoms. For ice at 0°C, a value of 0.12 A is obtained. From Eq. (19) or Fig. 3 one may then obtain a mean spread of the OH frequencies. For ice this mean spread is about 300–400 cm^{-1}, which is in satisfactory agreement with experiment. Classically this model is then capable of explaining the broadness of the OH bonds due to hydrogen bonding. Merrifield has given a similar explanation for the broadenss of the OH bands.[11] Cross, Burnham, and Leighton have also called attention to the large amplitude associated with the O---O motion.[5]

[11] R. E. Merrifield, Ph.D. thesis, Massachusetts Institute of Technology (1952).

DISCUSSION

This simple model of the hydrogen bond is adequate to predict OH frequency shifts, OH bonded distances, and hydrogen bond energies from independent measurements of the O---O distance. By graphically combining the predicted curves of Figs. 3 and 4 one may obtain a curve which relates hydrogen bond energy

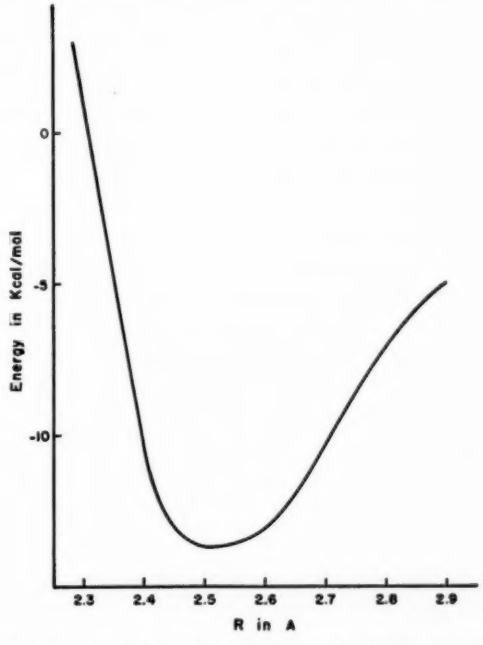

FIG. 9. The potential energy curve for the O---O motion of hydrogen bonds in oxalic acid.

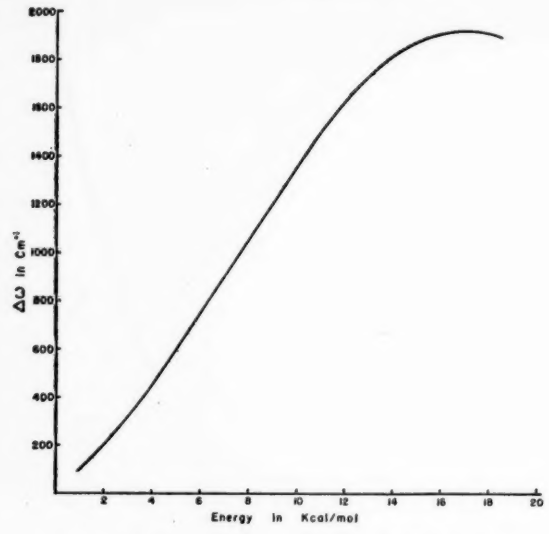

FIG. 10. O—H frequency shift as a function of hydrogen bond energy.

to OH frequency shift, thus eliminating the necessity of relying on measured values of the O - - - O distances. This curve is given in Fig. 10.

This model is applicable to other types of hydrogen bonding such as F—H - - - F, O—H - - N, and N—H - - - O. Calculations on these types are in progress and the results are encouraging. In particular this model should be adequate to predict hydrogen bond energies in proteins and related substances.

In its present form this simple model does not explain the multiple structure of some of the OH bands found by infrared studies. Of course, it says nothing about the effect of hydrogen bonding on the OH bending frequency or the frequencies of other nearby functional groups, which are known to be altered on formation of a hydrogen bond. Without modification the proposed model is incapable of handling bent hydrogen bonds and is not directly applicable to hydrogen bonding in liquid systems. Indications are that these latter cases may be handled by an extension of the model.

In any case it is surprising that such a simple model can adequately correlate and predict a number of the main features associated with hydrogen bonding.

Since the nature of hydrogen bonding has not been completely elucidated, it is logical to ask if this model is able to suggest new information about its basic explanation. The answer to this question depends to a large extent on the interpretation which is given to the potential function (1). Since this function is adequate to describe the properties of covalent bonds and not particularly suited to ionic or strongly polar bonds, it would seem that the forces playing an important role in hydrogen bonding are essentially the same as those applicable to ordinary covalent bonds. The latter are adequately described only in terms of quantum theory, and thus the commonly accepted explanation of the hydrogen bond in terms of classical electrostatic forces would appear unsatisfactory. The most important terms in the potential function used here are unlike ones used in electrostatic models which again implies that such forces have only a minor effect on the main features of the hydrogen bond. The electrostatic term used here does not make a major contribution to the energy but does allow a closer approach of the oxygen atoms resulting in more favorable distance factors. Because of the successful application of assumptions (c) and (f), it would appear that the potential function used would be most consistent with a resonance model illustrated by the resonance forms

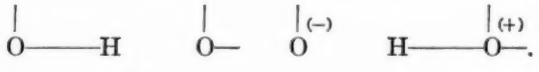

I II

Quantum-mechanically the wave function for this model would be

$$\psi = a_{\mathrm{I}}\psi_{\mathrm{I}}(RO{-}\mathrm{H}\ OR_2) + a_{\mathrm{II}}\psi_{\mathrm{II}}(RO^{-}\ \mathrm{H}{-}O^{+}R_2).$$

Here the classical electrostatic interactions would be described by ψ_{I} and the resonance contribution by ψ_{II}. Such a model has been proposed by others but with the exception of HFH^{-} the constant a_{II} has generally been considered so small that the $a_{\mathrm{II}}\psi_{\mathrm{II}}$ term could be neglected.[12] This model suggests that the resonance term is more important than now generally supposed.* Some investigators now prefer a quantum-mechanical model but most still consider the electrostatic one as the most likely explanation. A large number of papers have considered both sides of this question.[1,12–14]

We wish to express our appreciation to Professor R. C. Lord for several helpful discussions and to Professor R. E. Rundle and Dr. K. Nakamoto for sending us data in advance of publication. This work was supported in part by the Office of Ordnance Research, Contract DA-072-ORD-677.

[12] C. S. Coulson, *Valence* (Oxford University Press, New York, 1952), p. 303.

* *Note added in proof.*—The potential function (1) which forms the basis for the one-dimensional model of the hydrogen bond proposed here may be derived from a simple quantum-mechanical model [E. R. Lippincott, J. Chem. Phys. **23**, 643 (1955)].

[13] R. S. Mulliken, J. Phys. Chem. **56**, 801 (1952).

[14] Nukasawa, Tanaka, and Nagakura, J. Phys. Soc. Japan **8**, 792 (1953).

Treatment of Isotopic Exchange Reactions Having Complex Mechanisms*

R. A. MARCUS
Department of Chemistry, Polytechnic Institute of Brooklyn, Brooklyn 1, New York
(Received October 26, 1954)

The reaction rate *vs* time data of isotopic exchange reactions have been shown by previous work to obey a first-order rate law, neglecting differences in isotopic reactivity. A simple method, of use in reactions having complex mechanisms, is developed for relating this first-order rate constant to the rate constants of elementary steps in the process. The method involves examining the progress of specified atoms through the reaction sequence, and is applicable regardless of the number of exchange positions of the reactants, or of whether or not one isotope is present in tracer amounts. These results are used to reinterpret some data on the deuteration of diborane.

INTRODUCTION

DURING the past few years there has been a considerable amount of research on the rates of isotopic exchange reactions. Neglecting differences in isotopic reactivity, simple[1] calculations show that the rate at which the over-all isotopic composition of any chemical species in these reactions approaches its final value should obey a first-order rate law, regardless of their mechanism. A chemical species is defined here as a class of compounds differing only in their isotopic composition. This conclusion that the rate of formation of an equilibrium distribution of the isotopes among the reactants from an initially nonequilibrium distribution should be first order has been abundantly confirmed experimentally. The explicit form of the rate law[1] is given by

$$Rt=-\frac{ab}{a+b}\ln(1-F), \tag{1}$$

where a and b denote the concentrations of exchangeable atoms in the two reactants A and B, in gram atoms per liter say, R denotes the rate per unit volume at which atoms in A pass over to positions in B, and F denotes the fraction of exchange at time t. The rate per unit volume at which atoms in B pass over to positions in A must of course equal R. Furthermore, F is defined as $(x_a^0-x_a)/(x_a^0-x_a^\infty)$, where x_a, x_a^0, x_a^∞ denote the fractions of exchangeable atoms in A which are present as a particular isotope, α say, at time t, 0, and ∞.

When the mechanism of the exchange reaction is complex in that the over-all reaction is composed of several elementary steps, a problem of major interest is the relation of the quantity estimated from the experimental data, R, to the rate constants of the elementary steps and to the concentration of the reactants. In the present paper a simple method of obtaining this relation is presented and compared with other methods which have been, or could be used. Application of this technique to some recent data is made.

* This work was supported in part by the Office of Naval Research under Contract No. Nonr 839(09).

[1] A. C. Wahl and N. A. Bonner, *Radioactivity Applied to Chemistry* (John Wiley and Sons, Inc., New York, 1951), p. 7, give references to the original proof of H. McKay and to other derivations; G. M. Harris, Trans. Faraday Soc. **47**, 716 (1951).

THEORETICAL TREATMENT

General Discussion

It is useful to recall for purposes of continuity the simple proof[1] of Eq. (1). From the definitions of x_a and R it follows that the rate per unit volume in which atoms in A of the recognizable isotopic type, α say, pass over to positions in B is Rx_a and the rate at which atoms in B of the same isotopic type pass over to positions in A is Rx_b, where x_b is the fraction of exchangeable B atoms which are of the isotopic type α. Thus the net rate at which these atoms pass from A to B is

$$-\frac{d}{dt}(ax_a)=R(x_a-x_b) \tag{2}$$

where x_a and x_b are related by the material balance equation

$$ax_a+bx_b=ax_a^\infty+bx_b^\infty=(a+b)x_a^\infty, \tag{3}$$

which involves the fractions at infinite time. The second part of this equation follows from the fact that at equilibrium, i.e. at $t=\infty$, the fraction of exchangeable atoms of species A, x_a^∞, which are of the isotopic type α equals the corresponding fraction x_b^∞ in the species B. It immediately follows from the elimination of x_b between Eqs. (2) and (3) that

$$-\frac{dx_a}{dt}=R\frac{a+b}{ab}(x_a-x_a^\infty). \tag{4}$$

Equation (1) then results when Eq. (4) is integrated from $t=0$ to $t=t$.

One method of obtaining a detailed interpretation of R, which has been used in tracer studies of reactions having complex mechanisms, is applicable to mechanisms involving only one slow step. For example, it can be applied to reaction systems having several rapidly attainable equilibria which form intermediates, followed by a slow reaction between these intermediates (or between an intermediate and a reactant). The rate R is simply the rate expression for the reaction of these intermediates. It therefore involves their concentrations and these may be expressed in terms of the stoichiometric concentrations of the reactants using the appro-

priate equilibrium constant expressions. This method is simple and extremely useful but it is nevertheless of limited applicability.

If one of the isotopes is present in tracer amounts, denoted as the labeled isotope, then another more general way of obtaining the relation between R and the rate constants of the elementary steps could involve setting up expressions for the rates of formation and disappearance of each of the labeled reactants and intermediates. Once again a first-order law can be shown to result, only now the first-order constant has the desired form. It explicitly contains the rate constants of the elementary steps and is, generally, some function of the concentrations of the reactants. This method, however, becomes increasingly laborious with increasing complexity of the reaction mechanism, and a related, though appreciably simpler method of evaluating R is developed in the next section.

If both isotopes are present in comparable amounts but each type of molecule present contains at most one exchangeable atom, then a somewhat similar procedure to that used for the tracer case may be employed, or the procedure discussed in the following paragraph may be used.

When the isotopes are present in comparable amounts and at the same time the reactants have several exchangeable positions, many isotopically different compounds are formed, some isotopically isomeric with the intermediates and some with the reactants. In the case of complex mechanisms this enormously complicates any attempt to solve the equations for the rate of change of concentration of each of the many isotopically distinguishable molecules present.[2] For example, because of this isotopic multiplicity, it would be necessary to consider a large number of reactions, of the order of one hundred, in treating the exchange reaction of B_2H_6 with D_2 to be described later. In the present paper attention will be focused on the more limited but simpler problem of interpreting in terms of a detailed mechanism the rate of change of the over-all isotopic composition of any chemical species, i.e., of any class of compounds differing only in their isotopic composition. To accomplish this, it is first observed that this rate of isotopic exchange is given by Eq. (1), for the derivation of that equation was seen to be quite general. The problem then becomes one of evaluating the constant R occurring in this equation, in terms of the rate constants of the elementary steps of a suitable detailed reaction mechanism. To do this we note that R is independent of isotopic composition; therefore, its value for this apparently more complicated case, where the amounts of the isotopes are comparable and the reactants have several exchangeable positions, is the same as that for the case where one of the isotopes is present in tracer amounts. *That is, R for the complicated case may be evaluated by determining it for the tracer case.* Some methods for doing this have already been mentioned while in the following section a general simple treatment, valid for both cases, will be developed.

[2] An exception to this comment may be found in initial rate studies, for initially only relatively few distinguishable molecules are present.

Evaluation of R

General

In order to relate R to the rate constants of the elementary steps of the isotopic exchange reaction between A and B and to the initial concentrations, the progress of certain atoms through the reaction sequence from A to B will be followed. This will be done by labeling a certain, very small number of atoms which are initially in the A-type molecules say. This number of labeled atoms is taken to be so small that the number of molecules, A-type or otherwise, containing two labeled atoms per molecule is negligible and that the chance of a reaction between two molecules, each containing one labeled atom, is also negligible.

Let A^* be the concentration of those A-type molecules which at time t have one labeled atom each. An artifice which we find simplifies considerably the detailed evaluation of R will now be introduced. We will let the label* be such that by definition it vanishes when the specified atom enters a position in a B-type molecule, but not when the specified atom merely enters a position in one of the intermediates. Therefore A^* is actually the number of specified atoms per unit volume which at time t have *never* reached a position in a B-type molecule. It follows that A^* will decrease steadily with time from its initial value at $t=0$ to zero at $t=\infty$. The simplification resulting from the introduction of this artifice is that reactions involving the redissociation of a B molecule containing what would have been a labeled atom need not be considered for the evaluation of R. Detailed examples of this simplification are described later.

In a time interval, t, $t+dt$ a number of these labeled atoms per unit volume, $-dA^*$, will enter the species B. That is, this is the number when there are A^* labeled atoms available per unit volume. The number entering per available labeled atom present per unit time is therefore $(-dA^*/dt)/A^*$. Moreover, this is the probability per unit time that *any* given exchangeable atom in an A-molecule will enter a B-molecule. Now R is the number of A-atoms entering positions in the species B per unit volume per unit time, there being a atoms of species A per unit volume available, or R/a is the number of A-atoms entering B-molecules per available atom per unit time. Therefore, it follows that

$$\frac{R}{a}=-\frac{1}{A^*}\frac{dA^*}{dt} \tag{5}$$

which is the desired relation between R and A^*.

As an example of the detailed calculation of $-dA^*/dt$, and therefore of R, the isotopic exchange reaction be-

tween B_2H_6 and D_2 will be treated and compared with the experimental data.[3] The reaction between B_2H_6 and B_2D_6 has also been studied experimentally.[3] Its treatment presents some new problems since here there is only one chemical species and its over-all isotopic composition cannot change during the course of the reaction. A method of handling such a case is proposed and the results are compared with the experimental data.

Reaction of D_2 with B_2H_6

The system used to study this exchange reaction contained as reactants B_2H_6 and D_2. As a result of reaction there were presumably produced the following compounds: all possible substituted diboranes, B_2H_5D, $B_2H_4D_2 \cdots B_2D_6$, there being some twenty-four of these, all possible substituted borines, BH_3, BH_2D, BHD_2, BD_3, and the hydrogens, HD and H_2. The reaction was studied[3] by essentially analyzing for the total deuterium content present in the hydrogen chemical species after various reaction times. The rate-time data were found to obey the first-order rate law and the first-order rate constant showed a rather peculiar dependence on the initial concentrations.

A possible mechanism for this reaction which will be discussed here involves four basic steps; but, if this mechanism is written in terms of all the distinguishable compounds present (previously enumerated), the number of elementary reactions which contribute to the over-all exchange process is of the order of one hundred. However, as previously mentioned, the first-order rate data can be interpreted, neglecting differences in isotopic reactivity[4] and making only one further approximation,[5] by evaluating the constant R which appears in Eq. (1), using the method outlined in the previous section. The basic ideas underlying this approach to the problem can be summarized in the following way. These experimental data were actually obtained in a system having comparable amounts of the different isotopes and also having numerous isotopically different compounds. Then R was determined[3] from the data with the aid of Eq. (1). Now, R, for the case where one isotope is present in trace amounts, has the same value as R for this more complicated case. Therefore, if it is desired to derive a theoretical expression for R in terms of a detailed reaction mechanism and to compare it with the experimental value, it can be imagined that the reaction was performed under tracer conditions, although the more complex conditions were actually used. This is then done by labeling a small number of atoms and following their progress through the reaction mechanism.

A possible mechanism serving as a basis for this calculation is given by the following set of equations, similar from the viewpoint of chemical species involved to a mechanism previously suggested[3]:

$$B_2H_6 \underset{k_{-1}}{\overset{k_1}{\rightleftharpoons}} 2BH_3, \tag{6}$$

$$BH_3+HH^* \underset{k_{-2}}{\overset{k_2}{\rightleftharpoons}} BH_3^*+H_2, \tag{7}$$

$$BH_3^*+B_2H_6 \xrightarrow{k_3} B_2H_6+BH_3, \tag{8}$$

$$BH_3^*+BH_3 \xrightarrow{k_4} B_2H_6. \tag{9}$$

The labeled atoms are taken to be initially in hydrogen-type molecules so that A^* is H_2^* here. Let (H_2^*) and (BH_3^*) denote the concentration of H_2 and BH_3 molecules containing a labeled atom at time t. It is emphasized that this labeled atom is not necessarily an isotope but merely a device for the evaluation of the constant R. The label vanishes when the atom reaches a position in a B-type molecule. Once R is evaluated Eq. (1) may be applied to give the rate of change of the over-all isotopic composition of any chemical species.

Because of the disappearance of the label when the atom enters a position in B, i.e., because of the definition of a labeled atom, the reverse of reactions (8) and (9), reforming BH_3^*, should not be considered in the reaction scheme used to evaluate R. Reaction (8) is a reaction whereby the labeled atom of the borine disappears from this species to become part of a diborane molecule.

It follows from this reaction sequence that

$$\frac{-d(H_2^*)}{dt}=k_2(BH_3)(H_2^*)-k_{-2}(BH_3^*)(H_2) \tag{10}$$

where (BH_3) and (H_2) denote molar concentrations. Using a steady-state relation for BH_3^* we have

$$\frac{d}{dt}(BH_3^*)=0=k_2(BH_3)(H_2^*) - (k_{-2}H_2+k_3B_2H_6+k_4BH_3)(BH_3^*). \tag{11}$$

Eliminating BH_3^* from Eqs. (10) and (11) it follows that

$$R=-\frac{a}{(H_2^*)}\frac{d(H_2^*)}{dt}=\frac{k_2ca}{k_{-2}a/2(k_4c+k_3b/6)+1} \tag{12}$$

[3] P. C. Maybury and W. S. Koski, J. Chem. Phys. **21**, 742 (1953); P. C. Maybury, Dissertation, The Johns Hopkins University, Baltimore, Maryland (1952).

[4] We should like to comment on the neglect of differences in isotopic reactivity in the application of the first-order Eq. (1) to the experimental data. Inasmuch as the data actually obeyed a first-order equation, it may be inferred that the major effect of any difference in isotopic reactivity is on the value of the constant R which appears in Eq. (1). This effect will be considered in an approximate manner in the latter part of this paper.

[5] There is at small times some transient state which is neglected in the application of Eq. (1) to the data. However, the approximation made in neglecting this transient state is justified by the fact that first-order behavior was observed. It may be further remarked that the proposed mechanism is a chain mechanism, and the transient state in gas phase chain reactions would be expected to be established almost immediately.

where we have set $c=(BH_3)$, $a=2(H_2)$, and $b=6(B_2H_6)$, since a and b denote concentrations in gram atoms per liter while (H_2) and (B_2H_6) denote molar concentrations.

The constant k_2/k_{-2} is the equilibrium constant of reaction (7). It can be evaluated in terms of the partition functions of the components of this equilibrium. After due cancellation, only a product of symmetry numbers remains, so that

$$\frac{k_2}{k_{-2}}=\frac{\sigma_{BH_3}\sigma_{H_2}^*}{\sigma_{BH_3}^*\sigma_{H_2}}=\frac{6\times 1}{2\times 2}=\frac{3}{2}. \tag{13}$$

A further simplification of Eq. (12) can be made if the rate of termination of BH_3^* chains in this chain process, $k_4c(BH_3^*)$, is appreciably less than the rate of propagation, $k_3(BH_3^*)b/6$. This is generally true for chain reactions. A comparison of Eq. (12) with the data leads to the same conclusion here. Thus this equation becomes

$$R=\frac{k_2b^{\frac{1}{2}}(k_1/6k_{-1})^{\frac{1}{2}}}{2k_2/k_3+b/a} \tag{14}$$

where the equilibrium relation, $k_{-1}c^2=k_1b/6$, has been introduced.

According to this equation, R is independent of a and proportional to $b^{\frac{1}{2}}$ when a is relatively high such that $2k_2/k_3 \gg b/a$. When a is relatively low, i.e., when $2k_2/k_3 \ll b/a$, then R is proportional to a and also to $b^{\frac{1}{2}}$. This behavior was observed experimentally[6] with the exception of the square-root dependence on the diborane concentration at low a which has not yet been tested. It would be interesting to restudy experimentally this aspect of the problem.

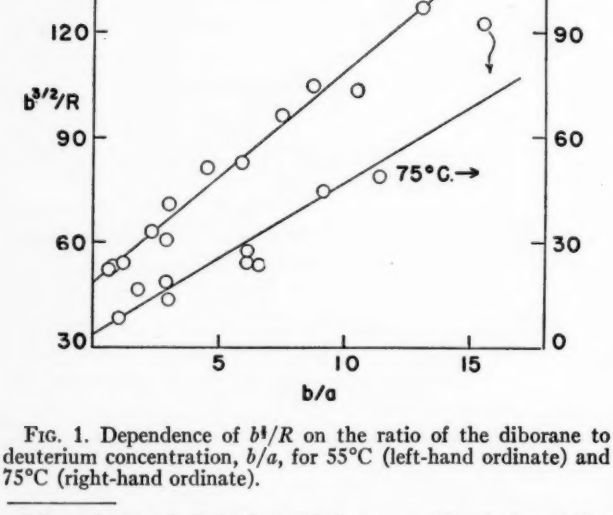

FIG. 1. Dependence of $b^{\frac{1}{2}}/R$ on the ratio of the diborane to deuterium concentration, b/a, for 55°C (left-hand ordinate) and 75°C (right-hand ordinate).

[6] See reference 3. It is observed that our a, H_2, is denoted by b there, and conversely.

According to Eq. (14) a plot of $b^{\frac{1}{2}}/R$ *vs* b/a should be a straight line whose ratio of slope to intercept is $k_3/2k_2$. Within experimental error this plot is found to be linear as seen from Fig. 1. At 55°C, k_3/k_2 is estimated in this manner to be 0.25. At 75°C this ratio is definitely higher, but its exact value as inferred from Fig. 1 is seen to be uncertain. It would appear that the reaction of a borine with diborane has a somewhat higher activation energy than that of borine with hydrogen. This is rather unexpected. When R is independent of a, $R=k_3(k_1b^3/6k_{-1})^{\frac{1}{2}}/2$, and the activation energy E_{act} for the over-all reaction becomes

$$E_{act}=E_3+\frac{\Delta H_1}{2} \tag{15}$$

where ΔH_1 is the heat of reaction of (6). Furthermore, E_{act} equals 20.4 ± 2 kcal mole^{-1}.

The foregoing analysis shows that the peculiar dependence of R on a and b can be consistent with a homogeneous mechanism. It had earlier been assumed[3] that this behavior was evidence for heterogeneous reaction. Actually the reaction is at least slightly heterogeneous, the rate increasing somewhat less than twofold at 55°C when the surface was increased tenfold, while at 75°C the rate was essentially unchanged. Such a slight surface effect will not affect the general agreement obtained above. Naturally, this does not rule out any heterogeneous mechanism consistent with these experimental observations, but there does not appear to be any need for invoking it at the present time.

It is interesting to note that the reaction rate was appreciably reduced at 55°C and at 75°C, five- or sixfold in some cases, by the addition of CO_2 or N_2 though not of He. While this might, as previously suggested,[3] be evidence for a surface reaction, an interesting alternative might be that the unsaturated borine is, possibly, partially associated with such molecules, thus reducing its reactivity. The effect of added gases on this and on other, equally slow, reactions of diborane is therefore of considerable interest.

Reaction of B_2D_6 with B_2H_6

In the exchange reaction between B_2H_6 and B_2D_6, the percentage deuterium in a given chemical species cannot change, there being but one such species, diborane. Thus the arguments of the previous sections cannot be applied to the treatment of data on this reaction without some further modification, and the modified treatment of these results presented here will be somewhat less rigorous.

Presumably many isotopic isomers of diborane are formed during the reaction, ranging from B_2H_6, B_2H_5D $\cdots$ to B_2D_6. The rate of disappearance of B_2H_6 in mixtures initially equimolar with respect to the two reactants, B_2H_6 and B_2D_6, was followed[3] by measuring the decrease in intensity of the infrared absorption band

at 974 cm^{-1}, associated with a vibration of two BH_2 groups with respect to each other. In this vibrational mode the terminal hydrogens move and the bridge hydrogens remain stationary. The intensity of this absorption band should decrease when any of the four terminal hydrogens changes positions with a deuterated atom. Experimentally the rate of decrease of intensity of this band obeys, at least approximately, a first-order relation.

For purposes of interpretation of these data the group of four terminal positions of the hydrogens in diborane is regarded as forming one species and the two bridge positions, another. It follows that the rate of change of deuterium content in either of these species would obey the first-order Eq. (1), neglecting differences in isotopic reactivity, where a and b denote the concentrations of the terminal and bridge species in gram atoms per liter. Inasmuch as there are twice as many terminal atoms as bridge atoms, $a=2b$ and this equation becomes

$$Rt=-\frac{a}{3}\ln(1-F) \tag{16}$$

where R, defined in a previous section, is the rate per unit volume at which atoms of one species assume positions in the other species.

Now one isotopic isomer of the terminal species is that member containing hydrogens in all four terminal positions. It does not necessarily follow that this member would obey the first-order relation Eq. (16), where $(1-F)$ would now be the ratio $(p_t-p_\infty)/(p_0-p_\infty)$, the p's denoting partial pressure of this constituent at the designated times 0, t, and ∞. However, it seems reasonable to suppose that this would approximately be the case and this will constitute the major assumption of this section.

In order to calculate R, we label a very small number of atoms such that

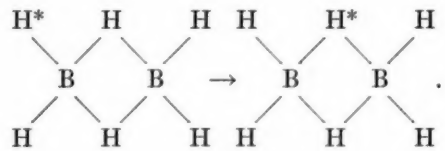

I II (17)

Each labeled atom is initially in a terminal position, as in I, say, no molecule having more than one labeled atom. The rate at which these atoms enter a bridge position II is then estimated. As before, the subsequent fate of any labeled atom once it has entered the other species (here the bridge positions) is not relevant to the calculation of R and for this reason the reverse of certain steps in the following mechanism is not considered in the calculation. The label in the species II is preserved only to indicate that the labeled atom entered a diborane molecule in the bridge position. A possible mechanism for the self-deuteration, similar structurally to that suggested by Maybury and Koski[3] is as follows:

$$B_2H_6 \underset{k_{-1}}{\overset{k_1}{\rightleftharpoons}} 2BH_3, \tag{6}$$

$$I \underset{k_{-1}'}{\overset{k_1}{\rightleftharpoons}} BH_3^*+BH_3, \tag{18}$$

$$BH_3^*+BH_3 \overset{k_{-1}''}{\rightarrow} II, \tag{19}$$

$$BH_3^*+B_2H_6 \overset{k_3'}{\rightarrow} BH_3+II, \tag{20}$$

$$BH_3^*+B_2H_6 \underset{k_3'''}{\overset{k_3''}{\rightleftharpoons}} BH_3+I, \tag{21}$$

$$BH_3+I \overset{k_3^{IV}}{\rightarrow} BH_3+II. \tag{22}$$

We let I denote the concentration of labeled atoms present in form I at any time t; I decreases with time from a value equal to the initial number of labeled atoms at $t=0$ to zero at $t=\infty$.

According to the aforementioned mechanism we have

$$-\frac{dI}{dt}=\frac{dII}{dt}=(k_{-1}''c+k_3'B_2H_6)(BH_3^*)+k_3^{IV}cI. \tag{23}$$

A steady-state equation for (BH_3^*) is

$$\frac{d(BH_3^*)}{dt}=0=(k_1+k_3'''c)I-(BH_3^*) \times[(k_{-1}'+k_{-1}'')c+(k_3'+k_3'')(B_2H_6)]. \tag{24}$$

Introducing this equation for (BH_3^*) into Eq. (23) we have

$$-\frac{1}{I}\frac{d(I)}{dt}=\frac{(k_{-1}''c+k_3'B_2H_6)(k_1+k_3'''c)}{(k_{-1}'+k_{-1}'')c+(k_3'+k_3'')B_2H_6}+k_3^{IV}c. \tag{25}$$

Now, the k_{-1}'s differ only by a small numerical factor at most, as do the k_3's. As in the previous section, we let $k_{-1}c \ll k_3B_2H_6$ and since $k_1B_2H_6=k_{-1}c^2$ it follows also that $k_1 \ll k_3c$. Thus Eq. (25) becomes

$$-\frac{1}{I}\frac{dI}{dt}=\left(\frac{k_3'k_3'''}{k_3'+k_3''}+k_3^{IV}\right)c. \tag{26}$$

Inasmuch as all k_3's are approximately equal the right-hand side is about k_3c. A somewhat more accurate figure is[7] $k_3c/6$. The total rate of exchange R of the

[7] The relative values of the various k_3's can be calculated as follows. It is emphasized that symmetry effects, not isotopic effects, are being estimated in this footnote. The ratio k_3''/k_3''' is the equilibrium constant of (21) and is estimated from the symmetry numbers of the components to be 4/3. Also $k_3''=2k_3'$ since there are twice as many equivalent collision complexes, resulting from a collision of a BH_3^* and a B_2H_6, which lead to I as compared

terminal atoms per unit volume is $(-a/I)(dI/dt)$ since $(-1/I)dI/dt$ is the rate of exchange for a given terminal atom and since there are a terminal atoms per unit volume. Combining this with Eqs. (16) and (26) we obtain a first-order rate constant, k, for the rate of disappearance of the 974 cm^{-1} band.

$$k=\frac{1}{t}\ln(1-F)=k_3c/2=k_3(k_1/k_{-1})^{\frac{1}{2}}(B_2H_6)^{\frac{1}{2}}/2 \quad (27)$$

where (B_2H_6) is the sum of concentrations of all diborane type molecules, in gram moles per liter. The square root dependence of Eq. (27) has been verified experimentally.[3] According to Eq. (27), the activation energy of this reaction is $(E_3+\Delta H_1/2)$, the same as that for the deuteration of diborane at relatively high pressures of deuterium, if isotopic effects be neglected. This too has been verified within experimental error, the activation energy for the self-deuteration reaction being 21.8±3 kcal mole^{-1}. However the absolute rate of the self-deuteration reaction is substantially faster than the deuteration reaction, the value of $k_3(k_1/k_{-1})^{\frac{1}{2}}$ at 44°C inferred[8] from the former reaction being about three hundred fold greater than that estimated from the latter process. No effect of added Pyrex surface or of inert gases was found for the self-deuteration reaction, perhaps because it is so rapid that a much larger variation of these factors would be needed to obtain an effect comparable to that observed for the deuteration reaction. It is of interest to speculate as to the reason for this relative rapidity of the self-deuteration reaction. First, the mechanisms discussed may be incorrect, but, inasmuch as they make several predictions, they can be further tested, at least partially. Second, if the assumption mentioned in reference 7 were in error, this factor could be reduced to 300/2.5, a still rather high value. Again, the reaction vessel of these two systems differed, the self-deuteration reaction having been studied in an infrared absorption cell with its salt windows, and with its walls of unspecified composition. It is also possible that in the deuteration reaction the rate of change of deuterium content of either of the reactants is slower than the rate of disappearance of the 974 cm^{-1} absorption band. It would be of interest to re-examine this reaction using both methods of analysis simultaneously. Another possible reason lies in isotopic effects.[4] If B_2D_6 dissociates more readily than B_2H_6 into borines then the self-deuteration reaction will presumably proceed at a lower temperature, depending upon the isotopic effect of k_3. The over all activation energy would almost undoubtedly also be lower but could equal the other activation energy within the experimental error. At the prevailing temperatures, a difference in reaction rate of a factor of one hundred can be equivalent to a difference in activation energy of 3 kcal mole^{-1}. On the basis of a recent assignment of infrared bands[9] we have estimated the relative equilibrium constants for the dissociation of B_2H_6 and of B_2D_6 into BH_3 and DB_3, respectively. If one assumes the BH-stretching and bending frequencies in borine to be the average values observed for the terminal hydrogens in diborane, (for B_2H_6, 2563 cm^{-1} and 1179 cm^{-1} respectively, and for B_2D_6, 1921 cm^{-1} and 905 cm^{-1}) then the ratio of the equilibrium constants is about unity. However, this assumption is open to question since the terminal BH-bonds in B_2H_6 are presumably approximately tetrahedral, while the BH-bonds are probably trigonal in BH_3. If the bonds in borine are actually stiffer than those in diborane, then B_2H_6 is more stable than B_2D_6 with respect to dissociation into borines. In this connection it is interesting to observe that the CH-stretching frequencies in ethane, which has tetrahedral CH-bonds, are greater than those in ethylene, which has trigonal bonds. The CH bending frequencies are, on the other hand, in the reverse order. It would be of interest to see if the rate of reaction of B_2D_6 with H_2 proceeds at a lower temperature than the reaction of B_2H_6 with D_2. A comparative study of some of the other reactions of B_2H_6 and B_2D_6 whose mechanisms appear to involve a preliminary dissociation into borines is also relevant.

with those leading to *II*. Further, the sum of these two constants $(k_3'+k_3'')$ must equal k_3 since an effective collision must produce *I* or *II*, and k_3, the rate constant for (8), is actually equal to the number of effective collisions. In this manner it is concluded that $3k_3'=3k_3''/2=2k_3'''=k_3$. The value of k_3^{IV}/k_3, depends on the exact nature of the collision complex and can be shown to lie between 0 and ¼. It will be ignored in our approximate treatment, the error being at most a factor of 2.5.

[8] In the application of the data to Eq. (14) it was seen that in the lower b/a range at 55°C the rate of the deuteration reaction was a direct measure of $k_3(k_1/k_{-1})^{\frac{1}{2}}$, so that the latter could be inferred at once from the reaction rate. From the comparison of the data obtained at 55°C and 75°C and given earlier, it appears that this approximation (which amounts to neglecting, in Eq. (14), b/a in comparison with $2k_2/k_3$) becomes increasingly valid at lower temperatures, 45°C for example. The value of b/a used at 45°C was about 2, while $2k_2/k_3$ should at least equal 8, the value at 55°C estimated previously. That is, at 45°C the value of $k_3(k_1/k_{-1})^{\frac{1}{2}}$ could be inferred directly from the observed reaction rate.

It may be remarked that the large difference in rates of self-deuteration and deuteration reactions will prevail at other adjacent temperatures, for the temperature coefficients of both reactions were seen to be essentially the same.

[9] R. C. Lord and E. Nielsen, J. Chem. Phys. **19**, 1 (1951).

Color Centers in Alkali Halides Containing NO_2^- Ions in Small Concentration

E. HUTCHINSON AND P. PRINGSHEIM
Chemistry Division, Argonne National Laboratory, Lemont, Illinois
(Received September 17, 1954)

Alkali halide single crystals (KBr, KCl, NaBr, and NaCl) containing NO_2^- ions at various concentrations, from 0.5 to 0.007 mole percent, were grown by the Kyropoulos method. At high NO_2^- concentrations the typical NO_2^- band appears in the absorption spectrum with peak wavelengths between 280 and 260 mμ depending on the nature of the base material. The production of F-bands by exposure to x-rays is completely suppressed in these crystals at room temperature and greatly inhibited at −190°C. Instead of the F-band, a continuous band (C-band) is produced with a wavelength nearly coincident with the NO_2^- band, but not showing at low temperature the vibrational structure characteristic of the latter. Other less important new absorption bands appear in the red and the ultraviolet. At lower NO_2^- concentrations F-bands begin to appear in competition with the C-bands. The bleaching of the various absorption bands by light absorbed in them is investigated and discussed. NaCl seems to differ from the other halides in so far as in this crystal the production of the F-band is greatly enhanced by NO_2^- in concentrations which in KBr greatly inhibit the formation of F-centers.

INTRODUCTION

It has been mentioned in a preceding paper[1] that the absorption spectrum of KBr containing small amounts of $NaNO_2$ shows a band at 382 mμ which at −190°C is resolved into a sequence of narrower peaks and is characteristic of the NO_2^- ion. Earlier, in an unpublished experiment, P. H. Yuster in this laboratory made the observation that if a little $NaNO_3$ is added to the melt, no F-band could be produced in the resulting KI crystal by exposure to x-rays, but that instead a weak broad band with peak a little below 400 mμ appeared in its absorption spectrum measured at room temperature.

Several papers of the Goettingen school deal with alkali halides contaminated with alkali nitrates and nitrites.[2] Among these investigators only Smakula treated the influence of an additon of $NaNO_3$ on the formation of F-centers, and this only for NaCl at $NaNO_3$ concentrations of 0.01 to 0.1 mole percent in the melt and probably less than 1/10 of this concentration in the crystal. He assumes that the peak wavelength and half-width of the F-band are not altered by the impurity and measures only the intensity at the band peak after various exposure times as a function of the $NaNO_3$ concentration. His rather surprising result that the intensity of the band is practically independent of the foreign admixture after short periods of irradiation but is greatly enhanced by the presence of small amounts of $NaNO_3$ after long lasting exposures, was not given an interpretation in the paper.

By investigating the infrared spectra, Maslakowez found that by adding nitrates or nitrites to the melts of alkali halides the resulting crystals always contain NO_3^- and NO_2^- ions, apparently in an equilibrium in which the relative NO_2^- concentration increases with increasing melting temperature of the salt (KI, KBr, KCl, NaCl). The concentrations which he used were fairly low (he mentions only the weight percent added to the melt), certainly a good deal lower than in some of our experiments in which the concentration of NO_2^- in the crystal was determined by the usual colorimetric method.[3] One sample of relatively high and one of much lower concentration were prepared with KBr and KCl as base material. The data are collected in Table I.

KBr AND KCl WITH HIGH $NaNO_2$ CONCENTRATION

Figure 1 shows the absorption spectrum in the range from 400 to 300 mμ of a KBr crystal of type *I* [KBr(*I*) of Table I] with the characteristic NO_2^- band near 375 mμ. The common origin of this band and the band with nearly identical structure observed in $NaNO_3$ crystals containing an admixture of $NaNO_2$, cannot be doubted. It is further corroborated by the fact that a similar band occurs in the spectrum of KCl(*I*), only slightly shifted towards the ultraviolet (Fig. 1, curve *c*); in $NaNO_3$ the band is displaced even more, by about 20 mμ to shorter wavelengths. Even in the absorption spectrum of a sample of KCl, into the melt of which nitrate instead of nitrite had been introduced, the NO_2^- band appeared with good intensity, while the NO_3^- band at about 300 mμ was completely missing. As far as this part of the ultraviolet spectrum provides a definite conclusion, the conversion of NO_3^- into NO_2^- would be complete in this case, not quite in agreement with Maslakowez's infrared analysis.[2] In the infrared spectra of our high concentration KBr(*I*) and KCl(*I*)

TABLE I. NO_2^- concentration in alkali halides.

	KBr		KCl		NaCl		
	I	*II*	*I*	*II*	*I*	*II*	NaBr
$g/g \times 10^3$	2.15	0.062	2.58	0.045	0.22	0.57	0.83
Mole percent	0.58	0.016	0.42	0.0073	0.027	0.071	0.185

[1] P. Pringsheim, J. Chem. Phys. **23**, 369 (1955).
[2] I. Maslakowez, Z. Physik **51**, 696 (1928); A. Smakula, Nachr. Ges. Wiss. Goettingen 110 (1929); E. Mollwo, Nachr. Ges. Wiss. Goettingen **3**, 149 (1939); W. Honrad, Ann. Physik **29**, 421 (1937); S. Apkinar, Ann. Physik **37**, 429 (1940).
[3] Hennig, Lees, and Matheson, J. Chem. Phys. **21**, 664 (1953).

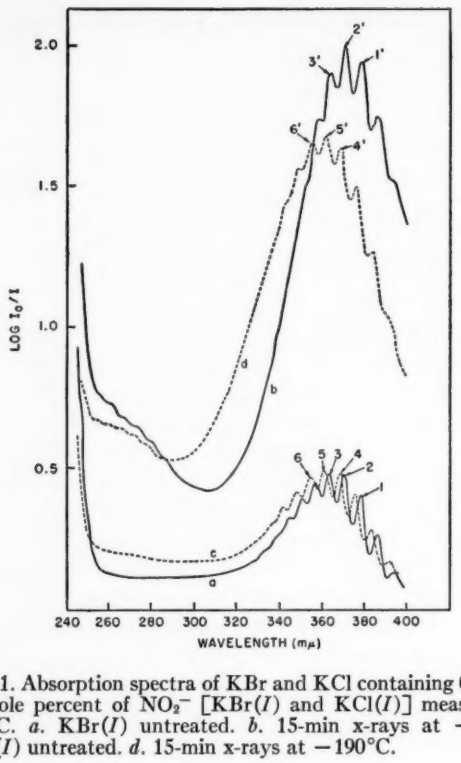

FIG. 1. Absorption spectra of KBr and KCl containing 0.56 and 0.42 mole percent of NO_2^- [KBr(I) and KCl(I)] measured at −190°C. *a*. KBr(I) untreated. *b*. 15-min x-rays at −190°C. *c*. KCl(I) untreated. *d*. 15-min x-rays at −190°C.

the regions in the neighborhood of 7.2μ and 8μ were completely opaque, so that it is not possible to decide whether the absorption of 7.2μ is caused by the "weak" NO_2^- or the strong NO_3^- band.[4]

Besides the NO_2^- band, curves *a* and *c* of Fig. 1 show a steep rise below 250 mμ which with great probability can be ascribed to the short wavelength absorption band of the NO_2^- ion with peak in the vicinity of 200 mμ, which is at least several hundred times stronger than the band at 350 mμ.[5]

Curves *b* and *d*, respectively, represent the alteration produced in the absorption spectra of KBr(I) and KCl(I) by exposure to x-rays at −190°C: a strong additional absorption is superimposed upon the NO_2^- band. The structure of this band itself remains practically unchanged, except for a shift in the intensity distribution between the individual peaks, as best visualized by comparing the relative heights of the peaks numbered 1, 2, 3 or 4, 5, 6 with those numbered 1′, 2′, etc. This is due to the fact that the additional absorption corresponds to continuous bands with peaks at 380 mμ for KBr and at 360 mμ for KCl. These bands (Fig. 2, *a* and *c*) are the typical "NO_2^-" color center bands and shall be called C-bands in this paper. In different base materials their exact peak wavelengths vary somewhat more than those of the NO_2^- bands themselves. Moreover they are not quite symmetrical and drop at a much slower rate at their long wavelength side than on the short wavelength side.

In addition to the C-bands a fairly strong absorption showing an indication of vibrational structure is produced between 300 and 250 mμ by the exposure to x-rays at −190°C; below 250 mμ it merges with the short wavelength NO_2^- band. In the far red end of the KBr(I) spectrum a band of low intensity is formed between 700 and 800 mμ; its peak at 750 mμ has an intensity less than 5 percent of that of the C-band. The existence of an analogous band in the spectrum of KCl could not be ascertained directly, but was made probable by bleaching experiments.

No trace of an F-band was produced in KBr(I) after 30 minutes of x-ray exposure at −190°C, while in "pure" KBr an optical density of 2.0 is obtained at the peak of the F-band under the same conditions. Although the NO_2^- concentration in KCl(I) was only slightly smaller than in KBr(I) (Table I), the formation of the C-band was appreciably less effective and, on the other hand, a low, but unmistakable F-band appeared in this case at 540 mμ after x-ray exposure at −190°C.

If after x-ray exposure at −190°C crystals of KBr(I) or KCl(I) are warmed up to room temperature, they are bleached almost completely to the initial state represented by curves *a* and *c* of Fig. 1, but for a small increase of absorption in the region of the NO_2^- band, which may or may not be due to a remainder of the C-band. A similar small increase in the absorption in the same region (and no other visible effect) is produced by irradiating the crystals with x-rays at room temperature. If KBr(I), after irradiation with x-rays at −190°C, is exposed to red light of wavelength 750 mμ, the red band is completely bleached out and about 60 percent of the C-band vanishes; but on the long wavelength

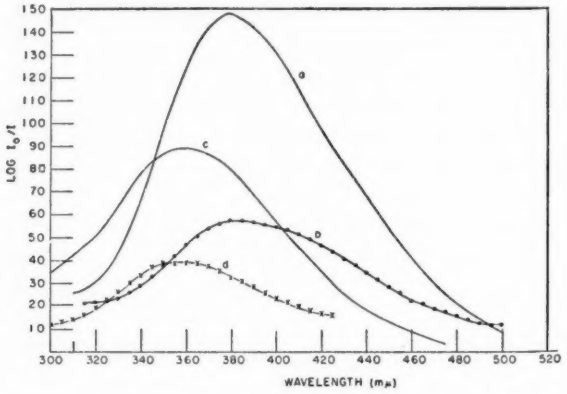

FIG. 2. Color center bands (C-bands) in KBr and KCl at −190°C. *a*. Additional absorption produced in KBr(I) by 15-min x-rays at −190°C. *b*. Additional absorption produced in KBr(II) by 15-min x-rays at −190°C. *c*. Additional absorption produced in KCl(I) by 15-min x-rays at −190°C. *d*. Additional absorption produced in KCl(II) by 30-min x-rays at −190°C.

[4] The absorption in the near infrared in these crystals was so strong that a number of bands in the region between 3 and 6μ not known before could be identified. These measurements were made in collaboration with Dr. S. Gordon and will be continued by him.

[5] According to Mollwo, see reference 2, the steep rise below 250 mμ should be ascribed to a KO-bond. Although nothing is known concerning the absorption by such a "bond," the existence of the short wavelength NO_2^- absorption band is a well-established fact.

side of the C-band, between 400 and 600 mμ, an apparently continuous absorption remains visible, which before the bleaching was hidden under the strong C-band (Fig. 3). The continuous absorption below 300 mμ is not affected by the exposure to red light. The C-band in KCl(*I*) does not respond to red light, but can be bleached by exposure to infrared between 0.8 and 1.2μ.

By C-light not only the C-band but also the red band and the ultraviolet absorption below 300 mμ are bleached out in KBr(*I*) at −190°C. The analogous effects are produced in KCl(*I*) and moreover in this case the low F-band present in the spectrum disappears too. If, on the other hand, the KCl(*I*) sample is exposed to F-light, the absorption in the C-band drops slightly, while the F-band disappears.

KBr AND KCl WITH LOW NO_2^- CONCENTRATION

In the absorption spectra of KBr(*II*) and KCl(*II*) (see Table I) no bands characteristic of the NO_2^- ions can be perceived in the near ultraviolet; only by the steep rise in absorption below 250 mμ is their presence indicated. One-hour exposure of KBr(*II*) to x-rays at room temperature does not produce a trace of an F-band which, under the same conditions appears with fairly high intensity (optical density 1.0) in the spectrum of pure KBr. If the same sample (No. 3 in Table II) is subsequently x-rayed for 30 minutes at −190°C, a clear-cut F-band appears, while the *F'*-band formed under similar conditions in pure KBr is missing. Instead, a band with peak at 380 mμ emerges which must be identified as a C-band; it is represented in Fig. 2 by curve *c* and the analogous band in KCl(*II*) by curve *d*.

Although the regularity is not complete, because different samples, even when cleaved from the same single crystal, may not contain exactly the same concentration of NO_2^-, Table II shows that with increasing time of x-ray exposure the intensity of the F-band increases at a much higher rate than the intensity of the C-band. It seems that the latter tends to a saturation value which may be explained by the assumption that only a restricted number of NO_2^- centers are available for the formation of C-centers.

TABLE II. Optical densities of peaks of various bands of KBr(*II*) after various treatments at −190°C.

No.	Treatment	F	C	275 mμ	255 mμ
4	40 min x-rays	0.65	0.72	0.61	0.55
	2 min F-light	0.04	0.67	0.60	0.55
	30 min C-light	0.06	0.23	0.30	0.40
	30 min x-rays	1.02	0.70	0.82	0.74
3	30 min x-rays	0.82	0.61	...	...
	1 hour x-rays	1.24	0.66	0.78	0.65
5	1.5 hours x-rays	1.18	0.81	0.96	0.85
	0.5 min F-light	0.06	0.75	0.94	0.50
	15 min C-light	0.14	0.21	0.45	0.50
6	2 hours x-rays	1.50	0.70	1.18	1.00

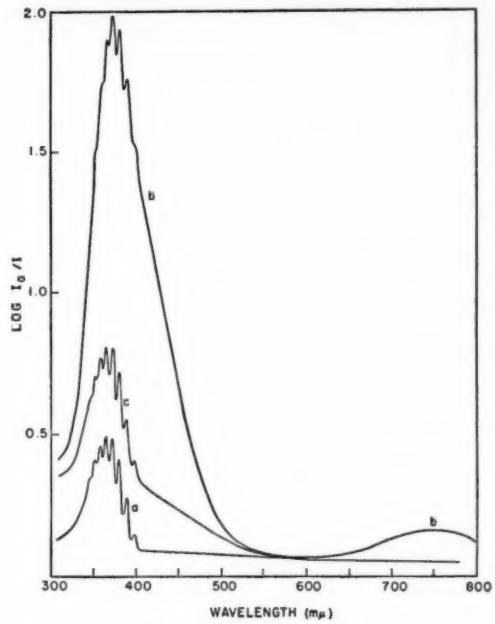

FIG. 3. Bleaching of the C-band in KBr(*I*) by red light at −190°C. *a*. KBr(*I*) untreated. *b*. 15-min x-rays at −190°C. *c*. 15 min bleached with red light at −190°C.

After being x-rayed once and bleached with C-light, sample No. 4 seems to have gained in its ability to form F-centers. It must also be mentioned that sample No. 3, before being x-rayed at −190°C, had been exposed without any visible effect for 1 hour to x-rays at room temperature.

Besides the F- and C-bands in KBr(*II*), a fairly strong absorption in x-rayed KBr(*II*) below 300 mμ, is incompletely resolved into two peaks at 275 mμ and 255 mμ. In this range KCl(*II*) shows only a rather weak slowly rising continuous absorption after x-ray exposure at −190°C. The C-band is also relatively much weaker in KCl(*II*) than in KBr(*II*), while the F-band, even after only 15 minutes' x-ray exposure at −190°C, acquires a very high intensity. By warming up these crystals to room temperature all x-ray-induced bands in the absorption spectra of KBr(*II*) and KCl(*II*) are destroyed. Their F-bands are also much more easily bleached by F-light at −190° than the F-bands in "pure" crystals. The radiation from an Hg AH6 lamp, passed through a Bausch and Lomb interference filter transmitting 600 mμ and a Corning Filter 3482, reduced in 30 seconds the F-band of KBr(*II*) No. 5 by 95 percent, while the C-band dropped only by 7.5 percent and the ultraviolet peaks remained quite unaltered. By exposure of the same crystal to C-light, the ultraviolet band peaks are bleached by different relative amounts (as shown in Table II for sample 4 and 5), the C-band is greatly decreased (in the case of sample No. 5 by 78 percent), and the absorption in the F-band is appreciably *increased*. The same phenomenon could be obtained even in a more striking manner with KCl(*II*) samples (Table III).

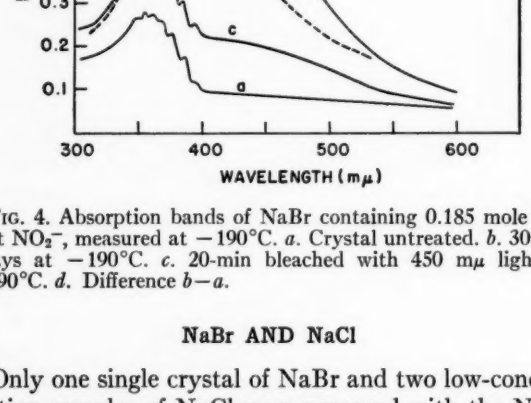

FIG. 4. Absorption bands of NaBr containing 0.185 mole percent NO_2^-, measured at −190°C. *a*. Crystal untreated. *b*. 30-min x-rays at −190°C. *c*. 20-min bleached with 450 mμ light at −190°C. *d*. Difference *b*−*a*.

NaBr AND NaCl

Only one single crystal of NaBr and two low-concentration samples of NaCl were prepared with the NO_2^- concentrations listed in Table I. NaBr is highly hygroscopic, and nothing is found in the literature with respect to its behavior under x-ray irradiation beyond the spectral location of its F-band at room temperature at about 530 mμ.[6] The yield of F-centers in "pure" NaBr is low. When x-rayed at −190°C for several hours it exhibits hardly a trace of an F-band; the yield is only a little better at dry ice temperature, and at room temperature twenty times as long exposures are needed to produce an F-band of the same intensity as in KBr. Adding small amounts of a divalent ion, such as Ca^{++}, to the melt greatly increases its colorability.*

The concentration of NO_2^- in our NaBr samples was lower than in KBr(*I*) and KCl(*I*) but still high enough to produce in the absorption spectrum not only the steep rise below 250 mμ but also a band with peak at about 360 mμ which, when recorded at −190°C, showed the characteristic structure of the NO_2^- band (Fig. 4*a*). Thirty minutes' exposure to x-rays at −190°C enhances this absorption band very appreciably (Fig. 4*b*) without increasing the intensity contrast in the structure. As in the case of KBr and KCl this is caused by the superposition of a continuous absorption band with its peak nearly coinciding with that of the NO_2^- band. Furthermore, as in the other instances a new continuous absorption appears between 280 and 250 mμ, while no trace of an F-band is found.

The strong shoulder on the long wavelength side of the NO_2^- band after x-ray irradiation in Fig. 4*b* seems to be a new feature not observed in the spectra of KBr(*I*) and KCl(*I*). However, the difference curve *d* in Fig. 4, obtained by subtacting *a* from *b*, may easily represent a C-band which is only a little more displaced in the direction of greater wavelengths than in KBr. At any rate this whole band is bleached uniformly when the crystal is exposed to light of a wavelength corresponding to any part of the band. Light of a wavelength well on the short wavelength side of the NO_2^- band and light of 450 mμ at the center of the apparent shoulder produce exactly the same effect, which for the first of these cases is represented by curve *c* of Fig. 4. In both cases the continuous absorption below 300 mμ drops simultaneously by relatively equal amounts. As in all other instances the C-band very nearly disappears when the crystal is warmed up to room temperature.

In the preparation of the NaCl crystal the relative quantity of $NaNO_2$ introduced into the melt was as large as or greater than in KBr(*I*) and KCl(*I*) (nearly 2 percent and 4 percent, respectively in weight). Nevertheless, according to the colorimetric analysis, the concentration in the finished crystals was quite low, as listed in Table I. Thus it seems that NaCl, perhaps because of its higher melting point, is not able to incorporate as great amounts of NO_2 ions as the potassium halides. Even so the molar concentration in the crystals was larger than in KBr(*II*) and KCl(*II*). However, while the F-center yield by x-ray irradiation at −190°C was still four times lower in KBr(*II*) than in "pure" KBr and while it was of about the same order of magnitude in KCl(*II*) and "pure" KCl, it was much higher in both NaCl samples than in "pure" NaCl, the colarability of which is small at −190°C. This result is interesting in connection with Smakula's paper mentioned in the introduction and will be investigated more completely.

In agreement with the behavior of the potassium halides of low NO_2^- concentration the NaCl(NO_2^-) samples exhibit no trace of the NO_2^- band at about 360 mμ before exposure to x-rays, while the steep rise below 250 mμ is observed also in this instance. After x-ray irradiation at −190°C, however, a shoulder appears on the short wavelength side of the F-band corresponding to the superposition upon the latter of a band with peak near 360 mμ. Moreover the F-band shows at its long wavelength side a tail reaching beyond 700 mμ. This tail vanishes when the crystal is exposed for a short time to red light (λ=650 mμ), and simultaneously the intensity of the F-band, instead of being enhanced, is lightly decreased, while the hypothetical C-band at 360 mμ drops even by a greater amount, (Fig. 5, curve *b*). Curve *c* of Fig. 5 represents the

TABLE III. Optical density in peaks of F- and C-bands of KCl(*II*) after various treatments at −190°C.

KCl(*II*) sample	No. 2		No. 4	
Treatment	F	C(V_1)	F	C(V_1)
30 min x-rays	1.82	0.32	2.35	0.60
10 min F-light	0.22	0.22	0.40	0.50
15 min C-light	0.55	0.11	0.74	0.32
15 min C-light	0.58	0.09	0.77	0.28

[6] R. Ottmer, Z. Physik **46**, 798 (1928).
* Unpublished.

absorption spectrum of the crystal at −190°C after it was warmed up for some time to room temperature. In contradistinction to the potassium halides KBr(*II*) and KCl(*II*) the F-band retains a very appreciable intensity in this case and the same is true for the shoulder at 360 mμ.

DISCUSSION OF THE EXPERIMENTAL RESULTS

The C-band produced in alkali halides by x-ray irradiation at low temperature can be ascribed to the same type of center which is responsible in $NaNO_3$ for the appearance of a similar band called, "NO_2^- color center band" in a preceding paper. It is almost certainly an electron surplus band due to electrons released by the action of x-rays from the matrix lattice ($NaNO_3$, KBr, etc.) and trapped in some other location. The electron capturing probability by these new centers must be fairly high, since by their presence the formation of F-centers can be completely suppressed in KBr and greatly inhibited in KCl, and since F′-centers are not produced even when the concentration of NO_2^- is quite low. It is quite certain that the appearance of the band is connected with the presence of the NO_2^- ions, and thus the trapping centers are probably located in the immediate vicinity of these ions. Two interpretations seem to be possible. Either, as in F-centers, the trapped electron itself forms the C-center with its characteristic absorption frequency, or the normal absorption mechanism of the NO_2^- ion, causing the relatively weak band with vibrational structure near 360 mμ, is perturbed by the electron captured in its neighborhood in such a way that its transition probability is greatly enhanced and its vibrational structure completely blurred out. The first interpretation can hardly be accepted. It is highly improbable that an electron captured in some vacancy of $NaNO_3$, KBr, KCl, or NaBr should always give rise to a band nearly coinciding with the NO_2^- band in this lattice. The second assumption which was discussed to some length in the preceding paper, seems to be more acceptable, although it is by no means better than a vague suggestion.

If two bands, one of which is an electron surplus band, are bleached by light absorption in each of the two bands, the second band is either a "hole band" (or V-type) or it is due to the perturbation by the electron surplus center of another absorbing mechanism; for instance the fundamental absorption (α,β type). The intensity of a band of the latter type must always vary exactly in parallel with the intensity of the electron surplus band. The red band appearing in the absorption spectrum of KBr(*I*) x-rayed at −190°C is bleached simultaneously with a part of the C-band by red light as well as by C-light. The same seems to hold for an infrared band of KCl(*I*) and for the long wavelength tail of the F-band of NaCl(NO_2^-). Since only a part of the C-band disappears with the complete bleaching of the red band, the latter cannot be of the α,β type: it must be a V-band, although none of the V-bands

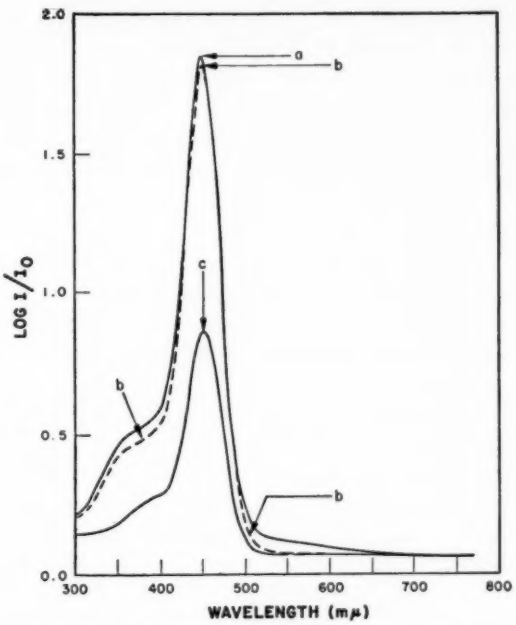

FIG. 5. Absorption spectrum of NaCl containing 0.071 mole percent of NO_2^-[NaCl(*II*)] measured at −190°C. *a*. After 30-min x-rays at −190°C. *b*. 5-min exposure to red light at −190°C. *c*. Warmed to room temperature.

known in "pure" KBr, but connected somehow with the presence of NO_2^- ions in the lattice. If the C-centers are photochemically produced electron surplus centers, corresponding V-centers must exist which might, but need not, be of the same character as in the pure alkali halides. The ultraviolet absorption below 300 mμ which can be bleached by F-light, but is not affected by red light in the case of KBr(*I*), must also be ascribed to V-centers; probably several V-bands of different stabilities are superimposed upon each other in this spectral range.

According to an earlier paper the F-band in pure KCl is bleached by F-light at −190°C with low efficiency.[8] The exceedingly high efficiency of F-light bleaching for the F-bands in KBr(*II*) and KCl(*II*) at −190°C favors the assumption that new very unstable V-centers must take part in these processes which most probably do not occur by raising F-electrons into the conduction band of the normal lattice, but rather by tunneling these electrons from the F-center to the new unknown V-centers.

The situation is complicated by the fact that in KCl the C-band coincides exactly with the V_1-band of "pure" KCl, while in KBr the two bands overlap sufficiently that light absorbed in the one can also excite the centers corresponding to the other. This explains why in KCl(*I*) the C-band drops somewhat when the low F-band is bleached out by F-light. The same phenomenon is much more impressive in the low concentration crystals, in KBr(*II*) and especially in

[8] Casler, Pringsheim and Yuster, J. Chem. Phys. **18**, 1564 (1950).

KCl(*II*), as shown in Table III. When the very strong F-band is bleached by F-light, apparently the C-band loses some of its intensity, but really it is the V_1-band hidden under the C-band which disappears. If by subsequent bleaching of the C-band by C-light the intensity of the F-band increases again, electrons lost by the C-centers must be restored to the F-centers. This is perhaps the most conclusive argument in favor of the electron surplus character of the C-centers.

We want to thank Mrs. M. Rauh for having made the colorimetric analyses of the various crystals used in this investigation.

THE JOURNAL OF CHEMICAL PHYSICS VOLUME 23, NUMBER 6 JUNE, 1955

Collision Excitation of Molecular Vibrations in Halogen-Substituted Methanes*

THOMAS D. ROSSING† AND SAM LEGVOLD
Department of Physics and the Engineering Experiment Station, Iowa State College, Ames, Iowa
(Received August 9, 1954)

Departures from the equilibrium between vibrational and translational energies in gases are characterized by relaxation times which depend upon the ease with which vibrations may be excited or de-excited by collisions. The de-excitation process has been discussed by various authors on the basis of the relative velocity of approach of two colliding molecules and on the basis of the relative energy of approach.

The dispersion of ultrasound has been measured in fourteen halogen-substituted methanes and compared with existing data. Binary collisions were found to be responsible for the excitation of vibrations, and all the gases were found to have a single relaxation time indicating a strong intermodal coupling. The probability, in a collision, of exciting or de-exciting molecular vibrations was found to depend upon the relative energy of approach of the molecules. Molecules with the same number of halogen substitutions resemble each other in this respect. The data suggest that the colliding molecules might form a complex molecule with a short lifetime during which energy exchange takes place readily.

I. INTRODUCTION

SINCE 1930, a number of investigators have used acoustic interferometers to measure the rates of vibrational excitation in diatomic and triatomic gas molecules. More recently, improvements in electronic circuits have made similar measurements possible in polyatomic gases which have very short relaxation times and whose regions of ultrasonic dispersion lie at rather high frequencies.

In this paper the excitation of vibrations in the halogen-substituted methanes is discussed and compared with a similar process in diatomic and triatomic molecules.

II. VIBRATIONAL EXCITATION BY COLLISIONS

A. Relaxation Theory

If a gas is composed of $\bar{n}$ molecules per unit volume, n_1 with vibrations in the first excited state, and n_0 with vibrations in the ground state, the continuous exchange of molecules between states 0 and 1 may be characterized by the equation

$$\frac{dn_1}{dt}=f_{01}n_0-f_{10}n_1, \tag{1}$$

in which f_{01} specifies the number of 0→1 transitions per ground state molecule per second and f_{10} the corresponding number of 1→0 transitions per excited molecule.

When the gas is in equilibrium, $dn_1/dt=0$, and therefore, according to the principle of detailed balancing, the total numbers of transitions in each direction are equal. At equilibrium

$$n_1=n_0e^{-h\nu/kT}, \tag{2}$$

and so

$$f_{01}=f_{10}e^{-h\nu/kT}, \tag{3}$$

in which ν is the frequency of molecular vibrations.

Since $\bar{n}=n_1+n_0$ at all times, (1) may be written:

$$\frac{dn_1}{dt}+n_1(f_{01}+f_{10})=f_{01}\bar{n}. \tag{4}$$

Since $\bar{n}$ is constant, the solution to this differential equation for nonequilibrium is

$$n_1=c_1+c_2e^{-(f_{01}+f_{10})t}. \tag{5}$$

The relaxation time of this process, when only the ground and first excited states are considered, can be seen to be

$$\theta=\frac{1}{f_{01}+f_{10}}. \tag{6}$$

θ is the time necessary for the departure from equilibrium to be reduced to $1/e$ of its initial value. Some

*Work supported by National Advisory Committee for Aeronautics.

† Present address: Remington Rand Inc., Engineering Research Associates Division, St. Paul, Minnesota.

authors have erroneously assumed that $h\nu/kT \gg 1$ and $f_{01} \ll f_{10}$, and hence that $\theta \simeq 1/f_{10}$. At vibrational frequencies less than $\nu = 1.5 \times 10^{13}$ sec^{-1} (corresponding to $\bar{\nu} = 500$ cm^{-1} in spectroscopic wave numbers), this assumption leads to error.

If the average number of collisions which a molecule makes per second is denoted by $\mathfrak{R}$, f_{01} and f_{10} may be written in terms of P_{01} and P_{10}, the probabilities that a molecule in the ground or first excited state will be excited or de-excited, respectively, in a collision:

$$f_{01} = P_{01}\mathfrak{R} \quad \text{and} \quad f_{10} = P_{10}\mathfrak{R}. \tag{7}$$

Z_{01} and Z_{10}, the reciprocals of P_{01} and P_{10}, will give the mean collision lifetimes of the ground and the first excited states, respectively. Substitution of (3) and (7) into (6) produces:

$$\theta = \frac{1}{\mathfrak{R}P_{10}(1+e^{-h\nu/kT})} = \frac{1}{\mathfrak{R}P_{01}(1+e^{h\nu/kT})}. \tag{8}$$

Therefore,

$$\frac{Z_{01}}{Z_{10}} = \frac{1+e^{h\nu/kT}}{1+e^{-h\nu/kT}}, \tag{9}$$

or

$$Z_{01} = Z_{10}e^{h\nu/kT}. \tag{10}$$

In case $h\nu \ll kT$ (not realizable at ordinary temperatures),

$$Z_{01} \simeq Z_{10}. \tag{11}$$

B. Prediction of P_{10}

Landau and Teller[1] have developed a theory which has been very successful in explaining energy transfer probabilities in relatively simple molecules. They write an expression for the probability of de-excitation of a vibrating molecule p_{10} in a single collision when the relative velocity of approach of the molecules lies within the range v to $v+dv$:

$$p_{10} = \alpha e^{-2\pi\nu s/v}. \tag{12}$$

α is a steric factor which gives the probability that a collision will find the molecules favorably oriented for excitation or de-excitation, s is the range of intermolecular forces, and ν the vibrational frequency. Bethe and Teller[2] integrate (12) over a molecular velocity distribution to obtain

$$\begin{aligned} P_{10} &= C\sigma e^{-\sigma}, \\ \sigma &= 0.090(\bar{\nu}s)^{\frac{2}{3}}(\mu/T)^{\frac{1}{3}}, \\ C &= 4/3^{\frac{1}{3}}\alpha. \end{aligned} \tag{13}$$

In (13), μ is the reduced molecular weight of the colliding molecules, $\bar{\nu}$ is the vibrational frequency in cm^{-1}, s is measured in units of 10^{-9} cm, and T is in degrees Kelvin.

Recent theory by Schwartz, Slawsky, and Herzfeld,[3] based on the approach of Zener, makes use of an exponential repulsion and a one-dimensional model. These authors arrive at a somewhat more complicated expression for P_{10} which, they point out, has essentially the same dependence upon μ, $\bar{\nu}$, and T as the theory of Landau and Teller. A later paper by Schwartz and Herzfeld[4] extends this technique to a three-dimensional model which slightly modifies this expression. Recently Fogg, Hanks, and Lambert[5] have measured the vibrational relaxation times of several halo-methane vapors and have calculated the number of collisions necessary to excite the lowest modes of vibration. At least four of these gases appear to fit an empirical relation of the form $P_{01} = e^{-X\nu_1}$ in which ν_1 is the frequency of the lowest vibrational mode and X is a proportionality constant characteristic of the particular group of gases. This suggests that the probability of vibrational excitation depends upon the energy of approach of the colliding molecules rather than upon the velocity of approach. An energy excitation theory, based on the above suggestion, will now be further developed by examination of the deactivation process.

It may be assumed that the probability p_{10} of de-exciting a vibrating molecule in a given collision can be written in terms of the relative energy of approach ϵ of the colliding molecules:

$$\begin{aligned} p_{10} &= \alpha \quad \epsilon \geq \epsilon^* \\ &= 0 \quad \epsilon < \epsilon^*. \end{aligned} \tag{14}$$

In the above equation, α is the steric factor, and ϵ^* is some minimum relative energy of approach which must be exceeded in order to produce de-excitation. If it is assumed that the mode of lowest frequency ν_1 is the first to be de-excited, ϵ^* may be written: $\epsilon^* = nh\nu_1$, where n is some constant.

Integration of (14) from $\epsilon = \epsilon^*$ to $\epsilon = \infty$ gives the probability of de-excitation of a single collision:

$$\begin{aligned} P_{10} &= \alpha e^{-\epsilon^*/kT}\left(\frac{\epsilon^*}{kT}+1\right) \\ &= \alpha e^{-nh\nu_1/kT}\left(\frac{nh\nu_1}{kT}+1\right). \end{aligned} \tag{15}$$

The corresponding probability for excitation may be written:

$$P_{01} = \alpha e^{-(n+1)h\nu_1/kT}\left(\frac{nh\nu_1}{kT}+1\right). \tag{16}$$

[1] L. Landau and E. Teller, Physik. Z. Sowjetunion **10**, 34 (1936).
[2] H. A. Bethe and E. Teller, "Deviations from thermal equilibrium in shock waves," Report X-117, Aberdeen Proving Ground (1942).
[3] Schwartz, Slawsky, and Herzfeld, J. Chem. Phys. **20**, 1591 (1952).
[4] R. N. Schwartz and K. F. Herzfeld, J. Chem. Phys. **22**, 767 (1954).
[5] Fogg, Hanks, and Lambert, Proc. Roy. Soc. (London) **A219**, 490 (1953).

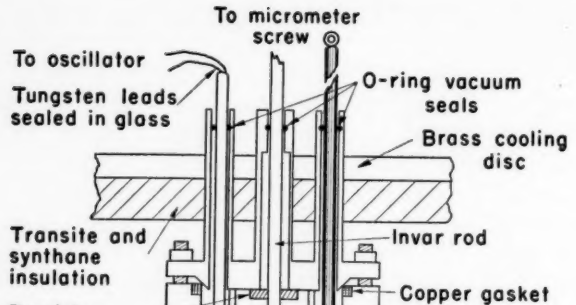

FIG. 1. Interferometer cup showing crystal mounting.

The above relations picture vibrational excitation and de-excitation as an involved process requiring a certain minimum energy of approach. It is tempting to assume that vibrational excitation and de-excitation take place only when a molecule is able to penetrate very deeply into the force field of another, the penetration requiring a certain amount of energy. It is even possible that the collision partners form a compound molecule with a very short lifetime, during which energy may pass readily between translational and vibrational degrees of freedom. The process of formation of the compound molecule would require a certain minimum amount of energy. It should be noted that the probabilities for the excitation and de-excitation processes differ by a factor $e^{-h\nu_1/kT}$. Fogg, Hanks, and Lambert[5] have apparently treated them as being the same.

Trace catalysts may still exist for gases which obey the energy excitation theory, but gases which catalyze diatomic and triatomic gases may not produce the same result in polyatomic gases. Hydrogen and helium apparently are strong catalysts in diatomic and triatomic gases, because they have a very high velocity at ordinary temperatures. In order to be a catalyst in a gas obeying the energy excitation theory, however, a gas molecule must be able to penetrate the force field of another easily, or form a compound molecule readily, and have a fairly large steric factor.

III. DISPERSION OF SOUND

When sound of high frequency is transmitted adiabatically through a gas whose relaxation time is of the same order as the period of an acoustic vibration, a dispersion in the velocity occurs together with a high anomalous absorption. This dispersion, caused by the failure of the vibrational and translational energies to maintain equilibrium with each other, provides a method to measure accurately the vibrational relaxation time of a gas.

The square of the velocity of sound in an ideal gas which has a single relaxation time is developed by Richards[6] and other authors:

$$V_{\text{ideal}}^2=\frac{RT}{M}\left(1+R\frac{C_0+\omega^2\theta^2C_\infty}{C_0^2+\omega^2\theta^2C_\infty^2}\right). \tag{17}$$

In the above, ω is 2π times the acoustic frequency, R is the universal gas constant, M is the molecular weight, and C_0 and C_∞ are the heat capacities below and above the dispersive region, respectively. The inflection point of the curve represented by (17) can be found by differentiation:

$$\omega_{\text{inf}}=\frac{C_0}{\theta C_\infty}. \tag{18}$$

A similar equation may be written for a gas which obeys

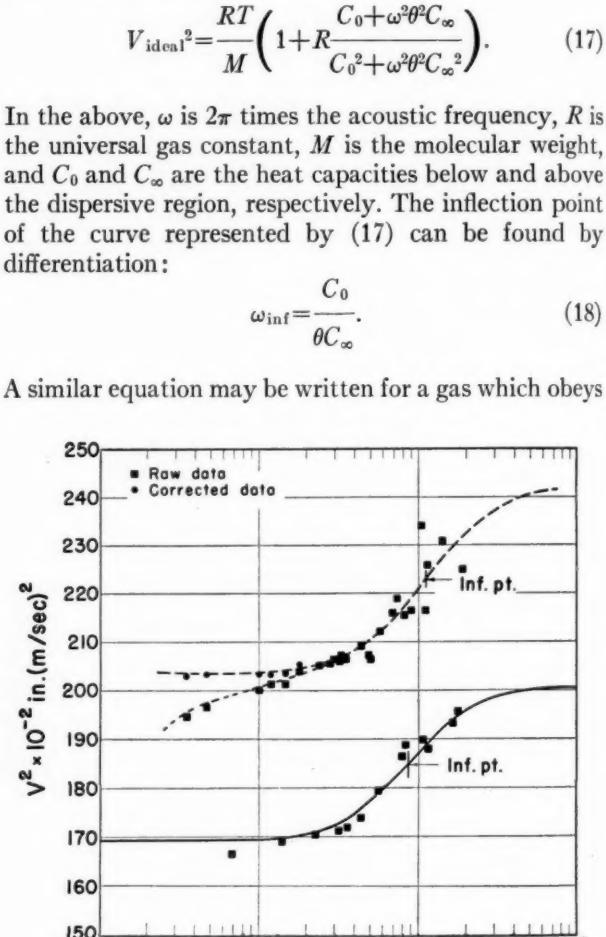

FIG. 2. Velocity dispersion in $CBrClF_2$ (——) and CCl_3F (- - -).

the equation of state of Beattie and Bridgman:

$$V_{BB}^2=\frac{1}{M}[RT+2\bar\rho(RTB_0-A_0)+3\bar\rho^2(A_0a-RTB_0b)]$$
$$+\frac{R^2T}{M}[1+2\bar\rho B_0+\bar\rho^2(B_0^2-2B_0b)]$$
$$\times\left[\frac{C_0+\omega^2\theta^2C_\infty}{C_0^2+\omega^2\theta^2C_\infty^2}\right], \tag{19}$$

in which A_0, a, B_0, and b are the Beattie-Bridgman constants, and $\bar\rho$ is the density. Equations similar to (19) have been developed by Beyer[7] and others using van der Waals' equation of state.

[6] W. T. Richards, Revs. Modern Phys. **11**, 36 (1939).
[7] R. T. Beyer, J. Acoust. Soc. Am. **24**, 714 (1952).

A. Multiple Dispersion

If different modes of vibration were excited with different relaxation times, or if all vibrational transitions did not occur with the same frequency as those between the ground state and the first excited state, a second relaxation time might result. That all transitions between the states of a given mode occur with the same relaxation time has been shown theoretically by Landau and Teller.[1] If, however, the coupling between different modes of vibration is so weak that they must be excited independently by collisions and therefore possess different relaxation times, a step-shaped velocity dispersion curve would result.

Pielemeier[8] and Buschmann and Schäfer[9] have reported a possible second dispersive region in carbon dioxide, but unfortunately at room temperature the

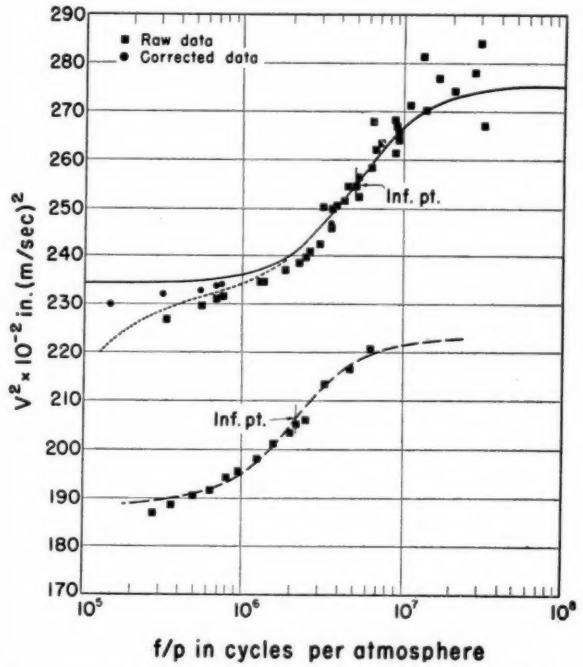

FIG. 3. Velocity dispersion in CCl_2F_2 (——) and $CBrF_3$ (– – –).

degenerate deformation mode contributes nearly all the specific heat. Any steps which might exist on the velocity dispersion curve due to the other modes would be difficult to detect. Alexander and Lambert[10] found three dispersive regions in acetaldehyde, but a later article by Lambert and Rowlinson[11] points out that the multiple dispersions are due to errors in calculation resulting from an ungrounded assumption with respect to dimerization.

Detection of multiple dispersion due to a lack of

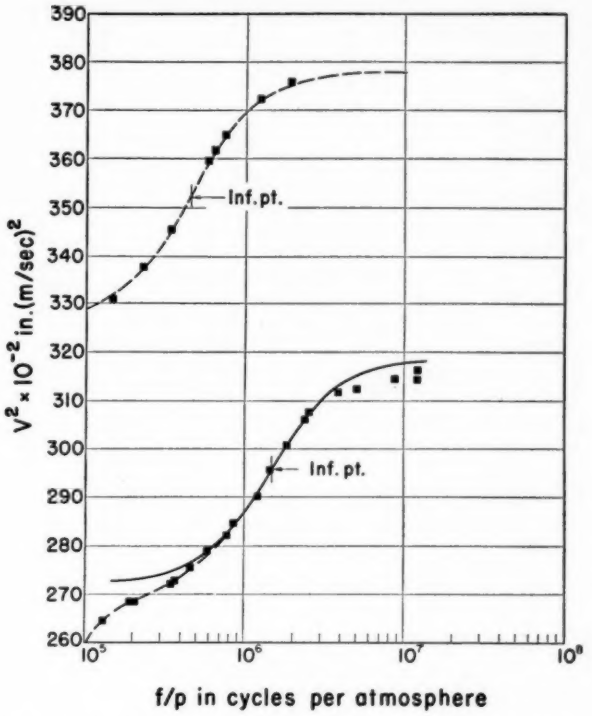

FIG. 4. Velocity dispersion in $CClF_3$ (——) and CF_4 (– – –).

intermodal coupling, if it exists, might be most probable in molecules such as the halogen-substituted methanes having several modes of low frequency which can be excited at room temperatures. On the other hand, if intermodal coupling is strong enough so that energy is transferred readily from one mode to another, only a single relaxation time will be observed. Presumably this will be the relaxation time of the mode of lowest frequency.

B. Multiple Collisions

In general, a certain average number of collisions are required to excite or de-excite the molecular vibrations in a given gas. Since the number of binary collisions is proportional to the pressure of the gas, the relaxation time will be inversely proportional to the pressure when binary collisions are responsible for vibrational excitation; if triple collisions are primarily responsible, the relaxation time will be inversely proportional to the square of the pressure, and so forth.

In equations dealing with acoustic dispersion, the independent variable is invariably $\omega\theta$ rather than ω. Hence, if the relaxation time θ is inversely proportional to pressure, the dispersion curve may well be drawn with $\log f/p$ as the abscissa instead of $\log f$. This is a great advantage in experimental work since it provides a method of obtaining a continuous range of "frequencies" without changing the frequency of the sound source. Of course it must first be ascertained which type of collision is responsible for vibrational excitation so that the correct pressure dependence is used.

[8] W. H. Pielemeier, J. Acoust. Soc. Am. **15**, 22 (1943).
[9] K. F. Buschmann and K. Schäfer, Z. physik. Chem. **B50**, 73 (1941).
[10] E. A. Alexander and J. D. Lambert, Proc. Roy. Soc. (London) **A179**, 499 (1942).
[11] J. D. Lambert and J. S. Rowlinson, Proc. Roy. Soc. (London) **A204**, 424 (1950).

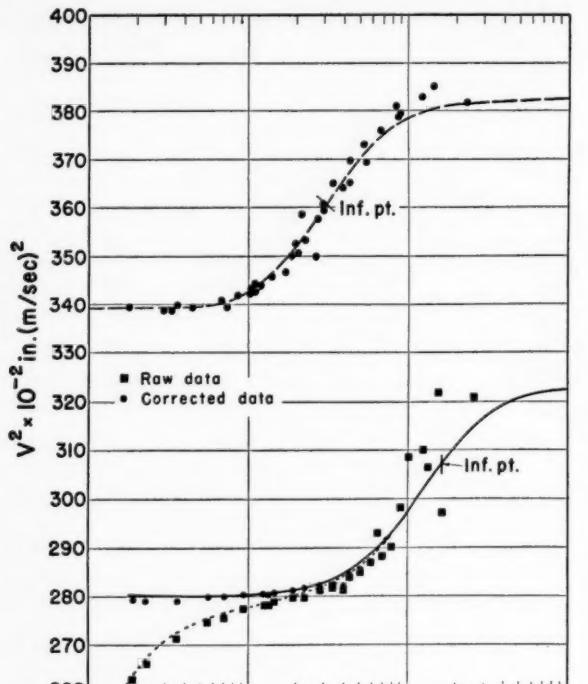

FIG. 5. Velocity dispersion in $CHCl_2F$ (——) and $CHClF_2$ (– – –).

No conclusive evidence has been presented supporting any importance of collisions of orders above the second. Walker[12] suggested that certain data of previous investigators, involving COS with added quantities of helium and argon, might be interpreted on the basis that triple collisions are of greater importance than the binary type. Walker, Rossing, and Legvold[13] later report that triple collisions are not important in the excitation by He, A, and N_2 of N_2O, which is very similar in structure to COS.

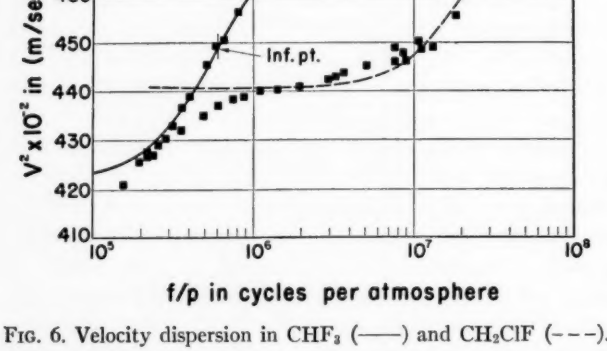

FIG. 6. Velocity dispersion in CHF_3 (——) and CH_2ClF (– – –).

[12] R. A. Walker, J. Chem. Phys. **19**, 494 (1951).
[13] Walker, Rossing, and Legvold, "The role of triple collisions in the excitation of molecular vibrations in nitrous oxide," Natl. Advisory Comm. Aeronaut. Tech. Notes 3210 (1954).

IV. EXPERIMENT

The velocity of sound has been measured by means of an interferometer of the Pierce type. A cross section of the acoustic chamber used to measure wavelengths is shown in Fig. 1. A gold-plated, X-cut quartz crystal is clamped in its nodal plane and is driven at its resonant frequency by an electrical oscillator. An optically flat reflector is driven by a micrometer screw having a least count of 0.001 mm. The crystal and reflector are maintained parallel within 0.01 wavelength by three leveling screws. The chamber and the gas handling system are vacuum tight.

The oscillator circuit is a variation of the Pierce circuit and drives the crystal at a very constant frequency and amplitude. The frequency of the crystal is determined by heterodyning the output of the oscillator with the output of some convenient broadcast station to produce a beat note in the audiofrequency range. Most of the measurements in this paper were made using a 300 kc crystal, although a 1000 kc crystal was sometimes employed. Changes in the electrical impedance of the crystal, due to changes in the acoustic field as the reflector moves, were detected electronically. This scheme of detection proved to be much more sensitive than the usual method of metering the grid or plate circuit of the oscillator. A similar method of detection has been employed in a two crystal system by Loomis and Hubbard[14] and others.

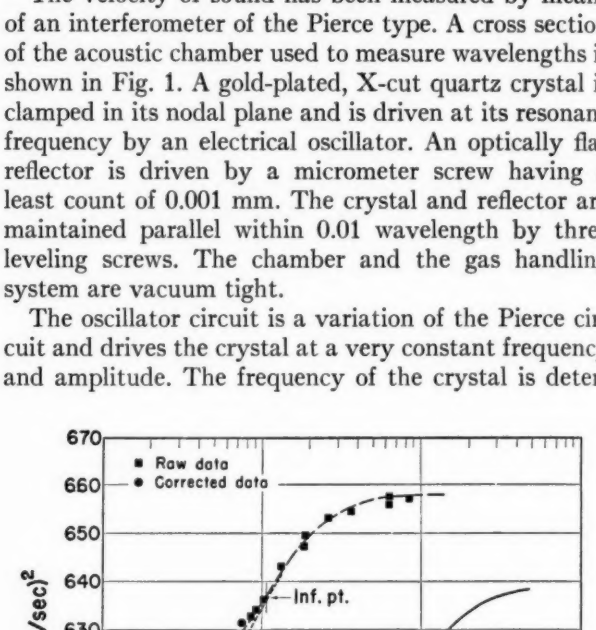

FIG. 7. Velocity dispersion in CH_2F_2 (——) and CH_3Cl (– – –).

The velocity of sound was measured at a variety of f/p ratios and the values of V^2 plotted in Figs. 2–9.

[14] A. L. Loomis and J. C. Hubbard, J. Opt. Soc. Am. and Rev. Sci. Instr. **17**, 295 (1928).

TABLE I. Relaxation times and collision lifetimes.

Gas	$\bar{\nu}_1$ cm^{-1}	$\bar{\nu}_1 M^{\frac{1}{3}}$	C_1 cal/mol °K	C_{vib} cal/mol °K	V_0^2 ideal $\times 10^{-2}$ m/sec	$\theta \times 10^6$ sec	$\theta_1 \times 10^6$ sec	$\mathcal{R} \times 10^{-9}$ sec^{-1}	Z_{10}
CH_3Br	611	328	1.03	2.26	326.2	7.5±0.3	3.4 ±0.1	10.79±0.22	386±14
$CHClF_2$	369	227	1.45	5.99	336.4	9.5±0.7	2.3 ±0.2	9.98±0.20	268±24
CH_3Cl	732	300	0.78	1.84	614.0	20.4±1.1	8.6 ±0.5	10.91±0.22	966±67
CCl_3F	244	202	4.05	10.63	203.8	4.0±0.4	1.5 ±0.2	11.79±0.24	234±31
$CBrClF_2$	200	188	1.85	10.24	169.3	5.0±0.4	0.9 ±0.1	9.66±0.48	121±15
CF_4	437	256	2.93	6.91	327.2	75.6±0.8	32.1 ±0.3	6.84±0.34	2460±125
CH_2F_2	532	245	1.19	2.32	594.4	3.0±0.3	1.5 ±0.2	9.81±0.49	159±24
CH_2ClF	358	206	1.56	3.46	441.0	1.0±0.1	0.45±0.05	11.20±0.56	60±7
$CClF_3$	356	237	3.16	8.16	272.4	23.9±0.6	9.3 ±0.2	11.28±0.23	1240±37
$CHCl_2F$	274	198	1.72	6.76	281.9	2.5+0.4	0.6 ±0.1	11.48±0.57	89±14
CHF_3	508	263	2.48	4.78	422.1	47.9±1.8	24.9 ±0.9	8.34±0.42	2260±140
CCl_2F_2	260	201	1.76	8.63	234.4	7.8±0.6	1.6 ±0.1	10.31±0.21	212±14
CBr_2F_2	165	179	1.88	10.55	133.2	2.9±0.3	0.50±0.05	9.34±0.47	68±8
$CBrF_3$	297	239	4.24	9.84	188.6	19.6±0.1	8.4 ±0.1	8.05±0.40	840±43

V_{ideal}^2 was plotted for each gas using (17) with an arbitrary value of θ. This curve was then shifted along the f/p axis until it best fit the experimental data, since the effect of changing θ is merely to shift the entire curve along this axis. For those gases in which the dispersive region occurred at low frequencies and for which the Beattie-Bridgman constants were known, the V_{BB}^2 curve has been drawn as a dotted line using (19). The experimental values of V^2 were then corrected to ideal gas behavior by adding the correct value of $V_{ideal}^2 - V_{BB}^2$. Nearly all the values of V^2 are the result of ten independent determinations of wavelength.‡

The gases used in the experiment were of the highest purity available. $CHClF_2$, $CHCl_2F$, CCl_2F_2, CH_3Cl, CH_3Br, CCl_3F, and $CClF_3$ were purchased from the Matheson Company. $CBrF_3$, CH_2ClF, CH_2F_2, CBr_2F_2, $CBrClF_2$, CF_4, and CHF_3 were furnished by the Jackson Laboratory of E. I. du Pont de Nemours and Company. Several of the above gases were stored in cylinders as gas over liquid; these were withdrawn in their liquid phase to minimize contamination by air and noncondensible gases. Others were liquified, by use of the liquid nitrogen cold trap, and then evaporated into the system after pumping off all noncondensible vapor. The close fit of the low-frequency experimental data to the calculated values of V_0^2 demonstrates the high degree of purity of the gases used.

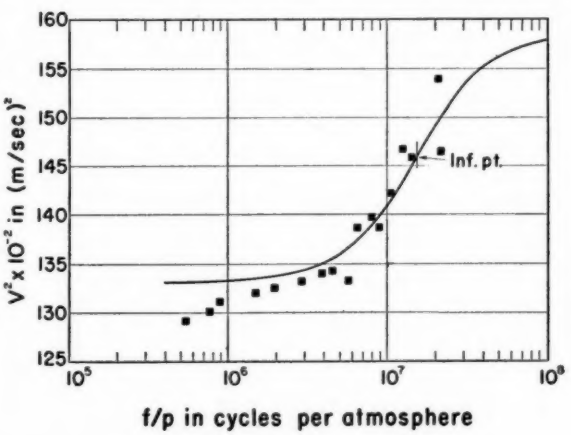

FIG. 8. Velocity dispersion in CBr_2F_2.

‡ *Note added in proof.*—The inflection point for $CHCl_2F$ in Fig. 5 is obviously in error. It should be at $V^2 = 302.5 \times 10^2$ m^2/sec^2. The correct data appear in Table I. Point 10 in Fig. 11 would now move up on the curve.

Since it was observed that none of the dispersion curves showed any evidence for the existence of multiple relaxation times, it was assumed that the lowest vibration was excited with its characteristic relaxation time, and that the energy passed freely to the other modes. Thus the relaxation time of the lowest mode θ_1 should be given by the expression

$$\theta_1 = \theta \frac{C_1}{C_{vib}}, \tag{20}$$

in which C_1 is that part of C_{vib} corresponding to the lowest vibrational mode. Values of θ_1 were calculated from (20) and appear in Table I as well as corresponding values of the collision lifetime Z_{10} and the collision rate per molecule $\mathcal{R}$.

V. RESULTS

A. Experimental Results

It may be noted in Figs. 2–9 that none of the gases measured showed multiple dispersive regions. This

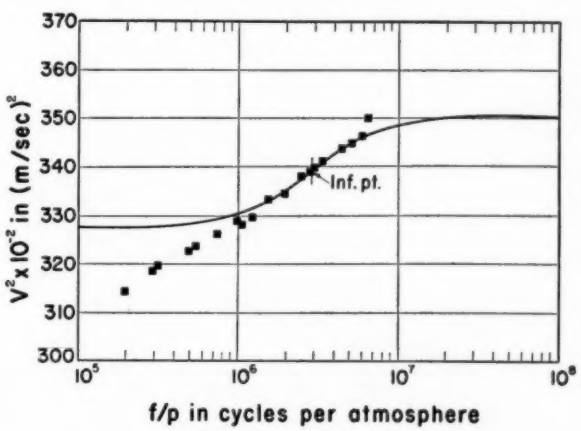

FIG. 9. Velocity dispersion in CH_3Br.

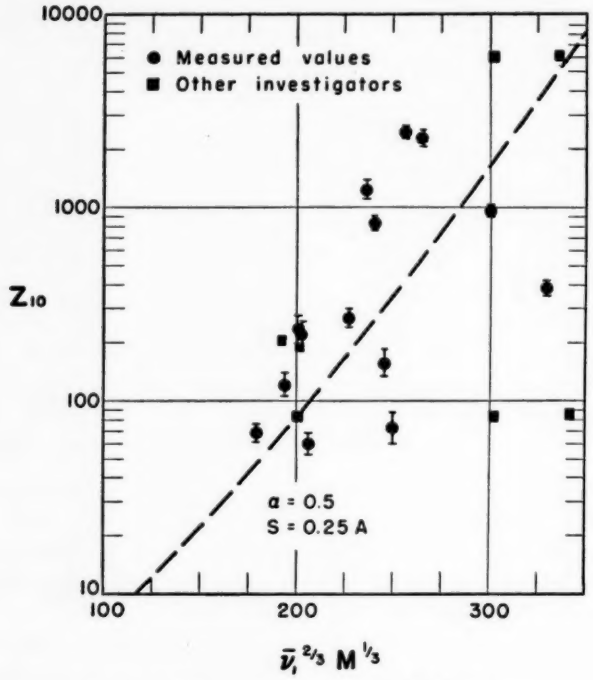

FIG. 10. Z_{10} interpreted by Landau-Teller theory.

indicates that intermodal coupling is relatively strong in these molecules, and the assumption made by the use of (20) is justified. Furthermore, since the use of f/p along the axis of abscissas yields the proper form of dispersion curve, the excitation and de-excitation of molecular vibrations must be brought about principally by binary collisions.

Following the result of Landau and Teller given by (13), Z_{10} has been plotted against $\bar{\nu}_1^{\frac{1}{3}}M^{\frac{1}{3}}$ in Fig. 10. Theoretical curves were drawn using various values of s and α. The particular curve shown in Fig. 10 has $s=0.25$ A and $\alpha=0.5$. This value of s is about $\frac{1}{8}$ the diameter of the colliding molecules and therefore is not reasonable. A similar curve drawn with $s=1$ A or more will not fit the data regardless of the α used. It therefore appears that the theory of Landau and Teller does not fit the de-excitation of molecular vibrations in these gases.

In Fig. 11, Z_{10} has been plotted against $\bar{\nu}_1$ in accordance with (15) and the energy excitation theory. Curves have been drawn using the values $\alpha=1/12$, $n=1.5$, 1.8, 2.8, and 3.8. The value of n to be used apparently depends upon the number of hydrogen atoms replaced from the methane molecule. On the other hand, the single value of α may be used regardless of the molecule considered. The quantity $nh\nu_1$ gives the minimum energy of approach necessary to excite or de-excite the vibrations of the molecule. This is presumably the energy necessary for the molecules to penetrate deeply into each other's force fields or to form a compound molecule as previously suggested.

Fogg, Hanks, and Lambert[5] have measured the relaxation times of some of the halogen-substituted methanes. Their values for Z_{10} were computed from their relaxation data by making the assumption that $h\nu \gg kT$ and hence that $Z_{10} \simeq \mathcal{R}\theta_1$. At values of $\bar{\nu}<500$ cm^{-1}, this is not true and leads to error in Z_{10} at low frequencies. In accordance with (8), their values for Z_{10} have been multiplied by a factor $1+e^{-h\nu_1/kT}$. The values of Z_{10}, thus corrected, are recorded in Table II.

The above data were taken at temperatures of about 373°K. The temperature correction predicted by (15) has been used to correct Z_{10} to 300°K; these values are

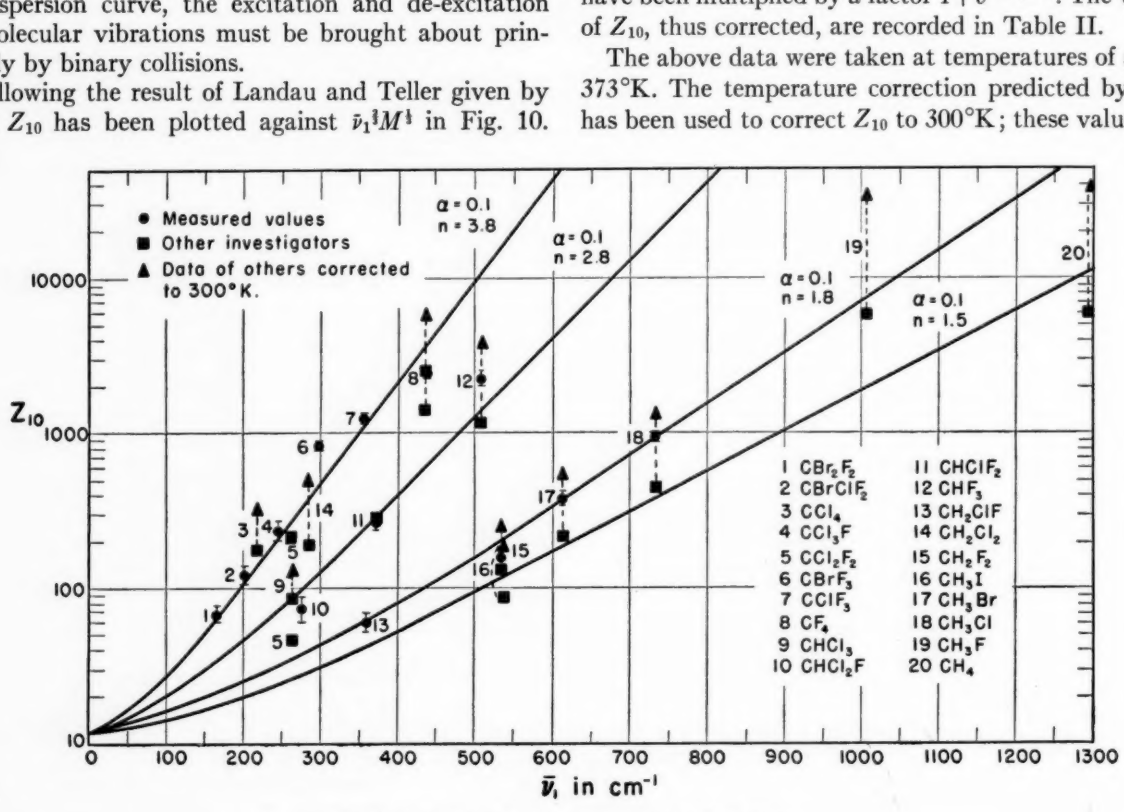

FIG. 11. Z_{10} interpreted by energy excitation theory.

TABLE II. Data of other investigators.

Gas	Investigator	T °K	$\theta \times 10^6$ sec	Z_{10}	Z_{10} $T=300°K$	$\bar{\nu}_1$ cm^{-1}	$\bar{\nu}_1[M]$
CH_3I	Fogg, Hanks, Lambert	373	4.5	86	176	533	342
$CHCl_3$	Fogg, Hanks, Lambert	383	2.8	83	139	260	200
CH_2Cl_2	Fogg, Hanks, Lambert	373	8.4	204	466	283	192
CH_3F	Fogg, Hanks, Lambert	373	320	6070	29 400	1048	336
CCl_4	Fogg, Hanks, Lambert	373	8.3	191	348	218	197
CH_3Br	Fogg, Hanks, Lambert	373	10	202	468	611	328
CH_2F_2	Fogg, Hanks, Lambert	373	5.5	136	278	532	248
CHF_3	Fogg, Hanks, Lambert	373	42	1200	3720	508	263
CH_3Cl	Fogg, Hanks, Lambert	373	18	424	1200	732	300
	Griffith	295	20.2	956			
	Petralia	287	20.2	956			
CF_4	Fogg, Hanks, Lambert	373	66	1580	6210	437	256
	Byers	293	76	2480			
CH_4	Eucken and Aybar	382	84	6000	36 000	1306	302
CCl_2F_2	Huber and Kantrowitz	297	2	49		260	201
	Griffith	292	8	218			
$CHClF_2$	Griffith	294	10	282		369	227

also recorded in Table II. The corrections thus calculated, however, were invariably larger than the differences between these points and the calculated Z_{10} curves. The values of Z_{10} for 373°K and also the values predicted for 300°K are shown in Fig. 11.

Several other authors have measured relaxation times in some of the halogen-substituted methanes. Byers,[15] Eucken and Aybar,[16] and Petralia[17] have used acoustic interferometers to measure relaxation times; Griffith[18] and Huber and Kantrowitz[19] have made measurements using Kantrowitz-type impact nozzles. Their data are also reported in Table II, and the corresponding values of Z_{10} are plotted in Fig. 11. Where the measurements were made at temperatures more than a few degrees removed from 300°K, the data are corrected to this temperature by use of (15).

The fact that use of (15) gives too large temperature corrections might suggest that the steric factor α is a function of temperature. It is reasonable to assume that α, being a geometrical probability, is dependent upon the speed at which the molecules are rotating, which in turn is a function of temperature. The period of a rotation of a typical molecule is 10^{-12} second, which is of the same order as the duration of a molecular collision.

VI. CONCLUSIONS

On the basis of the data reported in this paper, the following conclusions may be drawn:

1. Intermodal coupling is so strong in the halogen-substituted methanes, that once the vibrational mode of the lowest frequency is excited, the energy passes readily into the other modes.

2. Only binary collisions are important in the excitation of vibrations in the halogen-substituted methanes within the limits of observation.

3. The probability, in a given collision, of exciting or de-exciting molecular vibrations in the halogen-substituted methanes appears to depend upon the relative energy of approach of the colliding molecules rather than upon their relative velocity as the Landau-Teller theory predicts. In particular, the probability of excitation or de-excitation appears to be negligible unless the relative energy of approach exceeds $\epsilon^* = nh\nu_1$, where n is characterized by the number of hydrogen atoms replaced. ν_1 is the lowest vibrational frequency.

4. The excitation of vibrations in polyatomic organic molecules may be a complex process involving the formation of a compound molecule with a very short lifetime.

5. The steric factor probably depends upon temperature through its dependence upon rotational velocity.

VII. ACKNOWLEDGMENTS

The authors wish to thank Mr. Robert Amme and Mr. Sigurds Arajs for their assistance in taking the large amount of data required. They also wish to thank Dr. R. S. Hansen of the Iowa State College Department of Chemistry for his very enlightening suggestions. Several of the test gases were made available by the Jackson Laboratory of the E. I. du Pont de Nemours Corporation, and special thanks are due Dr. R. C. McHarness of that laboratory for his courtesy.

[15] W. H. Byers, J. Chem. Phys. **11**, 348 (1943).
[16] A. Eucken and S. Aybar, Z. physik. Chem. **B46**, 195 (1940).
[17] S. Petralia, Nuovo cimento **9**, 351 (1952).
[18] W. Griffith, J. Appl. Phys. **21**, 1319 (1950).
[19] P. W. Huber and A. Kantrowitz, J. Chem. Phys. **15**, 275 (1947).

Theory of Normal Paraffin Liquids

MICHIO KURATA AND SIN-ITI ISIDA*
Department of Industrial Chemistry, Faculty of Engineering, Kyoto University, Kyoto, Japan
(Received October 5, 1954)

A hole theory of *n*-paraffin liquids, which is the same in mathematical form as Flory's theory of polymer solutions, is developed to derive the relationships between the physical constants and the number of carbon atoms *n*. If the number of segments in a molecule is equal to $n^{\frac{1}{2}}$, quantitative agreements between the theory and the observations can be shown for the critical temperature, the critical pressure, the boiling temperature and the heat of vaporization. It is also possible to give theoretical foundations for some empirical rules recently proposed by Grunberg and Varshni.

INTRODUCTION

ON the basis of Egloff's critical review[1] of physical constants of hydrocarbons, many attempts have recently been made by Grunberg,[2,3] Mitra,[4] and Varshni[5,6] to establish the relationships between the critical constants and the boiling point and the number of carbon atoms of *n*-paraffins. All of these, however, are purely empirical relationships and the theoretical evidences are not sufficiently obvious.

As is well known, as the number of carbon atoms increases, the physical constants of the *n*-paraffins (C_nH_{2n+2}) show increasing deviation from the values expected from the law of corresponding states; for example, both the ratio of the boiling temperature to the critical temperature and the Kamerlingh-Onnes constant increase with the number of carbon atoms, while their values for methane coincide well with those for the ideal monoatomic liquids such as argon. In this connection, it seems reasonable to consider that the deviation of this kind mainly originates in the change of molecular shape from sphere to rod, because the effect of the molecular association can be entirely neglected in the present case.

In this paper, we shall develop a theory of the *n*-paraffin liquids based on the lattice model, and discuss the critical constants, the boiling point and the heat of vaporization in correlation with the number of carbon atoms. The Flory expression for the configurational entropy[7] which have been presented for the solution of flexible chain polymers seems to be effectively applicable to the present problem with only slight modifications.

LIQUID MODEL AND THE EQUATION OF STATE

In order to obtain the simple analytical results we shall adopt a lattice model which is usually called the hole theory of liquids. In the hole theory of the usual form, the entire system is divided into *cells* whose volume is approximately the same as that of a molecule, and the partition function of the system is set up assuming that the probability of simultaneous entries of more than two molecules into one cell can entirely be neglected, because of a repulsive force between molecules. This model is fit to deal with monoatomic liquids such as argon, and polyatomic-molecular liquids such as methane, the shape of which is regarded as a sphere; but this model is not fit for applying to liquids of rod-like molecules such as the *n*-paraffins. We, therefore, shall employ in this paper a modified model of liquids as stated below in an attempt to discuss effects which arise as a result of the deviation from sphere in the shape of molecule.

At the outset, choosing a size of a cell which is independent of the chain length of the molecules, let τ represent the volume of a cell. The τ is assumed to be of a volume somewhat larger than that of a methane molecule. Consequently, one molecule of *n*-paraffin having the number n of carbon atoms occupies some consecutive cells, the number of which is denoted by x. If there are N molecules in the entire system of the volume V, the number of vacant cells which are conveniently called "*holes*" is given by $\{(V/\tau)-xN\}$.

In consideration of the aforementioned, the system now in question will be mathematically the same as a solution consisting of N rod-like polymers and $\{(V/\tau)-xN\}$ single-site solvent molecules. Therefore, if we neglect for a while the difference between short and long chains, the theory of the solution of flexible chain polymers already presented can be applied to the present system without any essential alteration. If, for the sake of simplicity, the Flory approximation[7] is adopted in calculating the configurational entropy, the Helmholtz free energy F of the present system will be written as follows:

$$F=Nf+kT[\{(V/\tau)-xN\}\ln\{1-(\tau xN/V)\}+N\ln(\tau xN/V)]+(z\psi/2)(V-\tau xN)(\tau xN/V), \quad (1)$$

where k is the Boltzmann constant, T the absolute temperature, z the number of the nearest neighbor cells, f the free energy related to the intramolecular freedoms, and ψ represents the increase of the free energy in the

* Present address: Technical Division, Asahi-Dow Company, Nobeoka, Miyazaki, Japan.

[1] G. Egloff, *Physical Constants of Hydrocarbons* (Reinhold Publishing Corporation, New York, 1939).

[2] L. Grunberg and A. H. Nissan, Nature **161**, 170 (1948); Trans. Faraday Soc. **44**, 1013 (1948).

[3] L. Grunberg, J. Chem. Phys. **22**, 157 (1954).

[4] S. S. Mitra, J. Chem. Phys. **21**, 2234 (1953); **22**, 156 (1954).

[5] Y. P. Varshni, J. Chem. Phys. **21**, 2235 (1953).

[6] Y. P. Varshni, J. Chem. Phys. **21**, 1400 (1953); **22**, 150 (1954); Y. P. Varshni and S. N. Srivastava, J. Chem. Phys. **22**, 349 (1954).

[7] P. J. Flory, J. Chem. Phys. **12**, 425 (1944).

TABLE I. Critical temperature, the Kamerlingh-Onnes constant, and the boiling temperature of the n-paraffins.

n	T_c (°K) calculated values Eq. (11)	Eq. (21)	Eq. (18)	T_c (°K) obs.	P_c (atmos) obs.	nP_c/T_c	kT_c/P_cv_c calc	obs.	obs./calc	T_b (°K) Eq. (33)	obs.
1	203.8	204.4	239.2	190.7	45.8	0.240	2.59	3.44	1.33	111.5	120.1
2	300.6	299.2	322.4	305.3	48.8	0.320	2.64	3.56	1.35	184.7	183.3
3	369.3	368.1	381.7	368.8	43.0	0.349	2.67	3.64	1.36	230.9	232.7
4	423.5	422.8	429.2	426.2	36.0	0.338	2.69	3.71	1.38	272.6	274.3
5	468.4	468.4	469.7	470.4	33.04	0.351	2.71	3.76	1.39	309.1	310.4
6	506.8	507.4	505.1	508.0	29.63	0.350	2.72	3.83	1.41	342.0	342.7
7	540.5	541.4	536.8	540.0	26.89	0.348	2.73	3.86	1.41	371.5	371.9
8	570.5	571.4	565.3	569.4	24.66	0.346	2.74	3.88	1.41	397.6	398.7
9	597.4	598.4	591.7	595.4	22.86	0.345	2.75	3.88	1.41	423.6	423.4
10	621.9	623.1	616.1	619.3	21.24	0.343	2.75	3.89	1.41	447.0	446.2
11	644.3	645.6	639.4	642.6	19.92	0.341	2.76	3.90	1.41	470.0	467.7
12	664.9	666.2	660.9	663.8	18.59	0.336	2.76	3.90	1.41	489.0	488.0
13	684.0	684.9	681.2	683.2	17.55	0.334	2.77	3.90	1.41	507.0	506.8
14	702.2	702.7	700.8	701.0	16.56	0.330	2.77	3.90	1.41	525.5	525.2
15	718.9	718.9	718.9	717.6	15.75	0.328	2.78	3.90	1.40	543.5	542.0
16	734.8	734.2	736.9	734.3	15.10	0.329	2.78	3.90	1.40	560.5	558.3
17	749.6	748.5	753.6	749.3	14.41	0.327	2.79	3.90	1.40	576.0	573.7
18	763.4	762.2	769.8	763.2	13.83	0.326	2.79	3.90	1.40	590.0	588.6
19	777.0	774.6	785.5	776.0	13.43	0.329	2.79	3.90	1.40	603.0	602.4

following rearrangement:

$$\text{(Segment pair)}+\text{(Hole pair)} \rightarrow 2\times\text{(Segment}-\text{hole pair)}. \quad (2)$$

Here the term "segment" means an element of the hydrocarbon chain, the size of which is equal to that of a cell, and the "segment pair" means a pair of neighboring cells, each of which is occupied by a segment. Letting v represent the volume V/N per molecule, the pressure P and the chemical potential μ of a molecule may be written as

$$P=-\left(\frac{\partial F}{\partial V}\right)_{T,N}=-\frac{kT}{\tau}\left\{\ln\left(1-\frac{x\tau}{v}\right)+(x-1)\frac{\tau}{v}\right\}-\frac{z\psi}{2\tau}\left(\frac{x\tau}{v}\right)^2, \quad (3)$$

$$\mu=\left(\frac{\partial F}{\partial N}\right)_{T,V}=f+kT\left\{\ln\left(\frac{x\tau}{v}\right)-x\ln\left(1-\frac{x\tau}{v}\right)-(x-1)\right\}+\frac{zx\psi}{2}\left(1-\frac{2x\tau}{v}\right). \quad (4)$$

Of course, the equation of state (3) reduces to that of the ideal gas for large v.

CRITICAL CONSTANTS

As is well known, the critical point of liquids is given by

$$(\partial P/\partial v)_T=0, \quad \text{and} \quad (\partial^2 P/\partial v^2)_T=0. \quad (5)$$

The substitution of Eq. (3) in Eq. (5) gives

$$T_c=(z\psi_c/k)\{x/(x^{\frac{1}{2}}+1)^2\}, \quad (6)$$

$$\tau x/v_c=1/(x^{\frac{1}{2}}+1), \quad (7)$$

and

$$\tau P_c/kT_c=\ln\{1+(1/x)^{\frac{1}{2}}\}-\{(2x^{\frac{1}{2}}-1)/2x\}, \quad (8)$$

where T_c, P_c, and v_c represent the critical temperature, the critical pressure and the critical volume per molecule, respectively, and ψ_c represents the value of the interaction parameter ψ at the critical temperature. These results are identical with the ones which have already been presented for the consolute critical point of chain polymer solutions.

Now, denoting the energy and the entropy terms in ψ by ϵ and s, respectively, and assuming, for simplicity's sake, that both ϵ and s are independent of the temperature, we can put[8]

$$\psi=\epsilon-Ts, \quad \text{and} \quad \psi_c=\epsilon-T_cs. \quad (9)$$

The substitution of this equation in Eq. (6) yields the following expression for the critical temperature:

$$1/T_c=\{(k/z\epsilon)+(s/\epsilon)\}+(2k/z\epsilon)\{(1/2x)+(1/x^{\frac{1}{2}})\}. \quad (10)$$

As is shown in Table I, the observed values of T_c agree very well with that derived from the following expression which is the same in form as Eq. (10):

$$1/T_c=0.000543+0.002909\{(1/2n)+(1/n^{\frac{1}{2}})\}. \quad (11)$$

[8] It being unnecessary to take into consideration the interaction energy of the "hole pair" and the "segment-hole pair," the ϵ in Eq. (9) can be regarded as energy sufficient to separate one segment pair, while the s involves contributions from a change in the free volume of segment associated with the separating process of the segment pair. (The s is also supposed to involve a correction of the Flory mixing entropy.)

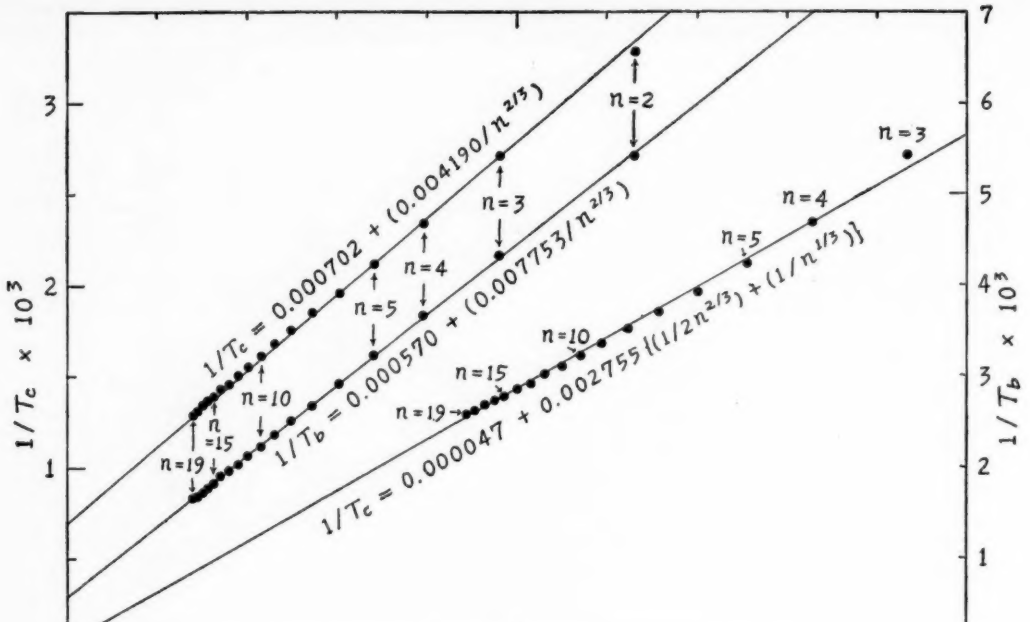

FIG. 1. Critical temperature T_c and the boiling temperature T_b at 1 atmos. Circles show the observed values.

If the neglect of the difference between short and long chains leads us to no critical error in the calculation of thermodynamic properties, it seems to be reasonable to assume that $x=n$. The good correspondence of Eq. (11) with the experimental data seems to apparently prove the above simple assumption. There is, however, an important defect in this assumption, because, if $x=n$, the density at the critical point ρ_c ($\propto n\tau/v_c$) expected from Eq. (7) will decrease to zero with increasing n in contradiction to the observation that ρ_c is almost the same for all the n-paraffins. This constancy of ρ_c seems to be more estimable as judgment data of the theory than the linearity of $1/T_c$ such as Eq. (11), therefore we must modify the simple assumption that $x=n$, even though it yields the excellent empirical equation (11).

Now let us assume that $x^{\frac{1}{3}}=n$ and examine the results derived from the assumption by making comparison with the experimental data. The basis of this assumption will be discussed later.

Substituting this in Eq. (7), and denoting by ρ_0 the density of the cell occupied by the segment, we obtain

$$\rho_c=n\tau\rho_0/v_c=\rho_0 n^{\frac{1}{3}}/(n^{\frac{1}{3}}+1), \tag{12}$$

which does not conflict with the observation mentioned above.

Expanding Eq. (8) in a power series of $1/x$, and setting $x=n^{\frac{1}{3}}$, we find

$$\tau P_c/kT_c=1/3x^{\frac{1}{3}}=1/3n, \tag{13}$$

or

$$nP_c/T_c=k/3\tau. \tag{14}$$

The requirement of the equation that the ratio, nP_c/T_c, is to be independent of the carbon number is satisfied with good accuracy by the experimental data as is shown in Table I, and we can find

$$k/3\tau=0.337 \text{ (atmos. cm}^{-2}\text{ degree}^{-1}). \tag{15}$$

In a crude treatment such as the present theory, it being justified to think that the molecular weight M is also proportional to the number of carbon atoms, Eq. (15) may be rewritten as

$$MP_c/T_c=\text{Constant independent of } n. \tag{16}$$

This is nothing but the expression recently proposed by Grunberg.[3]

The combination of Eq. (7) with Eq. (8) gives the Kamerlingh-Onnes constant,

$$kT_c/P_cv_c=1/[(n^{\frac{1}{3}}+1)\{n^{\frac{2}{3}}\ln(1+n^{-\frac{1}{3}})-n^{\frac{1}{3}}+\tfrac{1}{2}\}]. \tag{17}$$

Although the agreement between the calculated and the observed values is not sufficient, quantitatively speaking, Eq. (17) reproduces fairly well the tendency that the constant increases gradually and converges on a definite value as the number of carbon atoms increases. In Table I we also listed the ratio of the observed values to the calculated values, which does not depend on n very much.

The relationship between the critical temperature and the number of carbon atoms can be given, under the

assumption of $x=n^{\frac{1}{3}}$, by

$$1/T_c=\{(k/z\epsilon)+(s/\epsilon)\}+(2k/z\epsilon)\{(1/2n^{\frac{1}{3}})+(1/n^{\frac{1}{3}})\}. \quad (18)$$

If this equation should agree with the observation, the plot of $1/T_c$ against $\{(1/2n^{\frac{1}{3}})+(1/n^{\frac{1}{3}})\}$ would give a straight line. In fact, the demand for this linearity is satisfied tolerably, though not perfectly as in the case of Eq. (11), by the observation as shown in Fig. 1, where the observed values are plotted by open circles. In Table I are also tabulated the calculated values of T_c which is obtained by Eq. (18) with

$$\{(k/z\epsilon)+(s/\epsilon)\}=0.000047,$$

and

$$2k/z\epsilon=0.002755. \quad (19)$$

The modern theory of gases enables us to define with good accuracy the potential energy of the intermolecular interaction by using the experimental data of the second virial coefficient or the viscosity coefficient. According to the results, the potential energy has a minimum in the neighborhood of the intermolecular distance 4.3 A in the case of methane molecule, the depth of the minimum is approximately 140 k.[9] On the other hand, the distance d between the nearest neighbor cells is given by

$$\begin{aligned} d&=0.86\tau^{\frac{1}{3}} \text{ (diamond lattice)},\\ &\quad 1.00\tau^{\frac{1}{3}} \text{ (simple cubic lattice)},\\ &\quad 1.12\tau^{\frac{1}{3}} \text{ (face-centered cubic lattice)}. \end{aligned} \quad (20)$$

We can estimate the value of d by using Eqs. (19) and (15), and the value of ϵ by using Eq. (19). As is shown in Table II, if z is assumed to be $4\sim6$ the values of d and ϵ generally settle, judging from the values of the intermolecular potential of methane referred to before, within the reasonable range.

In addition, so far as the number of carbon atoms ranges from one to twenty, a linear relationship holds between $\{(1/2n)+(1/n^{\frac{1}{3}})\}$ and $1/n^{\frac{1}{3}}$; therefore, Eq. (11) can be rewritten as

$$1/T_c=0.000702+(0.004190/n^{\frac{1}{3}}). \quad (21)$$

This equation seems to be excellent as an empirical equation. The values of T_c calculated by Eq. (21) are shown in Fig. 1 and in Table I in comparison with the observed values.

BOILING POINT AND THE HEAT OF VAPORIZATION

The conditions for equilibrium between the vapor phase and the liquid phase are expressed by stipulating equalities of the pressures and of the chemical potentials in the two phases; that is,

$$P_g=P_l, \quad \text{and} \quad \mu_g=\mu_l, \quad (22)$$

[9] For example, J. E. Lennard-Jones, Proc. Roy. Soc. (London) A112, 214 (1936); Hirschfelder, Bird, and Spotz, J. Chem. Phys. 16, 968 (1948).

TABLE II. Values of the interaction parameters, d and ϵ.

Lattice type	z	d(A)	ϵ/k (°K)
Diamond lattice	4	4.4	182
Simple cubic lattice	6	5.2	121
Face-centered cubic lattice	12	5.8	60

where the subscripts g and l are adopted to indicate the vapor and the liquid phases, respectively. Letting v_g and v_l represents the volume per molecule in each phase, we find the equations for equilibrium condition

$$\ln\left(1-\frac{x\tau}{v_g}\right)+(x-1)\frac{\tau}{v_g}+\frac{z\psi}{2kT}\left(\frac{x\tau}{v_g}\right)^2 =\ln\left(1-\frac{x\tau}{v_l}\right)+(x-1)\frac{\tau}{v_l}+\frac{z\psi}{2kT}\left(\frac{x\tau}{v_l}\right)^2, \quad (23)$$

$$\frac{1}{x}\ln\left(\frac{x\tau}{v_g}\right)-\ln\left(1-\frac{x\tau}{v_g}\right)+\frac{z\psi}{2kT}\left(1-\frac{2x\tau}{v_g}\right) =\frac{1}{x}\ln\left(\frac{x\tau}{v_l}\right)-\ln\left(1-\frac{x\tau}{v_l}\right)+\frac{z\psi}{2kT}\left(1-\frac{2x\tau}{v_l}\right). \quad (24)$$

As these are two simultaneous equations involving two independent variables, v_g and v_l, it should be possible to calculate v_g and v_l, and to determine the binodial curve representing isothermal two-phase equilibrium densities. If the value of v_g thus obtained is substituted in Eq. (3), the vapor pressure will be obtained as a function of the temperature, but such calculations are practically impossible to carry out because of the mathematical difficulty.

If we are concerned only with the temperatures lower than the boiling point, molecular density of the vapor phase is extremely small, and then v_g is sufficiently large in comparison with either v_l or $x\tau$. In this case, Eq. (3) yields the equation of state of the ideal gas,

$$P=kT/v_g, \quad (25)$$

and Eqs. (21) and (22) yield

$$\ln\left(\frac{v_l}{v_g}\right)=(x-1)\left(\frac{x\tau}{v_l}\right)-\frac{xz\psi}{2kT}\left(\frac{x\tau}{v_l}\right)\left(2-\frac{x\tau}{v_l}\right). \quad (26)$$

Combining Eq. (25) with Eq. (26), we obtain the expression for the vapor pressure P:

$$\ln P=\ln\left(\frac{kT}{v_l}\right)+(x-1)\left(\frac{x\tau}{v_l}\right)-\frac{xz\psi}{2kT}\left(\frac{x\tau}{v_l}\right)\left(2-\frac{x\tau}{v_l}\right). \quad (27)$$

If, for simplicity's sake, the number of holes in liquid phase is assumed to be negligible at low temperatures,

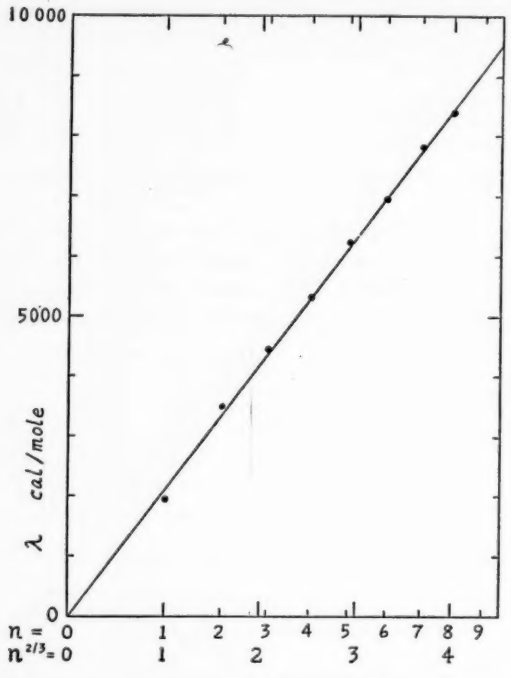

FIG. 2. Heat of vaporization λ of the *n*-paraffins. Circles show the observed values, and the line represents Eq. (29).

v_l can be replaced approximately by $x\tau$, and we obtain

$$\ln P=\ln(kT/x\tau)+x\{1+(zs/2k)\}-1-x(z\epsilon/2kT). \quad (28)$$

Using again the assumption that $x=n^{\frac{2}{3}}$ in Eq. (28), we find the following expression for the heat of vaporization:

$$\lambda=n^{\frac{2}{3}}(z\epsilon/2). \quad (29)$$

This relation shows satisfactory agreement with the experimental data which is represented by black circles in Fig. 2, and we find

$$z\epsilon/2=2115 \text{ cal/mole}. \quad (30)$$

If z is 12, one finds that $\epsilon=176k$; this seems to lie within reasonable range in comparison with the interaction energy of methane molecule. Although we must assign different values to z at the critical and the boiling points in order to obtain reasonable value of ϵ, the adjustment of parameters of this kind has been frequently made in lattice theories of liquids.

Furthermore, if the vapor pressure is expressed in terms of atmosphere, $\ln P$ becomes zero at the boiling point T_b, and therefore, we can easily obtain the following equation after some rewritings:

$$1/T_b=\{(2k/z\epsilon)+(s/\epsilon)\}+(A/n^{\frac{2}{3}}), \quad (31)$$

with

$$A\equiv(2k/z\epsilon)\{\ln(kT_b/n^{\frac{2}{3}}\tau)-1\}. \quad (32)$$

As $T_b/n^{\frac{2}{3}}$ does not sharply depend on n, we may regard A as a constant. In fact, the experimental values of T_b agree very well with the calculated ones by using the following equation as shown in Table I.

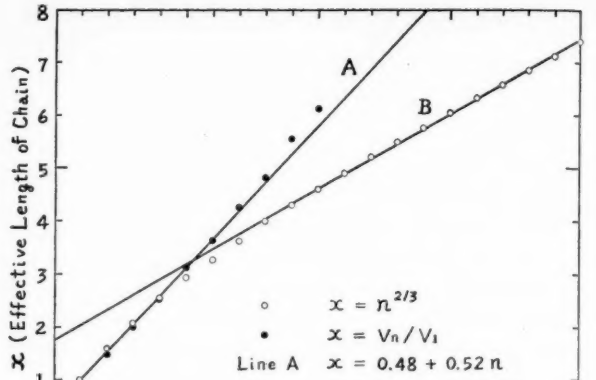

FIG. 3. Empirical relations between effective chain length and the number of carbon atoms.

$$1/T_b=0.000570+(0.007753/n^{\frac{2}{3}}). \quad (33)$$

In Fig. 1, the experimental and the calculated values of T_b are represented by closed circles and a full line respectively.

Combining Eq. (33) with the empirical equation (21) of T_c, and eliminating $(1/n^{\frac{2}{3}})$ from them, we obtain

$$1/T_c=(0.5404/T_b)+0.000394, \quad (34)$$

which is just the relation empirically presented by Varshni.[5]

In addition, it must be noted that the substitution of the simpler assumption $x=n$ for $x=n^{\frac{2}{3}}$ fails in deriving proper expressions for the boiling point and the heat of vaporization.

DISCUSSION

In consideration of the aforementioned results, it seems possible to presume that the hole theory having the similar form as the theory of chain polymer solution is adequate as the zeroth approximation for the *n*-paraffin liquids, though the assumption that $x=n^{\frac{2}{3}}$ should be regarded as entirely empirical.

Now let us consider the reason why the assumption $x=n^{\frac{2}{3}}$ gives the proper expressions for various quantities. As the end effect due to the difference of the sizes between the end and the intermediate segments, $-CH_3$ and $-CH_2-$, cannot be ignored for the chains with small n, it seems reasonable to assume that x is given by

$$x=a+bn, \quad (35)$$

but not by $x=n$. If Egloff's data[1] of the molecular volume V_n at the boiling point are adopted to determine the constants a and b, we find

$$x=V_n/V_1=0.48+0.52n, \quad (36)$$

where the subscripts represent the number of carbon atoms. In Fig. 3, the values of V_n/V_1 and Eq. (36) are

shown by closed circles and the line A, respectively, in comparison with $n^{\frac{1}{2}}$ which is shown by open circles. From the figure, we can find that $n^{\frac{1}{2}}$ lies closely on the line A when n is small. This nature of the relation $x=n^{\frac{1}{2}}$ may probably be one of the reasons why it is properly used.[10]

For large n $(5\leq n\leq 20)$, the relation $x=n^{\frac{1}{2}}$ deviates from A line but approaches to another line B in Fig. 3; i.e.,

$$x=1.75+(n/3.5). \tag{37}$$

As is well known, the Flory approximation gives an overestimated virial coefficient of osmotic pressure for solutions containing flexible chains, and, in order to avoid difficulties of this kind, it is necessary to underestimate the degree of polymerization by a factor of three or five.[7,11] The relation, $x=n/3.5$, for long chains which is obtained from Eq. (37) does not conflict with the above statement, for x can be regarded as a degree of polymerization of the n-paraffins. Therefore, the coincidence of the relation $x=n^{\frac{1}{2}}$ with Eq. (37) can also be considered as a reason for our success.

In conclusion, we express sincere thanks to Professor Mikio Tamura and Dr. Hiroshi Fujita of the Kyoto University for their continued interest and encouragements, and to Dr. Ryoichi Kikuchi of the University of Chicago for his kind help with publication. Thanks are tendered also to the Ministry of Education of the Japanese Government for a grant-in-aid.

[10] It must be noted here that rod-like chains should more nearly agree with the Flory equation than do flexible chains. Therefore, the shorter the n-paraffins, the better agreement between theory and observation can be expected if the end effect of chain is taken into consideration.

[11] This procedure corresponds to the assuming that a solvent molecule or a segment of polymers occupies three or five lattice points [see also Kurata, Tamura, and Watari, J. Chem. Phys. **23**, 991 (1955)].

THE JOURNAL OF CHEMICAL PHYSICS VOLUME 23, NUMBER 6 JUNE, 1955

General Relation between Potential Energy and Internuclear Distance for Diatomic and Polyatomic Molecules. I

ELLIS R. LIPPINCOTT AND RUDOLPH SCHROEDER
Department of Chemistry, Kansas State College, Manhattan, Kansas

(Received September 7, 1954)

A general relation between potential energy and internuclear distance is proposed which is applicable to the ground states of diatomic and polyatomic molecules. The relation has the form $V=D_e[1-\exp(-n\Delta r^2/2r)]\times[1+af(r)]$, where the parameter n is defined by the equation $n=k_e r_e/D_e$. For large values of r, the $f(r)$ term assumes the form of a Lennard-Jones (6–12) repulsive potential. With $a=0$ the function assumes a simple form which is numerically easier to use and much more accurate than the Morse function. By using the simple function dissociation energies are readily calculated with greater accuracy than hitherto possible through the use of bond lengths, force constants, and anharmonicity constants. Independent empirical methods are given for evaluating the parameter n and with its use anharmonicity constants as well as dissociation energies may be calculated more accurately than was possible previously. The use of the general relation gives improved correlations and predictions of the five spectroscopic constants r_e, k_e, D_e, $\omega_e x_e$, and α_e. The wide application of these potential functions to a large number of molecules indicates that the potential energy curves for most molecules have a general form to which the proposed relation is a reasonable approximation. The application of the proposed functions to strongly ionic or charged molecules has not been fully investigated.

INTRODUCTION

ANY adequate theory of chemical binding should allow the derivation of a potential energy function describing the internuclear law of force. In general, it should be possible to obtain such functions from the first principles of quantum theory. However, except for the simplest systems[1–3] these methods have not yielded satisfactory potential energy functions. The reason for this stems from the difficulty in handling polyelectronic problems in quantum theory. Solutions of the differential equations involved are not obtainable in closed form and in order to make the problem tractable, it is necessary to make simplifying assumptions and to use approximate methods. To date these assumptions and approximations have had the effect of removing from quantum theory the possibility of predicting potential energy functions which would quantitatively describe the internuclear law of force and correlate a number of bond properties such as force constant, dissociation energy, bond length, anharmonicity constant, etc. Many semiempirical quantum-mechanical calculations of electronic energies of molecules have

[1] E. Teller, Z. Physik **61**, 458 (1930).
[2] H. M. James and A. S. Coolidge, J. Chem. Phys. **1**, 825 (1933).
[3] A. Meckler, J. Chem. Phys. **21**, 1750 (1953).

been given.[4–9] In general such calculations have been limited to the equilibrium configuration of the molecule or to a limited range of points in the neighborhood of this point.

Because of these difficulties many investigators have proposed empirical potential energy functions. The Morse function[10] has been the most useful of these, partly because of its simplicity and partly because solutions of the anharmonic oscillator problem are readily obtained when this function is used for the potential energy in solving the Schrödinger wave equation. However, the Morse function only approximately represents the actual potential energy curve as determined from experimental data for most diatomic molecules. At the expense of simplicity several modified Morse functions have been proposed.[11–13] Examples of these are the Coolidge, James, and Vernon function and the Hulburt and Hirschfelder function. Other proposed functions are those of Kratzer, Rydberg,[14] Manning and Rosen,[15] Pöschl and Teller,[16] Hylleraas,[17] Linnett,[18] Sutherland,[19] and Frost.[20] Recently Frost and Musulin have proposed a semiempirical function which was obtained after making use of certain theoretical criteria.[21] Although they have only applied it to the H_2 and H_2^+ molecules it appears to have a number of promising features.

There are a number of conditions which an adequate potential function should satisfy, of which the most important are:

I. The potential energy should become very large as the internuclear distance r approaches zero.

II. For large values of r the value of the function should approach the dissociation energy of the bond D_e.

III. For the equilibrium value of the internuclear distance r_e the value of the function should be zero.

Since there are an infinite number of functions which will satisfy these conditions, we add five additional conditions or criteria for an acceptable function:

IV. The function should contain terms which at large distances describe the Van der Waals energies of interaction.

V. The function should adequately represent the actual potential energy curve as determined from experimental data.

VI. The function should allow prediction of one or more quantities such as dissociation energy D_e, anharmonicity constant $x_e\omega_e$, etc. from the remaining spectroscopic constants.

VII. The function should be general and represent the potential energy curves for large classes of diatomic molecules and not just a few favorable examples.

VIII. The function should be applicable to polyatomic as well as to diatomic molecules.

Condition V emphasizes the fact that although conditions I, II, and III are necessary conditions for an acceptable potential function, they are not sufficient conditions. Condition VI offers a check on the function and also demands that it be a useful one.

The difficulty of obtaining a function which satisfies condition VII is well known and has led some investigators to suggest that there is no general potential function applicable to all molecules. The failure to obtain functions which fulfill condition VII is also partially responsible for their lack of application to polyatomic molecules. To be sure, the vibrational motions of a large number of polyatomic molecules have been adequately described in terms of a number of different type of force fields such as the valence force field, central force field, etc. However, all these force field models are only valid for small displacements of the nuclei and in no case has it been possible to relate quantitatively such quantities as bond dissociation energy and force constant k_e, etc.

Although all of the aforementioned potential functions satisfy or approximately satisfy the first three conditions, they are all inadequate in most of the additional conditions. An example of a function which satisfies condition VI but not the remaining conditions is the Morse function.

The Morse function is

$$V=D_e[1-e^{-\beta\Delta r}]^2, \tag{1}$$

where $\Delta r=r-r_e$ and $\beta=\omega_e(2\pi^2c\mu/D_eh)^{\frac{1}{2}}$.

By solving the Schrödinger wave equation using this potential, Morse obtained the following expression[10]:

$$D_e=\omega_e^2/4\omega_ex_e. \tag{2}$$

Thus from the fundamental frequency ω_e and the anharmonicity constant ω_ex_e, the dissociation energy may readily be calculated. However, when the calculated D_e values are changed to D_0 values and compared with the values determined from experimental data agreement is not obtained, as is readily apparent in Table I, where the average percent deviation is 26.4. This lack of agreement thus implies that the Morse function does

[4] G. W. Wheland, J. Am. Chem. Soc. **63**, 2025 (1941).
[5] Glasstone, Laidler, and Eyring, *The Theory of Rate Processes* (McGraw-Hill Book Company, Inc., New York, 1941), Chap. III.
[6] R. S. Mulliken, J. Phys. Chem. **56**, 295 (1952).
[7] W. Moffitt, Proc. Roy. Soc. (London) **A210**, 224, 245 (1951).
[8] G. G. Hall, Proc. Roy. Soc. (London) **A205**, 541 (1951).
[9] C. C. J. Roothaan, Revs. Modern Phys. **23**, 69 (1951).
[10] P. M. Morse, Phys. Rev. **34**, 57 (1929).
[11] Coolidge, James, and Vernon, Phys. Rev. **54**, 726 (1938).
[12] H. M. Hulburt and J. O. Hirschfelder, J. Chem. Phys. **9**, 61 (1941).
[13] M. L. Huggins, J. Chem. Phys. **3**, 473 (1935); **4**, 308 (1936).
[14] R. Rydberg, Z. Physik **73**, 376 (1932).
[15] M. F. Manning and N. Rosen, Phys. Rev. **44**, 953 (1933).
[16] G. Pöschl and E. Teller, Z. Physik **83**, 143 (1933).
[17] E. A. Hylleraas, Z. Physik **96**, 661 (1935).
[18] J. W. Linnett, Trans. Faraday Soc. **36**, 1123 (1940); *ibid.* **38**, 1 (1942).
[19] G. B. B. M. Sutherland, J. Chem. Phys. **8**, 161 (1940); Proc. Indian Acad. Sci. **8**, 341 (1938).
[20] A. A. Frost and B. Musulin, J. Am. Chem. Soc. **76**, 2045 (1954).
[21] A. A. Frost and B. Musulin, J. Chem. Phys. **22**, 1017 (1954).

not approximate the actual experimental curve adequately as demanded by condition V.

An example of a function which is adequate in condition V but not VI is the Hulburt and Hirschfelder function.[12] This function is

$$V=D_e[(1-e^{-\beta\Delta r})^2+c\beta^3(\Delta r)^3e^{-2\beta\Delta r}(1+b\beta\Delta r)], \quad (3)$$

where β may be evaluated in the same manner as it is for the Morse function. The parameters b and c must be evaluated from the remaining spectroscopic constants. One of the advantages of this function is that these parameters may readily be evaluated in terms of the five readily available spectroscopic constants ω_e, D_e, $\omega_e x_e$, r_e, and α_e (vibrational-rotational coupling constant). When compared with the actual potential energy curves for particular diatomic molecules this function gives good agreement. However, this agreement has been obtained by using all the important and readily available spectroscopic data and thus little new information may be predicted from it. Most of the more useful potential functions have this same property. The difficulty is a serious one for little has been gained if one uses all relevant available data to construct a function, since one of its important characteristics should be the ability of such a function to predict unknown quantities.

The purpose of this paper is to present a general potential energy function which reasonably satisfies conditions I through VIII and to apply it by correlating and predicting a large amount of spectroscopic data for molecules in their ground states. The general form of this function has been presented previously.[22] It is

$$V=D_e[1-\exp(-n\Delta r^2/2r)][1+af(r)], \quad (4)$$

where D_e=dissociation energy referred to the bottom of the potential curve, $\Delta r=r-r_e$, r_e=equilibrium bond distance, and a=constant. The quantity $f(r)$ is a function of r chosen such that $f(r)=\infty$, where $r=0$ and $f(r)=0$ when $r=\infty$. This function is conveniently discussed in two sections. In the first section we will discuss this function when the constant a is put equal to 0. This separation arises naturally because for many purposes the $f(r)$ term is unimportant and it is a great advantage to be able to work with such a simple function. In the second section we will make the function more general by including the $f(r)$ term and illustrate the application of the resulting more general function.

SIMPLE FUNCTION

The simple function is

$$V=D_e[1-\exp(-n\Delta r^2/2r)]. \quad (5)$$

This differs from most other proposed functions in that an exponential term in $1/r$ is used as well as one in r.

By imposing the conditions for stability that $(V')_{eq}=0$ and $(V'')_{eq}=k_e$, the following relation can be derived defining the parameter n:

$$D_e=k_e r_e/n. \quad (6)$$

Here k_e is the force constant referred to zero displacement of the nuclei. This relation is better illustrated if the exponential term in Eq. (5) is first expanded and this followed by a power series expansion of the $1/r$ and $1/r^2$ terms, giving

$$V=(nD_e/2r_e)\Delta r^2-(nD_e/2r_e^2)\Delta r^3+(nD_e/2r_e^3-n^2D_e/8r_e^2)\Delta r^4. \quad (7)$$

The potential function (5) was obtained from the knowledge that relation (6) was experimentally valid when used with Eq. (11), followed by integration on using the condition that $(V'')_{eq}=k_e$. This integration process is not unique, however, and one may obtain a large number of functions which are consistent with relation (6). A decision as to which function to use can be made by using them to predict the energy levels of an anharmonic oscillator. These levels are usually represented as

$$E=hc\omega_e(v+\tfrac{1}{2})-hc\omega_e x_e(v+\tfrac{1}{2})^2+hc\omega_e y_e(v+\tfrac{1}{2})^3\ldots. \quad (8)$$

For most diatomic molecules the frequency ω_e and anharmonicity constant $\omega_e x_e$ are available, while for some of the more extensively studied molecules the $\omega_e y_e$ is also available. The problem of checking possible potential functions then reduced to one of solving the anharmonic oscillator wave equation using the desired potential function.

We have not obtained an exact solution of the wave equation for the function (5). Fortunately there are

TABLE I. A comparison of the proposed simple potential function with the Morse function.[a]

Molecule	D_0(kcal/mole) observed	Simple potential function D_0(kcal/mole) from Eq. (9)	Deviation (%)	Morse function D_0(kcal/mole) from Eq. (2)	Deviation (%)
As_2	91.3	90.4	1.0	116.9	28.1
CH	80.0	71.6	10.5	86.7	8.4
ClI	49.6	54.7	10.3	71.2	45.6
CO	210.5	195.0	7.4	247.0	17.4
Cs_2	10.5	10.3	1.9	15.6	48.6
H_2	103.2	102.0	1.2	111.0	7.6
HBr	86.4	85.7	0.8	107.0	23.8
HCl	102.0	95.7	6.2	119.0	16.6
HI	70.4	71.9	2.1	92.7	31.7
I_2	35.6	40.9	14.9	53.5	50.3
K_2	11.8	13.6	15.3	17.2	45.7
KH	42.8	39.7	7.2	46.0	7.5
N_2	224.8	214.0	4.8	273.0	21.8
NO	149.4	142.2	4.8	182.0	21.8
OH	100.5	93.9	6.6	116.0	15.5
O_2	117.0	114.0	2.6	146.0	24.8
P_2	116.0	119.0	2.6	154.0	32.0
S_2	101.4	102.0	0.6	133.0	31.3
SO	118.5	114.0	3.8	146.0	23.1
Se_2	81.9	79.5	3.0	102.9	26.4
		Average	5.4	Average	26.4

[a] Unless otherwise stated data for these computations were taken from G. Herzberg, *Spectra of Diatomic Molecules* (D. Van Nostrand Company, Inc., New York, 1950) pp. 502–581.

[22] E. R. Lippincott, J. Chem. Phys. **21**, 2070 (1953).

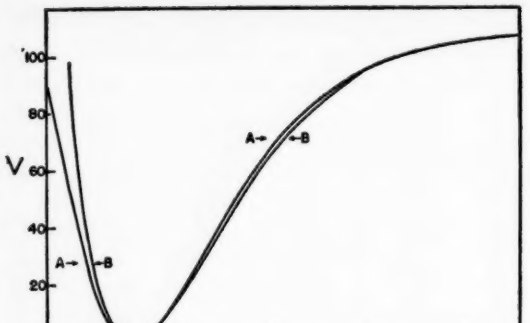

FIG. 1. A plot of potential energy V in kcal/mole, against bond length for H_2 where curve A is calculated from the proposed simple function, Eq. (5), and curve B represents the experimental curve.

several adequate approximate methods for solving the wave equation which yield the energy levels to any desired degree of accuracy. We have used two, the perturbation method and the W.B.K. method as used by Dunham.[23] With the latter we have made extensive use of the analysis given by Coolidge, James, and Vernon[11] as well as that of Hulburt and Hirschfelder.[12] With the perturbation method the quadratic terms of Eq. (7) may be using as the zero-order harmonic oscillator approximation and the cubic and quartic terms as the perturbing potential. By carrying out this approximation to the second order and comparing the resulting energy levels with Eq. (8), the following expression for D_e in terms of k_e, r_e, and $\omega_e x_e$ is obtained:

$$D_e(\text{ergs/molecule}) = k_e/[(64\pi^2 c\mu\omega_e x_e/3h) - 1/r_e^2]. \quad (9)$$

By using (6) to eliminate D_e, one is able to obtain an expression for $\omega_e x_e$ as a function of r_e and n, namely,

$$\omega_e x_e = 3h(n/r_e + 1/r_e^2)/64\pi^2 c\mu. \quad (10)$$

The use of the Dunham method gives the same results.

Equation (9) does not depend on any arbitrarily evaluated constants and it can be used to check the acceptability of the simple potential function. In Table I we have used Eq. (9) to calculate the D_0 values $(D_e - Nhc\omega/2)$ of the 20 diatomic molecules where the experimental dissociation energy is known with an accuracy of ± 2 percent and where the $\omega_e x_e$ value has been given to three significant figures. The average percent deviation of 5.4 percent is quite reasonable and is considerably better than the 26.4 percent error obtained for the same set of calculations using the Morse function and relation (2). This comparison with the Morse function has been given because it is one of the few other functions from which similar calculations of dissociation energies may be made without using empirically evaluated parameters. A plot of the potential curve for H_2 using Eq. (5) is given in Fig. 1 along with the experimentally determined curve (see references 38 and 39). For values of r greater than r_e, there is reasonable agreement with the experimental energies, the predicted energies being somewhat high. For values of r less than r_e, there is considerable deviation from the observed energies.

A comparison of the simple function with the Morse function is given for Br_2 in Fig. 2. For values of r greater than r_e, the Morse function gives much too large a binding energy, where for values of r less than r_e, it would appear that the simple function gives too much binding energy.

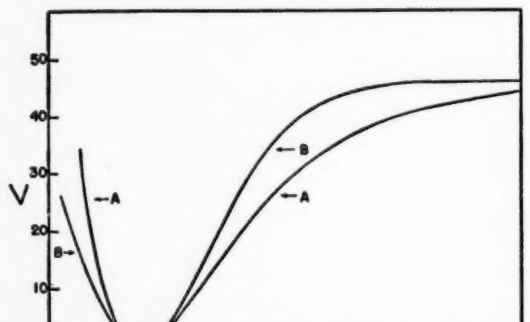

FIG. 2. A plot of potential energy V in kcal/mole, against bond length for Br_2 where curve A is calculated from the Morse function, and curve B is calculated from the simple proposed function, Eq. (5).

[23] J. L. Dunham, Phys. Rev. **41**, 713 and 721 (1932).

EVALUATION OF THE PARAMETER n

Although Eq. (9) is quite useful for calculating dissociation energies when accurate $\omega_e x_e$ values are known, there is a large number of diatomic molecules as well as most polyatomic molecules where the $\omega_e x_e$ values are only approximately known or not known at all. If we are to apply this function to these molecules it is important that we base our calculation of dissociation energies on quantities other than the anharmonicity constants.

To do this we propose to evaluate the parameter n without using known values of D_e, k_e, and r_e. Relation (6) may then be used to calculate one of the latter quantities from the remaining two. For the most part we will be concerned here with the calculation of D_0 (from D_e). The evaluation of n may be accomplished in a number of ways. We will describe two here.

(a) It has been found that n may be calculated by means of the following empirical relation:

$$n = n_0(I/I_0)^{\frac{1}{4}}_A (I/I_0)^{\frac{1}{4}}_B \text{ cm}^{-1}, \quad (11)$$

where $(I/I_0)_A$ and $(I/I_0)_B$ are the ionization potentials of atoms A and B, respectively, relative to those of the corresponding atoms in the same row and first column of the periodic table. For H atoms I/I_0 has been assigned the value 0.88. For most molecules where the binding is primarily covalent and including all molecules of the

fourth, fifth, sixth, and seventh columns of the periodic table, n_0 has the value $6.32 \cdot 10^8$. For the diatomic alkali metal and alkali hydrides, n_0 had the value $4.21 \cdot 10^8$. Indications are that there are characteristic values of n_0 for the molecules involving the transition elements and for molecules where the binding is primarily ionic as in the alkali halide molecules. However, the calculation of n values and the application of the simple function to strongly polar molecules or to ones carrying a charge such as HF, NaCl, CH^+, O_2^+, etc. has not been fully investigated.

Relation (11) was intuitively arrived at by realizing that the wave function for a hydrogen-like atom involves an exponential in $I^{\frac{1}{2}}$ and that this form should carry over approximately to an exponential in the product $(I)^{\frac{1}{2}}_A(I)^{\frac{1}{2}}_B$ for the wave function for a molecule AB. This then indirectly implies that the potential energy as a function of internuclear distance should also involve an exponential in $(I)^{\frac{1}{2}}_A(I)^{\frac{1}{2}}_B$.

It can be argued that n should be defined in terms of electronegativities. We have defined such a relation and its use gives results which are not quite as good as those obtained from Eq. (9). Since ionization potentials are more readily available and more accurately known we have used these in our calculations.

In Table II we have calculated the dissociation energies (D_0) for a number of molecules where k_e and r_e values are readily available and for which the experimental D_0 values are reasonably well known. The average percent deviation of 4.4 is lower than that obtained by using Eq. (9) with $\omega_e x_e$ values, but is still significantly greater than the experimental error with which D_e, r_e, and k_e are known for these molecules. This emphasized the fact that the use of the simple functions is limited by the accuracy with which the $\omega_e x_e$ values are known as well as by the approximate nature of the function itself.

In Table III we have made similar calculations of the dissociation energies of alkali metal and alkali hydride molecules. For those molecules where the predicted D_0 value can be compared with corresponding experimental values the average percent error is 4.3 which is surprisingly low.

Relation (6) is equally applicable to bonds of polyatomic molecules and it has been found that the predicted dissociation energies for a large number of polyatomic molecules agree with the corresponding thermochemically determined quantities with an average error of less than 5 percent. The application of this function to polyatomic molecules will be described in a second paper.

Since n has been evaluated separately it now may be used in Eq. (10) to predict $\omega_e x_e$ values from r_e values. It is significant and convenient that for these calculations one does not need k_e or D_e. The calculated and observed values of $\omega_e x_e$ are given in Table II, the average percent error being 5.5.

TABLE II. The calculation of dissociation energies and anharmonicity constants from the parameter n [Eq. (11)].[a]

Molecules	D_0(kcal/mole)	Deviation (%)	$\omega_e x_e$ (cm^{-1}) from Eq. (10)	$\omega_e x_e$ (cm^{-1}) observed	Deviation (%)
As_2	85.1	6.8	1.19	1.12	0.6
Br_2	46.6	2.4	1.25		
C_2	133.8		11.2	11.7	4.3
CH	79.6	0.5	61.4	64.3	4.5
ClBr	48.4	6.9			
Cl_2	57.8	1.4	2.98		
ClF	58.0	3.7	6.25		
ClI	49.7	0.2	1.61	1.46	10.3
CO	208.8	0.8	12.7	13.5	5.9
F_2	43.9		98.1		
HBr	81.5	5.7	47.3	45.2	4.6
HCl	95.9	6.0	50.7	52.0	2.5
H_2	103.4	0.2	117.5	118.0	0.4
HI	73.9	0.7	41.3	39.7	3.3
IBr	44.1	5.5	0.92	0.78	18.0
I_2	41.5	16.6	0.63	0.61	3.3
N_2	209.7	6.7	14.8	14.5	2.1
NO	156.1	4.5	12.8	14.0	8.6
OH	109.1	8.6	72.1	82.8	12.9
O_2	123.9	5.9	11.1	12.1	8.3
P_2	111.5	3.9	3.02	2.80	7.9
S_2	104.8	3.4	2.77	2.85	2.8
SO	116.9	1.4	5.96	6.12	2.6
Se_2	78.0	4.8	1.08	1.06	1.9
		Average 4.4			Average 5.5

[a] See footnote a in Table I.

(b) A second method of calculating dissociation energies from n can be accomplished through the use of Eq. (6). This equation can be used to define an n value for each element of the periodic table. These n values will be considered as a characteristic property of each element in the table. The n value for a molecule then can be calculated from the geometric mean of those of

TABLE III. The dissociation energies of alkali hydride and metal molecules calculated from k_e, r_e, and n.[a]

Molecule	$k \cdot 10^4$ (dynes/cm)	Calculated D_0^0 (kcal/mole)	Observed D_0^0 (kcal/mole)	Deviation (%)
Cs_2	0.691	10.5	10.3	2.0
CsH	4.67	40.3	42.8	5.8
K_2	0.984	13.0	11.8	10.2
KH	5.61	42.6	42.8	0.5
Li_2	2.55	22.5	23.7	5.1
LiH	10.26	56.4	57.7	2.2
LiCs	1.09[b]	13.6		
LiK	1.48[b]	16.2		
LiRb	1.29	15.0		
Na_2	1.716	17.7	16.8	5.4
NaH	7.82	51.0	50.7	0.6
NaK	1.30[b]	15.3	14.4	6.2
NaCs	1.08[b]	13.65		
Rb_2	0.81	11.6	11.3	2.7
RbH	5.14	42.5	42.8	0.7
RbNa	1.20[b]	14.5	13.2	9.9
RbCs	0.753[b]	11.0		
				Average 4.3

[a] See footnote a in Table I.
[b] Values of k_e and r_e used for these computations were taken from W. Gordy, J. Chem. Phys. 14, 308 (1946).

H 5.57			
C 12.8	N 15.9	O 17.3	F 22.2
Si 9.0 (est)	P 13.0	S 13.3	Cl 16.3
Ge 9.5 (est)	As 13.5	Se 13.6	Br 17.6
Sn 10 (est)	Sb 15.7	Te 16 (est)	I 18.4
Pb 10 (est)	Bi		

FIG. 3. Periodic table of n-values ($\times 10^{-8}$).

the respective atoms making up the bond. Thus,

$$n_{AB}=(n_A n_B)^{\frac{1}{2}}. \tag{12}$$

In Fig. 3 we give a periodic table of some of the more readily available n-values. These n-values may then be used to calculate the dissociation energy of any bond not used in making up the periodic table of n-values. We have made these calculations for the same molecules as given in Table II and have tabulated the results in Table IV. The average error when compared with the corresponding experimental quantities is 4.8.

The simple potential, as used here, satisfies all the eight conditions listed for an acceptable function except I. When we put the limiting value of $r=0$ in Eq. (5) we obtain $V=D_e$ and not $V=\infty$. Although this defect is not serious for a number of purposes, it must be corrected if one is to have an acceptable general potential function.

If one uses Eq. (5) as the potential energy and solves the problem of the rotating anharmonic oscillator by the W.B.K. method as given by Dunham,[23] one is able to calculate a value for the vibrational-rotational coupling constant α_e. A surprising feature of Eq. (5) is that it predicts for all molecules

$$\alpha_e=0. \tag{13}$$

Although this feature represents a definite limitation on Eq. (5), in some respects it is a favorable one. First it is rather convenient to have a potential function which predicts zero coupling between vibrational and rotational motion, as it may then be used as a first approximation to a more general function. Second since bonds in polyatomic molecules usually have values of α_e which are much smaller than the corresponding α_e values for diatomic molecules, it may be that Eq. (5) represents an improved approximation to potential curves for bonds in polyatomic molecules. The results obtained for polyatomic molecules[24] would seem to suggest that this is perhaps one reason why the simple function is applicable to polyatomic molecules, although certainly not the only one.

[24] E. R. Lippincott, 125th Meeting of the Am. Chem. Soc., Kansas City, March, 1954.

It is interesting that Eq. (6) implies that, with constant k and n, the dissociation energy is directly proportional to the bond length. This is contrary to the commonly accepted ideas that, other things being equal, the bond energy (which is the same as dissociation energy for diatomic molecules) is the greater the smaller the bond length.[25] This concept has arisen because of the difficulty of comparing bond energy with bond length for the same or the nearly same force constant. Since k is usually greater the smaller the bond lengths, bonds with small r usually have relatively large dissociation energies. However, this is only true because of the overriding importance of k in Eq. (6).

PREDICTION OF DISSOCIATION ENERGIES

The accuracy, with which the simple potential function has predicted the dissociation energies and anharmonicity constants for diatomic molecules where these quantities are already well known, justifies its use in predicting the dissociation energies of unknown molecules. In particular there are a number of important diatomic molecules where two or more known values have been proposed for the dissociation energies. In some cases the widely different values have been known experimentally with considerable accuracy. The proposed potential function should be able to definitely distinguish which values are the correct ones.

N_2

Two values have been proposed for the dissociation energy of N_2. A value of 170.2 kcal/mole has been favored until recently by Herzberg, while Gaydon has favored the considerably higher value of 225.1 kcal/mole. Our predictions from both relation (6) and Eq. (9) are

TABLE IV. Dissociation energies calculated from periodic table of n's.

Molecule	Observed D_0 in kcal/mole[a]	Calculated D_0 in kcal/mole	Deviation (%)
CH	80.0	82.8	3.5
CH^+	83.0	75.4	9.2
BrF	50.5	52.0	3.0
ClBr[b]	52.1	47.8	8.3
ClF	60.3	57.6	4.5
ClI	49.6	46.0	7.3
CO	210.5	207.1	1.6
HBr	86.4	80.7	6.6
HCl	102.4	95.0	7.2
HI	70.4	68.3	3.0
IBr[b]	41.9	40.2	4.1
N_2^+	201.2	199.6	0.8
NO	149.4	157.3	5.3
OH	100.5	105.5	5.0
O_2^+	149.4	151.5	1.4
SO	118.5	111.6	5.8
		Average	4.8

[a] See footnote a in Table I.
[b] Radii estimated with aid of table of covalent bond radii. Linus Pauling *Nature of the Chemical Bond* (Cornell University Press, Ithaca, New York, 1948), p. 164.

[25] M. L. Huggins, J. Am. Chem. Soc. **75**, 4126 (1953).

close to Gaydon's value of 225.1 kcal/mole (see Tables I and II). On the basis of the potential function there seems to be little doubt that this is the correct dissociation energy for N_2. The average of the predicted values is 212 kcal/mole.

NO

Values of 122.3 and 149.7 kcal/mole have been proposed for the dissociation energy of NO depending on whether D_0 for N_2 is taken as 170.2 or 225.1 kcal/mole, respectively. Since the latter value for N_2 appears definitely established, the dissociation energy of NO should be 149.7 kcal/mole. The predictions given in Tables I, II, and IV verify this value remarkably well.[26] Their average is 152 kcal/mole.

CO

Four values have been proposed for the dissociation energy of CO: 159,[27] 210.8 (Herzberg),[28] 221.5 (Hagstrum),[29] and 256.1 (Gaydon).[30] The calculated values from relation (6) (n evaluated by either method) and from Eq. (9) are 195, 209, and 207 kcal/mole, respectively. This would then be consistent with the value proposed by Herzberg as well as that proposed by Hagstrum. The potential function appears to favor slightly the 210.8 kcal/mole value. The average of the predicted values from Tables I, II, and IV is 204 kcal/mole.

C_2

Several widely different values have been proposed for the dissociation energy of C_2. The three most discussed values are 83 (Herzberg),[31,32] 114 (Brewer, Gilles, and Jenkins),[33] and 139 (Glockler) kcal/mole, respectively.[34] The average of the predicted values from Eqs. (6) and (9) is 132 and favors a value near that proposed by Glockler.

F_2

Widely different values for the dissociation energy of F_2 have been proposed.[35] Until recently a value near 60 kcal/mole has been used. More recent work suggests a much lower D_0, values ranging from 35 to 45 having been given.[36] Calculations from the potential function definitely indicate that the lower value is correct. The predicted value from Eq. (6) is 43.9 kcal/mole.

TABLE V. Dissociation energies predicted from periodic table of n's.

Molecule	Landolt-Bornstein[a] observed D_0 in kcal/mole	Herzberg[b] observed D_0 in kcal/mole	Predicted D_0 in kcal/mole
AsN[c]	115±25	(149.9)	120.0
AsO[c]	113±2.5	≤115.3	112.4
CP	140±25	(159.1)	135.0
CS	165±25	(179.9)	143.1
CSe[c]	115±25	(156.8)	123.5
ClO[c]	53±7	43.8	54.9
GeBr[c]	58±10	(69.2)	51.7
GeCl[c]	62±10	(92.2)	58.7
GeO	125±25	(113.0)	140.1
GeS[c]	115±12	(129.1)	114.7
GeSe[c]	88±12	(94.4)	103.6
GeTe[c]	67±10	(73.8)	66.1
NBr[c]	58±12	(69.2)	52.3
NS[c]	115±25	(136.0)	125.9
PN	138±18	(145.3)	150.6
PO	143±12	(143.0)	129.3
PbH	41±5	≤36.7	49.3
PbO	76±10	(99.2)	94.5
PbS	69±12	(108.4)	89.2
PbSe[c]	80±25	(108.4)	78.0
PbTe[c]	80±25	(80.7)	59.8
SbN[c]	71±12	(110.7)	106.4
SbO[c]	74±10	(87.6)	89.1
SeO[c]	80±25	(124.5)	92.0
SiBr[c]	69±12	(85.3)	51.2
SiCl[c]	76±12	(92.2)	66.9
SiF[c]	88±10	(110.7)	78.5
SiN	(104±10)	(103.8)	119.3
SiO	185±25	(170.6)	160.5
SiS	147±7	(152.2)	109.9
SiSe[c]	127±12	(133.8)	113.2
SiTe[c]	115±15	(126.8)	86.9
SnO	180±25	(129.1)	111.8
SnS	67±2.5	≤69.2	79.4
SnSe[c]	92±12	(106.1)	89.7
SnTe[c]	80±12	(96.9)	71.2
TeO[c]	62.8	(62.9 or 79.6)	82.3

[a] Values taken from Landolt-Bernstein *Zahlenwerte und Funktionen aus Physik, Chemie, Astronomie, Geophysik, Technik* (Springer-Verlag, Berlin, 1951), Vol. I, pp. 26–35.
[b] See footnote a in Table I.
[c] Radii estimated with aid of table of covalent bond radii. Linus Pauling *Nature of the Chemical Bond* (Cornell University Press, Ithaca, New York, 1948), p. 164.

In Table V we have tabulated the predicted dissociation energies, from the periodic table of n-values, for a large number of molecules for which such data have been previously known with little or no certainty. In some, but not all, cases the predicted dissociation energies lie within the estimated error of the experimental value. We will refrain from predicting the dissociation energies of such strongly polar molecules and HF, BCl, CaCl, NaCl, SbCl, PbCl, etc.

MORE GENERAL RELATION BETWEEN POTENTIAL ENERGY AND INTERNUCLEAR DISTANCE

The simple potential function will now be modified to make it more general by inclusion of the $[1+af(r)]$ term. This quantity must be chosen such that condition I is satisfied and in such a way that the resulting function will correlate or allow a prediction of vibrational-

[26] A. G. Gaydon, Proc. Phys. Soc. (London) **56**, 95 and 160 (1944).
[27] R. Schmid and L. Gero, Z. physik Chem. **B36**, 105 (1937); Physik. Z. **39**, 460 (1938). J. G. Valatin, Phys. Rev. **74**, 350 (1948).
[28] G. Herzberg and R. Schmid, Phys. Rev. **52**, 467 (1937). G. Herzberg, Chem. Rev. **20**, 145 (1937); J. Chem. Phys. **10**, 306 (1942).
[29] H. D. Hagstrum, Phys. Rev. **72**, 947 (1947). H. G. Howell, Nature **163**, 773 (1949).
[30] A. G. Gaydon and W. G. Penney, Proc. Roy. Soc. (London) **A183**, 374 (1949).
[31] J. C. Fox and G. Herzberg, Phys. Rev. **52**, 638 (1937).
[32] G. Herzberg, Phys. Rev. **70**, 762 (1946).
[33] Brewer, Gilles, and Jenkins, J. Chem. Phys. **16**, 797 (1948).
[34] G. Glockler, J. Chem. Phys. **21**, 1242 (1953).
[35] L. Hass and C. W. Beckett, Natl. Bur. Standards Rept. No. 1435 (February 1, 1952).
[36] H. W. Wise, J. Phys. Chem. **58**, 389 (1954).

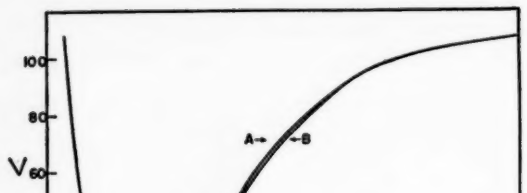

FIG. 4. A plot of potential energy V in kcal/mole, against bond length r in cm, for H_2 where curve A is calculated from the general proposed function, Eq. (15), and curve B represents the experimental curve.

rotational coupling constants. At large distances it should give a Van der Waals energy of interaction. These adjustments must be made without losing the desirable features of the simple potential function. This latter requirement is surprisingly difficult.

To accomplish this we will use a power series in the quantity $[1-\exp(-b^2n\Delta r^2r^{11}/2r_e^{12})]^{\frac{1}{2}}$. Since the most important quantities which we wish to correlate do not depend on the coefficients of powers of Δr beyond the 4th, it is sufficient to use only three terms of this series. Thus

$$1+af(r)=1+(-1)a \times\{(r_e/r)^6[1-\exp(-b^2n\Delta r^2r^{11}/2r_e^{12})]^{\frac{1}{2}} -(r_e/r)^{12}[1-\exp(-b^2n\Delta r^2r^{11}/2r_e^{12})]\} \quad (14)$$

or for the general function

$$V=D_e[1-\exp(-n\Delta r^2/2r)] \times\{1+(-1)a(r_e/r)^6[1-\exp(-b^2n\Delta r^2r^{11}/2r_e^{12})]^{\frac{1}{2}} +a(r_e/r)^{12}[1-\exp(-b^2n\Delta r^2r^{11}/2r_e^{12})]\}. \quad (15)$$

For large values of r this function takes the form

$$V=D_e[1-\exp(-n\Delta r^2/2r)]\{1+a[-(r_e/r)^6+(r_e/r)^{12}]\},$$

where $f(r)$ takes the form of a Lennard-Jones (6–12) Van der Waals potential.[37] The major spectroscopic constants may be correlated with or without the use of a Van der Waals potential for large values of r. However, the shape of the potential curve from Eq. (15) will not be in reasonable agreement with the observed curve unless $f(r)$ assumes the form of a Van der Waals potential for large values of (r). The predicted potential curve for H_2 calculated from Eq. (15) is compared with the observed curve[14,37,38] in Fig. 4.

It is possible to introduce additional flexibility into Van der Waals term through the use of additional parameters and thus improve the correspondence between the predicted and experimental curves. However, there is no readily available experimental data which may be used to evaluate these parameters for atoms which are involved in bond formation and, since such parameters do not affect the correlation or prediction of the five major spectroscopic constants, they were not introduced into Eq. (15).

On expanding the exponential terms of Eq. (15) followed by an expansion of the terms involving inverse powers of r, one obtains

$$V=D_e(nr_e/2)(\Delta r^2/r_e^2)\{1-[1+ab(nr_e/2)^{\frac{1}{2}}]\Delta r/r_e +[1-nr_e/4+3(ab/2)(nr_e/2)^{\frac{1}{2}} +ab^2nr_e/2]\Delta r^2/r_e^2\}. \quad (16)$$

By comparing (16) with (7) the effect of the additional terms in (15) on the simple potential function can be studied.

The form of (14) was arrived at intuitively by considering the effect of powers of nr on the predicted value of the vibrational-rotational coupling constant α_e. Several related forms of (14) would be adequate in that they can be chosen such that the same terms in (16) will be obtained up to the 4th power in Δr.

The acceptability of Eq. (15) depends on whether it can be shown that it satisfies the eight conditions listed for an acceptable function. Since Eq. (15) contains two additional constants, a and b, its usefulness depends on the ease with which they may be evaluated. In particular, for Eq. (15) to be a general potential function both a and b should be true constants for all molecules and not be parameters which depend on the particular bond properties of the molecule under consideration. This has been one of the difficulties of most potential functions presented previously. It will be shown here that ab is constant within 10 percent for a large class of diatomic molecules and that b is constant to 3.0 percent for all diatomic molecules.

To check Eq. (15), we need to use this potential and obtain the energy levels of a nonrigid anharmonic oscillator. This must be done by an approximate

TABLE VI. Calculated values of constants ab and b.[a]

Molecule	ab	b	Molecule	ab	b
AlH	0.608	1.035	KH	0.436	1.164
AuH	0.588	1.067	LiH	0.496	1.055
BiH	0.614	1.050	NaH	0.563	0.978
CdH	0.451	1.144	N_2	0.618	1.091
CH	0.556	1.041	N_2^+	0.672	1.023
ClI	0.612	1.081	NO	0.616	1.050
CO	0.594	1.027	OH	0.555	1.082
CuH	0.563	1.050	O_2	0.618	1.061
HBr	0.542	1.060	O_2^+	0.706	1.038
HCl	0.564	1.065	PbH	0.507	1.160
HCl^+	0.651	0.987	P_2	0.574	1.034
HF	0.601	0.995	RbH	0.567	0.983
H_2	0.426	1.068	S_2	0.624	1.073
HI	0.584	1.120	SO	0.634	1.093
HgH	0.462	1.035	SbH	0.458	1.154
I_2	0.607	1.068	ZnH	0.423	1.008
InH	0.634	1.076			

[a] See footnote a in Table I.

[37] J. E. Lennard-Jones, Proc. Roy. Soc. (London) **A106**, 463 (1924).

[38] H. Beutler, Z. physik. Chem. **B27**, 287 (1934).

method. We will apply the results of the W.B.K. method as obtained by Dunham.[23] He was able to solve this problem by writing the potential in the form

$$V=a_0\xi^2[1+a_1\xi+a_2\xi^2+\cdots]hc, \tag{17}$$

where $\xi=\Delta r/r_e$. The energy levels of the nonrigid anharmonic oscillator may be compared with the expression for the energy levels in terms of the spectroscopic constants ω_e, $\omega_e x_e$, B_e, α_e, γ_e, etc. These are for a diatomic molecule

$$E_{\text{vib-rot}}=hc\omega_e(v+\tfrac{1}{2})-hc\omega_e x_e(v+\tfrac{1}{2})^2 +hc\omega_e y_e(v+\tfrac{1}{2})^3+B_vJ(J+1)hc -D_vJ^2(J+1)^2hc+\cdots, \tag{18}$$

where

$$B_v=B_e-\alpha_e(v+\tfrac{1}{2})+\gamma_e(v+\tfrac{1}{2})^2+\cdots,$$
$$D_v=D_e+B_e(v+\tfrac{1}{2})+\cdots.$$

Here B_v is the rotational constant, the subscript v referring to the vibrational state v, and subscript e to the equilibrium bond length. The quantity D is a rotational constant representing the influence of the centrifugal force. Dunham found that a comparison of the two expressions for the energy levels[23] gives for the constants in Eq. (17)

$$a_0=\omega_e^2/4B_e, \tag{19}$$

$$a_1=-1-\alpha_e\omega_e/6B_e^2, \tag{20}$$

$$a_2=5/4a_1^2-2\omega_e x_e/3B_e. \tag{21}$$

Equations (19), (20), and (21) may be used with the values of a_0, a_1, and a_2 obtained from Eq. (16). A comparison of (16) with (17) shows that for the general potential function

$$a_0=D_e n r_e/2 \tag{22}$$

$$a_1=-1-ab(nr_e/2)^{\frac{1}{2}} \tag{23}$$

$$a_2=1-nr_e/4+(3/2)ab(nr_e/2)^{\frac{1}{2}}+ab^2nr_e/2. \tag{24}$$

These equations used with (19), (20), and (21) give

$$D_e=\omega_e^2/2nr_eB_e, \tag{25}$$

$$\alpha_e=(6abB_e^2/\omega_e)(nr_e/2)^{\frac{1}{2}}, \tag{26}$$

$$x_e\omega_e=1.5B_e[0.25+nr_e/4+ab(nr_e/2)^{\frac{1}{2}} +(5a^2b^2-ab^2)nr_e/2]. \tag{27}$$

Equation (25) is equivalent to relation (6) of the simple potential function, since $B_e=h/8\pi^2\mu r_e^2c$ and $k_e=4\pi^2\mu\omega_e^2c^2$. Equation (26) can be used to define and evaluate the constant ab. It is convenient that ab depends only on n, ω_e, r_e, and α_e. We have evaluated the constant ab for the molecules listed in Table VI. For a large number of these molecules, ab appears to have a value of 0.57. This is particularly true of molecules which involve primarily covalent binding and which do not involve H. Because ab is approximately constant Eq. (26) may be used to calculate α_e from r_e and n. The quantity n may be obtained from Eq. (6) or from one or the other of the independent methods given to evaluate it. The calculated and predicted values of α_e are given in Tables VII and VIII. In nearly all cases the calculated values of α_e are an improvement over those obtained by similar calculations from the

TABLE VII. Calculation of vibrational-rotational coupling constants.[a,b,c]

Molecule	Morse function α_e (cm^{-1})	Morse function Deviation (%)	α_e (cm^{-1}) observed	New potential function using Eq. (26)[a] α_e (cm^{-1})	New potential function using Eq. (26)[a] Deviation (%)
Br_2	0.000351	27.6	0.000275	0.000308	12.0
CH	0.484	9.4	0.534	0.546	2.2
CO	0.0167	4.6	0.0175	0.0167	4.6
Cl_2	0.00190	11.8	0.0017	0.00145	14.7
ClF	0.00675	55.0	0.00436	0.00434	0.5
H_2	1.89	38.5	3.07	4.10	33.6
HBr	0.213	5.8	0.226	0.236	4.4
HCl	0.267	16.0	0.302	0.303	0.3
HI	0.232	26.8	0.183	0.178	2.7
I_2	0.000107	8.6	0.000117	0.000110	6.0
N_2	0.0172	8.0	0.0187	0.0172	8.0
NO	0.0158	11.2	0.0178	0.0164	7.9
O_2	0.015	6.3	0.0160	0.0145	9.4
OH	0.626	12.3	0.714	0.728	2.0
P_2	0.00143	0.7	0.00142	0.00140	1.4
S_2	0.0015	6.3	0.0016	0.00145	9.4
SO	0.00569	1.2	0.00562	0.00503	10.5
Se_2	0.00041	48.0	0.00027	0.000263	2.6
	Average	16.5		Average	7.3

[a] The n-values used are defined by Eq. (6).
[b] See footnote a in Table I.
[c] A value of 0.567 was used for the constant ab.

TABLE VIII. Predicted values for the vibrational-rotational coupling constant α_e.[a-d]

Molecule	Observed α_e (cm^{-1})	Calculated α_e (cm^{-1})	Molecule	Observed α_e (cm^{-1})	Calculated α_e (cm^{-1})
AlBr	0.000853	0.000774	HgH	0.312	0.382
AlH	0.188	0.175	ICl	0.000536	0.000494
AlO	0.00575	0.00498	InH	0.145	0.130
AuH	0.214	0.205	KH	0.0673	0.0875
BaH	0.0655	0.0852	LiH	0.213	0.245
BCl	0.00646	0.00520	MgH	0.167	0.166
BeF	0.0168	0.0147	MgH^+	0.206	0.207
BeH	0.300	0.411	MgH_2	0.0654	0.0624
BeH^+	0.294	0.360	N_2^+	0.0202	0.0171
BeO	0.0190	0.0190	NaH	0.135	0.137
BiH	0.148	0.137	O_2^+	0.0194	0.0160
BO	0.0165	0.0144	OH_2	0.295	0.281
C_2	0.0168	0.0175	PbH	0.144	0.161
CaH	0.096	0.026	PN	0.00577	0.00517
CdH	0.218	0.275	RbH	0.072	0.0719
CH_2	0.212	0.216	SiN	0.00567	0.00553
CP	0.00597	0.00512	SiO	0.00494	0.00423
CS	0.00625	0.00506	SiS	0.00149	0.00123
CuH	0.249	0.252	SrH	0.081	0.101
HH_2	1.99	2.69	TlH	0.154	0.132
H_2H_2	1.05	1.46	ZnH	0.250	0.335
HCl^+	0.318	0.278	ZnD^+	0.107	0.086
HF	0.770	0.738			

[a] The n-values used are defined by Eq. (6).
[b] See footnote a in Table I.
[c] A value of 0.567 was used for the constant ab.
[d] There are certain classes of molecules in this table where a different value of the constant ab would be more suitable for calculating the α_e values.

Morse function.[39] These values are also listed in Table VII.

Since the only additional information needed to evaluate ab other than that used to evaluate n is α_e, it is sometimes convenient to treat ab as a parameter when using it in Eq. (27). The use of this latter equation depends on the extent to which b is a constant since to evaluate it requires n, $\omega_e x_e$, and α_e. In Table VI we have tabulated b for all molecules listed there from n, $\omega_e x_e$, and α_e. In this case n was obtained from Eq. (6). For most molecules b has the value 1.06_5 and is remarkably constant, the average percent deviation being 3.0.

The constancy of b and to a lesser extent ab, despite the wide range of bond types involved, shows that most molecules have a universal form for their potential energy curves and that Eq. (15) is a good general approximation to the "true" potential function.

Since b has the fixed value 1.06_5, Eq. (27) may now be used in two ways. It is possible first to calculate $\omega_e x_e$ from n and α_e (n being obtained in the most convenient way), or second to calculate n from α_e and $\omega_e x_e$. This value of n may then be used with (6) to obtain D_e and thus D_0. In Tables IX and X we have tabulated the calculated and predicted values of $\omega_e x_e$. The agreement is remarkable where reliable spectroscopic data is available, and represents a large improvement over the values calculated by means of the simple function, the calculated values in this case already being quite good. The average percent deviation from the observed values in Table IX is 2.3 percent. It would appear that except for the most elaborately studied molecules that the calculated $\omega_e x_e$ values are possibly within the experimental error of the observed values. This excellent agreement is further evidence for the general validity of Eq. (15).

The dissociation energies calculated from b, $\omega_e x_e$, and α_e are given in Table XI. The average percent deviation between calculated and observed values is 4.6. This percent deviation is two times larger than the average percent deviation of 2.3 in obtaining the $\omega_e x_e$ values by the reverse calculations with (27). This error is surprisingly large and is caused primarily by the fact that the calculated dissociation energies of a few molecules may be in error possibly due to the use of incorrect $\omega_e x_e$ or α_e values. In particular the calculation of D_0 values by this method involves relatively small differences of quantities involving $\omega_e x_e$ and α_e. Because of this, a relatively small error in $\omega_e x_e$ or α_e will produce a magnified error in the calculation of dissociation energies. For example, a 5 percent error in $\omega_e x_e$ will sometimes produce a 15 percent error in D_0. Since both $\omega_e x_e$ and α_e represent quantities which themselves are relatively small corrections to the energy levels of a nonrigid anharmonic oscillator, it is not surprising that the calculation of dissociation energies from quantities involving relatively small differences of these produces a magnified error. In particular the calculations of a first-order quantity such as D_0 from the small difference of two second-order quantities is not very practical unless these latter quantities are known with a high degree of accuracy. Although for a number of elaborately studied molecules $\omega_e x_e$ and α_e are known with high accuracy (it is these which produce good agree-

TABLE IX. Calculated values of $\omega_e x_e$ for the general potential function.[a,b]

Molecule	$\omega_e x_e$ (cm^{-1}) calculated	$\omega_e x_e$ (cm^{-1}) observed	Deviation (%)
C_2	12.0	11.7	2.7
CH	62.0	64.3	3.6
CD	33.7	34.7	2.9
ClI	1.493	1.467	1.9
CO	12.93	13.46	4.1
HBr	44.9	45.2	0.7
HCl	53.4	52.0	2.5
H_2[c]	130.4	131.7	1.0
HO	97.7	95.0	2.8
D_2	64.3	64.1	0.3
HI	42.3	39.7	6.5
I_2	6.16	6.13	0.5
N_2	14.6	14.5	0.7
NO	13.8	13.97	1.4
OH	84.4	82.8	1.9
OD	46.8	44.2	5.9
O_2	12.03	12.07	0.3
P_2	2.71	2.80	3.2
S_2	2.87	2.85	0.7
SO	6.22	6.12	1.6
		Average	2.3

[a] The n-values used are defined by Eq. (6).
[b] See footnote a in Table I.
[c] Data used for H_2 computations were taken from H. C. Urey and G. K. Teal, Revs. Modern Phys. **7**, 34 (1935).

[39] C. L. Pekeris, Phys. Rev. **45**, 98 (1934).

TABLE X. Anharmonicity constants predicted by the general potential function.[a,b,c]

Molecule	$\omega_e x_e$ (cm^{-1}) calculated	$\omega_e x_e$ (cm^{-1}) observed	Molecule	$\omega_e x_e$ (cm^{-1}) calculated	$\omega_e x_e$ (cm^{-1}) observed
AgH	33.2	34.1	K_2	0.333	0.354
AlBr	1.45	1.28	KH	12.5	14.6
AlH	28.4	29.1	Li_2	2.84	2.59
AlO	6.39	7.12	LiH	21.5	23.2
AuH	43.0	43.1	MgH	24.9	31.5
BaH	16.1	16.0	MgD	13.5	16.1
BCl	5.13	5.11	MgH^+	34.3	30.2
BeF	8.12	9.12	N_2^+	16.4	16.14
BeH	40.8	35.5	Na_2	0.718	0.726
BeH^+	37.3	39.8	NaH	18.3	19.7
BiH	30.5	31.6	O_2^+	15.4	16.5
BO	10.9	11.77	PbH	32.0	29.8
CaH	21.1	19.5	PN	6.22	6.98
CdH	50.4	46.3	RbH	13.0	14.15
CP	6.11	6.86	SiN	6.58	6.56
CS	5.13	6.5	SiO	5.65	6.05
CuH	36.4	37.0	SiS	2.64	2.56
HCl^+	49.6	53.5	SrH	18.6	17.0
HF	86.2	90.1	TlH	26.3	22.7
HgH	80.1	83.0	ZnH	52.0	55.1
InH	25.0	24.7	ZnD^+	23.2	19.8

[a] The n-values used are defined by Eq. (9).
[b] See footnote a in Table I.
[c] The value used for the constant b was 1.065.

ment), there are a large number of diatomic molecules as well as most polyatomic molecules where $\omega_e x_e$ and α_e are known only approximately or not at all. We therefore, in general, will not be concerned with calculating D_0 from α_e and $\omega_e x_e$, except in the cases where the experimental values of these quantities are known with sufficient accuracy.

Equation (15) is not unique in that it is the only modification of the simple potential function which will produce good results. However, it is the best of a relatively large number of similar functions with which we have worked. In particular all these have the property that it is not very practical to calculate dissociation energies from $\omega_e x_e$ and α_e, whereas the reverse calculation is readily made.

DISCUSSION

The simple potential function (5) has the advantage of simplicity and ease of manipulation as well as general applicability to polyatomic as well as diatomic molecules. Its use with ionic molecules or ones with large dipole moments has not been fully investigated. There is some indication that similar methods can be devised to handle such molecules. Numerical calculations are more readily made from it than they are from the less accurate Morse function because the former only involves one exponential term while the use of the latter involves two because of the squaring process. The significant difference between this function and previously proposed functions is that it introduces an exponential term in $1/r$. This function can be used to predict dissociation energies and anharmonicity constants from n, r_e, and k_e with greater accuracy than previously possible through the use of relation (6) and one of the two methods proposed for obtaining n. If it is desirable to calculate dissociation energies without using the parameter n, this can be accomplished through the use of k_e, $\omega_e x_e$, and r_e.

The general potential function has the advantage that it retains all the desirable characteristics of the simple function and relation (6) and at the same time gives an improved correlation between D_e, k_e, $\omega_e x_e$, r_e, and α_e. It has been possible to predict values of both $\omega_e x_e$ and α_e more accurately than hitherto possible. Since calculated values of b and to a lesser extent a are nearly constant, this function suggests that the actual potential curves for all molecules are of the same general form, to which (15) is a good approximation. Finally the proposed function satisfies all seven conditions prescribed for an acceptable potential function. The additional terms in this function have the convenient property of reducing to a Lennard-Jones (6–12) Van der Waals potential for large values of r.

TABLE XI. Calculated D_0 values using the general potential function from $\omega_e x_e$, α_e, B_e and b.[a,b]

Molecule	D_0 (kcal/mole) calculated	Deviation (%)	Molecule	D_0 (kcal/mole) calculated	Deviation (%)
CH	81.7	2.1	HCl	100.0	2.0
CH^2	73.6	9.1	HI	85.0	20.6
ClI	5.12	3.2	I_2	35.3	0.8
CO	186.0	11.4	N_2	225.0	0.0
H_2	105.7[c]	0.7	NO	138.0	7.4
H^1H^2	110.3	6.1	O_2	114.0	2.6
H^1H^3	104.0	0.3	OH	103.4	2.9
H_2^2	105.7	0.7	P_2	105.4	9.2
H_2^3	105.4	0.6	S_2	102.8	1.4
HBr	83.6	3.2	SO	124.6	5.1
				Average deviation	4.6

[a] Value of b used is 1.065.
[b] See footnote a in Table I.
[c] Data taken from H. C. Urey and G. K. Teal, Revs. Modern Phys. **7**, 34 (1935).

The success of the application of these two functions to polyatomic molecules has prompted us to use these as a starting point for an attack on other problems. In particular it has been possible to obtain a one-dimensional model of hydrogen bonding based on the simple potential function, which allows a successful prediction of hydrogen bond energies, OH stretching frequency shifts, OH bonded distances, etc. We have also made encouraging progress on estimating heats of sublimation and activation energies of chemical reactions.

The applicability of the periodic table of n-values suggests that it defines a molecular or atomic property. We are attempting to investigate the relation of this n-value to other such properties such as electronegativity, electron affinity, etc.

At present no simple theory of the chemical bond has been presented which is adequate for predicting a potential function. The simplicity of Eq. (5) suggests that it should be possible to formulate an adequate simple model for most chemical bonds.*

We wish to acknowledge financial support from an Office of Ordnance Research contract.

* *Note added in proof.*—The simple potential function, Eq. (5), has been derived from a quantum-mechanical model through the use of shifted delta functions [E. R. Lippincott, J. Chem. Phys. **23**, 603 (1955)]. In this note parts of the exponential terms in Eqs. (3) and (4) have been omitted. The correct equations are

$$E=(-g^2m/2\hbar^2)[1+e^{-c(a_0+a_1/R+R)}]^2 \quad (3)$$

and

$$c=(mg/\hbar^2)[1+e^{-c(a_0+a_1/R+R)}]. \quad (4)$$

Liquid Surface Tension Measurements by Analysis of Solid-State Curvatures; The Surface Tension of Liquid Germanium

R. C. SANGSTER* AND J. N. CARMAN, JR.†
Research and Development Department, Semiconductor Division, Hughes Aircraft Company, Culver City, California
(Received October 18, 1954)

A procedure based upon zone-melting techniques has been developed for determining liquid-gas surface tension coefficients for liquids at their melting points by analysis of the surface curvatures of solid specimens. The method can give standard deviations of the mean of the order of ±1 percent. It has been calibrated with lead and cadmium to be valid to within at least ±5–10 percent. The most important factors limiting its range of applicability are crystallographic forces which produce facets on the solid and the difficulty of producing and maintaining a clean liquid-gas surface. The surface tension of liquid germanium at its melting point, 934.5°C, in contact with helium or nitrogen has been found to be 632±5 dyne/cm, in good agreement with a previously reported value.

THEORY

THE possibility of determining the surface tension of a liquid by the study of solid specimens was initially indicated by observations made during the operation of a zone-melting furnace[1] for the purification of germanium. (See Figs. 1 and 2.) In this furnace a long ingot in a graphite boat is drawn through a narrow heat zone, causing a molten section to be swept along the length of the ingot. Soon after the beginning of a run on a uniform ingot, a state of dynamic equilibrium is attained in which as much metal melts at the leading edge of the zone as freezes out behind and in which the geometrical relationships of molten zone and ingot are constant. Under these conditions, the shape of a lateral cross section of the refrozen ingot is determined by the shape of the liquid surface at the solid-liquid interface.

The shape of the liquid-gas surface at a solid-liquid-gas boundary in equilibrium is determined by the fundamental equation for the surface of separation of two fluids,[2]

$$\gamma\left(\frac{1}{R_1}+\frac{1}{R_2}\right)=C+gz(D_1-D_2), \tag{1}$$

and by the boundary conditions which must hold at the line of intersection of three surfaces in local equilibrium,[3]

$$\gamma_{12}/\sin\theta_3=\gamma_{23}/\sin\theta_1=\gamma_{13}/\sin\theta_2. \tag{2}$$

In these equations $\gamma=\gamma_{12}$=coefficient of liquid-gas surface tension; R_1 and R_2 are the radii of curvature of the liquid-gas surface along two mutually perpendicular arcs; C is a constant of integration; g is the acceleration due to gravity; z is the vertical height of a point on the surface measured from a fixed point, z being positive when measured toward the concave side of the curve; D_1 and D_2 are the densities of the lower and upper fluids, respectively; γ_{23} and γ_{13} are the coefficients of solid-liquid and solid-gas surface tension; and θ_1, θ_2, and θ_3 are the angles defined in Fig. 3. The effect of Eq. (2) is to determine one of the radii of curvature which enter Eq. (1): If the solid-liquid interface is plane and perpendicular to the axis of the ingot, as has been assumed in Fig. 1, the triangle of forces of Fig. 3 is the same over the full width of the ingot so that θ_2 is constant. It is reasonable physically, and could probably be rigorously established mathematically, that constancy of the angle θ_2 under the conditions existing in these experiments implies that the radius of curvature of the liquid-gas interface in a direction normal to the solid-liquid-gas boundary is also essentially constant at this boundary. The boundary conditions for longitudinal sections cut normal to the solid-liquid-gas junction are essentially the same for any portion of the liquid zone (except possibly very near the wall of the boat), since the slope of the liquid surface is constant at the junction and since the slope

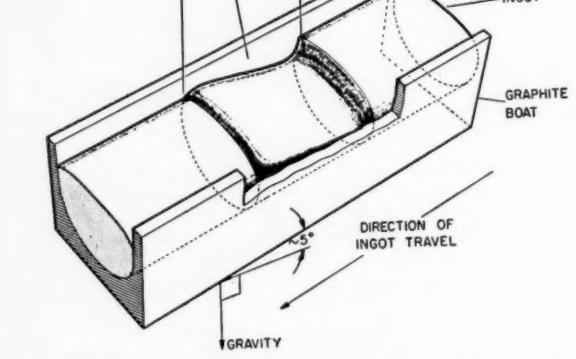

FIG. 1. Schematic diagram of an ingot in a zone-melting furnace. The boat is inclined as shown to compensate for the decrease in volume of germanium upon melting.

* Present address: Texas Instruments Incorporated, 6000 Lemmon Avenue, Dallas, Texas.
† Present address: Pacific Semiconductors, Inc., 10451 W. Jefferson Blvd., Culver City, California.
[1] W. G. Pfann, J. Metals 4, 747 (1952).
[2] N. K. Adam, *Physics and Chemistry of Surfaces* (Oxford University Press, London, 1941), third edition, pp. 9, 365–367, 382–383.
[3] W. Shockley, editor, *Imperfections in Nearly Perfect Crystals* (John Wiley and Sons, Inc., New York, 1950), p. 379.

and curvature are zero at any reasonably large distance away from the interface, not too close to the other interface. Since the slope at the solid-liquid-gas junction is in addition known to be small, it is physically improbable that there can be significant variation in the longitudinal curvature at this boundary (see Fig. 2). Because of the complexity of the mathematics and because the assumptions on which it is based are only approximately satisfied experimentally, the mathematics of this situation has not been rigorously worked out.

If one of the radii of curvature in Eq. (1) can be regarded as a constant, the equation then becomes essentially two-dimensional and amenable to exact mathematical treatment. On the assumption that the

FIG. 2. Photograph of the freezing interface during the zone-melting of a cadmium ingot (liquid zone at right). The boat and furnace tube in this case are both made of Vycor. The heating coil is being drawn along the furnace tube toward the right. The ingot is approximately one inch in width. The rough ingot surface at the left indicates the extreme perturbations which can be introduced by crystallographic forces in cadmium. (The perturbations observed for lead and germanium were insignificant.) An oxide film has smoothed out the ingot surface near the present position of the interface.

solid-liquid-gas junction is essentially a plane, cross-sectional curve, its size and shape can be determined by taking a lateral cross section of the ingot. This lateral cross section (neglecting thermal contraction effects due to the difference between the temperature at which the measurements are made and the melting point of the material[4]) will be identical to that of the liquid at the interface, and the two-dimensional form of Eq. (1) can be applied to permit the evaluation of the constant of integration and the coefficient of liquid-gas surface tension. Direct observation indicates that the assumptions on which this treatment is based are at

[4] The authors wish to acknowledge the assistance of Dr. J. R. Macdonald of Texas Instruments Incorporated, in pointing out that the thermal contraction of the ingot had been ignored in their original deviation.

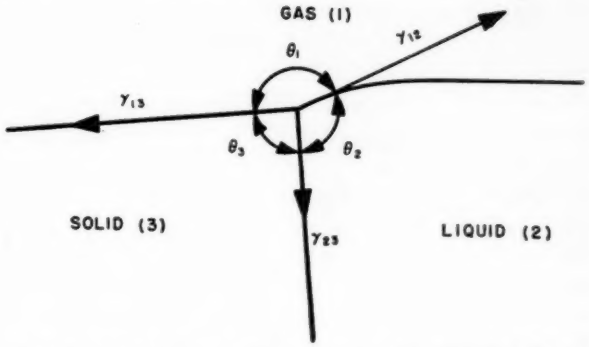

FIG. 3. Triangle of surface forces at a three phase junction.

least approximately valid, and the consistency of the fit which can be attained between the theoretical expressions and the experimental curves implies that no serious errors exist.

The major sources of experimental error are contamination of the liquid-gas surface and specific crystal orientation forces which cause facets to form on the solid. The first can be minimized by cleanliness and by keeping away from oxidizing atmospheres. The second when present can be only partially controlled, by attempting to minimize the size of the crystal grains.

In addition to zone-melt ingot cross sections, several samples of solid germanium were studied which had frozen from small pools of the liquid resting on graphite surfaces. Superficially at least, these samples showed some regions in which the surface configuration appeared to be due predominantly to surface-tension forces, particularly around the edges where the initial freezing occurred. In these regions, one of the radii of curvature, essentially the radial distance from the center of the pool, was again almost constant and almost negligible. Cross sections of these samples were so chosen that the deviations from constancy could be ignored and that the constants of integration see [Eq. (3)] were essentially the same as for the ingot cross sections. It was found that the pool and ingot cross sections could then be fitted to each other to yield composite curves of the type shown in Fig. 4. The basic justification for using these composite curves is the internal consistency of the curves and of the numerical data derived from them.

Recasting the fundamental surface tension equation [Eq. (1)] for the two-dimensional case of Fig. 4 gives

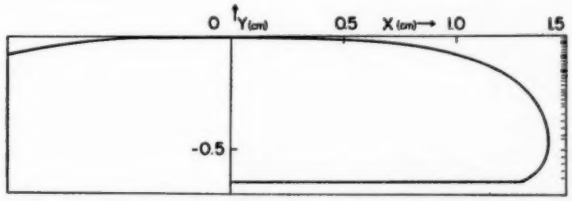

FIG. 4. Cross section of a surface-tension determined germanium surface.

the relation

$$\rho g y+\alpha\gamma=\frac{-\delta\gamma\ddot{y}}{(1+\dot{y}^2)^{\frac{3}{2}}} \tag{3}$$

where $-y$ is the distance below the highest point of the surface cross section; $\dot{y}$ is the slope of the surface; $\ddot{y}$ is the space rate of change of the slope; δ represents $\ddot{y}/|\ddot{y}|$; ρ is the density of the liquid; g is the acceleration due to gravity, 979.6 cm/sec^2 in Los Angeles[5]; α equals $\ddot{y}$ evaluated at the highest point on the surface (the origin); and γ is the coefficient of surface tension for the liquid-gas interface. Integration of Eq. (3) yields

$$\gamma=\frac{\rho g}{2}\frac{y^2}{1-\alpha y+\delta(1+\dot{y}^2)^{-\frac{1}{2}}} \tag{4}$$

or

$$w=\frac{2\gamma}{\rho g}\left(1-\alpha\frac{w}{y}\right) \tag{5}$$

where

$$w=\frac{y^2}{1+\delta(1+\dot{y}^2)^{-\frac{1}{2}}}. \tag{6}$$

Both y and $\dot{y}$ are quantities which can be easily measured experimentally. (It must be kept in mind that the y values must be corrected for the contraction of the ingot in cooling to room temperature from the melting point.) From the values thus found w and $-w/y$ can be computed directly. A plot of w *versus* $-w/y$ yields $2\gamma/\rho g$ as the intercept and $\alpha(2\gamma/\rho g)$ as the slope. Since ρ and g are known quantities, such a plot permits the evaluation of both the surface tension coefficient γ and the constant of integration α.

EXPERIMENT

Liquid-gas surface tension coefficients have been determined for lead, cadmium, and germanium. The first two materials were studied to check the method, while the latter was the substance of primary interest.

For germanium, shadowgraph enlargements (20×) were made of the cross sections of four ingots and of three "frozen pools." All but two of the enlargements fitted well the original from which the curve of Fig. 4 was copied. Combining the two exceptional cases yielded a curve that differed only slightly from that of Fig. 4. Similar cross-sectional enlargements were obtained for the lead and cadmium samples.

On these enlargements coordinate lines were ruled to correspond to suitably distributed values of y, corrected for the thermal contraction of the ingot in cooling from the melting point, and at each intersection of a coordinate line with the curve, the tangent to the curve was drawn. Measurement of the intercepts of the tangent lines with appropriate vertical and horizontal axes then permitted calculation of the slopes $\dot{y}$. For each pair of values $(y, \dot{y})$, w and $-w/y$ were calculated using Eq. (6). From lines fitted to the plots of w *versus* $-w/y$ the intercepts $2\gamma/\rho g$ and slopes $\alpha(2\gamma/\rho g)$ were evaluated numerically. Insertion of the appropriate values for ρ and g then permitted calculation of the surface tension coefficients γ and the constants of integration α.

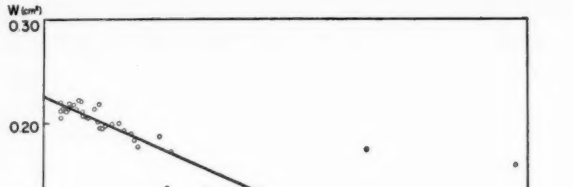

FIG. 5. Plot of parameters determining the surface tension coefficient for the surface shown in Fig. 4. The values of y for which points are plotted are indicated at the right in Fig. 4.

In Fig. 5 is shown the line fitted to the plot of w *versus* $-w/y$ for the germanium cross-sectional curve of Fig. 4. The surface tension coefficient computed from the intercept is 631 dyne/cm. The value of the α parameter is -0.096 cm^{-1}. The surface tension coefficients computed for the individual points $(y,\dot{y})$ by using Eq. (4) with this value of α gave an average value for γ of 632 dyne/cm with a standard deviation of the mean of 4 dyne/cm; five points for which y was very small and the accuracy of determination of $\dot{y}$ very low were omitted in computing this average.

The points in the plot of w *versus* $-w/y$ made for the other, exceptional, germanium cross-sectional curve deviated considerably from the theoretical straight-line form. With the extreme assumptions that could reasonably be used in fitting a straight line to these points (i.e., in the one case fitting a line to the whole set of points, and in the other merely to the points in the region close to the vertical axis), the values found for the surface tension coefficient were 623 and 646 dyne/cm, respectively.

The density of liquid germanium[6] at its melting point was taken as 5.575 g/cm^3. The average thermal expansion coefficient between room temperature and the melting point was taken as 6.6×10^{-6}/°C.[7] The gas phase in all cases was either nitrogen or helium at 1 atmos pressure.

The surfaces studied were very clean and in all probability characteristic of pure liquid germanium. The effects of floating contaminants were eliminated by cleanliness and by studying sections in which such contamination was not present. It is improbable that any oxide film was present, since the reaction product of traces of oxygen and germanium is volatile at the melting point of germanium. While crystallographic

[5] C. D. Hodgman, editor, *Handbook of Chemistry and Physics* (Chemical Rubber Publishing Company, Cleveland, 1949), 31st edition, p. 2675. Value for 30°30′ north, at sea level.

[6] Klemm, Spitzer, Lingenberg, and Junker, Monatsh. Chem. **83**, 629 (1952).

[7] E. M. Conwell, Proc. Inst. Radio Engrs. **40**, 1327–1337 (1952).

orientation effects were present, they could be neglected, primarily because the crystal grains were small compared to the size of the samples studied.

The value indicated by these calculations for the coefficient of surface tension of liquid germanium at its melting point, 934.5°C,[8] in contact with nitrogen or helium is 632 dyne/cm, with a standard deviation of the mean of about 5 dyne/cm. The electrical resistivity of the germanium used was for the most part of the order of 20 ohm cm, indicating an impurity level in the parts-per-hundred-million range. The surface tension value reported here is consistent with that determined by Keck and Van Horn,[9] 600±15–30 dyne/cm. The higher precision obtained in the present case is probably valid, since the values determined for surface tension coefficients are more often below the true values than above: since the present value is somewhat higher than that previously reported, it probably is a somewhat better approximation of the true value.

For lead in contact with vacuum, an average of the surface tension coefficients calculated for five different cross sections was 424±10 dyne/cm (327.4°C). The literature value[10] is 442 dyne/cm. The only feasible technique found for obtaining a clean lead surface was to scrape off the oxidized surface layer mechanically just before using the material. An attempt to eliminate the oxide by operating in a hydrogen atmosphere was not successful. It is probable that the surface tension value obtained is low due to a slight residual contamination of the surface by lead oxide. Even so, the mean value agrees with that from the literature to within about 4 percent and to within the limits implied by the experimental standard deviation.

For cadmium in contact with a hydrogen atmosphere, the value found by averaging the surface tension coefficients determined for the two most valid cross sections was 525±30 dyne/cm (321°C) (literature value 564–611).[10] The surface was clean: premelts were made and the ingots were etched thoroughly with aqua regia; in addition, it was found that with a very hot zone the oxide film left by etching was reduced by the hydrogen atmosphere. However, when a clean surface was achieved, crystallographic effects became pronounced (see Fig. 2). Only two cross sections taken near the beginning of the ingot were usable. One taken too near the beginning was perturbed by the three-dimensional curvature present at the end of the ingot.

Density and melting point data for lead and cadmium were obtained from the *Liquid Metals Handbook*.[10] Thermal expansion coefficients were taken from Lange's *Handbook of Chemistry*.[11]

The authors wish to acknowledge the assistance of Miss C. M. Taylor and Mrs. P. E. Stello in carrying out much of the experimental work and analysis for the lead and cadmium samples.

[8] D. M. Van Winkle, this laboratory, private communication.
[9] P. H. Keck and W. Van Horn, Phys. Rev. **91**, 512 (1953).
[10] R. N. Lyon *et al.*, *Liquid-Metals Handbook* (U. S. Government Printing Office, Washington, 1952), second edition, pp. 40–41.
[11] N. A. Lange, *Handbook of Chemistry* (Handbook Publishers, Inc. Sandusky, Ohio, 1952), eighth edition, pp. 125–131.

Low Resolution Electronic Spectrum of Hexamethylbenzene with Application to Benzene*

RICHARD C. NELSON† AND WILLIAM T. SIMPSON
Department of Chemistry, University of Washington, Seattle, Washington
(Received October 20, 1954)

The crystal spectrum of hexamethylbenzene has been obtained using polarized light in the region 1725–2800 A and the results including extinctions for out-of-plane absorption are interpreted. The vapor spectrum has been determined in the region 1300–2800 A and the solution spectrum down to 2150 A. The vapor spectrum shows a new band at 2350 A. A suggestion is made for determining quantum numbers in the Rydberg series formula.

INTRODUCTION

THE spectrum of hexamethylbenzene is closely similar to that of benzene itself; moreover hexamethylbenzene is a solid at room temperature, and its crystal structure has been worked out.[1] This makes possible a study of the polarization of absorption over the electronic bands, and provides valuable information about benzene itself.[2] When the present research was begun it had been proposed that the 2000 (angstrom units understood) band of benzene might be polarized out-of-plane (Rydberg series of the type $2p \rightarrow 3s$)[3] and the original intention was to check this point. Then sometime later Lyons and Craig published the result of a brief investigation in which the long wavelength tail of the hexamethylbenzene absorption at *ca* 2375 was shown to be in-plane.[4] This result probably already answered the original question put by Hammond, Price, Teegan, and Walsh, since the absorption at 2375 in solid hexamethylbenzene no doubt is in the zero-zero region of a band which corresponds to the 2000 band of benzene.

In the present investigation the approach is different from that of Lyons and Craig in that the measurement of polarization of absorption has been carried out down to 1725. This not only gives a check of their result, but also information over the whole band, as well as over the strong band farther in the ultraviolet. Further, the vapor spectrum of hexamethylbenzene has been obtained and the results interpreted as implying the existence of a new electronic transition. In addition the extinction has been determined quantitatively (though not with high accuracy) which has necessitated some work in solution. The quantitative extinctions over the entire range 2800–1700 A for in-plane and out-of-plane absorption can, it is believed, be given satisfactory interpretation. Finally Hammond, Price, Teagan, and Walsh's suggestion[3] is examined and general consideration given the problem of what quantum numbers to use in the formulas representing Rydberg series.

In the Experimental part, which comes next, a description of the determination respectively of crystal, vapor and solution spectra is given.

EXPERIMENTAL

The Crystal Spectrum

The vacuum spectrograph which was used for both the crystal and vapor spectra has been described previously in the literature.[5] Modifications were necessary to polarize the radiation and to accommodate a crystalline sample.

The light was polarized by transmission through a quartz Wollaston prism, without binder, 4 mm thick and 7 mm high.[6] The height is that required to intercept the entire beam of light when the prism is placed 13 cm from the slit between the slit and the grating. The thickness is that necessary to provide adequate separation (2 mm center to center) of the two polarized beams on the photographic plate. The prism was found to transmit by itself to about 1550 but for crystals of hexamethylbenzene the practical lower limit was found to be approximately 1725.

A crystal holder was designed so that the crystalline sample, which was mounted upon an optically polished quartz cover slip,[7] could be covered with a similar cover slip and pressure applied to the sandwich thus formed while allowing no rotary motion of the cover slips. The slightest slipping of the cover slips upon one another would shatter the fragile crystal. The entire crystal holder fit into a cylindrical cavity between the source and the slit and immediately preceding the slit. The source was a Lyman tube[8] which was attached to the spectrograph through an o-ring, enabling the crystal holder to be easily inserted and removed. Once the crystal holder was in place the extinction directions of

* This research was supported in part by the Air Research and Development Command, Contract No. AF 18(600)–375.

† Eastman Kodak Predoctoral Research Fellow, 1952–1953. Present address: Shell Oil Company, Martinez, California. This paper is taken from the writer's Ph.D. thesis.

[1] L. O. Brockway and J. M. Robertson, J. Chem. Soc. 1324 (1939).

[2] Scheibe, Hartwig, and Muller, Z. Electrochem. **49**, 372 (1943).

[3] Hammond, Price, Teegan, and Walsh, Discussions Faraday Soc. **9**, 53 (1950).

[4] L. E. Lyons and D. P. Craig, Nature **169**, 1102 (1952).

[5] H. D. Hunt and W. T. Simpson, J. Am. Chem. Soc. **75**, 4540 (1953), and Noyes, Duncan, and Manning, J. Chem. Phys. **2**, 721 (1934).

[6] The prism was purchased from Karl Lambrecht, 4318 North Lincoln Avenue, Chicago 13, Illinois.

[7] The Thermal Syndicate Ltd., 14 Bixley Heath, Lynbrook, New York.

[8] R. E. Worley, Rev. Sci. Instr. **13**, 67 (1942).

the crystal were set parallel to the directions of polarization as defined by the prism.[9] Next, the holder was clamped in place by screwing down upon it the anode-cooling-fin of the Lyman tube.

The crystalline sample was a single crystal, four to five tenths of a micron thick and large enough to completely cover the slit of the spectrograph. The thickness was determined under the polarizing microscope from the known refractive indices and Newton's colors. It was found that large, thin crystals could be grown more easily when sublimed onto cloth than when sublimed in the conventional manner onto glass. The procedure was to form with three loosely woven cotton laboratory towels three horizontal compartments above one another in a large beaker. The cloth which formed the top of the upper compartment covered the top of the beaker. The hexamethylbenzene, which had been sprinkled over the bottom of the beaker before inserting the cloths, was vaporized by heating the beaker on a hot plate. When all of the compound had vaporized, the heat was turned off, the beaker well wrapped with towels and allowed to stand for at least two hours. At the end of that time many large, thin, well-formed crystals could be found, especially in the upper compartment. The well-defined angles of these single crystals made it easy to identify the prominent crystal face as the *bc* face.

The spectra were taken with between 50 and 2000 flashes of the Lyman tube at voltages which varied from $12\frac{1}{2}$ to 17 kv for different exposures.

Above 2250 the spectrum obtained in the vacuum spectrograph was overlapped and extended to longer wavelengths by the use of a monochromator-photomultiplier instrument assembled in this laboratory by Dr. A. C. Albrecht. The spectra obtained by the two methods required a 1 percent change in the density of the photographic blank to be put into agreement. The crystal spectrum was taken in the region above 2400 as a check on that reported by Scheibe, Hartwig, and Muller.[2] This was of interest particularly because of the rather large amount (10 percent) of out-of-plane absorption found by those workers in that region.

The Vapor Spectrum

The vapor spectrum was taken in two parts, one above 1850 and the other below 1850 (onset of oxygen absorption). This division was necessary because of the inability of the vacuum spectrograph to hold a vacuum sufficient to eliminate oxygen absorption, after the pumps had been turned off for the length of time required to attain vapor pressure equilibrium.

The method for the region below 1850 was to allow vapor from a heated bulb, which had previously been evacuated, to flow into the spectrograph while the pumps were running. The forward part of the spectrograph was also heated to delay condensation of the vapor, but the rear part was cooled in order that all of the hexamethylbenzene would condense on the walls and the baffle system before it reached the grating. Since the spectrum was not photographed at equilibrium, absolute extinction coefficients would not be directly determined. However, this spectrum overlapped the spectrum above 1850 for which absolute extinction measurements could be made. By fitting the two curves together, absolute values were obtained below 1850.

Above 1850 the presence of oxygen in the spectrograph did not matter. For that region the method was to place solid hexamethylbenzene throughout the spectrograph, apply a partial vacuum to speed the attainment of equilibrium, and, in order to produce a higher vapor pressure, heat the entire room to 40°C. The room was allowed to stand over night at that temperature. From the known vapor pressure-temperature relationship for hexamethylbenzene,[10] the concentration of the vapor and hence absolute extinction coefficients could be calculated. As a check on the spectrum obtained by this method, the spectrum above 1850 was rephotographed with the hydrogen lamp from the Beckman D.U. Spectrophotometer replacing the Lyman tube. The photographic plates used in all work with the vacuum spectrograph were Eastman 103–0, U.V., V.S., X-Thin. The plates were developed for four minutes at 20°C in Eastman X-Ray Developer which gave a gamma of approximately unity at 2000. Calibration curves were determined at least once for each emulsion number. The variation of gamma with wavelength was appreciable above 2000, but in agreement with that which has been reported in the literature.[11]

The method for determining gamma was to vary the number of flashes of the Lyman tube rather than the intensity. This method would give the true gamma only if the "reciprocity law" were obeyed. There is theoretical evidence for the assumption that the reciprocity law is obeyed for a series of flashes of extremely short duration. That assumption was made for exposures with the Lyman tube and found to be valid at least for the region above 2250 by the method described in the following paragraphs. The calibration curves for exposures with the hydrogen lamp gave gamma values about 0.85 times those for exposures with the Lyman tube.[11a]

The vapor spectrum was also taken above 2250 in

[9] It is known that Beer's law is obeyed for light polarized along the extinction directions. We had attempted to obtain information using other orientations but decided experiments of this type would not be fruitful. The reader can understand this point by thinking of the hexamethylbenzene crystals as pieces of Polaroid. If incident polarized light is set parallel, to pass through a Polaroid, any absorption spectrum recorded would be for the electron vibration direction of essentially no absorption. If the Polaroid is rotated by 45° the intensity would be cut in half but the spectrum recorded would be the same.

[10] Nitta, Seki, and Chihara, J. Chem. Soc. Japan, Pure Chem. Sect. **70**, 387 (1949).

[11] P. Lee and G. Weissler, J. Opt. Soc. Am. **43**, 512 (1953).

[11a] If the Schwartzchild constant for the exposures with the Lyman tube is assumed to be unity, this makes the constant for the continuous source 0.85, which is a typical value.

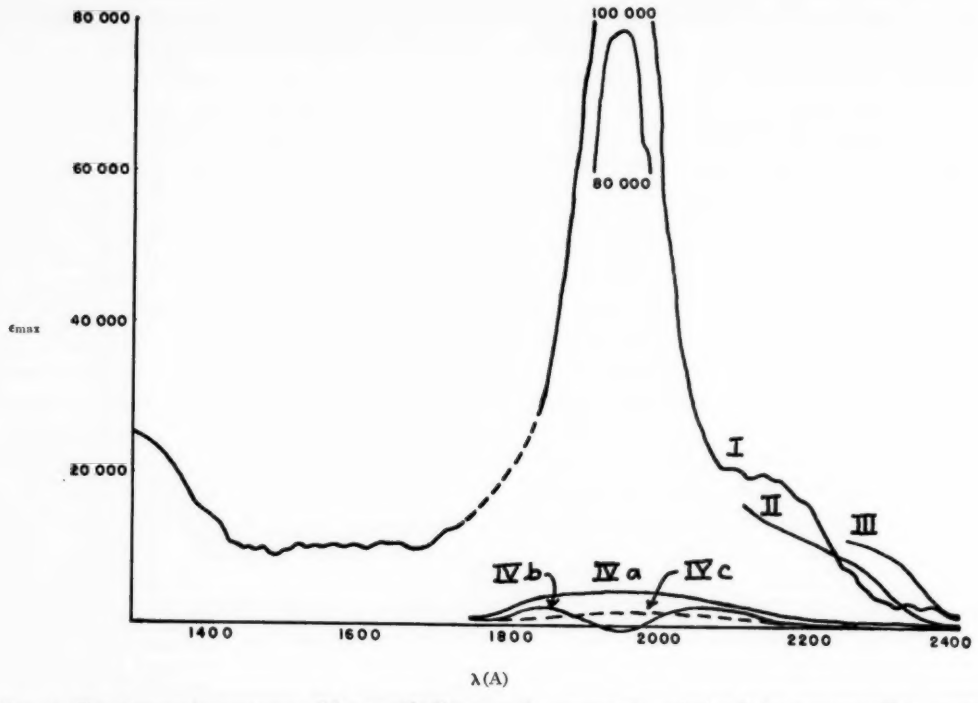

FIG. 1. The electronic spectrum of hexamethylbenzene. I—vapor; II—solution in iso-pentane; III—crystal, parallel to the molecular plane; IVa—crystal, perpendicular to direction for curve III; IVb—crystal, perpendicular to the molecular plane as essentially derived from approximate equation $\epsilon_{II} = (3/2)\epsilon_{vapor}$; IVc—crystal, perpendicular to the molecular plane, smoothed.

the Beckman Spectrophotometer. This was made possible by a special attachment, made available to us by Professor D. M. Ritter, designed so that two 20 cm cells could be placed alternatively in the light beam of the spectrograph while being immersed in hot water. A temperature of 73°C gave a suitable concentration of vapor in the cell (densities varied from 0.07 at 2500 to 0.57 at 2250). A correction of 0.06 density unit (3 to 4 percent) in the photographic blank was required to put the spectra obtained by the two different methods into agreement. The shapes of the two curves were nearly identical. This indicates that the values of gamma used in the photographic determinations were correct, and that the reciprocity law holds for the short exposures of the Lyman tube.

The Solution Spectrum

Although the solution spectrum to 2150 of hexamethylbenzene had been published,[12] it was decided, because of the importance of the spectrum in that region, to repeat the experiment. The spectrum was taken with a Cary, Model 11S, Recording Spectrophotometer with purified Phillips Pure Grade iso-pentane as the solvent.

For all of the spectra, Eastman Kodak white label hexamethylbenzene which had been purified by at least one sublimation was used.

In the next section the spectra are presented and the important features noted. The general significance of the results is mainly discussed in a succeeding section.

[12] Scheibe, Backenkohler, and Rosenberg, Ber. **59B**, 2617 (1926).

RESULTS

Figures 1 and 2 show the results of the final determinations of spectra. The similarity of the vapor spectra of hexamethylbenzene and that of benzene confirms the assumption that information obtained about the spectrum of one can be applied to the spectrum of the other. Although four different spectra were traced both manually and automatically (two manually on a Hilger microdensitometer and all four automatically on a Kip microdensitometer), no Rydberg members were detected. This result is not surprising in view of the known increase in diffuseness of such series with methyl substitution.[3]

It will be noted that there is one particular in which the vapor spectra of benzene and hexamethylbenzene do not agree. Between the 2200 and 2700 bands of hexamethylbenzene (which correspond to the 2000 and 2500 bands of benzene) there appears another band (2350) which does not appear in the benzene spectrum. It was in order to confirm the presence of this band that the spectrum was repeated; first with the hydrogen lamp from the Beckman D.U. Spectrophotometer as a source, and then in the Beckman Spectrophotometer itself. The presence of the new band in all the experiments obviates any possibility of its generation through errors in gamma or failure properly to take account of reciprocity failure with the Lyman source. The method

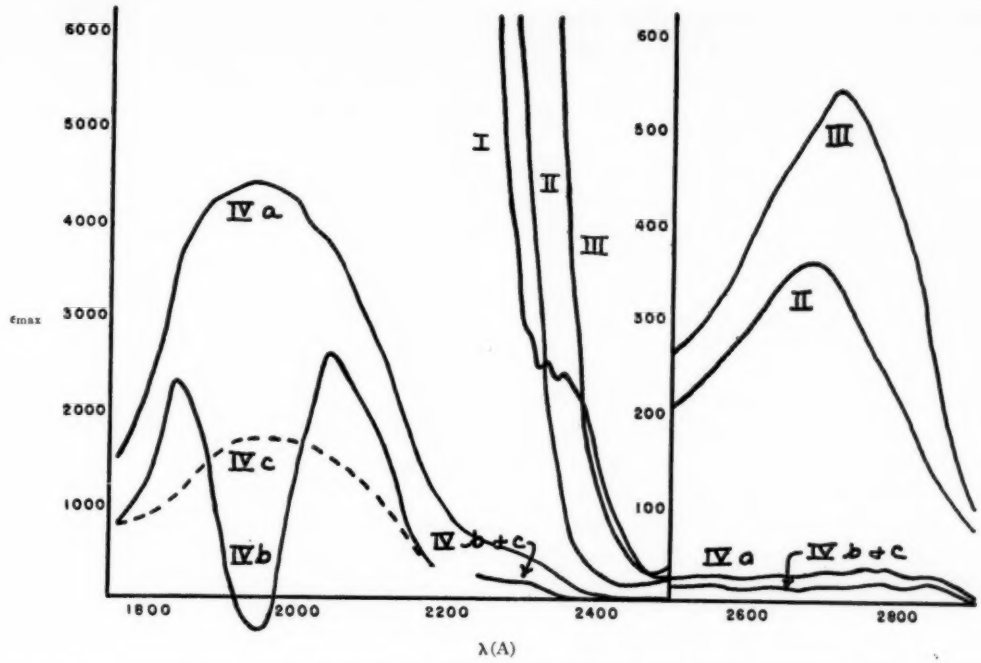

FIG. 2. The electronic spectrum of hexamethylbenzene at ten and one hundred times magnification compared with Fig. 1. Labeling the same as in Fig. 1.

for the spectrophotometric experiment was to trace through the spectrum taking readings every two millimicrons, then to return reading at intermediate wave lengths. The elapsed time between the readings at 2500 and 2480 and that at 2490 was close to an hour; nevertheless, the points of the return tracing fell exactly on the curve defined by the initial tracing. This fact not only serves to show that vapor pressure equilibrium had been attained in the sample cell, but almost entirely eliminates any possibility that the new band is a result of a compound produced by photodecomposition. The inference is that there is an extra electronic state observed in hexamethylbenzene, though to argue from "new band" to "extra electronic state" admittedly requires further experimentation.

The solution spectrum of hexamethylbenzene had been published earlier[12] with no indication of a new band. For that reason determination of the solution spectrum was repeated, and no band was found. This tends to confirm that the band was not caused by an impurity in our material. The maximum extinction coefficient of the new band is about 2400. Now even if the absorption band of an hypothetical impurity were as strong as the 1950 band of hexamethylbenzene ($\epsilon_{max} \approx 100\,000$), the percentage of impurity would have to exceed two. Because of the initial purity of the compound and the additional purity introduced by sublimation, it is felt that this percentage is much too high, and that impurities cannot be a significant factor.

The crystal spectrum of hexamethylbenzene shows conclusively that the 2000 A band of benzene is polarized predominantly parallel to the plane of the molecule and cannot, therefore, be assigned solely to a perpendicular Rydberg transition. It also shows, as was expected, that the 1800 band of benzene is predominantly polarized in the same direction. The percentage of perpendicular absorption in the 2700 band is found to be near 3 percent rather than 10 percent as reported by Scheibe, Hartwig, and Muller. Also the shape of the out-of-plane absorption curve for the band no longer follows that of the in-plane curve. The maximum extinction coefficient for light polarized perpendicular to the molecular plane in the region of the 2500 band is 20. In contrast, the amount of perpendicular absorption in the regions of the 2200 and 2700 bands is appreciable, and it is of interest to know the extent of that absorption.

The spectrum recorded by the light which has passed through the crystal in the extinction direction which is parallel to the b axis is entirely determined by in-plane absorption of the molecule. On the other hand, the spectrum recorded by the light which has passed through the crystal in the extinction direction which is perpendicular to the b axis is not entirely due to the extinction of the molecule perpendicular to the molecular plane. Because the molecules are tilted, 10°18′ from the propagation vector of the light,[1] the spectrum recorded when the plane of polarization is perpendicular to the b axis contains a small contribution from in-plane absorption. The value for the extinction coefficient perpendicular to the molecular plane is actually given by the expression

$$\frac{\epsilon_{\perp} - \cos^2(79°42')\epsilon_{\parallel}}{\cos^2(10°18')},$$

where $\epsilon_{\perp}$ and $\epsilon_{\parallel}$ refer to directions perpendicular and

parallel to the b axis. Above 2250 $\epsilon_{\parallel}$ can be obtained directly from experiment. Below 2250 its value must be approximated. The assumption is made that

$$\epsilon_{\text{vapor}} = (2/3)\epsilon_{\parallel} + (1/3)\epsilon_{\perp} \approx (2/3)\epsilon_{\parallel}.$$

Curve IVb is the curve obtained by correcting the measured curve (IVa) in this manner. It is obvious that the amount of correction near the peak of the 1950 band is too large. This indicates that this band is not as sharp when the compound is in the crystalline state as when it is in the vapor state. The integrated intensity of the band, however, should remain nearly the same in the two states. This would mean that while the correction is too large near the peak of the band it is too small on the edges of the band. Curve IVc is drawn so as to intercept equal areas above and below itself with curve IVb. This should be an approximate representation of the true absorption of the hexamethylbenzene molecule perpendicular to the plane of the ring. The value of the extinction coefficient in the vapor spectrum which would be necessary to bring curve IVb into coincidence with curve IVc at its peak is 58 000 rather than the observed 98 000. This is in good agreement with the variance observed in the condensed phase (solution) and vapor spectra of benzene—46 000 for the maximum extinction coefficient in solution as compared with 79 000 for the vapor. The larger values for hexamethylbenzene agree with the trend toward greater intensity with methyl substitution.

In summary, the vapor spectrum shows general agreement with benzene except for a new band ($\epsilon_{\max} \approx 2400$). The out-of-plane absorption is quite small over the entire region percentagewise, but nevertheless is appreciable on an absolute basis ($\epsilon_{\max} \approx 200$ for the 2200 band, and 1800 for the 1950 band). We now examine the significance of these results in the light of the theoretical work on benzene electronic states.

DISCUSSION

As noted by Lyons and Craig, and now confirmed for the whole band, the 2200 band (2000 band of benzene) is not polarized out-of-plane. The question as to whether or not the transition is NV (valence shell) or an in-plane Rydberg series member is not answered by this research; but Albrecht and Simpson have recently found that the transition is $A_{1g} \rightarrow B_{1u}$,[13] which along with much previous experimental and theoretical work, marks the transition as NV.

The next question is whether or not there might still be an out-of-plane Rydberg member in the 2200 region. We have calculated a transition moment for $2p \rightarrow 3s$ using a reasonable effective Z (3.2) and find $\sim$0.1 A. The area under the corrected *perpendicular* absorption from 1700 to 2350 corresponds to $\sim$0.3 A; so that the answer must be yes, there could be a Rydberg member after all (note however that the perpendicular absorption in the 2200 region is only a small fraction of the total absorption, 1700–2350). The simple intensity criterion employed here is not often used with all the confidence that it may deserve. If we had used the criterion we might not have attempted to test the 2200 band to see if it was out-of-plane in the first place, as it has an intensity corresponding to a transition moment *ca* five times the calculated value of 0.1 A for $2p \rightarrow 3s$. A particularly sure observation of a related nature is that the 1950 band (1800 band of benzene) must be allowed *in-plane*, as the molecules are not thick enough for the development of sufficient transition moment out-of-plane. (Each component of the degenerate pair has a transition moment of $\sim$1.3 A, as computed from the vapor spectrum area.)

We have seen that there is enough out-of-plane intensity in the region 1700–2350 to account for a Rydberg member; nevertheless this does not mean that there is a Rydberg member in the region. In the next section it is shown that it is not necessary to adhere to the theoretical argument for an out-of-plane Rydberg member. We may therefore use as a working hypothesis the idea that the perpendicular absorption is a natural part of the NV bands themselves.

Many fairly strong NV bands must have appreciable out-of-plane "backgrounds," as indeed is formally implied by the well-known Sponer-Teller treatment. The fact that the out-of-plane intensity can be considerably higher than for individual Rydberg members means that a large number of states (perhaps prominently including the continuum) are contributing. This is not surprising, because empirically the out-of-plane polarizability is of the order of the in-plane, if somewhat smaller. Therefore it is useful to think of a resultant band or frequency (in the sense of the one-term dispersion formula) which is about as strong as the NV bands. Let us assume now that the perpendicular absorptions at 1950, 2200, and 2700 all arise by borrowing from a single transition, and use the resonance denominator concept quantitatively.

If the 1950 and 2200 bands are assumed to borrow from the resultant band with equal effectiveness, then using the observed crystal out-of-plane intensities one locates the resultant band at 1725. Using this position and again assuming equal borrowing effectiveness one calculates for $\epsilon_{\max}$ at 2700 a value of 90. The observed value is 20 and this discrepancy is in accord with theory. That is, in benzene itself transition to the B_{1u} state (2200 band of hexamethylbenzene) can be made allowed out-of-plane by a single vibration in the upper state, but the state of B_{2u} (2700 band of hexamethylbenzene) needs to mix with a vibration which doesn't exist in the molecule.

Another though not a new argument, using resonance denominators, can be made for the in-plane or, essentially, total vapor absorption. It is assumed that the

[13] A. C. Albrecht and W. T. Simpson, J. Chem. Phys. (to be published). See also A. C. Albrecht and W. T. Simpson, J. Chem. Phys. **21**, 940 (1953), where the 2600 band of benzene is shown to be $A_{1g} \rightarrow B_{2u}$.

2700 and 2200 bands borrow from the 1950 band with equal matrix elements, as is suggested by the fact that for benzene the same vibrations mix E_{1u} with B_{1u} and B_{2u}. The in-plane intensities then depend solely on the resonance denominators. Using the observed 2700 intensity one calculates for the 2200 band $\epsilon_{max}=6000$. From Fig. 1, curve I, it can be seen that this value is about right, if correction is made for the tail of the 1950 band.

The last part of the discussion is about the new band at 2350 found in the vapor spectrum. The most obvious consideration is that more experimental work needs to be done, particularly to determine whether the band persists in such a set of derivatives as to show that it also belongs to benzene. It is tempting to suggest that the band may be a transition to the E_{2g} upper state which comes in when orbital theories are extended.[14] The absence of the band in solution or in the crystal may be linked up with a red shift of the 2200 band, or even the 1950 band, together with no shift or even a blue shift for the new band, assuming that in the condensed phase the new band is hidden under the other absorption.

QUANTUM NUMBERS IN RYDBERG SERIES

In this final section a suggestion is made about the quantum numbers in the Rydberg formula for unsaturated molecules. When the suggestion is applied to benzene it does away with the need for postulating absorption in the neighborhood of 2000 as arising from a Rydberg type transition. To begin, we review briefly the argument given by Hammond, Price, Teegan, and Walsh.

The apparent first observed frequency (wavelength 1600) considered to be out-of-plane is given by[3]

$$\text{I.P.}-\nu=R/(4-1.03)^2.$$

The expression is written with four as the principal quantum number because on physical grounds an appreciable negative quantum defect needs to be assumed. [Otherwise the right side would have to be $R/(3-0.03)^2$.] From the fact that the π electrons in benzene have $n=2$ it is supposed that there should be observed a band given by $R/(3-1.03)^2$, (wavelength ≈ 2146) so that the 1600 band is postulated to be really the second member of the out-of-plane series.

Let us now attempt to refute the argument. We may positively characterize the molecular orbital reached in the first out-of-plane transition. It is essentially a linear combination of $3s$ atomic orbitals with phases to match the originating orbital (highest filled benzene π orbital), hence with one nodal plane perpendicular to the plane of the molecule. After this step the orbitals are characterized in what is called "fused atomic orbital" description. The originating orbital becomes $3d$. That is, when the $2p$ atomic orbitals are moved to a common point of origin, as for a united atom approach, two nodal planes remain: one in the plane of the molecule, and one perpendicular to it. Similarly, the orbital reached in the first out-of-plane transition becomes $4p$. Note that the separated atom approach is used in building up the molecule, in the conventional way. Only then are the atomic orbitals fused.

The fused atomic orbital description gives the selection rules, but certainly not the energy of the electron in the originating molecular orbital. The energy is best thought of as described by $n=2$, modified by overlap forces to give bonding. The energy of the orbital reached in the transition likewise may be thought of as described by $n=3$. However energy considerations are not germane to the problem of deciding whether there is a transition given by $R/(3-1.03)^2$. The important point is the nodal character of the wave functions and the Pauli exclusion principle.

As n increases the fused atomic orbital approach becomes increasingly accurate, and gives the wave functions correctly in the limit. Consider an orbital which has a high enough quantum number to be hydrogen-like, with a true quantum number of n. Then as the quantum number is successively lowered the hydrogen-like quality disappears but the fused atomic orbital description remains appropriate for keeping track of the quantum number. At $n=4$ the orbital is certainly no longer hydrogen-like but has spread out into what is a linear combination of $3s$ atomic orbitals on the carbons. The quantum number is four because the fused atomic orbital description of this orbit is $4p$. The next lower orbital, $3p$ in this description, is filled (it is a linear combination of $2s$ carbon orbitals) so that the series stops at $n=4$. It is believed that only for the fused atomic orbital description is it required on physical grounds that there be an appreciable negative quantum defect. [Hence there is no objection to writing the series so that the 1600 band is represented by $R/(3-0.03)^2$ provided one does not misinterpret the virtual vanishing of the quantum defect].

It is concluded that the adoption of the form

$$R/(n-1.03)^2 \quad n=3,4,5\cdots$$

is incorrect in that the member $n=3$ represents transition to an already filled orbital. Generalizing, if there is to be invoked the necessity of an appreciable negative quantum defect, a fused atomic orbital approach should be used for the determination of the principal quantum number. Application of this idea seems to make simpler the understanding of Rydberg series in a number of unsaturated molecules, but this point is still under investigation.

[14] See for example Parr, Craig, and Ross, J. Chem. Phys. **18**, 156 (1950).

Analysis of Spin-Spin Multiplets in Nuclear Magnetic Resonance Spectra

H. M. McConnell, A. D. McLean, and C. A. Reilly
Shell Development Company, Emeryville, California

(Received October 18, 1954)

A systematic procedure is developed for the analysis of the spin-spin multiplets that are observed in the high-resolution NMR (nuclear magnetic resonance) spectra of liquids. It is shown how the symmetry properties of nuclear spin functions can be used to simplify the interpretation of NMR multiplets in terms of the empirical quantities, chemical shifts, and spin-spin coupling constants. It is also pointed out that when NMR multiplets have been properly interpreted in terms of these empirical quantities, it is then possible to predict theoretically relative intensities of multiplets to the same degree of precision as that involved in the measurement of multiplet frequency separations.

As an example the multiplet splittings of the H^1 and F^{19} resonances in 1,1-difluoroethylene are analyzed using the procedure proposed in the present paper.

INTRODUCTION

TWO magnetic nuclei in a molecule can exert two distinct magnetic forces on one another. The direct magnetic dipole-dipole interactions are responsible for the large line widths observed in the nuclear magnetic resonance (NMR) spectra of solid materials.[1] A much weaker indirect magnetic interaction between nuclei is responsible for the so-called "spin-spin" multiplets that are observed in the high resolution NMR spectra of liquid samples.[2] For liquids, the linewidth broadening by direct magnetic dipole-dipole interaction is greatly reduced because the energy of this interaction is averaged to zero by the high-frequency molecular motions characteristic of normal liquids.[3]

Multiplicities in the resonance signal from a given nuclear species can also arise because of differences in the magnetic shielding of chemically nonequivalent nuclei.[4] However, multiplets due to spin-spin interactions can be distinguished from the "chemical shift" multiplets in that the former are field independent whereas the latter are proportional to the applied magnetic field intensity.[2]

The numbers and relative intensities of the spin-spin multiplets can be accounted for empirically if the energy of interaction between any two magnetic nuclei in a molecule is taken to be proportional to the dot product of the spins of the two nuclei $\mathbf{I}_i \cdot \mathbf{I}_j$.[2] The constant of proportionality is called the spin-spin coupling constant J_{ij}, so that the energy of interaction of nuclei i and j is $J_{ij}\mathbf{I}_i \cdot \mathbf{I}_j$.

Gutowsky, McCall, and Slichter[2] have shown that for many molecules there is a simple relation between the observed multiplet splittings, their intensities, and the coupling constants. For example, the F^{19} resonance of PF_3 is a simple symmetrical doublet corresponding to the two equally probable "spin-up" and "spin-down" orientations of the P^{31} nucleus in the applied magnetic field. The P–F coupling constant J^{PF} is simply equal to the multiplet separation (in cps). The P^{31} resonance in PF_3 is split into a symmetrical quartet with relative intensities 1:3:3:1. This multiplet pattern corresponds simply to the four possible components of the total F_3 spin along the field axis: $-\frac{3}{2}\hbar$; $-\frac{1}{2}\hbar$; $+\frac{1}{2}\hbar$; $+\frac{3}{2}\hbar$, and the relative intensities correspond to the threefold statistical weights of the $-\frac{1}{2}\hbar$ and $+\frac{1}{2}\hbar$ states of the F_3 group. Again the multiplet separations are simply equal to J^{PF}.

As will be seen from the discussion in the present paper, such simple multiplet analyses are possible only for (1) a few simple rigid and symmetrical molecules and (2) those molecules for which rapid internal rotation effectively increases the symmetry. For many other relatively simple substances, and for a host of complex compounds, the analysis of multiplet splittings and relative intensities in terms of coupling constants and chemical shifts is by no means trivial. For example, the simple symmetrical 1,1-difluoroethylene molecule, $CF_2=CH_2$ (to be discussed later in this paper), shows at least eight distinct signals in *both* the H^1 and F^{19} resonance spectra. As another example, it may be mentioned that we have observed *fifty-two* distinct signals in the F^{19} resonance spectrum of a slightly more complex substance, perfluoropropylene; $CF_3CF=CF_2$. The purpose of the present paper is to propose what we believe to be a systematic and useful procedure for the analysis of multiplet splittings and intensities in terms of chemical shifts and coupling constants. According to this procedure, the Zeeman energy levels of an assembly of molecular nuclei are classified as to their angular momenta and symmetry properties. Just as in other fields of spectroscopy, this type of classification greatly facilitates the factorization of the secular equation which determines the energies of the nuclear spin states; in addition this classification provides a convenient formulation of the spectroscopic selection rules.

[1] See, for example, R. V. Pound, Phys. Rev. **79**, 685 (1950); **82**, 343 (1951); R. Livingston, J. Chem. Phys. **20**, 1170 (1952); N. A. Schuster and G. E. Pake, Phys. Rev. **81**, 157, 886 (1951).
[2] Gutowsky, McCall, and Slichter, J. Chem. Phys. **21**, 279 (1953).
[3] Bloembergen, Purcell, and Pound, Phys. Rev. **71**, 466 (1947).
[4] W. D. Knight, Phys. Rev. **76**, 1259 (1949); W. C. Dickinson, Phys. Rev. **77**, 736 (1950); W. G. Proctor and F. C. Yu, Phys. Rev. **77**, 717 (1950).

I. OUTLINE OF THE METHOD

The present quantum-mechanical procedure for the analysis of NMR spectra is, in outline at least, quite similar to the methods that have been extensively employed in other fields of spectroscopy (e.g., infrared, ultraviolet, etc.). According to these methods the exact Hamiltonian for the energy of a molecule is simplified in some way so as to give an approximate Hamiltonian; the approximate Hamiltonian is chosen to be as accurate as possible and, at the same time, to be such that the Schrödinger equation can be solved exactly and conveniently. The zero-order energies and wave functions thus obtained are then used as a starting point for a more accurate calculation of energies and wave functions using, in so far as possible, a complete, exact Hamiltonian. This latter calculation is, in many cases, greatly simplified by selecting the zero-order wave functions to be eigenfunctions of all those molecular properties that commute with the complete Hamiltonian. Molecular symmetry and spin or rotational angular momenta are typical of such molecular properties. The exact wave functions and energies are also commonly classified according to such molecular properties inasmuch as the spectroscopic selection rules are generally conveniently formulated in terms of such classifications. Also the classification of energy states according to these molecular properties often enable one to predict how transition energies and intensities will behave under specified perturbations.

In the remainder of the present section there are given the exact and approximate Hamiltonians that are used for calculating the Zeeman energies of a system of magnetic nuclei in a molecule where there is (indirect) spin-spin coupling. The classification of the zero-order spin functions for a molecule in terms of symmetry and spin angular momenta is discussed in Secs. II and III. Section IV describes how such classifications simplify the solution of the secular equation for the energies. Section V gives a formulation of the spectroscopic selection rules. As an example of the application of these methods, Sec. VI presents an analysis of the high-resolution NMR spectra of 1,1-difluoroethylene.

In the present work we shall regard all NMR signals as arising from radiation induced transitions between stationary state energy levels. The calculation of the energy levels, and the derivation of the spectroscopic selection rules are based on the Hamiltonian[5] given in the following equations:

$$\mathcal{H}=\mathcal{H}^{(0)}+\mathcal{H}^{(1)}, \tag{1}$$

where

$$\mathcal{H}^{(0)}=\frac{1}{2\pi}\sum_i \gamma_i H_i I_z(i), \tag{2}$$

$$\mathcal{H}^{(1)}=\sum_{i<j} J_{ij}\mathbf{I}(i)\cdot\mathbf{I}(j). \tag{3}$$

[5] This Hamiltonian is discussed by Gutowsky, McCall, and Slichter (reference 2), and by N. F. Ramsey and E. M. Purcell, Phys. Rev. **85**, 143 (1952) and N. F. Ramsey, Phys. Rev. **91**, 303 (1953).

In Eqs. (1), (2), and (3) the complete Hamiltonian $\mathcal{H}$ is the sum of two terms $\mathcal{H}^{(0)}$ and $\mathcal{H}^{(1)}$. The $\mathcal{H}^{(0)}$ gives the sum of the magnetic interactions of all nuclei with the externally applied (stationary) magnetic field, and the $\mathcal{H}^{(1)}$ gives the sum of the spin-spin interactions of all pairs of nuclei. In Eq. (2), γ_i is the magnetogyric ratio of nucleus i, H_i is the stationary magnetic field acting at nucleus i, and $I_z(i)$ is the component of the spin angular momentum vector of i along the stationary field which is here taken to be the z-axis. In Eq. (3), J_{ij} is the spin-spin coupling constant between nuclei i and j. The spin angular momentum vector of nucleus i is $\mathbf{I}(i)$.

For convenience in comparisons with experimental data all energies are here expressed in cycles per second. All spins $[\mathbf{I}(i)]$ are expressed in units of $\hbar$ and so the quantities $\mathbf{I}(i)$ and $I_z(i)$ are dimensionless and J_{ij} is in cycles per second.

Only nuclei with spin $\frac{1}{2}$ will be considered here; extension of the equations and results to systems containing nuclei with spin greater than $\frac{1}{2}$ is straightforward provided there are no complications due to quadrupole coupling.

We let Φ_i and Φ_i^0 be the stationary state eigenfunctions of $\mathcal{H}$ and $\mathcal{H}^{(0)}$, respectively, and let $\mathcal{E}_i$ and $\mathcal{E}_i^{(0)}$ be the corresponding eigenenergies. Our problem will then be to solve the secular equation,

$$|\mathcal{H}_{mn}-\mathcal{E}\delta_{mn}|=0 \tag{4}$$

for the eigenenergies. In (4),

$$\mathcal{H}_{mn}=(\Phi_m^0|\mathcal{H}|\Phi_n^0), \tag{5}$$

and $\delta_{mn}=1$ if $m=n$ and $\delta_{mn}=0$ if $m\neq n$. The exact eigenfunctions of the complete Hamiltonian are expressed in terms of the Φ_n^0 by the equations

$$\Phi_m=\sum_{n=1}^{M} a_{mn}\Phi_n^0, \tag{6}$$

where the a_{mn} are obtained from the solutions of the M simultaneous equations,

$$\sum_{n=1}^{M}[\mathcal{H}_{mn}-\delta_{mn}\mathcal{E}_m]a_{mn}=0. \tag{7}$$

The order of secular equation (4) is 2^p, where p is the number of nuclei in the molecule with spin $\frac{1}{2}$. Evidently then Eq. (4) can only be useful for obtaining the energies $\mathcal{E}_n$ for molecules with, say, $p\geq 5$, when the secular equation is easily factored. Sections II and III discuss the manner in which the Φ_n^0 are to be selected so as to achieve the optimum factoring of secular equation (4).

The solutions of (4) give the energies in terms of the coupling constants J_{ij}, the γ_i, and the H_i. A later section on selection rules, Sec. V, then permits one to determine which of the transition frequencies $\mathcal{E}_m-\mathcal{E}_n$ are observable.

TABLE I. Zero-order spin functions for equivalent nuclei.

No. nuclei	Group symmetry	Spin function	Designation
2	$D_{\infty h}$	$(\alpha\alpha)$	$^3(A_{1g})_1$
2	$D_{\infty h}$	$\frac{1}{\sqrt{2}}(\alpha\beta+\beta\alpha)$	$^3(A_{1g})_0$
2	$D_{\infty h}$	$(\beta\beta)$	$^3(A_{1g})_{-1}$
2	$D_{\infty h}$	$\frac{1}{\sqrt{2}}(\alpha\beta-\beta\alpha)$	$^1(A_{2u})_0$
3	D_{3h}	$(\alpha\alpha\alpha)$	$^4(A_1')_{\frac{3}{2}}$
3	D_{3h}	$\frac{1}{\sqrt{3}}(\alpha\alpha\beta+\alpha\beta\alpha+\beta\alpha\alpha)$	$^4(A_1')_{\frac{1}{2}}$
3	D_{3h}	$\frac{1}{\sqrt{3}}(\beta\beta\alpha+\beta\alpha\beta+\alpha\beta\beta)$	$^4(A_1')_{-\frac{1}{2}}$
3	D_{3h}	$(\beta\beta\beta$	$^4(A_1')_{-\frac{3}{2}}$
3	D_{3h}	$\frac{1}{\sqrt{6}}(\alpha\alpha\beta+\alpha\beta\alpha-2\beta\alpha\alpha)$ $\frac{1}{\sqrt{2}}(\alpha\alpha\beta-\alpha\beta\alpha)$	$^2(E')_{\frac{1}{2}}$
3	D_{3h}	$\frac{1}{\sqrt{6}}(\beta\beta\alpha+\beta\alpha\beta-2\alpha\beta\beta)$ $\frac{1}{\sqrt{2}}(\beta\beta\alpha-\beta\alpha\beta)$	$^2(E')_{-\frac{1}{2}}$
4	D_{4h}	$(\alpha\alpha\alpha\alpha)$	$^5(A_{1g})_2$
4	D_{4h}	$\frac{1}{2}(\alpha\alpha\alpha\beta+\alpha\alpha\beta\alpha+\alpha\beta\alpha\alpha+\beta\alpha\alpha\alpha)$	$^5(A_{1g})_1$
4	D_{4h}	$\frac{1}{\sqrt{6}}(\alpha\alpha\beta\beta+\alpha\beta\beta\alpha+\beta\alpha\alpha\beta+\beta\beta\alpha\alpha$ $+\alpha\beta\alpha\beta+\beta\alpha\beta\alpha)$	$^5(A_{1g})_0$
4	D_{4h}	$\frac{1}{2}(\beta\beta\beta\alpha+\beta\beta\alpha\beta+\beta\alpha\beta\beta+\alpha\beta\beta\beta)$	$^5(A_{1g})_{-1}$
4	D_{4h}	$(\beta\beta\beta\beta)$	$^5(A_{1g})_{-2}$
4	D_{4h}	$\frac{1}{2}(\alpha\alpha\alpha\beta-\alpha\alpha\beta\alpha+\alpha\beta\alpha\alpha-\beta\alpha\alpha\alpha)$	$^3(B_{2g})_1$
4	D_{4h}	$\frac{1}{\sqrt{2}}(\alpha\beta\alpha\beta-\beta\alpha\beta\alpha)$	$^3(B_{2g})_0$
4	D_{4h}	$\frac{1}{2}(\beta\beta\beta\alpha-\beta\beta\alpha\beta+\beta\alpha\beta\beta-\alpha\beta\beta\beta)$	$^3(B_{2g})_{-1}$
4	D_{4h}	$\frac{1}{\sqrt{2}}(\alpha\alpha\alpha\beta-\alpha\beta\alpha\alpha)$ $\frac{1}{\sqrt{2}}(\alpha\alpha\beta\alpha-\beta\alpha\alpha\alpha)$	$^3(E_u)_1$
4	D_{4h}	$\frac{1}{\sqrt{2}}(\alpha\alpha\beta\beta-\beta\beta\alpha\alpha)$ $\frac{1}{\sqrt{2}}(\alpha\beta\beta\alpha-\beta\alpha\alpha\beta)$	$^3(E_u)_0$
4	D_{4h}	$\frac{1}{\sqrt{2}}(\beta\beta\beta\alpha-\beta\alpha\beta\beta)$ $\frac{1}{\sqrt{2}}(\beta\beta\alpha\beta-\alpha\beta\beta\beta)$	$^3(E_u)_{-1}$
4	D_{4h}	$\frac{1}{\sqrt{12}}(\alpha\alpha\beta\beta+\alpha\beta\beta\alpha+\beta\alpha\alpha\beta+\beta\beta\alpha\alpha$ $-2\alpha\beta\alpha\beta-2\beta\alpha\beta\alpha)$	$^1(A_{1g})_0$
4	D_{4h}	$\frac{1}{2}(\alpha\alpha\beta\beta-\alpha\beta\beta\alpha-\beta\alpha\alpha\beta+\beta\beta\alpha\alpha)$	$^1(B_{1g})_0$

II. ZERO-ORDER SPIN FUNCTIONS FOR GROUPS OF CHEMICALLY EQUIVALENT NUCLEI

Let us consider a molecule which contains only one group of chemically equivalent nuclei of spin $\frac{1}{2}$ (e.g., CH_3Br). We shall refer to this group as group A. For group A we may write the Hamiltonian in the form

$$\mathcal{H}(A)=\mathcal{H}^{(0)}(A)+\mathcal{H}^{(1)}(AA), \tag{8}$$

$$\mathcal{H}^{(0)}(A)=\frac{1}{2\pi}\gamma_A H_A F_z(A), \tag{9}$$

$$\mathcal{H}^{(1)}(AA)=\sum_{i<j} J_{ij}{}^{AA}\mathbf{I}(A_i)\cdot\mathbf{I}(A_j), \tag{10}$$

$$F_z(A)=\sum_i I_z(A_i). \tag{11}$$

In solving secular equation (4) either for a molecule containing only group A, or for a molecule containing additional groups of chemically equivalent nuclei $(B,C,\cdots)$, it is of great convenience to choose the eigenfunctions of $\mathcal{H}^{(0)}(A)$ to be also eigenfunctions of all those operators which commute with $\mathcal{H}(A)$. These operators include $F_z(A)$, $F^2(A)$, and $R_i(A)$, where

$$\mathbf{F}(A)=\sum_i \mathbf{I}(A_i) \tag{12}$$

and where the $R_i(A)$ are the covering operations of the point group to which A belongs. As an example of the operations $R_i(A)$ consider the three chemically equivalent protons in a CH_3 group (group A). The Hamiltonian for this system is formally identical to that of three bare protons arranged in an equilateral triangle. In this case $\mathcal{H}^{(0)}(A)$ and $\mathcal{H}(A)$ commute with the covering operations of the point group D_{3h}.[6]

Represent the exact eigenfunctions of $\mathcal{H}^{(0)}(A)$ and $\mathcal{H}(A)$ by $\Phi_m{}^0(A)$ and $\Phi_m(A)$. These functions, or linear combinations of them, may be classified according to their behavior with respect to the covering operations of the point group to which group A belongs. In the case of the three nuclei with spin $\frac{1}{2}$ and arranged as in

[6] The group notation used throughout the present paper is that of Eyring, Walter, and Kimball, *Quantum Chemistry* (John Wiley and Sons, Inc., New York, 1944).

CH_3 with D_{3h} effective symmetry, there are four spin functions of A_1' symmetry and two pairs of spin functions belonging to the symmetry degenerate representations E'.

Since $F^2(A)$ and $F_z(A)$ also commute with $\mathcal{H}^{(0)}(A)$ and $\mathcal{H}^{(1)}(AA)$, and with one another, and also with $R_i(A)$, the functions $\Phi_m{}^0(A)$ and $\Phi_m(A)$ can be chosen to be simultaneous eigenfunctions of all these operators. Actually, instead of classifying the spin functions $\Phi_m{}^0(A)$ and $\Phi_m(A)$ according to their eigenvalues of the operator $F^2(A)$, it is more convenient to use the multiplicity S, which is related to the eigenvalue of $F^2(A)$ by the equation

$$F(F+1)=\frac{S^2-1}{4}, \tag{13}$$

where $F(F+1)$ is the eigenvalue of $F^2(A)$ in the state for which S is the multiplicity.

In Table I there are given $\Phi_i{}^0(A)$ functions for two nuclei with $D_{\infty h}$ symmetry, three nuclei with D_{3h} symmetry, and four nuclei with D_{4h} symmetry.

The functions given in Table I are easily derived using standard group-theoretical methods; the functions are eigenfunctions of $F^2(A)$, $F_z(A)$, and $R_i(A)$. The symbols in Table I which are used to identify the spin functions are defined according to the following scheme:

$$^S(X)_M. \tag{14}$$

In (14), S is the multiplicity defined according to (13), M is the eigenvalue of $F_z(A)$, and X gives the designation of the particular representation of the group to which the spin function belongs.

In the following tables and text we use the convention that in all products of single nucleus spin functions the nuclei are written in serial order; i.e., the product spin function $\alpha\alpha\beta\alpha$ is $\alpha(1)\alpha(2)\beta(3)\alpha(4)$. Also, since the spins are expressed in units of $\hbar$,

$$I_z(1)\alpha(1)=\tfrac{1}{2}\alpha(1),$$
$$I_z(1)\beta(1)=-\tfrac{1}{2}\beta(1).$$

III. ZERO-ORDER SPIN FUNCTIONS FOR MOLECULES WITH NONEQUIVALENT NUCLEI

Let us next consider a molecule containing more than one group of chemically equivalent nuclei, say groups $A,B,C,\cdots$. In this case the Hamiltonian can be written in the form,

$$\begin{aligned}\mathcal{H}(AB\cdots)=&\mathcal{H}^{(0)}(A)+\mathcal{H}^{(0)}(B)+\cdots\\&+\mathcal{H}^{(1)}(AA)+\mathcal{H}^{(1)}(BB)+\cdots\\&+\mathcal{H}^{(1)}(AB)+\cdots,\end{aligned} \tag{15}$$

where

$$\mathcal{H}^{(1)}(AB)=\sum_{i,j} J_{ij}{}^{AB}\mathbf{I}(A_i)\cdot\mathbf{I}(B_j) \tag{16}$$

and the other terms in (15) are similar to those defined for Eqs. (8)–(11). Except for degenerate spin functions, the zero-order spin functions corresponding to the solution of the Hamiltonian may be taken as simple products

$$\Phi_m{}^0(AB\cdots)=\Phi_p{}^0(A)\Phi_q{}^0(B)\cdots. \tag{17}$$

In cases of degeneracies one may, in general, take linear combinations of products of the type given in (17). The eigenenergies of $\mathcal{H}^{(0)}(A)+\mathcal{H}^{(0)}(B)+\cdots$ are

$$\mathcal{E}_m{}^{(0)}(AB\cdots)=\mathcal{E}_p{}^{(0)}(A)+\mathcal{E}_q{}^{(0)}(B)+\cdots. \tag{18}$$

The only operators which *always* commute with $\mathcal{H}^{(0)}(A)+\mathcal{H}^{(0)}(B)+\cdots$ and $\mathcal{H}(AB\cdots)$ are $F_z(AB\cdots)$ and $R_i(AB\cdots)$, where

$$F_z(AB\cdots)=F_z(A)+F_z(B)+\cdots, \tag{19}$$

and $R_i(AB\cdots)$ are all those covering operations for the entire molecule $AB\cdots$; i.e., those covering operations common to the point groups of groups $A,B,\cdots$. Only in certain special cases, to be discussed later, do other operators commute with $\mathcal{H}(AB\cdots)$. In designating the complete nuclear spin functions for molecules containing more than a single group of equivalent nuclei, we shall use the same notation as that proposed in the previous section *except* that the multiplicities will no longer be given. In such cases the multiplicities are deleted because $F^2(AB\cdots)$ does not commute with $\mathcal{H}(AB\cdots)$. If for a particular molecule there is more than one spin function belonging to the same representation of the molecular point group, and having the same eigenvalues of $F_z(AB\cdots)$, then these states will be distinguished by labeling arbitrarily these spin functions. For example, in $CH_2{=}CF_2$ there are four states with $(A_1)_0$ symmetry and these are labeled arbitrarily according to the scheme: $1(A_1)_0$, $2(A_1)_0$, $3(A_1)_0$, and $4(A_1)_0$.

Table II shows the detailed products which are used

TABLE II. Zero-order spin functions for two nuclei in group A, two nuclei in group B, and C_{2v} molecular symmetry.

$\Phi_i{}^0(A-D_{\infty h})$	$\Phi_j{}^0(B-D_{\infty h})$	$\Phi_m{}^0(AB-C_{2v})$[a]
$^3(A_{1g})_1$	$^3(A_{1g})_1$	$1(A_1)_2$
$^3(A_{1g})_0$	$^3(A_{1g})_1$	$1(A_1)_1$
$^3(A_{1g})_1$	$^3(A_{1g})_0$	$2(A_1)_1$
$^3(A_{1g})_{-1}$	$^3(A_{1g})_1$	$1(A_1)_0$
$^3(A_{1g})_1$	$^3(A_{1g})_{-1}$	$2(A_1)_0$
$^1(A_{2u})_0$	$^1(A_{2u})_0$	$3(A_1)_0$
$^3(A_{1g})_0$	$^3(A_{1g})_0$	$4(A_1)_0$
$^3(A_{1g})_0$	$^3(A_{1g})_{-1}$	$1(A_1)_{-1}$
$^3(A_{1g})_{-1}$	$^3(A_{1g})_0$	$2(A_1)_{-1}$
$^3(A_{1g})_{-1}$	$^3(A_{1g})_{-1}$	$1(A_1)_{-2}$
$^1(A_{2u})_0$	$^3(A_{1g})_1$	$1(B_2)_1$
$^3(A_{1g})_1$	$^1(A_{2u})_0$	$2(B_2)_1$
$^3(A_{1g})_0$	$^1(A_{2u})_0$	$1(B_2)_0$
$^1(A_{2u})_0$	$^3(A_{1g})_0$	$2(B_2)_0$
$^1(A_{2u})_0$	$^3(A_{1g})_{-1}$	$1(B_2)_{-1}$
$^3(A_{1g})_{-1}$	$^1(A_{2u})_0$	$2(B_2)_{-1}$

[a] Note that the $\Phi_m{}^0(AB)$ are products of $\Phi_i{}^0(A)$ and $\Phi_j{}^0(B)$ listed on the same row.

TABLE III. Spin states for three nuclei in group A, three nuclei in group B, and D_{3h} molecular symmetry.

Symmetry	Number of states
$(A_1')_3$	1
$(A_1')_2$	2
$(A_1')_1$	4
$(A_1')_0$	6
$(A_1')_{-1}$	4
$(A_1')_{-2}$	2
$(A_1')_{-3}$	1
$(A_2')_1$	1
$(A_2')_0$	2
$(A_2')_{-1}$	1
$(E')_2$	2
$(E')_1$	5
$(E')_0$	6
$(E')_{-1}$	5
$(E')_{-2}$	2

in obtaining the zero-order spin functions for a molecule with C_{2v} symmetry containing two nuclei in group A and two nuclei in group B.

To illustrate this procedure a little further, let us consider the zero-order spin functions corresponding to a molecule with D_{3h} symmetry and having three nuclei in group A and three nuclei in group B. By using the information containing in Table I for the zero-order spin functions for group A and group B, and by using the group multiplication table for the D_{3h} point group, one can show that the molecule $(AB-D_{3h})$ will have zero-order spin functions corresponding to the various symmetries given in Table III. Explicit formulas for all of the states listed in Table III (in terms of α's and β's) are easily obtained as products of the spin functions listed in Table I (under D_{3h}) except in those cases which involve products of pairs of degenerate E' spin functions. In this latter case, for which $E'\times E'=A_1'+A_2'+E'$, one must take linear combinations of the four possible products of each member of the degenerate E' states which correspond to A_1', A_2', and E'.

IV. SOLUTION OF THE SECULAR EQUATION

The solution of the secular equation (4) can now be greatly simplified by using zero-order spin functions of the type described in the two previous sections. This simplification is achieved by specifying those conditions under which the nondiagonal matrix elements in (4) are zero, i.e., those conditions for which $\mathcal{H}_{mn}=0$ when $m\neq n$.

Let the symbol Q stand for all those operators that commute with the complete Hamiltonian $\mathcal{H}(AB\cdots)$ and also $\mathcal{H}^{(0)}(A)+\mathcal{H}^{(0)}(B)+\cdots$. The class Q will always include $R_i(AB\cdots)$ and $F_z(AB\cdots)$, but in special cases other operators will be included in the class Q.

The zero-order spin functions have been chosen to be eigenfunctions of Q so that

$$Q\Phi_m^0=Q_m\Phi_m^0. \tag{20}$$

Therefore, we have in general

$$\mathcal{H}\Phi_m^0=\sum_n \mathcal{H}_{nm}\Phi_n^0, \tag{21}$$

$$Q\mathcal{H}\Phi_m^0=\sum_n \mathcal{H}_{nm}Q_n\Phi_n^0, \tag{22}$$

and

$$Q_m\sum_n \mathcal{H}_{nm}\Phi_n^0=\sum_n \mathcal{H}_{nm}Q_n\Phi_n^0. \tag{23}$$

According to (23), $\mathcal{H}_{mn}=0$ unless $Q_m=Q_n$. One can also show that, in general, $\mathcal{H}_{mn}=0$ when m and n are members of a degenerate (E) set provided that the degenerate functions are orthogonal.

Since the class Q always includes $R_i(AB\cdots)$ and $F_z(AB\cdots)$ for any molecule, we always know that $\mathcal{H}_{mn}=0$ if Φ_m^0 and Φ_n^0 belong to different representations of the same point group, or if Φ_m^0 and Φ_n^0 have different eigenvalues of $F_z(AB\cdots)$.

For example, we can now immediately say that the secular equation for a molecule with C_{2v} symmetry having two nuclei in group A and two nuclei in group B (compare Table II) will exactly factor into two 1×1 determinants [the $1(A_1)_2$ and $1(A_1)_{-2}$ states], five 2×2 determinants [involving $(A_1)_1$, $(A_1)_{-1}$, $(B_2)_1$, $(B_2)_0$, and $(B_2)_{-1}$ states] and one 4×4 determinant [involving the four $(A_1)_0$ states]. In many cases the solutions of the factored secular equation can be quite well approximated by perturbation theory.

The starting spin functions $\Phi_m^0(AB)$ will be represented as in Table II [e.g., $3(A_1)_0$] and the corresponding exact functions $\Phi_m(AB)$ or the perturbation theory approximation to the exact functions $\Phi_m(AB)$ are represented in the same manner except that a prime will be placed after the first index [e.g., $3'(A_1)_0$].

It may be of interest to point out that there are some relatively simple rules that can be used in the evaluation of nonzero matrix elements involving spin-spin interactions. In the evaluation of a matrix element of the type

$$(\Phi_m^0|\sum_{i,j} J_{ij}\mathbf{I}(i)\cdot\mathbf{I}(j)|\Phi_n^0)$$

there occur many terms of the type

$$(\psi_p|\sum_{i<j} J_{ij}\mathbf{I}(i)\cdot\mathbf{I}(j)|\psi_q),$$

where the ψ_p and ψ_q are single products of spin functions such as $\alpha\beta\alpha\alpha\cdots$. These integrals are easily evaluated by the equations

$$(\psi_p|\sum_{i<j} J_{ij}\mathbf{I}(i)\cdot\mathbf{I}(j)|\psi_p)=\tfrac{1}{4}\sum_{i<j} J_{ij}T_{ij}, \tag{24}$$

where $T_{ij}=+1$ if spins i and j are parallel, and $T_{ij}=-1$ if spins i and j are antiparallel.

$$(\psi_p|\sum_{i<j} J_{ij}\mathbf{I}(i)\cdot\mathbf{I}(j)|\psi_q)=\tfrac{1}{2}UJ_{ij}, \tag{25}$$

where $U=1$ if ψ_p only differs from ψ_q in the permutation of spins i and j, and $U=0$ in all other cases.

For some molecules still other operators belong to the class Q. This is true for a few simple substances (such as PF_3 mentioned in the Introduction) and is also true for many molecules having rapid internal rotations. Let us consider a molecule containing a group of equivalent nuclei A and another group of equivalent nuclei B, and having internal rotation such that $J_{ij}^{AB}=J^{AB}$ for all i, j. An example of this would be CH_3-CF_3, where rapid internal rotation about the C−C single bond effectively averages to zero all the instantaneous differences between the various H−F coupling constants. The complete Hamiltonian for the molecule under consideration is then given by

$$\begin{aligned}\mathcal{H}=&\mathcal{H}^{(0)}(A)+\mathcal{H}^{(0)}(B)\\&+\mathcal{H}^{(1)}(AA)+\mathcal{H}^{(1)}(BB)\\&+J^{AB}\mathbf{F}(A)\cdot\mathbf{F}(B).\end{aligned}\tag{26}$$

For the Hamiltonian in (26), the following operators belong to the class Q: $R_i(A)$, $R_i(B)$, $F^2(A)$, $F^2(B)$, $\mathcal{H}^{(1)}(AA)$, $\mathcal{H}^{(1)}(BB)$ as well as $R_i(AB)$ and $F_z(AB)$. Moreover, the zero-order spin functions discussed in the previous sections are eigenfunctions of these operators. Thus, for the Hamiltonian in (26) we have that, for $m\neq n$,

$$\mathcal{H}_{mn}=J^{AB}(\Phi_m^0(AB)\,|\,\mathbf{F}(A)\cdot\mathbf{F}(B)\,|\,\Phi_n^0(AB)).\tag{27}$$

Equation (27) may be rewritten in the form

$$\begin{aligned}\mathcal{H}_{mn}=J^{AB}&(\Phi_i^0(A)\,|\,\mathbf{F}(A)\,|\,\Phi_j^0(A))\\&\times(\Phi_p^0(B)\,|\,\mathbf{F}(B)\,|\,\Phi_q^0(B)),\end{aligned}\tag{28}$$

where

$$\Phi_m^0(AB)=\Phi_i^0(A)\Phi_p^0(B)\tag{29}$$

and

$$\Phi_n^0(AB)=\Phi_j^0(A)\Phi_q^0(B).$$

We note that $\mathcal{H}_{mn}=0$ unless:

(1) $\Phi_i^0(A)$ and $\Phi_j^0(A)$ belong to the same representation of the symmetry group of the A group of equivalent nuclei; i.e., these two functions must have the same eigenvalues of $R_i(A)$.

(2) $\Phi_i^0(A)$ and $\Phi_j^0(A)$ have the same multiplicity.

(3) $(F_z(A))_i=(F_z(A))_j\pm1$, where

$$F_z(A)\Phi_i^0(A)=(F_z(A))_i\Phi_i^0(A).\tag{30}$$

(4) Conditions (1)–(2) hold also for $\Phi_p^0(B)$ and $\Phi_q^0(B)$ and $(F_z(B))_p=(F_z(B))_q\mp1$.

(5) $(F_z(AB))_m=(F_z(AB))_n$.

It is easily shown that all the diagonal matrix elements of $J^{AB}(\mathbf{F}_A\cdot\mathbf{F}_B)$ are given by the equation,

$$\begin{aligned}(\Phi_m^0(AB)\,|\,&J^{AB}\mathbf{F}(A)\cdot\mathbf{F}(B)\,|\,\Phi_m^0(AB))\\&=J^{AB}(F_z(A))_i(F_z(B))_p.\end{aligned}\tag{31}$$

In the section on selection rules, it will be shown that for those classes of molecules corresponding to the Hamiltonian in (26), it is not necessary to calculate eigenvalues of $\mathcal{H}^{(1)}(AA)$ and $\mathcal{H}^{(1)}(BB)$ since these eigenvalues do not affect the observed spectra.

V. SELECTION RULES

The probability $P(m\rightarrow n)$ (in $\sec^{-1}$) that a nuclear system undergoes the transition $m\rightarrow n$ (i.e., $\Phi_m\rightarrow\Phi_n$) is given by the equation[7]

$$P(m\rightarrow n)=\frac{8\pi^3}{h^2}(\mu_x)_{mn}{}^2\rho_\nu,\tag{32}$$

where

$$\mu_x=\hbar\sum_i\gamma_iI_x(i)\tag{33}$$

and

$$(\mu_x)_{mn}=(\Phi_m\,|\,\mu_x\,|\,\Phi_n).\tag{34}$$

In (32), ρ_ν is the energy density per unit frequency range arising from the oscillatory radio-frequency field in the x-direction.

For a molecule containing groups of chemically equivalent nuclei, $A,B,\cdots$, one condition that $(\mu_x)_{mn}$ be different from zero is

$$(F_z(AB\cdots))_m-(F_z(AB\cdots))_n=\pm1.\tag{35}$$

This is our first selection rule and is the familiar requirement for magnetic dipole radiation. Additional selection rules are derived by the following considerations.

Of the operators Q which commute with the complete Hamiltonian $\mathcal{H}$, there will be a subclass Q', which also commute with μ_x:

$$Q'\mu_x-\mu_xQ'=0.\tag{36}$$

One then has the set of selection rules that if $(\mu_x)_{mn}\neq0$ then $Q_m'=Q_n'$, or conversely if $Q_m'\neq Q_n'$ then $(\mu_x)_{mn}=0$ and the $m\rightarrow n$ transition is forbidden.

For any arbitrary nuclear system the only operations which always belong to Q' are the symmetry operations $R_i(AB\cdots)$. We therefore have the general selection rule: If the $m\rightarrow n$ transition is allowed, then the upper and lower energy state spin functions belong to the same representation of the molecular point group. If the spin functions of the upper and lower energy states belong to different representations of the molecular point group, the transition is forbidden.

For example, referring to Table II, we see that in this particular case transitions of the type $1'$, $2'$, $3'$, $4'(A_1)_0\rightarrow1'$, $2'(A_1)_1$ are all allowed (although some may be weak in many cases). It is extremely interesting to note that some of these allowed transitions correspond to "combination bands"; i.e., signals can be expected at principal frequencies other than the resonance frequency of group A, $(1/2\pi)\gamma_AH_A$ or the resonance frequency of group B, $(1/2\pi)\gamma_BH_B$. These will, however, be of very low intensity except when $|\gamma_AH_A-\gamma_BH_B|\sim|J^{AB}|$. For example, the energy of the allowed $2'(A_1)_0\rightarrow1'(A_1)_1$ transition contains the term, $1/2\pi\times[2\gamma_BH_B-\gamma_AH_A]$ and corresponds to the simultaneous "flip" of three nuclei. Of course transitions of the types $(A_1)_{-1}\rightarrow(A_1)_{+1}$ and $(B_2)_0\rightarrow(A_1)_1$ are always

[7] A derivation of the corresponding equation for electric dipole radiation is given in Chapter VIII of reference (6).

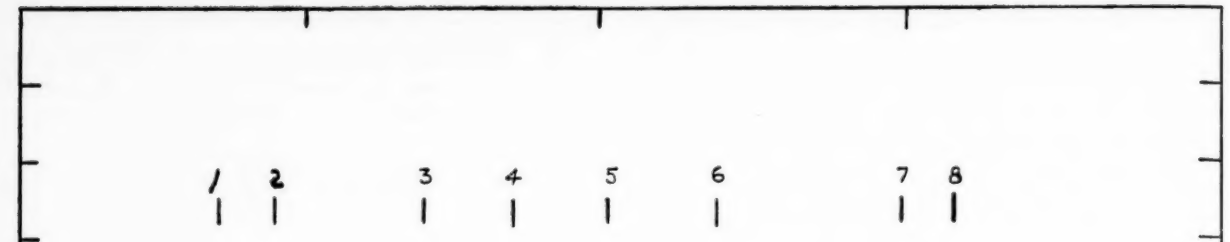

FIG. 1(a). The fluorine NMR spectrum of 1,1-difluoroethylene. The abscissa is the applied sweep field in milligauss. (1 mgauss=4.00 cps.)

forbidden irrespective of the relative magnitudes of $|\gamma_A H_A - \gamma_B H_B|$ and $|J^{AB}|$.

For those molecules for which the Hamiltonian in (26) is appropriate, still other selection rules apply. In this case, for an allowed transition $m \rightarrow n$, one must have $(R_i(A))_m = (R_i(A))_n$, $(R_i(B))_m = (R_i(B))_n$. The operators $\mathcal{H}^{(1)}(AA)$ and $\mathcal{H}^{(1)}(BB)$ also belong to the class Q' for the Hamiltonian in (26) and $(\mathcal{H}^{(1)}(AA))_m = (\mathcal{H}^{(1)}(AA))_n$, and $(\mathcal{H}^{(1)}(BB))_m = (\mathcal{H}^{(1)}(BB))_n$. Therefore since there is no change in the energy of interaction between equivalent nuclei during an allowed transition, these interactions do not give rise to multiplets. Also, since $F^2(A)$ and $F^2(B)$ belong to the class Q', there is no change in the multiplicities of the spin functions for groups A and B during an allowed transition.

To illustrate these rules let us consider the spin functions given in Table II and consider that the Hamiltonian in equation (26) is applicable. In this case, for example, transitions $1'(A_1)_0 \rightarrow 1'(A_1)_1$ and $1'(A_1)_1 \rightarrow 1'(A_1)_2$ are allowed, whereas transitions $3'(A_1)_0 \rightarrow 1'(A_1)_1$ and $3'(A_1)_0 \rightarrow 2'(A_1)_1$ are forbidden.

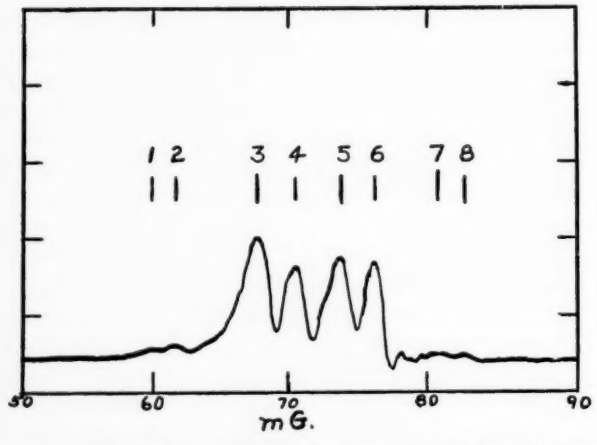

FIG. 1. (b) The proton NMR spectrum of 1,1-difluoroethylene. The abscissa is the applied sweep field in milligauss. (1 mgauss =4.26 cps.)

VI. EXAMPLE: 1,1-DIFLUOROETHYLENE

The purpose of the present section is to illustrate the application of the general methods outlined in the present paper to the analysis of the high-resolution NMR spectrum of $CH_2=CF_2$. The H^1 and F^{19} resonance spectra of this substance are given in Figs. 1 (a) and (b), and it will be noted that each spectrum shows four strong signals and four weak signals. The signals have been labeled 1–8 in Figs. 1 (a) and (b). These spectra were obtained with a Varian high-resolution NMR spectrometer at a fixed frequency of 40 mc and magnetic fields of 9396 and 10 000 gauss for the H^1 and F^{19} resonances, respectively.

The Hamiltonian corresponding to Eq. (15) for $CH_2=CF_2$ is

$$\begin{aligned}\mathcal{H}=&\gamma_H H_H(I_z(H_1)+I_z(H_2))\\&+\gamma_F H_F(I_z(F_1)+I_z(F_2))\\&+J_{11}{}^{HF}\mathbf{I}(H_1)\cdot\mathbf{I}(F_1)+J_{12}{}^{HF}\mathbf{I}(H_1)\cdot\mathbf{I}(F_2)\\&+J_{21}{}^{HF}\mathbf{I}(H_2)\cdot\mathbf{I}(F_1)+J_{22}{}^{HF}\mathbf{I}(H_2)\cdot\mathbf{I}(F_2)\\&+J_{12}{}^{HH}\mathbf{I}(H_1)\cdot\mathbf{I}(H_2)+J_{12}{}^{FF}\mathbf{I}(F_1)\cdot\mathbf{I}(F_2).\end{aligned}\quad(37)$$

Since $CH_2=CF_2$ has C_{2v} symmetry, we have

$$J_{11}{}^{HF}=J_{22}{}^{HF},$$
$$J_{12}{}^{HF}=J_{21}{}^{HF},$$

where the H^1 and F^{19} nuclei have been labeled according to the system

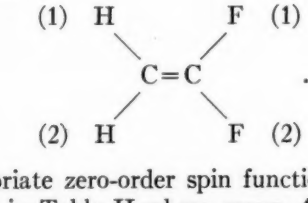

(I)

The appropriate zero-order spin functions for (I) are those listed in Table II where group A comprises the H_1 and H_2 nuclei and group B the F_1 and F_2 nuclei. As indicated in a previous section, the secular determinant for this problem exactly factors into two 1×1,

five 2×2, and one 4×4 determinants. Since, for this problem $|\gamma_H H_H - \gamma_F H_F| \sim 2.4\times10^6$ cps, and the J's are ~40 cps, the solutions of the 2×2 and 4×4 determinants are accurately approximated by perturbation theory.

When first-order perturbation theory is used the secular determinant further factors into twelve 1×1 and two 2×2 determinants. The two 2×2 determinants arise from accidental degeneracies in the $3(A_1)_0$ and $4(A_1)_0$, and $1(B_2)_0$ and $2(B_2)_0$ states. Transition frequencies are readily obtained from these determinants and the frequencies of *allowed* transitions are given in Table IV for the resonance lines of the H^1 nuclei. The multiplet splittings (and relative intensities) for the F^{19} resonance spectra are theoretically identical to those of the H^1 nuclei. Table IV employs the following definitions:

$$\begin{aligned} K &= J_{12}{}^{HH} + J_{12}{}^{FF}, \\ L &= J_{11}{}^{HF} - J_{12}{}^{HF}, \\ M &= J_{12}{}^{HH} - J_{12}{}^{FF}, \\ N &= J_{11}{}^{HF} + J_{12}{}^{HF}. \end{aligned} \tag{38}$$

Table IV shows that there are ten distinct allowed transitions in the H^1 (as well as F^{19}) resonance spectra for $CH_2=CF_2$. In Figs. 1 only eight distinct transitions are observed. We find that the observed spectrum is accounted for if we make the following assignments:

$$\begin{aligned} J_{12}{}^{HH} &\approx 4 \text{ cps}, \\ J_{12}{}^{FF} &= 37 \text{ cps}, \\ J_{11}{}^{HF} &\approx 1 \text{ cps}, \\ J_{12}{}^{HF} &= 34 \text{ cps}. \end{aligned} \tag{39}$$

For these J values the transitions $2'(A_1)_{-1} \rightarrow 3'(A_1)_0$ and $2'(B_2)_0 \rightarrow 2'(B_2)_1$ and $(3'(A_1)_0 \rightarrow 2'(A_1)_1$ and $2'(B_2)_{-1} \rightarrow 2'(B_2)_0)$ are separated by about <2 cps and are therefore not resolved in Fig. 1. The numbers listed in Eqs. (39), were determined directly from measured multiplet splittings and the theoretical expressions for the transition energies given in Table IV. Actually, on the basis of the theoretical equations and the observed spectrum in Figs. 1, there is in fact no way of deciding whether the coupling constant of 37 cps is equal to $J_{12}{}^{FF}$ or $J_{12}{}^{HH}$, or whether the coupling constant of 34 cps is $J_{12}{}^{HF}$ or $J_{11}{}^{HF}$. The assignments in Eqs. (39) were made on the basis of comparison of these coupling constants with multiplet splittings in other molecules, to be described elsewhere. Also, it is not possible to distinguish between positive and negative values of the coupling constants.

TABLE IV. Proton multiplet spectrum for $CH_2=CF_2$.

Band No.	Transition	Transition energy[a] Theoretical (cps)	Observed	Theoretical relative intensity
1	$4'(A_1)_0 \rightarrow 2'(A_1)_1$	$\frac{1}{2}K+\frac{1}{2}(K^2+L^2)^{\frac{1}{2}}$	48	0.11
2	$2'(B_2)_{-1} \rightarrow 1'(B_2)_0$	$-\frac{1}{2}M+\frac{1}{2}(M^2+L^2)^{\frac{1}{2}}$	40	0.14
3	$1'(A_1)_1 \rightarrow 1'(A_1)_2$ $1'(A_1)_0 \rightarrow 1'(A_1)_1$	$\frac{1}{2}N$ $\frac{1}{2}N$	17.5	2.00
4	$2'(A_1)_{-1} \rightarrow 3'(A_1)_0$ $2'(B_2)_0 \rightarrow 2'(B_2)_1$	$-\frac{1}{2}K+\frac{1}{2}(K^2+L^2)^{\frac{1}{2}}$ $\frac{1}{2}M+\frac{1}{2}(M^2+L^2)^{\frac{1}{2}}$	6.5	1.74
5	$3'(A_1)_0 \rightarrow 2'(A_1)_1$ $2'(B_2)_{-1} \rightarrow 2'(B_2)_0$	$\frac{1}{2}K-\frac{1}{2}(K^2+L^2)^{\frac{1}{2}}$ $-\frac{1}{2}M-\frac{1}{2}(M^2+L^2)^{\frac{1}{2}}$	−6.5	1.74
6	$1'(A_1)_{-1} \rightarrow 2'(A_1)_0$ $1'(A_1)_{-2} \rightarrow 1'(A_1)_{-1}$	$-\frac{1}{2}N$ $-\frac{1}{2}N$	−17.5	2.00
7	$1'(B_2)_0 \rightarrow 2'(B_2)_1$	$\frac{1}{2}M-\frac{1}{2}(M^2+L^2)^{\frac{1}{2}}$	−40	0.14
8	$2'(A_1)_{-1} \rightarrow 4'(A_1)_0$	$-\frac{1}{2}K-\frac{1}{2}(K^2+L^2)^{\frac{1}{2}}$	−48	0.11

[a] These transition energies are measured relative to the principal resonance frequency at $(1/2\pi)\gamma_H H_H$.

In Table IV there is no serious mixing of the starting functions except in the case of $3'(A_1)_0$ and $4'(A_1)_0$, and $1'(B_2)_0$, and $2'(B_2)_0$, and so the final functions listed with these exceptions are essentially the same as the corresponding starting functions. The zeroth-order perturbation wave functions for the aforementioned two sets are:

$$\begin{aligned} 3'(A_1)_0 &= C_1 3(A_1)_0 + C_2 4(A_1)_0, \\ 4'(A_1)_0 &= C_2 3(A_1)_0 - C_1 4(A_1)_0, \\ 1'(B_2)_0 &= C_3 1(B_2)_0 + C_4 2(B_2)_0, \\ 2'(B_2)_0 &= C_4 1(B_2)_0 - C_3 2(B_2)_0, \end{aligned} \tag{40}$$

where

$$\begin{Bmatrix} C_1 \\ C_2 \end{Bmatrix} = \left[\frac{L^2}{2[K^2+L^2 \mp K(K^2+L^2)^{\frac{1}{2}}]}\right]^{\frac{1}{2}},$$

$$\begin{Bmatrix} C_3 \\ C_4 \end{Bmatrix} = \left[\frac{L^2}{2[M^2+L^2 \mp M(M^2+L^2)^{\frac{1}{2}}]}\right]^{\frac{1}{2}}.$$

The theoretical relative intensities were calculated using these wave functions and the experimentally determined coupling constants in Eqs. (39). It is quite likely that these theoretical relative intensities are more precise than those which can be obtained experimentally at present with available instrumentation. Table IV also gives the experimental values of the multiplet separations listed for the H^1 resonances according to the numbering used in Fig. 1(b). The observed F^{19} multiplet separations were equal to those of H^1 to within the experimental accuracy (1 cps).

Absorption Cross Sections of Methane and Ammonia in the Vacuum Ultraviolet

H. SUN AND G. L. WEISSLER
Department of Physics, University of Southern California, Los Angeles 7, California
(Received October 22, 1954)

Absorption cross sections of methane and ammonia for electromagnetic radiation in the range from 1300 A to 374 were obtained with a two-meter radius of curvature, grazing incidence vacuum spectrograph. For methane 85 wavelengths were measured. Starting from $\sigma=14$ Mb (1 Mb$=10^{-18}$ cm^2) at 1300 A, the absorption first increased slowly and then rose more rapidly to a maximum of $\sigma=56$ Mb at 960 ± 278 A corresponding to the first ionization potential of methane. The absorption then decreased gradually to 14 Mv at 374 A. The total f-value pertaining to the transitions of $2p$-electrons was found to be 6.1. For ammonia, 100 wavelengths were measured. Band absorption appeared at longer wavelengths. The continuous absorption began near 1210 A and extended to the shorter wavelengths. The structure of the absorption contour suggested the existence of two ionization continua: a weaker one with maximum $\sigma=21$ Mb at 1130 ± 20 A and a larger one with its maximum of 34 Mb at 730 ± 20 A. These two maxima corresponded to the ionization limits of the outer electrons of ammonia. The total f-value was found to be 5.9.

INTRODUCTION

ABSORPTION spectra of methane and ammonia in the vacuum ultraviolet have been studied by several investigators. For methane, Duncan and Howe[1] found a continuous absorption between 1450 A and 850 A. Wilkinson and Johnston[2] working in the range from 1850 A to 1370 A found that the absorption began to be observable at 1450 A increasing to a value of the coefficient of 70 cm^{-1} at 1370 A. Dalgarno[3] made a theoretical calculation of the photoionization cross section between 946 A and 500 A by the use of a neon-like wave function which will be compared to the experimental results presented here.

The absorption of gaseous ammonia at room temperature begins at 2200 A and extends to the vacuum ultraviolet region.[4,5] Duncan[6] extended these investigations to 850 A and found a system of bands at wavelengths longer than 1160 A and a continuous absorption for shorter wavelengths. These bands were classified into four electronic transitions. The maxima of the intensities in the four transitions had the wavelengths of 1905 A, 1538 A, 1288 A, and 1178 A respectively. The present work deals with the absorption cross sections of methane and ammonia between 1306 A and 374 A.

APPARATUS AND EXPERIMENTAL PROCEDURE

The investigations on the absorption cross sections of methane and ammonia were carried out with a grazing incidence vacuum spectrograph. A grating with a radius of curvature of two meters and ruled with 14 405 lines per inch, had a plate factor of from 2.5 A per mm, at 500 A to 3.5 A per mm at 1300 A. A constant intensity line emission source[7] supplied the required light from a condensed ac spark discharge, which passed through a quartz capillary of two millimeters in diameter. Lines of different wavelengths ranging from 1300 A to 374 A were used. Air, argon, and freon were used in the source, and their pressures ranged from 15 to 100 microns with breakdown potentials from 1500 to 8000 volts and one to three sparks per cycle. Listed in Table I are the photographic densities, D, of four different exposures of the same air line. The exposure times were constant and the spectrograph tank was maintained at high vacuum. A condenser of 0.018 μfd connected across the source gap was charged every cycle to a potential at which the spark would pass through the quartz capillary of the discharge tube. The results of Table I show that the source was constant to within 2.5 percent.

Eastman spectroscopic plates, type 103a–0, sensitized for the ultraviolet by a thin layer of fluorescent lacquer, were used. For each individual plate, a calibration curve was obtained using light of wavelength 3150 A as discussed by Weissler, Lee, and Mohr.[8] This yielded a relationship between the photographic density and the natural logarithm of the time of exposure. It has been shown[9] that the reciprocity law and constant quantum efficiency were valid between light of 3150 A and vacuum ultraviolet radiation used in these experiments. After the calibrated plate was introduced into the spectrograph, the tank was pumped out to a pressure of less than 0.1 micron. Then the absorbing gas was allowed to flow into the tank until the pressure was 100 microns and pumped out again. This was repeated several times to rinse out any residual air and other contaminating gases. In the meantime, the source tube was adjusted for steady-state operation. Four identical time exposures were taken for different pressures of the absorbing gas in the tank. The time of exposure for

[1] A. B. F. Duncan and J. P. Howe, J. Chem. Phys. **2**, 851 (1934); G. Moe and A. B. F. Duncan, J. Am. Chem. Soc. **74**, 3140 (1952).
[2] P. G. Wilkinson and H. L. Johnston, J. Chem. Phys. **18**, 190 (1950).
[3] A. Dalgarno, Proc. Phys. Soc. (London) **A65**, 663 (1952).
[4] S. W. Leifson, Astrophys. J. **63**, 70 (1926).
[5] J. K. Dixon, Phys. Rev. **43**, 711 (1933).
[6] A. B. F. Duncan, Phys. Rev. **47**, 822 (1935) and **50**, 700 (1936).
[7] P. Lee and G. L. Weissler, J. Opt. Soc. Am. **42**, 80 (1952).
[8] Weissler, Lee, and Mohr, J. Opt. Soc. Am. **42**, 84 (1952).
[9] P. Lee and G. L. Weissler, J. Opt. Soc. Am. **43**, 512 (1953).

different plates lasted from five to thirty minutes. The pressure for each exposure was measured by a calibrated mercury McLeod gauge, to which a liquid-nitrogen or dry-ice trap was attached to prevent contamination from mercury vapor. A thermocouple and a Philips gauge were two auxiliary instruments for pressure measurement. The pressures in all experiments were smaller than 35 microns. Both spectrograph tank and source tube were maintained in a state of dynamic equilibrium by continuous pumping and supplying of new gases. A value of 5 percent has been estimated for the accuracy of the pressure measurements.

The light beam from the source passed through the primary slit of 30 microns width into the spectrograph tank which was either at a high vacuum or contained the absorbing gas at various pressures. There the grating dispersed the light and reflected it onto the photographic plate. From the progressively decreasing densities of the source lines with increasing pressures of the absorbing gas, the absorption coefficients or cross sections could be evaluated according to standard procedure.

Methane and ammonia, supplied by the Matheson Company in cylinders, were purified by repeated condensations and fractional distillations. By using freezing agents of suitable cooling temperature, either higher or lower boiling point impurities could be removed. A liquid-nitrogen trap was used to condense methane while allowing gases of lower boiling point uncollected, such as N_2 and H_2, to be pumped off. Impurities of higher boiling points such as ethane and carbon dioxide were frozen out by passing the evaporated methane through an alcohol-ice trap which was obtained by the addition of liquid nitrogen into alcohol. The process can be repeated by exchanging the positions of the two traps. Usually, the gases were purified three times. For ammonia, traps of dry ice and salted ice water were used. The purities of methane and ammonia were higher than 99.0 percent and 99.9 percent respectively as stated by the supplier.

EXPERIMENTAL RESULTS AND DISCUSSION

I. Methane

As the pressures of the absorbing gases in this work were low, not over 40 microns, they could be considered as ideal gases. Lambert's and Beer's law lead to the equation

$$I=I_0e^{-(kT_0pL/p_0T)}=I_0e^{-\alpha p},$$

where

$$\alpha=\frac{kT_0L}{p_0T} \quad \text{and} \quad k=n_0\sigma.$$

I_0 is the intensity of the incident light, I the intensity of the transmitted light, L the length of the absorption path, k the absorption coefficient in cm^{-1} at standard conditions of p_0T_0, σ the absorption cross section, n_0 the number of molecules per cm^3, p and T the pressure and temperature of the absorbing gas. The quantity α is equal to the slope of the straight line obtained by plotting $\log_e I_0/I$ against p. From α either k or σ can be calculated.

The absorption cross sections, σ, of methane obtained from six plates are listed in Table II and Fig. 1,

TABLE I. Constancy of the light source with spectrograph tank at high vacuum.

Wavelength (A) of the line measured		D_1	D_2	D_3	D_4	Standard deviation	Probable error percent
1306.0	OI	0.88	0.91	0.91	0.90	0.014	1.0
1304.9	OI	0.92	0.94	0.96	0.97	0.022	2.0
1302.2	OI	1.03	1.06	1.05	1.04	0.014	0.9
1152.1	OI	1.47	1.49	1.46	1.51	0.024	1.1
979.8	NII	3.61	3.62	3.66		0.036	0.7
977.0	CIII	3.04	3.14	3.26		0.11	2.4
574.7	NII		1.52	1.54	1.54	0.01	0.4

TABLE II. Absorption cross sections of methane. (The number in ( ) following the value for σ indicates the number of photographic plates used to evaluate σ. Each plate contained four exposures at different pressures of the absorbing gas.)

Wavelength (A)		σ Mb	Wavelength (A)		σ Mb
1306.0	OI	14 (2)	871.1	AIII	42 (1)
1304.9	OI	14 (2)	864.7	CIII	42 (1)
1302.2	OI	14 (2)	851.6	CIII	44 (1)
1275.1	NII	16 (2)	850.6	AIV	43 (1)
1243.3	NI	18 (3)	840.0	AIV	41 (1)
1217.6	OI	19 (1)	835.1	OIII	42 (2)
1215.7	Hα	16 (1)	834.6	OII	48 (1)
1206.9	SiII	18 (1)	833.7	OII	46 (2)
1200.7	NI	19 (2)	833.3	OII	43 (3)
1200.2	NI	20 (2)	796.7	OII	42 (2)
1199.5	NI	19 (1)	776.7	OII	42 (1)
1184.5	NIII	20 (2)	775.9	OII	39 (1)
1183.0	NIII	23 (2)	772.9	NIII	43 (2)
1176.4	CII	25 (1)	772.4	NIII	38 (1)
1175.5	CII	23 (1)	771.9	NIII	43 (2)
1152.1	OI	19 (1)	771.5	NIII	39 (2)
1135.0	NI	19 (3)	765.1	NIV	40 (2)
1134.4	NI	19 (3)	764.5	NIV	36 (2)
1085.5	NII	29 (2)	763.3	NIV	36 (2)
1084.6	NII	27 (2)	747.0	NII	35 (1)
1071.8	CIII	32 (1)	745.8	NII	39 (2)
1065.9	CII	31 (1)	686.3	NIII	36 (2)
1037.0	CII	31 (2)	685.0	NIII	32 (2)
1036.3	CII	31 (2)	660.3	NII	33 (3)
991.5	NII	29 (3)	645.2	NII	29 (2)
989.8	NII	38 (2)	644.8	NII	32 (2)
979.8	NIII	41 (3)	644.6	NII	27 (2)
977.0	CIII	44 (2)	644.1	NII	36 (2)
961.5	CII	56 (1)	629.4	NII	35 (1)
958.5	FI	60 (1)	629.2	NII	36 (1)
955.5	FI	56 (1)	617.1	OII	34 (2)
954.8	FI	56 (1)	616.3	OII	31 (2)
951.9	FI	56 (1)	600.6	OII	31 (1)
932.0	AIII	48 (1)	599.6	OIII	31 (2)
924.3	NIV	42 (2)	582.2	OII	25 (2)
923.2	NIV	46 (3)	581.0	OII	25 (2)
916.7	NII	49 (1)	580.4	OII	25 (2)
916.0	NII	46 (1)	538.3	OII	23 (2)
887.4	AII	38 (1)	537.8	OII	24 (2)
883.2	AIII	39 (1)	508.2	OIII	23 (2)
879.6	AIII	41 (1)	507.7	OIII	25 (2)
875.8	AIII	45 (1)	374.3	NIV	14 (1)

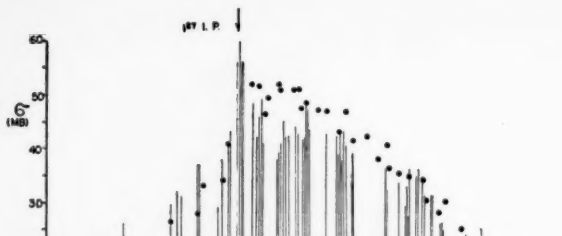

FIG. 1. Absorption cross sections of CH_4. The solid lines represent the measured values of σ, and circles are Ditchburn's data.

which shows a continuous absorption with $\sigma=14$ Mb* at 1300 A increasing slowly up to 980 A where the absorption rises steeply to a peaked maximum with σ equal to 56 Mb at 960 ± 20 A and decreases gradually to $\sigma=14$ Mb at 374 A. Using a Lyman continuum as a source revealed no obvious discreet absorption bands.

The results are in good agreement with those of Ditchburn,[10] whose values are also shown by circles in Fig. 1, and with the direct photoionization measurements by Wainfan, Walker, and Weissler.[11] The wavelength corresponding to maximum absorption, 960 ± 20 A or $12.9_{-0.1}^{+0.4}$ ev was identified with the first ionization potential of methane. Recent electron impact experiments[12–14] gave the value of 13.07 ± 0.02 ev. According to Mulliken's model[15] the electron configuration of methane is $1s^2\ 2s^2\ 2p^6$, where the p-electrons are rather loosely bonded to the nucleus in comparison with the $1s$-, $2s$-electrons. Therefore the first ionizing process of methane must correspond to the removal of a $2p$-electron from the nuclei. The present measurements may be compared with the theoretical work of Dalgarno[3] as shown in Table III. Dalgarno considered the methane molecule as quasi-atomic and used neon-like wave functions in his calculations. The values obtained by him are of the same order of magnitude (within 40 percent) as those of this work; they are somewhat larger than the experimental ones in the region near the spectral head. However, the relative difference becomes smaller at the short wavelength end. A part of the discrepancy might be due to the fact that exchange effect was neglected in the theoretical calculations.†

At the long wavelength side a σ value of 14 Mb at 1300 A agrees roughly with an extrapolation of the work by Wilkinson and Johnston.[2] Moe and Duncan[1] determined absolute absorption cross sections between 1450 A and 1050 A and found a flat maximum between 1300 A and 1200 A with $\sigma=22$ Mb (our value at 1243.3 A: $\sigma=18$ Mb). Below 1100 A their data agreed closely with those presented here. The continuous absorption contour obtained from the work presented here showed only the barest indication of a maximum at approximately 1180 A. The application of a quasi-atomic model to methane seems strongly supported for the region of its ionization continuum. However, the continuous absorption at wavelength longer than the ionization limit cannot be explained on the basis of this assumption. In the atomic case, the absorption at longer wavelengths should be zero except for discrete absorption of Rydberg series bands. It seems unlikely that the observed continuous absorption at the long wavelength side of the ionization limit is the tail part of the dissociation continuum of methane. Recent data on the dissociation of methane[16] showed the following:

$$CH_4=CH_3+H-101 \text{ kcal (4.4 ev or 2880 A)};$$
$$CH_3\approx CH_2+H-\ 87 \text{ kcal (3.8 ev or 3260 A)};$$
$$CH_2\approx CH+H\ -125 \text{ kcal (5.4 ev or 2300 A)};$$
$$CH\ =C\ \ +H-\ 80 \text{ kcal (3.5 ev or 3600 A)}.$$

Because of the absence of Frank-Condon curves for the transitions involved, the probable position of the maximum of the dissociation continuum cannot be guessed at. However, the results of Wilkinson and Johnston[2] showed that methane had no appreciable absorption between 1850 A to 1450 A. This might mean that the dissociation continuum of methane ended in the wavelength region longer than 1850 A. The absorption starting at 1450 A and increasing to a value of 2.6 Mb at 1370 A could be extrapolated and joined to the long wavelength side of the absorption curve of the present work. It is therefore felt that the continuous absorption (below 1450 A) is not a portion of the dissociation continuum. The existence of the continuous absorption at wavelengths longer than 960 A might be explained by the influence of coupling between vibration and electronic motion as discussed by Sponer and Teller.[17] Using again the quasi-atomic model, one would expect a

TABLE III. Experimental and theoretical absorption cross sections of methane between 946 A and 500 A.

Wavelength (A)	σ (Mb) experimental	σ (Mb) theoretical
946	56	94
834	41	77
715	36	57
625	30	42
556	26	33
500	22	24

* Mb=1 megabarn=10^{-18} cm^2.

[10] R. W. Ditchburn, private communication, submitted to Proc. Roy. Soc. (London).

[11] Wainfan, Walker, and Weissler (to be published).

[12] Lossing, Tickner, and Bryce, J. Chem. Phys. **19**, 1254 (1951).

[13] J. J. Mitchell and F. F. Coleman, J. Chem. Phys. **17**, 44 (1949).

[14] M. B. Koffel and R. A. Lad, J. Chem. Phys. **16**, 420 (1948).

[15] R. S. Mulliken, Phys. Rev. **40**, 55 (1932).

† A. Dalgarno, private communication, 1953.

[16] K. J. Laidler and E. J. Casey, J. Chem. Phys. **17**, 1087 (1949).

[17] H. Sponer and E. Teller, Revs. Modern Phys. **13**, 75 (1941).

Rydberg series of bands at the long wavelength side of the ionization limit. In the region near the series limit many electronic states are present which usually are degenerate because of the symmetric structure of the molecule and should be split due to the vibration of the nuclei. For a molecule like methane, a stable symmetrical configuration requires a nondegenerate electron wave function in the initial state. Subject to the selection rules for this kind of molecule, the absorption takes place only from a nondegenerate ground state to a degenerate higher level which does not have the same symmetry as the former. Many nontotally symmetrical vibrations would be excited simultaneously. Thus the spectrum will have a rather complicated appearance. If, moreover, the equilibrium positions differ considerably in the two states, the number of bands might be increased so greatly that the spectrum *appears* continuous.

TABLE IV. Absorption cross sections of ammonia. (The number in ( ) following the value of σ indicates the number of photographic plates used to evaluate σ. Each plate contained four exposures at different pressures of the absorbing gas.)

Wavelength (A)	σ Mb	Wavelength (A)	σ Mb
1036.0 OI	27 (4)	765.1 NIII	33 (3)
1034.9 OI	8.2 (4)	764.5 NIII	36 (4)
1032.2 OI	15 (4)	763.3 NIII	36 (4)
1276.2 NII	4.5 (2)	747.0 NII	33 (1)
1275.1 NII	5.6 (2)	746,8 NII	31 (1)
1243.3 NII	3.6 (2)	740.2 AII	35 (1)
1200.7 NI	7.8 (3)	730.9 AII	34 (1)
1200.2 NI	7.8 (3)	725.5 AII	32 (1)
1199.5 NI	7.8 (3)	723.4 AII	34 (1)
1184.5 NIII	17 (1)	718.5 OII	34 (2)
1183.0 NIII	18 (1)	703.9 OIII	35 (2)
1135.0 OI	23 (2)	702.9 OIII	35 (2)
1134.4 NII	22 (2)	702.3 OII	33 (2)
1084.6 NII	20 (3)	686.3 NIII	29 (4)
1084.0 NII	19 (3)	685.8 NIII	31 (4)
1037.0 CII	20 (2)	685.5 NIII	31 (4)
1036.0 CII	19 (2)	685.0 NIII	33 (4)
991.5 NIII	20 (1)	673.0 NII	32 (2)
989.8 NIII	19 (2)	672.0 AII	32 (2)
988.8 OI	23 (2)	671.9 AII	31 (2)
979.8 NIII	25 (3)	670.9 AII	31 (2)
977.0 CIII	24 (3)	666.0 AII	32 (1)
924.3 NIV	24 (2)	664.6 AII	30 (1)
923.5 NIV	26 (2)	661.9 AII	30 (1)
923.2 NIV	23 (2)	660.3 NII	28 (3)
923.0 NIV	23 (2)	645.2 NII	28 (3)
922.5 NIV	23 (2)	644.8 NII	30 (3)
916.7 NII	21 (3)	644.6 NII	31 (2)
916.0 NII	20 (3)	644.1 NII	31 (1)
915.9 NII	21 (1)	643.3 AIII	28 (1)
887.4 AIII	35 (2)	641.8 AIII	31 (1)
883.2 AIII	32 (2)	641.4 AIII	27 (1)
879.6 AIII	27 (2)	637.3 AII	34 (2)
878.7 AIII	26 (2)	635.2 NII	35 (1)
875.5 AIII	29 (2)	617.1 OII	31 (2)
871.1 AIII	30 (2)	616.3 OII	32 (2)
850.6 AIII	35 (2)	604.2 AII	31 (1)
843.8 AIV	34 (2)	599.6 OIII	27 (2)
840.0 AIV	35 (2)	582.2 NII	29 (1)
835.3 OIII	32 (4)	581.0 OII	29 (1)
835.1 OIII	30 (2)	580.4 OII	28 (1)
833.7 OIII	32 (2)	555.1 OII	27 (1)
833.3 OII	31 (4)	539.9 OII	31 (1)
832.8 OII	32 (4)	539.4 OII	26 (1)
796.7 OII	33 (3)	539.2 OII	28 (1)
776.0 OII	33 (4)	538.3 OII	28 (1)
773.0 NIII	34 (3)	511.5 AII	24 (1)
772.4 NIII	34 (2)	503.7 AII	29 (1)
771.9 NIII	33 (3)	374.3 OIII	17 (1)
771.5 NIII	33 (3)	374.1 OIII	20 (1)

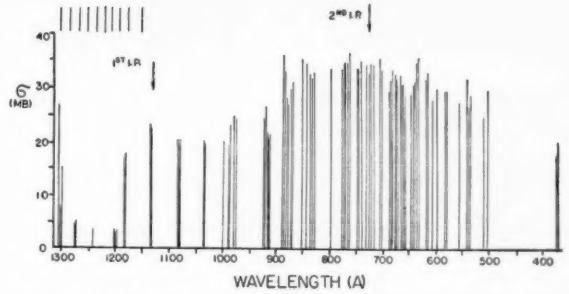

FIG. 2. Absorption cross sections of NH_3. The solid lines represent the measured values of σ, and bands are shown in the upper left part.

The oscillator strength or f-value for methane in the measured region from 1300 A to 374 A was found to be 5.5 by integrating the area under a curve obtained by plotting the absorption coefficient k *versus* wave number. According to the sum rule, the total f-value of the whole spectrum should be equal to the number of electrons which take part in the transitions, i.e., 6, due to the six $2p$-electrons. Dalgarno integrated from the wavelength at the ionization limit to zero wavelength and gave the theoretical f-value as 6.3. The f-value for wavelengths longer than 1300 A was obtained by connecting the absorption contour of this work with Wilkinson's value, $k=70$ cm^{-1}, at 1370 A and was found to be 0.04. At wavelengths shorter than the present measurements, namely 374 A, the absorption was still rather large. By extrapolating the absorption curve to zero wavelength and integrating the area of the extrapolated portion of the curve, a value of 0.57 was found. The total f-value for all transitions is then 6.1 which is in good agreement with the sum rule, Dalgarno's estimate and Friberg's dispersion data[18] ($f_1=0.42$ at $\lambda_1=1255$ A and $f_2=5.08$ at $\lambda_2=753$ A).

II. Ammonia

Figure 2 and Table IV show the absorption cross sections of ammonia measured from five plates in the spectral region from 1300 A to 374 A. From the large fluctuation of values of σ of the closely spaced successive lines at 1306.0 A, 1304.9 A, and 1302.9 A, it can be concluded that absorption in this region is due to bands. Figure 2 shows that the continuous absorption starts at about 1210 A and extends toward the shorter wavelengths. Several plates showed clearly the absorption bands of ammonia when photographed with a Lyman continuum. The results of these plates agree with the earlier observations of Duncan[6] in the region between 1300 A and 1170 A. The absorption bands are sketched

[18] S. Friberg, Z. Physik **41**, 378 (1927).

TABLE V. Statistical error of σ measurements.

Wavelength (A)		σ Mb (Individual measurement)					σ Mb (Average and standard deviation)	Probable error in percent
				CH_4				
1306.0	OI	16			12	14	±2.8	14
1243.3	NI	16	19		18	18	±1.6	6
1135.0	NI		17	16	25	19	±5.0	18
1084.6	NII		29	25		27	±2.8	7
1036.3	CII			29 32		31	±2.2	5
991.5	NII		29	29	29	20	±0	0
979.8	NIII	35	41		48	41	±6.5	11
923.2	NIV		50	43	46	46	±3.5	5
833.3	OII		47	41	41	43	±3.4	5
764.4	NIV		36		36	36	±0	0
763.3	NIV		35		37	36	±1.4	3
660.3	NIII	30	36		33	33	±3.0	6
616.3	OII		33		28	31	±3.6	8
538.3	OII	22			24	23	±1.4	4
				NH_3				
1306.0	OI	27	28	29	25	27	±1.7	4
1243.2	NII	3.0		4.1		3.6	±0.8	17
1134.2	NII	21		22		22	±1.0	3
1084.6	NII	17		25	17	20	±4.7	16
979.8	NIII	24		28	22	25	±3.2	9
916.0	NII	17		25	17	20	±4.7	16
871.1	AIII	32	28		30	30	±2.8	6
835.3	OIII	36	24	37	30	32	±6.1	13
796.7	OII		32	37	30	33	±3.6	7
776.0	OII		32	31 37	32	33	±2.7	6
686.3	NIII		21	27 36	31	29	±6.3	15
660.3	NII		24	31	29	28	±3.6	9
644.8	NII		23	32	35	30	±6.3	14
599.6	OIII			30	25	27	±3.6	9

in the top of Fig. 2. Recently, Watanabe[19] measured the absorption cross sections of NH_3 between 2000 A and 1070 A. His results generally agree with the data obtained here in the overlapping region. The absorption curve seems to be composed of two parts with a minor maximum at 1130±20 A and a major one at 730±20 A with σ equal to 21 Mb and 34 Mb respectively. Both maxima are rather flat. The wavelength of the first maximum, corresponding to 11.0±0.2 ev, can be identified with the first ionization potential of ammonia. Values obtained from electron impact measurements[20,21] were 11.2 ev. Duncan[6] found that his Rydberg series limit was 11.6 ev, approximately. The second maximum at 730±20 A corresponds to 17.0±0.5 ev. From this maximum on toward shorter wavelengths the absorption falls gradually to 18 Mb at 374 A.

The electronic structure of the ammonia molecule may be compared with that of the nitrogen atom, which has the form $1s^2\,2s^2\,2p^3$. According to Mulliken,[22] when a nitrogen atom and three hydrogen atoms combine to form an ammonia molecule, the two $1s$-electrons of the nitrogen atom become the two innermost electrons of the ammonia molecule. Omitting these two electrons, the electronic configuration of the ground state of ammonia is $(sa_1)^2(\pi e)^4(za_1)^2$. The orbital sa_1-electron is primarily a $2s$-orbital of the nitrogen atom and it is only very slightly influenced by the bonding between the nitrogen and hydrogen atoms. One of the $2p$-electrons of the nitrogen atom and three electrons of hydrogen atoms form the four πe-electrons which are strongly bonded. The two za_1-electrons are nonbonding. Using this configuration, the two absorption maxima in the spectrum may be explained. The first one at 11.0 ev must correspond to the removal of a za_1-electron and the second one at 17.0 ev to that of a πe-electron.

The f-value in the range measured was found to be 4.9. Assuming that the whole absorption spectrum is the superposition of two continua due to za_1- and πe-electrons, the sum rule indicates that the f-value of the transitions due to excitation of all za_1- and πe-electrons should be six. Extrapolation from 374 A towards shorter wavelengths resulted in an f-value of 1.0, thus yielding a total f-value of 5.9, close to that predicted by the sum rule. The agreement is not so good with the data derived from dispersion measurements[18] where $f_1=0.072$ at 1968 A and $f_2=3.68$ at 874 A.

In Table V, the statistical errors of the absorption cross sections of methane and ammonia are listed for some wavelengths. These errors were calculated directly from the value of σ for the same line from different plates.

The greatest statistical error in this table is 18 percent. A detailed analysis of the uncertainty in the experimental results due to all possible causes has been made.[23] It was found that the upper limit of the overall experimental errors was at most 25 percent and on the average 10 percent. For many lines, the accuracy is higher yet.

The authors wish to thank Professor R. W. Ditchburn for his many helpful discussions and for making his unpublished results on CH_4 absorption available for quotation. The assistance of the Office of Naval Research is also gratefully acknowledged.

[19] K. Watanabe, J. Chem. Phys. **22**, 1564 (1954).
[20] J. H. Bartlett, Phys. Rev. **33**, 169 (1929).
[21] C. A. Mackay, Phys. Rev. **24**, 319 (1924).
[22] R. S. Mulliken, J. Chem. Phys. **1**, 492 (1933) and **3**, 506 (1935).
[23] H. Sun, Dissertation, June, 1953, The University of Southern California.

Letters to the Editor

THIS section will accept reports of new work, provided these are terse and contain few figures, and especially few half-tone cuts. The Editorial Board will not hold itself responsible for opinions expressed by the correspondents. Contributions to this section should not exceed 600 words in length and must reach the office of the Editor not later than the 15th of the second month preceding that of the issue in which the Letter is to appear. No proof will be sent to the authors. A publication charge of $10.00 per Letter is made which, when honored, will entitle the Institution to 100 free reprints.

Note on Hyperconjugation

Y. I'HAYA
Department of Chemistry, Tokyo University of Education, Otsuka, Tokyo, Japan
(Received April 5 1955)

IN several computations which have been carried out on the MO theory of hyperconjugation, the choice of semiempirical parameters, particularly of corrected term δ for the Coulomb integral of H_2 or H_3 quasi-atom, seem to be considerably arbitrary. The values of δ proposed by several authors to date are divided into two main classes, namely, the values in the neighborhood of -0.2[1-5] and -0.5.[6-8] Among these only Muller, Pickett, and Mulliken[7] give a theoretical explanation on the basis of LCAO MO theory and their argument is very satisfactory from a qualitative viewpoint. Still it seems desirable to quantify it. When they estimated the binding energy of an H_2 quasi-π group orbital of the form $1s-1s$, there should have been added to an atomic integral (I_H in their paper) a term ω (see below) as mentioned in the note added in proof in their paper. The following computation including this term ω appears to give a more quantitative basis for determining such a parameter.

According to LCAO MO theory[9] the orbital energy (or binding energy) of an antibonding $1s-1s$ MO is approximately given by

$$\epsilon_{1s-1s}\approx\alpha_H-\beta_{HH}/(1-S_{HH})$$

where

$$\alpha_H=\epsilon_{1s}+\omega, \quad \omega\approx\int u_b aa+\tfrac{1}{2}(J_{aa}+J_{ab}),$$

$$\beta_{HH}\approx\int u_b ab-S_{HH}\int u_b aa+\int aa|ab-\tfrac{1}{2}S_{HH}(J_{aa}+J_{ab}),$$

and

$$J_{aa}=\int aa|aa, \quad J_{ab}=\int aa|bb.$$

Here a and b denote two hydrogen atoms separated 1.780 A from each other (assuming tetrahedral configuration in CH_2 or CH_3 group), u_b is approximately the potential energy function for an electron in a field of the positive ion H_b^+, and S_{HH} is the overlap integral between hydrogen atoms a and b.

Using the Slater-type AO's with the effective nuclear charge unity,[10] we get the following integral values:

$$J_{aa}=-17.00 \text{ ev}, \qquad J_{ab}=-7.89 \text{ ev},$$

$$\int u_b aa=-8.04 \text{ ev}, \qquad \int u_b ab=-4.11 \text{ ev},$$

$$\int aa|ab=-3.36 \text{ ev}, \qquad S_{HH}=0.282.$$

With these values and $\epsilon_{1s}=-13.595$ ev, we find

$$\alpha_H=-9.19 \text{ ev} \quad \text{and} \quad \beta_{HH}=-1.98 \text{ ev},$$

then

$$\epsilon_{1s-1s}=-6.42 \text{ ev}.$$

This may be recognized as the Coulomb integral of a quasi-$1s-1s$ AO of H_2 or H_3 and be compared with Coulomb integrals of $2p\pi$ AO's of the other atoms in unsaturated molecule with which to be hyperconjugated.

When ϵ_{1s-1s} is required to be related to the Coulomb integral of the $2p\pi$ carbon AO in benzene (for example, hyperconjugations in toluene, benzenium ion, etc.), the former is found to be slightly smaller than the latter (α_c(sepc.) $=-7.2$ ev) in absolute magnitude and is written as

$$\epsilon_{1s-1s}=\alpha_c+\delta\beta_{cc}.$$

If we use the spectroscopically determined values $\alpha_c=-7.2$ ev and $\beta_{cc}=-2.56$ ev,[11] δ is found to be approximately -0.3.

Another point to be added is as follows: as far as this value and the group overlap value 0.541[12] between C and H_2 or H_3 are used, the assumption that γ is proportional to S seems to be not adequate and it should be assumed that β is proportional to S as proposed by Mulliken and Rieke.[13] A detailed computation of hyperconjugation including the above determined parameter will be published in the near future.

[1] G. W. Wheland, J. Am. Chem. Soc. **64**, 900 (1942).
[2] Pullman, Mayot, and Berthier, J. Chem. Phys. **18**, 257 (1950).
[3] H. C. Longuet-Higgins and R. G. Sowden, J. Chem. Soc. 1404 (1952).
[4] C. A. Coulson, Proc. Phys. Soc. (London) **45**, 933 (1952).
[5] H. H. Jaffe, J. Chem. Phys. **20**, 778 (1952).
[6] C. A. Coulson and V. A. Crawford, J. Chem. Soc. 2052 (1953).
[7] Muller, Pickett, and Mulliken, J. Am. Chem. Soc. **76**, 4770 (1954).
[8] Y. I'Haya (to be published).
[9] R. S. Mulliken, J. Chim. Phys. **46**, 497 (1949).
[10] For such a larger internuclear separation where the overlap is appreciably small, effective nuclear charge for hydrogen atom may be considered essentially unity.
[11] C. C. J. Roothaan and R. S. Mulliken, J. Chem. Phys. **16**, 118 (1948); R. S. Mulliken, J. Chim Phys. **46**, 675 (1949), Table XVIII.
[12] See reference 8, Sec. III of Part I.
[13] R. S. Mulliken and C. A. Rieke, J. Am. Chem. Soc. **63**, 1770 (1941).

Dimorphism of *Para*-Dichlorobenzene*

G. A. JEFFREY AND W. J. MCVEAGH†
The University of Pittsburgh, Pittsburgh 13, Pennsylvania
(Received March 28, 1955)

THE literature relating to the structure of $p\cdot Cl-C_6H_4-Cl$ between room temperature and the melting point (53°C) is somewhat confusing. The original observation[1] of a sudden contraction in volume indicated a lattice change at 39.5°C, and later this received some measure of confirmation from the report[2] of an inflection in the cooling curve at that temperature. Other investigators,[3-5] who were attempting to interpret the low-frequency spectra, maintained that a change took place at 32°C with the onset of molecular rotation. This interpretation was criticized on the basis of work in the same field[6-8] and from an x-ray study,[9] which appeared to show that only one crystal lattice existed over the temperature range 18–45°. On the other hand, the velocity of a phase transformation measured[10] by direct observation of a single crystal enclosed in a capilliary gave a transition temperature at 30.8°C. It was also observed that the low-temperature form could remain indefinitely superheated up to 34°C and sometimes remained unchanged for some time at 8–9° above the transition point. More recently this phase change has been detected by the chlorine nuclear quadrupole coupling[11,12] with the transition temperature close to 32°C.

We have confirmed the existence of the high-temperature β form by optical and x-ray examination and have characterized it as triclinic with a unit cell $a=6.844$, $b=5.960$, $c=3.978$ A, $\alpha=91°25'$, $\beta=98°40'$, $\gamma=92°30'$, $V=160.2$ A,^{3} containing one molecule. This cell has half the volume of that for the room temperature monoclinic α form reported by Hendricks[13] and there is at least a superficial similarity in the cells which have approximately equal b- and c-axes.

The single crystals of the triclinic form were obtained by sublimation from about 40° on to a cooler surface. Under these conditions both forms are obtained as plates, the α on (100) and the β on (010). The β form tended to be the more elongated in the direction of the c-axis and often appeared as flat needles. The crystals can be easily distinguished since the β form has oblique extinction at 28° to the c-axis direction. When a crystal of one form was partly transformed to the other ($\alpha\rightarrow\beta$ by heating to 40°C $\beta\rightarrow\alpha$ by cooling below 0°C), the reversible phase transformation

was observed through the polarizing microscope to correspond with the description of the $\alpha-\beta$ transition reported in the kinetic study of the Russian workers.[10]

We found no evidence of the trimorphic monoclinic forms with transitions at 25° and 29°C reported briefly in 1914.[14]

So far our x-ray study shows no evidence to support Saksena's postulate[5] that the high-temperature phase is disordered due to excitation of free rotation about an axis normal to the molecular plane.

A detailed analysis of the room temperature form has been completed by Croatts, Bezzi, and Bua.[15] We are undertaking an analysis of the triclinic crystals to ascertain the mechanism of the phase change and also to establish a more complete structural correlation with the nuclear quadrupole data.

* Work done jointly in the Sarah Mellon Scaife Radiation Laboratory and the Chemistry Department and assisted by a grant from the National Science Foundation, Washington, D. C.

† Present address: Gulf Research and Development Company, Pittsburgh 30, Pennsylvania.

[1] K. Beck and K. Ebbinghaus, Ber. deut. chem. Ges. **39**, 3870 (1906).
[2] A. N. Campbell and L. A. Proden, J. Am. Chem. Soc. **70**, 553 (1948).
[3] M. Vuks, Compt. rend. acad. sci. U.R.S.S. **1**, 73, (1936).
[4] A. Rousset and R. Lochet, J. phys. radium **3**, 146 (1942).
[5] B. D. Saksena, J. Chem. Phys. **18**, 1653 (1950).
[6] S. C. Sirkar and J. Gupta, Indian J. Phys. **10**, 473 (1936).
[7] C. S. Venkateswaran, Proc. Indian Acad. Sci. **8A**, 448 (1938).
[8] S. C. Sirkar, J. Chem. Phys. **20**, 742 (1952).
[9] S. C. Sirkar and J. Gupta, Indian J. Phys. **11**, 283 (1937).
[10] V. I. Danilov and D. E. Ovsienko, Doklady Akad. Nauk. S. S. S. R. **73**, 1169 (1950).
[11] C. Dean and R. V. Pound, J. Chem. Phys. **20**, 195 (1952).
[12] B. C. Lutz, J. Chem. Phys. **22**, 1618 (1954).
[13] S. B. Hendricks, Z. Krist. **84**, 85 (1933).
[14] F. Wallerant, Compt. rend. **158**, 385 (1914).
[15] Croatts, Bezzi, and Bua, Acta Cryst. **5**, 825 (1952).

On the Specific Adsorption of Ions in the Electrical Double Layer

DAVID C. GRAHAME
Department of Chemistry, Amherst College, Amherst, Massachusetts
(Received April 13, 1955)

IN the Stern theory of the electrical double layer it is assumed that the number of ions specifically adsorbed at an interface is to the number of ions of the same kind in solution as the number of adsorption sites is to the number of free places for the ion in solution multiplied by a Boltzmann factor, $e^{-w_i/kT}$, where w_i is the energy of specific adsorption. Unfortunately the ratio of the number of sites to the number of free places in solution cannot readily be defined or evaluated. In an earlier publication[1] the writer suggested that this ratio is given by $2r$, where r is the radius of the adsorbed ion, but this suggestion is now withdrawn. It was based upon the supposition that if a centimeter cube be divided into smaller cubes of dimensions $2r$, the small cubes on one face of the centimeter cube will represent adsorption sites whereas the remainder of the small cubes represent free places in the solution. The defect in this argument lies in the fact that when the center of an ion wanders into one of the cubes called adsorption sites it is not immediately in a potential well of depth w_i, as is implied by the subsequent use of the Boltzmann factor.

There will now be given a more general solution to the problem as follows. Let $V(r)$ be the average potential energy of an ion at a distance r from the plane interface. Consider an increment of distance dr. Then the excess of ions in this increment, per unit of area, will be

$$dn^i = n_{0i} \exp[-V(r)/kT]dr - n_{0i}dr \qquad (1)$$

where n_{0i} is the concentration of ions of type X_i in the interior of the solution. The total excess per unit of area is accordingly

$$n^i = n_{0i}\int_0^\infty \{\exp[-V(r)/kT]-1\}dr. \qquad (2)$$

The potential energy function $V(r)$ is composed of two parts, one electrostatic and one chemical, and as usual it is not possible to separate these parts experimentally or even conceptually. Also, $V(r)$ will be approximately a Morse function, but since the introduction of this function into Eq. (2) leads to an integral not expressible in terms of tabulated functions, it has been suggested[2] that a parabolic well be employed instead. This requires omission of the constant 1 from Eq. (2) to take account of the fact that $\exp[-V(r)/kT]$ now goes to zero, rather than to unity, as $r\to\infty$. The lower limit of integration is changed to $-\infty$ for a similar reason. If r_0 is the value of r at the minimum of $V(r)$, the suggested form of $V(r)$ is therefore

$$V(r) = V(r_0) - \tfrac{1}{2}(r-r_0)^2(\partial^2 V/\partial r^2)_{r=r_0}, \qquad (3)$$

where $(\partial^2 V/\partial r^2)_{r=r_0}$ is minus the force constant of the "bond" holding the adsorbed ion to the surface. The subscript $r=r_0$ is superfluous for a parabolic potential well but is written here to denote the manner in which $\partial^2 V/\partial r^2$ would be chosen in another case.

Putting Eq. (3) into Eq. (2) with the aforementioned changes gives after integration

$$n^i = n_{0i}[-2\pi kT/(\partial^2 V/\partial r^2)_{r=r_0}]^{\frac{1}{2}} \exp[-V(r_0)/kT]. \qquad (4)$$

Although $V(r_0)$ and $(\partial^2 V/\partial r^2)_{r=r_0}$ are both unknown, it is possible to adopt a semitheoretical relationship between these variables by use of the Morse function and a reasonable value of the constant a, whereupon they can both be evaluated from measured values of n^i.

The fact that the adsorbed ions are quantized in their vibration relative to the surface suggests the possibility of an alternative treatment by the methods of statistical mechanics. It is considered by the writer that the quantization of the motion does not render the above treatment significantly less valid or useful, however.

[1] D. C. Grahame, Chem. Rev. **41**, 441 (1947), Eq. (82).
[2] Private communication from Professor Carl Wagner, to whom the author wishes to express his gratitude for this suggestion and for the permission to use it.

Proton Resonance in Barium Chlorate Monohydrate

R. D. SPENCE
Department of Physics, Michigan State College, East Lansing, Michigan
(Received April 5, 1955)

THE unit cell of $Ba(ClO_3)_2\cdot H_2O$ contains six water molecules. The proton resonance signal from the hydration waters is a simple well resolved doublet indicating that all the $p-p'$ (proton-proton) directions are the same. By rotating crystals about the crystallographic axes it was found that the $p-p'$ vectors are parallel to the (010) plane. Determinations on four crystals gave an average value of the angle between the c-axis and the $p-p'$ vector of 124°±1.5° (i.e., 30.5° below the positive a-axis since $\beta=93.5°$ for this crystal). The maximum splitting in the (101) plane gives a value of 1.56 A° for the $p-p'$ distance. The components of the doublet show an anisotropic line width which appears to arise from a dipole-dipole interaction among four protons which lie at the corners of parallelograms parallel to the (010) plane and which are associated with nearest neighbor water molecules.

The crystal structure of this compound has been examined by Kartha.[1] From his results it would appear that if the protons lay on lines connecting the water oxygens and the nearest oxygens of appropriate chlorate groups the $p-p'$ vector would make an angle of 113.6° with the c-axis as compared to the value of 124° given by the present experiment. While other workers[2] have shown that in certain crystals the protons may lie off the 0–0 directions, it seems rather unlikely in the present compound.

In addition to the doublet structure most of the crystals showed a rather weak narrow central line. The intensity of this line relative to that of the doublet components varies from crystal to crystal and may be due to minute amounts of water trapped in the crystal during its growth.

[1] G. Kartha, Proc. Indian Acad. Sci. **36**, 501 (1952).
[2] Itoh, Kusaka, Kiriyama, and Yabumoto, J. Chem. Phys. **21**, 1895 (1953).

Comparison of the Approximate Solutions for Free Neutral Atoms

T. TIETZ
Nicolas Copernicus University, Torun, Poland
(Received March 31, 1955)

THE method of Thomas-Fermi treats the atomic electron as a gas at zero temperature, obeying Fermi-Dirac statistics. This leads to the equation[1]

$$\frac{d^2\Phi}{dx^2}=x^{-\frac{1}{2}}\Phi^{\frac{3}{2}}. \tag{1}$$

The boundary conditions for neutral atoms are

$$\begin{aligned}\Phi&=1 \quad \text{for} \quad x=0\\ \Phi&\to 0 \quad \text{for} \quad x\to\infty.\end{aligned} \tag{2}$$

The comparison of the different approximate solutions of the Thomas-Fermi equation would be facilitated if there existed a measure for the approximation degree of any approximate solution. For this measure Umeda[2] has proposed the numerical value of the variational integral

$$I(\Phi)=\int_0^\infty[(\Phi')^2+\tfrac{4}{5}\Phi^{5/2}/x^{1/2}]dx, \tag{3}$$

evaluated by putting the given approximate solution in place of Φ. For Miranda's[3] exact solution, direct numerical quadrature of (3) gives the value

$$I=1.3625, \tag{4}$$

which should of course be the limiting minimum value of I. Since the minimization of I is equivalent to the integration of the Thomas-Fermi equation, the better approximate solution should result in the smaller numerical value of I. The general formula,

$$\Phi=\frac{1}{(1+ax)^\alpha};\quad \alpha>\tfrac{1}{5} \tag{5}$$

is now being studied on the basis of the approximation degree (private communication of Professor K. Umeda) previously mentioned. If we take[4] $\alpha=2$, $\alpha=7/5$, and $\alpha=9/5$, we obtain

$$\alpha=2;\begin{cases}I=1.3663\\ a=0.569272\end{cases}\quad \alpha=7/5;\begin{cases}I=1.3636\\ a=0.881206\end{cases} \tag{6}$$

$$\alpha=9/5;\begin{cases}I=1.3650\\ a=0.645996.\end{cases}$$

Comparing the values to the standard value $I=1.3625$ we see that the formula for $\alpha=2$, $\alpha=7/5$, and $\alpha=9/5$ is of fairly high approximation degree. Table I gives a comparison of the various approximations, *viz*, Baker[5] approximation Φ_{Ba}, Sommerfeld[6] approximation Φ_{So}, Buch-Caldwell-Fermi[7] approximation $\Phi_{Fe,Bu}$, and our approximation $_{I}\Phi_{Ti}$ for $\alpha=2$; $_{II}\Phi_{Ti}$ for $\alpha=7/5$ and $_{III}\Phi_{Ti}$ for $\alpha=9/5$. We have limited the values to three significant decimal places, which are sufficient for our purposes.

TABLE I.

x	$\Phi_{Fe,Bu}$	Φ_{So}	Φ_{Ba}	$_{I}\Phi_{Ti}$	$_{II}\Phi_{Ti}$	$_{III}\Phi_{Ti}$
0.01	0.985	0.969	0.985	0.991	0.988	0.989
0.03	0.959	0.931	0.959	0.968	0.970	0.966
0.08	0.902	0.860	0.902	0.915	0.909	0.913
0.1	0.882	0.836	0.882	0.895	0.888	0.893
0.2	0.793	0.741	0.793	0.806	0.797	0.804
0.3	0.721	0.667	0.720	0.729	0.721	0.726
0.4	0.660	0.607	0.659	0.663	0.655	0.661
0.5	0.607	0.556	0.606	0.605	0.600	0.604
0.6	0.562	0.514	0.561	0.555	0.553	0.555
0.9	0.453	0.412		0.437	0.442	0.438
1.0	0.425	0.385		0.407	0.413	0.408
1.4	0.333	0.302		0.310	0.327	0.313
1.8	0.268	0.244		0.245	0.265	0.251
2.0	0.244	0.221		0.219	0.241	0.225
2.5	0.194	0.176		0.170	0.196	0.177
3.0	0.157	0.143		0.137	0.163	0.144
4.0	0.108	0.099		0.0931	0.121	0.101
4.5	0.093	0.084		0.0788	0.106	0.0863
5.0	0.079	0.073		0.0676	0.0942	0.0746
10.0	0.024	0.023		0.0223	0.0410	0.0269
20.0	0.0058	0.0056		0.00652	0.0167	0.00874

From Table I we see that the well-known Sommerfeld asymptotic formula is not a better approximation. It has a sufficient foundation in regard to the asymptotic behavior, while the March[8] formula is obviously an improved approximate solution. The Sommerfeld approximation is relatively complicated. More details will be published elsewhere.

In conclusion the writer wishes to thank Professor Dr. Kwei Umeda for friendly private comments.

[1] L. H. Thomas, Proc. Cambridge Phil. Soc. **23** (1926); E. Fermi, Rend. reale acad. Naz. Lincei **6**, 602 (1927). P. Gombás, *Die statistische Theorie des Atoms* (Verlag Julius Springer, Wien, 1949).
[2] K. Umeda, J. Phys. Soc. Japan, **9**, 290 (1954).
[3] C. Miranda, Mem. R. Acad. d'Italia **5** (1934).
[4] T. Tietz, J. Chem. Phys. **22**, 2094 (1954); Ann. Physik **15**, 186 (1955).
[5] E. Baker, Phys. Rev. **36**, 630 (1930).
[6] A. Sommerfeld, Rend. reale acad. Naz. Lincei **15**, 788 (1932).
[7] V. Bush, and S. H. Caldwell, Phys. Rev. **38**, 1898 (1931).
[8] N. H. March, Proc. Cambridge Phil Soc. **46**, 356 (1950).

Electron Theory of Metals and Hydrogen Overvoltage

PAUL RÜETSCHI* AND PAUL DELAHAY
Department of Chemistry, Louisiana State University, Baton Rouge, Louisiana
(Received March 28, 1955)

IT was recently pointed out[1] that differences in hydrogen overvoltage, η, from one metal to another for given electrolysis conditions primarily depend on the heat, $D(M-H)$, of adsorption of atomic hydrogen. The η–$D(M-H)$ relationship is approximately linear. Other quantities such as work function, lattice constant, etc., have been considered in the comparison of overvoltages for different metals. It is shown below that these observations can be correlated to the $\eta-D(M-H)$ relationahip.

The heat of adsorption of atomic hydrogen can be calculated by[2]

$$D(M-H)=\tfrac{1}{2}\{D(M-H)+D(H-H)\}+23.06(X_M-X_H)^2, \tag{1}$$

where D's are the bond energies and X's the electronegativities. Characteristics of the metal appear in $D(M-M)$ and X_M. The latter is approximately 0.355ϕ, ϕ being the work function of the metal.[3,4] Furthermore, $D(M-M)$ can be computed from the heat of sublimation L of the metal, and L can be correlated to parameters characterizing the metal. Thus, $L\approx 3\phi/5$ for the alkali metals, copper, silver, and gold[5] and $D(M-H)$ depends on ϕ. The relationship between L and ϕ for other metals is more involved, but the simple equation $L\approx 3\phi/5$ suffices to indicate a trend. The $\eta-\phi$ dependence observed by Bockris[6] can thus be accounted for qualitatively; L and consequently $D(M–H)$ increases with ϕ, and since η decreases with increasing values of $D(M-H)$, the overvoltage decreases with increasing work function.

The energy of sublimation L for Na, K, etc., is proportional[5] to the power $\frac{3}{2}$ of the free electron density, and consequently an increase in electron density in the electrode causes a decrease in overvoltage. This conclusion is verified experimentally.[7] Conversely, large lattice constants and large compressibilities correspond to relatively low electron densities and high overvoltages.

Another approach in correlating overvoltage to electrode material can be followed by applying the expression for ϕ derived by Wigner and Bardeen.[8] The expression contains the cohesive energy of the metal, and consequently the bond energy $D(M-H)$ can be expressed in terms of the work function. Still another approach would be to apply Mulliken's treatment of charge-transfer-no-bond adsorption.[9,10]

These various treatments show that hydrogen overvoltage (or exchange current) can be correlated to various quantities characterizing the electrode material. However, the resulting relationships would probably be more complicated than the

$\eta - D(M-H)$ dependence which follows more directly from the kinetic treatment. A detailed treatment will be published.

We are indebted to Dr. W. Oldekop for valuable comments on the electron theory of metals.

* Postdoctoral fellow, 1953–54, on a project sponsored by the Office of Naval Research.

[1] P. Rüetschi and P. Delahay, J. Chem. Phys. **23**, 195 (1954).
[2] D. D. Eley, J. Phys. Chem. **55**, 1016 (1951).
[3] D. P. Stevenson, J. Chem. Phys. **23**, 203 (1955).
[4] R. S. Mulliken, J. Chem. Phys. **2**, 782 (1934); **3**, 573 (1935).
[5] H. Frölich, *Elektronentheorie der Metalle* (Verlag Julius Springer, Berlin, 1936), pp. 256–285.
[6] J. O'M. Bockris and E. C. Potter, J. Electrochem. Soc. **99**, 169 (1952).
[7] M. J. Brabers, thesis, Delft, 1954.
[8] F. Seitz, *The Modern Theory of Solids* (McGraw-Hill Book Company, New York, 1940), p. 399.
[9] R. J. Mulliken, J. Am. Chem. Soc. **74**, 811 (1952); J. C. P. Mignolet, J. Chem. Phys. **21**, 1298 (1953).
[10] Matsen, Makrides, and Hackerman, J. Chem. Phys. **22**, 1800 (1954).

On the Entropy of Mixing of Liquid Solutions

A. Englert-Chwoles
Faculty of Sciences, University of Brussels, Brussels, Belgium
(Received March 4, 1955)

MANY binary mixtures of polyatomic nonpolar molecules with approximately central field of forces show an important excess entropy [Table I (B)], which at first may be attributed to the following causes:

(*1*) *Order-disorder effect.*—This leads to a negative, and practically negligible excess entropy.[1,2]

(*2*) *Changes in the rotational (or orientational) partition function on mixing.*—The contributions of this effect to Ts_e and to g_e are of the same order of magnitude and of the same sign.[3]

(*3*) *Effect of the change in the motion of molecules around their equilibrium position.*—The corresponding excess entropy is mainly related to the volume change on mixing.[4–6]

Let us consider in more detail the excess entropy resulting from this effect and calculated by the cell model assuming an intermolecular potential independent of orientation. We also assume that

$$\epsilon_{AB}{}^{*2}=\epsilon_{AA}{}^{*}\epsilon_{BB}{}^{*} \quad r_{AB}{}^{*}=(r_{AA}{}^{*}+r_{BB}{}^{*})/2, \tag{1}$$

where $\epsilon_{ij}{}^{*}$ and $r_{ij}{}^{*}$ are coordinates of the minimum of the curve describing the interaction between molecules i and j as function of their distance apart. Experimental data on second-virial coefficient of mixtures of simple gases[7] and even of complicated polyatomic molecules[8] justify the use of (1).

For a *solution composed of molecules of the same size* ($r_{AA}{}^{*}=r_{BB}{}^{*}$, but $\epsilon_{AA}{}^{*}\neq\epsilon_{BB}{}^{*}$), Ts_e is of opposite sign to, and of the order of 10 percent to 50 percent of g_e; at zero pressure $v_e<0$, $Ts_e<0$, $g_e>0$.[4,6] For a *solution composed of molecules of different size* ($r_{AA}{}^{*}\neq r_{BB}{}^{*}$, and $\epsilon_{AA}{}^{*}\neq\epsilon_{BB}{}^{*}$), for sufficiently large differences in diameters, when $|(r_{BB}{}^{*}-r_{AA}{}^{*})/r_{AA}{}^{*}|>\frac{1}{2}|(\epsilon_{BB}{}^{*}-\epsilon_{AA}{}^{*})/\epsilon_{AA}{}^{*}|$ both the excess volume and excess entropy became positive.[5,6]

The aforementioned conclusions are valid when $\epsilon_{AB}{}^{*}\approx(\epsilon_{AA}{}^{*}+\epsilon_{BB}{}^{*})/2$, as is the case for homopolar solutions as long as (1) is valid.

It is to be noticed, that the structure of a solution of molecules of the same size is very similar to that of pure liquids, the order-disorder effects being small; while the structure of a solution of molecules of different size can no longer be considered as identical to that of the pure liquids.

It has not as yet been possible to draw definite conclusions as to the origin of the excess entropy, since experimental data on the excess entropy of mixtures of molecules of similar size were lacking.

We have measured the heat of mixing of one such system, namely CCl_4+neopentane at 0°C. As the vapor pressure and the excess volume of CCl_4+neopentane at 0°C were already measured in our laboratory,[9] all the excess properties of this system are at present known. The heat of mixing is for a mole fraction 0.5, 75±5 cal/mole^{-1}.[10]

The experimental excess properties of mixtures of globular molecules and the parameters of the central force field, estimated from critical ratio, virial coefficients, heats of vaporization, densities, and viscosities, are given in Table I. The comparison of these data lead to following conclusions:

The excess entropy seems to depend rather strongly on the excess volume: for the four mixtures of molecules with $v_e>0$, $Ts_e>0$, and $Ts_e\approx g_e$, whereas for the mixture CCl_4+neopentane with $v_e<0$, we obtained a very small and probably negative value of Ts_e and $Ts_e\ll g_e$.

The sign and the relation between the excess properties and their dependence upon the intermolecular forces are, for all systems studied, correctly predicted by the cell theory assuming (1) and a central force law. The observed negative entropy (−1±8

TABLE I.

A. Solution of molecules of the same size, $|(r_{BB}{}^{*}-r_{AA}{}^{*})/r_{AA}{}^{*}|\ll|(\epsilon_{BB}{}^{*}-\epsilon_{AA}{}^{*})/\epsilon_{AA}{}^{*}|$.

$AA+BB$	$(\epsilon_{BB}{}^{*}-\epsilon_{AA}{}^{*})/\epsilon_{AA}{}^{*}$	$(r_{BB}{}^{*}-r_{AA}{}^{*})/r_{AA}{}^{*}$	v_e cm^{3}mole^{-1}	Ts_e cal mole^{-1} for a mole fraction 0.5	g_e
neopentane +cyclohexane[a]	0.30	0.00	−1.0		+44
$CO+CH_4$[b]	0.44	+0.04	−0.3		+28
neopentane +CCl_4[a,c]	0.30	−0.04	−0.5	−1	+76
neopentane +benzene[a]	0.32	−0.08	−0.5		+135

B. Solutions of molecules of different size, $|(r_{BB}{}^{*}-r_{AA}{}^{*})/r_{AA}{}^{*}|>\frac{1}{2}|(\epsilon_{BB}{}^{*}-\epsilon_{AA}{}^{*})/\epsilon_{AA}{}^{*}|$.

$AA+BB$	$(\epsilon_{BB}{}^{*}-\epsilon_{AA}{}^{*})/\epsilon_{AA}{}^{*}$	$(r_{BB}{}^{*}-r_{AA}{}^{*})/r_{AA}{}^{*}$	v_e cm^{3}mole^{-1}	Ts_e cal mole^{-1} for a mole fraction 0.5	g_e
$SiCl_4+CCl_4$[d]	0.07	−0.04	+0.015	+13	+20
CCl_4+benzene[e,f]	0.02	−0.04	+0.01	+7	+19
cyclohexane +benzene[f,g]	0.02	−0.08	+0.65	+115	+76
cyclohexane +CCl_4[f,h]	0.00	−0.04	+0.16	+20	+17

[a] See reference 9.
[b] Mathot, Staveley, Young, and Parsonage (to be published).
[c] See reference 10.
[d] S. E. Wood, J. Am. Chem. Soc. **59**, 1510 (1937); R. D. Vold, J. Am. Chem. Soc. **59**, 1515 (1937); J. H. Hildebrand and J. M. Cartner, J. Am. Chem. Soc. **54**, 3592 (1932).
[e] B. G. Cheesman and B. Whittaker, Proc. Roy. Soc. (London) **A212**, 406 (1952).
[f] For references on g_e and v_e see S. E. Wood and J. A. Gray, J. Chem. Am. Soc. **74**, 3729 (1952).
[g] Scatchard, Thicknor, Goates, and McCartney, J. Am. Chem. Soc. **74**, 3721 (1952).
[h] D. S. Adcock and M. L. McGlashan, Proc. Roy. Soc. (London) **A226**, 266 (1954).

cal mole^{-1}) of CCl_4+neopentane seems slightly smaller than that calculated by the cell model ($-10+5$ cal mole^{-1})[4,6] but these two values agree within the experimental uncertainties. It should, however, be pointed out that a difference between calculated and experimental value should be expected due to the neglected orientational forces.

We are much indebted to Professor Prigogine, who suggested the present work, for constant advice and interest. We are indebted to Dr. Tompa for his help in the experimental part of this work.

[1] L. Sarolea, J. Chem. Phys. **21**, 182 (1953).
[2] Z. W. Salzburg and J. G. Kirkwood, J. Chem. Phys. **20**, 1538 (1952).
[3] J. A. Pople, Discussions Faraday Soc. **15**, 35 (1953).
[4] O. Prigogine and V. Mathot, J. Chem. Phys. **20**, 49 (1952).
[5] I. Prigogine and A. Bellemans, Discussions Faraday Soc. **15**, 80 (1953).
[6] Prigogine, Bellemans, and Englert-Chwoles (to be published).
[7] E. A. Gugenheim, *Mixtures* (Oxford University Press, New York, 1952) Chap. VIII.
[8] F. G. Walbroeck (to be published).
[9] V. Mathot and A. Desmyter, J. Chem. Phys. **21**, 782 (1953).
[10] A detailed description of the measurements will be published in Bull. soc. chim. Belge.

Mass Spectrometric Detection of Radicals in the Mercury Photosensitized Decomposition of Acetone

J. B. FARMER,* F. P. LOSSING, D. G. H. MARSDEN,* AND E. W. R. STEACIE
Division of Pure Chemistry, National Research Council, Ottawa, Canada
(Received March 24, 1955)

A NUMBER of studies of the reactions and properties of free radicals have been made by various authors using mass spectrometers modified to permit continuous sampling of a stream of radicals and other products resulting from the pyrolysis of reactants in furnaces and on hot filaments, from the action of hydrogen atoms, or from combustion flame reactions.[1] Owing to the relatively high temperatures usually prevailing in the production of the radicals, most of these studies have of necessity been confined to radicals having considerable thermal stability. This limitation could to a large extent be removed if the radicals could be produced at much lower temperatures such as are found in photolytic reactions. The absorption coefficients of nearly all organic compounds are so small, however, that very little energy can be transferred to a reactant carried at a high rate of flow through a reaction zone of reasonable proportions. Since the walls of the reaction vessel would absorb at least as much of the useful radiation as would the reactant at such low pressures, the use of external reflectors to increase the path length would improve the situation only slightly.

A way out of this difficulty would be to take advantage of the large absorption coefficient of mercury vapor for 2537 A resonance radiation as has been done in the extensive studies of photosensitized reactions. Some preliminary experiments have been made to examine the feasibility of this proposal.

The photosensitized decomposition of acetone, using 2537 A radiation from a low-pressure mercury lamp, has been carried out in a quartz reactor attached to the ionization chamber of a mass spectrometer. Acetone carried at a few microns pressure in a stream of helium saturated with mercury vapor was passed through a quartz tube surrounded by a water-cooled mercury lamp of cylindrical form. After traversing the illuminated zone the stream of gas passed over a quartz cone containing a small orifice,through which a sample of gas entered directly into the ionization chamber of the mass spectrometer. On irradiation, the decrease in the parent peak of the acetone showed that a considerable fraction had been decomposed during the time taken to traverse the illuminated zone (about 0.002 sec). Under some conditions the extent of decomposition reached 80 percent. Using low-energy electrons suitable for the detection of free radicals,[2] CH_3 radicals were found to be present in considerable abundance. An increase in the mass 43 peak upon illumination, when using electrons of energy insufficient to produce CH_3CO^+ from acetone or biacetyl, showed that CH_3CO radicals were also present.

The dimerization products of these radicals, ethane and biacetyl, were also found in considerable amounts. Cooling the illuminated zone with a blast of air increased the yield of biacetyl, suggesting that the temperature in the reactor was sufficiently high to dissociate an appreciable fraction of the CH_3CO radicals. This is not surprising in view of their low thermal stability.[1b] The formation of CO in large amounts also suggested the decompositon of CH_3CO radicals, either by a thermal reaction, or by a further collision with an excited mercury atom. Ketene was also identified as a product as well as small amounts of CH_4 and H_2. No indications of the presence of the acetonyl radical CH_3COCH_2 could be obtained. It is hoped that with some modifications this apparatus can be of use in studying the mechanisms of a number of photosensitized reactions and also the reactions and properties of radicals such as CH_3CO which are too unstable to be produced by thermal means.

The authors would like to express their appreciation of the invaluable assistance of Mr. G. Ensell, who designed and constructed the mercury lamp and the reactor.

* National Research Council Postdoctorate Fellow.
[1] For reviews see (a) A. J. B. Robertson, *Mass Spectrometry* (Methuen and Company, Ltd., London, 1954), and (b) E. W. R. Steacie, *Atomic and Free Radical Reactions* (Reinhold Publishing Corporation, New York, 1954).
[2] G. C. Eltenton, J. Chem. Phys. **15**, 455 (1947).

Ground State of the Helium Hydride Ion

ARTHUR A. EVETT
Department of Physics, Yale University, New Haven, Connecticut
(Received March 24, 1955)

THE variational method developed by James and Coolidge for molecular hydrogen has been applied to the ground state of the helium hydride ion $(HeH)^+$, extending the earlier work of Coulson and Duncanson[1] and of Toh.[2] Several terms not considered previously in the power series expansion in elliptical coordinates were found to be very effective in increasing the binding energy. The wave functions considered were of the type $\Psi=\sum_i c_i\psi_i$ with $\psi_i=e^{-1.375(\xi_1+\xi_2)}[\xi_1{}^{m_i}\xi_2{}^{n_i}\eta_1{}^{j_i}\eta_2{}^{k_i}\rho^{p_i}+\xi_1{}^{n_i}\xi_2{}^{m_i}\eta_1{}^{k_i}\eta_2{}^{j_i}\rho^{p_i}]$. The symbolism agrees with that used in the earlier work.

TABLE I.

Term No. i	Exponents $mnjkp$	Term No. i	Exponents $mnjkp$
1	00000	13	00050
2	00010	14	10030
3	00110	15	10200
4	00020	16	10300
5	10000	17	00120
6	10100	28	00130
7	00001	19	00220
8	10010	20	00230
9	00011	21	11000
10	00030	22	20000
11	00040	23	10001
12	10020		

Table I gives the values of the exponents for the 23 terms considered in the function Ψ. Coulson and Duncanson[1] had used terms 1–5, 7, while Toh[2] had included terms 1–12. It should be noted, however, that terms 1 and 3 are twice those of Toh.

Table II shows the binding energy values obtained for several internuclear separations with 20-term and 23-term wave functions. These energy values indicate that the equilibrium internuclear separation is about $1.44a_0$. The fundamental vibration frequency was computed to be 3600 cm^{-1}, leading to a corrected dissociation energy of 1.68 ev. This is considerably greater than the value of about 1.05 ev reported by Toh for a 12-term function. Employing

TABLE II.

Internuclear Separation (a_0)	Binding energy (e^2/a_0) Terms 1–20	Terms 1–23
1.20	−2.9559	
1.30	−2.9674	
1.40	−2.9713	−2.9730
1.44	−2.9716	
1.50	−2.9710	
1.60	−2.9673	−2.9687

an ionic-polar Wang-type function, Coulson and Duncanson[1] arrived at a value of 2.10 ev, which they considered to be an upper limit because of decreased flexibility of their wave function at large internuclear separations. The value of 1.68 ev represents a lower limit so the actual corrected dissociation energy of $(HeH)^+$ can be placed with some confidence in the range 1.75–2.05 ev.

TABLE III.

Term No. i	$R=1.40a_0$ c_i	$R=1.44a_0$ c_i
1	1.677	1.662
2	−2.675	−2.765
3	0.804	0.777
4	2.118	2.306
5	−0.3413	−0.4152
6	0.5712	0.6292
7	0.3654	0.3377
8	0.0026	0.1010
9	−0.5731	−0.5499
10	−0.9539	−1.064
11	0.5933	0.5991
12	0.3253	0.2170
13	−0.1796	−0.1861
14	−0.1526	−0.1103
15	−0.2532	−0.3442
16	0.1827	0.2254
17	−1.728	−1.710
18	0.3382	0.3570
19	0.4576	0.4700
20	−0.2066	−0.2226

Table III lists the coefficients c_i for the normalized 20-term function at internuclear separations of $1.40a_0$ and $1.44a_0$.

A more detailed presentation of these results will be published later.

[1] C. A. Coulson and W. E. Duncanson, Proc. Roy. Soc. (London) **A165**, 90 (1938).
[2] S. Toh, Proc. Phys. Math. Soc. Japan **22**, 119 (1940).

Absence of Hydrogen Bonding in an Alcohol-Fluorohydrocarbon System

R. S. McDONALD, J. H. GIBBS, AND J. R. LADD
General Electric Research Laboratory, Schenectady, New York
(Received March 28, 1955)

THE hydrides of nitrogen, oxygen, and fluorine (H_3N, H_2O, HF) form hydrogen bonds. The organic compounds of nitrogen and oxygen [e.g., $(CH_3)_3N$, $(CH_3)_2O$] act as proton acceptors in hydrogen bond formation. This communication describes some evidence concerning the proton accepting properties of an alkyl fluoride.

The system benzyl fluoride-benzyl alcohol was chosen because of the stability and nonvolatility of the former and the fact that any reaction involving interchange of functional groups between these two compounds would leave the system unchanged.

The benzyl fluoride was prepared by the method of Bernstein, Roth, and Miller.[1] A sharp band of moderate intensity at 3680 cm^{-1} was present in the spectrum of the purified benzyl fluoride. The position of this band did not shift when 10 percent pyridine was added, indicating that the band is not due to an OH bearing impurity.

The spectrum of a 3 percent (by volume) solution of benzyl alcohol in benzyl fluoride was compared with the spectra of similarly dilute solutions of benzyl alcohol in both proton accepting (anisole) and nonproton accepting (toluene) solvents. The concentration was a compromise between that required to eliminate completely hydrogen bond formation between alcohol molecules, and that required to obtain OH bands of intensity comparable to that of the 3680 cm^{-1} band of benzyl fluoride. The path length was 0.36 mm. The spectra were measured with a Perkin-Elmer Model 21 spectrophotometer using a sodium chloride prism.

The O−H stretching frequency characteristic of isolated benzyl alcohol OH groups was found to be 3610 cm^{-1} from the benzyl alcohol-toluene spectrum. An OH stretching frequency due to hydrogen bonds between pairs of alcohol molecules was found at 3460 cm^{-1}.[2] The 3610 cm^{-1} free OH band was much more intense than the 3460 cm^{-1} bonded OH band.

In a 5 percent solution of benzyl alcohol in anisole the OH frequency was 3520 cm^{-1}. The very small shift of the OH frequency from the free OH value indicates a very weak hydrogen bond between anisole and benzyl alcohol. No free OH band (e.g., at 3610 cm^{-1}) was observed in this solution.

The spectrum of a 3 percent solution of benzyl alcohol in benzyl fluoride was essentially the same as the corresponding spectrum of benzyl alcohol in toluene. The strong narrow free OH band was again observed at 3610 cm^{-1}. The weaker band occurring at 3460 cm^{-1} was again attributed to OH–OH rather than OH–F on the basis of the following observations. In a 1 percent solution, the 3610 cm^{-1} band was approximately $\frac{1}{3}$ as strong as in the 3 percent solution, while the 3460 cm^{-1} band was only $\frac{1}{9}$ as strong as in the 3 percent solution. Dilution would have had the same effect on the intensity of OH−F bands as on that of free OH bands in these systems containing excess benzyl fluoride.

The similarity of the benzyl alcohol spectrum in benzyl fluoride to that in toluene and the contrast with that in anisole indicates that there is little if any OH−F hydrogen bonding in this alcohol-fluorohydrocarbon system.

[1] Bernstein, Roth, and Miller, J. Am. Chem. Soc. **70**, 2310 (1948).
[2] Smith and Creitz, J. Research Natl. Bur. Standards **46**, 145 (1951), have shown that the 3460 cm^{-1} band in dilute solutions of alcohols in nonpolar solvents is due to alcohol-alcohol dimers.

Diffusion of Zinc in Crystalline Zinc Oxide*

E. A. SECCO AND W. J. MOORE
Department of Chemistry, Indiana University, Bloomington, Indiana
(Received April 13, 1955)

THE diffusion of zinc in crystals of zinc oxide has been measured from 900 to 1025° in an atmosphere of zinc vapor. The ZnO crystals, incorporating radioactive Zn^{65}, were prepared by the method of Scharowsky.[1] A 50 mg sample of the crystals was weighed into a small quartz bucket, which was suspended in a cylindrical quartz vessel. After addition of enough pure zinc to give the requisite vapor pressure during the diffusion process, the vessel was evacuated and sealed. The ZnO sample contained about 1000 individual acicular crystals, with a mean thickness of 0.01 mm and a selected narrow distribution of thicknesses. After each successive diffusion anneal the bucket was withdrawn, and the residual radioactivity of the ZnO was determined. The diffusion coefficient D of Zn in ZnO was calculated by an adaptation of the method of Zimens,[2] and the use of an appropriate solution of the diffusion equation given by Wilson.[3] The fact that the measured exchange rate is diffusion-controlled was established by the good fit of the data with the theoretical diffusion curves, and by experiments in which the cross sections of the ZnO crystals were varied.

At 1 atmos zinc pressure, it was found that $D=4.8\exp(-73.0$ kcal/RT)cm^2sec^{-1}. This result corresponds to $\Delta H^*=70.5\pm3.0$ kcal and $\Delta S^*=8.1\pm2.3$ cal deg^{-1} for the parameters of the Eyring diffusion equation[4] with $\lambda=3.21$ A. Variation of zinc pressure from

0.2 to 2.9 atmos indicated that D varies as $P_{Zn}^{0.65}$. This dependence suggests that the diffusing species is the singly dissociated interstitial zinc ion, Zn^+. The D *vs* P_{Zn} curve does not pass through the origin, indicating that there may be some mechanism other than solution from the vapor for forming excess zinc in ZnO crystals at low zinc pressure. This observation is consistent with the results of Lindner,[5] who found a D for Zn in sintered ZnO heated in air which is very close to our figure. A structural interpretation of these results, and a correlation with the solubility of Zn in ZnO and the oxidation kinetics of zinc, will be included in the detailed account of this investigation to be published later.

* This work has been carried out under U. S. Atomic Energy Commission contract.

[1] E. Scharowsky, Z. Physik **135**, 318 (1953).
[2] K. Zimens, Arkiv Kemi, Mineral. Geol. **20A**, No. 18 (1945).
[3] A. H. Wilson, Phil. Mag. **39**, 48 (1948).
[4] Glasstone, Laidler, and Eyring, *The Theory of Rate Processes* (McGraw-Hill Book Company, Inc., New York, 1941), p. 524.
[5] R. Lindner, Acta Chem. Scand. **6**, 457 (1952).

Third-Order Conjugation Energies

Y. I'HAYA
Department of Chemistry, Tokyo University of Education,
Otsuka, Tokyo, Japan
(Received April 5, 1955)

In a previous paper,[1] the third-order conjugation (second-order hyperconjugation) energies computed for various carbon-carbon bond lengths were appreciably less than the Mulliken, Rieke, and Brown[2] (M. R. B.), Roberts and Skinner[3] (R. S.), and even than the Coulson and Crawford[4] (C. C.) values. Although we have no method of directly examining these energies, the parameter δ the Coulomb integral correction term for quasi-π orbital has been successfully determined on the basis of theoretical treatment, hence it seems interesting to rescrutinize the third-order conjugation energies.

The third-order conjugation energies $E_3(CJ)$ per bond per dimension are computed for various bond lengths by solving the secular determinants for ethane or ethylene and the methyl group,[5] and are listed in Table I. Here the following should be noted: (1) the assumption that β is proportional to S is taken here, while in the previous work γ was assumed to be proportional to S, (2) δ value -0.3 determined theoretically in the preceding letter is used, while the previous work has been done with the δ value of -0.5, (3) the theoretically computed overlap integral of the group orbitals of C$-$H$_3$ or C$-$H$_2$($S^*=0.541$) is used, and not the empirical value determined in the previous paper, and (4) all secular determinants involve overlap integrals for adjacent atoms but not non-neighbor interactions as before.

TABLE I. Third-order conjugation energies, in units of $|\beta|$.

r(C$-$C), A	E_3(CJ)	r(C$-$C), A	E_3(CJ)
1.55	0.0157	1.39	0.0266
1.53	0.0169	1.35	0.0303
1.46	0.0214	1.33	0.0323

Using these third-order conjugation energies, theoretically corrected conjugation energy of benzene becomes -1.0383β. The value β obtained by comparison of this and empirical conjugation energy for benzene (75 kcal) is found to be -72.2 kcal (-70.0 kcal in the previous work). In Table II, the third-order conjugation energies converted into kcal are compared with those of the other authors and the previous work.

TABLE II. Comparison of third-order conjugation energies in kcal.

r(C$-$C), A	1.55	1.53	1.46	1.39	1.35	1.33
M. R. B.	...	1.35	2.37	3.93	5.00	5.54
R. S.	2.50	2.76	3.98	5.60	...	7.40
C. C.	0.68	...	0.90	1.14	1.30	1.38
Previous work	0.08	0.09	0.12	0.15	...	0.18
Present work	1.13	1.22	1.55	1.92	2.19	2.33

The considerably larger values in the second and third rows of Table II is no doubt due to the neglecting of the overlap integrals. The extremely smaller values of the previous work may be ascribed to the fact that γ was assumed to be proportional to S and δ was taken as -0.5. The intermediate and fairly satisfactory values of rows 4 and 6 are different in the method of computations; the present work has been done with the conditions (1)–(4), while Coulson and Crawford assumed that γ is proportional to S, S^*/S is 2.5, and δ is neglected. Of course we cannot say which is the better value, but from the viewpoint of the quantitative treatment which has been done as nonempirically as possible, the present work would seem to be more satisfactory than any other previous computations.

[1] Y. I'Haya (to be published in Bull. Chem. Soc. Japan).
[2] Mulliken, Rieke, and Brown, J. Am. Chem. Soc. **63**, 41 (1941).
[3] J. S. Roberts and H. A. Skinner, Trans. Faraday Soc. **45**, 339 (1949).
[4] C. A. Coulson and V. A. Crawford, J. Chem. Soc. **1953**, 2052 (1953).
[5] See reference 1, Sec. IV of Part II.

Theory of the Taylor-Benedict-Strong Effect*

GILBERT AMAT† AND MARK GOLDSMITH
Department of Physics and Astronomy, The Ohio State University, Columbus, Ohio
(Received March 21, 1955)

TAYLOR, Benedict, and Strong,[1] in calculating the vibrational constants of CO_2, have observed that the theory of Fermi-Dennison resonance corrected to second order does not lead to results in complete agreement with experiment. These authors discovered that satisfactory agreement is obtained if one supposes that the resonance energy W, which had been previously assumed equal[2] to $K_{122}/2^{\frac{1}{2}}$, is in reality a function of the vibrational quantum numbers. As an empirical form of this function, they have proposed:

$$W^2=W_0^2\{1-\beta_2[(V_2+2)^2-l_2^2]^{\frac{1}{2}}V_1^{\frac{1}{2}}-2\beta_2-\beta_3V_3\}, \qquad (1)$$

where $Wo=K_{122}/2^{\frac{1}{2}}$; β_2 and β_3 are adjustable parameters independent of the quantum numbers.

The Taylor-Benedict-Strong effect has subsequently been used by other authors qualitatively to rationalize difficulties encountered in the calculation of the rotational constants[3] of CO_2 and the vibrational constants[4] of N_2O.

Now it can be shown that the variation of W with the vibrational quantum numbers is easily explained if one computes the vibrational Hamiltonian to third order. In the usual first- or second-order[5] theory, the resonance energy enters the calculation through the matrix elements:

$$(V_1,V_2,l_2,V_3,\cdots|H'|V_1-1,\ V_2+2,\ l_2,\ V_3,\ \cdots)=W_0Z \qquad (2)$$

where $Z=(\frac{1}{2})[(V_2+2)^2-l_2^2]^{\frac{1}{2}}V_1^{\frac{1}{2}}$. The transformed third-order Hamiltonian H_3', however, contains terms in $R_1R_2R_2R_2R_2$, $R_1R_1R_1R_2R_2$, and $R_1R_2R_2R_sR_s$ (where we have designated by R_i either the ith normal coordinate or its conjugate momentum) whose nonvanishing matrix elements, $(V_1,V_2,l_2,V_3,\cdots|V_1-1, V_2+2, l_2, V_3, \cdots)$, are respectively of the types: $Z(a+bV_2+cl_2)$, $Z(d+eV_1)$, and $Z(f+gV_s)$ where a, b, $\cdots$ g are constants independent of the V_i and l_2.

Since it may also be shown that H_3' has neither diagonal nor $(V_1,V_2,l_2,V_3|V_1-2,\ V_2+4,\ l_2,\ V_2\cdots)$ matrix elements which are nonvanishing, it follows that to perform a calculation which is correct to third order, one needs only to replace W_0 in Eq. (2) by

$$W'=W_0(1-\beta_0'-\beta_1'V_1-\beta_2'V_2-B_i'l_2-\beta_3'V_3\cdots) \qquad (3)$$

where the β's are complicated combinations of the anharmonic force constants, the constants[2] $\zeta_{s\sigma,s'\sigma'}{}^{\alpha}$ and $a_{s\sigma}{}^{\alpha\beta}$, the moments of inertia, and the fundamental frequencies. The calculation of these coefficients is in progress at present and forms part of our general study of third-order rotation-vibration energies.

In principle therefore it would seem to us desirable to use

$$(V_1, V_2, V_3, l_2 | H | V_1 - 1, V_2 + 2, l_2, V_3) = W'Z \qquad (4)$$

rather than to obtain the value of these matrix elements from the empirical equation (1) although the latter, due to the presence of the arbitrary parameters β_2 and β_3, has been found adequate in practice to explain the existing experimental data.

* This research was supported in part by Contract N6-onr-22526 NR403, with the Office of Naval Research.

† Foreign Operations Administration Fellow (1954–55) on leave from the Laboratoire d'Infrarouge P.C.B., Paris.

[1] Taylor, Benedict, and Strong, J. Chem. Phys. **20**, 1884 (1952).

[2] K_{112} designates the coefficient of the potential energy term in $q_1(q_{21}^2 + q_{22}^2)$. Throughout the present discussion, we shall use the notation of H. H. Nielson, Revs. Modern Phys. **23**, 90 (1951). It should be observed that formula (1), as given here, differs from the corresponding equation in reference (1) because of a difference in definition of V_2.

[3] G. Herzberg and L. Herzberg, J. Opt. Soc. Am. **43**, 1037 (1953).

[4] G. Amat and M. L. Grenier-Besson, J. phys. radium **15**, 591 (1954).

[5] The matrix elements (2) are obtained from the first-order Hamiltonian; it should be observed that the second-order Hamiltonian has no nonvanishing matrix elements of this type.

Microwave Spectrum of Cyclopentanone

JAMES H. BURKHALTER
Department of Physics, University of Georgia, Athens, Georgia
(Received March 16, 1955)

THE R-branch lines identified by Erlandsson[1] in the microwave spectrum of cyclopentanone have been remeasured to frequency standard accuracy, and the rotational constants determined. If one neglects centrifugal distortion corrections, all the energy levels involved, except the 4_{04} and 4_{22} levels, are quadratic or of lower order in the asymmetry parameter κ. Thus, eight of the ten lines listed in Table I are expressible as explicit functions of A, C, and κ. Any three of these lines can be used to determine a set of values of these constants without recourse to approximation methods. Using the measured values of the absorption frequencies reported in Table I, the rotational constants have been determined for several sets of these lines. The 4_{04} and 4_{22} levels were then calculated, using the continued fraction method of King, Hainer, and Cross.[2] In all cases, calculations were carried out to at least one decimal place further than reported, to prevent accumulated rounding off errors. The analysis yielding the best agreement with experiment yields the rotational constants listed in Table II. The calculated line frequencies of Table I are derived from these constants.

TABLE I.

Transition	Observed frequency, mc/sec	Calculated frequency, mc/sec
$2_{12} \rightarrow 3_{22}$	17 287.54	17 286.63
$2_{20} \rightarrow 3_{21}$	17 952.40	17 952.71
$2_{11} \rightarrow 3_{12}$	18 576.78	18 577.10
$3_{13} \rightarrow 4_{14}$	20 867.76	20 867.76
$3_{03} \rightarrow 4_{04}$	21 568.33	21 568.07
$3_{22} \rightarrow 4_{23}$	22 911[a]	22 910.94
$3_{31} \rightarrow 4_{32}$	23 346.37	23 346.37
$3_{30} \rightarrow 4_{31}$	23 469.59	23 469.02
$3_{21} \rightarrow 4_{22}$	24 388.86	24 389.65
$3_{12} \rightarrow 4_{13}$	24 512.22	24 512.22

[a] Measured with wave meter only.

The absorption lines were observed with a Stark modulation spectroscope. The frequency standard used was of the Unterberger-Smith type,[3] and was monitored by comparison to radio station WWV. The interpolation receiver used was calibrated at each reading. The absorption lines were measured at the limit of vanishing Stark field, and corrections were made for relative phase shift of the frequency markers and lines, by sweeping in both directions with equal sweep voltages, and averaging results. It is believed that the experimental rms error is considerably better than the rms discrepancy of 0.48 mc/sec between the calculated and observed values of Table I. It appears, therefore, that centrifugal distortion effects are not entirely negligible.

TABLE II. Rotational constants.

$A = 6621.440$ mc/sec
$B = 3351.994$ mc/sec
$C = 2410.217$ mc/sec
$\kappa = -0.5527298$.
$I_a = 76.3354$ amu $-A^2$
$I_b = 150.7908$ amu $-A^2$
$I_c = 209.7114$ amu $-A^2$
$\Delta = I_a + I_b - I_c = 17.4148$ amu $-A^2$.

[1] Gunnar Erlandsson, J. Chem. Phys. **22**, 563 (1954).
[2] King, Hainer, and Cross, J. Chem. Phys. **11**, 27 (1943).
[3] R. R. Unterberger and W. V. Smith, J. Sci. Instr. **19**, 580 (1948).

Number of X-Ray Diffraction Groups

WERNER NOWACKI
*Department of Mineralogy, University of Berne, Switzerland**
(Received October 6, 1954)

UNDER this title C. D. West[1] published a note of the number of x-ray diffraction groups in which it is pointed out that there exist 122 and not 120 different diffraction groups as indicated by Buerger,[2] Zhdanov and Pospelov,[3] and Nowacki.[4] Now this question of the number of different diffraction groups depends on the definition of a diffraction group. If one merely considers Laue *symmetries* together with an observed set of absent spectra and if one calls "diffraction group" the totality of all space groups which show the same Laue symmetry and the same set of absent spectra, then there exist 120 different diffraction groups. If in addition the absolute lengths of the vectors aa' (see West[1]) are determined, then one is led to 122 diffraction groups (diffraction units would be a better designation, because the word group should be reserved for a group in the mathematical sense). This latter point is equivalent to say (for C_{3v}^1, C_{3v}^2f.e.) that the d-value of the mirror planes $(//c)$ is $a/2$ for $C_{3v}^1 - P3m1 - P_a3m$ (see Nowacki[5]) and $(a/2)\sqrt{3}$ for $C_{3v}^2 - P31m - P_c3m$. But the determination of absolute lengths is something new, which leads further than a Laue symmetry.

The writer was glad to discuss this problem with Dr. C. D. West at the 3rd International Congress of Crystallography in Paris.

* Contribution No. 80.

[1] C. D. West, J. Chem. Phys. **22**, 150–151 (1954).
[2] M. J. Buerger, *X-Ray Crystallography* (1942).
[3] G. Zhdanov and V. Pospelov, Zhur. Eksptl. i Teort. Fiz. **15**, 703–708 (1945).
[4] W. Nowacki, *Fouriersynthese von Kristallen* (1952).
[5] W. Nowacki, Schweiz. Mineralog. Petrog. Mitt. **32**, 186–212 (1952) (allgmeine Auslöschungseinheiten).

Crystallographic Formalism IB: Reply to Nowacki's Letter "The Number of X-Ray Diffraction Groups"

C. D. WEST
Polaroid Corporation, Cambridge 39, Massachusetts
(Received January 4, 1955)

THIS note is written as one of a series in which a previous letter[1] is designated as IA. I agree that there have been advanced two different concepts concerning the number of kinds of crystal units that can be distinguished by x-ray diffraction, the earlier one leading so far as is now known to 120 units, and the later one of IA leading so far as is now known to 122 units. As a satisfactory name for the earlier concept, I adopt Nowacki's name "extinction unit" ("Auslöschungseinheit"). For the later concept I now replace my previous name "diffraction group" by the name "diffraction unit," in accordance with the suggestion of Nowacki in the preceding letter.

The earlier concept of extinction unit in current usage by other writers is explained in the "1952 International Tables for X-Ray Crystallography," p. 52. To the writings already cited as listing the extinction units according to this earlier concept may be added

another recent book.[2] To describe the later concept of diffraction unit, I now propose the following definition: those collections of symmetry operations which can be distinguished, identified, set and coded, conveniently and without ambiguity, as they are found in real three-dimensional single crystals, by so-called qualitative Friedel diffraction of x-rays alone. A further sharpening of this statement may become desirable or necessary from experience.

The units answering to the two different concepts have been coded in substantially the same international symbolism. The information carried by the symbolism must therefore differ for the two concepts. The parts of the symbolism that require examination are first, the Laue symmetry symbol, and second the lattice symbol. I consider that the information carried by both of these parts of the symbol, as they are found in current usage, is unduly indefinite, and I accordingly put more definite meanings on them as follows.

With the Laue symmetry symbol, I associate a definite set of lattice vectors taken in a definite order, and designated for convenience by letters such as *abc*, *caa'*, *aa'a''*, etc. My writing of the Laue symmetry symbol presupposes a knowledge, arrived at unambiguously through diffraction, of both the absolute length and the Laue symmetry of every one of the lattice vectors, and of setting of the lattice as regards the nontrivial symmetry operations of the Laue group.

With the lattice symbol I associate a lattice which has been completely identified as belonging to one of the fourteen lattice groups, set and described by diffraction. My writing of the lattice symbol thus again presupposes a knowledge of the absolute lengths of all of the lattice vectors of the lattice.

The older concepts of crystal lattices and extinction units in current usage by other writers have given rise to undesirable complications in the literature of crystallography, complications which become avoidable through the adoption of the newer and more definite concepts proposed here. Some evidence for this veiw is found in IA, and more comes out of a closer examination of such a pair of space groups as C_{3v}^1 and C_{3v}^2. We agree that these two belong to a single *extinction* unit. Nowacki[3] has implied that to separate this pair in real crystals one can resort to a more sophisticated concept based on diffraction, i.e., an implication diagram. But before there had been advanced any clear ideas of extinction units, diffraction units, or implication diagrams it had been established[4] that such a pair of space groups as D_3^1 and D_3^2 (which in this respect are similar to C_{3v}^1 and C_{3v}^2) could be separated by elementary methods, using only qualitative Friedel diffraction of x-rays. That the two space groups in question do come out in different *diffraction* units is simply a convenient way of restating the conclusion of Barnes and Wendling.*

[1] C. D. West, J. Chem. Phys. **22**, 150 (1954).
[2] A. I. Kitaigorodsky, *Rentgenostrukturny Analiz* (Moscow/Lenigrad, 1950).
[3] W. Nowacki, *Fouriersynthese von Kristallen*, (Basel, 1952) p. 177.
[4] E.g., by Barnes and Wendling, Z. Krist. **99**, 152 (1938) and other papers.
* *Note added in proof, May 2, 1955.*—Since writing the above reply I learn that M. A. Porai-Koshits already in 1951 published definitions and descriptions of two different kinds of "diffraction groups," which correspond respectively to the foregoing 120 "extinction units" and 122 "diffraction units." This 1951 work therefore anticipates both my 1954 Letter as well as the first question raised in W. Nowacki's comment above. Apparently it does not touch on Nowacki's second question, i.e., the propriety of associating the word "group" with the concepts in question. [G. B. Boky i M. A. Porai-Koshits, Prakt. Kurs Rentgenostrukturnovo Analiza, Moskva, (1951), str. 281–300.]

Sensitized Luminescence of Zinc Sulfide Phosphors Activated with Copper and Manganese

SHIGEO SHIONOYA
Faculty of Engineering, Yokohama National University Yokohama, Japan
(Received April 11, 1955)

THE sensitized luminescence has been one of the most interesting problems in the field of crystalline phosphors in recent years. However, this phenomenon has been investigated almost

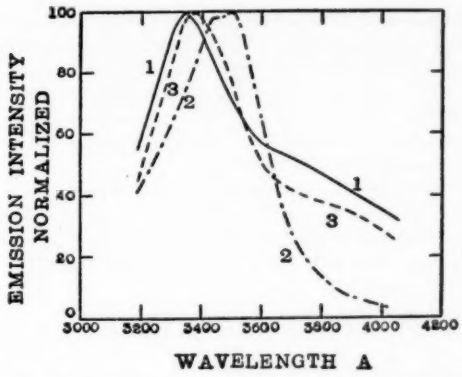

FIG. 1. Excitation spectra for (1) Cu emission of ZnS:Cu, (2) Mn emission of Zn:Mn, and (3) Mn emission of ZnS:(Cu+Mn).

only for the nonphotoconducting phosphors and not for the photoconducting ones such as ZnS phosphors. In the photoconducting phosphors, the sensitization due to the following two mechanisms may possibly take place. The first is the resonance transfer of excitation energy from sensitizer to activator as in the nonphotoconducting phosphors,[1] and the second is the transfer of photoelectrons through the conduction band simultaneously accompanied with the migration of holes through the filled band.[2] In order to examine whether Mn incorporated in ZnS phosphor is sensitized by an impurity incorporated as sensitizer, ZnS:(Cu+Mn) phosphors were prepared and their emission spectra, excitation spectra, and photoconductivities measured.

A series of samples was prepared, in which Cu concentration was fixed to be 3×10^{-6}g/gZnS and Mn concentration was varied from zero to 3×10^{-3}g/gZnS. These were fired at 1200°C for 1 hr in the air with the flux of NaCl(0.02g/gZnS).

The emission spectra were measured under 3650 A excitation with a glass monochromator of constant deviation type and a photomultiplier, photocurrent being amplified by a dc amplifier. The samples containing less than 2×10^{-4} Mn show the Mn emissions scarcely observable, those containing $4\sim8\times10^{-4}$ Mn show distinctly both the Cu and Mn emissions, and those containing more than 1.5×10^{-2} Mn show the predominant Mn emissions, while the Cu emissions almost disappear. The emission peaks of Cu and Mn are located at about 5200 A and 5800 A, respectively.

The excitation spectra were measured with a quartz monochromator of Littrow type using a tungsten incandescent lamp as the excitation source. The samples were set behind the exit slit, and their emissions were detected with a photomultiplier and a dc amplifier, Cu and Mn emissions being isolated from each other with filters, namely, Matsuda V−Y1+V−B2 for Cu and V−02 or V−R3 for Mn.

The results are given in Fig. 1, including those for ZnS:Mn (Cu not incorporated). All samples have an excitation peak near 3400 A, which is regarded as the one due to the absorption of host crystal, since this wavelength corresponds to the fundamental absorption edge of ZnS crystal.[3,4] ZnS:Cu has, in addition, the excitation band regarded as the one due to the absorption of Cu impurity, the peak of which seems to be located at about 3800 A. These results are nearly in agreement with those of Bube.[3] While Mn in ZnS:Mn has only the host excitation band, Mn in ZnS:(Cu+Mn) has, in addition, the excitation band due to Cu. This result shows that Mn is really sensitized by Cu. According to Bube[3] ZnS:Mn has, in addition to the host excitation band, four excitation peaks due to the forbidden transition within Mn^{+2} ion itself in the wavelength region 3900∼5100 A. However, they were not found in the present phosphors, which seems to be probably due to the effect of impurity, especially oxygen.

Photoconductivity cells were made by packing the phosphor powders between a conductive glass and an aluminium plate. Photocurrents induced by applying dc electric field (280 v/cm) under 3650 A excitation were detected with a sensitive amplifier

and a galvanometer. It was found that the photoconductivities of the samples with relatively large Mn concentrations and distinctly observable Mn emissions are by far smaller than those of the samples with relatively small Mn concentrations and scarcely observable Mn emissions.

Further work on this problem is in progress, and the sensitization mechanism will be discussed later.

The author wishes to express his thanks to Professor S. Makishima, Mr. Y. Kotera, and Assistant Professor K. Oshima for their encouragements and discussions, and to Mr. S. Kamiya, Mr. W. Ichise, and Mr. K. Amano for their assistance in the experimental works.

[1] D. L. Dexter, J. Chem. Phys. **21**, 836 (1953).
[2] N. F. Mott and R. W. Gurney, *Electronic Processes in Ionic Crystals* (1940), p. 207.
[3] R. H. Bube, Phys. Rev. **90**, 70 (1953).
[4] W. W. Piper, Phys. Rev. **92**, 23 (1953).

Crystal Growth and Coercive Forces of Variously Prepared Ni Powders

WELBY G. COURTNEY
Chemical Construction Corporation, c/o Stamford Research Laboratories, American Cyanamid Company, Stamford, Connecticut
(Received March 16, 1955)

AN increase in the coercive force H_c of a crystallized material by growth in a magnetic field (m.f.) can most readily be attributed to an influence in the incorporation of new material into the substrate crystal lattice.[1] Since this deposition reaction is probably the most obscure of the sequence of reactions comprising crystal growth, any correlation between H_c and growth in a m.f. may be useful in clarifying the incorporation process.

Experimentally, a freshly prepared, cold, aqueous solution variously containing 0.05−1M $NiSO_4$, 1−6M NH_3, 0.5−1M $(NH_4)_2SO_4$, and a reducing agent, 0.05−1M NaH_2PO_2(**I**) or 100–500 psi H_2pp, was sealed into a glass tube or SS bomb and placed in an oil bath controlled at 185–225±5°C. Ni metal powder formed within an hour in this temperature range. Reductions were performed in magnetic fields of 0–1200 oersteds using a permanent magnet.

Reduction by **I** outside a m.f. (neglecting the earth's field) gave irregular stringed agglomerates of metal particles, 1–3 microns wide by 10–50 microns long; while reduction in a 1200 oersted field gave smooth, straight, 1–3 by 50–500 micron agglomerates (Fig. 1). All agglomerates were chains of 1–3 micron particles which were each composed of several primary particles. Variation in reagent concentrations and temperature did not noticeably affect agglomeration. X-ray examination of **I**-prepared powders showed no appreciable particle orientation. Products contained 2 percent P. Reduction by H_2 both in and outside a field gave 10–50 micron irregular flocs of 1-micron primary metal particles.

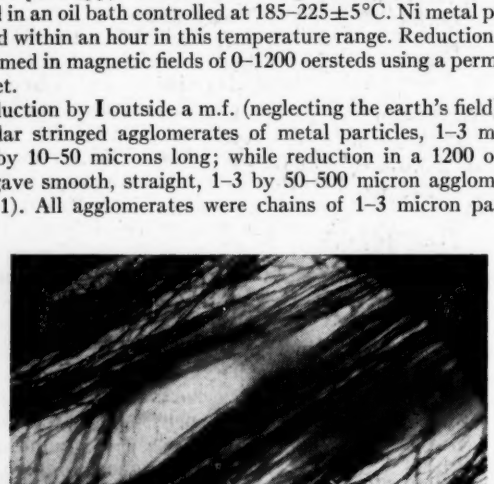

FIG. 1. Ni powder prepared by reduction of aqueous $NiSO_4-NH_3-(NH_4)_2SO_4$ solution with NaH_2PO_2 in a 1200-oersted magnetic field. Magnification = 75×.

Coercive forces (in oersteds) at ambient temperature were: 17±5 for H_2-prepared powder produced in and outside a field; 75±5 for **I**-prepared powder produced outside a field (see Weil and Marfoure[2]); and 110±10 for **I**-prepared powder produced in a 1200-oersted field, thus far below the H_c of 3150 predicted for Ni powder with shape anisotropy.[3] Any stringed agglomerates were previously magnetically aligned parallel to the measuring field. The transition in the direction of easy magnetization in Ni from ⟨111⟩ to ⟨100⟩ directions at about 200°C[4] may obscure these results, but reduction with **I** at 185° and 225° gave powders with similar H_c values.

The increase in H_c when reduction with **I** occurred in a m.f. indicates that the field affects crystal growth, but conclusions as to modification of growth rate or crystal habit were not permitted. The apparent lack of effect of a m.f. on H_c in growth by H_2 reduction compared to the marked effect in **I** reduction suggests that the deposition mechanisms in the two cases may be qualitatively different.

I-prepared powders were magnetically saturated by only a 600-oersted field (compared to 2100 oersteds for a multidomain particle), but deductions based upon saturation[5] are probably not applicable to the impure powders prepared here. Experimental error does not warrant a conclusion about saturation for the H_2-prepared powder.

The marked variation in particle agglomeration in **I**- and H_2-prepared powders cannot be discussed since the factors affecting colloid stability,[6] e.g., double layer repulsion potentials and particle concentrations, are completely unknown for these systems at the reaction temperatures. Accentuation of linear agglomeration in **I**-prepared powder by a m.f. of only 5 oersteds suggests that magnetic forces directed particle agglomeration.[7] Linear agglomeration because of a repulsion potential minimum along a "biparticle" axis[8] seems less likely.

The writer is pleased to acknowledge the advice and assistance of Dr. H. M. Hulburt, Mr. J. J. Shaw, and numerous people of the Stamford Research Laboratories, American Cyanamid Company.

[1] A. Perrier and C. Mermod, Helv. Phys. Acta **11**, 362 (1954).
[2] L. Weil and S. Marfoure, J. phys. radium **8**, 358 (1947).
[3] C. Kittel [Revs. Modern Phys. **21**, 541 (1949)] reviews the magnetics of fine particles.
[4] D. Kirkham, Phys. Rev. **52**, 1163 (1937).
[5] Kittel, Galt, and Campbell, Phys. Rev. **77**, 725 (1950).
[6] H. R. Kruyt, *Colloid Science* (Elsevier Publishing Company, Inc., New York, 1952), Vol. I.
[7] D. Biescher and A. Winkel, Naturwiss. **25**, 420 (1937).
[8] A. G. L. Rees, J. Phys. & Colloid Chem. **55**, 1340 (1951).

Calculation of Electrostatic Binding Energies in Systems of Isotropic Ions

CHESTER T. O'KONSKI
Department of Chemistry and Chemical Engineering, University of California, Berkeley 4, California
(Received February 25, 1955)

IT has been shown[1] that ionic polarizabilities lead to substantial contributions to binding energies in cases where the structure is such that large electric fields exist at the ions. The usual computation for the electrostatic part of the binding energy involves a determination of the induced moments from polarizabilities and the computed electric fields at each ion, followed by the summation of pair potentials between ions and induced dipoles, and the work of formation of the dipoles.[1] Quadrupole and higher terms, which may be important in some cases, have been ignored because of lack of information regarding the induced multiple moments.

For isotropic ions, the general expression to induced dipole

terms may be written

$$V_e=\tfrac{1}{2}\Sigma'\frac{Z_iZ_je^2}{r_{ij}}-\Sigma'\frac{Z_ie}{r_{ij}^3}(\underline{\mu}_j\cdot\mathbf{r}_{ij})$$
$$-\tfrac{1}{2}\Sigma'\left\{\frac{3}{r_{ij}^5}(\underline{\mu}_i\cdot\mathbf{r}_{ij})(\underline{\mu}_j\cdot\mathbf{r}_{ij})-\frac{(\underline{\mu}_i\cdot\underline{\mu}_j)}{r_{ij}^3}\right\}+\Sigma\frac{\mu_i^2}{2\alpha_i},\quad(1)$$

where the sums for the first three terms are over all i and j except $i=j$, Z_ie is the charge on the ion i, $\underline{\mu}_i$ is the induced moment, and $\mathbf{r}_{ij}$ is the vector pointing from the ion i to the ion j. The four terms correspond respectively to charge-charge, charge-dipole, and dipole-dipole potentials, and the work of formation of the induced dipoles.

For cases involving more than two ions, direct computations from (1) became tedious, especially because of the last two sums, which involve second-order terms in μ. To simplify this equation, we may insert α_iE_i for one of the μ_i in the last term. In vector notation, recalling that the field and dipole directions coincide, one obtains

$$\frac{\mu_i^2}{2\alpha_i}=\frac{(\underline{\mu}_i\cdot\mathbf{E}_i)}{2}=\tfrac{1}{2}\sum_j\left\{\frac{Z_je(\underline{\mu}_i\cdot\mathbf{r}_{ij})}{r_{ij}^3}+\frac{3(\underline{\mu}_{ij}\cdot\mathbf{r}_{ij})(\underline{\mu}_j\cdot\mathbf{r}_{ij})}{r_{ij}^5}-\frac{(\underline{\mu}_i\cdot\underline{\mu}_j)}{r_{ij}^3}\right\}.\quad(2)$$

Substituting this into (1) and rearranging, we find

$$V_e=\tfrac{1}{2}\Sigma'\frac{Z_iZ_je^2}{r_{ij}}-\tfrac{1}{2}\Sigma'\frac{Z_ie(\underline{\mu}_j\cdot\mathbf{r}_{ij})}{r_{ij}^3}.\quad(3)$$

This may be written

$$V_e=\tfrac{1}{2}\Sigma_iZ_ie\varphi_i,\quad(4)$$

where

$$\varphi_i=\sum_j\left\{\frac{Z_je}{r_{ij}}-\frac{(\underline{\mu}_j\cdot\mathbf{r}_{ij})}{r_{ij}^3}\right\}.\quad(5)$$

Numerical computations are simpler with Eq. (3) because the second sum is just one-half the second sum of (1), and there are no terms above first power in μ.

It is seen that φ_i is the potential at the ion i produced by all the other ions and induced dipoles in the final configuration of the system. Thus, when the effects of the induced dipoles are included in the expression for φ_i, Eq. (4), which is rigorously correct for a system of nonpolarizable particles, also yields the correct result for isotropic polarizable particles. It is anticipated that this result is general, i.e., that multipolar contributions need be included only in φ_i to make binding energy computations of a higher order of accuracy. This would require knowledge of multipolar polarizabilities and solution of the electric field problem to appropriate derivatives of E. Although the multipolar coefficients are not yet avaialble, it appears that in certain instances experimental nuclear electric quadripole resonance data might be useful in obtaining the quadrupole terms.

[1] See, e.g., M. Born and W. Heisenberg, Z. Physik **23**, 388 (1924); E. S. Rittner, J. Chem. Phys. **19**, 1030 (1951); C. J. F. Böttcher, *Theory of Electric Polarization* (Elsevier Publishing Company, Inc., Amsterdam, 1952).

Structure and Calculation of the Binding Energy of Gaseous Alkali Halide Dimers

CHESTER T. O'KONSKI AND WILLIAM I. HIGUCHI
Department of Chemistry and Chemical Engineering, University of California, Berkeley 4, California
(Received February 25, 1955).

As the properties of alkali halide monomers can be explained on the basis of an electrostatic model,[1] expressions have been developed for a proposed dimer structure, employing the formulation of an accompanying note[2] for the binding energy, which includes all Coulombic and induced dipole interactions. Because the leading terms are the Coulomb interactions, it is evident that the energetically favored configuration of the ions will be the symmetrical planar arrangement of Fig. 1. Proceeding as usual,[3] the the electric field problem was solved for this structure. The field

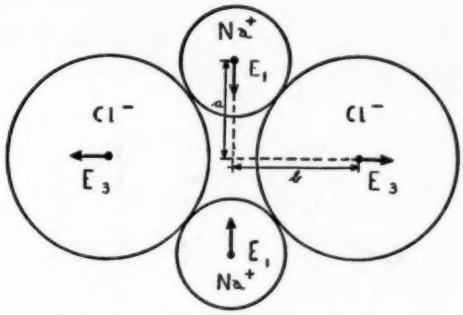

FIG. 1. Proposed structure for the NaCl dimer. Arrows are field vectors. To scale.

equations are

$$E_1(1+\alpha_1/4a^3)=Ze\{2a/(a^2+b^2)^{3/2}-1/4a^2\}$$
$$+6ab\alpha_3E_3/(a^2+b^2)^{5/2},\quad(1)$$
$$E_3(1+\alpha_3/4b^3)=Ze\{2b/(a^2+b^2)^{3/2}-1/4b^2\}$$
$$+6ab\alpha_1E_1/(a^2+b^2)^{5/2}.$$

E_1 and E_3 are the magnitudes of the electric field intensities at the cation and anion, respectively, α_1 and α_3 are the corresponding ionic polarizabilities, $2a$ and $2b$ are the intercationic and interanionic separations, Ze is the ionic charge, and units are cgs. The directions of the electric field and induced dipole vectors are shown in Fig. 1.

The expression for the electrostatic part of the binding energy is

$$V_e=Ze(\varphi_1-\varphi_3),$$
$$\varphi_1-\varphi_3=-Ze\{4/(a^2+b^2)^{\frac{1}{2}}-1/2a-1/2b\}$$
$$+\{1/4a^2-2a/(a^2+b^2)^{\frac{1}{2}}\}\alpha_1E_1$$
$$+\{1/4b^2-2b/(a^2+b^2)^{\frac{1}{2}}\}\alpha_3E_3.\quad(2)$$

As an example, numerical computations have been carried out for $(NaCl)_2$. Employing the polarizability values given recently,[4] it was found that the maximum binding energy at constant internuclear separation, $r=(a^2+b^2)^{\frac{1}{2}}=2.59$ A, was obtained with $b/a=1.35\pm0.05$ A, which corresponds to an apex angle of $105\pm2°$ at the sodium ion. The effects upon the angle of the London attractive forces,[5] and the short range quantum-mechanical repulsions,[6] between the anion pairs and between the cation pairs were found to be negligible. Therefore it was necessary to include only the Coulombic and induced dipole interactions in the determination of the angle. The energy of formation of the dimer from the ions was calculated as a function of r. Neglecting the zero-point energy, estimated to be a few hundredths of an electron volt, the energy of formation of the dimer from ions at 0°K may be written

$$V=V_e+V_r+V_L,\quad(3)$$

where V_e is the electrostatic binding energy, V_r is the repulsion enregy, and V_L is the London attractive energy. Following Rittner,[1] the repulsive potential function $A\exp(-r/\rho)$ was used, so $V_r=4A\exp(-r/\rho)$. The recent value,[7] $r_e=2.3606$ A, was employed in determining $A=2530$ ev, and $\rho=0.311$ A. V_L, computed with the new polarizability values,[4] and the London constants from Rittner's work, turned out to be very small. The minimum energy $V=-13.12$ ev, was obtained at $r=2.59\pm0.01$ A. Employing the recent parameters[4,7] and Rittner's equations, a binding energy of 5.63 ev was obtained for the NaCl monomer. This is equal to the experimental value obtained in the usual manner from the dissociation energy of the molecule into neutral atoms, the first ionization potential, and the electron affinity.[8] Then at 0°K for the reaction

$$2NaCl=(NaCl)_2,$$
$$\Delta E=-1.86\text{ ev}.$$

Experimental results for the structure and binding energies of the dimers are not yet published, but some indications have

been obtained in molecular beam experiments.[9] Comparison of experiment with theory should lead to interesting conclusions regarding the applicability of the idealized electrostatic model in the induced dipole approximation.

[1] E. S. Rittner, J. Chem. Phys. **19**, 1030 (1951).
[2] C. T. O'Konski, J. Chem. Phys. **23**, 1174 (1955).
[3] See e. g., C. J. F. Böttcher, *Theory of Electric Polarization* (Elsevier Publishing Company, Inc., New York, 1952).
[4] Tessman, Kahn, and Shockley, Phys. Rev. **92**, 890 (1953).
[5] These were estimated by the method of F. London, Z. Physik **63**, 245 (1930).
[6] The exponential potential was employed, with parameters given by M. L. Huggins and J. E. Mayer, J. Chem. Phys. **1**, 643 (1933).
[7] Honig, Mandel, Stitch, and Townes, Phys. Rev. **96**, 629 (1954).
[8] A. G. Gaydon, *Dissociation Energies* (Chapman and Hall, Ltd., London, England, 1953), pp. 93 and 228.
[9] R. C. Miller, Quarterly Reports, Columbia Radiation Laboratory, December 31, 1952; March 31, June 30, August 31, October 30, 1953; January 30, April 30, July 30, 1954.

Molecular Structure of Diborane Tetrachloride, B_2Cl_4

MASAO ATOJI, WILLIAM N. LIPSCOMB, AND P. J. WHEATLEY*
School of Chemistry, University of Minnesota, Minneapolis 14, Minnesota
(Received March 23, 1955)

AN extension of Walsh's theory[1] of the structure of simple molecules would predict a planar B_2Cl_4 molecule of D_{2h} symmetry, since the molecule would utilize the same molecular orbitals as N_2O_4 or the oxalate ion. On the other hand, the Raman and infrared spectra,[2] and the electron diffraction data[3] have been interpreted as favoring a molecule of D_{2d} symmetry. In an attempt to resolve this discrepancy we have completed an x-ray diffraction study of a single crystal of B_2Cl_4 at $-165°$C.

There are four B_2Cl_4 molecules in an orthorhombic unit cell with

$$a = 11.900 \text{ A},$$
$$b = 6.281 \text{ A}, \text{ and}$$
$$c = 7.690 \text{ A}.$$

The space group is $D_{2h}^{15}-Pbca$, which requires the molecule to have a center of symmetry. The atomic parameters refined by two-dimensional (F_o-F_c) syntheses are:

	x/a	y/b	z/c
Cl_1	0.0900	−0.2363	0.1810
Cl_2	−0.1475	−0.2268	0.0507
B	-0.014_5	-0.120_5	0.059_0

The molecular symmetry is thus found to be $D_{2h}-mmm$, within the experimental errors. The interatomic distances and bond angles are shown in Fig. 1.

The B−Cl bond distance, 1.72 A±0.02 A, is essentially that of a single bond. The B−B bond distance, 1.80 A±0.04 A, considerably longer than the single B−B bond distance of 1.60 A,[4] is similar to the lengthened N−N bond in N_2O_4.[5]

This weak bond is consistent with the course of the reaction between B_2Cl_4 and ethylene.[6] Moreover, it would suggest considerable freedom of rotation of the BCl_2 groups in the gaseous and liquid phases. Although we can only state with confidence that B_2Cl_4 is planar in the solid state, we feel that a reinvestigation of the Raman, infrared, and elctron diffraction data, in terms of a planar molecule with a large degree of torsional motion, is desirable.

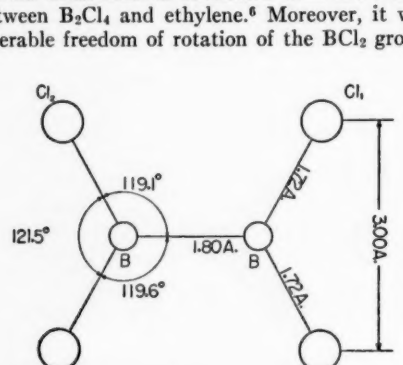

FIG. 1.

We would like to thank Professor H. I. Schlesinger and Dr. G. Urry for providing us with the sample of B_2Cl_4 and for advice on handling the substance.

It is a pleasure to acknowledge support of this research by the U. S. Office of Ordnance Research.

* On leave of absence from the University of Leeds.
[1] A. D. Walsh, J. Chem. Soc. **1953**, 2260 (1953).
[2] Linevsky, Shull, Mann, and Wartik, J. Am. Chem. Soc. **75**, 3287 (1953).
[3] K. Hedberg (unpublished data).
[4] K. Hedberg, J. Am. Chem. Soc. **74**, 3486 (1952).
[5] J. S. Broadley and J. M. Robertson, Nature **164**, 915 (1949).
[6] Urry, Kerrigan, Parsons, and Schlesinger, J. Am. Chem. Soc. **76**, 5299 (1954).

Simplified SCF Calculation for Fulvene

HIDEO KON
Department of Chemistry, Tohoku University, Sendai, Japan
(Received March 18, 1955)

AMONG the recent developments in the study of MO theory, Pariser and Parr's semiempirical ASMO method[1] is found useful for practical purposes. The electronic structure of fulvene is treated here, as in the previous papers,[2] by this method in conjunction with Roothaan's SCF scheme.[3] The SCF MO's obtained in this way may be helpful in giving some indication of availability of the method, because fulvene is known to have a dipole moment in its ground state to be compared with theoretical value.

The calculation is made along lines similar to those of the preceding paper, so that details are not given here, except that (1) the Coulomb penetration integrals $(p:qq)$ neglected in the previous calculation are taken into account, numerical values of which are computed by the formula of Parr and Crawford,[4] (2) the bond length values which are obtained by Wheland and Mann[5] in their iterative LCAO MO method, are assumed as a reasonable first approximation, and (3) the configuration interaction is allowed for only to such an extent as in Pariser and Parr's article, i.e., between the two low excited configurations.

The calculated results for the ultraviolet spectrum and dipole moment (μ) due to π electrons are compared in Table I with those of previous authors[6,7] and with experimental results. The agreement with experimental values is satisfactory. It is to be noted that the correct estimation of $(p:qq)$ is essential for obtaining the right order of magnitude of dipole moment and neglect of $(p:qq)$ causes too small a μ value. Introduction of the configuration interaction reduces the calculated oscillator strength to about $\frac{1}{3}$ of the value before the interaction, whereas the electronic excitation energy is not affected so much (4.0 ev before interaction). Remembering that in the previous work, very close coincidence with observation was obtained for the excitation energies of various molecules without taking account of configuration interaction, the corresponding value, 4.0 ev, of the present calculation seems unsatisfactory. This is a situation in contrast also to the case of Pullman *et al.*,[8] where much improvement is brought about on the calculated $N \rightarrow V$, energy of trans-butadiene by revising the monocentric Coulomb repulsion integral, with configuration interaction being ignored. Thus it appears that attention must be paid

TABLE I. Calculated ultraviolet spectrum and dipole moment.

	$^1A_1 \rightarrow {}^1B_2$ ev	f[a] cgs	μD	Method
Berthier	4.95	0.013	1.13	SCF
Julg-Pullman	4.52	0.014	3.25	ASMO CI
This paper	3.71	0.012	1.64	...
Experimental[b]	3.4	0.012	1.2	...

[a] Calculated with $\nu_{exp.}$
[b] See reference 7.

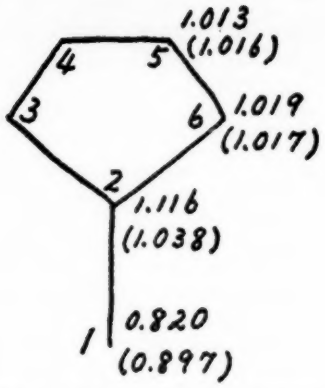

FIG. 1. π electron distribution of fulvene.

in this case to what has been left out (for example, the configuration interaction in a more rigorous way), besides the mere revision of integral values.

The distribution of π electrons obtained from the SCF MO is shown in Fig. 1, the figures in brackets being the corresponding values obtained by Berthier[6] as the result of rigorous SCF calculation. As can be seen there, these two sets agree very well with each other with slight difference at 1 and 2 positions. Thus it may be said that the present method of calculation, i.e., Pariser-Parr approximation plus the SCF method of Roothaan, yields fairly good approximate MO's of the ground state. Further details will be published elsewhere.

The writer is grateful to Professor H. Tominaga for his kind guidance during the course of this work.

[1] P. Pariser and R. G. Parr, J. Chem. Phys. **21**, 466 767 (1953).
[2] J. A. Pople, Trans. Faraday Soc. **49**, 1375 (1953); H. Kon, Bull. Chem. Soc. Japan **27**, 566 (1954), and the succeeding to be published.
[3] C. C. J. Roothaan, Revs. Modern Phys. **23**, 69 (1951).
[4] R. G. Parr and B. L. Crawford, J. Chem. Phys. **16**, 1049 (1948).
[5] G. W. Wheland and D. E. Mann, J. Chem. Phys. **17**, 264 (1948).
[6] G. Berthier, J. chim. phys. **50**, 344 (1953).
[7] A. Julg and A. Pullman, J. chim. phys. **50**, 460 (1953).
[8] A. Pullman (private communication).

Nuclear Quadrupole Resonances of Sb^{121} and Sb^{123}

R. G. BARNES,* *Physics Department, University of Delaware, Newark, Delaware*
AND
P. J. BRAY,† *Physics Department, Rensselaer Polytechnic Institute, Troy, New York*

(Received April 11, 1955)

PURE quadrupole resonances of Sb^{121} and Sb^{123} were first detected by Dehmelt and Kruger[1] in $SbCl_3$ at 83°K. Two resonances arise from the Sb^{121} isotope with nuclear spin $I=5/2$ and three resonances from Sb^{123} with $I=7/2$. The present letter reports $Sb^{121,123}$ resonances in antimony trioxide, triphenylstibine, isopropyl antimonite, and room temperature measurements in the trichloride. The I^{127} measurements in bismuth and antimony triiodide are included.[2]

Measured frequencies and signal-to-noise ratios are listed in Table I. Table II contains, as functions of temperature, the derived constants and asymmetry parameters evaluated with the aid of recent theory.[3]

The asymmetry parameter at the antimony nuclei in Sb_2O_3 is zero within experimental accuracy at both liquid-nitrogen and room temperature. This compound has a cubic low-temperature form below 570°C made up of Sb_4O_6 molecules.[4,5] The similar As_2O_3 crystalline solid[6] is cubic above −13°C and monoclinic below.[7] Both forms contain As_4O_6 molecules. No discontinuity has been observed in frequency or appearance of the As^{75} quadrupole resonance as it is brought slowly through the reported transition temperature and some 40°C higher. Work at temperatures progressively higher than room temperature is in progress on both compounds.

TABLE I.

Compound	Isotope	Frequency in Mcps at 77°K	S/N	Frequency in Mcps at other temp.	S/N
Sb_2O_3	Sb^{121}	166.45 ±0.04	20	165.33 ±0.05	7–8
		83.21 ±0.04	8	82.66 ±0.03	5
	Sb^{123}	151.89 ±0.05	3–4	150.54 ±0.04	3
		101.01 ±0.05	5–7	100.41 ±0.04	3–5
		50.511 ±0.002	10–12	50.195 ±0.002 (T=23°C)	4
$Sb(C_6H_5)_3$	Sb^{121}	156.200 ±0.010	4–5	153.020 ±0.040	2
		152.471 ±0.010	4–5	150.040 ±0.045	2
		78.274 ±0.010	3	76.659 ±0.034	4–5
		76.912 ±0.008	3⁻	75.550 ±0.038	4–5
	Sb^{123}	142.174 ±0.010	2		
		138.859 ±0.010	2		
		94.741 ±0.010	3	92.915 ±0.045	2
		92.267 ±0.010	3	90.950 ±0.050	2
		47.841 ±0.018	3⁻	46.65 ±0.06	weak
		47.545 ±0.030	1½	(T=21°C)	
$Sb(C_3H_7O)_3$	Sb^{121}	167.570 ±0.030	7	164.730 ±0.050	2–3
		85.804 ±0.030	4		
	Sb^{123}	101.111 ±0.035	3–4	(T=195°K)	
$SbCl_3$	Sb^{121}	114.300 ±0.011[a]		112.490 ±0.020	20
		59.709 ±0.006[a]		58.170 ±0.006	15
	Sb^{123}	104.460 ±0.010[a]		102.520 ±0.020	2
		68.648 ±0.007[a]		67.791 ±0.006	3
		39.094 ±0.004[a]		37.410 ±0.004	8
SbI_3	I^{127}	174.509[b]	20–40	172.920 (T=147°K)	3
				172.075 (T=195°K)	1½
BiI_3	I^{127}	201.380 ±0.070	10–12	197.160 ±0.070	3–4
		111.320 ±0.070	3	106.805 ±0.065 (T=20°–22°C)	2

[a] At 83°K; see reference 1.
[b] See reference 12.

Although the resonance frequencies of antimony trioxide and isopropyl antimonite are unusually similar, the existence of structure differences or bond strains in $Sb(C_3H_7O)_3$ is evident from the large asymmetry parameter in this compound. Furthermore, $Sb(C_3H_7O)_3$ hydrolyzes to Sb_2O_3 on exposure to moisture.

While the Bi^{209} resonances in bismuth triphenyl are singlets,[8] the corresponding As^{75} and $Sb^{121,123}$ resonances are doublets, indicating two crystallographically nonequivalent positions for antimony and arsenic atoms in the respective unit cells. At one of these positions in $Sb(C_6H_5)_3$ the asymmetry parameter is essentially temperature-independent, whereas at the other, ϵ is several times larger and noticeably temperature dependent. In the latter case, the value $\epsilon=0.08$ is comparable to the 0.09 value observed in the bismuth compound.

Application of the bond switching analysis employed[9] for AsI_3 to the asymmetry data for BiI_3 yields a Bi−I−Bi angle of 85.1° (at 21°C), in poor agreement with the value 90.7° calculated from the crystallographic data.[9,10] In the case of SbI_3 intensive search has failed to locate the high-frequency iodine line. This is particularly surprising in view of the large signal obtained for the resonance reported by Schawlow.[11] Only one resonance would be present if the asymmetry parameter at the I^{127} nucleus were unity (the value is 0.18 in AsI_3 and 0.29 in BiI_3). With the assumption that $\epsilon=1$, the bond-switching analysis leads to an Sb−I−Sb angle of 70.5°, which would seem very unlikely.[9,10]

No Sb or Bi resonances have been detected so far in SbI_3 and BiI_3. These compounds have the same layer structure as AsI_3 in which the As^{75} resonance occurs at approximately 116 Mcps.[12] However, the octahedra of iodine atoms surrounding the metal atoms in these compounds may be nearly perfect.[13] The field gradient at the Sb or Bi position would vanish if the octahedron were exactly perfect.

No resonances were found in several samples of BiI_3 provided in crystalline powder form by several suppliers. The listed resonances were observed in samples consisting of pea-sized chunks, and vanish

TABLE II. [a]

Compound	Isotope	eqQ/h Mcps 77°K	eqQ/h Mcps room T	ϵ 77°K	ϵ room T	$\alpha(10^{-4}°C^{-1})$ eqQ/h	$\alpha(10^{-4}°C^{-1})$ ϵ
Sb_2O_3	Sb^{121}	554.83±0.13	551.10±0.2	0.000	0.000	0.31	0.0
	Sb^{123}	707.11±0.3	702.70±0.3	0.000	0.000	0.29	0.0
$Sb(C_6H_5)_3$	Sb^{121}	520.84±0.12	510.37±0.25	0.026	0.026	0.93	0.0
		509.00±0.12	500.68±0.25	0.080	0.070	0.75	5.8
	Sb^{123}	664.18±0.40	650.73±0.45	0.018	0.022	0.93	0.0
		648.56±0.40		0.083			
$Sb(C_3H_7O)_3$	Sb^{121}	560.66±0.25		0.138			
$SbCl_3$	Sb^{121}	383.69±0.17	376.98±0.19	0.189	0.165	0.82	6.0
	Sb^{123}	489.34±0.30	482.05±0.30	0.187	0.163	0.69	5.9
BiI_3	I^{127}	682.18±0.47	665.86±0.46	0.290	0.258	1.1	5.1

[a] $\alpha(eqQ/h)=[1/(eqQ/h)]\Delta(eqQ/h)/\Delta T$ and $\alpha(\epsilon)=[1/\epsilon]\Delta\epsilon/\Delta T$.

if the chunks are ground into crystalline powder. Apparently the resonances are smeared out by dislocations generated in cold working.[14,15] The observed resonances are unusually broad, presumably because of the same defects. Further work in annealing studies and growth of defect-free crystals is in progress on this compound.

All resonances were detected with frequency modulated super-regenerative oscillators and were displayed on cathode-ray oscilloscopes.

* Research supported by the Office of Ordnance Research and the Research Corporation.
† Research supported by a grant from the National Science Foundation and a grant-in-aid from the Rensselaer Polytechnic Institute Research Grants Committee.
[1] H. G. Dehmelt and H. Kruger, Z. Physik **130**, 385 (1951).
[2] A preliminary report of this work by R. G. Barnes and P. J. Bray appears in Bull. Am. Phys. Soc. **30**, No. 1, 43 (1955).
[3] M. H. Cohen, Phys. Rev. **96**, 1278 (1954).
[4] M. J. Buerger and S. B. Hendricks, J. Chem. Phys. **15**, 600 (1937).
[5] The orthorhombic form existing above 570°C can, however, exist as a metastable phase even at room temperature. This phase consists of infinite double molecular chains.
[6] H. Kruger and U. Meyer-Berkhout, Z. Physik **132**, 221 (1952).
[7] A. F. Wells, *Structural Inorganic Chemistry* (Oxford University Press, London, 1950).
[8] Robinson, Dehmelt, and Gordy, Phys. Rev. **89**, 1305 (1953).
[9] Kojima, Tsukada, Ogawa, Shimauchi, and Abe, J. Phys. Soc. Japan **9**, 805 (1954).
[10] See reference 7 and references therein.
[11] A. L. Schawlow, J. Chem. Phys. **22**, 1211 (1954).
[12] R. G. Barnes and P. J. Bray, J. Chem. Phys. **23**, 407 (1955).
[13] R. W. G. Wyckoff, *Crystal Structures* (Interscience Publishers Inc., New York, 1948).
[14] N. Bloembergen and T. J. Rowland, Acta Met. **1**, 731 (1953).
[15] G. D. Watkins and R. V. Pound, Phys. Rev. **89**, 658 (1953).

Erratum: Nuclear Quadrupole Resonances of As^{75}

[J. Chem. Phys. **23**, 407 (1955)]

R. G. BARNES, *Physics Department, University of Delaware, Newark, Delaware*
AND
P. J. BRAY, *Physics Department, Rensselaer Polytechnic Institute, Troy, New York*

THE As^{75} in $AsCl_3$ resonance reported as 78.950±0.030 Mcps at 77°K in the above-named paper has now been obtained at 147°K and 195°K. Measured values are 78.02±0.03 and 77.171±0.015 Mcps, respectively. The temperature coefficient $\alpha=(1/\nu)(\Delta\nu/\Delta T)=1.83\times10^{-4}°C^{-1}$.

The liquid nitrogen temperature measurement of the As^{75} resonance in $AsBr_3$ was incorrectly reported in the above-named paper. Redetermination of the value yields 63.540±0.008 Mcps which is in agreement with other recently reported values.[1] The temperature coefficient $\alpha=1.66\times10^{-4}°C^{-1}$ is very similar to that obtained in $AsCl_3$. Both values differ markedly from the 0.25 $\times10^{-4}°C^{-1}$ found in the layer structure compound AsI_3. Crystalline $AsBr_3$ is known to consist of distinct pyramidal molecules.[2]

[1] Kojima, Tsukada, Ogawa, Shimauchi, and Abe, J. Phys. Soc. Japan, **9**, 805 (1954).
[2] N. V. Sidgwick, *The Chemical Elements and Their Compounds* (Oxford University Press, New York, 1950), Vol. 1.

Reinterpretation of Electron Impact Experiments in CO, N_2, NO, and O_2

HOMER D. HAGSTRUM
Bell Telephone Laboratories, Murray Hill, New Jersey
(Received April 11, 1955)

EARLIER[1] it appeared possible to interpret all the electron impact data in CO, N_2, NO, and O_2 in terms of $D(CO)=9.6$ ev, $D(N_2)=7.4$ ev, $D(NO)=5.3$ ev, $D(O_2)=5.1$ ev, and $EA(O)=2.2$ ev, and the assumption that the only possible excited state of O^- lies very near the positive energy continuum.[2] Recently, however, several experiments indicate strongly that $D(N_2)=9.76$ ev, $L(C)=170$ kcal/mole, and thus $D(CO)=11.1$ ev.

From the first it has been possible to interpret the appearance potential for N^+ ions of zero initial energy from $N_2(A_0=24.3$ ev) in terms either of $D(N_2)=9.76$ ev or 7.38 ev.[1,3,4] (See Table I.) But if we use the higher value of $D(CO)$ and the value $D(NO)=6.49$ ev required if $D(N_2)=9.76$ ev, and continue to assume that $EA(O)=2.2$ ev, we must conclude that many large errors exist in the electron impact data for CO and NO.[5] Very recently, however, Branscomb and Smith,[6] in a convincing photodetachment experiment, have obtained a new value for $EA(O)=1.45\pm0.15$ ev. We investigate here to what extent this new value for $EA(O)$ permits reinterpretation of electron impact data in CO, NO, and O_2 using the so-called higher values of $D(CO)$ and $D(NO)$.

Using the values $D(CO)=11.1$ ev, $D(N_2)=9.76$ ev, $D(NO)=6.49$ ev, and $EA(O)=1.45$ ev, one calculates the appearance potentials, A_0, for ions of zero initial energy listed in Table I. For CO, N_2, and NO the experimental A_0 values listed are those of the author.[1] In general these agree well with other values.[3,7,8] For O_2 the data for the processes yielding O^+ ions are Thorburn's,[9] which differ considerably from the author's earlier measurements.[1] It appears quite certain that the O^+ and O^- appearance potentials from the earlier work[1] are relatively correct but that an error was made when calibrating the absolute energy scale relative to the appearance of O_2^+. Thus if we calibrate the energy scale as Thorburn did using the first appearance potential of O^- of 4.7±0.1 ev,[10] we obtain the values of A_0 given in parentheses in Table I in essential agreement with Thorburn.

In interpreting the process yielding O^+ ions in CO it is necessary to assume that the other product is the C^- ion observed by Chupka and Inghram[5] and by Lagergren,[11] and that $EA(C)=1.5$ ev.[2] Evidence to date indicates that C^- is much less abundant than O^+ (C^- was not observed in the earlier work[1] although O^+ was of workable intensity), a result which needs further clarification if the only process starting at 23.2 ev is that yielding C^-+O^+. If $D(CO)$

TABLE I. Calculated and experimental dissociation limits.

Process	Calc. A_0	Exp A_0	Ref.
$CO(X^1\Sigma^+)\rightarrow C(^3P)+O^-(^2P^0)$	9.66	9.6±0.2 (O^-)	1,7
$\rightarrow C^+(^3P^0)+O^-(^2P^0)$	20.92	20.9±0.2 (C^+)	1,7
		21.1±0.2 (O^-)	1,7
$\rightarrow C^+(^2P^0)+O(^3P)$	22.37	22.8±0.2 (C^+)	1,7
$\rightarrow C^-(^4S^0)+O^+(^4S^0)$	23.22	23.2±0.2 (O^+)	1[a]
$N_2(X^1\Sigma_g^+)\rightarrow N^+(^3P)+N^4(S^0)$	24.30	24.3±0.2 (N^+)	1,3
$NO(X^2\Pi)\rightarrow N(^4S^0)+O^-(^2P^0)$	5.04	5.3±0.4 (O^-)	1
$\rightarrow N^+(^3P)+O^-(^2P^0)$	19.68	19.9±0.2 (N^+)	1
		19.8±0.2 (O^-)	1
$\rightarrow N^+(^3P)+O(^3P)$	21.03	21.7±0.2 (N^+)	1,8
$\rightarrow N(^4S^0)+O^+(^4S^0)$	20.10	20.6±0.2 (O^+)	1
$O_2(X^3\Sigma_g^-)\rightarrow O(^3P)+O^-(^2P^0)$	3.63	3.2 (O^-)	9
$\rightarrow O^+(^4S^0)+O^-(^2P^0)$	17.24	16.9±0.2 (O^+)	9
		(17.2±0.2) (O^+)	1[b]
		17.1±0.2 (O^-)	9
		(17.0±0.2) (O^-)	1[b]
$\rightarrow O^+(^4S^0)+O(^3P)$	18.69	18.9±0.2 (O^+)	9
		(19.2±0.2) (O^+)	1[b]
$\rightarrow O^{+*}(^2D^0)+O^-(^2P^0)$	20.57	20.5±0.2 (O^+)	9
		20.2±0.2 (O^-)	9
		(20.4±0.2) (O^-)	1[b]

[a] Assuming the products are C^- and O^+.
[b] Corrected as indicated in the text.

$=11.1$ ev, the process yielding unexcited $C+O^+$ should first appear at 24.7 ev. It is possible that both processes occur but that the bombarding electrons have not been sufficiently homogeneous in energy to show the onset of the second process.

Study of Table I indicates that the new value for EA(O) makes possible a satisfactory interpretation of the processes yielding O^- from CO and NO. In all cases the O^- ion is formed in its ground electronic state. Also one need not assume that the dissociation fragments possess minimum kinetic energy greater than zero in these processes in O_2.[9] However, sizable discrepancies exist between calculated and experimental values of A_0 for the processes yielding a positive ion and a neutral fragment. A similarly difficult situation exists in the interpretation of the process yielding $O+O^-$ in O_2. Here Marriott's dissociation limit of 3.2 ev, although the highest of several measurements,[7,12] is much too low.

[1] H. D. Hagstrum, Revs. Modern Phys. **23**, 185 (1951)[CO, N_2, NO, O_2].
[2] H. S. W. Massey, *Negative Ions* (Cambridge University Press, New York, 1950), second edition; O^-, p. 15, C^-, p. 18, O^{-*}, p. 20.
[3] W. W. Lozier, Phys. Rev. **44**, 575 (1933); **45**, 840 (1934) [N_2].
[4] In recent electron impact work the energies at which additional breaks occur above the first onset indicate that the products at the first break are in fact unexcited. E. M. Clarke, Can. J. Phys. **32**, 764 (1954); J. F. Burns, (private communication).
[5] W. A. Chupka and M. G. Inghram, J. Phys. Chem. **59**, 100 (1955).
[6] L. M. Branscomb and S. J. Smith (private communication), Letter to be published in *The Physical Review*.
[7] W. W. Lozier, Phys. Rev. **46**, 268 (1934) [CO, O_2].
[8] E. E. Hanson, Phys. Rev. **51**, 86 (1937) [NO].
[9] R. Thorburn, Report of Conference on Applied Mass Spectroscopy, Institute of Petroleum, London (1955) p. 185.
[10] This potential measured by Marriott relative to O_2^+ and reported by Thorburn (reference 9) is generally agreed to correspond to a minimum kinetic energy of the O^- ions greater than zero. It thus does not locate the dissociation limit for the dissociative attachement process.
[11] C. R. Lagergren (private communication).
[12] Marriott, Thorburn, and Craggs, Proc. Phys. Soc. (London) **B67**, 437 (1954).

Temperature Dependency of the Statistical Segment Size of Polyethylene*

RICHARD J. VOLUNGIS† AND RICHARD S. STEIN
Department of Chemistry, University of Massachusetts, Amherst, Massachusetts
(Received March 11, 1955)

THE difference between the principal polarizabilities of the statistical segment of an ideal stretched cross-linked rubber is given by the equation[1-3]

$$(b_{\parallel}-b_{\perp})=\frac{45knT\Delta}{2\pi(n^2+2)^2\sigma},$$

where $b_{\parallel}$ and $b_{\perp}$ are the polarizabilities of the statistical segment along and perpendicular to the contour of the chain, k is Boltzmann's constant, n is the average refractive index of the polymer, T is the absolute temperature, Δ is the birefringence (the difference between the refractive index for light polarized along the stretching direction and for light polarized in a direction perpendicular to this), and σ is the stress in dynes per cm² of actual area. $(b_{\parallel}-b_{\perp})$ may be obtained from a simultaneous measurement of Δ and σ.[4]

The stress-birefringence of the polyethylene chain is of interest as this is representative of the "backbone" of vinyl polymer chains. A study of this property is complicated by the polymer being partly crystalline at temperatures below 115°C, and by rapid relaxation at temperatures above this.[5] This relaxation may be prevented by cross-linking the polyethylene.

The study reported here was conducted on a 5 mil thick film of DYNH polyethylene cross-linked by 15 mr of electron bombardment.‡ The sample was studied in a creep type experiment at temperatures between 120°C and 170°C in 20 microns vacuum (to prevent oxidation at the higher temperatures). The length, width, and optical retardation of this sample were measured as a function of temperature during heating and cooling cycles. Sufficient time was allowed between readings to permit the sample to attain equilibrium where no further changes occurred for a period of several days in trial experiments at constant temperature. The stress and birefringence were calculated from these data. There was no evidence of crystallinity above 120°C and the temperature dependency of stress was adequately described by the kinetic theory of elasticity[6] throughout the temperature range. The number of chains per cm³, N_c, remained essentially constant indicating that the material behaved as an ideal rubber.

It was found that $(b_{\parallel}-b_{\perp})$ decreased with increasing temperature (Fig. 1). If one assumes that $(b_{\parallel}-b_{\perp})$ is proportional to the length of the statistical segment, this would mean that the segment became shorter as the temperature was increased. This is to be expected if the planar transconfiguration of the chain is most stable at low temperatures but rotation about C−C bonds increases and the chain coils at higher temperatures. This behavior is different from that of polyisobutylene, for which $(b_{\parallel}-b_{\perp})$ is independent of temperature above −35°C.[7]

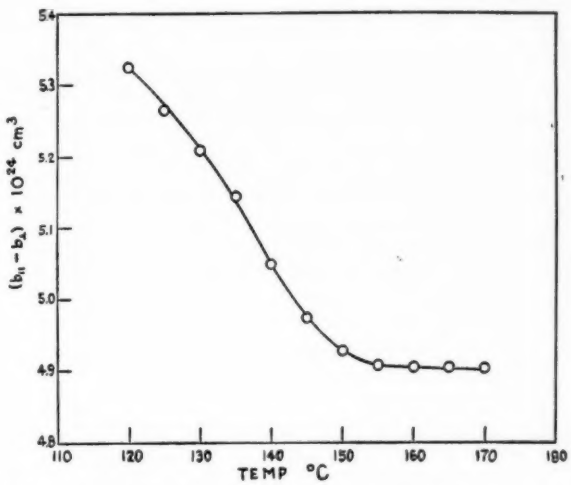

FIG. 1. The variation of $(b_{\parallel}-b_{\perp})$ with temperature for radiation cross-linked DYNH polyethylene in the rubbery state.

The distance between the ends of a free chain is proportional to the length of the statistical segment. The variation of the distance between ends with temprature depends upon the size and shape of the potential energy barrier opposing rotation about the C−C bonds.[8] One may choose values for the parameters Vm and x in the equation for the dependency of the potential on the rotation angle, ϕ,

$$V(\phi)=\tfrac{1}{2}V_m[x(1-\cos\phi)+(1-x)(1-\cos3\phi)]$$

in order to describe the variation of length and $(b_{\parallel}-b_{\perp})$ with temperature. Following Taylor[8] and assigning a shape factor of $x=0.26$, one can fit the data with a value of $Vm=6.4\pm0.7$ kcal per mole.

This value agrees quite well with that determined by Newman[9] from measurements of the variation of the width of proton magnetic resonance absorption bands with temperature for polyethylene, but is higher than the value of 4.1 kcal estimated from the thermodynamic data of Pitzer[10] on low molecular weight n-paraffin vapors.

* This work was supported in part by a contract with the Office of Naval Research.
† The contribution to this work by Mr. Volungis constitutes part of a thesis for the Degree of Master of Science at the University of Massachusetts.
[1] W. Kuhn and F. Grun, Kolloid-Z. **101**, 248 (1942); W. Kuhn, J. Polymer Sci. **1**, 380 (1946).
[2] L. R. G. Treloar, Trans. Faraday Soc. **43**, 277, 289 (1947).
[3] R. S. Stein and A. V. Tobolsky, Textile Research J. **18**, 201, 302 (1948).
[4] R. S. Stein and A. V. Tobolsky, J. Polymer Sci. **11**, 285 (1953).
[5] Stein, Krimm, and Tobolsky, J. Polymer Sci. **14**, 443 (1954).
[6] W. Kuhn, Kolloid-Z. **682** (1934).
[7] Stein, Holmes, and Tobolsky, J. Polymer Sci. **14**, 443 (1954).
‡ Supplied through the courtesy of the Chemical Division, General Electric Company, Pittsfield, Mass.
[8] W. J. Taylor, J. Chem. Phys. **15**, 412 (1947); **16**, 257 (1948).
[9] R. Newman, J. Chem. Phys. **18**, 1303 (1950).
[10] K. S. Pitzer, J. Chem. Phys. **8**, 711 (1940); Chem. Revs. **27**, 39 (1940); Ind. Eng. Chem. **36**, 829 (1944).

Some Anomalies in the Data on Coexistent Densities in the Region of the Critical Temperature

SIDNEY W. BENSON AND CHARLES S. COPELAND
Chemistry Department, University of Southern California, Los Angeles 7, California.
(Received April 14, 1955)

ALTHOUGH the critical temperature of a system seems to be a quite reproducible and directly observable property, the critical density seems somewhat elusive. The general procedure in use for establishing the critical density is to make use of the law of rectilinear diameters, that is, to plot the sum of the measured coexistent densities of liquid and vapor as a function of temperature and extrapolate, what appears to be an excellent straight line (in the neighborhood of the critical temperature) to the critical temperature and to then take the intercept as twice the critical density.

In the course of some of our work on critical phenomena we discovered that a virial expansion of the equation of state around the critical point could be used to derive an equation of the form $\phi_V+\phi_L-2=k_\phi(1-\theta)$ where ϕ_V and ϕ_L are the reduced coexistent volumes of vapor and liquid respectively.[1] A less detailed derivation has been shown to lead to a similar relation with $k_\phi=0$.[2,3] Interestingly enough, if the sums of the experimentally observed, specific volumes of coexistent liquid and vapor are plotted against temperature, the points fall on an excellent straight line for data within about 15–30°C of the critical temperature. In Fig. 1 are shown some plots of this kind for a representative selection of pure substances. For convenience the data are put in reduced form.

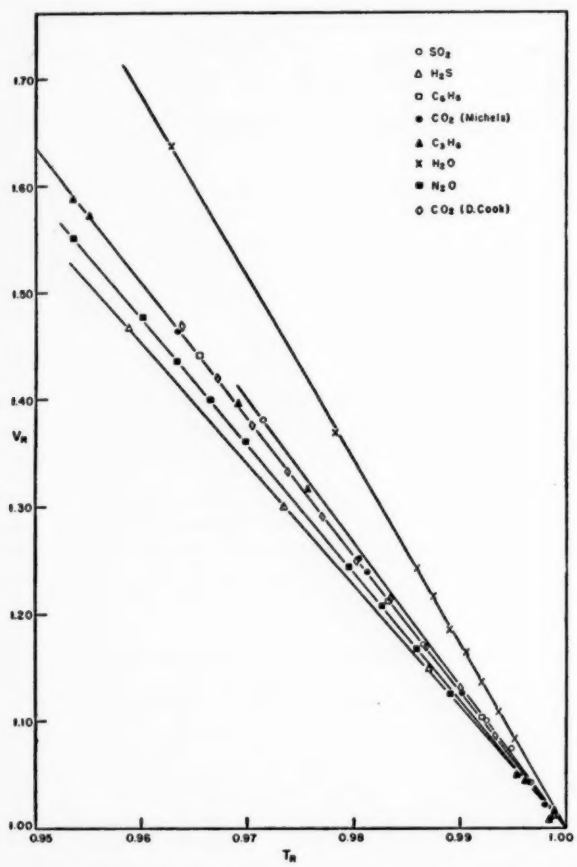

FIG. 1. Plot of the average of the coexistent volumes (ordinates) against reduced temperature (abscissa) for the substances shown in Table I. ○ = SO_2. △ = H_2S. □ = C_6H_6. ● = CO_2 (Michels *et al*). ▲ = C_3H_6. × = H_2O. ■ = N_2O. ◇ = CO_2 (Cook).

TABLE I. Comparison of critical densities obtained by extrapolation methods.

Substance	Volume extrapolation V_c(cc/g)	Volume extrapolation d_c'(g/cc)	Density extrapolation from lit., d_c(g/cc)	% difference $100(d_c-d_c')/d_c$
SO_2[a]	1.98	0.505	0.5240	+3.8
H_2S[b]	2.89	0.346	0.350	+0.6
C_6H_6[c]	3.49	0.286	0.298	+4.0
CO_2[d]	2.21	0.452	0.469	+3.5
C_3H_6[e]	4.37	0.228	0.233	+2.0
N_2O[f]	2.30	0.434	0.452	+4.0
H_2O[g]	3.22	0.310	0.323 (0.329)[h]	+4.2 (+6.1)[h]

[a] E. Cardoso and E. Sorrentino, J. chim. phys. **24**, 77 (1927).
[b] Reamer, Sage, and Lacey, Ind. Eng. Chem. **42**, 140 (1950).
[c] Gonowski, Arnick, and Hixson, Ind. Eng. Chem. **39**, 1348 (1947).
[d] Michels, Blaisse, and Michels, Proc. Roy. Soc. (London) **A160**, 358 (1937); D. Cook, Proc. Roy. Soc. (London) **A219**, 245 (1952). See also Fig. 2.
[e] W. E. Vaughan and N. R. Graves, Ind. Eng. Chem. **32**, 1252 (1940); C. A. Winkler and O. Maass, Can. J. Research **9**, 610 (1933).
[f] D. Cook, Trans. Faraday Soc. **49**, 716 (1953). These points have been fitted by a least squares method.
[g] J. H. Keenan and F. G. Keyes, *Thermodynamic Properties of Steam* (John Wiley and Sons, Inc., New York, 1936).
[h] E. H. Riesenfeld and T. L. Chang, Z. physik Chem. **B30**, 61 (1935).

Below a reduced temperature of 0.95, this sum of coexistent volumes begins to show deivations from the straight line relation.

The law of rectilinear densities, which seems to be obeyed experimentally over a much greater range of temperatures, is of course inconsistent with the law of rectilinear volumes presented above unless the temperature coefficient k_ϕ is zero or very small, so that within the accuracy of the data, the two laws appear to coincide.

A much more disturbing feature of the two laws however is that if the coexistent volumes are extrapolated to the critical temperature, the reciprocal of the intercept is not the same as that obtained from the intercept given by the law of rectilinear densities. This anomaly in the data is illustrated by the recent data of Cook on nitrous oxide which is shown plotted in Fig. 2. The dotted lines indicate the behavior which would have to be followed by the appropriate curve if the behavior of its conjugate curve were correct.

In Table I we have summarized the anomalies for the substances shown in Fig. 1. It can be seen that the density predicted by the law of rectilinear densities is about 4 percent higher for most

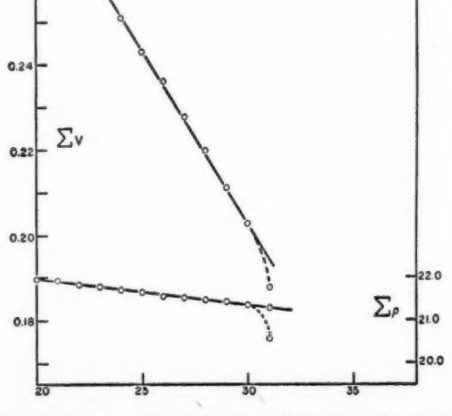

FIG. 2. Rectilinear lawa for CO_2. Data of D. Cook (see reference f of Table I). Upper line, sums of coexistent volumes (left-hand ordinates). Lower line, sums of coexistent densities (right-hand ordinates.) Abscissa, temperature in °C. Dotted lines indicate the maximum error in the linear extrapolations for each of the two laws.

substances than that given by the law of rectilinear volumes. This is beyond the experimental errors in the determinations. There are now a number of data for substances, taken within a few degrees of the critical. Unfortunately the known difficulties with gravitational density gradients tend to make these results unreliable and so we have not included points taken closer then $\frac{1}{2}$°C of the critical temperature.

There seems to be at present no compelling arguments either theoretical or experimental by which to resolve this anomaly in favor of one or the other extrapolation methods. One is forced to assume that, either there is a systematic discrepancy in volume (or density data) which reaches the order of magnitude of 4 percent near the critical, or that one or possibly both of these extrapolation methods is incorrect. Because the sums of the densities show so much smaller variations with temperature and thus fit a straight line over a much larger temperature range, one is strongly tempted to assume that it is the volume curve which will show deviations in the immediate vicinity of the critical. This is not, however, a really convincing argument.

We should like to express our indebtedness to the Office of Naval Research for their support.

[1] There is something strange about the expansion since the coefficient k_ϕ has the opposite sign to that found experimentally or even theoretically for such equations as van der Waals'.
[2] R. Fowler and E. A. Guggenheim, *Statistical Thermodynamics* (Cambridge University Press, Cambridge, England, 1949), Sec. 729.
[3] L. Landau and E. Lifschitz, *Statistical Physics* (Oxford University Press, Oxford, England, 1938), Sec. 50.

On Diffusion of Radioactive Ions in Ion Exchangers

SHINTARO SUGAI AND JIRO FURUICHI
Physics Department, Hokkaido University, Sapporo, Japan
(Received April 11, 1955)

IT seems that for the ion exchange reaction between an ion A originally in the solution and an ion B in an exchange resin, one or more of the following processes may be rate determining, namely, the diffusion of ion A or B in the solution, the diffusion of A or B in the resin, and the exchange reaction between A and B. Some authors have pointed out that especially when the concentration of A ion previously in the solution is greater than a certain degree, the most probable mechanism is bulk diffusion of the ions in the resin, but in cases when that concentration is very small, diffusion in the surface layers of the resin may be the rate determining factor.[1-3]

In order to gain more information on the aforementioned circumstances, the self-diffusion of calcium ions in a cation exchange resin, Dowex-50, was measured by the radioactive method in the present case, and E. Pitts' theory of radioactive ion exchange[4] was applied to the analysis of the results.

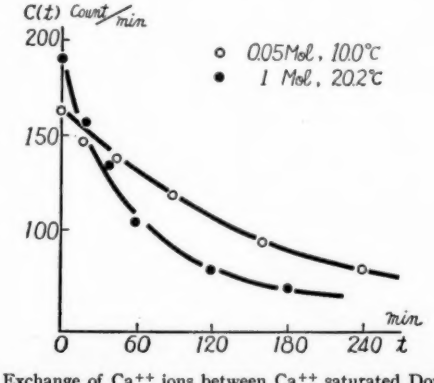

FIG. 1. Exchange of Ca^{++} ions between Ca^{++} saturated Dowex-50 and calcium chloride aqueous solution. $C(t)$ =radioactivity of solution and t=exchange time.

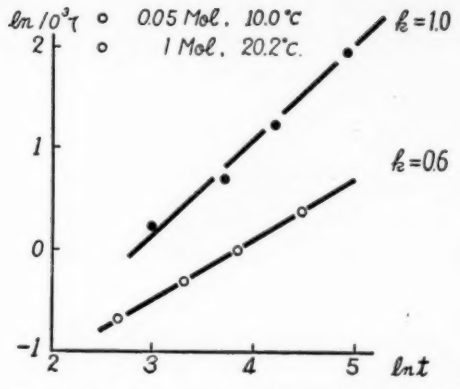

FIG. 2. The realtion between τ and t in two cases as shown in Fig. 1.

Recently, E. Pitts has developed the theory of radiaoctive ion exchange to analyze the exchange reaction of silver or halogen ions between silver-halide precipitates and silver or halogen solution as observed by A. Langer,[5] and pointed out a simple method to find the rate determining process in such cases.

In the present study, by an experimental method similar to that employed by A. Langer, calcium chloride saturated Dowex-50 was exchanged with the aqueous calcium chloride solution containing Ca^{45}.

In Fig. 1, some examples of exchange are indicated.

TABLE I. The values of k in various cases.

Size of resin mesh	Conc. of $CaCl_2$ mole/lit.	Temp. °C	k
30~40	1	1.0	1.0
30~40	1	20.2	1.0
20~30	2	10.8	1.2
20~30	1	9.0	1.0
20~30	0.5	12.5	1.0
40~50	0.05	10.0	0.6
40~50	0.008	11.0	0.7

According to E. Pitts, values of $Q(t)$, which are shown as below, can be also taken as a measure of exchange:

$$Q(t)=\frac{C(O)-C(t)}{C(O)-C(\infty)}. \tag{1}$$

Then the necessary condition is shown in Eq. (2), when diffusion in exchange resin is assumed to be the rate determining factor:

$$\ln\tau=k\ln t+\ln D/r^2 \qquad k=1, \tag{2}$$

where τ is a quantity determined by comparing the experimental $Q(t)$ and theoretical one and r is the radius of resin. Morever, the diffusion coefficient D can be also calculated by Eq. (2).

On the other hand, if the diffusion in the surface layers is important, $Q(t)$ must satisfy the condition that

$$\ln[1-Q(t)]\alpha-t. \tag{3}$$

Then, to check the solid diffusion condition (2), the relation between τ and t obtained from the results in Fig. 1 are plotted as in Fig. 2. Evidently, in the case of the use of 1-mole calcium-

TABLE II. The value of diffusion coefficient D and activation energy U in the cases of the use of 1-mole solution.

Size of resin mesh	Temp. °C	D 10^{-8} cm²/sec	U kcal/mole
30~40	1.0	0.84	
30~40	9.8	1.3	1.4
30~40	20.2	3.7	
30~40	30.7	4.0	

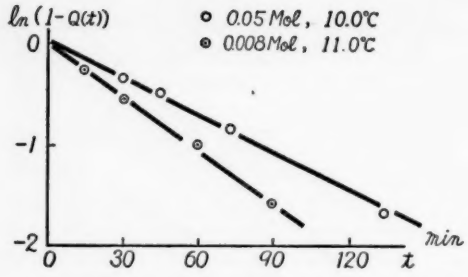

FIG. 3. Diffusion in surface film rate determining.

chloride solution, the value of the tangent is equal nearly to unity, so the main factor seems to be the bulk diffusion of calcium ion in the resin. However, in the case of the use of the dilute aqueous solution, the values of k are considerably smaller than unity.

In Table I, the values of k obtained in various cases are summarized. Certainly, the solid diffusion condition (2) is satisfied in all cases of the use of a more concentrated solution than 0.5 mole.

In Table II, the values of diffusion coefficient D in cases of the use of 1-mole solution and their temperature dependence are indicated.

Next, checking the surface diffusion condition (3) in the cases of the use of the dilute solution, the relation between $Q(t)$ and t are shown in Fig. 3. It is clear that in these cases surface diffusion may be very important.

More detailed considerations will be published later in another journal.

[1] Boyd, Adamson, and Mayer, J. Am. Chem. Soc. **69**, 2836 (1947); **72**, 4807 (1950).
[2] Merriam, Southworth, and Thomas, J. Chem. Phys. **20**, 1842 (1952).
[3] L. W. Holm, J. Chem. Phys. **22**, 1132 (1954).
[4] E. Pitts, J. Chem. Phys. **22**, 56 (1954).
[5] A. Langer, J. Chem. Phys. **10**, 321 (1942); **11**, 11 (1943).

Mercury Sensitized Decomposition of Ethylene

R. J. CVETANOVIĆ AND A. B. CALLEAR*
Division of Applied Chemistry, National Research Council, Ottawa, Canada
(Received March 21, 1955)

MERCURY sensitized decomposition of ethylene has been investigated by a number of workers. Bates and Taylor[1] suggested for the primary step an intramolecular decomposition into acetylene and hydrogen. LeRoy and Steacie[2] postulated initial formation of an excited ethylene molecule which could decompose or be deactivated by collisions

$$C_2H_4+Hg(^3P_1)\rightarrow C_2H_4^*+Hg(^1S_0), \quad (1)$$

$$C_2H_4^*\rightarrow C_2H_2+H_2, \quad (2)$$

$$C_2H_4^*+C_2H_4\rightarrow 2C_2H_4. \quad (3)$$

The proposed decomposition by a molecular process has recently been questioned and an intermediate formation of free radicals and atoms considered more probable.[3] For this reason we have carried out some experiments which appear to show in a conclusive manner that hydrogen and acetylene are formed by an intramolecular process.

Mercury sensitized decomposition of mixtures of ordinary and deuterated ethylene was carried out at room temperature to conversions not exceeding 4 percent. The result of a mass spectrometer analysis was: H_2 53.6 percent, D_2 45.2 percent HD 1.2 percent. The C_2D_4/C_2H_4 ratio was 1.54, the pressure 29.3 mm, the irradiation time 1 hour, and the amount of the three hydrogens produced 17.7 micromoles. In another experiment, with C_2D_4/C_2H_4 ratio of 1.22 at a pressure of 22 mm, 19.3 micromoles of acetylene were produced and the mass spectrometer analysis showed 39.1 percent C_2D_2, 59.1 percent C_2H_2, and 1.8 percent C_2DH. Almost exclusive formation of H_2 and D_2, as well as of C_2H_4 and C_2D_2,

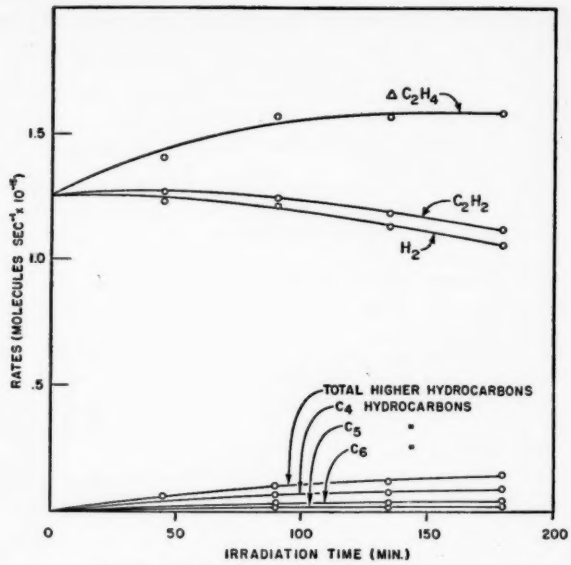

FIG. 1. Variation in reaction rates with time.

shows that these products are formed by an intramolecular process not involving intermediate formation of free radicals or atoms. The very small amounts of HD and C_2DH formed are probably due to incomplete deuterization of C_2D_4 used. The results also indicate that C_2H_4 decomposes more readily than C_2D_4. Experiments with C_2H_4 and C_2D_4 used singly have confirmed the pronounced isotopic effect. This and some other aspects of the process are being further investigated.

Primary occurrence of reactions (1) and (2) requires that the initial rates of ethylene consumption, of hydrogen and of acetylene formation should be identical and that the secondary products, resulting from hydrogenation of ethylene, should not be formed initially. Figure 1, based on mercury sensitized decomposition of 8.2 mm of ethylene in a static system, shows this to be the case. Some of the information in Fig. 1 overlaps and agrees well with the findings of LeRoy and Steacie.[2]

Darwent[4] pointed out that the above reaction scheme did not entirely agree with the observed dependence of rates on pressure. There was indication that the deactivating reaction (3) proceeded by ternary rather than binary collisions, or, alternately, that the excited ethylene molecules decomposed on the walls of the reaction vessel. Since the quantum yield decreased when mercury concentration was lowered, the latter explanation was considered to be the correct one. Direct light absorption measurements were not possible and a complete light absorption was assumed. With a mercury arc of similar construction, however, we find that the decreased yields are explainable by decreased light absorption, as measured by a phototube. A similar effect has been observed with n-butane.[5] In view of this the postulate of a heterogeneous decomposition of the excited molecules appears unnecessary. Callear and Robb have arrived at the same conclusion on the basis of experiments with a water-cooled mercury arc.[6]

Although reactions (1) and (2) of the foregoing mechanism seem to be well substantiated, there is need for a refinement of the deactivating reaction (3). At present, this can be done only on a highly speculative basis.

The authors are grateful to Dr. L. C. Leitch for preparation of deuterated ethylene and to Dr. A. Tickner for mass spectrometer analysis.

* National Research Council Postdoctorate Fellow, 1954–1955.
[1] J. R. Bates and H. S. Taylor, J. Am. Chem. Soc. **49**, 2438 (1927).
[2] D. J. LeRoy and E. W. R. Steacie, J. Chem. Phys. **9**, 829 (1941).
[3] G. B. Kistiakowski, Discussions Faraday Soc. **17**, 92 (1954).
[4] B. de B. Darwent, J. Chem. Phys. **19**, 258 (1951); *ibid.* **20**, 1673 (1952).
[5] R. J. Cvetanović, to be published in J. Chem. Phys.
[6] A. B. Callear and J. C. Robb, Discussions Faraday Soc. **17**, 21 (1954).

CONTENTS—Continued

Letters to the Editor:

Note on Hyperconjugation . . . . . Y. I'Haya 1165

Dimorphism of Para-Dichlorobenzene . . . . . G. A. Jeffrey and W. J. McVeagh 1165

On the Specific Absorption of Ions in Electrical Double Layers . . . David C. Grahame 1166

Proton Resonance in Barium Chlorate Monohydrate . . . . . R. D. Spence 1166

Comparison of the Approximate Solutions for Free Neutral Atoms . . . . . T. Tietz 1167

Electron Theory of Metals and Hydrogen Overvoltage . . . Paul Rasteski and Paul Delahay 1167

On the Entropy of Mixing of Liquid Solutions . . . . . R. Englert-Chwoles 1168

Mass Spectrometric Detection of Radicals in the Mercury Photosensitized Decomposition of Acetone . . . J. E. Farmer, F. P. Lossing, D. G. H. Marsden, and E. W. R. Steacie 1169

Ground State of the Helium Hydride Ion . . . . . Arthur A. Evett 1169

Absence of Hydrogen Bonding in an Alcohol-Thiocyanic-dissociation System . . . . . R. S. McDonald, J. H. Gibbs, and J. R. Ladd 1170

Diffusion of Zinc in Crystalline Zinc Oxide . . . . . E. A. Secco and W. J. Moore 1170

Third-Order Conjugation Energies . . . . . Y. I'Haya 1171

Theory of the Taylor-Benedict-Strong Effect . . . . . Gilbert Assat and Mark Goldsmith 1171

Microwave Spectrum of Cyclopentimine . . . . . James H. Burkhalter 1172

Number of X-Ray Diffraction Groups . . . . . Werner Nowacki 1172

Crystallographic Formalism III: Reply to Nowacki's Letter "The Number of X-Ray Diffraction Groups" . . . . . C. D. West 1172

Sensitized Luminescence of Zinc Sulfide Phosphors Activated with Copper and Manganese . . . . . Shigeo Shionoya 1173

Crystal Growth and Coercive Forces of Uniformly Prepared Ni Powders . Welby C. Courtney 1174

Calculation of Electrostatic Binding Energies in Systems of Isotropic Ions . . . . . Chester T. O'Konski 1176

Structure and Calculation of the Binding Energy of Gaseous Alkali Halide Dimers . . . . . Chester T. O'Konski and William I. Higuchi 1175

Molecular Structure of Dibutane Tetrachloride, B_2Cl_4 . . . . . Mamo Atoji, William N. Lipscomb, and P. J. Wheatley 1176

Simplified SCF Calculation for Polyenes . . . . . Hideo Kon 1176

Nuclear Quadrupole Resonances of Sb^{121} and Sb^{123} . . . . . R. G. Barnes and P. J. Bray 1177

Erratum: Nuclear Quadrupole Resonances of As^{75} . . . . . R. G. Barnes and P. J. Bray 1178

Reinterpretation of Electron Impact Experiments in CO, N_2, NO, and O_2 . . . . . Homer D. Hagstrum 1178

Temperature Dependency of the Statistical Segment Size of Polyethylene . . . . . Richard J. Volungis and Richard S. Stein 1179

Some Anomalies in the Data on Coexistent Densities in the Region of the Critical Temperature . . . . . Sidney W. Benson and Charles S. Copeland 1180

On Diffusion of Radioactive Ions in Ion Exchangers . . . Shintaro Sugai and Jiro Furuichi 1181
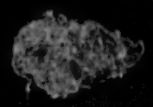
Mercury Sensitized Decomposition of Ethylene . . . . . R. J. Cvetanović and A. B. Callear 1182